NASA/CP—1999-208917

Fifth International Microgravity Combustion Workshop

Proceedings of a conference sponsored by
NASA Office of Life and Microgravity Sciences and Applications and the Microgravity Combustion Science Discipline Working Group
hosted by NASA Glenn Research Center and the National Center for Microgravity Research on Fluids and Combustion
Cleveland, Ohio
May 18–20, 1999

National Aeronautics and
Space Administration

Glenn Research Center

May 1999

Note that at the time of printing, the NASA Lewis Research Center was undergoing a name change to the NASA John H. Glenn Research Center at Lewis Field. Both names appear in these proceedings.

Available from

NASA Center for Aerospace Information
7121 Standard Drive
Hanover, MD 21076
Price Code: A23

National Technical Information Service
5285 Port Royal Road
Springfield, VA 22100
Price Code: A23

PREFACE

On behalf of the NASA Headquarters Microgravity Research Division and the Microgravity Combustion Science Discipline Working Group, we are pleased to present these proceedings of the Fifth International Microgravity Combustion Workshop. At the time we go to press we expect to welcome to the workshop over 250 presenters and participants from U.S. academia, industry, and government; and from at least 8 international partner countries. We come together for this workshop at the beginning of the International Space Station era, where the future of microgravity combustion science programs will unfold over the next few years. As we accelerate our preparations for the ISS, this book and the growing literature base cited herein provide a summary of the accomplishments of approximately forty space-flight experiment–missions (plus nearly countless drop tests and aircraft parabolas) and a valuable resource for the new experiment ideas of the future.

Since the Fourth International Microgravity Combustion Workshop in May of 1997, some important developments have occurred. We welcome to the enterprise of microgravity combustion science our new partner, the National Center for Microgravity Research in Fluids and Combustion, (NCMR) led by Professor Simon Ostrach and Mr. Thomas H. Cochran, whose contributions to the field predate the formation of the NCMR by more than three decades. The NCMR brings tremendous additional strength to the research capability of NASA in Cleveland, support for the growing international community of university, industry and government agency researchers, a revitalized outreach from fundamental combustion and fluids research to the U.S. industrial sector and a formal program for bringing the meaning of our work into the classrooms of the young researchers of tomorrow. This workshop is jointly hosted by NASA and the NCMR.

The NASA Lewis Research Center in Cleveland, Ohio has been renamed as the NASA John H. Glenn Research Center at Lewis Field (GRC). We honor this genuine space hero and U.S. Senator and the contributions of George Lewis, a hero in his own right in the wartime effort to develop aviation propulsion systems as the research director of NASA's predecessor, the National Advisory Committee on Aeronautics.

In the NASA Research Announcement process following the Fourth Workshop, 51 proposals were selected for funding from the 155 submissions; 10 as new spaceflight-definition experiments and the rest to conduct ground-based research. Two of these selections were from international proposals. This is the largest class of new microgravity combustion experiments ever selected, and we welcome the new participants to the program. Those among them who are initiating new programs (rather than renewals of earlier work) will present their research in the new poster session portion of the workshop, a dedicated time for discussion.

In the Microgravity Science Division of the NASA Glenn Research Center, we welcome Mr. Jack A. Salzman as the new Division Chief, Mr. Stephen N. Simons as the new Deputy Division Chief, and Dr. David L. Urban as the new Chief of the Microgravity Combustion Science Branch. Please join us in congratulating these new leaders.

While this is the second time our workshop proceedings have been available at the time of the workshop, we are happy with the results of our new innovation, viz., the electronic submission of papers. While about one-quarter of the authors required our assistance to achieve the desired format, the results are almost uniformly readable, and for the most part the authors

kept control over the final format of their paper. We appreciate the perseverance of the entire cadre of authors, and give our thanks both for their good cheer (mostly), and their creative use of this new technology. Please be sure to view the collection of papers on the workshop web site: http://www.ncmr.org/events/workshop.html, which was made possible by the conversion of the papers to the PDF format (which deconstructed means "portable document format," not one of the more colorful proposals we recently heard).

We have worked to improve the workshop program organization based on survey comments following the fourth workshop and on our own observations. In this fifth workshop, there are to be two parallel sessions rather than three, and more time for each paper. We've added a poster session, primarily for new participants in the program to interact more directly with the audience than might be possible in the lecture format. The workshop web site permitted on-line workshop registration and hotel reservations, plus updated schedule and logistics information without as many email prompts. Finally, we organized the workshop program with two new topics, "flammability and extinction," and "flame stability," which appeared as natural groupings of papers otherwise dispersed across the program.

We would like to thank the Combustion Institute's Sue Terpak for her very kind assistance in publicizing the workshop through the low cost method of email.

Our thanks are offered to the authors for providing the papers in a timely manner and to our colleagues at the NASA Glenn Research Center and the National Center for Microgravity Research on Fluids and Combustion for their many contributions. Assistance from the Logistics and Technical Information Division personnel at NASA Glenn Research Center in publishing this proceedings volume is gratefully acknowledged.

Finally, we thank Ann Heyward, Christine Gorecki, Norm Weinberg, Beatrix Norton, and Christina Klamer for their endless and indelible efforts to create this workshop.

Kurt R. Sacksteder
Microgravity Combustion Science Branch
Mail Stop 500-115
NASA Glenn Research Center
21000 Brookpark Road
Cleveland, OH 44135
(216) 433-2857
kurt.sacksteder@grc.nasa.gov

James S. T'ien
NCMR Senior Combustion Scientist and
Professor of Mechanical and Aerospace
Engineering
Case Western Reserve University
Cleveland, OH 44106
(216) 368-4581
jst2@po.cwru.edu

Microgravity Combustion Science Discipline Working Group:

Dr. Merrill King, Microgravity Combustion Enterprise Scientist, NASA Headquarters
Professor Chung K. Law, Princeton University (Chair)
Professor Robert Altenkirch, Mississippi State University
Professor Gerard Faeth, University of Michigan
Professor Jack Howard, Massachusetts Institute of Technology
Professor Robert Santoro, Pennsylvania State University
Professor Mitchell Smooke, Yale University
Professor Forman Williams, University of California—San Diego
Dr. Kurt Sacksteder, NASA Glenn Research Center

Plenary Papers

TABLE OF CONTENTS

Laminar Flames

NASA MICROGRAVITY COMBUSTION SCIENCE PROGRAM

Merrill K. King, NASA Headquarters, Code UG, Washington, DC 20546
merrill.king@hq.nasa.gov

5,-29

INTRODUCTION

Combustion has been a subject of increasingly vigorous scientific research for over a century, not surprising considering that combustion accounts for approximately 85% of the world's energy production and is a key element of many critical technologies used by contemporary society. Although combustion technology is vital to our standard of living, it also poses great challenges to maintaining a habitable environment. A major goal of combustion research is production of fundamental (foundational) knowledge that can be used in developing accurate simulations of complex combustion processes, replacing current "cut-and-try" approaches and allowing developers to improve the efficiency of combustion devices, to reduce the production of harmful emissions, and to reduce the incidence of accidental uncontrolled combustion. With full understanding of the physics and chemistry involved in a given combustion process, including details of the unit processes and their interactions, physically accurate models which can then be used for parametric exploration of new combustion domains via computer simulation can be developed, with possible resultant definition of radically different approaches to accomplishment of various combustion goals.

Effects of gravitational forces on earth impede combustion studies more than they impede most other areas of science. The effects of buoyancy are so ubiquitous that we often do not appreciate the enormous negative impact that they have had on the rational development of combustion science. Microgravity offers potential for major gains in combustion science understanding in that it offers unique capability to establish the flow environment rather than having it dominated by uncontrollable (under normal gravity) buoyancy effects and, through this control, to extend the range of test conditions that can be studied. It cannot be emphasized too strongly that our program is dedicated to taking advantage of microgravity to untangle complications caused by gravity, allowing major strides in our understanding of combustion processes and in subsequent development of improved combustion devices leading to improved quality of life on Earth.

Fire and/or explosion events aboard spacecraft could be devastating to international efforts to expand the human presence in space. Testing to date has shown that ignition and flame spread on fuel surfaces (e.g., paper, wire insulation) behave quite differently under partial gravity and microgravity conditions. In addition, fire signatures—i.e., heat release, smoke production, flame visibility, and radiation—are now known to be quite different in reduced gravity environments; this research has provided data to improve the effectiveness of fire prevention practices, smoke and fire detectors, and fire extinguishment systems. The more we can apply our scientific and technological understanding to potential fire behavior in microgravity and partial gravity, the more assurance can be given to those people whose lives depend on the environment aboard spacecraft or eventually on habitats on the Moon or Mars.

CURRENT PROGRAM

Currently, NASA's Microgravity Combustion Science program is supporting approximately sixty ground-based studies (including experimental studies utilizing drop-tower facilities and/or parabolic aircraft, along with analytical modeling efforts) and twenty projects which are utilizing or are expected to utilize extended duration testing in microgravity afforded by space-based experiments on sounding rockets or orbiting facilities (shuttle or space station). These studies can be divided into seven major categories: premixed gas flames; gaseous diffusion flames; combustion of individual fuel droplets, clusters of droplets, and sprays; combustion of individual solid particles and dust clouds; flame spread across liquid and solid fuel surfaces; smoldering combustion; and combustion synthesis. In addition, a number of advanced diagnostic instrumentation technologies are being developed for experimental microgravity studies, especially in the space environment, where there are severe constraints as regards volume, mass, and power. In a recent expansion of the scope of the program, we are also funding several studies whose main relevance lies in the area of access to space, rather than strictly microgravity, all related to spacecraft propulsion.

An overview of combustion experiments performed in space prior to the Microgravity Science Laboratory-1 (MSL-1) flights of April and July, 1997 was presented by this author and Dr. Howard Ross in the August, 1998 issue of the AIAA Journal (Volume 36, Number 8). Description of the experiments (Laminar Soot Processes, Structure of Flameballs at Low Lewis Numbers, and Droplet Combustion Experiment) conducted on that benchmark mission, along with preliminary results, were described in three accompanying articles by the investigators. Although the MSL-1 mission carried by far the most extensive set of space combustion experiments to date, the considerable earlier space experimentation aimed at determining the effects of microgravity on combustion processes included experiments on candle flames, combustion of fuel droplets positioned on support fibers, ignition and spread of flames across solid fuel surfaces, flame spread across liquid fuel pools, smoldering combustion, and production of soot in flames as related to fire detection. These experiments have been accompanied by numerous other microgravity experiments – providing thousands of test points – performed in the last decade in ground-based facilities such as drop towers and low-gravity aircraft in the United States, Europe, Russia, and Japan. A complete bibliography associated with these tests may be found on the Internet at http://www.lerc.nasa.gov/Other_Groups/MCFEP

To date, microgravity combustion studies have demonstrated major differences in structures of various types of flames from those seen in normal gravity. Besides the practical implications of these results to combustion efficiency (energy conservation), pollutant control (environmental considerations), and flammability (fire safety), these studies establish that better mechanistic understanding of individual processes making up the overall combustion process can be obtained by comparing of results gathered in microgravity with normal gravity tests, with potential for major improvements in design of combustion processes and hardware for use on earth as well as in space.

Future microgravity combustion experiments in space will be carried out mainly on the International Space Station (ISS) either in a dedicated Combustion Integrated Rack (CIR) with Experiment Unique Inserts or in the Microgravity Science Glovebox, a major upgrade from the Middeck Glovebox currently employed on the Shuttle. As is the case with all of the microgravity disciplines, the ISS will offer the ability to conduct a considerably larger number of microgravity combustion experiments per year, a big advantage over available opportunities on the space

shuttle; regular access to a laboratory in space should bring flight-based research more closely in line with experimentation done on Earth. The CIR performance requirement is to support an average of 5 typical combustion experiments (with many data points being obtained in each) per typical year within all known on-orbit and on-earth resource limitations, including budget. In addition, if the limiting resources are increased, the CIR shall be capable of supporting up to 15 experiments per year. Over its life cycle, the CIR shall be capable of supporting 80 percent of the combustion experiments selected into the flight program. Since CIR will be on-orbit for the life of the ISS, up to about 120 combustion experiments may eventually be conducted. Central to giving the CIR the required flexibility is the use of Principal Investigator (PI) unique combustion experiment hardware/software to customize the CIR to fully meet the PI's requirements. The CIR is scheduled for launch on UF-3 in October, 2002 and will begin its scientific work immediately. Seventeen combustion experiments are tentatively planned during the first three years of CIR operation.

Flight investigators in the NASA Microgravity Combustion Program often need to conduct reduced gravity experiments in ground-based facilities during the experiment definition and technology development phases of their programs; in addition, the duration of microgravity time available in ground-based facilities is adequate for completion of many studies without recourse to a spaceflight investigation. (Given the difference in cost, it is important that investigations be carried out in ground-based facilities where feasible.) The NASA ground-based reduced gravity research facilities include two drop towers (2.2 and 5.18 seconds of high-quality microgravity time) at the Lewis Research Center (LeRC) and a KC-135 aircraft (20-25 seconds of considerably lower quality microgravity time) that is based at JSC but flies 6-10 campaigns per year from LeRC. In addition, NASA has made arrangements to use, on a cooperative basis, a Japanese dropshaft facility in Hokkaido capable of providing 10 seconds of quality microgravity time.

HEDS ENTERPRISE

In early 1994, as part of an ongoing reorganization at NASA, the agency established six major enterprises, later reduced to four. In the current organization, the Microgravity Research Division of the Office of Life and Microgravity Sciences and Applications (OLMSA) has become part of the Human Exploration and Development of Space (HEDS) Enterprise. In January, 1996, a Strategic Plan for HEDS was put into place, and development of "roadmaps" for the future directions of activities within HEDS was initiated. The three major charges of the HEDS activities are (1) to advance and communicate scientific knowledge and understanding of the Earth, the solar system, the universe, and the environment of space for research, (2) to explore, use, and enable the development of space for human enterprise, and (3) to research, develop, verify, and transfer advanced aeronautics, space, and related technologies. While basic research into fundamentals is still considered to be vitally important to the program, there is a major shift of emphasis toward "mission-oriented" research; that is, research aimed at specific problems in combustion applications on Earth as well as under reduced or microgravity conditions. Thus, it is important that firmer linkages between the research being done using microgravity and applications to practical applications on Earth (e.g., increased efficiency of conversion of chemical energy contained in fuels to useful work, reduction of combustion-generated pollutants from automobile engines and other combustors, decreased fire and explosion hazards) be established for an increasing percentage of efforts funded under this program. In the past, we have asked our peer reviewers to judge proposals solely on scientific merit and microgravity relevance; for future

NRA's, we will extend the evaluation criteria to include responsiveness to specific areas of emphasis called out in these NRA's. The need for improved understanding of combustion phenomena to enable future space technologies and operations should be recognized as one of the primary opportunities of the discipline. Included are development of spacecraft combustion/propulsion systems, fire safety, use of *in-situ* resources, and power generation in extraterrestrial environments. Examples of local resource utilization-related processes include chemical reaction engineering for production of fuels and/or oxidizers, combustion of such products in a reduced-gravity environment, and fire safety during such operations. At a HEDS Technology Workshop held on August 5-7, 1997, several fire research areas of interest with respect to a manned Mars mission were defined.

UPCOMING MICROGRAVITY COMBUSTION NASA RESEARCH ANNOUNCEMENT

In the Microgravity Combustion Program at NASA, investigators are selected in response to a NASA Research Announcement (NRA) issued once every two years and are placed either in the Ground-based Category or in the Flight Definition Category. At this time, it is anticipated that an NRA will be released early in the Fall of this year (1999) with proposals being due approximately three months after the NRA release date; it is suggested that, even though distribution of postcards describing how to obtain the NRA will be made to an existing extensive distribution list, potential proposers contact this author to ensure that they are included on this list. As stated in NASA's Microgravity Research Program Strategic Management Handbook, the Microgravity Research Program mission is "to use the microgravity environment of space as a tool to advance knowledge; to use space as a laboratory to explore the nature of physical phenomena, contributing to progress in science and technology on Earth; and to study the role of gravity in technological processes, building a scientific foundation for understanding the consequences of gravitational environments beyond Earth's boundaries." The combustion science program seeks a coordinated research effort involving both space- and ground-based research, including both experimental and theoretical modeling efforts. Ground-based research forms the foundation of this program, providing the necessary experimental and theoretical framework for development of rigorous understanding of basic combustion phenomena. For proposals receiving awards in the Flight Definition category, the programs may proceed, following passing of a peer-reviewed Science Concept Review (SCR) and Requirements Definition Review (RDR) and acceptance of a Science Requirements Document (SRD) generated by the Principal Investigator, into the Flight Program. NASA is currently developing several types of flight hardware; brief descriptions of the planned capabilities are given in another paper. Experimental proposals for which none of the existing flight instruments is appropriate are also encouraged; however, it must be pointed out that experiments calling for facilities considerably outside of these envelopes will involve considerably more expense to NASA, a factor which must be taken into consideration in funding decisions. In addition, there is opportunity for Ground-Based investigators to participate as "guest" investigators in Glovebox Experiments on a Space Platform based on internal NASA review of proposals submitted in response to Glovebox Opportunity Announcements. [More details on these processes are available from the author.] Participation is open to U.S. and foreign investigators and to all categories of organizations: industry, educational institutions, other nonprofit organizations, NASA centers, and other U.S. Government agencies. Though NASA welcomes proposals from non-U.S. investigators, NASA does not fund principal investigators at

non-U.S. institutions.

Examination of the other papers included in this Workshop proceedings will provide the reader with a good idea of the current scope of our research program. However, future proposals are not limited to these topic areas; extension to combustion topics not currently included in the Microgravity Combustion program is strongly encouraged to help us in broadening the program scope. At this time, the Microgravity Combustion Science Discipline Working Group (external advisory group) is working with NASA personnel to develop a list of "fundamental data sets" needed for better understanding of basic combustion processes, testing of combustion models, and design of improved practical combustion devices. Included in this effort is an attempt to prioritize the resulting list in terms of both utility and need for microgravity in filling out the data set. Categories of data sets being considered include: Physico-Chemical Constants (e.g., thermal and mass diffusivity at high temperature and pressure of various species including combustion intermediates); Fundamental Combustion Parameters which are not System/Device Dependent (e.g., laminar burning velocities, extinction strain rates, soot inception points, Markstein lengths); Classical Well-Defined Benchmark Systems for Model Validation and Calibration (e.g., flame spread rates, Burke-Schumann flame shapes); and, Emerging Topics (e.g., spacecraft fire safety, SHS, flame-synthesized materials). It is anticipated that at least a preliminary prioritized data set list will be included in the upcoming NRA.

The total amount of funding for this program is subject to the annual NASA budget cycle. The Government's obligation to make awards is contingent upon the availability of appropriated funds from which payment for award purposes can be made and the receipt of proposals which the Government determines to be acceptable for an award under the upcoming NRA. For the purposes of budget planning, we have assumed that the Microgravity Research Division (MRD) will fund 0 to 3 flight experiment definition proposals from the upcoming NRA. These efforts are typically funded at an average of $150,000 to $175,000 per year. It is also anticipated that approximately 15-20 ground-based study proposals will be funded, at an average of about $80,000 to $100,000 per year, for up to 4 years.

Active research experience is one of the most effective techniques for attracting talented undergraduates to and retaining them in careers in mathematics, science, and engineering; accordingly, MRD is endeavoring to foster the career development of undergraduate students by offering optional supplements of approximately $5,000 per student per year to approved research tasks for undergraduate student research projects. These projects should involve undergraduate students in a meaningful way in ongoing research programs or in related sub-projects specifically designed for this purpose.

The principal elements considered in the evaluation of proposals solicited by this NRA are: relevance to NASA's objectives, intrinsic merit, and cost. Of these, intrinsic merit has the greatest weight, followed by relevance to NASA's objectives, of slightly lesser weight. Both of these elements have greater weight than cost. Responding to the following questions should be kept in mind by proposers:

1. Is microgravity of fundamental importance to the proposed study, either in terms of unmasking effects hidden under normal gravity conditions or in terms of using gravity level as an added independent parameter?
2. Do the issues addressed by the research have the potential to close major gaps in the understanding of fundamentals of combustion processes?

3. Is there potential for elucidation of previously unknown phenomena?
4. Is the project likely to have significant benefits/applications to ground-based as well as space-based operations involving combustion processes?
5. Is the project technologically feasible, without requirements for substantial new technological advances?
6. What is the potential of this project in terms of stimulating future technological "spin-offs"?
7. Are there strong, well-defined linkages between the research and HEDS goals

The evaluation process for the upcoming NRA will begin with a scientific and technical external peer review of the submitted proposals. NASA will also conduct an internal engineering review of the potential hardware requirements for proposals that include flight experiments. The external peer review and internal engineering review panels will be coordinated by the NASA Enterprise Scientist for Microgravity Combustion Science. Consideration of the programmatic objectives of this NRA will be factored in by NASA to ensure enhancement of program breadth, balance, and diversity; NASA will also consider the cost of the proposal. The MRD Director will make the final selection based on science panel evaluations and programmatic recommendations. Upon completion of all deliberations, a selection statement will be released notifying each proposer of proposal selection or rejection. Offerers whose proposals are declined will have the opportunity for a verbal debriefing regarding the reasons for this decision. It is anticipated that the review process should be complete by mid-2000, with awards occurring in late 2000 (early Fiscal Year 2001).

Space Station Utilisation Initiatives of the European Space Agency ESA/ESTEC

52-27

Ewald Kufner
Fluid- and Combustion Sciences Applications Co-ordinator

Directorate of Manned Spaceflight & Microgravity, ESA/ESTEC, Noordwijk,NL
Tel:+31(0)715653786; Fax:+31(0)715653661; e-mail: ekufner@estec.esa.nl

Introduction:
The overall strategic objective of ESA's Microgravity Applications Programme (MAP) is to generate a European activity using the International Space Station (ISS) as a facility for applications-oriented research and eventually for industrial R&D in the long-term. Applications of microgravity may be understood as the exploitation of the ISS for applied research and as a testbed for the development of technology and processes useful on Earth and for long-duration space flight.

Programme Strategy and Objectives:
The MAP has the objective of fostering and developing a first generation of applications-oriented projects, as far as possible with active participation of industry. These projects shall use existing microgravity platforms for precursor experiments that help develop and prepare experiment hardware for its later application on the ISS.

As a first step, this programme uses as much as possible European expertise and know-how by expanding ongoing basic research projects towards applications whenever possible. Sufficiently large European project teams are initiated, since they are essential to the efficient development, operation, and exploitation of facilities, and to carry out long term and coherent research and development programmes.

The overall approach to develop applications of microgravity can be summarised as follows:

- Identifying ongoing R & D activities where microgravity could be useful as a tool.
- Identifying and defining applications-oriented projects based on an assessment of ongoing activities and results obtained worldwide.
- Fostering the dialogue between the present traditionally scientific users and potential new users from non-aerospace industry.
- Soliciting proposals (Announcements of Opportunity/peer and expert evaluation).
- Exploiting precursor flight opportunities such as the traditional Drop Tower/Drop Tube, Aircraft, Sounding Rockets, Spacehab, and early ISS opportunities; maximum use is made of already existing and planned flight experiment hardware developed in other programmes.
- Co-ordinating with European national space agencies the development of flight experiment hardware and ground-based research financing.
- Fostering international co-operation with the U.S.A., Japan, Russia, and Canada.

Further Initiatives to Solicit new Projects:
The MAP tries to capitalise on the substantial investments made in Europe during the past 15 years in basic microgravity research. Building and expanding from this solid scientific basis and expertise appears to be very promising for the development of applications-oriented

microgravity research projects. With this philosophy in mind, seven Topical Teams have been founded in Spring, 1997. They have been addressing the following topics:

- The Influence of steady and alternating Magnetic Fields on Crystal Growth and Alloy Solidification.
- Convection and Pattern Formation in Morphological Instability during Directional Solidification.
- Metastable States and Phases.
- Equilibrium and Dynamic Properties of Adsorbed Layers.
- Dust Aggregation and Related Subjects.
- Double Diffusive Instabilities with Soret Effect
- Thermophysical Properties of Fluids.

Additionally, 5 new teams have been added in Spring, 1998, dealing with:

- Magnetic Fluids;
- Foams and Capillary Flows;
- Droplet/Particle Spray Cloud Combustion;
- Flame/Vortex Interactions;
- Combustion Synthesis.

The assignment of these teams is to form European Networks and to include researchers from industry in their discussion on procuring microgravity applications projects in their particular field.

Announcement of Opportunity 1998/1999:
ESA issued an Announcement of Opportunity (A. O.) on "Microgravity Research and Applications In Physical Sciences and Biotechnology" during November 1998 and February 1999. This A. O. solicited from European lead teams microgravity relevant research proposals that promised to contribute substantially to progress in science and technology. The proposals could concern basic or applications-oriented research programmes. Experiments could consider using Drop Towers/Tubes, Parabolic Flight Aircraft, Sounding Rockets, Getaway Specials, and the Spacehab for investigations, precursory to the main goal, using the ISS. The A. O. requested to announce planned proposals in Letters of Intent, which were due 15 December, 1998. The deadline for the submission of proposals was 28 February, 1999. ESA evaluates submitted proposals in co-operation with external peers and with its advisory bodies.

ESA issued the A. O. on a specifically installed MAP-Home Page, anybody with an Internet connection could access via the Web-address http://www.estec.esa.int/spaceflight/map/. In future, this MAP-Home Page will offer interested parties an easy access to descriptions of microgravity relevant facilities, ongoing and planned activities, and specifically, new A. O.s.

Besides issuing the A. O. on Internet, ESA initiated a mailing campaign by addressing 7194 European experts from academia and industry with a one page Article. Additionally, a Swedish industrial research institute forwarded information on the A. O. to its roughly 3600 industrial contact addresses. Paper copies of the A. O. were distributed upon request.

SPACE STATION UTILISATION INITIATIVES OF THE EUROPEAN SPACE AGENCY ESA/ESTEC: EWALD KUFNER

Statistical Analysis of the Letters of Intent:
The Letters of Intent (LOIs) had the purpose to inform ESA preliminarily about:

- the topics the proposals would refer to;
- the number of research proposals to be expected;
- the number of Topical Team proposals to be expected;
- the number of involved scientific and industrial institutions;
- the names of the team members;
- the number of basic research and applications oriented proposals;
- the national distribution of participating institutions.

Since not all LOIs contained the requested information, they only allowed for a rough statistical analysis, delivering the results the following tables summarise.

Number of received letters	212
Number of involved scientists	600
Number of industries	100
Basic research programmes	40%
Applications-oriented programmes	60%
Represented Countries	22

Trans-European distribution of the origin of the letters; this distribution does not reflect the nationalities of involved scientists or industries, but refers only to the nationalities of the submitting persons.

Germany	37%
Italy	17%
France	11%
Belgium	3.8%
Spain	3.8%
United Kingdom	2.8%
Switzerland	1.4%
The Netherlands	1.4%
Sweden	0.9%
Austria	0.5%
Denmark	0.5%
Greece	0.5%
Norway	0.5%

Additionally, Non-European experts sent 19% of the LOIs as the following table summarises:

Russia	12
Ukraine	2
Portugal	2
Canada	2
China	1

Hungary	1
Lithuania	1
Poland	1
USA	1

Topical Team Performance:
The above mentioned, in the field of Physical Sciences presently active, 12 Topical Teams submitted 28 letters with the following distribution:

Total number of teams	12
Total number of letters	28
Maximum number from one team	4
Minimum number form one team	1
Nomination of at least one industry partner	75%
No industry partner specified or basic research intention	25%

Microgravity Relevant Combustion Research Programmes:
The LOIs referring to Combustion Research Programmes addressed the topics:

Particle/spray/cloud combustion, flame-vortex interaction, soot formation, research in microgravity to enhance fire extinguishing on Earth, combustion properties of materials applied in space vehicles, combustion properties of premixed sprays, ignition extinction in microgravity, flame spread and flammability limits of diffusion flames.

Since the American FCF will be the only facility on the ISS being specifically devoted to combustion research, European experts are interested in using it. ESA, on behalf of its Member States, is therefore prepared to negotiate corresponding Barter Agreements; e. g. Europe provides inserts for the FCF also American experts can use.

We would like to point out that also experts from Non-ESA Member States can participate in European microgravity research programmes. The MAP-Home Page provides detailed information on ESA's relevant co-operation and funding policy.

OMIT THIS PAGE

Flammability/Extinction

53-29

SOLID INFLAMMABILITY BOUNDARY AT LOW SPEED (SIBAL)

James S. T'ien[1], Paul Ferkul[2], Kurt R. Sacksteder[3], Hsin-Yi Shih[1], Hasan Bedir[1], Paul S. Greenberg[3], Richard D. Pettegrew[2], Nancy Piltch[3], and David Frate[3]
[1]Case Western Reserve University, Cleveland, OH 44106
[2]National Center for Microgravity Research, Cleveland, OH 44135
[3]NASA Glenn Research Center, Cleveland, OH 44135

This research program is concerned with the effect of low-speed, concurrent flow on the spreading and extinction processes of flames over solid fuels. The primary objective is to verify the theoretically predicted extinction boundary, using oxygen percentage and flow velocity as coordinates. In particular, we are interested in the low-speed quenching limits and the existence of the critical oxygen flammability limit. Detailed flame spread characteristics, including flame spread rate, flame size, and flame structure are sought. Since the predicted flame behavior depends on the inclusion of flame and surface radiation, the measured results will also be used to assess the importance of radiative heat transfer by direct comparison to a comprehensive numerical model.

This project passed the Science Concept Review (SCR) in 1996. As a result, the experiment continues on the flight definition path, and is currently scheduled to be performed in the Space Station Combustion Integrated Rack (CIR). We present an overview of recent and ongoing work, including selected experimental and theoretical topics.

GLOVEBOX EXPERIMENTS

The SIBAL project took advantage of an opportunity to perform a Microgravity Glovebox space experiment in order to determine some long-duration burning behavior. The Forced Flow Flame Spread Test (FFFT) consisted of a test module, which was a miniature, low-speed wind tunnel; a hand-held control box; and individual fuel sample assemblies. The test module was a metallic duct with an inlet section, where air velocity measurements were made, and an outlet section where the fan that moves the air was located [1].

Flat sheets of paper fuel of different thicknesses were burned. Due to limitations in the size of this experiment, none of the flames reached steady state. General observations of flame spread rate, temperatures, and appearance were obtained, however. The flames were wide, dim, and mostly blue (see fig. 1 for an example). The wide flames were due to small airflow speed, and the dim blue flame color was due to slow oxygen transport. Flame spread rates increased as the flow speed increased, and were inversely proportional to sample thickness.

FLAME SPREAD MODEL

The model has been described in detail elsewhere [2] so only the broad features are presented here. The steady, Navier-Stokes equations are solved together with conservation of energy and reacting species. A one-step, second-order chemical reaction is assumed. Gas and solid phase radiation are included, and the gas properties are evaluated as a function of temperature.

The model was solved in two dimensions. A comparison is made with experiment in fig. 1. The fuel consumption rate contours are plotted next to the flame. These contours are the best indicator of the blue visible flame in models with one-step kinetics. In order to achieve the best agreement with experimental data, Grayson et al. [3] used $w_F = 0.1$ mg/s cm^3 to represent the

edge of the blue flame (minimum visible reaction rate) in related solid-fuel flame-spread modeling, and the same value is used here. The curvature of the visible flame is in good agreement with that of the computed reaction rate contour, even though the computed flame is steady while the observed flame did not yet reach steady state.

In concurrent-flow flame spread, however, it is well-known that in order to have a system for which the two-dimensional approximation is valid requires an excessively wide sample. Specifically, such a formulation applies for cases where the fuel is substantially wider than the flame length. This is a difficult condition to meet even for relatively small, concurrent-flow flames. Rather than attempt to build an experiment for which the two-dimensional approximation is valid, we instead developed a three-dimensional model. It is only in the initial stages, and additional work is forthcoming. While being more computationally intensive, this model can now examine the effect of varying fuel width on flame characteristics. The most obvious advantage for using a three-dimensional formulation is that the exact geometry of the experiment can be modeled.

FLAME RADIATION STUDIES

Because of the reduction of convection, radiation becomes an important heat transfer mechanism in microgravity flames. The accuracy and the affordability of computation models for radiation that can be coupled to the flame analyses are of general interest.

We have applied a variety of radiation models to a one-dimensional low-stretch diffusion flame with carbon dioxide and water vapor as the radiation participating media [4]. These include gray-gas, optical-thin, wide-band, narrow-band and spectral line weighted sum of gray gases (SLWSGG) models. Both the accuracy (in term of the radiative source, i.e., the divergence of radiative heat flux) and the relative computational times are compared. Computed results of the radiative source distribution for wide-band, narrow-band and SLWSGG show reasonable agreement with each other. Results from the optical-thin and gray-gas models with Planck mean absorption coefficient are shown to underestimate the self-absorption and overestimate the emission substantially for the low stretch flame. On the other hand, the relative computational times can be different by several orders of magnitude, the most time consuming being the narrow-band model.

Since the narrow-band model yields the more accurate spectral information among these models and is now affordable for one-dimensional flames, several computations have been carried out recently to study low-stretch flames. The narrow-band model was incorporated into a solid-fuel diffusion flame (PMMA) to investigate the flammability boundary as a function of ambient oxygen percentage and stretch rate and to study the effect of gas versus solid surface radiation [5]. In [6], a detailed account of the radiation absorption (self and across species) and emission are given including the contribution of MMA fuel vapor.

More recently, the narrow-band model has been combined with detailed chemical kinetics in the study of the flammability limit of hydrogen/oxygen gaseous diffusion flames at low pressure [7]. We have chosen an ambient pressure of 1.013 kPa with carbon dioxide as the diluent. The conditions studied are particularly relevant to Mars exploration. Fig. 2 shows the computed maximum flame temperature as a function of stretch rate with and without flame radiation. It is obvious from this figure that radiation is very important at low stretch rates. There are large drops of flame temperature at low stretch rates due to radiative losses and the flame temperature curve exhibits a peak at an intermediate stretch rate. Although this trend has been shown

previously with simplified models (either simplified kinetics or simplified radiation treatment or both), the present results with the narrow-band model and detailed kinetics are expected to be more accurate quantitatively.

Fig. 3 gives the flammability map using carbon dioxide diluent and stretch rate as coordinates. First, without radiation, the extinction boundary is monotonic with respect to stretch rate. From the trend of the computed boundary, there is no apparent low-stretch limit: when carbon dioxide dilution level is increased, the flame can still be made flammable at lower stretch rates. Furthermore, it is seen that the adiabatic system would cease to be flammable only when the carbon dioxide dilution is beyond 90% (obtained by extrapolating stretch rate to zero). With radiation, low-stretch quench limits exist and the trend of the extinction boundary is altered. This behavior helps to define an absolute carbon dioxide dilution level above which a flame can not exist at any stretch rate. The existence and the determination of this dilution level can be important from the point of view of fire safety. For the present diffusion flame at 1.013 kPa and an upstream temperature of 300 K, this dilution level is 81%, equal from both the fuel and the oxygen sides.

LOW-PRESSURE TUNNEL

We are constructing a combustion tunnel for use in normal gravity both to provide data for comparison to the model as well as to give guidance in the design of the ultimate space experiment. This vertical wind tunnel, measuring 11 cm x 11 cm, can be operated at reduced pressure to better simulate a flame burning in microgravity. The fuel, automatically supplied from a roll, will be fed in at the exact rate so that the flame will be fixed in space. Infrared and ultraviolet flame emissions will be imaged using video cameras and corresponding filters.

A central issue in this experiment is the choice of fuel. Mechanically, the fuel must be rollable both before and after combustion. Scientifically, the fuel must be well-characterized and burn in a uniform manner. These concerns are addressed by using a custom-woven fabric fuel, consisting mostly of pure cotton threads, but with some fiberglass threads woven in to provide support after combustion. The detailed specifications of the fuel are still being determined. In fact, the low-pressure tunnel will be used to refine the fuel properties to yield the optimal mechanical and scientific properties desired.

REFERENCES

[1] Sacksteder, K.R.: Forced Flow Flame Spreading Test: Preliminary Findings from the USMP-3 Shuttle Mission, Third United States Microgravity Payload: One Year Report, NASA CP-1998-207891 (1998).

[2] Shih, H.-Y. and T'ien, J. S.: Modeling Wall Influence on Solid-Fuel Flame Spread in a Flow Tunnel, presented at the AIAA 35th Aerospace Sciences Meeting, AIAA-97-0236 (1997).

[3] Grayson, G., Sacksteder, K.R., Ferkul, P. V., and T'ien, J.S.: Flame Spreading Over a Thin Solid in Low Speed Concurrent Flow: Drop Tower Experimental Results and Comparison with Theory, Microgravity Science and Technology, VII 2: 187 (1994).

[4] Bedir, H., T'ien, J. S., and Lee, H. S.: Comparison of Different Radiation Treatments for a One-dimensional Diffusion Flame, Combustion Theory and Modeling, v1, pp. 393-404 (1997).

[5] Rhatigan, J. K., Bedir, H. and T'ien, J. S.: Gas Phase Radiative Effects on the Burning and Extinction of a Solid Fuel, Combustion and Flame, v112, pp. 231-241 (1998).

[6] Bedir, H and T'ien, J. S.: A Computed Study of Flame Radiation in PMMA Diffusion Flame

Including Fuel Vapor Participation, The 27th Symposium (International) on Combustion, The Combustion Institute, to appear (1998).
[7] Shih, H.-Y., Bedir, H., T'ien, J. S., and Sung, C.-J.: Computed Flammability Limits of Opposed-Jet $H_2/O_2/CO_2$ Diffusion Flames at Low Pressures, J. of Propulsion and Power, to appear.

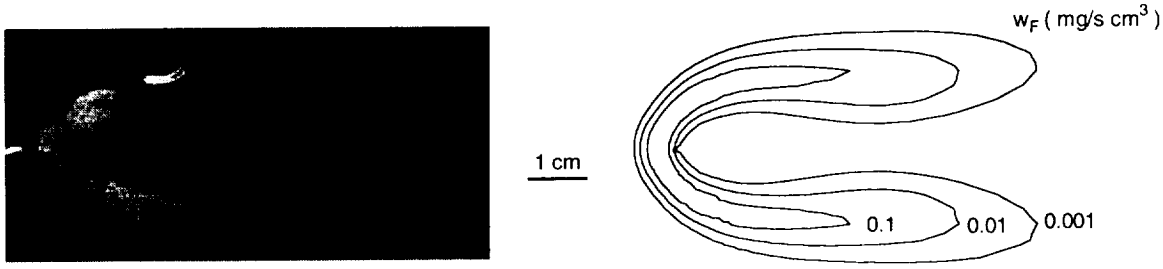

Figure 1. Concurrent-flow combustion of a paper sheet (half-thickness area density = 1.0 mg/cm^2): comparison of visible flame to numerically predicted fuel consumption rate contours. Flow is from left to right at 2 cm/s. Note that the flame is still shrinking in size, while the model results are steady.

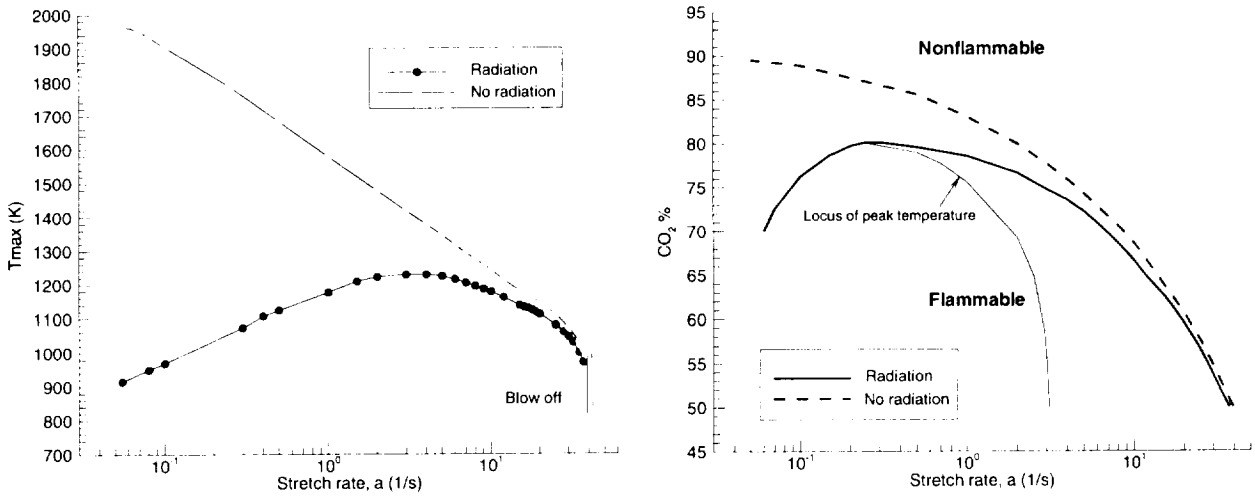

Figure 2. (Left) The maximum flame temperature of H_2/O_2 diffusion flames as a function of stretch rate (fuel side) at a total pressure of 1.013 kPa and 50% CO_2 dilution (same on the fuel and the oxygen sides), with and without the consideration of flame radiation.

Figure 3. (Right) Flammability boundary of $H_2/O_2/CO_2$ opposed-jet diffusion flame with and without the consideration of flame radiation. Total pressure: 1.013 kPa; upstream temperature: 300K.

SOME RECENT OBSERVATIONS ON THE BURNING OF ISOLATED N-HEPTANE AND ALCOHOL DROPLETS

F. L. DRYER,
Mechanical and Aerospace Engineering, Princeton University, Princeton, NJ 08544-5263

INTRODUCTION

In a joint program involving Prof. F.A. Williams of the University of California, San Diego and Dr. Vedha Nayagam of the National Center for Microgravity Research on Fluid and Combustion, the combustion of liquid fuel droplets having initial diameters between about 1 mm and 6 mm is being studied. The objectives of the work are to improve fundamental knowledge of droplet combustion dynamics through microgravity experiments and theoretical analyses. The Princeton contributions to the collaborative program supports the engineering design, data analysis, and data interpretation requirements for the study of initially single component, spherically symmetric, isolated droplet combustion studies through experiments and numerical modeling. The complementary UCSD contributions apply asymptotic theoretical analyses and are described in the published literature and in a companion communication in this volume [1].

Emphases of the Princeton work are on the study of simple alcohols (methanol, ethanol), alcohol/water mixtures, and pure alkanes (n-heptane, n-decane) as fuels, with time dependent measurements of drop size, flame-stand-off, liquid-phase composition, and finally, extinction. Ground based experiments have included bench-scale studies at Princeton and collaborative experimental studies in the 2.2 and 5.18 second drop towers at NASA-Glenn Research Center [2,3].

Spacelab studies have included fiber-supported droplet combustion (FSDC) experiments in the Glovebox facility with accompanying numerical analyses. Experiments include FSDC-1, performed on the USML-2 mission in October, 1995 (STS-73) [4,5,6,7] and FSDC-2, on the second flight of the MSL-1 mission in July, 1997 (STS-94) [8,9]. Droplets are tethered on very small diameter silicon fibers in these experiments, and combustion occurs in Space-Lab cabin air. The recent FSDC-2 experiments covered a number of different fuels, including methanol, methanol-water mixtures, ethanol, ethanol-water mixtures, methanol-dodecanol mixtures, n-heptane, n-decane and heptane-hexadecane mixtures; in addition to studying single droplets in quiescent atmospheres, the FSDC work investigated single droplets in forced convective flow of controlled velocities and droplet pairs. In total, there have now been more than 160 successful FSDC burns. The principal types of data obtained in FSDC-2 were back-lighted droplet regression data, wide-angle radiometer measurements during the combustion event, and extinction diameter at cessation of combustion [8]. Flame diameter information could also be estimated in these experiments from the locations of the flame intersections with the supporting fiber. Drop-drop interactions, flame elongation through convection, droplet and flame oscillation phenomena, staged combustion, and ignition phenomena could also be qualitatively studied. Only the quiescent combustion data on methanol, ethanol and alcohol/water isolated droplet burning are discussed here.

The first full facility droplet combustion experiments (DCE), were flown as DCE-1 on the MSL-1 mission in both the April 1997 flight (STS-83) [10,11] and the July 1997 flight (STS-94) [11,12]. The DCE-1 studies employed n-heptane as the fuel and addressed mainly the combustion of free-floated droplets, although some DCE tests also utilized a fiber support to obtain data for

comparison with FSDC results. The DCE-1 experiments were conducted primarily in oxygen-helium atmospheres at pressures of 1.00 atm., 0.50 atm. and 0.25 atm. In addition, four DCE data points were obtained in atmospheric pressure cabin air in the STS-94 flight, 2 for free droplets and 2 for fiber-supported droplets. Forty-four successful burns were obtained. The principal types of data obtained in these experiments were droplet diameter and flame diameter time histories and extinction diameters, as functions of initial oxygen index, inert, and pressure. Some initial computational comparisons with DCE-1 data for burning rate and flame/droplet diameter ratio are described in reference 12.

Additional experiments and analyses using the above fuels in drop towers and in space are planned as part of this continuing study. The space experiments include a third fiber supported droplet combustion experiment (FSDC-3) (various fuels) aboard a future shuttle flight and a second facility experiment (DCE-2) on free, isolated droplet combustion of methanol and methanol/water mixtures, in nitrogen/oxygen and nitrogen/oxygen/helium mixtures, presently under consideration for flight on the International Space Station.

SUMMARY OF RECENT RESULTS

Alcohols

The results from methanol/water droplet combustion experiments conducted on FSDC-1 and FSDC-2 were analyzed and compared against the predictions of a detailed numerical model [9]. The model used is fully time dependent, with consideration of detailed methanol oxidation chemistry, non-luminous radiative coupling, and water dissolution and vaporization from the liquid phase [7]. The effect of internal liquid phase motions observed in the experiments was approximated by enhancing liquid phase mass diffusive transport coefficients [13]. The model was found to quantitatively reproduce (without modifications or adjustments) measured burning rate, flame position histories, as well as extinction diameter, for a wide range of initial diameters and initial water content. The results showed that the effect of radiative heat loss is significant in experiments with initial diameters greater than 3 mm. Ironically, the initial droplet diameters that yield the most accurate temporal and spatial measurements (> 3 mm) are precisely those for which radiation heat loss becomes significant. Decreased burning rate and a non-linear increase in extinction diameter are observed with increasing initial diameter. Moreover, a critical radiative extinction diameter of 6 mm, predicted in a previous study for methanol droplet combustion in 1 atm. air, is verified experimentally. Fortunately, the effect of radiation loss is easily handled numerically in the case of methanol/water droplet combustion.

It should be noted here that FSDC experiments involving alcohol fuels potentially have aberrations present from the supporting filament (causing heat transfer to the droplet surface and inducing internal liquid phase motions), and from the fact that significant humidity exists in the cabin air. Water content of initially pure alcohol droplets may be modified during the formation, deployment and ignition phases of the experiment. Free and supported experiments on methanol and methanol water mixture droplets in DCE are presently in planning. Numerical studies using both nitrogen-oxygen and helium-nitrogen-oxygen mixtures have been performed to develop test matrix parameters for these future experiments. An optimal mixture ratio of nitrogen/helium mixture results in a minimum extinction diameter for droplet combustion in the same amount of oxygen and inert, pressure, and initial droplet size. The results demonstrate the competing issues of water dissolution and diffusive heat loss to the surroundings on droplet extinction.

Since the combustion of methanol creates virtually no soot, the radiative heat loss is caused solely by non-luminous thermal radiation from CO_2, CO and H_2O. In sooting fuels (e.g. alkanes,

aromatics, higher alcohols, etc.) the majority of the radiative heat loss is via continuum radiation from the soot itself, and it is very difficult to experimentally produce non-sooting conditions with these fuels. On the other hand, ethanol burns under some conditions with no soot being formed, and can be easily made to soot by raising the ambient pressure. Therefore, to accurately quantify the radiative heat loss in sooting droplet combustion, the complicated phenomena governing the production and thermophoretic collection of soot can be studied more easily using ethanol as fuel. Initial experiments on ethanol droplet burning were conducted as FSDC-2 [8]. Another communication in this volume considers this approach to the study of sooting in droplet combustion [14].

n-Heptane

Transient, spherically symmetric combustion of single and multicomponent liquid n-alkane droplets has been numerically simulated with a model that includes gas phase detailed multi-component molecular transport and complex chemical kinetics. A compact semi-detailed kinetic mechanism for n-heptane and n-hexadecane oxidation consisting of 51 species (including He, Ar, and N_2) and 282 reactions was developed to describe the gas phase chemistry [12]. The environment was considered to be non-sooting; however non-luminous, gas phase radiative heat transfer and conservation of energy and species within the liquid droplet interior were considered. Comparisons with experiments included predictions of the droplet regression rate, flame diameter and extinction diameter characteristics. No parameters were varied to obtain improved agreement with experiments.

Modeling results were found to be in reasonable agreement with small-diameter, droptower experiments, though slow convective effects and droplet sooting effects exist in the experimental data. Comparisons with isolated large-diameter free droplet data from DCE-1 (1 atm., He/O_2 mixtures and air) are reasonable for droplet gasification rate, flame/droplet radius, and flame extinction. Very small extinction diameters are predicted for small initial diameter droplets (< 1 mm). As droplet size is increased, or oxygen index is decreased, the model predicts decreasing gasification rates and for an appropriate range of parameters, radiative flame extinction.

Bi-component droplet combustion of n-heptane and n-hexadecane was also considered, again without treating issues related to sooting. Modeling results qualitatively reproduced experimentally observed, multi-stage, burning resulting from the volatility differential and diffusional resistance of the liquid components. Internal liquid convection effects were examined by parametrically varying an effective liquid mass diffusivity. Flame extinction was theoretically shown to be possible either in the initial or the secondary droplet-heating period, with subsequent, continuing vaporization of the more volatile component from the residual heat within the liquid phase. The latter was found to result in a slow, continuing vaporization of the residual droplet after combustion was extinguished. Analyses of the results of the DCE-1 experiments are continuing.

ACKNOWLDEGEMENTS

This work was supported by NASA under COOP No. NCC3-487. I gratefully acknowledge the contributions of and collaborations with fellow FSDC team members, Forman Williams, Ron Colantonio, Dan Dietrich, John Haggard, Sue Motil, Vedha Nayagam, and Ben Shaw, and fellow DCE team members, Forman Williams and Vedha Nayagam. I also wish to acknowledge the contributions at Princeton University of Anthony Marchese (Rowan University), Jordan Conley (Rowan University), Paul Michniewicz, Yolanda Stein, and Bradley Urban.

REFERENCES

1. F.A. Williams (1999). Flame Histories in Heptane Droplet Combustion. This proceedings.
2. Marchese, A.J., Dryer, F.L., Nayagam, M.V., and Colantonio, R. (1996). Microgravity Combustion of Methanol and Methanol/Water Droplets: Drop Tower Experiments and Model Predictions", 26th Symposium (Intn'l) on Combustion, The Combustion Institute, Pittsburgh, PA. p. 1209.
3. Marchese, A.J., Dryer, F.L., Nayagam, M.V., and Colantonio, R. (1996). Hydroxyl Radical Chemiluminescence Imaging and the Structure of Microgravity Droplet Flames, 26th Symposium (Intn'l) on Combustion, The Combustion Institute, Pittsburgh, PA. p. 1219.
4. Dietrich, D.L., Haggard, J.B. Jr., Dryer, F.L., Vedha-Nayagam, M., Shaw, B.D., and Williams, F.A. (1996). Droplet Combustion Experiments in Spacelab. 26th Symposium (Intn'l) on Combustion, The Combustion Institute, Pittsburgh, PA. p. 1201.
5. Dietrich, D.L., Dryer, F.L., Haggard, J.B., Jr., Nayagam,M.V., Shaw, B.D., and Williams F.A. (1997). Fiber Supported Droplet Combustion, L+1 Symposium for USML-2 Shuttle Mission, National Academy of Sciences, February, 10, 11. Published in Special Proceedings.
6. Zhang, B. L. and Williams, F. A. (1997). Theoretical Studies of Methanol Droplet Combustion Based on Results from the Shuttle Spacelab during the USML-2 Mission, Acta Astronautica 40, 829.
7. Marchese, A.J. and Dryer, F.L. (1997). The Effect of Non-luminous Thermal Radiation in Microgravity Droplet Combustion, Combust. Sci. and Tech., 124, 373.
8. Colantonio, R. O., Dietrich, D. L., Haggard, J. B., Jr., Nayagam, V., Dryer, F. L., Shaw, B. D., and Williams, F. A. (1998). Fiber Supported Droplet Combustion-2, L+1 Meeting of the MSL-1 Flight, Marshall Space Flight Center, Huntsville AL, August 25,26. Published in Special Proceedings.
9. Marchese, A.J., Dryer, F.L. and Colantonio, R. O. (1999). Radiative Effects in Space-Based Methanol/Water Droplet Combustion Experiments, 27th Symposium (Intn'l) on Combustion, The Combustion Institute, Pittsburgh, PA. 1999. p. 2627-2634.
10. Nayagam, V., Haggard, J. Colantonio, R., Marchese, A.J., Zhang, B.L., and Williams, F.A. (1998). N-Heptane Droplet Combustion in Oxygen Helium Mixtures at Atmospheric Pressure, AIAA Journal Proceedings, 36, 1369.
11. Dryer, F.L., Nayagam, V., and Williams, F. A. (1998). The Droplet Combustion Experiments on MSL-1, L+1 Meeting of the MSL-1 Flight, Marshall Space Flight Center, Huntsville AL, August 25,26. Published in Special Proceedings.
12. Marchese, A. J., Dryer, F. L. and Nayagam, V. (1999). Numerical Modeling of Isolated n-Alkane Droplet Flames: Initial Comparisons with Ground and Space-based Microgravity Experiments, Combust. Flame, 116: 432-459.
13. Marchese, A.J., and Dryer, F.L. (1996). Effect of Liquid Mass Transport on the Combustion and Extinction of Bi Component Liquid Droplets of Methanol and Water. Comb. and Flame, 105, 104.
14. Manzello, S.L., Hua, M., Choi, M.Y, and Dryer, F.L. (1999). Experiments and Model Development for the Investigation of Sooting and Radiation Effects in Microgravity Droplet Combustion, This Proceedings.

55-29

Dynamics and Structure of Weakly-Strained Flames In Normal- and Micro-gravity

HAI ZHANG, CHRISTINE M. VAGELOPOULOS & FOKION N. EGOLFOPOULOS
Department of Aerospace & Mechanical Engineering
University of Southern California
Los Angeles, California 90089-1453

Introduction

Strained laminar flames have been systematically studied, as the understanding of their structure and dynamic behavior is of relevance to turbulent combustion [e.g. 1,2]. Most of these studies have been conducted in opposed-jet, stagnation-type flow configurations. Flame studies in stagnation flows also allow for the determination of fundamental flame properties such as laminar flame speeds and extinction states [2,3] that can be also conveniently modeled in detail.

Studies at high strain rates are important in quantifying and understanding the response of vigorously-burning flames under conditions in which the transport time scales become comparable to the chemical time scales. Studies of weakly-strained flames can be of particular interest for all stoichiometries. For example, the laminar flame speeds for any equivalence ratio, ϕ, can be accurately determined by using the counterflow technique [2,3] only if measurements are obtained at very low strain rates [4]. Furthermore, near-limit flames can be only stabilized by weak strain rates. Previous studies [5,6] have shown that weakly-burning flames are particularly sensitive to chain mechanisms, thermal radiation, and unsteadiness.

The stabilization and study of weakly-strained flames is complicated by the presence of buoyancy that can render the flames unstable to the point of extinction. Such instabilities are caused either by the induced natural convection or the fact that higher density fluid can find itself on top of a lower density fluid. Thus, the use of microgravity (μg) becomes essential in order to provide meaningful insight into this important combustion regime.

Objectives

In view of the foregoing considerations, the main objectives of the program are to:

1. Experimentally determine the laminar flame speed at near-zero strain rates.
2. Experimentally determine the extinction limits of near-limit flames.
3. Experimentally determine the response of near-limit flames to unsteadiness and heat loss.
4. Introduce Digital Particle Image Velocimetry (DPIV) in microgravity.
5. Conduct detailed numerical simulations of the experiments.
6. Provide physical insight into the underlying physico-chemical mechanisms.

Experimental Approach

The counterflow configuration includes two opposing nozzles from which the reactant streams emerge and impinge on each other. Alternatively, strained flames can be established by impinging one jet on a flat plate [7]. The implementation of the stagnation flow technique in μg required the use of involved modifications compared to the normal-gravity configuration. Given that the duration of the experiments in the drop tower is 2.2 sec, the system was automated by using a tattletale-based electronic circuit. The ignition takes place at a higher (for fuel-lean mixtures) ϕ that is then reduced. Both air and fuel are stored in one-liter tanks under elevated pressures and their flow rates are controlled through calibrated sonic nozzles. In order to assure a better determination of the equivalence ratio at extinction, an approach was implemented in which the fuel reduction stops at a given time, and it is maintained constant throughout the rest of the drop. Thus, for a given strain rate, the minimum equivalence ratio that can sustain a flame is determined. Details of the μg experimental configuration are shown in Fig. 1.

While the fluid mechanics under μg conditions are described through a global strain rate, the studies in normal gravity involve the measurement of local strain rates through Laser Doppler Velocimetry (LDV). Furthermore, a Particle Streak Velocimetry (PSV) technique was developed

[8] in which velocities are determined by accurately measuring the lengths of the particle streaks. Currently, we are in the process of developing a DPIV technique appropriate for accurate velocity measurements in flames at normal gravity as well as in the 2.2-sec drop tower.

Numerical Approach

The numerical simulations of the experiments are conducted by using one-dimensional codes for freely-propagating [9] and stagnation-type flames [10]. The codes allow for the detailed description of chemical kinetics and molecular transport. Adding the effect of thermal radiation by using two approaches augmented the codes. The first includes the use of the Planck mean absorption coefficient at the optically thin limit [5,6]. The second includes the use of the detailed narrow-band radiation model, RADCAL, developed by Grosshandler [11]. This model can predict the spectral structure of various combustion products over a wide range of temperature, pressure, and pathlength. Both codes were also modified to allow for one-point continuation approach [e.g. 12] that allows for the solution around singular, turning-points.

Summary of Research

Studies have been conducted on the effect of downstream heat loss on the dynamics of strained premixed flames [7], the effect of strain rate and buoyancy on flame stability [13], the direct determination of laminar flame speeds [14], the extinction of near-limit flames [15], and the effects of unsteadiness on the flame response [6,16]. Results and discussion on near-limit flame extinction and the determination of laminar flame speeds are presented below.

Extinction of Near-Limit Lean Premixed Flames

This is an experimental and numerical study of the extinction of strained, near-limit, lean, laminar, premixed flames stabilized in an opposed-jet configuration. Previous studies [17,18] have revealed that the dependence of the extinction strain rate, K_{ext}, on the equivalence ratio, ϕ, depends on the mixture's Le number. Experiments were conducted in μg [17] and a C-shape behavior was found for lean CH_4/air mixtures, with Le<1. These results were numerically reproduced [18] and the bifurcation was found to be caused by the strain rate, as the strain rate increases, and to the synergistic effect of radiative losses and reduction of reaction intensity as the strain rate decreases for Le<1 mixtures. However, a quantitative discrepancy was found between the experiments and the simulations.

It was subsequently realized that the μg experiments of Ref. 17 were affected by upstream heat losses, as a small (1-cm) burner separation distance was used. Experiments for lean CH_4/air and C_3H_8/air mixtures were conducted by allowing for large separation distances (3-5 cm). These new data are shown in Fig. 2 along with numerical predictions that appear to be in better agreement as compared to the previous results [17,18]. Our experiments also confirm the previously observed dependence of K_{ext} on ϕ. The numerical simulations were conducted with and without upstream heat losses. It was found that upstream heat losses facilitate extinction. Figure 3 depicts the numerically determined variation of the maximum flame temperature with the global strain rate. Similarly to previous findings [18], two extinction limits are observed.

Direct Experimental Determination of Laminar Flame Speeds

The direct experimental determination of laminar flame speeds has not been previously achieved as a premixed flame must be stabilized in the laboratory either through stretch, curvature, and/or heat loss. Achieving ultra-low strain rates in the traditional stagnation flow technique is prohibited by a number of flame instabilities caused by buoyancy and pressure forces [14]. It was realized, however, that a flat flame undergoes a transition to a Bunsen flame as the flow rate is reduced and for relatively large nozzle-stagnation plane separation distance. Given that a flat flame is positively stretched while a Bunsen flame is negatively stretched [e.g. 2], it was hypothesized that as the flame undergoes that transition it must temporarily pass through a state of near-zero stretch. The schematic of transition is shown in Fig. 4.

Recording the flow velocity at locations around the vicinity of the transition region tested this hypothesis. As the flow rate is (slowly) reduced and the flame approaches the measuring point a

minimum velocity is reached, defined as a reference flame speed S_{ref}. The variation of S_{ref} with location x is shown in Fig. 5, and a "plateau" is observed just before the transition initiates. That "plateau" value is defined as the true laminar flame speed, S_u^0, as just before the transition initiates the lowest possible strain rate is obtained. Global strain rates were determined and values of the order of 5-10 s^{-1} were found. PSV measurements [8] of the local strain rate revealed values of the order of 10-30 s^{-1} for near-stoichiometric flames, which correspond to Karlovitz numbers $Ka \approx O(10^{-3})$. Laminar flame speeds were determined for atmospheric CH_4/air, C_2H_6/air, and C_3H_8/air mixtures. The present CH_4/air laminar flame speeds are shown in Fig. 6 along with values determined through linear extrapolations from data obtained in counterflow flames.

Measurements for very lean and very rich flames were not possible as the flame shape is curved upwards by buoyancy, as the forced convection is reduced. Thus, the transition is not possible and such measurements will be conducted under μg conditions with DPIV.

References

1. Peters, N.: *Prog. Energy Combust. Sci.* 10, pp. 221-252 (1984).
2. Law, C.K.: *Twenty-Second Symposium (International) on Combustion,* The Combustion Institute, Pittsburgh, 1988, pp. 1381-1402.
3. Law, C. K., Zhu, D. L. & Yu, G: *Twenty-First Symposium (International) on Combustion*, The Combustion Institute, Pittsburgh, 1986, pp. 1419-1426.
4. Vagelopoulos, C.M., Egolfopoulos, F.N. & Law, C.K., Twenty-Fifth Symposium (International) on Combustion, The Combustion Institute, Pittsburgh, 1994, pp. 1341-1347.
5. Law, C.K. & Egolfopoulos, F.N.: *Twenty-Fourth Symposium (International) on Combustion*, Combustion Institute, Pittsburgh, 1992, pp. 137-144.
6. Egolfopoulos, F.N.: *Twenty-Fifth Symposium (International) on Combustion*, Combustion Institute, Pittsburgh, 1994, pp. 1375-1381.
7. Egolfopoulos, F.N., Zhang, H. & Zhang, Z.: *Combust. Flame* 109, pp. 237-252 (1997).
8. Vagelopoulos, C.M. & Dimotakis, P.E.: "Application of Particle Streak Velocimetry in Flames," in preparation.
9. Kee, R. J., Grcar, J. F., Smooke, M. D. & Miller J. A.: A Fortran Program for Modeling Steady Laminar One-Dimensional Premixed Flames. Sandia Report SAND85-8240., 1985.
10. Egolfopoulos, F.N. & Campbell, C.S.: *J. Fluid Mech.* 318, pp 1-29 (1996).
11. Grosshandler, W. L.: RADCAL: A Narrow-Band Model for Radiation Calculations in a Combustion Environment. NIST Technical Note 1402 (1993).
12. Egolfopoulos, F.N. & Dimotakis, P.E.: "Non-Premixed Hydrocarbon Ignition at High Strain Rates," in press, *Twenty-Seventh Symposium (International) on Combustion.*
13. Vagelopoulos, C.M., Egolfopoulos, F.N. & Zhang, H.: "Dynamics and Stability Effects on Weakly-Strained Counterflowing Laminar Premixed Flames," paper No. 96F-110, Technical Meeting, *WSS/CI*, USC, Los Angeles, California, October 28-29, 1996.
14. Vagelopoulos, C.M. & Egolfopoulos, F.N.: "Direct Experimental Determination of Laminar Flame Speeds," in press, *Twenty-Seventh Symposium (International) on Combustion.*
15. Zhang. H. & Egolfopoulos, F.N.: "Detailed Studies on the Extinction of Near-Limit Premixed Flames," paper No. 98S-041, Technical Meeting, *WSS/CI*, UC Berkeley, Berkeley, California, March 23-24, 1998.
16. Zhang, H.: "An Experimental and Numerical Study of the Effects of Heat Loss and Unsteadiness on Laminar Strained Flames," Ph.D. Dissertation Thesis, USC, 1999.
17. Maruta, K, Yoshida, M, Ju, Y. & Niioka, T.: *Twenty-Sixth Symposium (International) on Combustion*, Combustion Institute, Pittsburgh, 1996, pp. 1283-1289.
18. Sung, C.J. & Law, C.K.: *Twenty-Sixth Symposium (International) on Combustion*, Combustion Institute, Pittsburgh, 1996, pp. 865-873.

Acknowledgments

This work is supported by NASA under Grant NAG3-1615 under the technical supervision of Dr. Fletcher Miller of the Lewis Research Center.

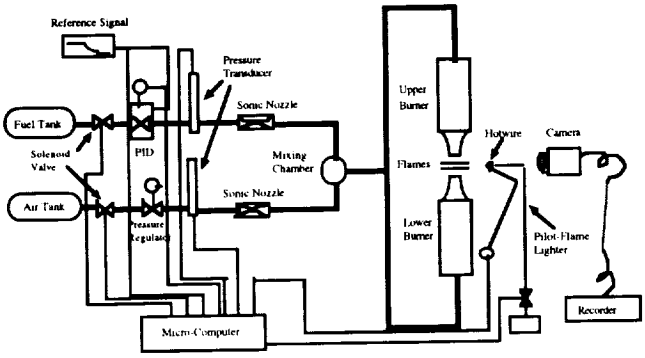

Fig. 1 Schematic of the microgravity experimental system

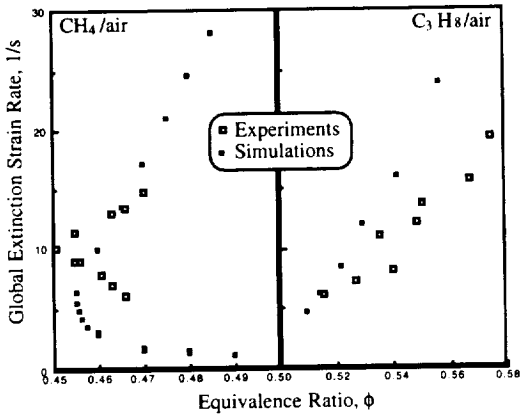

Fig. 2 Global extinction strain rates for lean flames

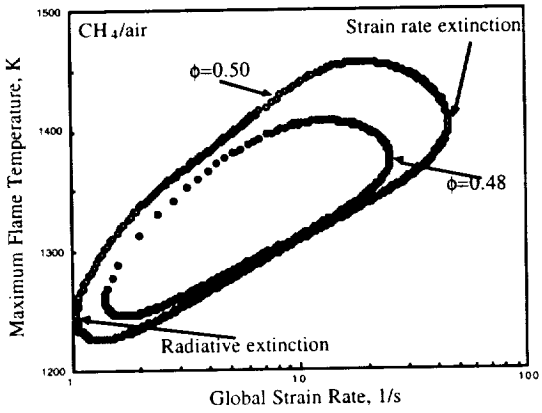

Fig. 3 Variation of flame temperature with global strain rate

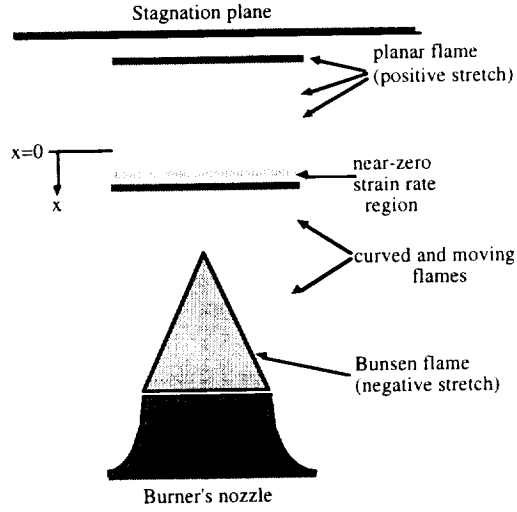

Fig. 4 Schematic of transition from flat to Bunsen flame

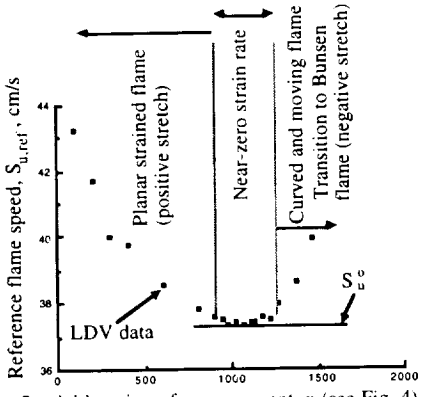

Fig. 5 Variation of $S_{u,ref}$ with spatial location and the definition of S_u^o

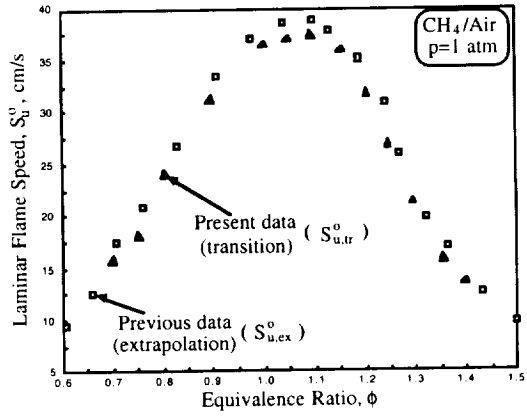

Fig. 6 Laminar flame speeds of CH_4/air flames

56-29

REFLIGHT OF THE SOLID SURFACE COMBUSTION EXPERIMENT: FLAME RADIATION NEAR EXTINCTION

R.A. Altenkirch[1], M.F. Bundy[2], L. Tang[1], S. Bhattacharjee[3], K. Sacksteder[4], and M.A. Delichatsios[5], [1]Mississippi State University, Office of Research, NSF Engineering Research Center for Computational Field Simulation, 617 Allen Hall, Mississippi State, MS 39762, altenkirch@research.msstate.edu, [2]Washington State University, School of Mechanical and Materials Engineering, Pullman, WA 99164, bundy@mme.wsu.edu, [3]San Diego State University, Department of Mechanical Engineering, San Diego, CA 92182, subrata@voyager5.sdsu.edu, [4]NASA Lewis Research Center, 21000 Brookpark Road, Cleveland, OH 44135, kurt.sacksteder@lerc.nasa.gov, [5]CSIRO Building, Construction & Engineering, North Ryde, NSW 2113, AUSTRALIA, michael.delichatsios@syd.dbce.csiro.au

INTRODUCTION

In flame spreading in quiescent and low-velocity opposing flows, effects of surface reradiation and flame radiation are important in establishing the spread rate and whether the flame, once ignited, survives to steady spread or extinguishes after a time long compared to the ignition event (Altenkirch *et al.*, 1999). A reflight of the Solid Surface Combustion Experiment (SSCE), supported by modelling, demonstrates that for thick, flat fuels, the ultimate fate of the flame is extinction rather than steady spread (West *et al.*, 1996; Altenkirch *et al.*, 1999). A mismatch between the thermal scale in the gas, driven by radiation, and the species diffusion scale, driven by mass diffusion, develops such that the high temperature regions of the flame are ultimately located in a region to which oxygen cannot be supplied at a sufficient rate to sustain reaction, and extinction occurs. Results of the experiment conducted on Space Shuttle mission STS 85 on 9 August 1997 are reviewed.

For the flat surface geometry, while the hydrodynamic phenomena associated with opposed-flow flame spread may be treated two dimensionally, the radiative effects are three dimensional, and so modelling the radiative processes, with the mismatch in dimensionality, is difficult. The cylindrical geometry, at least one long compared to the radius, provides a configuration in which the radiative processes for spread in the axial direction are two dimensional, thus simplifying the modelling. The cylindrical geometry allows for the development of more sophisticated radiative models without the complication of dimensionality concerns, e.g., discrete transfer, which is discussed in detail by Bundy (1998). Additionally, the cylindrical geometry results in a "focussing" of the heat transfer to the surface and may allow for steady spread for radii that for thick fuels of the same half-thickness there is no steady spread.

FLAT SURFACE EXPERIMENT

Results and analysis of this experiment are presented in detail elsewhere (Altenkirch *et al.*, 1999). The test apparatus was similar to that used in earlier experiments (West *et al.*, 1996), but with some notable changes. A single PMMA sample, 59.9 mm long, 3.18 mm thick, and 6.35 mm wide, more than twice the length of the earlier samples was used to obtain observations of the extended flame lifetime predicted by the numerical results. As before, the experiment was conducted inside a 39 liter chamber filled before flight with a mixture of 50% O_2, 50% N_2 at 1 atm.

The flame progress data were extracted from over 15,800 images from a video camcorder using an image analysis package developed by NASA (Klimek *et al.*, 1996). As predicted by

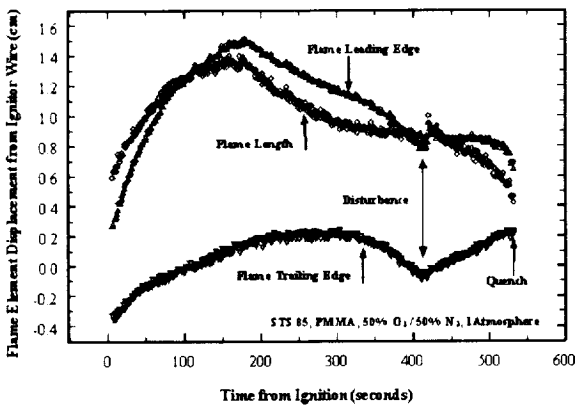

Fig. 1 Experimental flame location

the numerical model described in detail elsewhere (Altenkirch *et al.*, 1999), the flame leading edge advances at a continuously decreasing rate, stops, recedes and quenches. The trailing edge of the flame began over the back end of the sample and moved past and then away from the ignitor during the early phase of the flame lifetime. Later the trailing edge reversed direction and advanced toward the ignitor. In the original video, the ignitor wire appears to reach incandescent temperatures very briefly at this point. Thereafter, the trailing edge recedes from the ignitor and spreads forward upstream at a steady rate. The experimental results for the leading and trailing edge are shown in Fig. 1. Detailed discussion of the model results, which are consistent qualitatively with Fig. 1, are described by Altenkirch *et al.* (1999). The disturbance to which Fig. 1 refers was a bubble of fuel vapor apparently bursting, briefly ejecting a jet toward the flame. This fuel jet is visible in only two video frames (30 frames per s) indicating a maximum duration of less than $1/10^{th}$ s.

The interpretation of the experimental behavior of the leading edge of the flame is that local quenching occurs, and the leading edge retreats into a region of previously heated fuel. For the trailing edge the forward motion occurs because of heat loss near the trailing edge quenching the flame there, while the backward motion is interpreted to occur because the trailing edge spreads back into previously heated fuel as the leading edge approaches the trailing edge to heat the fuel and oxidizer there further while oxygen diffuses in. The trailing edge then moves forward again because the heat losses at the trailing edge are sufficient to quench the flame there again. Computationally, the trailing edge is not predicted to move backward; the heat losses and three-dimensional effects that occur in the trailing edge of the flame are modelled only approximately.

CYLINDRICAL GEOMETRY EXPERIMENTS

The hardware for the OFFS (Opposed-Flow Flame Spread) Glovebox experiments is shown in Fig. 2 and consists of two variable speed wind tunnels, eight fuel sample assemblies, and a control box. The miniature wind tunnels, OFFS Modules 1 and 2, provided opposing airflow. Module 1 provided flows in the range of 5-9 cm/s, and Module 2 was used for flows in the range of 2-5 cm/s.

Each fuel sample assembly consisted of a cellulosic fuel cylinder mounted on ceramic rods that were attached to the sample holder frame. The OFFS control box provided control of the Module fan speed, gas sampling for oxygen content, and fuel ignition.

Eight flame spread experiments were conducted aboard the MIR Space Station in March 1997 using the hardware described above. Three of the cellulose fuel samples were small diameter cylinders (7.5 mm), and five of the samples were large diameter cylinders (12 mm). The environmental conditions for each of the experiments were 1 atm pressure and 21% oxygen concentration (nominally station air). A summary of the experimental results is presented in the table below.

The SSCE-reflight used the same hardware as the original SSCE, except for the fuel sample assembly. Two fuel samples were used to represent three fuel geometries (Fig. 3). The first sample was a small diameter solid PMMA cylinder. The diameter of this sample was 2 mm, and the sample length was 44 mm. The second sample was a large diameter PMMA cylinder that was hollow at one end to provide a thin and thick configuration in one sample. The sample had a diameter of 6.4 mm and a length of 4 cm. The first 2 cm of the fuel was hollow with a wall thickness of 1 mm, and the second half of the fuel was solid.

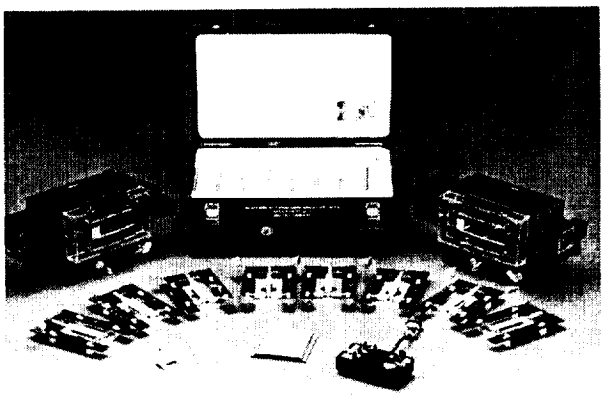

Fig. 2 OFFS hardware

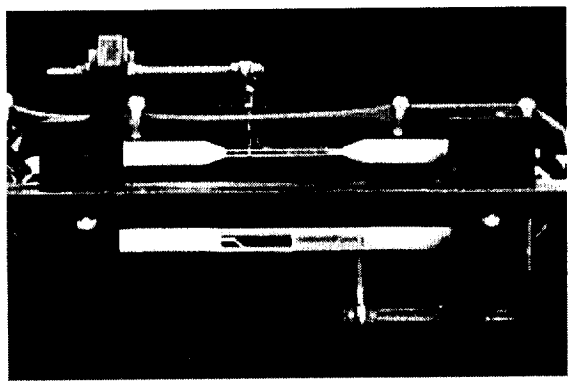

Fig. 3 SSCE cylindrical samples

Results from the OFFS and SSCE cylindrical experiments are summarized in the table below in terms of the experiments conducted and the spread rates. Additional detail is given by Bundy (1998). Spreading is steady and is predicted to be so for the cylindrical PMMA fuel in a quiescent environment for radii up to about 10 mm for 50% O_2, where as the 3.18 mm half-thickness flat sample exhibited the unsteady spread to extinction shown above.

CONCLUSIONS

We have demonstrated experimentally that flame spread over a thick, flat fuel in a quiescent, microgravity environment is inherently unsteady, with the ultimate fate of the flame being extinction. Modelling predicts this behavior for all O_2 concentrations up to pure oxygen for spread over PMMA at 1 am.

The results from the OFFS experiment in microgravity showed an apparent geometric flammability limit for cellulose fuel cylinders in a low opposed oxidizer flow. All three small diameter samples ignited and burned completely, while 4 of the 5 large diameter samples did not ignite, and the one sample that did ignite in a 9 cm/s flow extinguished when the flow velocity was reduced. The small diameter sample experiments showed an increase in flame spread rate when the flow velocity was increased from 2 cm/s to 5 cm/s, however the spread rate was

slowest at the flow velocity of 9 cm/s. A possible explanation for this unexpected decrease in spread rate for the fastest flow is that the sample was mounted with 5 gas-phase thermocouples, which may have quenched the flame enough to significantly lower its spread rate.

The results of the STS 91 Solid Surface Combustion Experiment showed the effects of cylindrical PMMA fuel geometry on flame spread in a quiescent microgravity environment. As predicted by the computations, the spread rate decreased as the fuel radius and then thickness were increased. The computed temperature, structure, and spread rates for the 3 cases compared reasonably well with the experiment in both quality and quantity.

Experiment	Measured Exp Spread Rate	Model Spread Rate
SSCE, Sample 1, PMMA R=1 mm, solid, Quiescent	3.11 mm/s	2.92 mm/s
SSCE, Sample 2, PMMA R= 3.2mm, τ=1 mm, Quiescent	0.93 mm/s	0.83 mm/s
SSCE, Sample 2, PMMA R= 3.2mm, solid, Quiescent	0.78 mm/s	0.61 mm/s
OFFS, Sample 1, cellulose R=7 mm, v_g=5 cm/s	0.11 mm/s	0.0925 mm/s
OFFS, Sample 2, cellulose R=7 mm, v_g=9 cm/s	0.049 mm/s	0.102 mm/s
OFFS, Sample 4, cellulose R=12 mm, v_g=9 cm/s	0.036 mm/s	0.0616 mm/s
OFFS, Sample 4, cellulose R=12 mm, v_g=7 cm/s	No flame	0.0532 mm/s
OFFS, Sample 4, cellulose R=12 mm, v_g=5 cm/s	No flame	0.0391 mm/s
OFFS, Sample 5, cellulose R=7 mm, v_g=2 cm/s	0.063 mm/s	0.0516 mm/s

ACKNOWLEDGEMENTS

The authors gratefully acknowledge support for this work through NASA Contract NAS3-23901 and Grants NCC3-354 and NCC3-564.

REFERENCES

Altenkirch, R.A., Tang, L., Sacksteder, K., Bhattacharjee, S., and Delichatsios, M.A. (1999). "Inherently Unsteady Flame Spread to Extinction over Thick Fuels in Microgravity," *Twenty-Seventh Symposium (International) on Combustion*, The Combustion Institute, Pittsburgh, in press.

West, J., Tang, L., Altenkirch, R.A., Bhattacharjee, S., Sacksteder, K., and Delichatsios, M.A. (1996). *Twenty-Sixth Symposium (International) on Combustion*, The Combustion Institute, Pittsburgh, pp. 1335-1343.

Bundy, M.F. (1998). "A Computational Model for Flame Spread Along Cylindrical Fuels in a Microgravity Environment," PhD Dissertation, Washington State University.

Klimek, R.G., Wright, T.W., and Sielken, R.S. (1996). "Color Image Processing and Object Tracking System," NASA Technical Memorandum, TM107144, 1996.

57-29

EDGE-FLAMES IN VON KARMAN SWIRLING FLOWS

Vedha Nayagam[1] and Forman A. Williams[2], [1]National Center for Microgravity Research, 21000 Brookpark Road, Cleveland, OH 44135, email:v.nayagam@grc.nasa.gov,[2]Center for Energy and Combustion Research, University of California, San Diego, La Jolla, CA 92093.

INTRODUCTION

Classical understanding of diffusion flames dictates that they, unlike the premixed flames, do not posses a characteristic propagation velocity and are constrained by stoichiometric requirements at the flame surface. However, it has been commonly observed that when local extinction occurs within a diffusion flame sheet, the edges that are formed propagate with distinct speeds. In general, the propagation speed of these edges depend on their geometrical shape (concave, convex, or straight) among other factors. Recently, Buckmaster [1, 2] investigated the dynamics of straight diffusion flame edges separating burning and quenched regions using simplified one-dimensional models. He showed that these flame edges can have positive, negative, or zero velocity depending on the Damköhler number of the equilibrium diffusion flame that support them. It was also shown that this unsteady flame-edge behavior is intrinsically linked to S-curve behavior of the diffusion flame with varying Damköhler number. When the system Damköhler number lies between the extinction and ignition limits, flame edges can propagate as an "ignition wave" or as a "failure wave," and for a critical Damköhler number remain as a stationary flame-edge.

We have extend Buckmaster's 1-d model to more general edge-flame configurations where the edges appear as "flame holes"[3] or as "flame disks" [4]. These two configurations along with the straight-edge case cover the entire range of possible edge-flame geometry observable in planar diffusion-flame sheets. A generalized map of edge-flame propagation velocities as function of the system Damköhler number and the edge-flame radius is presented. Experimentally we show that edge flames can be created using diffusion flames embedded in von Karman boundary layers [5]. In a von Karman boundary layer, the flow is generated by spinning a solid (fuel) disk in a quiescent ambient gas. Under normal gravity we were able to produce "flame disks" over a range of fuel-disk rotational velocities Ω varying from 0 to 20 revolutions per second, by orienting the burning surface of the fuel disk facing downward.

THEORETICAL

Consider a diffusion flame which is established by the intermixing of fuel and oxidizer supplied along the z-axis. Local extinctions can occur in the flame sheet due to perturbations in the strain rate leading to the formation of edge-flames. We consider two different edge-flame configuration: a "flame hole" where a steady flame surrounds a quenched region, and a "flame disk" where the quenched region surrounds a disk-shaped burning zone. Following Buckmaster we use activation-energy asymptotic techniques to derive expressions for edge speed as a function of system Damköhler number and the instantaneous radius of curvature. In this technique the region surrounding the edge is divided into three zones, namely, the uniform burning zone, a very thin reactive-diffusive zone at the edge, and the quenched zone. Expanding the dependent variables in terms of ε, the dimensionless activation energy, and suitably scaling the independent

variables and matching the results of each zone along the interface we obtain expression for the quasi-steady propagation speeds of the edges as a function of a reduced Damköhler number and the edge radius. The details of the analysis can be found in [3-4]. Table 1 summarizes the major results of the analysis where expressions for dimensionless edge-flame speed Pe $(=d\tilde{R}_f / d\tilde{\tau})$ are given implicitly through the reduced Damköhler number P^* and the dimensionless radius $\tilde{R}_f$. Note that a positive values Pe for a "flame hole" corresponds to an extinction wave, while it is an ignition wave for a "flame disk."

Table 1. Summary of 1-d model results for flame holes and flame disks.

Limits	*Flame Hole*	*Flame Disk*
	$P^* = k\left[1 - \dfrac{M[a+1,2,\zeta_f]}{M[a,1,\zeta_f]}\right]$	$P^* = -k\left[1 + \dfrac{U[a+1,2,\zeta_f]}{U[a,1,\zeta_f]}\right]$
$\tilde{R}_f \to \infty$	$P^* = \dfrac{1}{2}\left[\sqrt{Pe^2+4} - Pe\right]$	$P^* = \dfrac{1}{2}\left[\sqrt{Pe^2+4} + Pe\right]$
$\tilde{R}_f \to 0$	$P^* = \dfrac{k}{2}\left\{1 - \dfrac{1+\zeta_f}{[1-k\tilde{R}_f]}\right\}$	$P^* = -k\left[1 - \dfrac{1}{a\zeta_f[\log\zeta_f + \varphi(a)}\right]$

In Table.1 $M[a,1,\zeta]$ and $U[a,1,\zeta]$ are the two linearly independent confluent hypergeometric functions, also known as the Kummer functions, φ is the digamma function, $k = -1/2(Pe+\sqrt{Pe^2+4})$, $a = k/(2k+Pe)$, and $\zeta_f = \sqrt{Pe^2+4}\,\tilde{R}_f$. Figure 1 is a plot of the quasi-steady results shown in Table 1 for both flame holes and disks and illustrates the various regimes that are possible for planar edge flames. Note that as $\tilde{R}_f \to \infty$, the straight-edge results of Buckmaster are recovered. For large P^*, disks expand and holes shrink leading to a steadily burning flame. On the other hand for small P^*, disks shrink and holes expand leading to complete flame extinction. In the shaded region the holes shrink at a slower rate than the collapsing disks, i.e., failure waves catch up with ignition waves, a scenario that might lead to "flame strings." It can also be seen from the analysis that the only stationary solutions for flame edges correspond to a straight edge with $P^*=1$.

EXPEIMENTAL

A planar diffusion-flame sheet was created by igniting a spinning, PMMA fuel disk of 20 cm in diameter and 1.2 cm thickness in air. The burning surface of the fuel disk was oriented facing downward to avoid distortions of the flame by buoyancy effects. In this configuration the buoyancy forces aid the von Karman flow generated by the rotation of the fuel disk and the diffusion flame established within this mixed boundary-layer flow remained flat. Ignition was achieved by plying a butane torch across the face of the fuel plate after the desired spin velocity was established by a stepper motor controlled by a lap-top computer. Ignition duration was varied over a range, starting with a few seconds up to a minute. When long duration ignition was employed, the fuel disk was heated uniformly across its thickness, and a steady burning flame covering the entire face of the fuel disk was established for all rotational velocities of the fuel disk investigated under normal gravity. When short duration ignition was employed, however, only a

thin layer of the fuel surface was heated, and the in-depth heat loss from the fuel surface led to transient burning in the gas phase lasting several seconds. The dynamics of these transient, blue flames were recorded using an intensified-array video camera at a rate of 30 frames per second.

Starting with a fresh fuel disk, several runs were made using the same disk. Each run consisted of igniting the fuel disk and recording the transient flame behavior. During earlier runs, when only a thin layer of the fuel disk was heated, flame disks of finite radius were found to form and then shrink rapidly. Figure 2a shows the results forΩ=8 rps for several consecutive runs. After the disk was ignited several times it eventually becomes nearly uniformly heated and exhibited a growing flame disk. This is consistent with the 1-d model predictions, because as the fuel disk enthalpy increases, the effective enthalpy of vaporization decreases, the overall Damköhler number increases, and the flame edge transitions from a failure wave to an ignition wave as predicted by the model. Figure 3b shows the flame-disk radius as function of time for several different rotational speeds. Since the system Damköhler number is inversely proportional to the rotational velocity Ω, as the rotational velocity increases the edge speed decreases. According to the 1-d model prediction, for large flame-disk radius the product of flame-edge speed and rotational velocity should approach a constant. Figures 2b and 3b shows a plot ofΩPe as a function of $\tilde{R}_f$. As anticipated for large $\tilde{R}_f$ values the product approaches a constant. The 1-d model predicts that shrinking flame holes can be observed at high rotational speeds. However, only occasionally flame holes are observed in our experiments. This may be due to the fact that the radial velocity component, ignored in the model, plays a role in the behavior of the flame hole or the framing rate of the video camera is not sufficient to capture the flame-hole dynamics.

ACKNOWLEDGEMENTS

This work was supported by the NASA Microgravity Combustion Science Program. Stephen Hostler helped with the experiments and data analyses.

REFERENCES

1. Buckmaster, J. D., Edge-flames, *J. Eng. Math.* 31:269-284 (1997).
2. Buckmaster, J. D., Edge-flames and their Stability, *Combust. Sci. Tech.*, 115:41-68 (1996).
3. Nayagam, V., Balasubramaniam, R., and Ronney, P. D., Diffusion Flame Holes, *Combustion Theory and Modeling*, submitted , (1999).
4. Nayagam, V., and Williams, F. A., Diffusion-Flame Dynamics in von Karman Boundary Layers, in preparation, (1999).
5. Nayagam, V., and Williams, F. A., Stretched Diffusion Flames in von Karman Swirling Flows, 4th International Microgravity Combustion Workshop, NASA CP 10194, (1997).

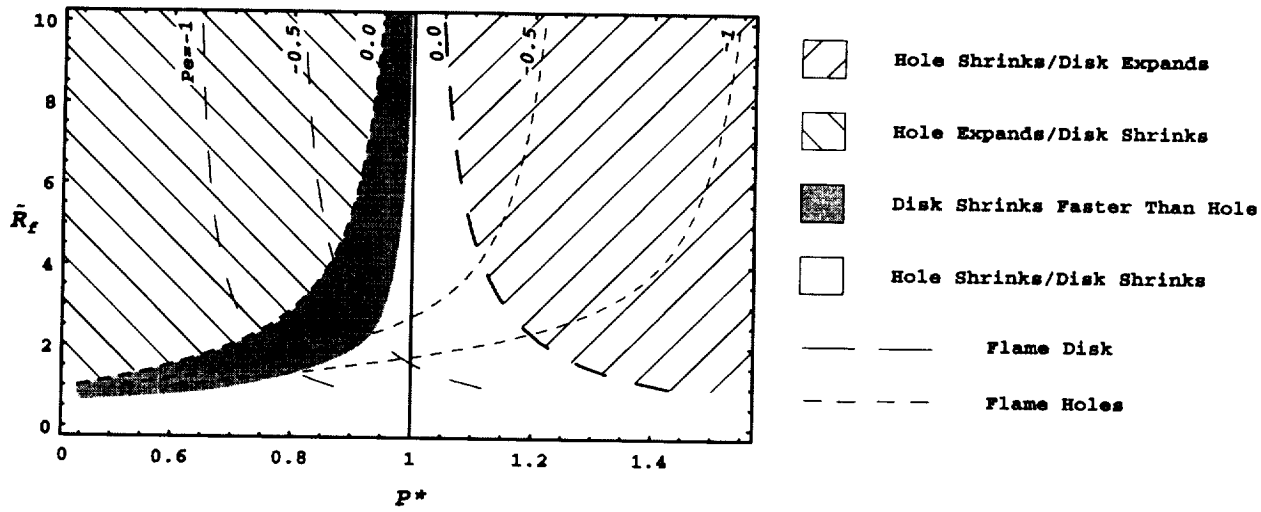

Fig. 1: Various edge-flame regimes predicted by the 1-d model

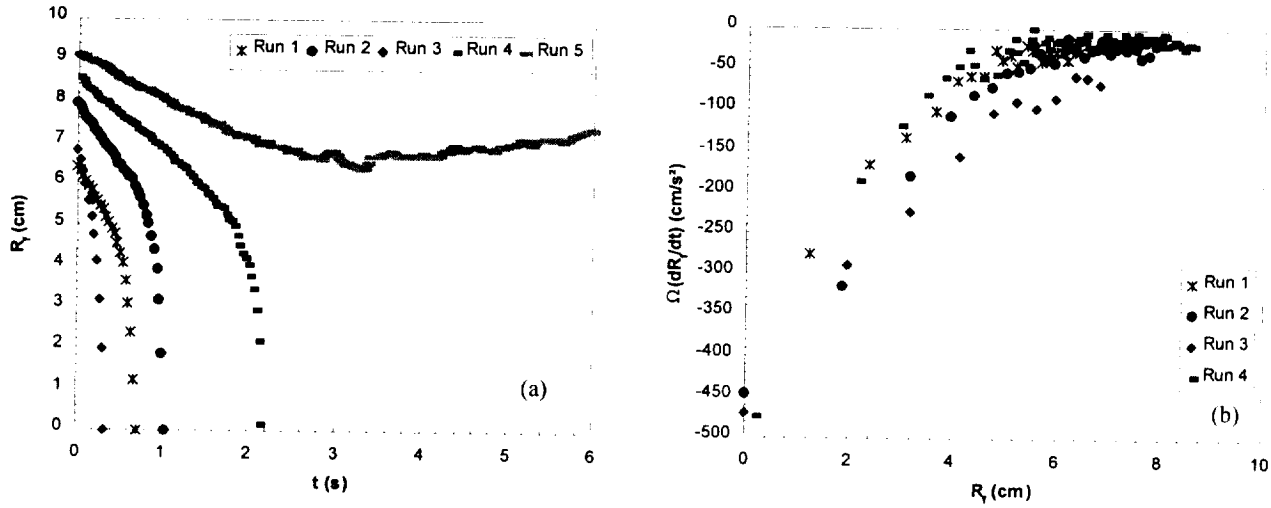

Fig. 2: Flame disk behavior at successive burns at a fixed angular velocity, $\Omega = 8$ revolutions per second (a) flame radius vs. time and (b) flame edge velocity multiplied by angular velocity vs. flame radius.

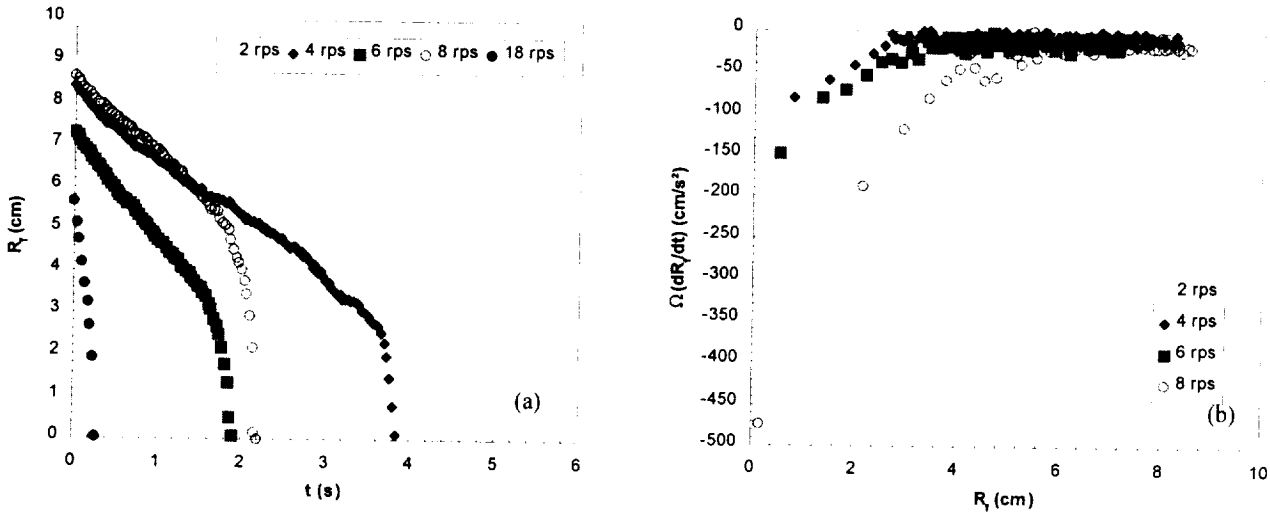

Fig. 3: (a) Flame radius vs. time and (b) flame edge velocity multiplied by angular velocity vs. flame radius

58-29

FLOW EFFECTS ON THE FLAMMABILITY DIAGRAMS OF SOLID FUELS: MICROGRAVITY INFLUENCE ON IGNITION DELAY

J. L. Cordova[1], D. C. Walther[1], A. C. Fernandez-Pello[1], T. Steinhaus[2], J. L. Torero[2], J. G. Quintiere[2], and H. D. Ross[3]

[1]Dept. of Mechanical Engineering, University of California, Berkeley, CA 94720-1740
[2]Dept. of Fire Protection Engineering, University of Maryland, College Park, MD 20742-3031
[3]NASA Glenn Research Center at Lewis Field, Cleveland, OH 44135-3191

INTRODUCTION

The possibility of an accidental fire in space-based facilities is a primary concern of space exploration programs. Spacecraft environments generally present low velocity air currents produced by ventilation and heating systems (of the order of 0.1 m/s), and fluctuating oxygen concentrations around that of air due to CO_2 removal systems. Recent experiments of flame spread in microgravity [1] show the spread rate to be faster and the limiting oxygen concentration lower than in normal-gravity. To date, there is not a material flammability-testing protocol that specifically addresses issues related to microgravity conditions. The present project (FIST) aims to establish a testing methodology that is suitable for the specific conditions of reduced gravity.

The concepts underlying the operation of the LIFT apparatus, ASTM-E 1321-93 [2-5], have been used to develop the *Forced-flow Ignition and flame-Spread Test* (FIST) [6]. As in the LIFT, the FIST is used to obtain the flammability diagrams of the material, i.e., graphs of ignition delay time and flame spread rate as a function of the externally applied radiant flux, but under forced flow rather than natural convection conditions, and for different oxygen concentrations. Although the flammability diagrams are similar, the flammability properties obtained with the FIST are found to depend on the flow characteristics.

A research program is currently underway with the purpose of implementing the FIST as a protocol to characterize the flammability performance of solid materials to be used in microgravity facilities. To this point, tests have been performed with the FIST apparatus in both normal-gravity and microgravity conditions to determine the effects of oxidizer flow characteristics on the flammability diagrams of polymethylmethacrylate (PMMA) fuel samples. The experiments are conducted at reduced gravity in a KC-135 aircraft following a parabolic flight trajectory that provides up to 25 seconds of low gravity. The objective of the experiments is to obtain data of ignition delay and flame spread rate at low flow velocities (0.1 to 0.2 m/s), which cannot be obtained under normal gravity because of the natural convection induced flows (~0.5 m/s). Due to the limited reduced gravity time, the data can only be obtained for high radiant fluxes, and are consequently limited in scope. These tests do, however, provide insight into the flammability diagram characteristics at low velocity and reduced gravity, and also into the implications of the flow-dependence of the flammability properties under environments similar to those encountered in space facilities.

NORMAL GRAVITY FLAMMABILITY DIAGRAMS

The flammability diagrams and fuel properties are obtained from a series of piloted ignition and flame-spread tests obtained with the FIST apparatus. The normal-gravity FIST apparatus consists of a rectangular combustion wind tunnel with a fuel sample mounted in one of the test section walls and an array of electrically heated radiant panels mounted in the opposite wall to that holding the fuel sample. The remaining two walls consist of quartz glass to permit optical imaging. The 560 mm long test section has a duct cross-section that is 127 mm wide by 100 mm high. The

fuel sample holder consists of a 25 mm thick Marinite section milled out to the fuel sample thickness such that the exposed fuel surface is mounted flush to the wall of the test section. A Nichrome wire igniter is located 10 mm downstream of the trailing edge of the fuel sample. Parallel to the fuel surface, a forced gas flow of a predetermined velocity and oxygen concentration is metered via critical (choked) flow nozzles and conditioned by a honeycomb filled settling section and converging duct. More detailed information on the experimental facility is provided in [7].

For the ignition delay experiments, the surface of the fuel is impulsively exposed to a uniform radiant heat flux ranging from 10 to 45 kW/m^2 with the pilot activated simultaneously. Experiments are conducted for flow velocities (measured prior to heating) which range from natural convection (~ 0.5 m/s) to 2.5 m/s. The *piloted ignition delay* of the solid fuel is recorded as a function of the given conditions, and plotted in diagrams of ignition delay versus radiant flux at the fuel surface, for different flow velocities and oxygen concentrations.

For the flame spread tests, a surface heat flux is used that decays from the critical value for ignition at the downstream edge of the fuel sample to a decreased flux at the leading edge of the sample. This spatial variation of the external flux allows for the flame spread rate dependence on the local incident heat flux to be determined with a minimum number of fuel samples. The fuel is ignited with the pilot once thermal equilibrium heating conditions have been reached. The corresponding flame spread rate is the maximum opposed spread rate attainable for the given flow conditions. A more detailed description of the experimental methods is provided in [7].

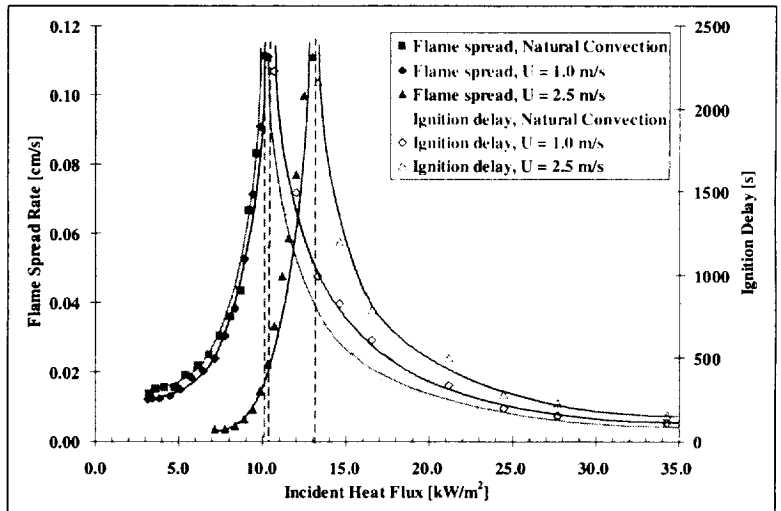

Figure 1. Flammability diagrams for different flow velocities.

Figure 1 shows the variation of the normal gravity flammability diagrams [7] for PMMA subject to natural convection conditions (no forced flow velocity) and forced air flow velocities of 1.0 and 2.5 m/s. Nominally, as the incident heat flux increases, the ignition delay decreases and spread rate increases. As the flow velocity increases, the convective cooling results in the increase of the ignition delay and reduction of the spread rate. The asymptotic value of the radiant flux below which piloted ignition does not occur (the *critical heat flux for ignition*) may also be read from Fig. 1 for different flow velocities. This critical value corresponds to the condition in which the heat losses from the fuel surface (which vary as a function of flow velocity) balance the external heat flux imposed prior to reaching the necessary solid gasification rate, thus preventing ignition. The critical heat flux also corresponds to that at which the fuel gasification is high enough prior to flame arrival so that the flame flashes across the material surface at near the premixed flame propagation rate. The flammability diagrams, as those of Fig. 1, together with a model for ignition delay and flame spread, may be used to obtain fire properties of the material such as the thermal inertia, critical heat flux for ignition, ignition temperature and flame spread constants. Clearly, these properties are a function of the flow velocity. Recent PMMA data for varying flow oxygen concentrations show that the ignition delay is independent

of the oxygen concentration for values larger than 30%, and increases as the oxygen concentration is decreased below this value until ignition is no longer possible for oxygen concentrations below 17% [8].

MICROGRAVITY FIST KC-135 EXPERIMENTS

The KC-135 microgravity FIST apparatus consists of an aluminum frame containing the sample positioning system, radiant panel arrays, and supporting instrumentation, that is housed within the Spacecraft Fire Safety Facility (SFSF) environmental chamber. A more detailed description of this facility can be found in [9]. The SFSF chamber has an internal volume of 36 L and has domed ends to provide a smooth oxidizer flow. Computer controlled solenoid valves regulate the flow rates and maintain a pressure of 1 atm throughout the chamber. The bottled oxidizer (zero air) is forced through a sintered bronze plate, providing uniform flows of up to 0.40 m/s and is exhausted through a PID controlled solenoid to the KC-135 overboard vent. The aluminum insert has a fixed array of temperature controlled radiant panels, a pair of Nichrome wire igniters, and a stepper motor to position the fuel sample cards. The fuel sample cards contain two 12 mm thick, 40 mm square PMMA samples with type K thermocouples located on both the front and rear surfaces. The sample cards are fixed to a mounting plate attached to the stepper motor and positioned by a data acquisition and control computer. A more detailed description of this facility can be found in [10].

Prior to entering the first parabolic trajectory, the heaters are brought to the desired temperature set point. During the pull-up of the trajectory, the oxidizer flow, ranging from 0.02 to 0.25 m/s, is set and the sample is moved into position. The igniters are manually activated at the beginning of the low gravity period and shut down when gravity levels are increased to ensure no ignition during the elevated gravity levels. The fuel samples are extinguished by reducing the chamber pressure to the overboard conditions. After both of the fuel samples have been burned, the chamber is flushed with the bottled oxidizer, vented, and the next sample card (10 total) is installed and positioned. Video recordings of the events are compared to the thermocouple histories to determine the ignition delay.

The available reduced low gravity period (~25 seconds) is shorter than the ignition delay in some cases. This requires that some fuel samples are subjected to the external radiant flux during the pull-up period resulting in some surface cooling by the induced buoyant flows, thereby limiting the testing range to high heat fluxes (low ignition times), 35 to 55 kW/m^2. The best effort was made to minimize the time period that the irradiated sample was subject to high gravity levels and the associated buoyant cooling. The results from these microgravity tests do, however, allow for extrapolation of the ignition branch of the flammability diagrams for low velocity flows that are not masked by buoyant flows. These data are how-

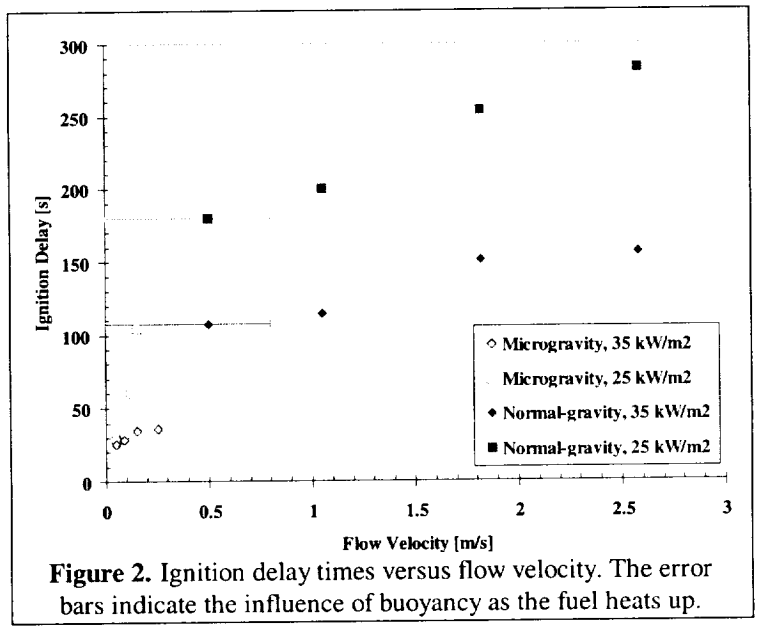

Figure 2. Ignition delay times versus flow velocity. The error bars indicate the influence of buoyancy as the fuel heats up.

ever subject to g-jitter and the resulting buoyant flows of the aircraft. Extended microgravity periods will allow for testing near the critical heat flux at oxidizer flow velocities below those attainable in normal gravity.

Preliminary microgravity ignition delay data are presented in Fig. 2. It is seen that at flow velocities below those induced by buoyancy (less than 0.5 m/s), ignition delay times reach values that are significantly below the minimums measured in normal-gravity buoyant flows. The reduction of ignition delay times under forced oxidizer velocities less than those induced by buoyant flow seems to indicate that the ignition process in these conditions is more strongly affected by surface heat losses than by the oxygen supply reduction associated with reduced convective transport rates. It is therefore necessary to examine how the interaction of these competing mechanisms affects the flammability properties of solid fuels.

CONCLUDING REMARKS

The normal gravity data indicate that the flammability properties of solid fuels are significantly affected by flow conditions. The ignition delay, critical heat flux, and the ignition temperature of the fuel decrease as the forced flow velocity decreases, until they reach minimum values determined by natural convection flows. The microgravity data obtained to date indicates that due to the absence of buoyancy this trend is continued in microgravity, and that consequently low velocity, microgravity conditions, are more hazardous from the point of view of ignition than natural convection conditions. Furthermore, they also indicate that results obtained from normal-gravity based flammability testing protocols cannot be directly extrapolated to microgravity conditions, and must be complemented by adequate microgravity tests and models in order to predict the actual flammability performance of materials in microgravity facilities.

Future work will examine the flammability behavior of composite materials. A laboratory polypropylene/glass fiber composite and commercial G10 epoxy/glass laminate are being tested in the normal gravity FIST apparatus and will be tested in a manner similar to the PMMA aboard the KC-135 low gravity aircraft.

ACKNOWLEDGMENTS

This work was funded by NASA Grants Nos. NCC3-478 and NAG-31961. The authors would like to acknowledge the efforts of the NASA Glenn Engineering and the NASA Reduced Gravity Aircraft teams. The help of M. Roslon and S. Olenick is greatly appreciated. Thanks are also due to Dr. J. Goldmeer and Dr. D. Urban for their loan of the Spacecraft Fire Safety Fac ility.

REFERENCES

[1] Olson, S. O., *Comb. Sci. Tech.*, **76**, pp. 223-249, 1991.
[2] ASTM-E 1321-93, *Annual Book of ASTM Standards*, **04-07**, pp. 1055-1077, 1993.
[3] Quintiere, J.G., *Fire and Materials*, **5**:2, pp. 52-60, 1981.
[4] Quintiere, J.G., Harkleroad, M., Walton, D., *Comb. Sci. Tech.*, **32**, pp. 67-89, 1983.
[5] Quintiere, J.G. and Harkleroad, M., NBSIR 84-2943, 1984.
[6] Cordova, J.L., Ceamanos, J., Fernandez-Pello, A.C., Long, R.T., Torero, J.L., and Quintiere, J.G, *4th Int'l Microg. Comb. Workshop*, **NASA CP-10194**, pp. 405-410, 1996.
[7] Cordova, J.L., Zhou, Y., Pfaff, C., Fernandez-Pello, A.C., Long, R.T., and Torero, J.L., *Proc. 5th ASME/JSME Joint Thermal Engin. Conf.*, **AJTE99-6244**, 1999.
[8] Pfaff, C., M.S. Report, University of California, Berkeley, 1998.
[9] Goldmeer, J.S., Ph.D. Dissertation, Case Western Reserve University 1996.
[10] Long, R.T., M. S. Thesis, University of Maryland at College Park, 1998.

59-29

COMBUSTION AND FLAMMABILITY CHARACTERISTICS OF SOLIDS AT MICROGRAVITY IN VERY SMALL VELOCITY FLOWS

C. Sánchez-Tarifa[1] and M. Rodríguez[2], [1] & [2] ETSI Aeronáuticos, Propulsion Dept., Plaza del Cardenal Cisneros, No. 3, 28040 Madrid (Spain). e-mail[1]: cstarifa@lmf.dmt.upm.es. e-mail:[2]: mrf@lmf.dmt.upm.es

INTRODUCTION

Fires still remain as one of the most important safety risk in manned spacecraft. This problem will become even more important in long endurance non orbital flights in which maintenance will be non existing or very difficult.

The basic process of a fire is the combustion of a solid at microgravity conditions in O_2/N_2 mixtures. Although a large number of research programs have been carried out on this problem, especially on flame spreading, several aspects of these processes are not yet well understood. It may be mentioned, for example, the temperature and characteristic of low emissivity flames in the visual range that take place in some conditions at microgravity; and there exists a lack of knowledge on the influence of key parameters, such as convective flow velocities of the order of magnitude of typical oxygen diffusion velocities.

The "Departamento de Motopropulsión y Termofluidodinámica" of the "Universidad Politécnica de Madrid, Escuela Técnica Superior de Ingenieros Aeronáuticos" is conducting a research program on the combustion of solids at reduced gravity conditions within O_2/N_2 mixtures. The material utilized has been polymethylmethacrylate (PMMA) in the form of rectangular slabs and hollow cylinders. The main parameters of the process have been small convective flow velocities (including velocity angle with the direction of the spreading flame) and oxygen concentration. Some results have also been obtained on the influence of material thickness and gas pressure.

The experimental program has been continuously supported by ESA, including three parabolic flight campaigns in the NASA KC-135 and one in the ESA Caravelle; a MiniTexus sounding rocket launched in 1995 and a Texus launching that would be carried out in November/December of this year.

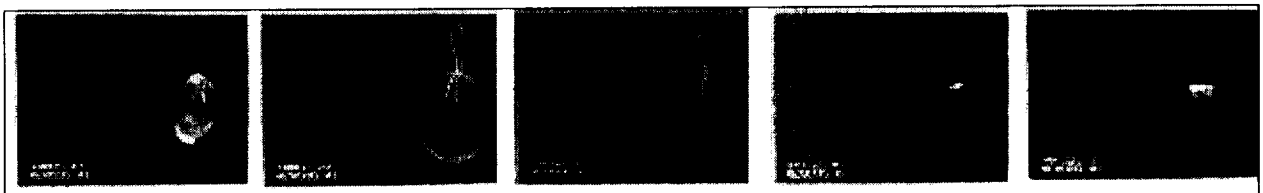

Flow Vel. $U_\infty = 0$ t = - 36.61 s since flow starts.	$U_\infty = 0$ t = - 34.77 s since flow starts.	$U_\infty = 0$ t = - 29.62 s since flow starts.	$U_\infty = 8$ mm/s t = + 0.32 s since flow starts.	$U_\infty = 12$ mm/s t = + 1.08 s since flow starts.

Fig. 1.-MiniTexus tests. PMMA hollow cylinder (ϕ = 6 mm). Wall thick = 2 mm. YO_2 = 40%. Pressure ≈ 100 kPa.

A considerable amount of information of flame spreading and flammability limits have already been obtained, as shown in the references. Some significant findings are also shown in Figs. 1 to 5. In Fig. 1 the ignition and combustion processes of a PMMA cylinder in an O_2/N_2 mixtures (40% O_2) are shown, obtained in the MiniTexus experiments. The premixed and diffusion flames are followed by a long period (30 s) in which the flame becomes non visible. Throughout this period the atmosphere is at rest. Then a forced air flow is started becoming visible the flame at very small velocities and within a very short time.

In Fig. 2 simultaneous video and infrared photographs of the combustion of a similar PMMA cylinder are shown, in a still O_2/N_2 mixtures (23% O_2). They where obtained in a parabolic flight (NASA KC-135). It may be pointed out that at 40% O_2 in the parabolic flight the flame was of a normal visible type, showing the influence of the different gravity level, when comparing these results with those obtained in the MiniTexus.

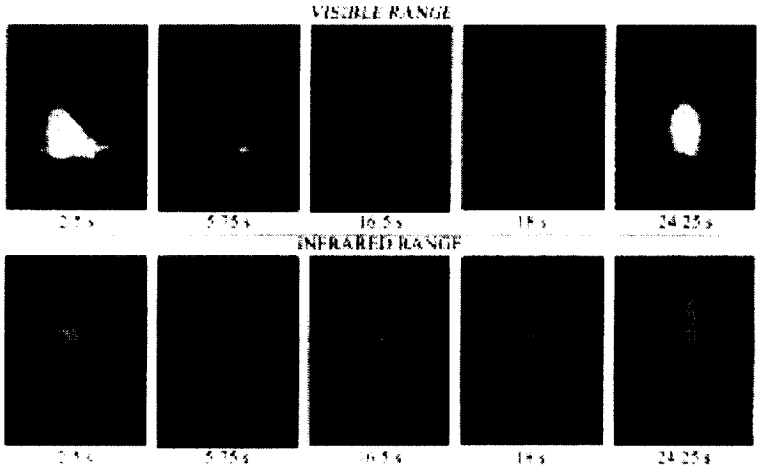

Fig. 2.-Parabolic flight. Simultaneous video and infrared photographs. ϕ = 6 mm. Wall thick. = 2 mm. Pressure 100 kPa. YO_2 = 23%.

In Figs. 3 and 4 some results of the influence of forced convection velocities and oxygen mass fraction on flame spreading velocity are shown. Finally, in Fig. 5 it may be seen the influence of the gravity level on the values of the spreading velocity.

Due to the very large number of inter-related parameters of the process: type of material, configuration, thickness, O_2 concentration, pressure, and convective flow velocity; the test matrix is very large and it would require a very long time and it would be very costly to accomplish the program utilizing sounding rockets (parabolic flights provide an insufficient gravity level and in drop towers the testing time is too short).

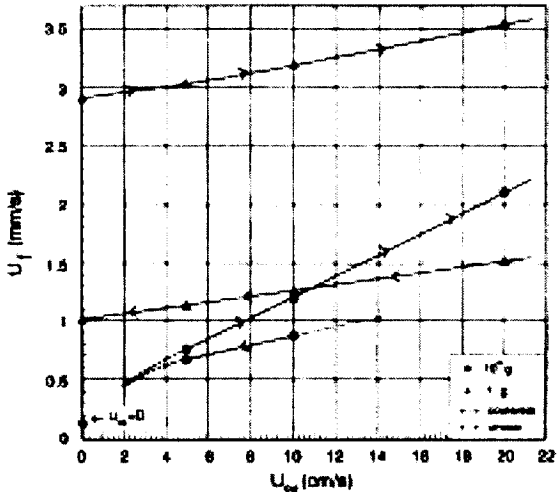

Fig. 3.-Flame spreading vs. forced flow velocity. MiniTexus results. ϕ = 6 mm. Wall thick. = 2 mm. P = 100 kPa. YO_2 = 40%. Flow incidence angle 45°

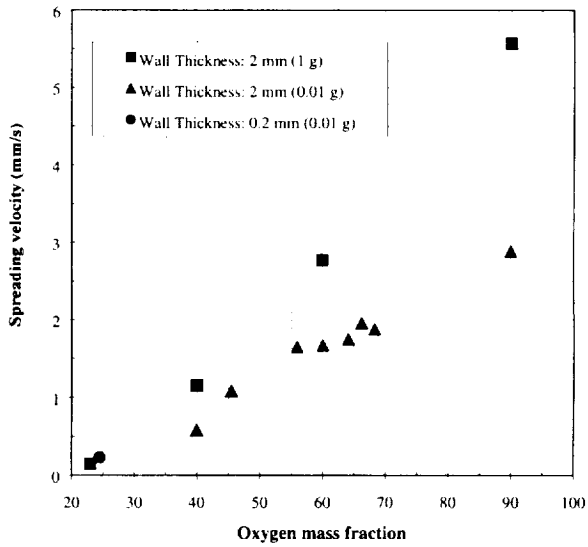

Fig. 4.- Influence of O_2 mass fraction on spreading velocity. Parabolic flight. ϕ = 4 mm. Wall thick. = 2 mm. Pressure 100 kPa.

Accordingly, a Proposal was submitted to NASA in June 1998, as a response to NRA-97-HEDS-01, requesting a research program on combustion of solids in O_2/N_2 mixtures to be carried out in the ISS US combustion module. This proposal has been approved by NASA.

RESEARCH PROGAM

The research program to be carried out in the ISS module would consist, in the first place, of the completion of the tests with PMMA material. In a second phase, materials utilized in manned space stations will be tested.

Specifically, the research program will be as follows:

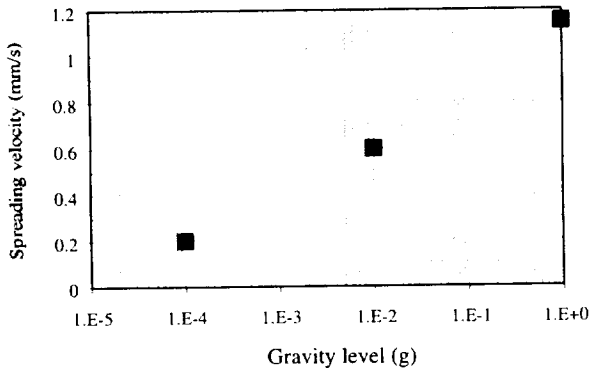

Fig. 5.- Influence of gravity level on flame spreading velocity. ϕ = 4 mm. Wall thick. = 2 mm. YO_2 = 40%. Pressure 100 kPa.

a) Completion of tests with PMMA samples (hollow cylinder mostly). Flammability limits and flame spreading velocities as function of flow velocity, O_2 concentration, thickness and, possibly, pressure. Determination of flame temperature and characteristics in the non-visible optical range. Ignition tests at low flow velocities.

b) Tests with materials utilized in spacecraft.

Flammability limit tests and flame spreading velocities as function of thickness oxygen concentration and flow velocities. Ignition tests at low flow velocities, and possibly flame extinction limits as function of pressure. Materials tested will be: foams and, in principle, one composite and one insulation blanket.

It may be pointed out that, actually, flammability limits will be approximately determined by obtaining extinction limits following the procedure described in the next paragraph.

The number of tests will be limited by the amount of gases available in the ISS module and by crew time. A final selection will have to be made.

An auxiliary test program will be carried out on the ground, parabolic flights and drop towers. These tests will be utilized for initial selection of materials and predetermination of the values of parameters, especially material thickness. Rough estimation of the values of ignition of flammability limits will also be determined. Finally, some fundamental combustion data of materials will be obtained by burning small spherical samples in drop towers.

COMBUSTION AND FLOW SYSTEM

The combustion chamber and flow system will be based, in principle, on the one being designed for the Texus 38 rocket. With this system it would be possible to change continuously, and in a controlled manner, the oxygen concentration from a maximum of 40% down to a value at which the flame extinguishes. Flow velocity would kept constant at a predetermined value at each tests.

This system has to be integrated in the gas supply system of the ISS module. This might possibly require important design changes in the Texus flow system. In addition, it is intended to perform tests with very small flow velocities, below 15 mm/s. This might require additional changes in the flow system which are already being evaluated.

The combustion chamber will be large enough to accommodate several cylinder or slabs to be investigated in each test run.

This combustion and flow system will be offered for utilization by the US and European

scientific community.

ACKNOWLEMENTS

Prof. A.C. Fernández-Pello of the Univ. of Cal., Berkeley will collaborate in the NASA Program. The continuous support given to these combustion research programs by the "Comisión de Investigación Cientifica y Técnica" and the "Plan Nacional de Investigación del Espacio" are fully appreciated. The data supplied by Dr. B. Lázaro, Project Manager for the design of Texus 38 module (SENER Company), is fully appreciated. Collaboration in previous research programs of Prof. J. Salvá, Ass. Prof. J. López Juste and Ass. Prof. G. Corchero, are fully appreciated

REFERENCES

[1] Sánchez Tarifa, C.; Corchero, G. & López Juste, G.: 37th International Astronautical Congress, Innsbruck, 1986.

[2] Tien, J. S.: Combustion and Flame, Vol. 65, N. 31, 1986.

[3] Olson, Sandra L.: NASA TM-100195, 1987.

[4] Sánchez Tarifa, C.; Corchero, G. & López Juste, G.: Applied Microgravity Technology (International Journal for Microgravity Research and Applications). Appl. microgravity tech. I, 1988.

[5] Olson, Sandra L.; Ferkul, P. V. & Tien, J. S.: Twenty Second Symposium (International) on Combustion. 1988.

[6] C. Sánchez-Tarifa, B. Lázaro and M. Rodríguez: Utilization of Sounding Rockets for Research in Microgravity Combustion. II Congreso Nacional de Ingeniería Aeronáutica, Madrid, Spain, Nov. 1993.

[7] Sánchez Tarifa, C.; Salvá, J. M. & López Juste, G.: ESA Symposium Proceedings on Space Station Utilization. Soc. Darmstadt, Germany, 1996.

[8] Altenkirch, R. A.; Bhattacharjee, S.; West, J.; Tang, L.; Sacksteder, K. & Delichatsios, M. A.: Solid Surface Combustion Experiment: Thick Fuel Results. Fourth International Microgravity Combustion Workshop, pp. 381-386, Cleveland, Ohio, 1997.

[9] Bhattacharjee, S.; Altenkirch, R. A.; Worley, R.; Tang, L.; Bundy, M.; Sacksteder, K. & Delichatsios, M. A.: Reflight of the Solid Surface Combustion Experiment: Opposed-Flow Flame Spread Over Cylindrical Fuels. Fourth International Microgravity Combustion Workshop, pp. 387-392, Cleveland, Ohio, 1997.

[10] Olson, Sandra L.; Altenkirch, R. A.; Bhattacharjee, S.; Tang, L. & Hegde, U.: Diffusive and Radiative Transport in Fires Experiment: DARTFire. Fourth International Microgravity Combustion Workshop, pp. 393-398, Cleveland, Ohio, 1997.

[11] T'ien, J. S.; Sacksteder, K. R.; Ferkul, F. V.; Bedir, H. & Hsin-Yi Shih: Solid Inflammability Boundary at Low Speed (SIBAL). Fourth International Microgravity Combustion Workshop, pp. 399-404, Cleveland, Ohio, 1997.

[12] Cordova, J. L.; Ceamanos, J.; Fernández-Pello, A. C.; Long, R. T.; Torero, J. L. & Quintiere, J. G.: Flow Effects on the Flammability Diagrams of Solid Fuels. Fourth International Microgravity Combustion Workshop, pp. 405-410, Cleveland, Ohio, 1997.

[13] C. Sánchez-Tarifa and G. López Juste: A Study of the Combustion Problems of Solid Materials at Conditions Existing in Space Stations; Second European Symposium on Utilisation of the International Space Station, ESTEC, Noordwijk, The Netherlands, Nov. 1998.

RADIANT EXTINCTION OF GASEOUS DIFFUSION FLAMES

Sean Berhan, Arvind Atreya and David Everest
Department of Mechanical Engineering & Applied Mechanics
University of Michigan; Ann Arbor, MI 48109
Kurt R. Sacksteder
NASA Lewis Research Center; Cleveland, OH 44135

INTRODUCTION

The absence of buoyancy-induced flows in microgravity (μg) and the resulting increase in the reactant residence time significantly alters the fundamentals of many combustion processes. Substantial differences between normal gravity (ng) and μg flames have been reported in experiments on candle flames [1, 2], flame spread over solids [3, 4], droplet combustion [5,6], and others. These differences are more basic than just in the visible flame shape. Longer residence times and higher concentration of combustion products in the flame zone create a thermochemical environment that changes the flame chemistry and the heat and mass transfer processes. Processes such as flame radiation, that are often ignored in ng, become very important and sometimes even controlling. Furthermore, microgravity conditions considerably enhance flame radiation by: (i) the build-up of combustion products in the high-temperature reaction zone which increases the gas radiation, and (ii) longer residence times make conditions appropriate for substantial amounts of soot to form which is also responsible for radiative heat loss. Thus, it is anticipated that radiative heat loss may eventually extinguish the "weak" (low burning rate per unit flame area) μg diffusion flame. Yet, space shuttle experiments on candle flames show that in an infinite ambient atmosphere, the hemispherical candle flame in μg will burn indefinitely [1]. This may be because of the coupling between the fuel production rate and the flame via the heat-feedback mechanism for candle flames, flames over solids and fuel droplet flames. Thus, to focus only on the gas-phase phenomena leading to radiative extinction, aerodynamically stabilized gaseous diffusion flames are examined. This enables independent control of the fuel flow rate to help identify conditions under which radiative extinction occurs. Also, spherical geometry is chosen for the μg experiments and modeling because: (i) It reduces the complexity by making the problem one-dimensional. (ii) The spherical diffusion flame completely encloses the soot which is formed on the fuel rich side of the reaction zone. This increases the importance of flame radiation because now both soot and gaseous combustion products co-exist inside the high temperature spherical diffusion flame. (iii) For small fuel injection velocities, as is usually the case for a pyrolyzing solid, the diffusion flame in μg around the solid naturally develops spherical symmetry. Thus, spherical diffusion flames are of interest to fires in μg and identifying conditions that lead to radiation-induced extinction is important for spacecraft fire safety.

EXPERIMENTS

The experiments were conducted in the 2.2 sec drop tower at the NASA Lewis Research Center. The drop-rig used is described in detail elsewhere [9]. Briefly, it consists of a cylindrical test chamber (0.38m dia.; 0.43m deep) that houses the spherical burner, the hot-wire igniter and the photodiodes and thermocouples used for making radiation and temperature measurements. The spherical burner (19mm dia.) was constructed from a low heat capacity porous ceramic material (93% porosity). Two gas cylinders (150 cc & 500 cc) were charged with various gases up to 45 psig and were used to supply the fuel to the porous spherical burner. Fuel flow rates to the burner were controlled by a calibrated needle valve and a gas solenoid valve was used to open and close the gas

line to the burner upon computer command. The test chamber also had a 125mm diameter Lexan window which enabled the camera to photograph the flame.

Several μg experiments under ambient pressure and oxygen concentration conditions, were conducted with methane (less sooty), ethylene (sooty), and acetylene (very sooty) fuels for flow rates ranging from 3 to 45 cm^3/s. However, in all the experiments conducted to-date, radiative extinction was not achieved within the 2.2 seconds μg time. The following measurements were made and collected by an onboard computer during these experiments: (i) *Flame radius* - this was measured from photographs taken by a color CCD camera. (ii) *Flame radiation* - this was measured by three photodiodes with different spectral characteristics varying from visible to IR. (iii) *Flame temperature* - this was measured by five S-type thermocouples and the sphere surface temperature was measured by a K-type thermocouple. In both cases $75\mu m$ diameter wire was used.

RESULTS

Two photographs for methane μg diffusion flames is shown in Fig.1. The experiment was conducted in air with a methane flow rate of 24 ml/sec. For all fuels (methane, ethylene and acetylene), initially the flame was blue (non-sooty) but becomes very bright yellow (sooty) under μg conditions. Later, as the μg time progresses, the flame grows in size and becomes orange and less luminous and the soot luminosity disappears. For the same fuel flow rate ($\approx$24 ml/s), methane flames eventually become blue (non-sooty) in approximately one second, ethylene flames became blue toward the end of the μg time (i.e. $\approx$2 sec) while acetylene flames remained luminous yellow throughout the 2.2 sec μg time. However, the luminosity of acetylene flames was considerably reduced toward the end of the μg time and would have also become blue given more time.

A possible explanation for this observed behavior is suggested by the planar light scattering measurements of soot of Ref.[6] and theoretical calculations of Ref.[7]. The soot scattering measurements of Ref.[6] clearly show that the amount of soot increases with time, reaches a maximum and then decreases. The calculations of Ref.[7] also show that the soot volume fraction first quickly increases and later decreases. Essentially, at the onset of μg conditions, initially a lot of soot is formed in the vicinity of the flame front resulting in a very bright yellow emission. As the flame grows, several events reduce the flame luminosity: (i) The high concentration of combustion products left behind by the flame front inhibits the formation of new soot and promotes soot oxidation. (ii) The primary reaction zone, seeking oxygen, moves away from the soot region and the soot is pushed toward the cooler regions by thermophoresis. Both these effects increase the distance between the soot layer and the reaction zone resulting in the formation of a soot shell. (iii) The dilution and radiative heat losses caused by the increase in the concentration of the combustion products reduces the flame temperature which reduces soot formation and the flame luminosity.

Figure 2 shows the measured flame radius, temperatures and radiation from methane and acetylene flames plotted against the μg time. For both flames, the flame radius measurements show that the growth rate is roughly proportional to $t^{1/3}$. The difference caused by the higher sooting tendency of acetylene which enables soot formation to persist for a longer time, is clearly seen in the radiation measurements.

ACKNOWLEDGMENTS

Financial support for this work was provided by NASA under contract number NAG3-482.

REFERENCES

1. *Dietrich, D. L., Ross, H. D. and T'ien, J. S.* "Candle Flames in Microgravity," Third Microgravity Combustion Workshop, Cleveland, Ohio, April, 1995.

2. *Ross, H. D., Sotos, R. G. and T'ien, J. S.*, Combustion Science and Technology, Vol. 75, pp. 155-160, 1991.

3. *T'ien, J. S., Sacksteder, K. R., Ferkul, P. V. and Grayson, G. D.* "Combustion of Solid Fuels in very Low Speed Oxygen Streams," Second International Microgravity Combustion Workshop," NASA Conference Publication, 1992.

4. *Ferkul, P., V.*, "A Model of Concurrent Flow Flame Spread Over a Thin Solid Fuel," NASA Contractor Report 191111, 1993.

5. *Jackson, G., S., Avedisian, C., T. and Yang, J., C.*, Int. J. Heat Mass Transfer., Vol.35, No. 8, pp. 2017-2033, 1992.

6. Tsue, M., Segawa, D., Kadota, T. and Yamasaki, H. *Twenty-Sixth (International) Symposium on Combustion*, The Combustion Institute, 1996, pp. 1251-1258.

7. *Atreya, A. and Agrawal, S.*, "Effect of Radiative Heat Loss on Diffusion Flames in Quiescent Microgravity Atmosphere," *Combustion & Flame*, (accepted for publication), 1997.

8. *Atreya, A, Agrawal, S., Sacksteder, K., and Baum, H.*, "Observations of Methane and Ethylene Diffusion Flames Stabilized around a Blowing Porous Sphere under Microgravity Conditions," AIAA paper # 94-0572, January 1994.

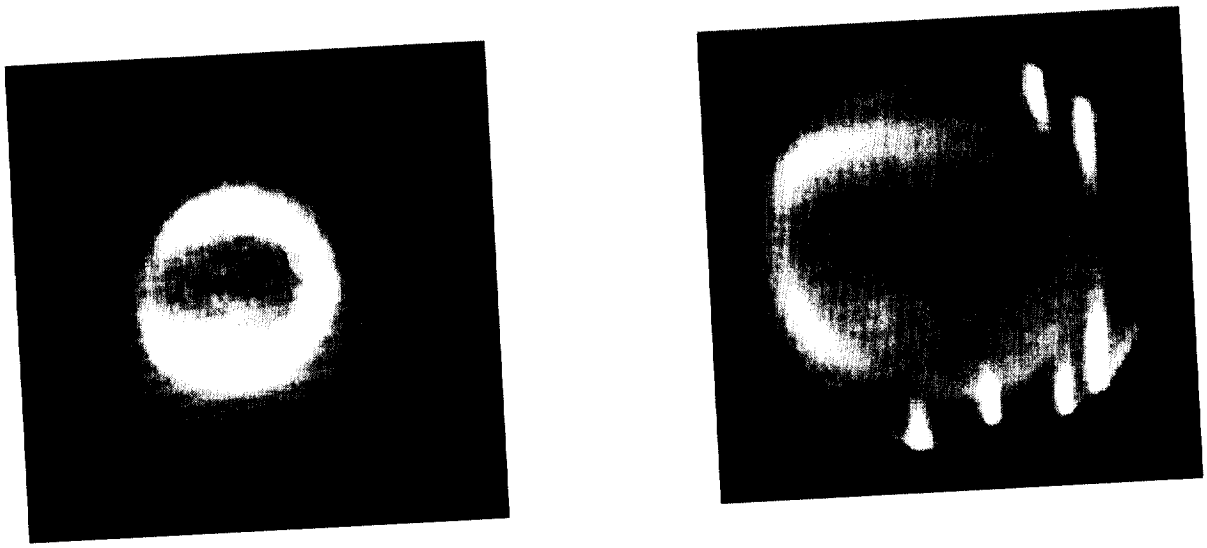

Figure 1: Photographs of methane μg diffusion flames around the 1.9 cm diameter porous ceramic sphere at 0.033 and 0.970 sec. For methane, the flames become blue and nearly invisible after 1 sec. For ethylene, the flames become blue at about 2 sec. Acetylene flames never became blue but were considerably less bright at 2.2 sec.

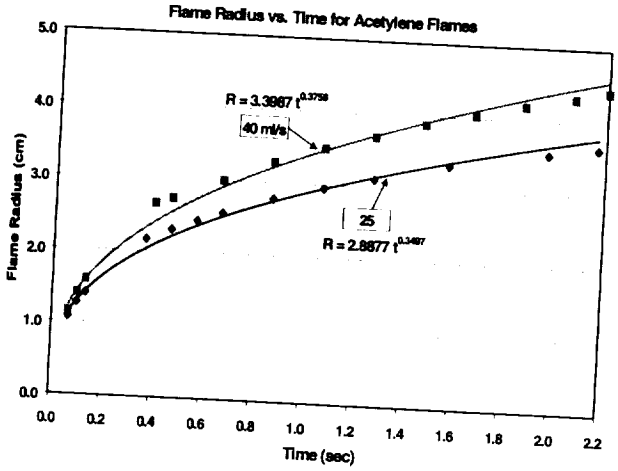
Flame Radius vs. Time for Acetylene Flames
Flame Radius (cm)
Time (sec)
R = 3.3987 t^0.3758
40 m/s
25
R = 2.8877 t^0.3497

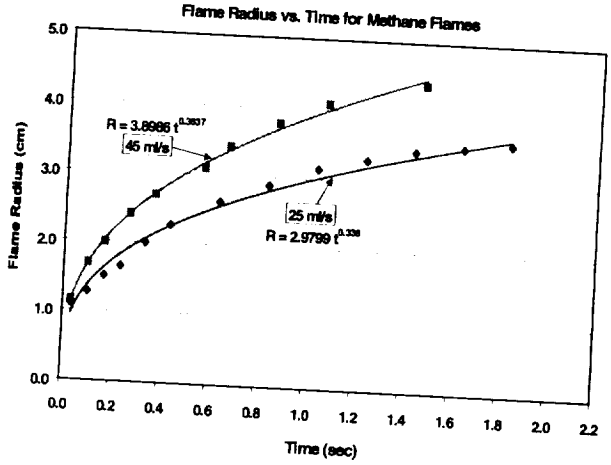
Flame Radius vs. Time for Methane Flames
Flame Radius (cm)
Time (sec)
R = 3.8986 t^0.3937
45 m/s
25 m/s
R = 2.9799 t^0.338

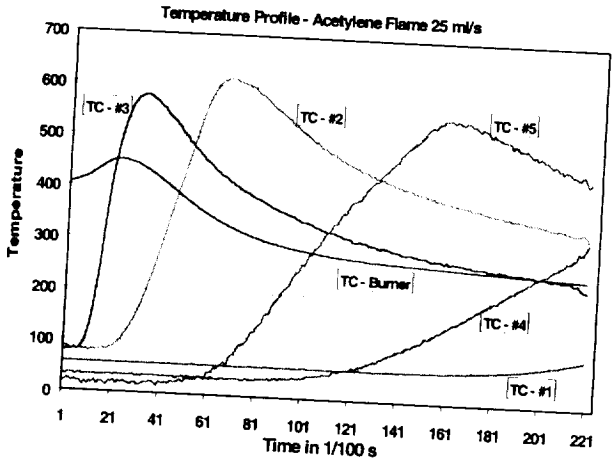
Temperature Profile - Acetylene Flame 25 ml/s
Temperature
Time in 1/100 s
TC - #3
TC - #2
TC - #5
TC - Burner
TC - #4
TC - #1

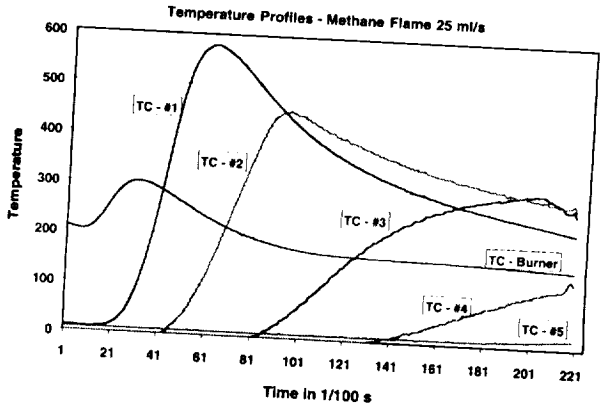
Temperature Profiles - Methane Flame 25 ml/s
Temperature
Time in 1/100 s
TC - #1
TC - #2
TC - #3
TC - Burner
TC - #4
TC - #5

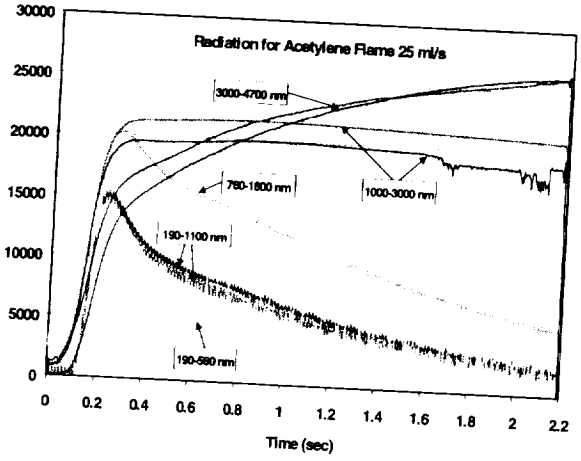
Radiation for Acetylene Flame 25 ml/s
Time (sec)
3000-4700 nm
780-1800 nm
1000-3000 nm
190-1100 nm
190-680 nm

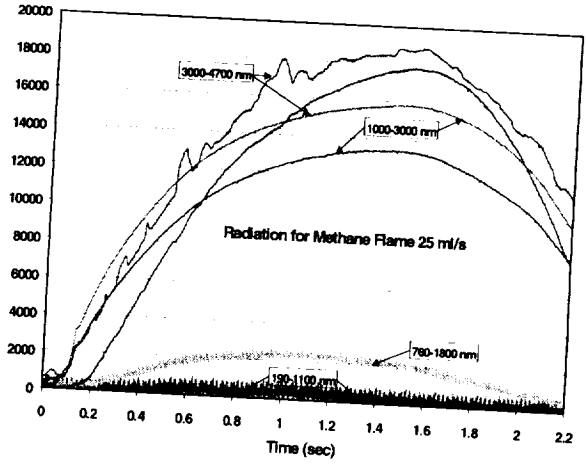
Radiation for Methane Flame 25 ml/s
Time (sec)
3000-4700 nm
1000-3000 nm
780-1800 nm
190-1100 nm

S1-27

Preliminary Results Of The Third Test Series Of Nonmetal Material Flammability Evaluation In SKOROST Apparatus On The Space Station Mir

A.V. Ivanov[1], V.F. Alymov[1], A.B. Smirnov[1], S.P. Shalayev[1], D.Ye.Belov[1], Ye.V. Balashov[2], T.V. Andreeva[2], A.V. Semenov[2], A.S. Melikhov[3], I.A.Bolodyan[3], and V.I. Potyakin[3]

[1]Keldysh Research Center, Moscow, Russia, [2]RSC-Energia, Korolev Russia. [3]All-Russian Institute for Fire Safety of Russian Federation Ministry of Internal Affairs, Moscow, Russia

INTRODUCTION

The work has been done according to the US/Russian Joint Project "Experimental Evaluation of the Material Flammability in Microgravity" a continued combustion study in the SKOROST test apparatus on the OS Mir. [1]. The objective of the project was to evaluate the flammability and flame-spread rate for the selected polymer materials in low velocity flow in microgravity.

Lately the issue of nonmetal material combustion in microgravity has become of great importance [2], based on the necessity to develop the fire safety system for the new International Space Station (ISS). Lack of buoyant flow in microgravity reduces oxygen transfer into the combustion zone, which leads to flame extinction when the flow velocity is less than the limiting flow velocity V_{lim} for the material. The ISS FGB fire-safety system was developed based on this phenomenon [1]. The existence of minimum flow velocity V_{lim} to sustain fire for the selected materials was determined both theoretically [3] and experimentally [4]. In the latter, it is shown that, even for thermally thin nonmetal materials with a very low oxygen index C_{lim} of 12.5% (paper sheets with the thickness of 0.1 mm), a limiting flow velocity V_{lim} exists at oxygen concentration C_{ox} = 17-21%, and is about 1.0 - 0.1 cm/sec. This might be explained by the relative increase in thermal losses due to radiation from the surface and from the gaseous phase [3].

In the second series of experiments in Skorost apparatus on Orbital Station Mir the existence of the limiting flow velocity V_{lim} for combustion was confirmed for PMMA and glass-epoxy composite strip samples 2 mm thick at oxygen concentration C_{ox} = 21.5%. It was concluded that V_{lim} depends on C_{ox}: for the PMMA sample with a low oxygen index of 15.5%, the limiting flow velocity V_{lim} was less than 0.5 cm/sec, and for the glass-epoxy composite sample with a high oxygen index of 19%, the limiting flow velocity V_{lim} was higher than 15 cm/sec.

As of now only those materials that maintain their integrity during combustion were investigated. The materials that disintegrate when burning present more danger for fire safety because the flame can spread farther with the parts of the structure, ejected melt drops, et cetera. Materials such as polyethylene are of great interest since they form a lengthy melt zone during the combustion in normal gravity. This melt zone generates drops of liquids that promote faster flame spread compared to usual combustion.

The preliminary results of polyethylene insulation flammability evaluation in microgravity are shown in the NASA Wire Insulation Flammability (WIF) experiment during Space Shuttle flight STS-50. [5]. A lot of interesting data was collected during the WIF test program. However, one of the most important results was that, in microgravity, the extinction of the polyethylene occurred almost immediately when the flow of relatively low oxygen concentration (C_{ox}=21%) was stopped.

The purpose of the work reported here is to expand the existing data base on material flammability in microgravity and to conduct the third series of the space experiment using Skorost

apparatus on Orbital Station Mir with melting polymers, which might increase the probability of fire and its propagation in ventilated microgravity environment of orbiting spacecraft.

TEST PROCEDURE

The Skorost test apparatus is a miniature wind tunnel. The fan generates a uniform airflow with the prescribed velocity V inside the Skorost combustion chamber (a tunnel of rectangular cross-section of 150×80 mm and length of 320 mm). The main parameter of apparatus performance V (velocity of the flow inside) can vary from 0 to 20 cm/sec. The flow velocity is controlled either by fan motor speed or by a damper setting according to the ground calibration of the flow in the combustion chamber. The air is drawn through the combustion chamber from the space station compartment; therefore, the oxygen concentration can not be controlled and is equal to the C_{ox} in the module Kvant at the time of the experiment. The Space Station on-board records indicated that oxygen concentration on Mir was elevated at the time of the experiment (October 15, 19, and 22 of 1998; C_{ox}=22.5%, 23.6%, and 25.4%; pressure was 95% atmospheric).

The samples of the test material were installed as cantilevers on two carousels inside the combustion chamber. Each carousel can accommodate six cylindrical samples 4-5 mm in diameter and 60 mm in length. Because of safety concerns, the crew was not allowed to open the combustion chamber, and samples were placed in the test position along the longitudinal axis of the chamber by the rotation of the carousel from the outside. The free end of the sample was ignited inside the chamber by a spiral electrical heater, and combustion occurred in the concurrent airflow. The test was observed through two windows with the size of 100×60 mm on side and top surfaces of the combustion chamber. Hi-8 and Betacam cameras videotaped the test.

Based on the results of the ground testing, three materials were selected for the flight experiment out of seven provided by the NASA Lewis Research Center: Delrin, PMMA, and high-density polyethylene (four cylindrical samples of each material—diameter of 4.5 mm and length of 60 mm). The main objective of the space experiment was to evaluate the effect of the flow of low velocity on the polymer material combustion in a microgravity environment of long duration and to determine 1) the minimum extinction flow rate for the material, *i.e.* the limiting velocity V_{lim} and 2) the flame-spread rate V_F versus the velocity of the concurrent flow V.

The test procedure specified a matrix of concurrent airflow velocity V from 8.5 cm/sec to 0.3 cm/sec. Twelve samples were tested during the experiment: four each of Delrin, PMMA, and high-density polyethylene. For each sample, the flow velocity was changed at prescribed position of the front of the flame along the length of the sample at 1/2, 1/3, or 1/6 of the initial sample length (60 mm). To guide the crew in fan mode switching each sample was marked at the appropriate length interval. When the flame front got to the last mark on each sample, the fan was shut off, and the time (τ_l) of flame extinction was recorded.

TEST RESULTS AND DISCUSSION

In the tests, it was observed that, when V is decreased, the size of the flame decreases as well; the flame becomes less bright, and the flame color changes from white, red-orange (PMMA, polyethylene) or white-blue (Delrin) to the dark-blue color. The flame becomes transparent and almost invisible, which means that the temperature of the flame decreases [2]. All selected materials demonstrated the formation of droplets of the melting products. The melt ball grew with time up to a final size of 2-2.5 initial diameters of the sample (4.5 mm).

The video of all 12 samples combustion was analyzed by computer, and data were collected. These data are time histories for various parameters to characterize the flame size and the material melting, the gap between the flame and the sample surface if any, et cetera. The flame-spread rate V_F and the rate of the material destruction were determined based on these data. Fig. 1 shows the function of V_F versus V. When the velocity of concurrent flow V decreases, the flame-spread rate decreases as well: from 0.5 - 0.75 mm/sec at V = 8.5 cm/sec to 0.05 - 0.1 mm/sec at V = 0.3 - 0.5 cm/sec. In [5] it is shown that the flame-spread rate along the surface of polyethylene insulation (0.375 mm thick) was significantly higher: V_F = 1.6 mm/sec at V = 10 cm/sec. This might be explained by the difference in the thickness and the initial temperature of the sample: d = 4.5 mm, t_0 = 20°C for the Skorost experiment, and δ = 0.375 mm, t_0 = 70-80°C for the Space Shuttle experiment [5].

The important characteristic of material flammability—limiting velocity V_{lim}—can be determined from the test modes and conditions for fire extinction process. Values for limiting velocities obtained in microgravity appeared to be lower than values [1] obtained on the ground but at suppressed convection. For example, for Delrin in microgravity, V_{lim} was less than 0.3 cm/sec; in a narrow-channel apparatus with the suppressed convection on the ground, V_{lim} = 0.55 cm/sec at C_{ox} = 21% and V_{lim} = 0.45 cm/sec at C_{ox} = 23%. For PMMA in microgravity, V_{lim} at C_{ox} = 23.6% and 25.4% was close to 0.5 cm/sec; in the narrow-channel apparatus, V_{lim} = 3.4 cm/sec at C_{ox} = 21% and V_{lim} = 2.4 cm/sec at C_{ox} = 23%. Again, when the flow was stopped in Skorost combustion chamber, the extinction of the PMMA samples happened very quickly: τ_1 = 5 - 15 sec, while in normal gravity the extinction time was longer (τ_1 = 30 sec). For polyethylene, in microgravity at C_{ox} = 25.4%, V_{lim} was close to 0.3 - 0.5 cm/sec; in the ground test, V_{lim} = 8.5 cm/sec at C_{ox} = 21% and V_{lim} = 3.5 cm/sec at C_{ox} = 23%. Polyethylene samples were still burning at V = 1 cm/sec when oxygen concentration was 23.5%, therefore V_{lim} < 1 cm/sec.

The space experiment indicated that the fire extinguishes faster in microgravity (τ_1 <13 sec) at flow shutoff than in normal gravity (τ_1 = 55 sec). All data obtained on V_{lim} and τ_1 indicate that, in microgravity when oxygen concentration is relatively low (C_{ox} = 21%), the molecular diffusion is not sufficient to sustain fire and the additional oxygen transport by forced convection into combustion zone is required. Therefore, a fire in the Space Station compartment might be extinguished by flow shutoff in microgravity.

The non-steady phenomena observed during the space experiment in the Skorost apparatus were due to constantly growing melt ball formation on the sample (almost of spherical shape for PMMA and Delrin or of ellipsoidal shape for polyethylene), and intensive (for Delrin and PMMA especially) boiling all over the volume of melting material. The results of measurements indicated that for majority of cases, the size of the melt drop will not reach the required size for the steady state, even for the time increment of 100 - 150 sec.

Delrin combustion in microgravity occurred with intensive boiling inside the foamy drop of melting material. The size of the gaseous bubbles sometimes was comparable to the size of the molten drop. Collapsing of the bubble happened with the ejection of the products of thermal destruction up to 4 - 5 cm in length. Those jets were burning and looked like the bright zones - flame tongues—ejected in the direction opposite to the flow. PMMA combustion occurred with the ejection of the gaseous products of thermal destruction as well. Jets of gaseous products of combustion were burning, and flame tongues of different length and brightness were formed.

Polyethylene combustion was the most stable one. Though bubble formation was noticeable in the semitransparent molten drop, combustion was steady, without significant spurts. However, when the flow velocity was close to limiting, the combustion became unstable: the flame front started to fluctuate with the frequency of 1.3 - 1.4 Hz (sample # 9, when V decreased from 8.5 cm/sec. to 0 cm/sec), and with the frequency of 2.3 Hz (sample #11, when flow velocity was 0.5 cm/sec and 0.3 cm/sec). When longitudinal flame fluctuations were observed, the measured velocity of flame wave movement in downstream direction was about 60 mm/sec, i.e. 100 higher than the flame-spread rate (V_F = 0.5 mm/sec) during stable combustion at the maximum velocity of the concurrent flow (V = 8.5 cm/sec). Oscillations of this type were observed before at the candle flame extinguishment in the Glovebox experiments on Orbital Station Mir and Space Shuttle.

ACKNOWLEDGEMENT

The work was supported by Contract NAS3-97160. The authors would like to thank their US colleagues M.Forkosh, R.Friedman, D.Hirsch, N. Goldin and Russian cosmonauts S.Avdeev and G.Podalka, who applied every effort to ensure the successful completion of the program.

REFERENCES

1. Ivanov, A.V., *et al.*: Study of Materials Combustion Processes in Microgravity. *Proc. Jt. Tenth Europ. and Sixth Russ. Symp. on Phys. Sci. in Microg.*, Moscow, June 1997, pp. 401-8.
2. King, M.K.; and Ross, H.D.: Overview of the NASA Microgravity Combustion Program. *AIAA Jour.*, vol. 36, 1998, pp. 1337-45.
3. T'ien, J.S.: Diffusion Flame Extinction at Small Stretch Rate: The Mechanism of Radiative Loss. *Comb. and Flame*, vol. 65, 1986, pp. 31-34.
4. Grayson, G.D., *et al.*: Flame Spreading Over a Thin Fuel in Low Speed Concurrent Flow. *Microg. Sci. Technol.* vol. 7., 1990, pp 187-192.
5. Greenberg, P.S., and Sacksteder, K.R.: The USML-1 Wire Insulation Flammability Glovebox Experiment. *Proc. 3rd Intern. Microg. Comb. Wkshop.* NASA CP 10174, 1995, pp. 237-41

Fig.1. Dependence of flame spread velocity V_F on airflow velocity V in microgravity.

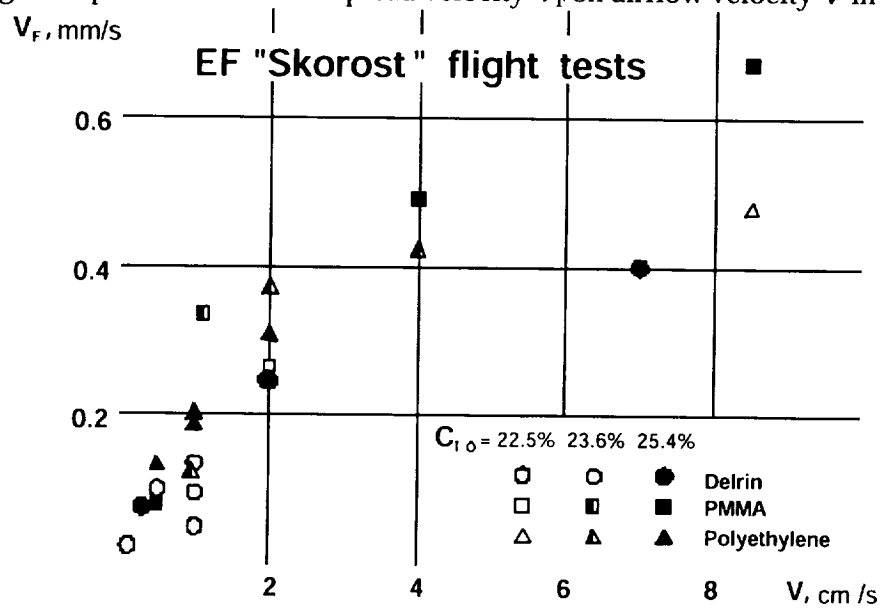

Laminar Flames

STUDIES OF PREMIXED LAMINAR AND TURBULENT FLAMES AT MICROGRAVITY (NASA Grant No. NAG3-2124)

M. Abid, K. Aung, P. D. Ronney, J. A. Sharif and M.-S. Wu
Department of Aerospace and Mechanical Engineering
University of Southern California, Los Angeles, CA 90089-1453

INTRODUCTION

Several topics relating to combustion limits in premixed flames at reduced gravity have been studied. These topics include: (1) flame balls; (2) numerical simulation of flame ball and planar flame structure and stability; (3) experimental simulation of buoyancy effects in premixed flames using aqueous autocatalytic reactions; and (4) premixed flame propagation in Hele-Shaw cells.

STRUCTURE OF FLAME BALLS AT LOW LEWIS-NUMBER (SOFBALL)

Successful flame ball experiments were conducted on the STS-83 and STS-94 Space Shuttle missions in 1997. Among the unexpected results were (1) flame balls survived much longer than expected based on pre-flight estimates – in most cases the entire 500 second test duration; (2) when multiple flame balls were present, they drifted apart from each other (although their "center of mass" was nearly motionless in many cases); (3) flame balls were very sensitive to small accelerations (typically 100 μg for 1 second) resulting from Orbiter vernier reaction control system (VRCS) thruster firings; and (4) remarkably, all flame balls in all mixtures tested produced between 1 and 2 Watts per ball of radiant power per ball.

The drift of adjacent flame balls was attributed to the enthalpy gradient each ball imposes on its neighbors. A model was developed by the PI in conjunction with J. D. Buckmaster. The slope of separation vs. time plots (*e.g.* Fig. 1), are close to the theoretically prediction of 1/3, and the quantitative agreement is reasonable considering the simplicity of the model. The mean and standard deviation of the slope for all relevant tests is 0.334 with a standard deviation of 0.060.

The flame balls were found to respond ballistically to VRCS impulses (Fig. 2). The impulse (change in velocity) imparted to the ball is about the same as the acceleration impulse (integral of acceleration over time). The ball velocity change is somewhat greater (by a factor of about 2) than the acceleration impulse. The maximum possible factor for a spherical bubble of fluid having very low density compared to the surrounding fluid is 2 because of the "added mass" effect. This change in velocity then decays on a time scale of tens of seconds, which is comparable to the viscous time scale associated with the flame ball and its surrounding hot gas field.

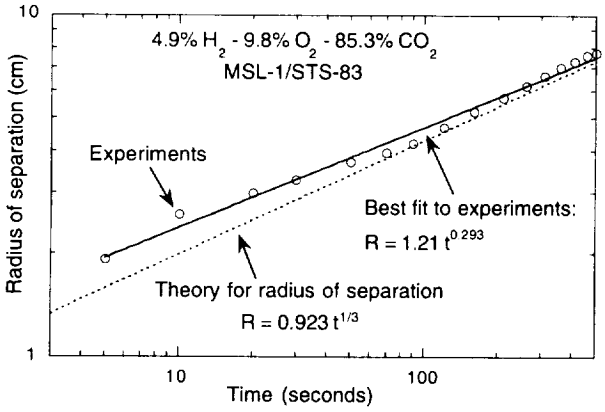

Figure 1. Examples of flame ball interactions resulting in mutual repulsion.

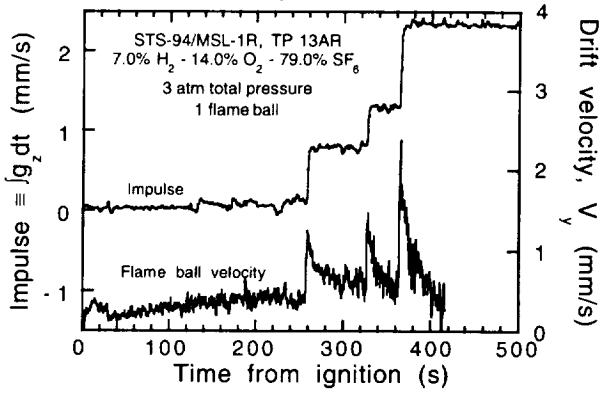

Figure 2. Effect of impulsive orbiter accelerations on flame ball drift velocity.

NUMERICAL SIMULATION OF FLAME BALL AND PLANAR FLAMES

In order to predict the properties of flame balls, a one dimensional, time-dependent flame code with detailed chemical and transport sub-models was employed to solve the usual

nonsteady equations for energy and species conservation in spherical geometry at constant pressure. It was found that the predicted flame ball radii using different chemical models vary widely, even though all of these models predict the burning velocities of steady plane flames quite accurately. Also, reabsorption of emitted radiation was found to be a dominant effect in mixtures diluted with CO_2 or SF_6, in that calculations assuming infinite absorption coefficient for the diluent showed much better agreement with experiment that calculations assuming optically-thin diluent radiation (Fig. 3).

A numerical study of premixed-gas flames in mixtures of CH_4, O_2, N_2 and CO_2 using detailed chemical and radiative emission-absorption models was conducted in conjunction with Prof. Yiguang Ju of Tohoku University in Sendai, Japan. It was found that reabsorption of emitted radiation led to substantially higher burning velocities and wider extinction limits than calculations using optically-thin radiation models, particularly when CO_2, a strong absorber, is present in the unburned gas (Fig. 4). Two heat loss mechanisms that lead to flammability limits even with reabsorption were identified: (1) differences in the absorption spectra of the reactant and product molecules and (2) the broadening of emission spectra at flame temperatures compared to ambient temperature. Via both mechanisms some net upstream heat loss due to radiation will always occur, leading to extinction of sufficiently weak mixtures. It is concluded that fundamental flammability limits can exist due to radiative heat loss, but these limits are strongly dependent on the emission-absorption spectra of the reactant and product gases and their temperature dependence, and cannot be predicted using gray-gas or optically-thin models.

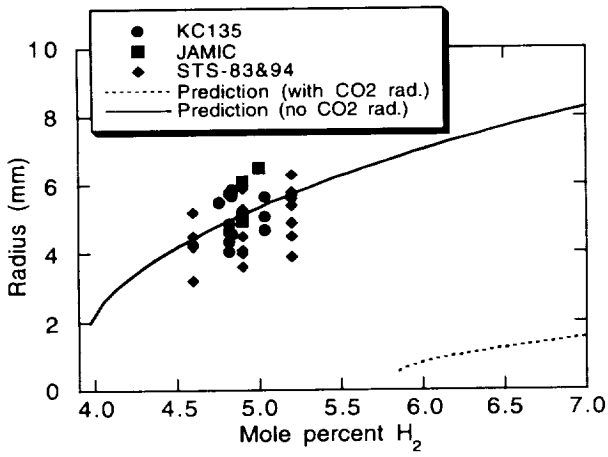

Figure 3. Predicted flame ball radii in H_2-O_2-CO_2 mixtures (H_2:O_2 = 1:2) including and excluding CO_2 radiation, along with measured flame ball radii from aircraft μg experiments, JAMIC drop-tower experiments, and the STS-83/94 space experiments.

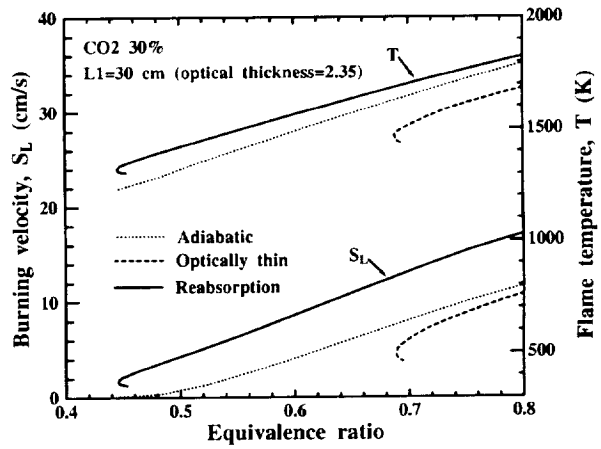

Figure 4. Predicted values of burning velocity and peak flame temperature in CH_4 - (0.21 O_2 + 0.49 N_2 + 0.30 CO_2) mixtures under adiabatic conditions, with optically-thin radiative losses, and including reabsorption effects.

"LIQUID FLAMES"

With NASA Code UG support, the PI has introduced the use of aqueous autocatalytic chemical reaction fronts for the experimental simulation of combustion processes. Theses fronts exhibit very little density change across the front, have simple chemistry, are unaffected by heat losses (since the front is nearly isothermal) and have high Schmidt numbers, allowing the front to remain "flamelet-like" even in the presence of very strong flow disturbances or turbulence. Thus, such fronts are very useful for experimental study of combustion under conditions far more readily simulated by available theoretical and numerical models.

Hele-Shaw cells are frequently employed to study buoyancy effects in fluid systems in a simple quasi two-dimensional geometry where the flow is governed by a linear equation (Darcy's law). Thus, autocatalytic reactions in Hele-Shaw cells represent the simplest possible

experimental realization of the interaction of a propagating front with buoyancy-induced convection. Fingering-type instabilities were observed (Fig. 5), which is very surprising since the classical Saffman-Taylor mechanism is not present (since there is no viscosity difference across the front). The fingering wavelength is independent of the front propagation rate (S_L) and the cell thickness (w) and is inversely proportional to the square root of the cosine of the angle of the cell from vertical. The only viable explanation of this behavior is a surface tension at the interface whose magnitude is about 0.005 dyne/cm – about 14,000 times smaller than a water-air interface.

An estimate of the magnitude of the buoyancy-induced flow disturbances was derived based on the Saffman-Taylor model, resulting in $u'/S_L \approx (\pi/12)g\delta w^2/\nu S_L$ where u' is the effective "turbulence intensity", g the gravitational acceleration, δ the fractional density change, and ν the kinematic viscosity. The "turbulent burning velocity" (S_T) is plotted as a function of U in Fig. 6. These results show that the Yakhot model $S_T/S_L = \exp((u'/S_L)/(S_T/S_L))^2$ fit the experimental data for this experiment, as it did our previous results from several different forced-turbulence flows. These results suggest a rather simple description of the role of buoyancy on the front propagation in this simple chemical and hydrodynamic system.

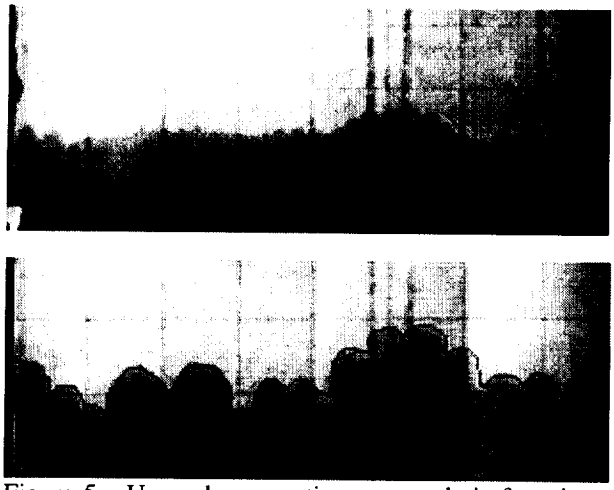

Figure 5. Upward propagating autocatalytic front in a Hele-Shaw cell. Cell thickness (w) = 1.0 mm, S_L = 0.17 mm/s. Upper image: 10 seconds after initiation; lower image: after reaching quasi-steady propagation condition. Width of cell is 200 mm.

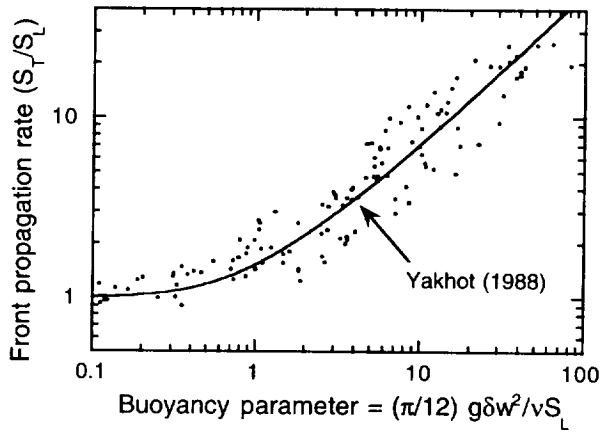

Figure 6. Correlation of wrinkled front speed (U_T) with buoyancy parameter (U_B).

PREMIXED-GAS FLAME PROPAGATION IN HELE-SHAW CELLS

As a complement to the experiments on chemical fronts in Hele-Shaw cells, premixed-gas flames in Hele-Shaw cells were also examined. Significantly, wrinkling was observed even for downward propagating (buoyantly stable) flames and flames having high Lewis number (diffusive-thermally stable) (Fig. 7a). The burning rates (S_T) of these flames are quite different from their laminar, unwrinkled values (S_L). Values of S_T/S_L in the quasi-steady stage were higher for upward vs. downward propagation, but only weakly dependent on Lewis and Peclet numbers (Fig. 7b). The first of these effects is consistent with the Joulin-Sivashinsky (JS) model, whereas the last is contrary to the JS predictions concerning the effects of heat losses. These results show that even for diffusively stable mixtures, at microgravity thermal expansion and viscosity changes across the front will lead to flame instabilities. These results also indicate that the behavior of flame propagation in narrow channels such as crevice volumes in premixed-charge internal combustion engines (the source of most unburned hydrocarbon emissions) may be quite different from that inferred from simple laminar flame experiments.

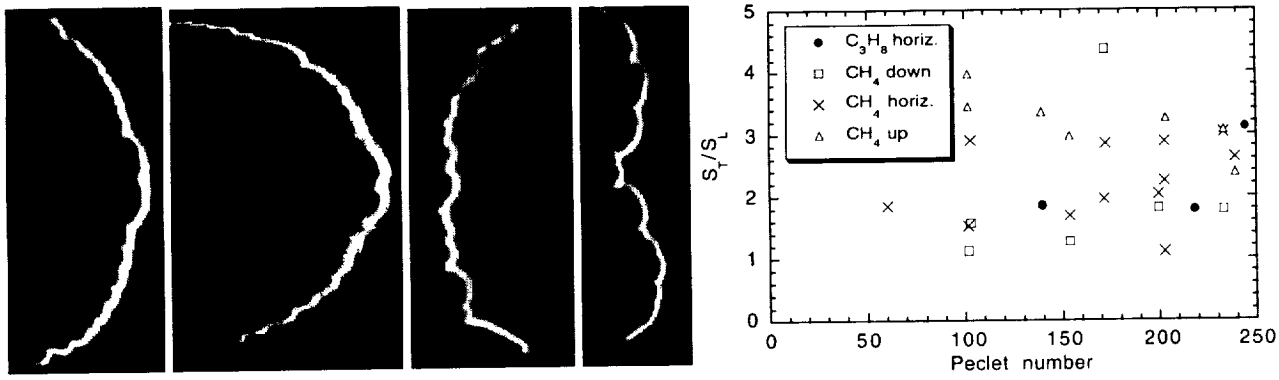

(a) (b)

Figure 7. Characteristics of flames in Hele-Shaw cells. (a) direct images (flames propagate from left to right.) Cell width (vertical direction in these images) 39 cm. Cell length (horizontal direction in these images) 60 cm, but images are cropped to show only flame front. Images from left to right: 7.2% CH_4 in air, horizontal propagation; 7.1% CH_4 in air, upward propagation; 7.1% CH_4 in air, downward propagation; 3.0% C_3H_8 in air, horizontal propagation. (b) Correlation of wrinkled front speed (S_T/S_L) with Peclet number.

PUBLICATIONS 1997-98

Liu, J.-B. and Ronney, P. D., "Premixed Edge-Flames in Spatially Varying Straining Flows," to appear in *Combustion Science and Technology* (1999).

Vedarajan, T. G., Buckmaster, J. D. and Ronney, P. D., "Two-dimensional Failure Waves and Ignition Fronts in Premixed Combustion," to appear in the *Twenty-Seventh International Symposium on Combustion* (1998).

Wu, M.-S., Liu, J. B. and Ronney, P. D., "Numerical Simulation of Diluent Effects on Flame Ball Structure and Dynamics," to appear in the *Twenty-Seventh International Symposium on Combustion* (1998).

Ju, Y., Masuya, G. and Ronney, P. D., "Effects of Radiative Emission and Absorption on the Propagation and Extinction of Premixed Gas Flames" to appear in the *Twenty-Seventh International Symposium on Combustion* (1998).

Buckmaster, J. D. and Ronney, P. D., "Flame Ball Drift in the Presence of a Total Diffusive Heat Flux," to appear in the *Twenty-Seventh International Symposium on Combustion* (1998).

Ronney, P. D., "Understanding Combustion Processes Through Microgravity Research," to appear in *Twenty-Seventh International Symposium on Combustion*, Combustion Institute, Pittsburgh, 1998 **(plenary paper).**

Ronney, P. D., "Premixed Laminar and Turbulent Flames at Microgravity," to appear in *Space Forum* (1998).

Ronney, P. D., "Flame Structure Modification and Quenching By Turbulence," *Combustion Science and Technology* (Japanese edition), Vol. 6 (Supplement), pp. 53-76, 1999.

Wu, M. S., Ronney, P. D., Colantonio, R., VanZandt, D., "Detailed Numerical Simulation of Flame Ball Structure and Dynamics," *Combustion and Flame*, Vol. 116, pp. 387-397 (1999).

Abid, M., Wu, M. S., Liu, J. B., Ronney, P. D., Ueki, M., K. Maruta, K., Kobayashi , H., Niioka, T. and VanZandt, D. M., "Experimental and Numerical Study of Flame Ball IR and UV Emissions," Combustion and Flame, Vol. 116, pp. 348-359 (1999).

Ronney, P. D., Wu, M. S., Pearlman, H. G. and Weiland, K. J., "Experimental Study of Flame Balls in Space: Results from STS-83," *AIAA Journal*, Vol. 36, pp. 1361-1368 (1998).

Aldredge, R. C., Vaezi, V. and Ronney, P. D., "Premixed-Gas Flame Propagation in Turbulent Taylor-Couette Flow," *Combustion and Flame*, Vol. 115, pp. 395-405 (1998).

D13-29

Gravitational Influences on Flame Propagation Through Non-Uniform Premixed Gas Systems

Fletcher J. Miller and John Easton, National Center for Microgravity Research, MS 110-3, Cleveland, OH, 44135-3191, fletcher@rosedbud.grc.nasa.gov
Howard D. Ross, NASA Glenn Research Center, MS 500-115, Cleveland, OH 44135.
Prof. Anthony Marchese, Rowan University, Glassboro, NJ, 08028-1701

INTRODUCTION

Flame propagation through non-uniformly premixed gases occurs in several common combustion situations. As summarized in [1], non-uniform premixed gas combustion has received scant attention compared to the more usual limiting cases of diffusion or uniformly premixed flames. It is the goal of this research to further our knowledge of layered combustion, in which a fuel concentration gradient exists normal to the direction of flame spread, in particular by focusing on the role that gravity plays. Gravity can affect flame propagation in at least three ways: through a hydrostatic pressure gradient, by altering the initial distribution of fuel vapor, and through buoyantly induced flows once ignition has occurred[1]. An understanding of the phenomena involved is important to fire safety, especially aboard spacecraft since no microgravity data exist. The data obtained will also be useful to verify theoretical models of this problem, which are easier to implement if buoyancy is neglected.

EXPERIMENTAL APPARATUS

Controlled Diffusion Time

The 1g experimental rig consists of a porous bronze fuel holder 76 cm long by 10 cm wide by 3.2 mm deep, inside a thermally controlled tray that is covered by an aluminum lid and gallery[1]. The recent addition of a spring loaded mechanism allows for precise and repeatable removal of the tray lid and ignition sequence so that different layer thicknesses can be formed by controlling the diffusion time[2].

Interferometric Fuel Vapor Measurements

Several problems were encountered with our Rainbow Schlieren System to used to measure the fuel vapor concentration [3]. Therefore, the decision was made to construct a Michelson interferometer to replace it. For quantitative work the finite fringe mode was used, and was achieved by tilting the reference beam return mirror about a vertical axis to give fringes perpendicular to the concentration gradient. A Fourier transform method based on the work of Takeda [4] was implemented to extract phase information from the interferograms and obtain the fuel concentration [3].

Drop Rig for Microgravity Measurements

A drop rig for use in the NASA Glenn 2.2 sec Drop Tower was completed and put into operation. It is similar in size to the 1g apparatus, and has two overhead cameras that view the flame from the top and from the side via a 45° mirror. The fuel tray is thermally controlled via a water bath. With the rig hanging at the top of the tower, the aluminum cover retracts automatically and the fuel holder is raised about 4 mm to seal against the bottom of the gallery. After a preset diffusion time, the rig is released and a hot wire is used to ignite the flame. Upon impact the fuel holder retracts and the lid closes to extinguish the flame.

EXPERIMENTAL RESULTS

Figure 1 shows the flame position as a function of time for several normal gravity cases with varying diffusion times, ranging from 1 second to 30 seconds. In all cases, the flame spread rate is constant after about 0.2 seconds after ignition, and the flame spreads steadily as expected. The flame spread rate increases with diffusion time due to increasing fuel vapor concentration and layer thickness above the frit. Further tests are needed to establish the upper limit of flame speed at this temperature. The flame fronts are for the most part flat as viewed from above, though they occasionally tilt to one side.

The fuel vapor concentration field during evaporation and ignition is measured with the interferometer described above. Fig. 2 contains a sample of this data taken for a temperature of 19 °C and a diffusion time of 10 sec. This allows us to determine the height of the lean-limit layer above the surface. We have noted that the flame, however, burns both below and above this height as it spreads, even accounting for fuel redistribution, indicating that a flame can be sustained at a fuel concentration below the "room temperature" lean limit if it is burning in proximity to a region with higher fuel vapor concentration.

Figure 3 has a summary of some results comparing μg flame spread with normal gravity flame spread rates near room temperature. For the same diffusion time, the microgravity flame appears to spread faster, though this must be considered a preliminary result, as more data are required to verify this trend. It is believed that without buoyancy causing hot gases to rise above the flame the gas thermal expansion is channeled in a more forward direction, which increases the flame, spread rate. Interestingly, this is in opposition to a stream-tube model developed for this problem, which did not consider buoyancy, that predicted higher velocities at 1g due to a hydrostatic pressure effect[5].

NUMERICAL MODEL

The numerical model used in this study is a two-dimensional (planar or axisymmetric), unsteady flame spread model developed at University of California, Irvine [6]. It has been used previously for modeling propanol, butanol, and to a limited extent, ethanol and decane in the subflash regime. Each of these fuels is treated with a global reaction mechanism.

The effects of gravity were examined by simulating ignition and flame spread across propanol-air mixtures at two initial pool temperatures in the superflash regime at normal gravity and at microgravity. Propanol was selected because the predictions of the model with this fuel agreed best with experiments that were done with subflash pools [6]. The tray was a 150-mm diameter pool with a liquid fuel depth of 1.6 mm, as was used in previous superflash experiments[7]. Ignition took place with an assumed symmetry about the centerline (zero gradient condition). The lower temperature of 27 C was selected because it is just above the flash point temperature of propanol-air, and would yield a lean flammable mixture throughout the initial gas phase. The higher temperature of 35 C was selected because it would yield a stoichiometric mixture somewhere in the initial gas phase. Diffusion is allowed to occur in 1g setting up a pre-ignition distribution of fuel vapor concentration that is consistent with experiments[7]. Kim et al [8] previously showed that the distribution of fuel vapor concentration above finite-size pools was gravity-dependent, with heavy fuel vapors spilling out over the tray edge and drawing air into the mixture. This has also been shown experimentally by tracking the layer height measured by the interferometer and noting that it reaches a steady state with the gallery ends open.

Figure 4 shows the flame position versus time for two initial temperatures, after central ignition. As expected, independent of gravity level, each flame's spread is very rapid and steady, consistent with experiments. Flame spread is more rapid at 35 C than at 27 C (70-80 cm/s versus 30-40 cm/s), due to the higher fuel vapor concentration initially in the gas phase. At both 27 C and 35 C, flame spread is predicted to be more rapid in microgravity than in normal gravity. This is due to the development of buoyant convection in the trailing portion of the normal-gravity flame. This creates a vortex above the pool surface, yielding high velocities in both the vertical and axial directions. More importantly, buoyancy forces divert some of the thermal expansion that accompanies combustion away from the direction of flame spread. In microgravity, the plume is absent, so the thermal expansion is directed in the direction of flame spread, and raises the speed of spread in agreement with the experiment conducted with ethanol.

ACKNOWLEDGEMENTS

We wish to acknowledge Ed White for his construction of the interferometer, Peter Politsky for the lid retraction mechanism, and Andy Jenkins, Ron Mileto, and Ken Burke for help on the drop rig.

REFERENCES

[1] F. J. Miller, E. B. White, and H. D. Ross, "Gravitational Influences on Flame Propagation Through Non-Uniform Premixed Gas Systems," presented at 4th International Microgravity Combustion Workshop, Cleveland, OH, 1997.
[2] P. Politsky, "Design and Testing of Automatic Lid Retractor and Ignitor for a Flame Spread Apparatus," : Case Western Reserve University, 1998.
[3] E. B. White, "Flame Propagation Through Fuel Vapor Concentration Gradients," : Case Western Reserve University, 1997.
[4] M. Takeda, H. Ina, and S. Kobayashi, "Fourier-transform method of fringe-pattern analysis for computer-based topology and interferometer," *Journal of the Optical Society of America*, vol. 72, pp. 156-160, 1982.
[5] M. Kaptein and C. E. Hermance, "Horizontal Propagation of Laminar Flames Through Vertically Diffusing Mixtures Above a Ground Plane," presented at 16th Symposium (Int'l) on Combustion, 1976.
[6] D. N. Schiller, H. D. Ross, and W. A. Sirignano, "Computational Analysis of Flame Spread Across Alcohol Pools," *Combust. Sci. Technol.*, vol. 118, pp. 205, 1996.
[7] H. D. Ross and R. G. Sotos, "An Investigation of Flame Spread over Shallow Liquid Pools in Microgravity and Nonair Environments," *23rd Symposium (International) on Combustion*, pp. 1649-1655, 1990.
[8] I. Kim, D. N. Schiller, and W. A. Sirignano, "Axisymmetric Flame Spread Across Propanol Pools in Normal and Zero Gravities," *Combustion Science and Technology*, vol. submitted, 1999.

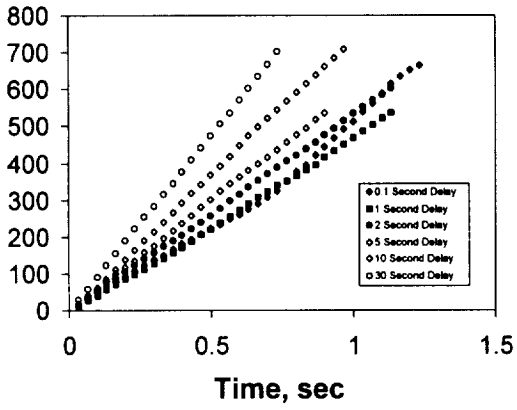

Figure 1. Flame position vs. time for various diffusion times for ethanol in normal gravity. Initial fuel temperature is 19 °C.

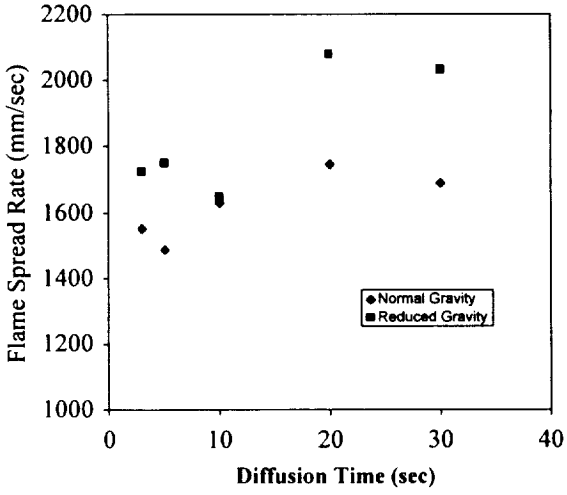

Figure 3. Flame velocity vs. diffusion time for normal and microgravity flames spreading over ethanol at 23 °C.

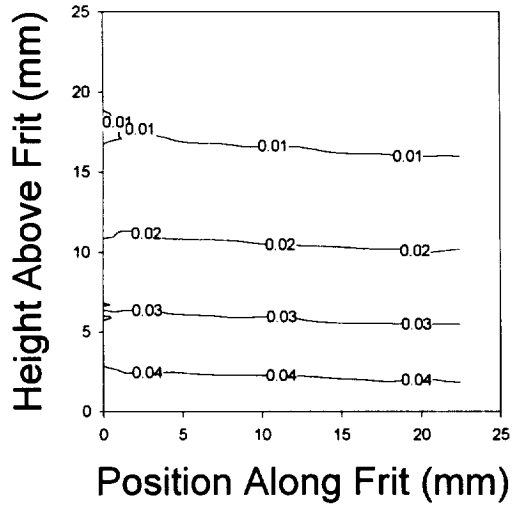

Figure 2. Ethanol concentration above a 19 °C normal gravity frit. The diffusion time is 10 seconds for this plot.

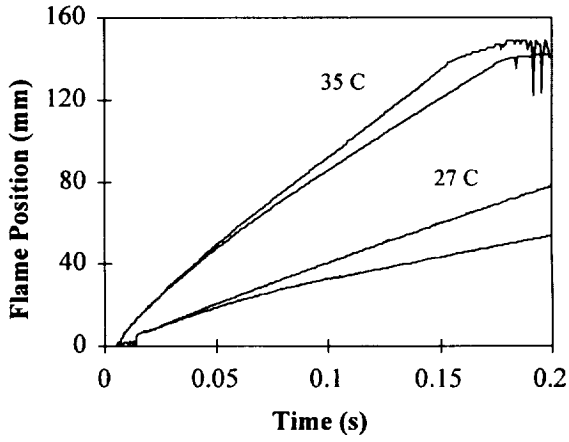

Figure 4. Predicted flame position vs. time for 1-propanol at two temperatures. Lower curves of each pair are for 1g conditions, upper for μg

SOOT FORMATION IN LAMINAR PREMIXED FLAMES

F. Xu, S.S. Krishnan and G. M. Faeth
The University of Michigan
Ann Arbor, Michigan

INTRODUCTION

Soot processes within hydrocarbon-fueled flames affect emissions of pollutant soot, thermal loads on combustors, hazards of unwanted fires and capabilities for computational combustion. In view of these observations, the present study is considering processes of soot formation in both burner-stabilized and freely-propagating laminar premixed flames. These flames are being studied in order to simplify the interpretation of measurements and to enhance computational tractability compared to the diffusion flame environments of greatest interest for soot processes (ref. 1). In addition, earlier studies of soot formation in laminar premixed flames used approximations of soot optical and structure properties that have not been effective during recent evaluations, as well as questionable estimates of flow residence times (ref. 1-3). The objective of present work was to exploit methods of avoiding these difficulties developed for laminar diffusion flames (ref. 1) to study soot growth in laminar premixed flames. The following description of these studies is brief, see refs. 2 and 3 for more details.

EXPERIMENTAL AND COMPUTATIONAL METHODS

The measurements were completed along the axis of flat flame burners operating at 100 kPa. The burner flows were surrounded by nitrogen shroud flows in order to avoid combustion of the fuel-rich soot-containing mixture with ambient air. Measurements are described in refs. 1-3; in addition H-atom concentrations were found using the deconvoluted Li/LiOH atomic absorption method. Test conditions included ethylene/air flames similar to Harris and Weiner (ref. 4) and methane/oxygen flames similar to Ramer et al. (ref. 5).

Flame properties were predicted using the detailed chemical mechanisms of Frenklach and coworkers (ref. 6) and Leung and Lindstedt (ref. 7). In addition, measurements were sufficient to resolve all quantities needed to evaluate the hydrogen-abstraction/carbon-addition (HACA) soot surface growth mechanisms of Frenklach and coworkers (ref. 6) and Colket and Hall (ref. 8).

RESULTS AND DISCUSSION

Measurements of soot and flame properties along the axis of a typical laminar premixed methane/oxygen flame are illustrated in Fig. 1. These results are for a fuel/oxygen, F/O, ratio of 1.15 but results at other conditions are similar. Increased distances from the burner cause increased streamwise velocities, u, due to buoyancy; increased soot volume fractions, f_s, due to soot nucleation and growth; increased soot primary particle diameters, d_p, due to soot growth; and decreased temperatures, T, in the soot growth region due to radiative heat losses; in contrast, gas species concentrations remain nearly constant because soot growth involves less than 0.02% of the available mass of carbon for the present test conditions.

Measured and predicted concentrations of major gas species for the methane/oxygen flames are illustrated in Fig. 2. Present measurements generally are in good agreement with the earlier measurements of Ramer et al. (ref. 5), and with both sets of predictions. Results at other flame conditions were similar (refs. 2 and 3). Taken together, it is encouraging that flame structure can be predicted reasonably well in the presence of soot.

A key property of the HACA soot growth mechanisms is the H-atom concentrations. Earlier predictions indicated that H-atom was essentially in thermodynamic equilibrium in the soot growth region of the test flames and this estimate was used to evaluate HACA mechanisms (refs. 2 and 3). Present work completed direct measurements of H-atom concentrations in methane/oxygen flames as plotted in Fig. 3. These results show that the mechanisms of Frenklach and coworkers (ref. 6) and Leung and Lindstedt (ref. 7) yield very nearly the same results, that these results are in very good agreement with estimates based on the assumption of local thermodynamic equilibrium, and that all these results are in excellent agreement with present H-atom measurements. This finding justifies estimates of H-atom concentrations used during earlier evaluations of HACA mechanisms of soot growth (refs. 2 and 3). H-atom concentrations decrease in response to the decreasing temperatures seen in Fig. 1, which is ultimately responsible for progressively decreasing soot growth rates through the HACA mechanism. Since the temperature reduction is mainly due to radiation from soot, soot formation itself ultimately controls maximum soot concentrations in these flames.

Present measurements were used to evaluate the HACA soot growth mechanisms of Frenklach and coworkers (ref. 6) and Colket and Hall (ref. 8). The results for the Colket and Hall mechanism are illustrated in Fig. 4, where the soot growth rate, w_g, is plotted as a function of their HACA reaction rate expression, R_{CH}, for both the ethylene/air and methane/oxygen flames. The predictions in this case are fitted by selecting an unknown steric factor for the HACA mechanism, finding a very plausible value of the steric factor of 0.9 with an uncertainty of 0.2. The resulting comparison between measurements and predictions is seen to be excellent. Notably, similar results were obtained using the HACA soot growth mechanism of Frenklach and coworkers (ref. 6) also finding very plausible (order of unity) values of the unknown steric factor in their HACA mechanism.

ACKNOWLEDGEMENTS

This research is sponsored by NASA Grants NAG3-1878 and -2048 under the technical management of Z.-G. Yuan of the National Center for Microgravity Research, NASA Glenn Research Center, Cleveland, Ohio and D. L. Urban of the Microgravity Science Division, NASA Glenn Research Center, Cleveland, Ohio.

REFERENCES

1. Sunderland, P. B., Köylü, Ü. Ö. and Faeth, G. M., Combust. Flame 100:310 (1995).
2. Xu. F., Sunderland, P.B. and Faeth, G. M., Combust. Flame 108:471 (1997).
3. Xu, F., Lin, K.-C. and Faeth, G. M., Combust. Flame 115:195 (1998).
4. Harris, S. J. and Weiner, A. M., Combust. Sci. Tech. 38:75 (1984).
5. Ramer, E. R., Merklin, J.F., Sorensen, C. M. and Taylor, T. W., Combust. Sci. Tech. 48:241 (1986).
6. Kazakov, A., Wang, H. and Frenklach, M., Combust. Flame 100:111 (1995).
7. Leung, K. M. and Lindstedt, R. P., Combust. Flame 102:129 (1995).
8. Colket, M. B. and Hall, R. J., *Soot Formation in Combustion* (H. Bockhorn, ed.), Springer-Verlag, Berlin, 1994, p. 442.

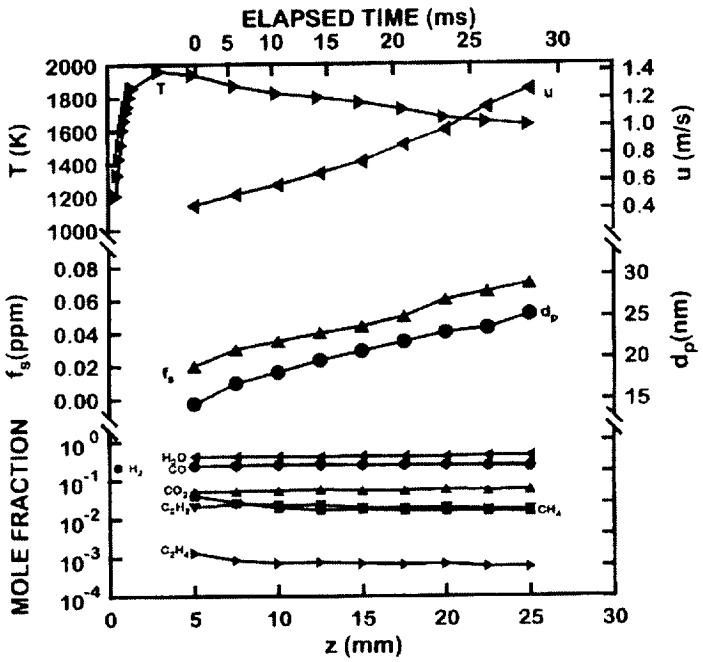

Fig. 1 Soot growth region of premixed methane/oxygen flame.

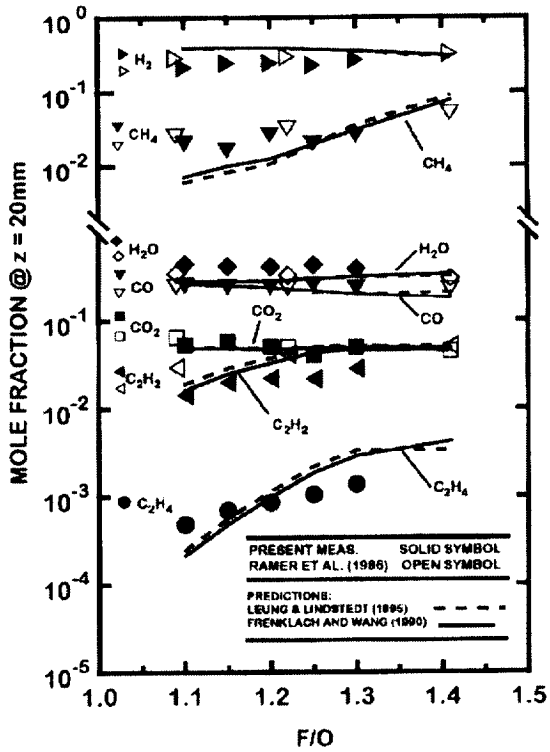

Fig. 2 Species concentrations in soot growth region of premixed methane/oxygen flames.

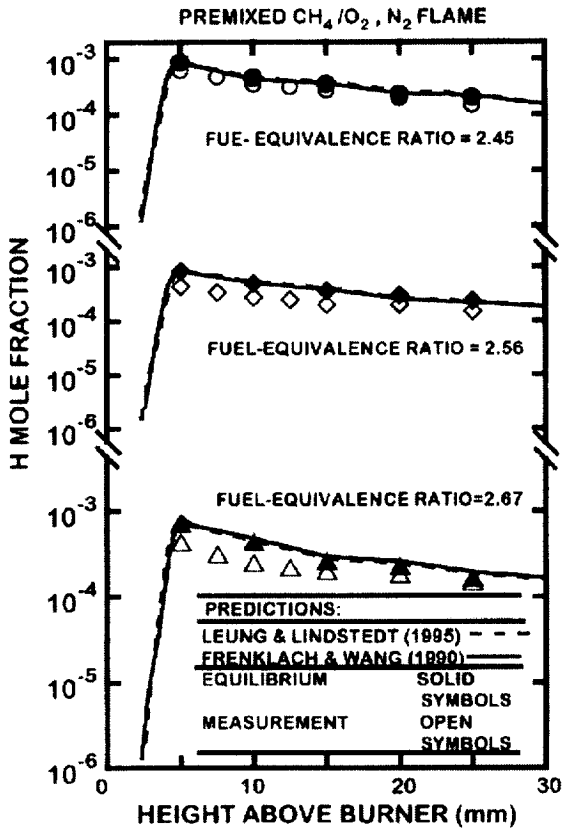

Fig. 3 H atom concentrations in soot growth region of premixed methane/oxygen flames.

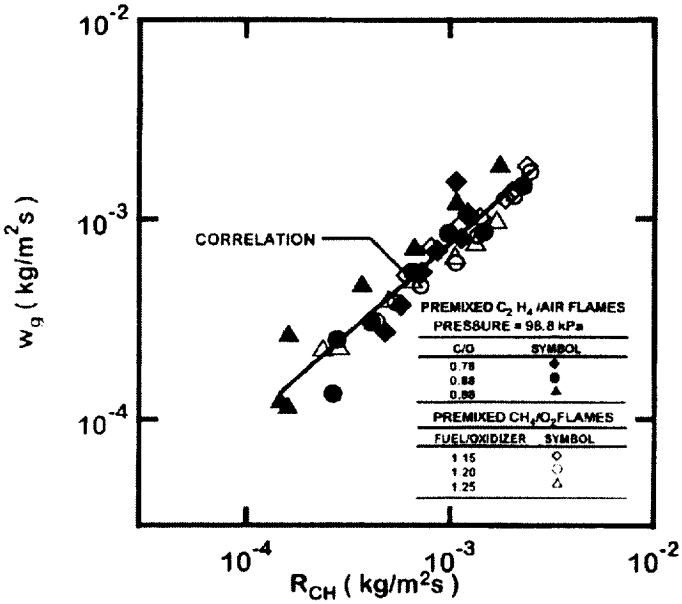

Fig. 4 Soot surface growth rates via the HACA mechanism.

A STUDY OF FLAME PROPAGATION ON WATER-MIST LADEN GAS MIXTURES IN MICROGRAVITY

S15-29

A. Abbud-Madrid, E. P. Riedel, and J. T. McKinnon
Center for Commercial Applications of Combustion in Space
Colorado School of Mines
Golden, CO 80401

INTRODUCTION

The use of water mists (very fine water sprays) for fire suppression is currently receiving increased attention as a replacement technology for halogen-based chemical agents—such as Halon 1301 (CF_3Br)—the manufacturing of which has been banned by the Montreal Protocol due to their high ozone depletion potential. Water mist technology has been found effective for a wide range of applications such as Class B pool fires, shipboard machinery, aircraft cabins, computers, and electronic equipment [1].

There are five distinct mechanisms by which water droplets may interact with a flame. First, the high enthalpy of vaporization of water (2450 kJ/kg) leads to heat removal from the flame front as the liquid droplets turn to steam. Second, as water vaporizes its volume increases approximately three orders of magnitude, which leads to the dilution of the oxygen and vaporized fuel required to maintain the flame. The third effect is the recombination of H-atoms and other radicals on the droplet surface. A fourth effect of water mists in fires is the retardation of surface propagation rates due to the wetting of walls and surfaces. The last potential impact of fine water mists affects the radiative propagation of the fire by forming an optically thick barrier to infrared radiation which prevents ignition of the unburned regions. Unfortunately, little fundamental information exists on the interaction of a flame with a water mist. To date, there is no widely accepted interpretation of the critical concentration of droplets required to suppress a flame or of the fundamental mechanisms involved in flame extinguishment by water mists.

One of the main obstacles to obtaining such understanding is the difficulty of providing a simple, well-defined experimental setup for the flame front/water mist interaction. Some of the difficulty stems from the problem of generating, distributing and maintaining a homogeneous concentration of droplets throughout a chamber while gravity depletes the concentration and alters the droplet size by coalescence and agglomeration mechanisms. Experiments conducted in the absence of gravity provide an ideal environment to study the interaction of water mists and flames by eliminating these distorting effects. In addition, microgravity eliminates the complex flow patterns induced between the flame front and the water droplets. The long duration and quality of microgravity in space flights provide the required conditions to perform the setup and monitoring of flame suppression experiments. Consequently, a series of experiments have been identified to be performed on the Combustion Module (CM-2) in the Space Shuttle. These consist of measuring the extinguishing capability of a water mist on a premixed flame propagating along a tube. These experiments should provide the necessary data to obtain further understanding of the water mist suppression phenomena that can be later used to design and manufacture appropriate fire suppression systems. In preparation for the orbital flights, experiments have been conducted on low-gravity ground facilities to obtain the preliminary data necessary to define the scientific objectives and technical issues of the spacecraft experiments.

EXPERIMENTAL APPARATUS AND RESEARCH APPROACH

The experimental apparatus used in both the normal- and low-gravity tests is shown in Fig. 1. The low-gravity experiments were conducted in NASA's KC-135 airplane in Houston, Texas. Gravity levels down to ±0.01 *g* are obtained during a typical 20-s parabolic maneuver. Up to 20 tests were conducted in a single flight for a total of 80 tests in a week-long flight campaign.

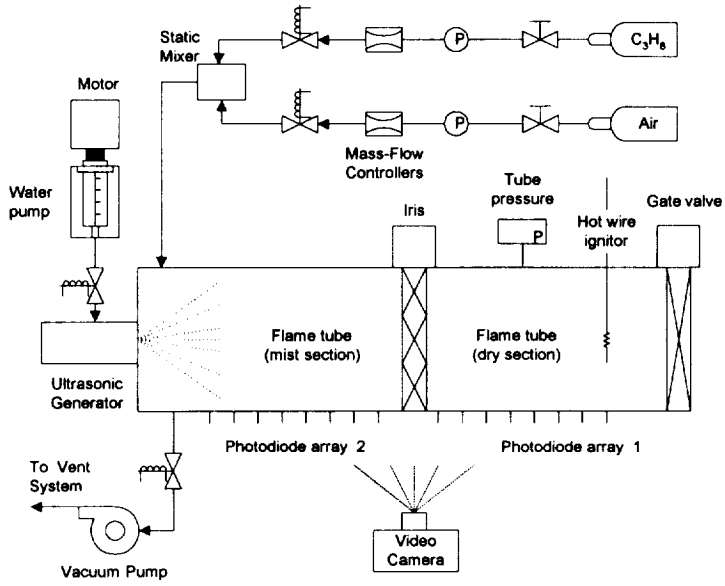

Figure 1. Experimental apparatus

In order to characterize the interaction of the water mist with the flame front, a premixed gas mixture of propane (C_3H_8) and air is loaded in a transparent cylindrical tube of approximately 6.35-cm diameter and 49.5-cm length. The C_3H_8-air mixture was chosen for its ease of ignition, high flame luminosity, and its wide used in many practical applications. In addition, two types of flame behavior are observed depending on mixture stoichiometry: continuous flames in lean mixtures and wrinkled flame fronts in rich mixtures. This behavior is caused by thermal-diffusive instabilities that depend on the Lewis number (*Le*) of the mixture. The two gases are introduced in the tube from separate tanks through a static mixer using mass flow controllers. A water mist generated by an ultrasonic atomizing system is introduced in one half of the tube separated by an iris from the dry region. The water concentration is determined by the volume of water delivered by the syringe pump. The iris opens and the mixture is ignited in the dry section while keeping the valve at that end of the tube open for an isobaric combustion process. In order to measure the fire suppression ability of a given water mist droplet size and concentration, the propagation velocity of the premixed flame is measured. The flame speed is measured by an array of photodiodes installed along the tube and by a video camera. Experiments are conducted with various equivalence ratios (ϕ) ranging from 0.6 to 2.0 and with several water-mist volumes from 0.25 to 1.00 mL. The mean diameter of the water mist droplets is 36 μm.

RESULTS

As mentioned above, the effect of water mist volume and equivalence ratio on the laminar flame speed is used as the measure of fire suppression efficacy. The influence of water mist on the shape and propagation behavior of flames is also explored. In the case of lean premixed

flames, a curved, continuous flame front propagates at a constant speed down the dry section of the cylindrical tube after ignition. Interestingly, for all lean equivalence ratios, the flame speed increases at first with low water-mist volumes and then decreases below its dry-region value for high water-mist volumes. This effect is shown in Fig. 2 for a C_3H_8-air mixture of $\phi = 0.8$. The speeds shown correspond to the flame front propagation velocity in the tube and not to the burning velocity of the mixture.

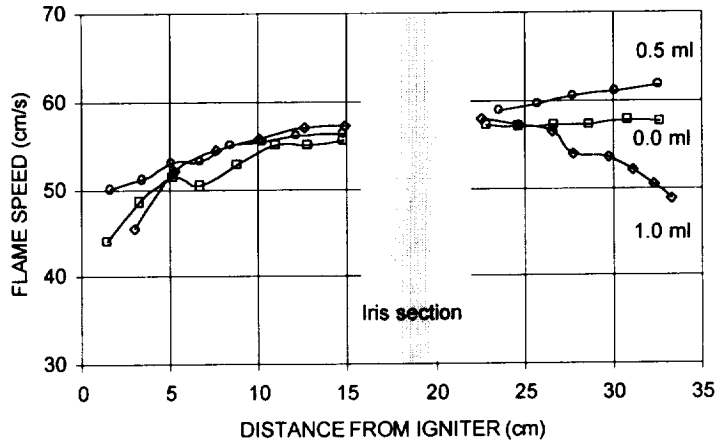

Figure 2. Effect of water mist (mean droplet diameter of 36 μm) on the flame speed of a C_3H_8-air premixed flame with equivalence ratio of 0.8.

This reversal of flame speed with water mist volume may be due in part to the heating of the unburned mixture ahead of the flame as a result of radiation absorption by the water droplets. At sufficiently low water-mist concentrations this preheating of the mixture may overcome the heat loss experienced by the flame due to the phase-change cooling and mixture dilution caused by the water mist. Alternatively, this behavior may be due to the short duration of reduced gravity in the airplane. The brief time allowed for water injection and dispersion in the airplane is not enough to generate a homogenous mist concentration and may also lead to residual convective currents generated by the mist injection. In addition the *g*-jitter present in parabolic flight may also contribute to the inability to obtain the desired experimental conditions. A few experiments were conducted with higher water concentrations. In these cases the flame front was distorted, slowed down, and eventually extinguished before reaching the end of the tube. Even under these extreme conditions of flame distortion and stretch, the flame front remains remarkably coherent and resilient due to the high *Le* number (1.78) of these lean mixtures.

The rich mixtures tested exhibited a wrinkled flame front immediately after ignition. This unstable behavior is caused by the unequal rates of diffusion of thermal energy and mass characteristic of a mixture with lower-than-unity Lewis number ($Le = 0.87$). These instabilities are accentuated by the quenching action of the water mist. Multiple local extinctions on the wrinkled flame front by water droplets result in increased flame curvature and consequently in larger reactant diffusion rates versus heat loss rates. As a result, the flame front breaks up into various cellular fronts that tend to propagate independently of each other. The highly curved cells acquire a higher temperature and higher resistance to extinction by water droplets. This in turn

promotes faster flame speeds for low water-mist concentrations. The inability to obtain a homogeneously distributed water concentration in the airplane experiments results in the formation of flame cells separating from the flame front and traveling at different propagation velocities. This non-coherent propagation makes it difficult to define a uniform flame front speed. A few tests were conducted with very rich mixtures (higher than ϕ=2.0) and high water volumes (higher than 1.0 mL). In these extreme cases, a few small cellular flames propagated through the non-homogeneous misted section at speeds lower than 5 cm/s.

CONCLUSIONS AND FUTURE WORK

A preliminary investigation of the effect of water mists on premixed flame propagation in a cylindrical tube under reduced-gravity conditions has been conducted to define the scientific and technical objectives of the experiments to be performed on the Space Shuttle microgravity environment. The inhibiting characteristics of several water mist concentrations in premixed propagating flames of propane-air mixtures at various equivalence ratios are studied. Two different types of flame behavior are found depending on the mixture stoichiometry. In the case of lean C_3H_8-air mixtures, the flame speed increases at first with low water-mist concentrations and then decreases below its dry value when higher water-mist volumes are introduced in the tube. This phenomenon may be due in part to the heating of the unburned mixture ahead of the flame as a result of radiation absorption by the water droplets. For rich C_3H_8-air mixtures, similar behavior of flame speed vs. water concentration is found but in this case is mostly due to the formation of cellular flames, which become more resistant to extinction by the water mist.

It is suspected that the unusual behavior observed in both of the above cases may be also due in part to the short duration and low quality of the reduced gravity available in the airplane. Consequently, the next stage of the Water Mist project (MIST) is the development of an experiment that will take advantage of the long duration and high-quality microgravity experienced in orbital flight. The MIST experiment is scheduled to fly on the STS-107 mission of the Space Shuttle in early 2001. During that mission, the MIST apparatus will be installed inside the Combustion Module (CM-2) along with other two combustion experiments. The final objective is to create a detailed map of flame speed, droplet diameter, water concentration, and equivalence ratio, which will give the appropriate set of parameters for flame suppression.

ACKNOWLEDGMENTS

This research is funded through the NASA Center for Commercial Applications of Combustion in Space (CCACS) at the Colorado School of Mines (CSM). We wish to acknowledge the invaluable help from the CCACS director, Frank Schowengerdt, and from the following graduate and undergraduate students: Francine Amon, Katie Squire, Erin Evans, Aragorn Earls, Jennifer Lawton, Sheli Babb, David Petrick, Tom Phare, and Richard Williams.

REFERENCES

1. Mawhinney, J.R. and Solomon, R., "Water Mist Fire Suppression Systems," in *The Fire Protection Handbook*, 18th ed., edited by A.E. Cote, Boston, National Fire Protection Association, 1997, pp. 216-248.

16-27

FLAME INVESTIGATION OF VERY LEAN PROPANE-AIR MIXTURES UNDER MICROGRAVITY

T.Kawakami, S.Okajima[1] and T.Sakuraya[2]College of Engineering Hosei University Kajino-cho, Koganei, Tokyo 184 Japan 2) Japan Space Utilization Promotion Center 3-30-16, Nishiwaseda, Shinjuku-ku, 169, Japan (kawakami@k.hosei.ac.jp, okajima@cm.me.hosei.ac.jp and sakuraya@jsup.or.jp)

INTRODUCTION

Experiments on combustion of very lean mixtures in the vicinity of lower flammability limits are very important from the viewpoint of development on the combustion system for low fuel consumption and low emissions with high load engines. However, accurate data on combustion characteristics of such mixtures are scarce due to difficulties inherent in conventional measuring techniques under normal gravity. It is well known that the flame behavior is strongly influenced by buoyancy under normal gravity. This influence is more pronounced in the near the lower flammability limits where flame speeds are very low. Consequently, the data such as burning velocity and flammability limits of extremely lean obtained by conventional measuring technique under normal gravity are suspect.

Thus, the present experiments have been carried out with quiescent mixtures for examining the irregular flame propagation and lower limits of flame propagation limit at very lean propane-air mixtures under microgravity.

These experiments were performed in the 490 m drop shaft of Japan Microgravity Center located in Kamisunagawa, Hokkaido, Japan.

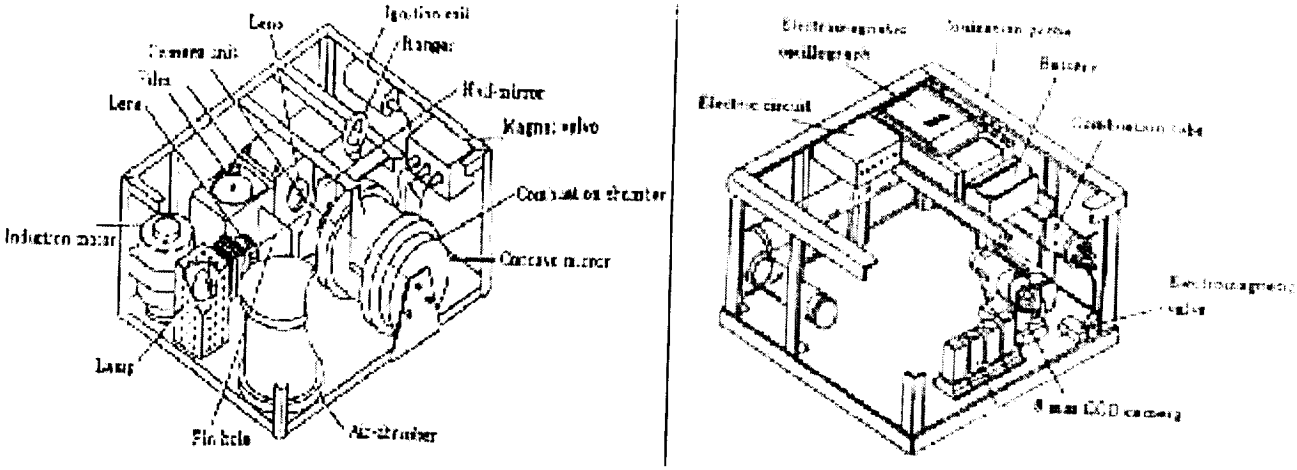

(a) Closed bomb • (b) Long tube

Fig. 1 Falling assembly

EXPERIMENTAL APPARATUS AND PROCEDURE

The falling assembly used for observation of the irregular flame propagation of very lean propane-air mixtures is shown in Fig. 1(a) and its size is 800×800×350 mm and weight is about 70 kg. It contains a cylindrical combustion bomb, an igniter, a schlieren photographic system and a camera unit.

In Fig.1(b) is shown the second falling assembly for determining the limits of flame propagation at very lean mixtures in a long tube and its size is 800×800×350 mm and weight is about 80 kg. It contains a glass tube, an electromagnetic oscillograph, six ionization probes and three CCD video cameras. The glass tube of 50 mm in initial diameter and 1500 mm in length is mounted horizontally inside the falling assembly.

Experiments were carried out at room temperature and 0.1 MPa. The fuel used is propane of 99.9 % purity. A mixture of 79 % nitrogen and 21 % oxygen by volume is used as a substitute for air.

EXPERIMENTAL RESULTS AND DISCUSSION

(1) Irregular flame propagation

Figure 2 shows the schlieren photographs of the flame propagation of propane-air under microgravity. Fig. 3 and 4 denote the flame speed with time from ignition of propane-air mixtures at •= 0.49 and 0.47 under microgravity. In these figures it can be seen that the flame speeds are somewhat irregular owing to the extreme lean state of mixtures. This fact indicated that the Lewis number, Le(=Di/•i, the ratio of mass diffusivity to thermal diffusivity) becomes larger than unity for lean mixture of propane in air. Flame propagation under such conditions will be limited by the relatively slower heat transfer rate from the flame front to the unburnt mixtures. As the mixture becomes leaner and leaner, enhanced diffusivity shifts Le to higher value and the poorer heat transfer conditions make the flame propagation irregular. [1),2)]

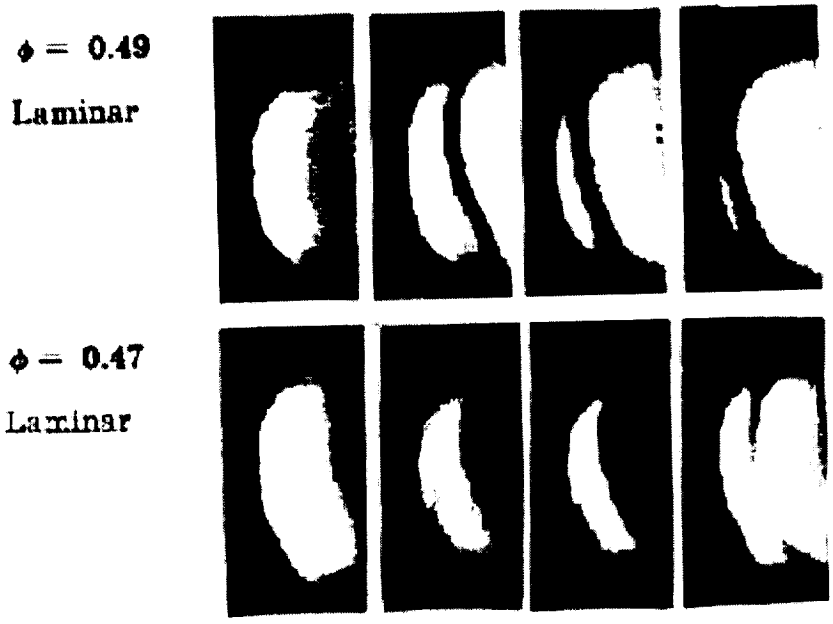

•Fig.2 Schlieren photograph

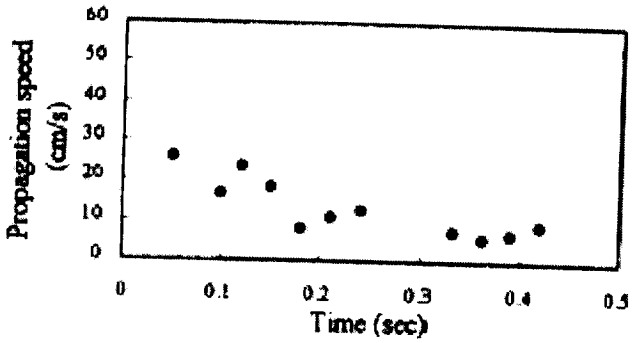

Fig. 3 Flame speed(•= 0.49)

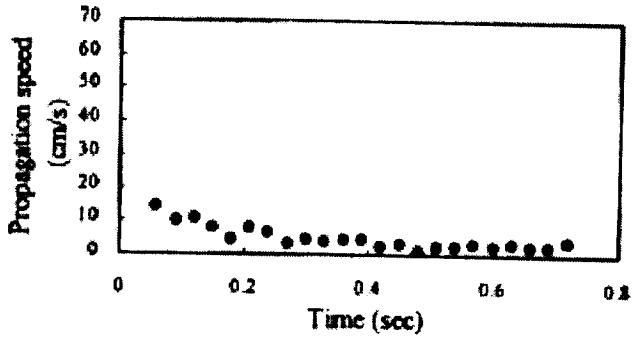

•••Fig. 4 Flame speed(•= 0.47)

(2) Propagation limit

Figures 5 and 6 show the direct color photographs of flame propagation of propane-air mixtures at equivalence ratio of 0.45 in a long tube under normal and microgravity, respectively. As seen from these photographs the flame shape of such mixtures under normal gravity is influenced by buoyancy, and hence the distortion of the flame shape from axial symmetry is markedly large. On the other hand under microgravity the flame remains symmetrical through out the combustion process. So it makes possible to determine the true values of the flame propagation limits from the microgravity experiment.

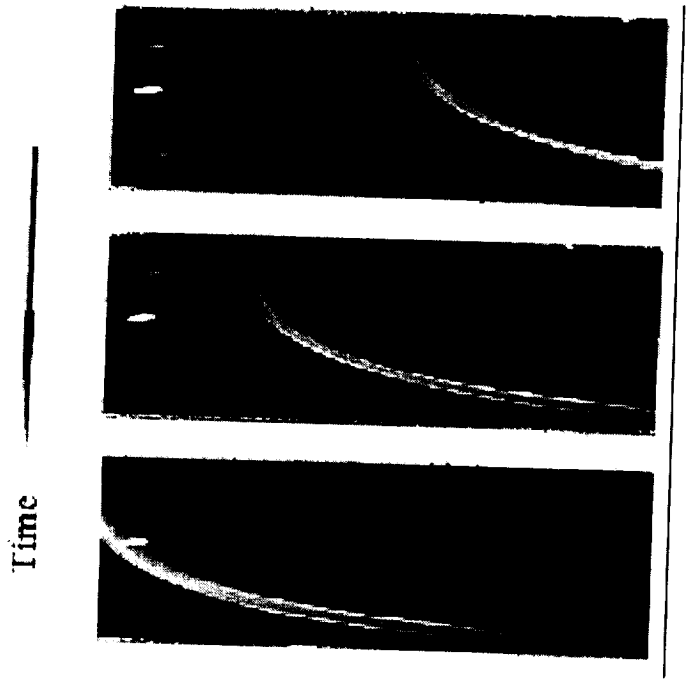

Fig. 5 Flame shape (normal gravity)

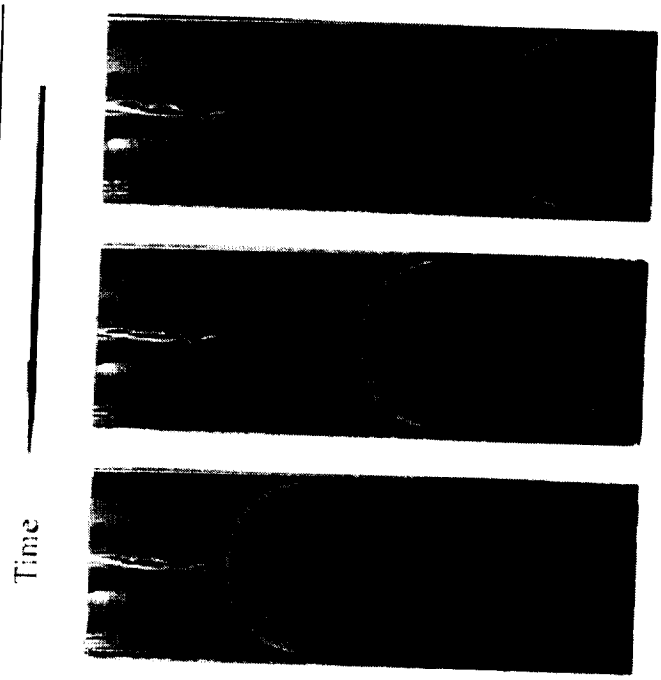

•••Fig. 6 Flame shape(microgravity)

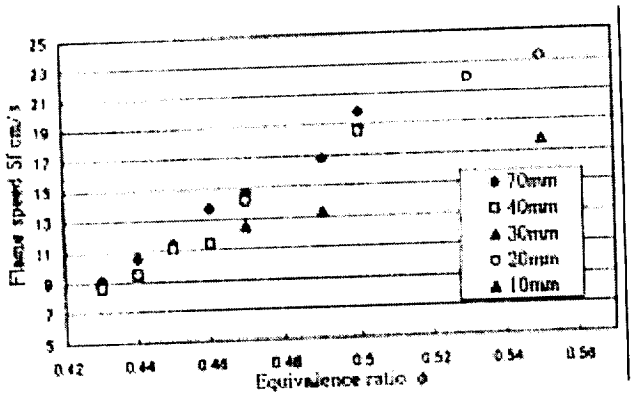

Fig.7 Flame speed(long tube)

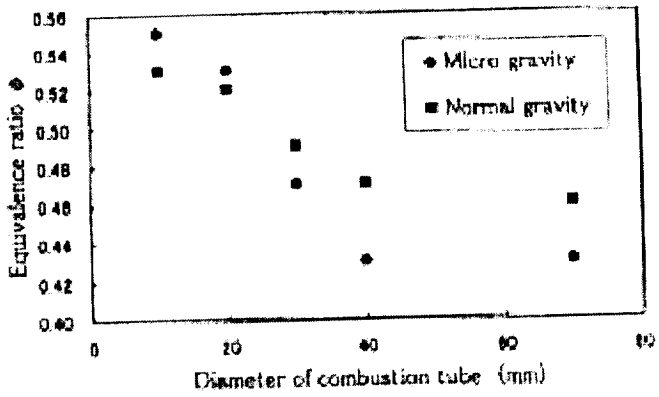

Fig. 8 Propagation limit

Fig. 7 shows the flame speed in a long tube of extremely lean propane-air mixtures with equivalence ratio under microgravity. It is found that from this figure that the flame speed decreases as equivalence ratio decreases and it increases with increasing inner diameter of combustion tube at same equivalence ratio. For more extreme lean mixtures of equivalence ratio less than 0.42, the flame propagation can not be observed at half length of combustion tube even when the observation time is 10 sec. So we can recognize that the minimum value of flame speed is about 9 cm/s at equivalence ratio of 0.43.

Figure 8 indicates the lower limits of flame propagation with diameter of combustion tube under microgravity. From this figure it can be seen that the lower limits of flame propagation are influenced by the variation of combustion tube diameter under both conditions of normal and microgravity and the values obtained under microgravity are shifted to lower values than that obtained under normal gravity. This fact denotes that the lower limits of flame propagation are influenced by radiative heat loss to walls of the combustion tube.

CONCLUSIONS

Experiments have been carried out to elucidate the irregular flame propagation and the limits of flame propagation of very lean propane-air mixtures under microgravity. The main conclusion are as follows: 1) The flame propagation of propane-air mixtures close to lower flammability is irregular even under microgravity. 2) Under microgravity the lower limits of flame propagation is shifted to lower value more than that obtained under normal gravity.

ACKNOWLEDGEMENTS

This study is carried out as part of project sponsored by "Japan Space Utilization Promotion Center(JSUP)" promoted by NASDA.

REFERENCES

1) Dunsky, C. M.:Twenty-Fourth Symp.(International) on Combustion, The Combustion Institute, Pittsburgh, pp.177-187, 1657(1991).
2) Sivashinsky, G. I., Fluid Mech., 179 (1983).

STRUCTURE AND TRANSIENT RESPONSE OF SPHERICAL FLAMES

C. K. Law, S. D. Tse, L. He, D. L. Zhu, and C. J. Sung
Department of Mechanical and Aerospace Engineering
Princeton University, Princeton, NJ 08544 USA

Introduction

The present research endeavor is concerned with gaining fundamental understanding of the configuration, structure, and dynamics of laminar flames in simple, well-defined flow fields such that the phenomena of interest can be studied without being unduly complicated and compromised by complex and sometimes non-quantifiable flow field effects. Consequently, microgravity, one-dimensional, spherically-symmetric flames are expected to yield data of high fidelity, which can be meaningfully interpreted as well as compared with numerical calculations for the understanding of the basic flame structure in general and flame chemistry and dynamics in particular. Moreover, such one-dimensional flames are readily amenable to theoretical study, through which the underlying physics of specific transient responses and their corresponding flame structures can be extracted.

We have recently extended our studies of the structures and transient responses of spherical flames along the following directions: (1) theoretical study of the role of flamefront motion in droplet burning to determine the range of validity of the classical quasi-steady theory in predicting the flame standoff ratio, as well as its implication on transient fuel vapor accumulation/depletion; (2) experimental and computational investigation of the influences of the gas-phase transient processes of fuel vapor accumulation and far-field diffusion on the flamefront movement and the attainment of steady state for burner-generated spherical diffusion flames, without the additional transient process of droplet surface regression; and (3) theoretical and numerical study of the dynamics involved in the transition from a propagating spherical flame to a stationary flame ball.

Role of Flamefront Motion and Criterion for Global Quasi-Steadiness in Droplet Burning

The classical ^{2}-law, formulated by assuming quasi-steady droplet vaporization for gas-phase density ρ much smaller than that of the liquid ρ , i.e. $\varepsilon = \rho/\rho \ll 1$, shows that the evaporation constant, $= \mathrm{d}r^2/\mathrm{d}$, and that the ratio, $\kappa = r/r$, of the instantaneous flame radius r to the droplet radius r , are constants as the droplet gasifies. However, it has also been observed that the standoff ratio and temperature of the flame may not be constant, implying failure of the classical ^{2}-law to describe the cumulative heat release. A number of studies have been subsequently carried out that attribute these phenomena to various effects of unsteadiness, which are not considered in the classical theory.

In the gas-phase analyses of the classical quasi-steady (CQS) theory and the far-field unsteady diffusion theory, it is assumed that the droplet surface regression velocity, non-dimensionalized by the gas velocity at the surface, $= (\mathrm{d}r/\mathrm{d})/$, is respectively zero and $\mathrm{O}(\varepsilon)$, and that the mass-flow rate across the reaction front, , is always the same as that at the droplet surface,

Implicit in such derivations is also the assumption that the non-dimensional flamefront velocity, $U \equiv (\mathrm{d}r/\mathrm{d})/$, is at most $\mathrm{O}(\varepsilon)$. However, in order for the standoff ratio κ to remain constant, the flame must spread with a non-dimensional velocity, $U \equiv (\mathrm{d}r/\mathrm{d})/ = \kappa (\mathrm{d}r/\mathrm{d})/$. Since the CQS theory predicts values of κ of up to 40 for hydrocarbon droplets burning in air, U can actually assume values substantially larger than $\mathrm{O}(\varepsilon)$. Consequently, by not explicitly considering the motion of the flamefront in the derivations, previous theories are not self-consistent and indeed violate mass conservation.

Considering that the ratio of the volume enclosed by the flamefront to that of the droplet is κ^3, a droplet-surface regression rate of $(dr/d) = \varepsilon$ produces a total mass-flow rate variation of the order of $\varepsilon\kappa^3$ between the droplet surface and the reaction front. As a result, the influence of this flamefront motion can be characterized by a quasi-steady parameter $\equiv \varepsilon\kappa^3$, such that the influence is large when it is O(1) and small otherwise.

Since $\kappa > 1$, the classical theory can be applied when $\varepsilon << 1$ and $\kappa = O(1)$. Thus the effect related to the motion of the reaction front becomes important for $\kappa \sim \varepsilon^{-1/3}$ or larger. For hydrocarbon droplet combustion in atmospheric air, $\varepsilon \sim (10^{-3}$ to $10^{-2})$ and the experimental standoff ratio κ typically varies from 5 to 20. The mass-flow rate variation is therefore of the order of 10^{-1} to 10^{2} indicating that the motion of the reaction front is, in general, important even if the combustion started out with the flame situated at the quasi-steady value such that the fuel vapor accumulation effect due to initial conditions is minimized.

By working in the flame coordinate and hence naturally allowing for this motion, and by further assuming gas-phase quasi-steadiness (in this coordinate), but neglecting far-field effects, calculated results show that the standoff ratio continuously increases with time for O(1) values of (Fig. 1), but approaches a constant, which is close to but exceeds the ^{2}-law prediction, when is sufficiently small (Fig. 2). Details of the work can be found in Ref. 1.

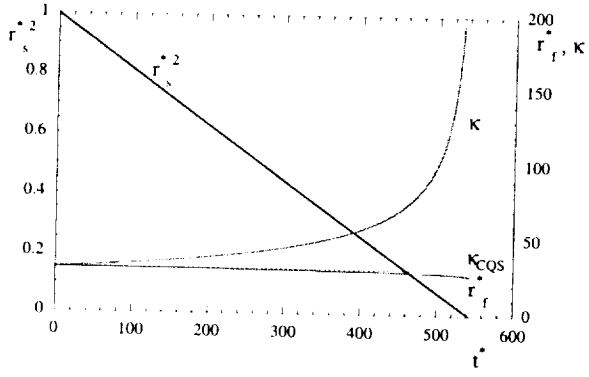

Figure 1. Heptane droplet (κ = 30, = 27) burning in the standard atmosphere. $^* = \tilde{} / \tilde{}_{,0}$, $^* = \tilde{} / \tilde{}_{,0}$, $t^* = t/(\tilde{}_{,0}/\tilde{}_{,0})$.

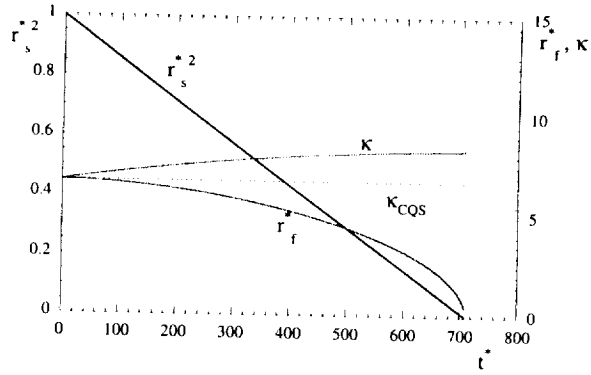

Figure 2. Ethanol droplet (κ = 6.7, = 0.3) burning in pure oxygen.

Microgravity Burner-Generated Spherical Diffusion Flames

The two main causes for the flame motion (gas-phase transient behavior) in droplet burning are droplet surface regression and mass accumulation due to initial displacement of the flame from an otherwise steady position. Furthermore, any flame motion itself, as well as the droplet surface regression process, can induce secondary far-field transient diffusion effects. In order to identify the role of each of these transient processes, it is essential that they are isolated to the extent possible. In the present investigation we have studied the motion of microgravity, spherical diffusion flames established by ejecting fuel/inert mixtures with constant mass-flow rates from a porous spherical burner into air. Therefore, effects caused by droplet heating and droplet surface regression are eliminated. As a result, the only transient processes that remain in operation are mass accumulation due to initial conditions and transient diffusion caused by the resulting flame motion. As such, steady-state combustion is achievable for the present system.

Experimental data of good quality have been obtained on the transient response, due to an impulsive step from normal-gravity to microgravity conditions, in the 2.2-s drop tower facility at the NASA Lewis Research Center. Figure 3 shows the development of a buoyancy-affected flame

into a nearly spherically-symmetric flame after the drop. The quality of the spherical diffusion flames produced is excellent, with 1.0 sphericity and 0.94 concentricity. Fully-transient computations with detailed chemistry and transport simulate well the experimental data of the flame expansion process (Fig. 4); however, although steady-state behavior should exist for such flames, the results indicate that steady-state flame behavior cannot be reached within the 2.2-s microgravity duration, for the fuels and mass-flow rates tested. As a result, longer durations of microgravity are needed in order to examine steady-state phenomena.

A simple scaling correlation, collapsing non-equidiffusion and finite chemistry effects into an effective-equidiffusive system with infinitely-fast chemistry for experimental and computational data, reveal that the transient flame expansion process can be approximately correlated for different fuel mixtures and mass-flow rates, showing that flames of smaller characteristic sizes approach steady-state faster. Additionally, the lack of correspondence of visible flame luminosity with the flame strength is also noted, and its implication on potential misinterpretation of flame extinction in the presence of decreasing flame luminosity is suggested. Details of this work can be found in Ref. 2.

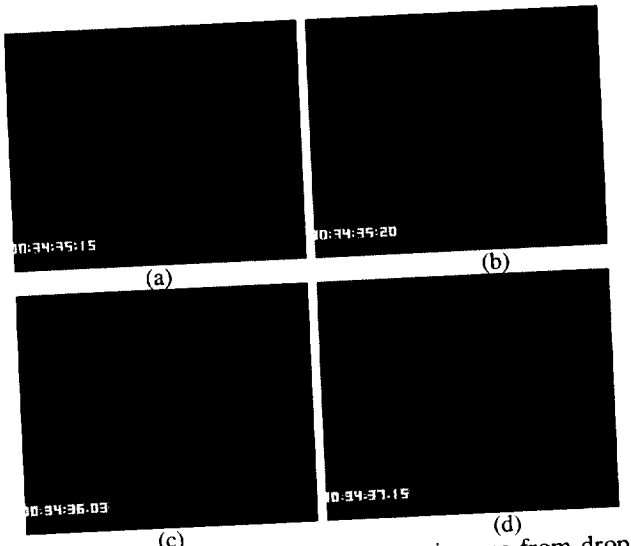

Figure 3. Spherical diffusion flame images from drop tower. 50%H_2-10%CH_4-40%N_2 at 0.0081 g/s. Time into μg: (a) 0.0 s; (b) 0.166 s; (c) 0.6; (d) 2.0 s.

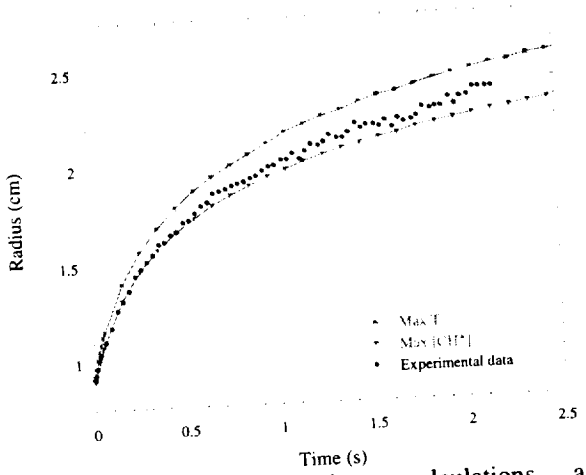

Figure 4. Fully transient calculations and experimental data for flame of Fig. 3. Calculated steady-state Max T radius is 4.72 cm.

Dynamics of Transition from Propagating Flame to Stationary Flame Ball

A theoretical and numerical study has revealed that the stationary flame ball (SFB) is a continuous extension of the propagating spherical flame and not an isolated phenomenon. The flame velocity-curvature relation depends strongly on transport and heat loss. As a result, three typical regimes exist: (i) when the heat loss is very small, the spherical flame expands outwardly and transforms asymptotically to a planar flame; (ii) when the heat loss is moderately large, the planar flame does not exist and the expanding flame quenches; and (iii) when the heat loss is large, the expanding spherical flame transforms to a stationary flame ball. A quasi-steady nonlinear relation between the instantaneous flame radius and flame velocity , obtained via both asymptotic analysis as well as numerical computation with constant density and one-step Arrhenius kinetics, shows that for sufficiently small heat loss, the flame velocity continuously varies from zero to the planar flame velocity. However, when the heat loss is larger than a critical value, the velocity-radius relation exhibits a turning point which may correspond to either flame extinction or reversal of the direction of propagation.

The flame radius, defined as the location of the maximum temperature, is plotted in Fig. 5 as a function of time for different values of heat loss, = 0, 0.5, 10 and 100. There are three regimes of the flame response respectively, separated by some critical values of heat loss, , and . Specifically, when the heat loss is very small, the flame ignited at the center decelerates asymptotically to the planar flame (see = 0 in Fig. 5). When < < , the flame radius first expands outwardly but then shrinks to the center. In these two cases, a stationary spherical flame ball cannot be established directly from the point ignition source. When < < , a spherical flame first expands outwardly, then shrinks, and finally stabilizes as a stationary spherical flame. Thus a stationary spherical flame ball can be reached directly from an expanding flame ignited by a point source. When the heat loss is very large, > , the flame is very difficult to ignite.

The corresponding maximum flame temperature is shown in Fig. 6. For = 0, the flame temperature decreases steadily to that of the planar flame. As the heat loss is increased to values larger than , = 0.5 and 10, the flame temperature first decreases slowly and then it drops very rapidly at around = 8 and 0.1 respectively, indicating clearly the occurrence of extinction of the flame front. Thus the shrinking of the "flame" radius, observed in Fig. 5 for this regime is simply the consequence of diffusive mixing of the non-reactive hot gas sphere with the cold ambience subsequent to flame extinction. Finally as is increased to 100, the temperature first decreases and then increases to that of the stationary flame ball. Details of this work can be found in Ref. 3.

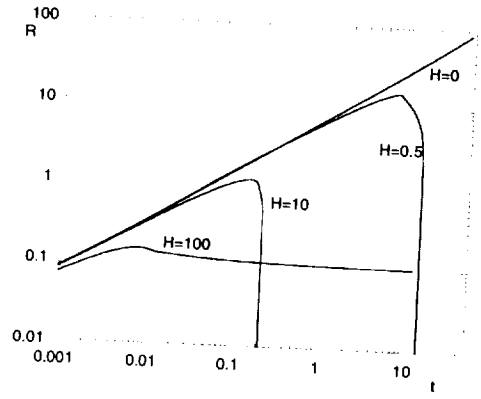

Figure 5. Trajectory of the flame front.

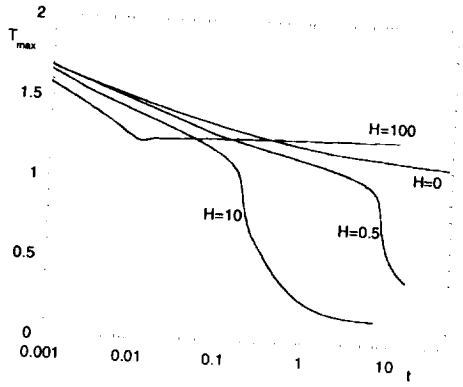

Figure 6. Maximum temperature of the flame.

References

1. He, L., Tse, S.D., and Law, C.K., "Role of Flamefront Motion and Criterion for Global Quasi-Steadiness in Droplet Burning,"
2. Tse, S.D., Zhu, D.L., Sung, C.J., and Law, C.K., "Microgravity Burner-Generated Spherical Diffusion Flames: Experiment and Computation," AIAA-99-0585, , (in press). , 1999.
3. He, L, and Law, C.K., "On the Dynamics of Transition from Propagating Flame to Stationary Flame Ball," AIAA 99-0325, , 1999.

PLANAR STRAIN-RATE-FREE DIFFUSION FLAMES: INITIATION, PROPERTIES, AND EXTINCTION

Francis Fendell[1], Suleyman Gokoglu[2], Harald Rungaldier[1], and Donald Schultz[3], [1]TRW Space and Electronic Group, Redondo Beach, CA, [2]NASA Glenn Research Center, Cleveland, OH, [3]Schultz Engineering Services, Middleburg Heights, OH.

INTRODUCTION

An effectively strain-rate-free diffusion flame constitutes the most vigorous laminar combustion of initially unmixed reactive gases. Such a diffusion flame is characterized by a relatively long residence time and by a relatively large characteristic length scale. If such a flame were also planar, providing high symmetry, it would be particularly suitable for experimental and theoretical investigations of key combustion phenomena, such as multicomponent diffusion, chemical kinetics, and soot inception, growth, and oxidation. Unfortunately, a planar strain-rate-free diffusion flame is highly disrupted in earth-gravity (*e.g.*, in a counterflow-diffusion-flame apparatus) because of the very rapid onset (~ 100 ms) of gravity-induced instability.

Accordingly, a specially dedicated apparatus was designed, fabricated, and initially checked out for the examination of a planar strain-rate-free diffusion flame in microgravity (Figure 1). Such a diffusion flame may be formed within a hollowed-out squat container (initially configured as 25 cm x 25 cm x 9 cm), with isothermal, noncatalytic, impervious walls. At test initiation, a thin metallic sheet (~ 1 mm in thickness) that separates the internal volume into two equal portions, each of dimensions 25 cm x 25 cm x 4.5 cm, is withdrawn, by uniform translation (~ 50 cm/s) in its own plane, through a tightly fitting slit in one side wall. Thereupon, diluted fuel vapor (initially confined to one half-volume of the container) gains access to diluted oxygen (initially with the same pressure, density, and temperature as the fuel, but initially confined to the other half-volume). After a brief delay (~ 10 ms), to permit limited but sufficient-for-flammability diffusional interpenetration of fuel vapor and oxidizer, burning is initiated by discharge of a line igniter, located along that side wall from which the trailing edge of the separator withdraws. The ignition spawns a triple-flame propagation across the 25 cm x 25 cm centerplane (Figure 2). When a diffusion flame is emplaced in the centerplane, any subsequent travel, and change in temperature, of that planar diffusion flame may be tracked, along with the effectively spatially uniform but temporally evolving pressure within the container. Eventually, nearly complete depletion of the stoichiometrically deficient reactant, along with heat loss to the container surfaces, effects extinction.

These data afford an opportunity to check theoretical models of diffusion and chemical kinetics under conditions ranging from intense burning to flame out, or, alternatively, to evolve simple empirical representations of these phenomena. Thus, the project sought to utilize microgravity testing to elucidate commonly encountered phenomenology, arising in the commonly-encountered mode of combustion (whether related to heating, manufacturing, boiling, and propulsion, or to uncontrolled, free-burning fire in structures and wildland vegetation), of those commonly utilized fuels usually categorized as gaseous fuels (such as hydrogen, natural gas, and propane, which are gaseous under atmospheric conditions).

PROJECT HISTORY: UNDERTAKING THE PRIMARY CHALLENGE OF PLANAR-FLAME EMPLACEMENT

A flight-experiment project entitled "Unsteady Diffusion Flames: Ignition, Travel, and Burnout" was initiated, as one of the combustion-science tasks of the NASA Microgravity Science Research Program, on July 10, 1994 (project acronym: SUBCORE). The primary challenge was (and remains) the initial emplacement of a planar diffusion flame between the initially segregated and quiescent reactants. A *convincing* demonstration entails planar-flame emplacement in *the actual experimental apparatus*. Time and resources expired before this goal was achieved; in fact, funding for the LeRC portion of the effort, sustained under the Space Station Utilization budget, was effectively terminated around December 1996. NASA Contractor Report 1999-208686 documents the appreciable progress achieved toward the goal during the nominal four-year period of performance that terminated on December 10, 1998.

Presently, a line igniter spark spawns a triple-flame propagation. Burning starts at one edge of the centerplane before burning begins at the opposite edge. Furthermore, the separator withdrawal induces a transient, recirculatory flow that enhances purely diffusive transport. Although these effects lead to initial transients, so that test initiation is not as ideal as with uniform ignition, we believe the transients can be minimized to meet the project challenge. However, means to achieve a more uniform ignition across the centerplane also warrants future exploration, because then a planar flame should form and persist, as has been demonstrated by numerical calculations.

OTHER EXPERIMENT MODIFICATIONS

In light of (extremely limited) microgravity-testing data, of approximate modeling, and of two-dimensional unsteady numerical simulations, we find that a significant amount of the hydrogen has reacted in 2 seconds for the scenario with contents initially at atmospheric pressure and temperature, effective equivalence ratio of 0.2, and 1 m/s separator-withdrawal speed. Accordingly, we have begun considering several modifications of the initially envisioned scenario of Figure 1.

One such modification addresses the fast depletion rate of hydrogen fuel. The temporal interval for data collection for a diffusively controlled phenomena is characterized by the ratio L^2/κ where L denotes the half height of the container and κ is a diffusion coefficient for species or heat. Clearly, both increasing the height of the apparatus L and decreasing the diffusion coefficient κ allow more diffusion-dominated testing time, for useful data collection prior to extinction. However, we are constrained by the requirement that planar symmetry persists only if the ratio $(\Delta\rho/\rho_{ref})gL^3/(\kappa\nu)$, where ρ denotes density, ν denotes kinematic viscosity, and g denotes the effective buoyant acceleration, is less than some critical value. The precise critical value, roughly 10^3, is rather uncertain for the scenario of Figure 1; the nominal choice L = 4.5 cm is conservative, and larger values may be accommodated. Alternatively, if we retain the current dimension for L but address circumstances involving a smaller value of the transport coefficient κ, we gain increased testing time, hopefully without disrupting the planarity. In more physical terms, exploring the hydrogen/oxygen diffusion flame affords an opportunity to examine

the consequences of differing diffusivities; selecting relatively rapidly diffusing hydrogen as the stoichiometrically deficient reactant results in a relatively brief testing interval (see below). However, examining a diluted-methane/diluted-oxygendiffusion flame, while affording a less pronounced opportunity to examine the consequences for combustion of differing diffusivities of the fuel and oxidizer species, does afford an opportunity to examine processes in a longer-duration test, including sooting. In this case, the highest-temperature soot furnishes an accessible indicator of flame position and temperature, whereas tracking a hydrogen/ oxygen diffusion flame may require an OH sensor.

In Figure 1 we consider fuel-deficient initial conditions, so the diffusion flame travels toward the end wall of the fuel-containing half-volume. This increases heat loss from the flame to the end wall, and the site of peak gas temperature in the container may not coincide with diffusion-flame position, at later times in a test. However, *testing with an initially stoichiometrically balanced presence of fuel and oxygen* allows the diffusion flame to hover near the centerplane $x = 0$, until reactant depletion (not heat loss) effects extinction. Then, the site of peak temperature continues to coincide closely with the flame position, and the burning persists longer. Though unrelated to the original objectives of SUBCORE, one can envision another experiment with a hydrocarbon fuel vapor in which soot might be subjected (deliberately) to various environments, promoting either surface growth or oxidation. In an initially-fuel-deficient scenario, relatively rapid oxidation would likely befall soot, owing to flame travel, while prolonged growth would occur in an initially excess-fuel scenario.

In Figure 1 we also consider effectively isothermal walls, so there is ready heat transfer from the gas contents. However, since the exothermicity derived from combustion of the contents of the container is $O(10\ kJ)$ or less, such heat transfer is deleterious to the persistence of vigorous burning. While achieving nearly perfectly adiabatic walls is not feasible (if it were, we could dispense with the large, 25 cm x 25 cm cross-section of the container), coating the walls to retard heat transfer significantly seems feasible. Furthermore, we suggest decreasing the initial pressure, which permits a faster speed of separator withdrawal for more uniform initiation, without increased risk of flow transition (since the Reynolds number is effectively proportional to the product of the pressure and the flow speed). We anticipate that a typical value of the pressure during much of a test might be 3-4 times the initial pressure. Hence, moderately decreasing the initial pressure to about one-quarter of an atmosphere neither incurs intrusion of atypical kinetics into a test of burning under nominally atmospheric conditions, nor compromises the vigor of the burn. In fact, adopting a reduced initial pressure would enhance the safety factor of the apparatus. Decreasing the initial pressure would also delay the onset of condensation at the walls of combustion-generated water vapor, just as raising the wall temperature rather modestly, to 330 K or 340 K.

We shall continue to pursue opportunities to demonstrate definitively the feasibility of the experiment.

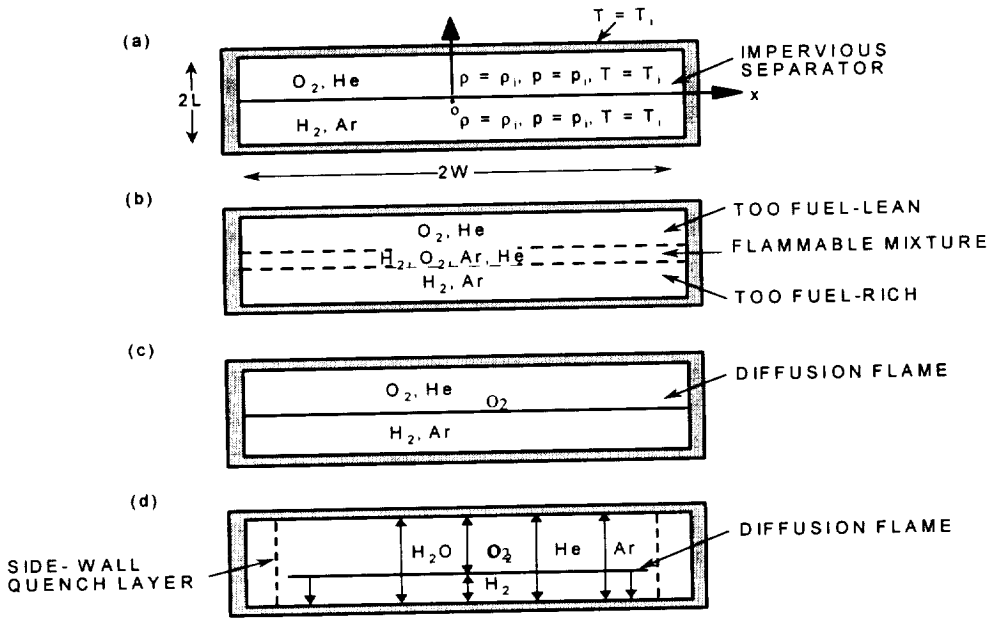

Figure 1. (a) Helium-diluted oxygen and argon-diluted hydrogen occupy half-volumes in a squat container. (b) Removal of the thin impervious separator initiates interpenetration of the reactants. (c) Ignition within the narrow layer of flammable mixture engenders a planar diffusion flame. (d) The planar diffusion flame travels into the half-volume of the deficient reactant (in early conception, the fuel), as the cold-wall-quench layers thicken in time.

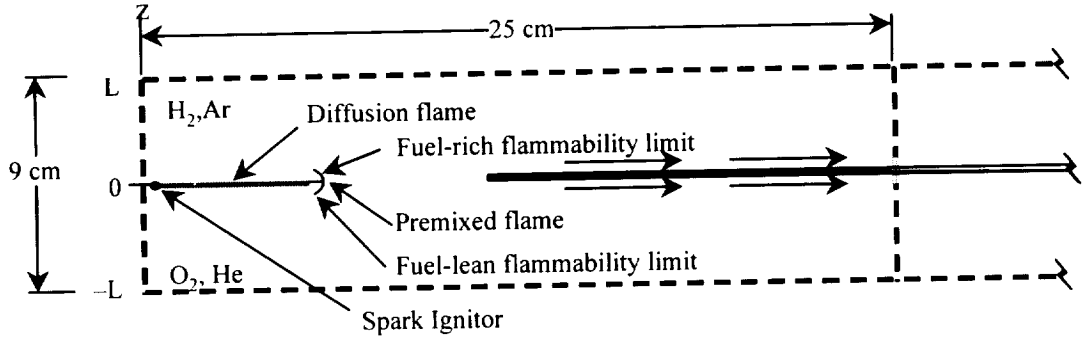

Figure 2. A triple flame propagates across the mid-height plane of the primary chamber, through the stratified mixture formed aft of the trailing edge of the separator. The diffusion flame engendered by the triple flame remains planar in microgravity. The separator is withdrawn from the primary chamber [by translation (at approximately uniform speed) in its own plane] through a tightly fitting slit in a sidewall.

CANDLE FLAMES IN MICROGRAVITY

D.L. Dietrich[1], H. D. Ross[1], J.S. T'ien[2], P. Chang[2], and Y. Shu[3]. [1]NASA Glenn Research Center, Cleveland, Ohio 44135 (Daniel.Dietrich@grc.nasa.gov), [2]Case Western Reserve University, [3]Cummins Diesel, Inc.

INTRODUCTION

This work is a study of a candle flame in a microgravity environment. The purpose of the work is to determine if a steady (or quasi-steady) flame can exist in a microgravity environment, study the characteristics of the steady flame, investigate the pre-extinction flame oscillations observed in a previous experiment in more detail, and finally, determine the nature of the interactions between two closely spaced candle flames. The candle flame in microgravity is used as a model of a non-propagating, steady-state, pure diffusion flame.

The present work is a continuation of two small-scale, space-based experiments on candle flames, one on the Shuttle and the other on the Mir OS[1]. The previous studies showed nearly steady dim blue flames with flame lifetimes as high as 45 minutes, and 1 Hz spontaneous flame oscillations prior to extinction. The present paper summarizes the results of the modeling efforts to date.

FLAME MODEL

The numerical model of the candle flame is two-dimensional and axisymmetric in the gas phase. While the model is relatively detailed in the gas phase by considering finite-rate chemistry and radiative loss, the detailed heat and mass transfer processes occurring in the porous wick are neglected. Specifically, we assume that the fuel evaporates from a small porous sphere with radius R, which is coated with a pure liquid fuel at its boiling temperature. This sphere is connected to an inert cone with a prescribed temperature distribution. The cone acts as a heat sink to simulate the flame quenching aspect of the candle wax. Fig. 1 shows the configuration of the sphere and cone.

The mathematical formulation utilizes a two-dimensional spherical coordinate system. The gas-phase model assumes: one-step, second-order overall Arrhenius reaction, constant specific heats and thermal conductivity, constant Lewis number for each species (although different species can have different constant Lewis numbers), ideal gas behavior and no buoyant force. Flame radiative losses from CO_2 and H_2O are accounted for by a gray gas treatment. The details of the formulation and results can be found in refs. 1-3.

COMPUTED RESULTS

The model predicts that the candle flame will reach steady state in an infinite ambient. The inner portion of the flame reaches steady state quickly, but the outer portion takes relatively much longer to reach steady state[4]. The time to reach steady state roughly scales with the diffusion time estimates (r^2/α or r^2/D), where r is the radial distance, and α and D are the thermal and mass diffusion coefficients of the gas, respectively. The gas phase at r = 5 mm (approximate flame location) reaches steady state in several seconds, but the far-field temperature and oxygen profiles can take tens of seconds to reach convergence. These results imply that it is possible to observe the approximate shape and dimension in short-duration microgravity tests for flames away from the extinction limit. It is not possible, however, to determine the extinction limit in short-duration microgravity tests, because the flame near extinction is sensitive to the changes in the outer part of the flame. Fig. 1 shows the contours of the fuel vapor reaction rate ($w_F = 0.2(10^{-3})$ g/cm^{3}s for a 0.6 mm radius sphere in varying oxygen ambients. The contours resemble the visible flames in the experiment except for a slight inward hook at the bottom. Decreasing the oxygen concentration

raises the flame base relative to the porous sphere, but does not substantially change the position of the flame top.

Decreasing the ambient oxygen concentration eventually leads to flame extinction. The model predicts that the limiting oxygen percentage depends on the diameter of the porous sphere and the rate of radiative loss (Fig. 2). Radiative losses shrink the flammable domain. The extinction boundary with radiation flattens out at large sphere diameters. We believe, based on related droplet studies[5], that this extinction boundary will curve up to form the so-called radiative quenching branch as the porous sphere diameter increases further, while the boundary without radiation decreases monotonically with increasing sphere size.

In the computation, the Lewis numbers for oxygen and fuel are 1.11 and 2.5, respectively. Because of the uncertainty regarding the appropriate value of the fuel Lewis number, we performed a parametric study where Le_F varied from 1.5 to 5. The bulk flame characteristics are rather insensitive to this variation in the fuel Lewis number. The fuel Lewis number appears in both the fuel diffusion equation and the boundary condition on the fuel surface. The effects of these two contributions tend to cancel each other with very little net effect on the flame. The flame, however, is very sensitive to changes in the oxygen Lewis number (but we are reasonably sure of its value). Fig. 3 shows the flammability map for a 0.6 mm radius sphere as a function of ambient oxygen mole fraction and Lewis number.

The numerical model also predicts the near-limit flame oscillation. The computation starts with a steady flame in a $Y_{0e} = 0.22$ ambient. If we lower the ambient oxygen by a very small amount (e.g., to $Y_{0e}= 21.875\%$), spontaneous flame oscillations will occur with a frequency around 0.63 Hz (see Fig. 4). This frequency scales with r_f^2 / D_F where r_f is the flame diameter and D_F is the diffusion coefficient of fuel vapor. The oscillation, once started, always increases in amplitude until flame extinction occurs. The rate of growth of oscillation depends on the magnitude or the rate of the ambient oxygen decrease. If this magnitude is small, the amplification rate is small, but more oscillatory cycles occur before extinction. Too large a decrease may result in flame extinction without oscillations. The dependence of the number of oscillation cycles on the rate (or the magnitude) of ambient oxygen decrease appears to be compatible with the results of the space experiments. In the Shuttle experiment, we had a smaller candle box with less open area, which accelerated the oxygen depletion rate. In these tests, typically only 5 to 6 cycles of near-limit oscillations were observed. In the *Mir* experiment, a larger and more open candle box resulted in as many a 90 cycles before extinction.

The oscillation results of the numerical model are consistent with existing one-dimensional near-limit flame stability models[6,7]. Both increasing heat loss and Lewis number (assumed to be the same for fuel and oxidizer) promoted flame instability in these models. The limited numerical experiments performed in this study are consistent with these trends. For example, in the basic case we studied here (R = 0.6 mm), when radiative loss is neglected, flame oscillation was not found. On the other hand, the oscillation in the candle flame was truly two-dimensional with a complex phase lag from point to point and between one physical variable and another. Among the three variables (T, Y_F, Y_O), the fuel vapor diffusion appears to control the oscillation frequency. Fig. 4 illustrates the oscillation of Y_F at five locations with the same angular position, but at different radial distances from the porous sphere. The phase angles between them illustrate the importance of fuel diffusion time. This is in contrast to the oxygen oscillations at the same points, which are almost in phase.

MODEL WITH REALISTIC WICK GEOMETRY

We have recently initiated a numerical analysis using a more realistic wick and candle shape as shown in Fig. 5. In this particular case, the wick length is 3.6 mm and diameter is 1.2 mm. Again, the liquid fuel coats the wick and the candle is inert. This new configuration is solved with a body-fitted coordinate using the associated transformed equations. Fig. 5 is the computed fuel vapor reaction rate contours. It compares reasonably well with the flame shape in Fig. 1. It appears that when the wick is short (compared with the flame diameter), the porous sphere/inert cone model is able to capture many of the essential features of the candle flames. The new formulation, however, will enable us to study flames with longer wicks and is a more realistic geometry when the condensed phase heat and mass transfer is added.

REFERENCES:

1. Dietrich,D.L., Ross, H.D., Shu, Y. and T'ien, J.S.: Candle Flames in Non-Buoyant Atmospheres, submitted.
2. Shu, Y.: M.S. Thesis, Case Western Reserve University (1998)
3. Shu,Y., T'ien, J., Dietrich, D. and Ross, H.: Modeling of Candle Flame and Near-Extinction Oscillation in Microgravity, First Asian-Pacific Conference in Microgravity Sciences, Wasada, Japan, May,1998. Proceedings, to appear.
4. King, M.K.: *Twenty-Sixth Sym. (Int.) on Combust.* p.1227 (1996).
5. Chao,B.H., Law, C.K., and T'ien, J.S.: *Twenty-third Sym. (Int.) on Combust.*, p.523 (1990).
6. Kirby, L.L. and Schmitz, R.A.: *Combust. And Flame*, 10, p.205 (1966).
7. Cheatham, S. and Matalon, M.: *Twenty-Sixth Sym.(Int.) on Combust.*,p.1063 (1996).

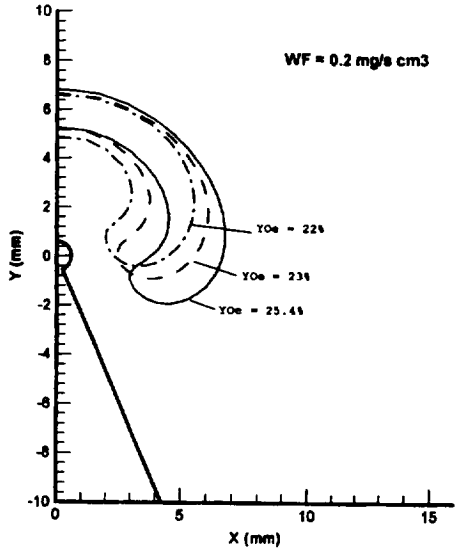

Fig. 1. The effect of ambient oxygen mole fraction on the flame shape.

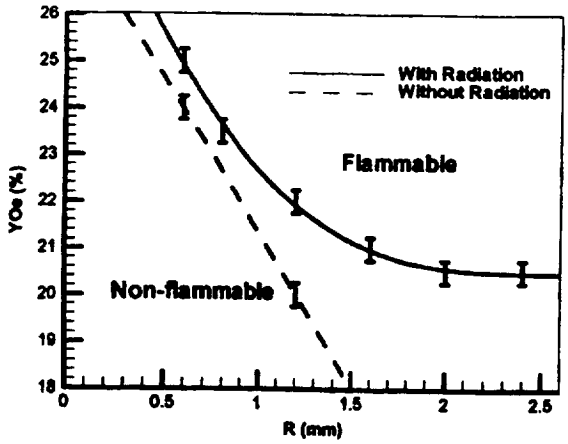

Fig. 2. Extinction boundary as a function of ambient oxygen concentration and sphere size.

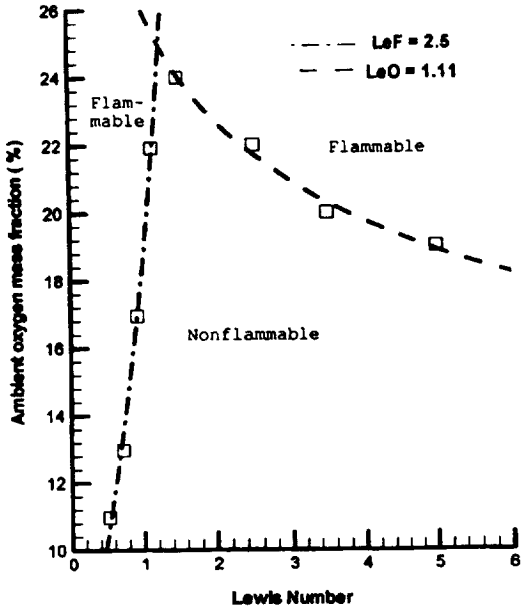

Fig. 3 Flammability map as a function of ambient oxygen mole fraction and Lewis number (fuel and oxygen).

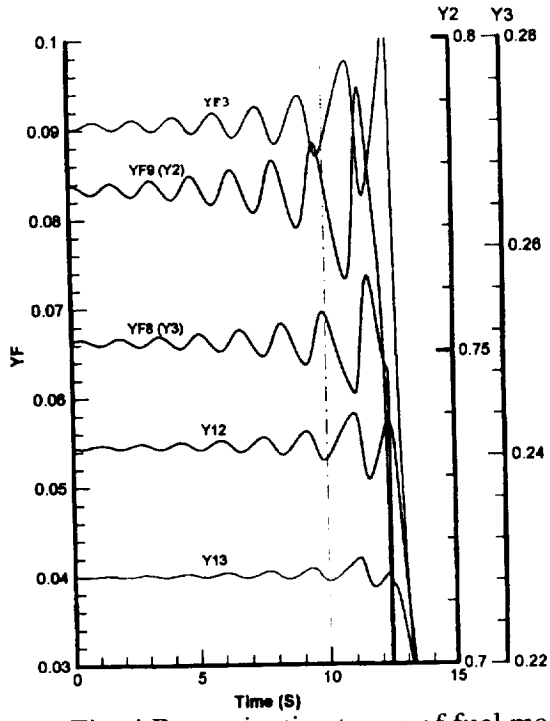

Fig. 4 Pre-extinction traces of fuel mass fraction at five radial points: θ =80° (from centerline). Sphere surface(pt. 9), and 2.6 mm(pt. 8), 5.2 mm (pt. 3),7.9 mm (pt. 12), and 9.2 mm (pt. 13) from the center.

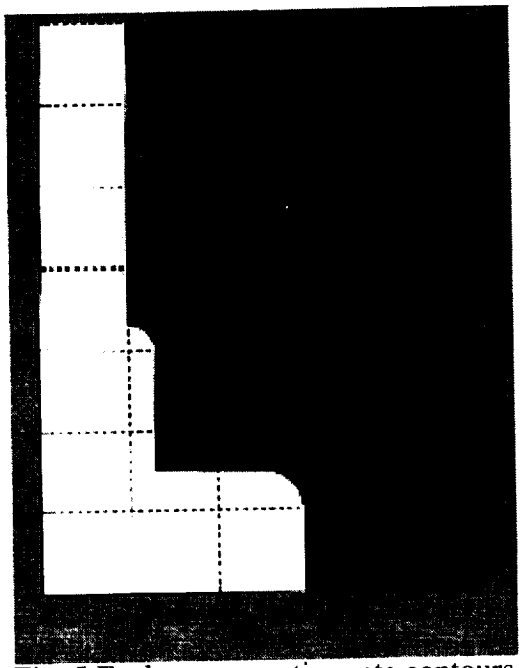

Fig. 5 Fuel vapor reaction rate contours (in unit: mg/s cm^3) for a candle with realistic wick shape. Y_{Oe} = 0.254.

HYDRODYNAMICS OF SPHERICAL FLOWS AND GEOMETRY OF PREMIXED FLAMES NEAR THE STAGNATION POINT OF AXISYMMETRIC VISCOUS COUNTERFLOWS

320-25

SIAVASH H. SOHRAB
Robert R. McCormick School of Engineering and Applied Science
Department of Mechanical Engineering
Northwestern University, Evanston, Illinois 60208

INTRODUCTION

Counterflow premixed flames play a significant role in the modeling of laminar flames [1-9]. This is in part motivated by the fact that stretched premixed flames simulate local flamelet dynamics within turbulent premixed flames [1, 10]. In the present study, the modified form of the Navier-Stokes equation for reactive fields introduced earlier [11] is employed to investigate the hydrodynamic of spherical flows embedded within counterflows. The geometry of premixed flames near the stagnation point is also determined. The predictions are in favorable agreement with the experimental observations and prior numerical studies.

HYDRODYNAMICS OF SPHERICAL FLOWS NEAR WITHIN COUNTERFLOWS

The symmetric forms of the conservation equations for energy, species concentrations and momentum are expressed as [11]

$$\frac{\partial \theta}{\partial t} + \mathbf{w}_c \cdot \nabla \theta = \alpha_m \nabla^2 \theta + \Lambda\, y\, e^{\beta(\theta - 1)} \tag{1}$$

$$\frac{\partial y}{\partial t} + \mathbf{w}_c \cdot \nabla y = D_m \nabla^2 y - \Lambda\, y\, e^{\beta(\theta - 1)} \tag{2}$$

$$\frac{\partial \mathbf{v}_c}{\partial t} + \mathbf{w}_c \cdot \nabla \mathbf{v}_c = \nu_m \nabla^2 \mathbf{v}_c - \mathbf{v}_c \Lambda\, y\, e^{\beta(\theta - 1)} \tag{3}$$

The hydrodynamics will be described by the *modified Navier-Stokes equations for reactive flows* given in Eq.(3) containing a reaction term [11]. In the conservation equations (1)-(3), the convective velocity $\mathbf{w}_c$ which is different from the local fluid velocity $\mathbf{v}_c$, to be further discussed in the following, and hence Eq.(3) is linear in $\mathbf{v}_c$. The dimensionless temperature, mass fraction, Damköhler number Λ are defined as

$$\theta = (T - T_u)/(T_b - T_u) \quad , \quad y = Y_F/Y_{Fu} \quad , \quad \Lambda \equiv (\nu_F W_F B/\Gamma)\, e^{-\beta/\chi} \tag{4}$$

Also, the dimensionless coordinates, time, and velocity are

$$z = z'/(\alpha/\Gamma)^{1/2} \quad , \quad r = r'/(\alpha/\Gamma)^{1/2} \quad , \quad t = t'\Gamma \quad , \quad \mathbf{w} = \mathbf{w}'/(\alpha\Gamma)^{1/2} \quad , \quad \mathbf{v} = \mathbf{v}'/(\alpha\Gamma)^{1/2} \tag{5}$$

where Γ is the rate of strain in the counterflow. The adiabatic flame temperature T_b, the Zeldovich number β, and the coefficient of thermal expansion χ are

$$T_b = T_u + (QY_{Fu}/\rho\nu_F W_F c_p), \quad \beta = E(T_b - T_u)/RT_b^2, \quad \chi = (T_b - T_u)/T_b \tag{6}$$

For ultra-simplified model of ideal gas, the diffusivities of heat, mass, and momentum are equal $\alpha_m = D_m = \nu_m$, such that θ, y, and $\mathbf{v}_c$ fields will become similar under identical boundary conditions and in the absence of reactions. The hydro-thermo-diffusive structure of counterflow premixed flames governed by Eqs.(1-3) has been discussed in a recent investigation [9].

According to the scale-invariant model of statistical mechanics [11], each statistical field is described by three distinguishable velocities respectively called the convective or system velocity **w**, the elemental velocity **v**, and the atomic velocity **u**. For example, at laminar cluster-dynamic LCD scale, the convective velocity is $\mathbf{w}_c = \mathbf{v}_e = \langle \mathbf{u}_e \rangle = \langle \mathbf{v}_c \rangle$ that is the mass-average of the mean cluster velocity. The element velocity is $\mathbf{v}_c = \mathbf{w}_m = \langle \mathbf{u}_c \rangle = \langle \mathbf{v}_m \rangle$ that is the mean cluster velocity. Finally, the atomic velocity is the velocity of individual clusters $\mathbf{u}_c = \mathbf{v}_m = \langle \mathbf{u}_m \rangle$, that is same as the mean molecular velocity $\mathbf{v}_m$. The convective velocity w is not *locally-defined*, since its value at any position depends on the value of $\mathbf{v}_c$ at other locations remote from this position. Since w is not locally-defined, it cannot occur in the *differential form within the equations* (1)-(3). This is because one cannot differentiate a function that is not locally, i.e. differentially, defined.

In view of the above discussions, at any given scale (n), the convective velocity must be determined from the solution of equation of motion at the next larger scale (n+1). For example, for the treatment of *cluster-dynamic* field described by Eq.(3), the convective velocity $\mathbf{w}_c = \mathbf{v}_e$ must be obtained from the solution of the momentum conservation equation at *laminar eddy-dynamic* LED scale given as [11]

Fifth International Microgravity Combustion Workshop, May 18-20, 1999, Cleveland , Ohio.

$$\frac{\partial \mathbf{v}_e}{\partial t} + \mathbf{w}_e \cdot \nabla \mathbf{v}_e = \nu_c \nabla^2 \mathbf{v}_e - \nu_c \Omega_e \qquad (7)$$

Now, the velocities ($\mathbf{w}_e = \langle \mathbf{v}_e \rangle, \mathbf{v}_e = \langle \mathbf{v}_c \rangle$) are receptively the convective and the local velocity at LED scale. We will not be concerned with the *reaction* (dissipation) term Ω_e in Eq.(7). One notes however, that in order to solve Eq.(7) for the local velocity $\mathbf{v}_e$, one requires the knowledge of yet another velocity $\mathbf{w}_e$, which is unknown. This unending chain continues to larger scales and constitutes the *closure problem* of the statistical theory of turbulence introduced earlier [11].

In order to achieve closure, we shall assume that the convective velocity at the scale of laminar fluid-element dynamics LFD is given as $\mathbf{w}'_e = \mathbf{v}'_f = \langle \mathbf{v}'_e \rangle = -2\,\Gamma_e \mathbf{z}'$, where Γ_e is the counterflow velocity gradient. Near the stagnation point (at the LFD scale), Eq.(7) under steady condition and in the absence of "reactions" $\Omega_e = 0$, simplifies to the one-dimensional form

$$2z_e \frac{d\mathbf{v}_e}{dz_e} + \frac{d^2\mathbf{v}_e}{dz_e^2} = 0 \quad , \quad z_e \equiv z'/(\nu_c/\Gamma_e)^{1/2} \quad , \quad \nu_c = \mu_c/\rho_c = \lambda_c \mathbf{v}_c/3 \qquad (8)$$

subject to the boundary conditions for symmetric counterflow $(\mathbf{v}'_e)_{-\infty} = -(\mathbf{v}'_e)_{\infty} = (\nu_c \Gamma_e)^{1/2}$

$$z_e \to \infty \qquad \mathbf{v}_e = \mathbf{v}'_e/\mathbf{v}'_{e\infty} = -1 \qquad (9a)$$

$$z_e \to -\infty \qquad \mathbf{v}_e = \mathbf{v}'_e/\mathbf{v}'_{e\infty} = 1 \qquad (9b)$$

with the solution

$$\mathbf{v}_e = \mathbf{w}_c = -\operatorname{erf} z_e \qquad (10)$$

that is schematically shown in Fig.1. If one now expands the solution (10) in the neighborhood of the stagnation plane $z_e \approx 0$ (but now at the LED scale), one obtains the linear velocity profile

$$\mathbf{v}_e = \mathbf{w}_c = \mathbf{w}'_c/\sqrt{\Gamma_e \nu_c} \approx -(2/\sqrt{\pi})\, z_e = -2\sqrt{\Gamma_e/(\pi \nu_c)}\, \mathbf{z}' \qquad (11)$$

that simplifies to

$$\mathbf{w}'_c = -2\Gamma_c \mathbf{z}' \quad \text{or} \quad \mathbf{w}_c = -2\mathbf{z}_c \quad z_c = z'/(\nu_m/\Gamma_c)^{1/2} \quad \nu_m = \mu_m/\rho_m = \lambda_m \mathbf{v}_m/3 \qquad (12)$$

and $\Gamma_c \equiv \Gamma_e/\sqrt{\pi}$. Thus, the expression for $\mathbf{w}'_c = -2\Gamma_c \mathbf{z}'$ assumes the same form as that for $\mathbf{w}'_e = -2\Gamma_e \mathbf{z}'$ discussed above. Hence, a *fractal* type of solution is encountered such that as one approaches the origin, one obtains a cascade of self-similar boundary layer solutions that are embedded within each other at increasingly smaller scales. As shown in Fig.1, the inner error-function solution within the boundary layer results in *displacement* of the outer error-function solution. This behavior has in fact been established by exact numerical solution of the viscous equations for finite-jet counterflows. The desired components of the *convective velocity* at LCD scale ($\mathbf{w}'_{cz}$, $\mathbf{w}'_{cr}$) that satisfy the continuity equation are given by

$$\mathbf{w}'_{cz} = -2\Gamma_c \mathbf{z}' \quad , \quad \mathbf{w}'_{cr} = \Gamma_c \mathbf{r}' \qquad (13)$$

where r' is the radial coordinate.

The classical solution of Hill describes the spherical flow produced by a single toroidal vortex in a droplet that is situated in a uniform flow [12]. Following the classical solution of Hill, a stream function was recently *postulated* to describe spherical flows produced by two toroidal vortices generated in a droplet that is located at the stagnation-point of a symmetric counterflow [13, 14]

$$\Psi = -r^2 z\,(1 - r^2 - z^2) \qquad (14)$$

, $\Psi = \Psi'/(\nu_m^3/\Gamma_c)^{1/2}$, that results in the streamlines shown in Fig.2. It was also shown that the above stream function can lead into a cascade of concentric spherical flows schematically shown in Fig.3. The components of the axial and the radial velocity are

$$v_z = -2z\,(1 - 2r^2 - z^2) \quad , \quad v_r = r\,(1 - r^2 - 3z^2) \qquad (15)$$

that result in the azimuthal component of dimensionless vorticity $\omega_\theta = \omega'_\theta/\Gamma_c$ given by

$$\omega_\theta = -14\, r\, z \qquad (16)$$

It is now shown that the *postulated* stream function in (14) that leads to the vorticity (16) is in fact a steady solution of the viscous vorticity equation deduced from the modified Navier-Stokes equation (3) in the absence of reactions. The modified Helmholtz vorticity equation corresponding to the modified Navier-Stokes equation is given as

$$\frac{\partial \omega_\theta}{\partial t} + \mathbf{w}_c \cdot \nabla \omega_\theta = \nu_m \nabla^2 \omega_\theta - \frac{\omega_\theta w_{cr}}{r} - \omega_\theta \Omega_e \qquad (17)$$

One notes that vorticity relates to the curl of the local velocity $\omega'_c = \nabla \times \mathbf{v}'_c$ and not that of the convective velocity $\mathbf{w}'_c$. For the convective velocity field, we consider the *inverse counterflow*

$$\mathbf{w}_{cz} = 2\mathbf{z} \quad , \quad \mathbf{w}_{cr} = -\mathbf{r} \qquad (18)$$

where the signs of velocities are just the opposite of those of the conventional counterflow given in Eq.(13). In inverse counterflows, the fluid flows radially inward, along the equatorial accretion disc, and is ejected axially as two axisymmetric polar jets (Fig.2). It is noted that the sign of the vortex-stretching term in Eq.(17) is opposite of that of the classical Helmholtz vorticity equation [12]. The reason for this is that the convective velocity w appearing in Eq.(17) has the opposite sign from that of the local velocity v appearing

in the classical Helmholtz vorticity equation. Therefore, while the radially-outward local flow v_r would tend to stretch the vortex, the radially-inward convective velocity $w_r = -r$ will tend to compress the vortex. Thus, radial diffusion of vorticity is prevented by the radially-inward convection, leading to a stable double-vortex spherical flow shown in Fig.2 .

For a steady problem, and in the absence of "reactions" $\Omega_e = 0$, Eq.(17) simplifies to

$$w_{cr}\frac{\partial \omega_\theta}{\partial r} + w_{cz}\frac{\partial \omega_\theta}{\partial z} = \nu_m\left[\frac{\partial^2 \omega_\theta}{\partial r^2} + \frac{\partial}{\partial r}\left(\frac{\omega_\theta}{r}\right) + \frac{\partial^2 \omega_\theta}{\partial z^2}\right] - \frac{\omega_\theta w_{cr}}{r} \qquad (19)$$

It is easy to verify that ω_θ in (16) with the velocity **w** in (18) indeed satisfies the modified viscous vorticity equation (19). In the vicinity of the stagnation point $r = z \approx 0$ (now at the scale of LCD), the velocity components (15) simplify as

$$v_z \approx -2z \qquad \text{near } r = z \approx 0 \qquad (20a)$$

$$v_r \approx r \qquad \text{near } r = z \approx 0 \qquad (20b)$$

that can be directly compared with the outer convective velocity **w** in (18). It is now clear that the convective velocity **w** in (18) may be considered as the local velocity near $r = z \approx 0$ (but at LED scale) deduced from the linearization of the velocity field of the next larger concentric spherical flow (see Fig.3) given as

$$w_{cz} = 2z(1 - 2r^2 - z^2) \qquad (21a)$$

$$w_{cr} = -r(1 - r^2 - 3z^2) \qquad (21b)$$

It is important to point out that the original outer spherical flow (21) is rotational with the azimuthal component of vorticity

$$\Omega_\theta = \nabla \times \mathbf{w}_c = 14\, r\, z = -\omega_\theta \qquad (22)$$

that has opposite sign of the vorticity within the inner sphere given in (16). However, when the outer flow in (21) is linearized near the stagnation point to obtain the local counterflow given by (18), one loses the flow vorticity in (22). In other words, the counterflow velocity field in (18) is irrotational, while the spherical flow in (21) is rotational. The stream function (14) is of fundamental significance since it allows an island of flow with vorticity ω_θ to exist within the large-scale counterflow which itself is vorticity free.

PREMIXED FLAME GEOMETRY NEAR THE STAGNATION-POINT OF A COUNTERFLOW

Given the convective counterflow velocity (13), the geometry of premixed flames stabilized in the vicinity of the stagnation-point can be determined from the solution of the equation governing the flame-front geometry [15]

$$\frac{\partial G}{\partial t} + \mathbf{w}_c \cdot \nabla G = v_f |\nabla G| \qquad (23)$$

The flame surface G(r, z, t) is expressed as

$$G = r - g(z, t) \qquad (24)$$

where $G = G'/(\alpha/\Gamma)^{1/2}$, $g = g'/(\alpha/\Gamma)^{1/2}$, and $v_f = v'_f/(\alpha\Gamma)^{1/2}$, where v'_f is the laminar flame propagation velocity. The unit vector normal to the flame surface and the convective velocity are

$$\mathbf{n} = \nabla G/|\nabla G| = (\hat{\mathbf{r}} - g_z\hat{\mathbf{z}})/\sqrt{(1 + g_z^2)} \qquad \text{and} \qquad \mathbf{w} = r\,\hat{\mathbf{r}} - 2z\,\hat{\mathbf{z}} \qquad (25)$$

For steady flame configurations, by substitutions from (25) in (23), one obtains

$$g_z^2(4z^2 - v_f^2) + 4rz\,g_z + r^2 - v_f^2 = 0 \qquad (26)$$

The above equation can be integrated directly, and the results when substituted in Eq.(24) gives the steady flame surface

$$G(r, z) = r + \frac{r}{4}\ln[4z^2 - B^2] + \frac{B}{\sqrt{4(x^2 - B^2)}}\,\text{Arctg}\left[\frac{4z}{\sqrt{4(x^2 - B^2)}}\right]$$

$$- \frac{r}{4}\ln\left[\frac{\sqrt{(x^2(1 - 2Bt' + x^2t'^2} + x^2t' + B}{\sqrt{(x^2(1 + 2Bt'' + x^2t''^2} + x^2t'' - B}\right] \qquad (27)$$

containing three parameters defined as

$$t' = 1/(2z - B) \quad , \quad t'' = 1/(2z + B) \quad , \quad B = v'_f/(\alpha\Gamma)1/2 \qquad (28)$$

The level surfaces of the above function with $v'_f = 2$ cm^2/s, $\Gamma = 200$ s^{-1}, and $\alpha = 1$ cm^2/s are shown in Fig.4. The calculated flame geometry agree with the observations of near extinction flames [7] and are in accordance with prior studies based on exact numerical solutions [16, 17]. The small flow recirculation zone near the stagnation point (Fig.4) is associated with the embedded local spherical flows discussed above. The influences of the three important parameters, namely v'_f, Γ, and ν require further examination.

ACKNOWLEDGMENT

This research is supported by NASA microgravity science program under grant NAG3-1863.

REFERENCES

1. Williams, F. A., *Combustion Theory*, 2nd Ed., Addison-Wesley, 1985, New York.
2. Buckmaster, J. D., and Ludford, G. S. S. *Theory of Laminar Flames*, Cambridge University Press, 1982, Cambridge.
3. Warnatz, J., Maas, U., and Dibble, R. W., *Combustion*, Springer, 1996, Berlin.
4. Liñán, A., *Acta Astronautica* 1:1007 (1974).
5. Daneshyar, H., Mendes-Lopes, J. M. C., and Ludford, G. S. S., *Nineteenth Symposium (International) on Combustion*, The Combustion Institute, Pittsburgh, 1983, p.413.
6. Tsuji, H., and Yamaoka, I., *Nineteenth Symposium (International) on Combustion*, The Combustion Institute, Pittsburgh, 1982, p.1533.
7. Ishizuka, S., and Law, C. K., *Nineteenth Symposium (International) on Combustion*, The Combustion Institute, Pittsburgh, 1982, p.327.
8. Sato, , J., *Nineteenth Symposium (International) on Combustion*, The Combustion Institute, Pittsburgh, 1982, p.1541.
9. Kurz, O., and Sohrab, S. H., Modified hydro-thermo-diffusive theory of laminar counterflow premixed flames. *Joint Western/Eastern States Section Meeting*, The Combustion Institute, Washington DC, March 15-17, 1999.
10. Peters, N., *Twenty First Symposium (International) on Combustion*, The Combustion Institute, Pittsburgh, 1986, p.1231.
11. Sohrab, S. H., Transport phenomena and conservation equations in multi-component chemically-reactive ideal gas mixtures. *ASME Proceedings of the 31 National Heat Transfer Conference*, HTD vol. 328, pp.37-60 (1996).
12. Panton, R. L., *Incompressible Flow* , Wiley, 1995, New York.
13. Pearlman, G. H. and Sohrab, S. H., Diffusion flame extinction and viscous hydrodynamics around rotating porous spheres with surface blowing. *Combust. Flame* 108:419-441 (1997).
14. Sohrab, S. H., Reactive hydrodynamics in rotating spherical and cylindrical geometry. *Fourth International Microgravity Workshop, May* 19- 21, 1997, Cleveland , Ohio.
15. Williams, F. A., Turbulent Combustion, in *The Mathematics of Combustion*, J. D. Buckmaster (Ed.), 1985, SIAM, Philadelphia.
16. Sheu, W. J., and Sivashinsky, G. I., Nonplanar flame configurations in stagnation point flow. *Combust. Flame* 84:221-224 (1991).
17. Brewster, M. E., Stationary premixed flames in a dual-source system. *Combust. Flame* 91:99-105 (1992).

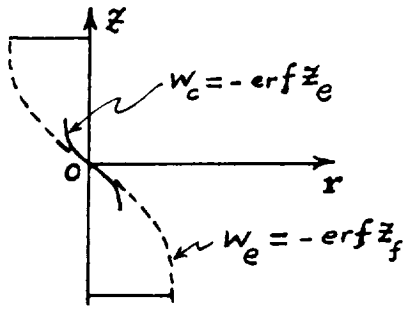

Fig.1 Counterflow velocity field with boundary layer.

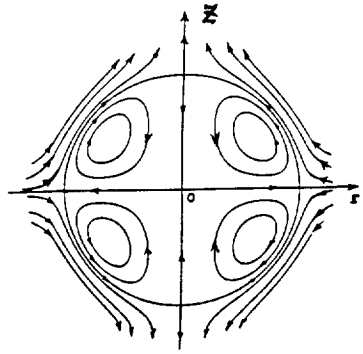

Fig.2 Spherical flow within an inverse counterflow.

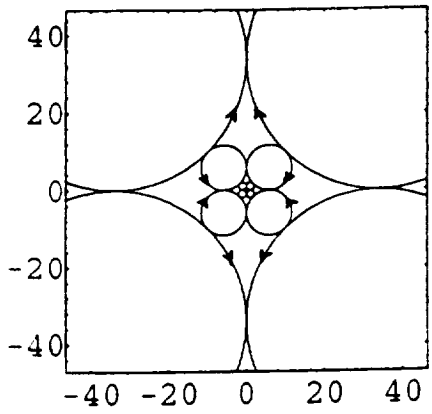

Fig.3 Cascade of concentric spherical flows.

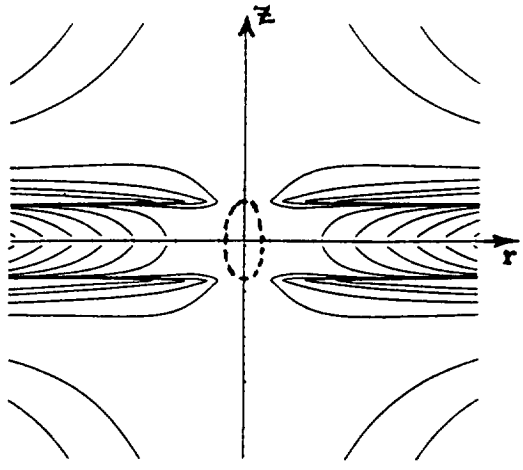

Fig.4 Premixed flame-geometry from Eq.(27).

S.21-25

EXPERIMENTAL OBSERVATIONS ON A LOW STRAIN COUNTER-FLOW DIFFUSION FLAME: FLOW AND BUOYANCY EFFECTS

J. A. Sutula[1], J. L. Torero[1] and O. A. Ezekoye[2], [1]Department of Fire Protection Engineering, University of Maryland, College Park, MD 20742-3031, jltorero@eng.umd.edu, [2]Department of Mechanical Engineering, University of Texas at Austin, Austin, TX 78712, dezekoye@mail.utexas.edu.

INTRODUCTION

Diffusion flames are of great interest in fire safety and many industrial processes. The counter-flow configuration provides a constant strain flow, and therefore is ideal to study the structure of diffusion flames. Most studies have concentrated on the high velocity, high strain limit, since buoyantly induced instabilities will disintegrate the planar flame as the velocity decreases [1,2]. Only recently, experimental studies in micro-gravity conditions have begun to explore the low strain regimes [3,4]. Numerical work has shown the coupling between gas phase reaction rates, soot reaction rates, and radiation [5,6]. For these programs, size, geometry and experimental conditions have been chosen to keep the flame unaffected by the physical boundaries. When the physical boundaries can not be considered infinitely far from the reaction zone discrepancies arise [4]. A computational study that includes boundary effects and accounts for the deviations occurring when the major potential flow assumptions are relaxed was presented by Borlik et al [7]. This development properly incorporates all heat loss terms and shows the possibility of extinction in the low strain regime.

A major constraint of studying the low strain regime is buoyancy. Buoyant instabilities have been shown to have a significant effect on the nature of reactants and heat transport, and can introduce instabilities on the flow that result in phenomena such as flickering or fingering. The counter-flow configuration has been shown to provide a flame with no symmetry disrupting instabilities for inlet velocities greater than 50 mm/s [3]. As the velocity approaches this limit, the characteristic length of the experiment has to be reduced to a few millimetres so as to keep the Rayleigh number ($Ra_L = (\beta g_o L^3 \Delta T)/(\alpha \nu)$) below 2000 [8].

In this work, a rectangular counter-flow burner was used to study a two-dimensional counter-flow diffusion flame. Flow visualisation and Particle Image Velocimetry served to describe the nature of the stagnation plane for strain rates smaller than 100 (1/s). These experiments were conducted with a non-reacting flow. Video images of a propane air diffusion flame were used to describe the behaviour of a diffusion flame in this regime. Flame geometry and pulsation frequency are described.

EXPERIMENT SETUP

The experimental study was conducted using two opposing porous burners. Through these burners, either fuel or oxidizer can be introduced. Each burner consists of a rectangular central chamber, rectangular external chamber, and rectangular honeycomb outlet face. The external chamber has dimensions of 12 cm by 9cm by 6 cm. The internal chamber has dimensions of 10 cm by 3 cm by 3 cm. When assembled, the central chamber is completely surrounded by the external chamber. The central chamber is used as the fuel or oxidizer inlet, while the external chamber is used to surround the fuel or oxidizer with a concurrent flow of an inert gas (i.e. Nitrogen). The rectangular honeycomb outlet face acts as a flow rectifier by creating a pressure drop as gases exit.

Four mass flow controllers were used to regulate gas flow to the burner system. Two mass flow controllers were set to regulate the flow of fuel and oxidizer, and two mass flow controllers were set to regulate the flow of Nitrogen gas. These mass flow meters were controlled through a computer-based analog control system composed of Labtech control software, used in conjunction with a CIO-DAC08 analog computer interface board by Omega.

A 0.5 watt red diode laser (670-690 nm) was used with the appropriate optics to create a laser light sheet. This laser light sheet was used to visually observe the flow characteristics of the burner system. A monochrome digital camera (COHU, INC.) with a narrow band filter (675 nm to 685 nm) was used to capture frame by frame images of smoke flow as well as seeding particle. Using a digital image processing software package by EPIX, XCAP, the camera was setup to capture images directly, and store them saved to a computer hard drive. The camera is able to capture up to 60 images in one second. The usage of all hardware will be discussed in the next section.

NON-REACTING FLOW

Commercial incense together with the Laser sheet was used to visualize the flow. Incense was only introduced through one burner at a time, and only through the inner flow. The co-flow remained unseeded. Tests were conducted seeding both burners independently and the images superposed. The digital camera was used to capture 75 monochrome gray scale images over a duration of 1.25 seconds. The saved digitized images were processed using XCAP image processing software. At each strain rate, 150 digital images were captured. Seventy-five images were captured when the top flow was seeded and 75 images were captured when the bottom flow was seeded. Each individual pixel of each individual image was then assigned a value of 1 or 0, depending on whether or not the image's pixel was above or below a certain monochrome threshold. In gray scale monochrome, a threshold of 0 refers to the color black, and a threshold of 255 refers to the color white. All other threshold values are various degrees of gray. The critical threshold for the smoke image processing was chosen to be 125. Any pixels with a value below this threshold was set to black (0). Any pixels with a value above this threshold was set to white (255). Once each individual picture has been adjusted to the appropriate threshold, the 75 images of the bottom flow are averaged together to one average image. Similarly, the 75 images for the top flow are averaged together. These final two images are then laid upon each other resulting in a measurable overlap that can be related to the strain at which the images are processed.

(a) (b)

Figure 1- Processed video images. Each figure corresponds to two averaged images (top seeded and bottom seeded) superposed. (a) Strain rate, a=2.8 s^{-1}. (b) Strain rate, a=7.0 s^{-1}.

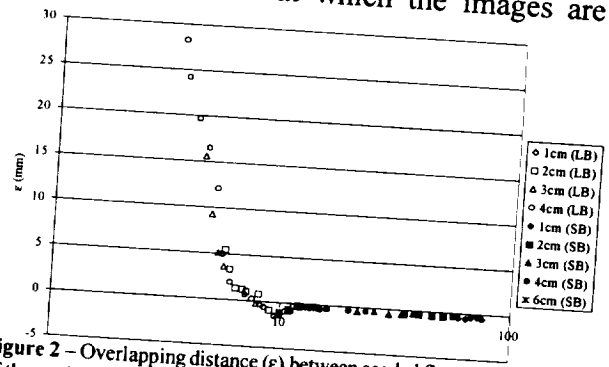

Figure 2 – Overlapping distance (ε) between seeded flows as a function of the strain (a).

Two examples of these images are presented in Figure 1. Figure 1(a) corresponds to a strain rate of a= 2.8 (s^{-1}) and Figure 1(b) for a= 7 (s^{-1}). It can be noticed that in Figure 1(a) the two images when superposed overlapped (white region), the overlapping distance is labeled ε. In

contrast Figure 1(b) shows that the zone labeled ε corresponds to an area towards which seeding particles are not transported (black region). Tests were then conducted at burner separations of 1-4 centimeters for characteristic velocities, U, less than 38 cm/s. Figure 2 shows the value of ε for different strain rates corresponding to these tests. It can be seen that for low strain rates the incense particles are convected into the opposing flow leading to overlapping seeded zones (ε>0). As the strain rate is increased, the size of this zone decreases until ε=0 at a=4 s^{-1}. For higher strain rates (a>4 s^{-1}), the flow behaves as predicted by the classical potential flow solution and a zone with no particles is observed, ε<0.

The same procedure was followed with larger particles and the velocity fields in one quadrant were determined by means of Particle Image Velocimetry. Figure 3 shows the PIV results for the top seeded flow at a strain rate of 6.35 and Figure 4 for a strain rate of 12.

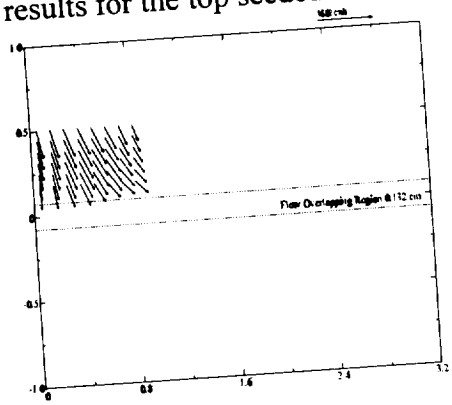

Figure 3 - Top seeded flow for strain a=6.35.

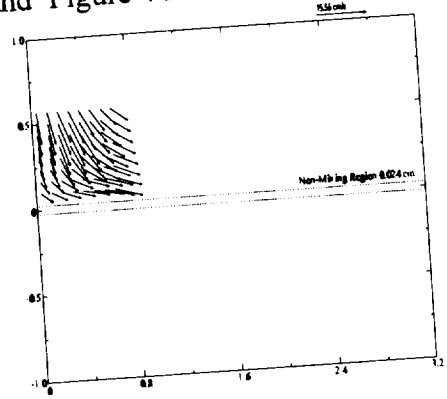

Figure 4 -Top seeded flow for strain a=12.

The above velocity vector plot depicts no velocity vectors beginning in the overlapping region. This is characteristic of the lower strain rates. Once the flow has entered this zone, identifying a primary orientation for the particles becomes difficult and no velocity vectors can be determined with certainty. Particles are present in this region but useful data can not be obtained. Though there are no velocity vectors present in the overlapping region, velocity vectors are observed entering into this region. These velocity vectors show clearly that the "y-component" of the velocity is still significant as the flow enters the overlapping region. Similarly, Figure 4 depicts no velocity vectors in the viscous region. At this strain rate, the velocity vectors are observed to curve away from the non-mixing region. In this case, the diminution of the magnitude of the "y-component" of the velocity is evident. The large particles fail to enter the viscous zone, therefore the particle density is negligible.

REACTING FLOW

Experiments were conducted using propane under strains similar to those presented above. The burner was configured such that propane was introduced into the reaction through the bottom central chamber, oxidizer was introduced through the top central chamber, and the two flows were surrounded by co-flows of nitrogen following through the top and the bottom external chambers.

It was observed that the diffusion flame pulsated with a frequency and amplitude linked to the strain rate and to the separation between the burners. To characterize this pulsation regime digitized images were employed. Fifteen images were digitized over a varying time period. By adjusting the rate of the camera, a full period of the flame pulse was captured within the image

sequence. The frequency of the pulse was then calculated by simply counting the number of frames between pulses and multiplying that by the number of frames between image captures. The amplitude of the pulses was also calculated from the digitized images. The amplitude was obtained by subtracting the position of the visible flame at the minimum displacement position from that at the maximum displacement location. The results are presented in Figure 5 and 6.

The pulsation frequency increases, at each separation, as the strain increases until a critical value is obtained. Beyond the critical value the pulsation frequency is not observed, Figure 5 shows the frequency value and amplitude as zero. The critical value corresponds well with the strain at which $\varepsilon=0$. The role of buoyancy can be captured by scaling the amplitude by the length scale and presenting it as a function of the Rayleigh number (Figure 6), the interactions between the flame and burner surface not allow a similar scaling for the frequency.

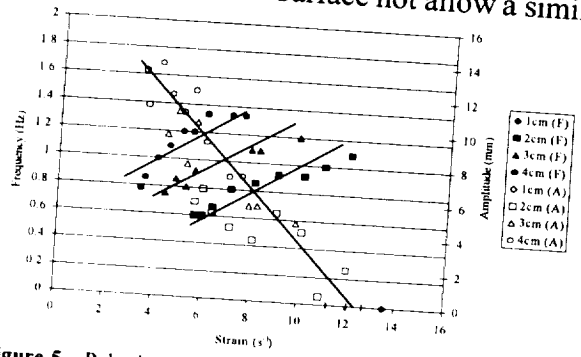

Figure 5 - Pulsation frequency and amplitude as a function of the strain rate (a).

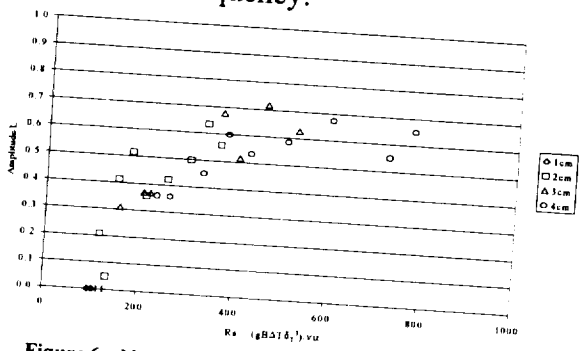

Figure 6 – Non-dimensional amplitude as a function of the Rayleigh number

CONCLUSIONS

A rectangular counter-flow burner was used to study a two-dimensional counter-flow diffusion flame. Flow-visualisation determined a critical strain at which the classical stagnation plane and viscous layer flow breaks down into overlapping flows. A diffusion flame corresponding to a viscous layer strain regime is characterised by and absence of pulsation. In contrast, as the strain rate is reduced and the flow enters the overlapping regime, buoyantly induced instabilities of decreasing frequency and increasing amplitude can be observed.

ACKNOWLEDGEMENTS

This work was funded by NASA Lewis Research Center under contract # NAG-31960.

REFERENCES

1. Puri, I.K. and Seshadri, K., *Combustion and Flame*, **65**, 137-150, 1986.
2. Law, C.K., *22nd Symposium (International) on Combustion*, 1381-1402, 1988.
3. Egolfopoulos, F.N., *25th Symposium (International) on Combustion*, 375-1381, 1994.
4. Egolfopoulos, F.N., *3rd Micro-Gravity Combustion Workshop*, NASA LeRC, 1995.
5. Atreya, A., Agrawal, S., Shamim, T., Pickett, K., Sacksteder, K. and Baum, H., *3rd International Micro-Gravity Combustion Workshop*, NASA LeRC, 1995.
6. Ezekoye, O.A. & Zhang, Z., *Combustion Science and Technology*, 106,4-6,363,1995.
7. Borlik, J., Ezekoye O.A. and Torero, J.L., 7th AIAA/ASME Heat Transfer Conference, HTD-Vol.357-1, 115-121, 1998.
8. Fendell, F. and Wu, F., *3rd International Micro-Gravity Combustion Workshop*, NASA LeRC, 1995.

BURSTING BUBBLES FROM COMBUSTION OF THERMOPLASTIC MATERIALS IN MICROGRAVITY

K.B. Butler, Building and Fire Research Laboratory, National Institute of Standards and Technology, 100 Bureau Drive Stop 8652, Gaithersburg, MD 20899-8652, kathryn.butler@nist.gov.

INTRODUCTION

Many thermoplastic materials in common use for a wide range of applications, including spacecraft, develop bubbles internally as they burn due to chemical reactions taking place within the bulk. These bubbles grow and migrate until they burst at the surface, forceably ejecting volatile gases and, occasionally, molten fuel. In experiments in normal gravity, Kashiwagi and Ohlemiller[1] observed vapor jets extending a few centimeters from the surface of a radiatively heated polymethylmethacrylate (PMMA) sample, with some molten material ejected into the gas phase. These physical phenomena complicated the combustion process considerably. In addition to the non-steady release of volatiles, the depth of the surface layer affected by oxygen was increased, attributed to the roughening of the surface by bursting events. The ejection of burning droplets in random directions presents a potential fire hazard unique to microgravity. In microgravity combustion experiments on nylon Velcro fasteners[1][2] and on polyethylene wire insulation[3], the presence of bursting fuel vapor bubbles was associated with the ejection of small particles of molten fuel as well as pulsations of the flame. For the nylon fasteners, particle velocities were higher than 30 cm/sec. The droplets burned robustly until all fuel was consumed, demonstrating the potential for the spread of fire in random directions over an extended distance.

The sequence of events for a bursting bubble has been photographed by Newitt et al.[4]. As the bubble reaches the fluid surface, the outer surface forms a dome while the internal bubble pressure maintains a depression at the inner interface. Liquid drains from the dome until it breaks into a cloud of droplets on the order of a few microns in size. The bubble gases are released rapidly, generating vortices in the quiescent surroundings and transporting the tiny droplets. The depression left by the escaping gases collapses into a central jet, which rises with a high velocity and may break up, releasing one or more relatively large drops (on the order of a millimeter in these experiments).

A better understanding of bubble development and bursting processes, the effects of bursting behavior on burning rate of the bulk material, and the circumstances under which large droplets are expelled, as well as their trajectories, sizes, and burning rates, is sought through computer modeling compared with experiment.

EXPERIMENTAL EVIDENCE

The combustion behavior of three types of thermoplastic spheres in microgravity, PMMA, polypropylene (PP), and polystyrene (PS), have been recently studied by Yang and Hamins[5] in a set of experiments flown on the NASA Lewis DC-9 Reduced-Gravity Aircraft. Figure 1 shows sequences from two events recorded during these experiments. In each case there is a sudden disturbance to the flame front, not noticeable in the previous frame. This disturbance decays slowly over the next few timeframes and is advected in the direction of a spherically

[1] Certain trade names and company products are mentioned in the text in order specify adequately the equipment used. In no case does such identification imply recommendation or endorsement by the National Institute of Standards and Technology, nor does it imply that the products are necessarily the best available for the purpose.

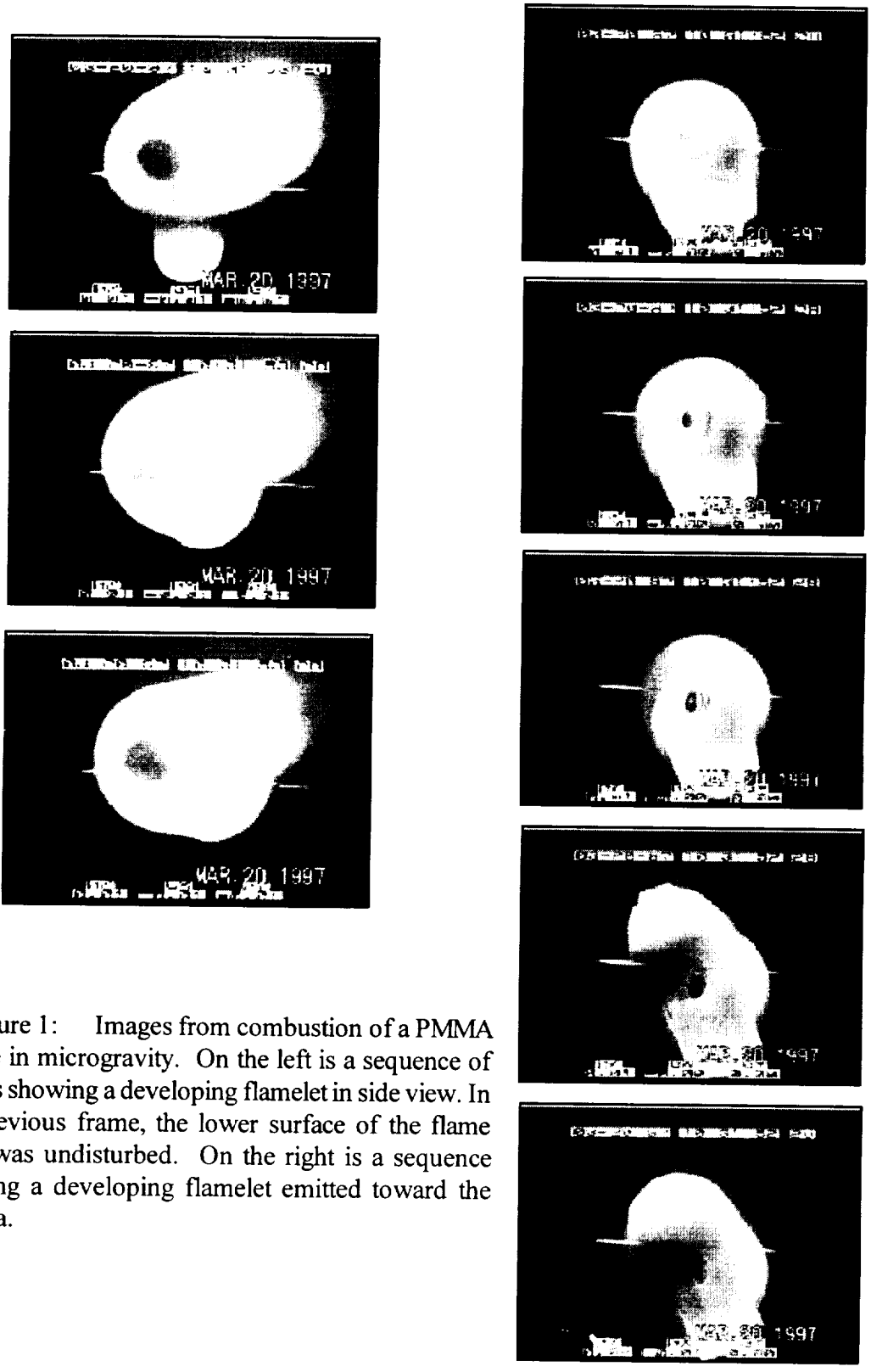

Figure 1: Images from combustion of a PMMA sphere in microgravity. On the left is a sequence of frames showing a developing flamelet in side view. In the previous frame, the lower surface of the flame front was undisturbed. On the right is a sequence showing a developing flamelet emitted toward the camera.

Figure 2: Trajectory of a particle emitted from a PP sphere.

asymmetric flow due to g-jitter. The structures displayed in these two sequences are similar to those of vortex-flame front interactions such as those reported by Roberts and Driscoll[6]. Events of this nature take place frequently during combustion for all three types of thermoplastics.

The ejection of a particle is displayed in Figure 2. Unlike the gaseous events shown in Figure 1, these events do not significantly distort the flame front, and the burning droplet travels in a straight line away from the sphere. Regrettably, the flame front surrounding the droplet is highly luminous, and droplet size could not be measured. Ejected particles were observed for PP but not for PMMA or PS, suggesting a dependence of droplet release on material properties.

MODELING

The bubble bursting process involves large interface deformations and topological changes. A model of this phenomenon must track the distortion of the fluid surface as the bubble approaches, the evolving distribution of the volatile gases released by the burst, the formation of a central jet of melted material, the potential breakup of the jet into one or more droplets, and the trajectory of these droplets away from the melt surface. In addition, the combusting thermoplastic problem must include heat transport and degradation chemistry.

In order to satisfy these requirements, the bubble bursting model applies a diffuse-interface approach based on extended irreversible thermodynamics[7]. This approach adds density gradients to the set of thermodynamic variables, allowing continuous variation of density between phases and providing the ability to follow complex motions of an interface without the need to explicitly track its location. The fluids treated by this model may be compressible, multiphase, and multicomponent. Balance equations of mass, momentum, and energy are rigorously satisfied, and the entropy of a material element of fluid increases or stays the same, as required by the second law of thermodynamics.

The model consists of three separate fluid components representing the polymer melt, a gas that is generated by chemical degradation of the polymer, and an unrelated gas outside of the melt. The effects of the growing bubble on the temperature and flow of its surroundings are included. Using this model, one or more bubbles are studied as they grow, travel toward a heated surface, and burst through the interface into the gaseous component. The formation of a jet is observed, and the

conditions under which the jet breaks up and melted material is released into the surroundings are determined. For those cases in which droplets are ejected, their size and velocity are determined.

FUTURE WORK

A three-dimensional model of a combusting thermoplastic sphere in microgravity, including heat transport and the nucleation, growth, and migration of multiple bubbles is under development[8]. Data obtained from the bursting bubble model on the release of gases and molten material for various types of thermoplastics will be added to this model.

ACKNOWLEDGMENTS

This work is supported by NASA Lewis Research Center under NASA Interagency Agreement C-32033-E. The author would like to thank Dr. Jiann Yang and Dr. Anthony Hamins for their insights into the experimental results and for permission to display some of their data. Dr. Nicos Martys provided much assistance on the development of the diffuse-interface model.

REFERENCES

1. Kashiwagi, T. and Ohlemiller, T.J., "A Study of Oxygen Effects on Nonflaming Transient Gasification of PMMA and PE During Thermal Irradiation," 19th Symposium (International) on Combustion, The Combustion Institute, 1982.

2. Olson, S.L. and Sotos, R.G., "Combustion of Velcro in Low Gravity," NASA TM 88970, 1987.

3. Greenberg, P.S., Sacksteder, K.R., and Kashiwagi, T., "The USML-1 Wire Insulation Flammability Glovebox Experiment," Third International Microgravity Combustion Workshop, NASA Lewis Research Center, Cleveland, Ohio, April 11-13, 1995, pp. 25-30.

4. Newitt, D.M., Dombrowski, N., and Knelman, F.H., "Liquid Entrainment 1. The Mechanism of Drop Formation from Gas or Vapour Bubbles," Trans. Instn. Chem. Engrs., 32:244-261, 1954.

5. Yang, J.C., Hamins, A., and Donnelly, M.K., "Reduced Gravity Combustion of Thermoplastic Spheres," NISTIR in preparation, 1999.

6. Roberts, W.L. and Driscoll, J.F, "A Laminar Vortex Interacting with a Premixed Flame: Measured Formation of Pockets of Reactants," Comb. and Flame 87:245-256, 1991.

7. Jou, D., Casas-Vazquez, J., and Lebon, G., Extended Irreversible Thermodynamics, Springer-Verlag, Berlin, 1993.

8. Butler, K.M.,"Numerical Modeling for Combustion of Thermoplastic Materials in Microgravity," Fourth International Workshop on Microgravity Combustion, NASA Lewis Research Center, Cleveland, Ohio, May 19-21, 1997, pp. 248-253.

INFLUENCE OF BUOYANT CONVECTION ON THE STABILITY OF ENCLOSED LAMINAR FLAMES

John E. Brooker[1], Kezhong Jia[2], Dennis P. Stocker[1] and Lea-Der Chen[2]
[1]NASA Lewis Research Center, Mail Stop 500-115, 21000 Brookpark Road, Cleveland, OH 44135, [2]Department of Mechanical Engineering, The University of Iowa, Iowa City, IA 52242

INTRODUCTION

Enclosed diffusion flames are commonly found in practical combustion systems, such as the power-plant combustor, gas turbine combustor, and jet engine after-burner. In these systems, fuel is injected into a duct with a co-flowing or cross-flowing air stream. In combustors, this flame is anchored at the burner (i.e., fuel jet inlet) unless adverse conditions cause the flame to lift off or blow out. Investigations of burner stability study the lift off, reattachment, and blow out of the flame. There have been numerous studies of flame stability [1-14]. Relatively few studies have investigated the stability of flames with an oxidizer co-flow [6-8], compared with the number of studies on (nearly) free jet diffusion flames [1-5,9-14]. The air flow around the fuel jet can significantly alter the lift off, reattachment and blow out of the jet diffusion flame. In normal gravity, however, the effects of the air flow on flame stability are often complicated by the presence of buoyant convection. A comparison of normal-gravity and microgravity flames can provide clear indication of the influence of forced and buoyant flows on the flame stability. The overall goal of the Enclosed Laminar Flames (ELF) research, described at the following URL site: *http://zeta.lerc.nasa.gov/expr/elf.htm*, is to improve our understanding of the effects of buoyant convection on the structure and stability of co-flow diffusion flames.

EXPERIMENT

The ELF hardware was designed and built to accommodate microgravity testing within the Middeck Glovebox (MGBX) facility. The facility, which has been used to conduct a variety of small and inexpensive experiments on several Space Shuttle missions, and the Russian space station *Mir*, is described at: *http://liftoff.msfc.nasa.gov/shuttle/usmp4/science/mgbx1.html*. In size, the experiment hardware is limited by the 35-liter volume of the glovebox working area, and the 180x220-mm dimensions of the main door. The ELF module is a miniature, fan-driven wind tunnel, equipped with a gas supply system. The module is 330x180x180 mm. A 1.5-mm diameter nozzle is located on the duct's flow axis. The cross section of the duct is nominally a 76-mm square with rounded corners. The forced air velocity can be varied from about 0.2 to 0.9 m/s. Honeycomb and screens are used to eliminate the fan-induced swirl. The fuel flow is established by a fixed pressure regulator and a mass flow controller. The fuel flow can be set to a nozzle exit velocity of up to 1.70 m/s. The flame is ignited with a replaceable hot-wire ignitor. A manually positionable rake is used to move 5 type-R thermocouples and 25 silicon carbide fibers across the duct. The fuel flow, fan voltage, air velocity, rake position, and two temperatures are displayed on the module front for operator viewing and video recording.

Multiple bottles (75-cc) are used to limit the amount of fuel within the glovebox. Each bottle is filled to 2.5 MPa (or 350 psig) with a 50/50 mixture (volume basis) of methane and nitrogen. Diluted methane is used because (a) the fuel and its combustion products are not toxic, (b) the combustion chemistry is well established, and (c) the flame is (nearly) soot-free. At standard state, the fuel's Schmidt number is about 0.7, suggesting that the flames may blow out immediately after

lift off based on the free-jet study of [1].

The primary operational variables are the fuel flow and air velocity. As such, the ELF tests are typically conducted where one velocity is held fixed and the other is varied to determine the velocity at lift off, reattachment, and blow out. Generally, the selected velocity is increased until the flame lifts off, is decreased until it reattaches to the nozzle, and then is increased again until it lifts off and blows out. Both velocities are controlled manually by potentiometers on a control box mounted outside of the glovebox. Therefore, the rate of change for the velocities is directly dependent on the operator. As the "ramp" rate can have a strong effect on the measured stability limits. Additional tests were conducted where attached flames were probed with the translating rake, but those temperature results are not reported in this paper.

The microgravity tests were conducted on the STS-87 Space Shuttle mission (November to December 1997). The ELF tests were conducted during two sessions, on flight days 10 and 12 of the 16-day mission. The microgravity results reported in this paper are from the second session only, during which the glovebox was open to the crew cabin via removal of the side doors and airlock port. The cabin pressure was 101.3±0.4 kPa (14.7 ± 0.06 psia), and the oxygen concentration was 21.56 ± 0.23% (with error bars based on instrument resolution). The normal-gravity comparison tests were conducted without the glovebox, with the module oriented such that the nozzle was pointed upward (i.e., aligned with the gravity vector). The normal-gravity tests were conducted in ambient air, at 98.6±0.3 kPa (14.3 ± 0.05 psia).

RESULTS AND DISCUSSION

Analysis of the results has yielded maps of the flame stability under microgravity and normal-gravity conditions, as shown in Fig. 1. These maps show the lift-off and blow-out boundaries, as functions of the fuel and air inlet velocities. The stability boundaries were selected based on visual inspection of the video data. However, classical definition of the lift-off condition as an abrupt jump of the flame base is not obvious in the ELF (experimental) video image, or in most of the numerical simulation results. The results thus suggest that the lift-off definition be revisited. The figure's axes are shown with "display" units along with "approximate" speed. The approximate speed is based on the scaling, which is nearly linear and the velocity ranges of the axes are of the order of 0 to 1.70 m/s and 0.15 to 0.60 m/s, for the fuel and air, respectively. It should be noted that during testing the fan was always powered, so there was a minimum air velocity on the order of 0.2 m/s.

The stability maps, Fig. 1, confirmed our hypothesis that higher velocities are required for lift-off and blow-out in microgravity compared to normal gravity. This hypothesis was based on the buoyant contribution to the velocity in normal gravity. In this study, most flames were on the order of 10 mm or less in height, whether in normal gravity or microgravity. As such, it is expected that the buoyant contribution to the axial velocity (in the region of the flame) would be on the order of 0.35 m/s, dependent on the flame size, and based on an estimation method of [16]. The data suggest that for a fixed fuel velocity, an increase in air velocity on the order of 0.15 m/s be required to induce lift off in microgravity (compared to normal gravity). As shown on Fig. 1, the increase in air velocity required to induce blow out in microgravity was nearly equal to the increase required to induce lift off. The air velocity increase was also relatively independent of the fuel flow, except at low fuel flows where lesser increases were required. Under those conditions, the buoyancy-induced velocity is diminished due to the small flame size.

From the stability maps, it can be seen that there is an intermediate "most stable" fuel velocity

where the greatest air velocity is required to cause lift off. This observation may have practical application in the design of combustors. There is a similar fuel velocity that is "most stable" in regards to blow out, as previously observed by [7-8], but it occurs at a lower value (than for lift off) regardless of the buoyancy condition. Comparison of the normal-gravity and microgravity maps reveals that both of these "most stable" fuel velocities occur at higher fuel velocities in microgravity. It is also observed that at low fuel velocities, the microgravity blow-out boundary exhibits a sharp decrease in the extinguishing air velocity with decreasing fuel velocity, whereas the normal-gravity curve shows a more gradual decrease.

At high fuel flows, it was found that the microgravity flames tend to immediately blow out after lift off, in agreement with the free-jet theory of [1]-- stable lifted flames are not possible for fuels with a Schmidt number of $0.5<Sc<1$. However, stable lifted flames were observed in microgravity at low fuel flows, and in normal gravity, despite the fuel's low Schmidt number. The discrepancy between the experimental data and the theory of [1] is presumably due to the differences in the flow condition; namely, the ducted flow versus a free jet, and a non-similar velocity profile versus a self-similar profile.

As expected, buoyant convection was found to have a relatively weak effect on the visible appearance of these flames, compared to its effect on their stability. After lifting, the flames generally became shorter and developed an outer, upwardly-turned, fuel-lean rim, essentially becoming hat shaped in appearance. An inner fuel-rich rim (i.e., triple flame structure) was never observed. Ultimately the flames would tend to flatten, becoming disk shaped, but still retaining the fuel-lean outer rim. Similar flame structure behavior has been reported in previous normal-gravity studies [1,4-5,9]. It was noted that the lifted flames had a somewhat tilted base, suggesting that the velocity profile across the duct may not be uniform, possibly due to the rake or another non-uniformity in the hardware.

Numerical simulation predicts a jump condition of the flame base for the fuel jet velocity at 0.2 m/s when the co-flow air velocity is increased to 0.11 m/s. The experimentally determined lift-off co-flow air velocity is 0.3 m/s when the fuel jet velocity is maintained at 0.2 m/s. It should be noted that in the region near the fuel jet velocity of 0.2 m/s, experiment shows a relatively flat lift-off co-flow air velocity as illustrated in Fig. 2. Hence ramping of the co-flow air velocity can introduce a larger uncertainty level in the determination of the lift-off air velocity. For the fuel jet velocity of 0.2 m/s, the predicted blow-out co-flow air velocity is 0.6 m/s; whereas the experimentally determined value was 0.4 m/s. Numerical simulation did not predict an obvious jump movement of the flame base when the fuel jet velocity is increased above 0.2 m/s. Effort of numerical simulation continues aimed at assessing the lack of the jump movement of the flame base.

ACKNOWLEDGEMENTS

The research was supported by the NASA Microgravity Research Division, Code UG, through Grant NAG3-1592 for the effort at The University of Iowa. Special thanks go to Mission Specialists, Dr. Kalpana Chawla (NASA) and Dr. Takao Doi (NASDA), for their interest and dedication during training and while conducting the investigation during the STS-87 mission.

REFERENCES

1. Chung, S.H. and Lee, B.J. *Combust. Flame*, 86:62 (1991).
2. Gollahalli, S.R., Sava, Ö. Huang, R.F., Rodriquez Azara, J.L. *21 Symp. (Int.) Combust.*, 1986, p. 1463.
3. Pitts, W.M. *22nd Symp. (Int.) Combust.*, The Combust. Inst., 1989, p. 809.

4. Sava, Ö. and Gollahalli, S.R. *J. Fluid Mech.*, 165:297 (1986).
5. Lee, B.J., Cha, M.S., and Chung, S.H. *Combust. Sci. and Tech.*, 127:55 (1997).
6. Dahm, W.J.A. and Mayman, A.G., *AIAA J.*, 28:7:1157 (1990).
7. Feikema, D., Chen, R.-H. and Driscoll, J.F. *Combust. Flame*, 80:183 (1990).
8. Feikema, D., Chen, R.-H. and Driscoll, J.F. *Combust. Flame*, 86:347 (1991).
9. Whol, K. Kapp, N.M., and Gazley, C. *3rd Symp. Combust. and Flame and Exp. Pheno.*, The Williams & Wilkins Co., 1949, p. 3.
10. Scholefiled, D.A. and Garside, J.E. *ibid*, p. 102.
11. Kalghatgi, G.T. *Combust. Sci. and Tech.*, 26:233 (1981).
12. Kalghatgi, G.T. *Combust. Sci. and Tech.*, 41:17 (1984).
13. Takahashi, F., Mizomoto, M., Ikai, S., and Futaki, N. *22nd Symp. (Int.) Combust.*, 1984, p. 295.
14. Eickhoff, H., Lenze, B., and Leuckel, W. *20th Symp. (Int.) Combust.*, The Combust. Inst., 1984, p. 311.
15. Burke, S.P. and Schumann, T.E.W. *Ind. Eng. Chem.*, 20:998 (1928).
16. Glassman, I. *Combustion* (3rd Ed.), Academic Press, 1996, p. 281.

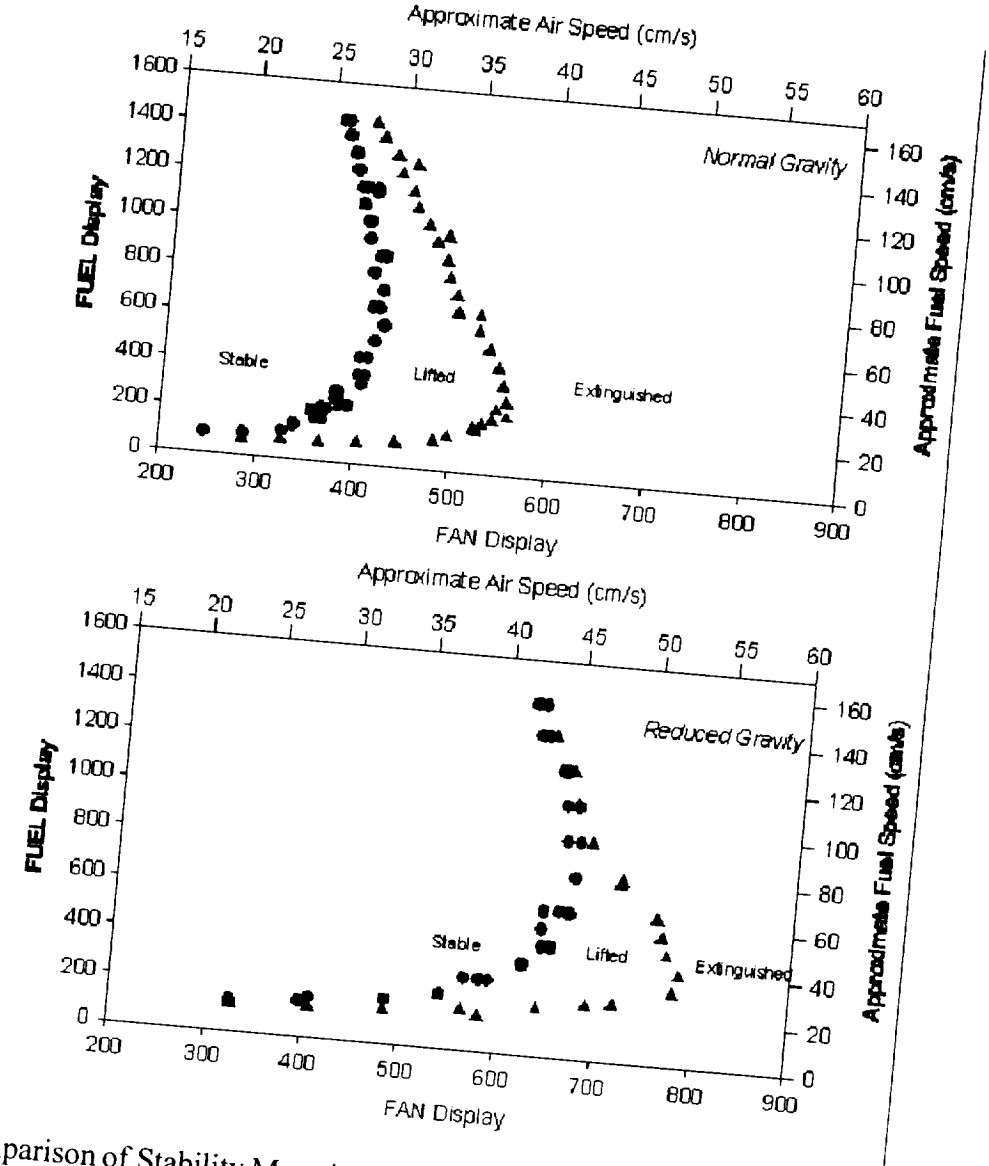

Figure 1. Comparison of Stability Maps in Normal Gravity and Microgravity Environment (circle denotes the lift-off and triangle the blow-out).

4-27

LAMINAR DIFFUSION FLAMES IN MICRO-GRAVITY: EXPERIMENTAL RESULTS LEADING TO MINI-TEXUS-6

T. Vietoris[1], P. Joulain[1] and J.L. Torero[2], [1]Laboratoire de Combustion et de Detonique, UPR9028 au CNRS, 86960 Futuroscope CEDEX, France, [2]Department of Fire Protection Engineering, University of Maryland, College Park, MD20742-3031

INTRODUCTION

Once a fuel is ignited the flame transfers heat to the surface and the combustible material pyrolyzes providing the necessary gaseous fuel to sustain the flame, this process is commonly referred as mass burning. In normal gravity, temperature gradients result in natural convective flows that are laminar when the scale is small, and transition to turbulence as the size of the fuel increases. In spacecraft, where buoyancy is negligible, the flow is limited to that induced by the ventilation system. Characteristic HVAC velocities are of the order of 0.1 m/s, therefore, the flow is expected to be laminar and parallel to the surface. The complex mixed flow fire scenario observed in normal gravity is reduced a classical combustion study, "The Emmons Problem" [1]. Natural constraints imposed by buoyancy and the differences between normal gravity fires and the laminar flame studied by Emmons have prevented validation of this model. The advent of long-term space facilities motivates revisiting the work of Emmons since this configuration represents a plausible fire scenario on board of a spacecraft.

Lavid and Berlad [2] incorporated the effect of buoyancy for a horizontal plate and Fernandez-Pello and Pagni [3] extended this analysis presenting a mixed flow parameter that applied to any orientation. Pagni and Shih [4] used the Emmons analysis to study the flame length. All these studies relied on the assumption of infinite chemistry, none of them address the issue of stability. Theoretical work related to stability has been restricted to blow-off limits [5].

Experimental work, using a gas burner explored the issues of stability and flow structure for velocities between 0.2 and 1.4 m/s [6]. Hirano et al. showed an upper limit for the free stream velocity and a lower limit for the fuel injection velocity. No mention of a lower limit for the oxidizer flow is made. A study conducted by Torero et al. [7] extended the range of velocities explored by Hirano et al. Thermal expansion and fuel injection resulted in separation of the boundary layer and the formation of 3-D flow patterns that altered the flame geometry but seemed to have only a minor stabilizing effect on the flame. Extinction at low strain rates was only observed for a minimum fuel injection velocity.

The subject of flame stability under micro-gravity conditions for free stream velocities smaller than 0.2 m/s has been addressed through flame spread studies with thin fuels [8]. Experiments with thick fuels, under these velocity regimes, are not very common since, in most cases, the micro-gravity time required is much longer than that available in ground based facilities. West et al. [10] conducted a series of quiescent flame spread studies over thermally thick PMMA and observed that the flame spread rate decreases with time never reaching steady state conditions. The present work addresses the stability of a diffusion flame under micro-gravity conditions for free stream velocities smaller than 0.2 m/s. The fuel used is PMMA and the experiments are conducted under normal and micro-gravity conditions. Extensive ground experimentation sets the basis for the Mini-Texus-6 sounding rocket experiment.

GROUND EXPERIMENT

A PMMA plate (50 mm x 50 mm x 10 mm) is mounted on a stainless steel plate which is

placed inside a horizontal combustion chamber (300 mm diameter). Different mixtures of O_2 and N_2 are supplied by a controlled mass flow meter through a chamber that serves to assure an homogeneous laminar flow. Two CCD cameras provide a side and top view of the flame. Temperatures are recorded by means of 5 type-K thermocouples melted into the top surface of the PMMA plate and 8 thermocouples placed vertically at the trailing edge of the plate. All thermocouples are 0.05 mm in diameter and their tip is placed at the plane of symmetry. The surface thermocouples are placed at 12, 20, 28, 36 and 44 mm from the trailing edge of the sample and the vertical thermocouples at 2, 5, 10, 15, 23, 31, 41, 53 mm from the fuel surface. Experiments were conducted on ground, on board of the Airbus A300 from CNES (25 sec. of μg) and at the ZARM Drop Tower (4.7 sec. of μg). Ignition was accomplished by means of an homogeneously distributed NiCr coil embedded in the fuel sample at the trailing edge. The propagation front was observed to be one dimensional for almost the integrity of the sample curving only 3-5 mm at the lateral edges of the sample.

MINI-TEXUS-6

Based on the experimental results obtained from ground based experiments a combustion chamber was designed for a Mini-Texus sounding rocket. The Mini-Texus consists of a 1050 mm x ϕ 500 mm payload weighing approximately 100 kg carried by and Orion and Nike rockets. This sounding rocket provides aproximatelly182 seconds of micro-gravity at a level of 10^{-5} g_0. The general characteristics of the combustion chamber are similar to those presented above and the diagnostic techniques used are listed in table 1. A schematic of the experimental configuration is presented in Figure 1.

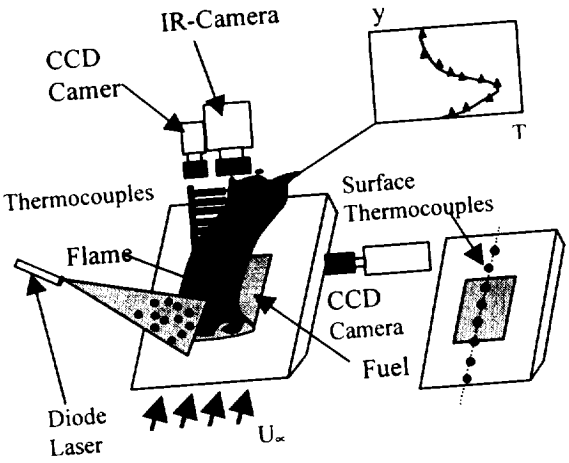

Figure 1 – Schematic of the Mini-Texus 6 experimental hardware

Process		Diagnostic
Flame Spread	**HEAT TRANSFER MECHANISMS**	
	Preheating Ahead of the Flame	Surface Thermocouples
		Infra-Red Camera
	MASS TRANSPORT MECHANISMS	
	The Leading Edge	
	Flow Structure	PIV
	Flame Geometry	CCD-Cameras
	The Trailing Edge	
	Extinction (Flame Geometry)	CCD-Camera
	Flame Length	CCD-Camera
Mass Burning	**HEAT TRANSFER MECHANISMS**	
	Upstream	Infra-Red Camera
		Surface Thermocouples
	Downstream	Surface Thermocouples
		Thermocouple Tree
	Flame Temperature	Infra-Red Camera
Flame Structure	Flame Geometry	CCD-Cameras
	Extinction	PIV
		Infra-Red Camera

Table 1 – Diagnostic Techniques

EXPERIMENTAL RESULTS

The different experimental conditions studied are presented in Figure 2. The oxygen concentration and free flow velocity was varied as indicated in the figure. As show by Figure 1, three different regimes can be observed and depend on the free stream velocity and oxygen

concentration. For oxygen concentrations above that of ambient and oxidizer velocity greater than 10 mm/s the flame is stable, is mostly yellow in color (significant soot oxidation) and remains very close to the fuel surface. Decreasing the oxygen concentration or the free stream velocity reduces the soot oxidation resulting in a bluer and less luminous flame. Oxygen concentration has a significant effect on the luminosity of the flame but the free stream velocity seems to control the color. As the velocity approaches the stability limits for 20-25% oxygen concentration the flame is almost invisible. A further decrease in the free stream velocity results in a sudden decrease in gas and solid phase temperatures which leads to extinction of the flame. Extinction was not observed in normal gravity for any of the conditions shown in Figure 2. The data points labeled as extinction, thus, represent extinction in less than 4.7 seconds, therefore can not be taken as an absolute extinction limit although, temperature traces clearly discriminated between stable and non-stable flames.

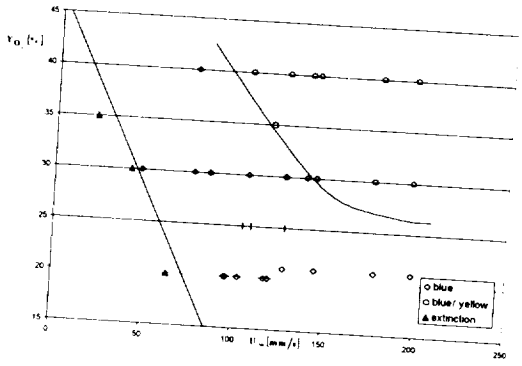

Figure 2 - Micro-gravity extinction limits and two different stable regimes.

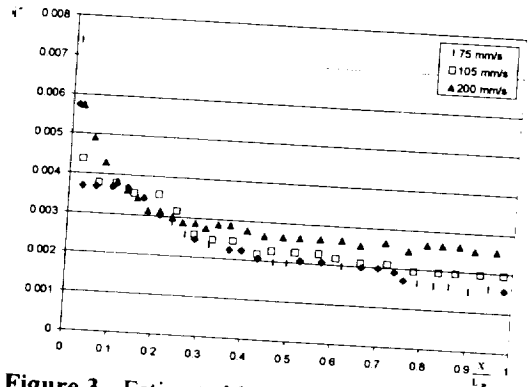

Figure 3 - Estimated heat flux (W/mm^2) for different forced flow velocities (Y_{O2}=40%).

Following boundary layer assumptions an estimate of the heat feedback from the flame to the fuel surface can be obtained by means of the following expression: $\dot{q}'' = -\lambda(T_P - T_F)/\delta_F$, where $\dot{q}''$ is the heat feedback per unit area, λ is an average thermal conductivity for air (λ=0.0257 W/m.K), T_P the surface pyrolysis temperature, T_F the flame temperature and δ_F the stand-off distance.

Single thermocouple histories do not allow a proper estimate of the pyrolysis temperature of the fuel therefore and average value was of 330°C was used. The thermocouple tree allowed to estimate an average flame temperature for the different experimental conditions. Both pyrolysis and flame temperatures were in agreement with values commonly found in the literature. The flame stand-off distance can be obtained by digitizing the video recordings and establishing a luminosity threshold to determine a flame boundary.

The estimated heat feedback to the fuel surface as a function of a scaled length, x/L_P, where L_P is the length of the pyrolyzing region and x the coordinate axis is presented in Figure 3. The heat flux to the surfaces reaches a maximum at the leading edge and decreases towards an almost constant value as the distance from the flame tip increases. For 200 mm/s the heat flux decreases smoothly with the distance from the leading edge reaching a constant value for x/L_P>0.4. For 105 mm/sec and the 75 mm/sec the increase in heat flux at the leading edge is not as obvious. For the lower velocities, an initial peak is followed by a plateau leading again to an almost constant value further downstream. A further decrease in the forced flow velocity results in a lower heat flux to the surface that eventually will lead to extinction.

The classical Blasius definition gives the following expression for the boundary layer thickness: $\delta_B = 5.5x / Re_x$, where x is the distance in the stream wise direction, $Re_x = U_\infty x / \nu$, U_∞ is the free stream velocity and ν the kinematic viscosity. The flame stand-off distance can be considered a constant fraction of the boundary layer thickness therefore the stand-off distance will be presented normalized by the boundary layer thickness, Figure 4. For the lower velocities, for $x/L_P<0.2$ the stand-off distance increases faster than the boundary layer thickness and for $x/L_P>0.2$ the stand-off distance is proportional to δ_B. The increase in the constant of proportionality with the flow is related to the increase of the fuel mass transfer [1].

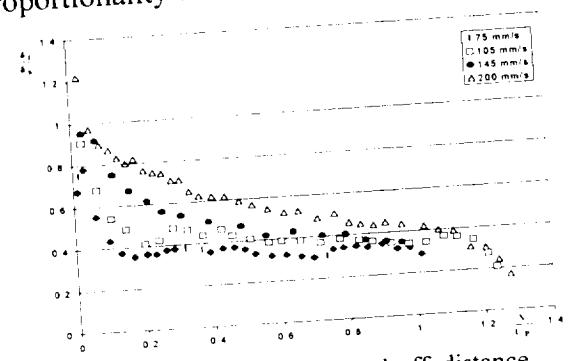

Figure 4 - Non-dimensional stand-off distance (Y_{O2}=40%).

The former case corresponds to the zone defined earlier as the blue flame regime and the latter to the blue/yellow zone. As described by Law and Faeth [8] for soot oxidation to occur, and a flame to emit yellow light, it is necessary for the flow stream lines to carry the soot particles formed at the fuel side close to the flame. As the flame exits the trailing edge of the fuel, the stand-off distance decreases as the fuel is consumed. This observation corresponds well with the concept of excess pyrolyzate[4].

CONCLUSIONS

Laminar diffusion flames were found to be unstable in the absence of a minimum oxidizer forced flow. The low velocity stability limit of the flame seems to be linked to a minimum fuel production. Fuel pyrolysis depends on the heat feedback from the flame thus relates to the characteristics and geometry of the flame. Two different regimes of stable flames have been identified, blue flames and yellow flames. Fuel supply is dominated by diffusion for blue flames, therefore, stand-off distance and flame length correspond well with classical theory. Convection of fuel towards the flame is of importance in yellow flames leading to discrepancies between theory and the present experiments. Mini-Texus 6 Experiments provided long term validation to these conclusions.

ACKNOWLEDGMENTS

This work was supported by CNES and ESA. Financial support for JLT was provided by the Minta Martin Research Foundation.

REFERENCES

1. Emmons, H., Z. Angew. Math. Mech., 33, 60, 1956.
2. Lavid, M. & Berlad, A.L., 16th Symposium (International) on Combustion, 1157-1568, 1976.
3. Fernandez-Pello, A.C. and Pagni, P.J., ASME-JSME Conference, Honolulu,4,1993.
4. Pagni, P.J. and Shih, T.M. 16th Symposium (International) on Combustion, 1329-1343, 1976.
5. Chen, H.C. and T'ien, J.S., Combustion Science and Technology, 50, 283-306, 1986.
6. Hirano, T., Iwai, K. and Kanno, Y., Astronautica Acta, 17, 811-818, 1972.
7. Torero, J.L., Bonneau, L., Most, J-M and Joulain, P 25th Symposium (International) on Combustion, 1701-1709, 1994.
8. Law, C.K. and Faeth, G. M. Prog. in Energy and Comb. Sci., 20, 1, 65-113, 1994.
9. West, J., Tang, L., Altenkirch, R.A., Bhattacharjee, S., Sacksteder, K. and Delichatsios, M.A. 26th Symposium (International) on Combustion, 1335-1343, 1996.

THE EFFECTS OF BUOYANCY AND DILUTION ON THE STRUCTURE AND LIFT-OFF OF COFLOW LAMINAR DIFFUSION FLAMES

Kevin T. Walsh, Marshall B. Long, and Mitchell D. Smooke

Yale University
Department of Mechanical Engineering
New Haven, CT 06520-8284

Technical Monitor: Karen Weiland
NASA Glenn Research Center, Cleveland, OH 44135

INTRODUCTION

The ability to predict the coupled effects of complex transport phenomena with detailed chemical kinetics in diffusion flames is critical in the modeling of turbulent reacting flows and in understanding the processes by which soot formation and radiative transfer take place. In addition, an understanding of the factors that affect flame extinction in diffusion flames is critical in the suppression of fires and in improving engine efficiency. The goal of our characterizations of coflow laminar diffusion flames is to bring to microgravity the multidimensional diagnostic tools available in normal gravity, and in so doing provide a broader understanding of the successes and limitations of current combustion models. This will lead to a more detailed understanding of the interaction of convection, diffusion and chemistry in both buoyant and nonbuoyant environments.

As a sensitive marker of changes in the flame shape, the number densities of excited-state CH ($A^2\Delta$, denoted CH*), and excited-state OH ($A^2\Sigma$, denoted OH*) are measured in μg and normal gravity. Two-dimensional CH* and OH* number densities are deconvoluted from line-of-sight chemiluminescence measurements made on the NASA KC-135 reduced-gravity aircraft. Measured signal levels are calibrated, post-flight, with Rayleigh scattering [1]. Although CH* and OH* kinetics are not well understood, the CH*, OH*, and ground-state CH distributions are spatially coincident in the flame anchoring region [2]. Therefore, the ground-state CH distribution, which is easily computed, and the readily measured CH*/OH* distributions can be used to provide a consistent and convenient way of measuring lift-off height and flame shape in the diffusion flame under investigation. Given that the fuel composition affects flame chemistry and that buoyancy influences the velocity profile of the flow, we have the opportunity to computationally and experimentally study the roles of fluids and chemistry. In performing this microgravity study, improvements to the computational model have been made and new calculations performed for a range of gravity and flow conditions. Furthermore, modifications to the experimental approach were required as a consequence of the constraints imposed by existing microgravity facilities. Results from the computations and experiments are presented in the following sections.

BURNER CONFIGURATION

The burner used in this experiment contains a central fuel jet (4 mm diameter) surrounded by coflowing air (50 mm diameter). The standard flow conditions, which have been measured and modeled extensively in normal gravity, consist of fuel composed of 65% methane diluted with 35% nitrogen by volume (denoted 65/35 in later discussion). The plug flow exit velocity of both fuel and coflow was 35 cm/s. These conditions produce a blue flame roughly 3 cm in length with a lift-off height of 5.5 mm in normal gravity. A wide range of flow conditions were examined in this study, with the fuel composition varied from 100% methane to a 40/60 CH_4/N_2 mixture in 5% increments, with all exit velocities held fixed at 35 cm/s.

COMPUTATIONAL APPROACH

The computational model used to compute the temperature field, velocities, and species concentrations, solves the full set of elliptic two-dimensional governing equations for mass, momentum, species, and energy conservation on a two-dimensional mesh [3]. The resulting nonlinear equations are then solved on an IBM RS/6000 Model 590 computer by a combination of time integration and Newton's method. The chemical mechanisms employed were GRI Mech 2.11 [4] and a simpler 26-species, C_2 hydrocarbon mechanism [5].

Flame structure was calculated over a range of flow conditions in both μg and normal gravity. The results of a computed solution at standard flow conditions (65/35) and normal gravity were used as a starting point. In subsequent calculations, the value of the gravitational acceleration (g) was reduced by 10 cm/sec^2 and a new solution calculated using Newton's method. Initial computations performed with different values for the gravitational constant indicate that buoyancy plays an important role in both the size and shape of the coflow laminar diffusion flame. Figure 1 shows the temperature isotherms for the 65/35 flame computed with g = 982.0 and 0.0 cm/sec^2. It is clear from the figure that, as the gravitational constant is lowered, the flame becomes shorter and broader in appearance. Computations at different flow conditions were performed by using the 65/35 flame as an initial condition and varying the fuel mixture in 5% increments.

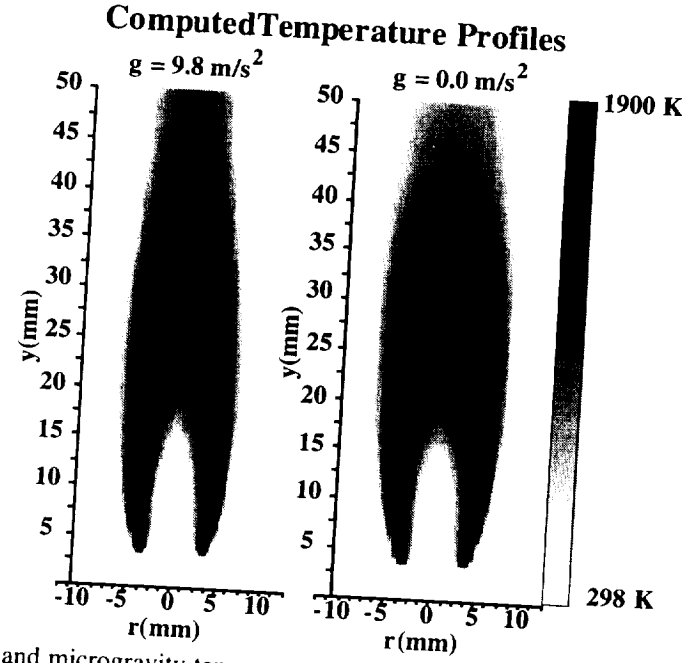

Figure 1. Normal and microgravity temperature profiles at 65/35 computed with GRI Mech 2.11

While large variations in g are important in illustrating the differences between normal gravity and microgravity flame structure, small variations in g are important in determining whether the flame will be stable enough for meaningful time-averaged measurements. During the low-g portion of the KC-135 parabolic trajectory, the value of the local acceleration can vary by as much as ±1% of Earth's gravity. To simulate this effect, the 65/35 flame was computed with a DC gravitational constant of ± 10 cm/s^2. These calculations, done prior to the experiments, suggested that the flame structure should be insensitive to such fluctuations for this coflowing geometry and fuel composition. These initial computations at standard flow conditions were performed with GRI Mech 2.11 as the kinetic mechanism, while the remaining calculations in this study used the simpler 26-species C_2 mechanism, which is in better agreement with measured lift-off at this flow condition.

EXPERIMENTAL SYSTEM

Several modifications to the laboratory-based experimental setup were required to make measurements on the KC-135. The burner and ignition system were housed inside a windowed pressure vessel to maintain standard atmospheric pressure. Spectrally-filtered, quantitative chemiluminescence images were collected with a f/4.5 UV camera lens and focused onto a cooled, unintensified CCD camera (Photometrics CH350). The camera/lens system was placed 50 cm away from the flame to ensure a wide depth of field, and high emission signal levels were collected with a 10 s exposure time. A color video camera (Sony XC-999) was used to give qualitative insight into flame structure and soot production, as well as monitor the stability of the flame in real time. During each low gravity maneuver on the KC-135, the combustion vessel pressure and airplane accelerometer signal were recorded simultaneously with the flame emission signal. The computer-controlled exhaust system kept the pressure inside the combustion vessel constant to better than 1%. All Rayleigh calibration was performed, post-flight, on the same optical setup. Details of this procedure are available in earlier work [2].

Emission measurements are integrated through the collection optics along the line of sight. Appropriate background images, taken for both CH* and OH* with the flame extinguished, are subtracted from the raw emission signal. Since our flame is axisymmetric and the imaging optics are configured such that the magnification changes by only 1% over the flame width, we can recover a two-dimensional, in-plane intensity distribution proportional to number density with the use of an algorithm that is equivalent to a two-point Abel deconvolution [6]. To make these measurements quantitative, further corrections and calculations are performed to account for quenching [7] and differences in the spectral profiles of the emission and Rayleigh signals [1]. These steps are not described in depth here, since the spatial location of the peak signal, rather that the absolute number density, is of primary interest in this study.

RESULTS

Although the gravitational acceleration produced by the KC-135 during low-g maneuvers is subject to both positive and negative unsteady forces (g-jitter), the flame anchoring region remained stable enough for careful emission measurements of both CH* and OH* for fuel compositions ranging from 50% to 100% methane. In dilute fuel blends (40%-55% N_2), the µg flame appeared as stable as a normal gravity flame. For richer fuel mixtures, which contained more than 75% methane by volume, the µg flames produced significant soot luminescence, which could be seen to fluctuate as a result of g-jitter. In the 100% methane flame, g-jitter causes the sooty region in the flame to "bounce", translate, and change shape considerably. Other µg measurements performed recently, involving Rayleigh thermometry and laser-induced incandescence (LII), will be better able to quantify these fluctuations and their relation to g-jitter.

Measured flame shape, as indicated by the spatial distributions of the CH* and OH* radicals, can change significantly between normal gravity and microgravity. In general, a microgravity flame is shorter, wider, and has a higher flame front curvature relative to its normal gravity counterpart. Additionally, the microgravity flame anchors closer to the burner surface. Although the OH* profile is more localized than that of CH*, similar gravity-induced changes in flame structure can be seen. Initial CH computations, performed at 65/35 with both GRI Mech 2.11 and the alternate mechanism, correctly predicted the buoyancy-related changes in flame shape and length while under-predicting the change in lift-off between normal gravity and µg. This can be seen back in Figure 1, where flame onset doesn't change between 0 g and 1 g. This discrepancy prompted further calculations, over a range of flow conditions and g-levels, performed with careful attention to convergence criteria.

We define the measured lift-off as the height above the burner where the maximum of OH* occurs, and similarly for CH in the computations. Since OH* is formed from ground-state CH, each maximum occurs in the same spatial location, as shown in earlier work [2]. We therefore have the ability to plot measured and computed lift-off heights, both in µg and normal gravity, as a function of diluent level in the fuel stream. This is shown below in Figure 2. Since methane is lighter than air, density effects provide normal gravity flames with a higher lift-off than µg flames

at a given flow condition. At 65/35, the predicted lift-off height agrees well with measurement at both 0g and 1g, in contrast to preliminary results. This shift illustrates the sensitivity of predicted lift-off height to the convergence tolerance used in the computation. Despite this success, the predicted normal gravity lift-off lacks the measured variation between 35% and 50% N_2. As the fuel dilution is increased beyond 50% in 1 g, the lift-off height becomes highly under-predicted, until the code predicts a stable flame for fuel mixtures (65% and 70% N_2) that do not ignite experimentally. Finally, the difference between computed normal and μg lift-offs does not

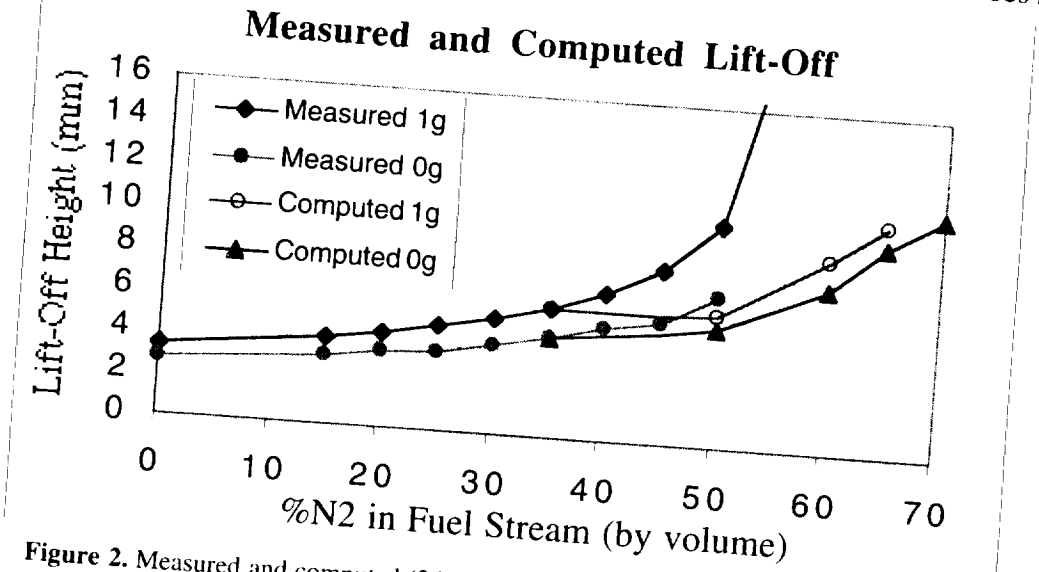

Figure 2. Measured and computed (26 species C_2 mechanism) lift-off heights in 0g and 1g.

match the measured curves, which separate increasingly as the fuel mixture is diluted.

A degree of sensitivity exists in experimental lift-off as well -- the details of burner design provide the measured onset of dilute flames with an uncertainty of one to two millimeters due to flame asymmetries. Nonetheless, the behavior of the computed lift-off as the fuel composition is varied suggests problems with this kinetic mechanism, which has been well validated in previous work at 65/35 [5]. Comparisons with other chemical mechanisms, notably the anticipated GRI Mech update, are planned in further studies.

ACKNOWLEDGEMENTS

The support of NASA under Grant NAG3-1939 is gratefully acknowledged. NASA Glenn personnel were extremely helpful from the early planning stages to the final nuts and bolts of flying the experiment successfully. In particular, we thank Jack Kolis, Eric Neumann, Karen Weiland, Joe Wilson, Jim Withrow, and John Yaniec.

REFERENCES

1. Luque, J. and Crosley, D.R., *Appl. Phys. B* 63:91-98 (1996).
2. Walsh, K. T., Long, M. B., Tanoff, M. A., and Smooke, M. D., *Twenty-seventh Symposium (International) on Combustion*, The Combustion Institute, Pittsburgh, PA, 1998, (in press).
3. Ern, A., Douglas, C. C., Smooke, M. D., *The International Journal of Supercomputer Applications*, Volume 9, No. 3, p. 167-186, (1995).
4. Bowman, C. T., Hanson, R. K., Davidson, D. F., Gardiner Jr., W. C., Lissianski, V., Smith, G. P., Golden, D. M., Frenklach, M., Wang, H., and Goldenberg, M.,: *GRI-Mech version 2.11*, http://www.gri.org, (1995).
5. Smooke, M.D., Xu, Y., Zurn, R.M., Lin, P., Frank, J.H., and Long, M.B., *Twenty-fourth Symposium (International) on Combustion*, The Combustion Institute, Pittsburgh, PA, 1992, pp. 813-822.
6. Dasch, C. J., *Appl. Opt.* 31:1146-1152 (1994).
7. Tamura, M., Berg, P.A., Harrington, J.E., Luque, J., Jeffries, J.B., Smith, G.P., and Crosley, D.R., *Combust Flame*, 114(3-4):502-514, (1998).

526-25

EFFECTS OF BUOYANCY IN HYDROGEN JET DIFFUSION FLAMES

A. K. Agrawal[1], K. Al-Ammar[1], and S.R. Gollahalli[1], and D.W. Griffin[2], [1]School of Aerospace and Mechanical Engineering, University of Oklahoma, Norman, OK 73019, [2]Fluid Physics Branch, NASA Lewis Research Center, Cleveland, OH 44135

INTRODCUTION

This project was carried out to understand the effects of heat release and buoyancy on the flame structure of diffusion flames. Experiments were conducted at atmospheric pressure in both normal gravity and microgravity conditions in the NASA LeRC 2.2 s drop tower. Experiments were also conducted in a variable pressure combustion facility in normal gravity to scale buoyancy and thus, to supplement the drop tower experiments. Pure H_2 or H_2 mixed with He was used as the jet fluid to avoid the complexities associated with soot formation. Fuel jet burning in quiescent air was visualized and quantified by the Rainbow Schlieren Deflectometry (RSD) to obtain scalar profiles (temperature, oxygen concentration) within the flame. Burner tube diameter (d) was varied from 0.3 to 1.19 mm producing jet exit Reynolds numbers ranging from 40 to 1900, and generating flames encompassing laminar and transitional (laminar to turbulent) flow structure. Some experiments were also complemented with the CFD analysis.

In a previous paper [1], we have presented details of the RSD technique, comparison of computed and measured scalar distributions, and effects of buoyancy on laminar and transitional H_2 gas-jet diffusion flames. Results obtained from the RSD technique [2, 3], variable pressure combustion chamber [4], and theoretical models [5] have been published. Subsequently, we have developed a new drop rig with improved optical and image acquisition [6]. In this set up, the schlieren images are acquired in real time and stored digitally in RAM of an onboard computer. This paper deals with laminar diffusion flames of pure H_2 in normal and microgravity.

RESULTS

Figure 1 shows the color schlieren images of a hydrogen gas-jet diffusion flame in normal and microgravity for d=1.19 mm and Re=70. The microgravity image was taken towards the end of the drop, when the flow field had attained a near steady state. In conformity with previous studies and as expected, we notice that the schlieren boundary in microgravity is wider than that in normal gravity. Also, the axial diffusion upstream of the burner exit is more significant in microgravity than that in normal gravity. Images in Fig. 1 were used to create contour plots of angular deflection shown in Fig. 2. The curvature of contours in Fig. 2 reveals large axial gradients near the burner exit that decrease gradually in the axial direction. The curvature is significantly higher in microgravity than that in normal gravity, suggesting that the axial diffusion is important for an accurate analysis of the near-burner region. The spacing between contours indicates radial gradient, which is smaller in microgravity because of the lack of the buoyant acceleration. Overall, the normal gravity flame is characterized as buoyancy-driven because the relatively slow diffusion process dominates in the absence of the buoyancy.

For a given jet exit Re, the ratio of jet momentum to the buoyant acceleration (i.e. the Froude number) increases with a decrease of the burner diameter. Thus, with a smaller burner, the flame is expected to approach non-buoyant conditions in normal gravity. This is observed experimentally for d=0.3mm and Re=70, as shown by the contour plots in Fig. 3. Note the similarity between microgravity flame in Fig. 2 (d=1.19mm) and normal gravity flame in Fig. 3 (d=0.3mm). The buoyancy effects, although small, are evident from the differences between the

normal and microgravity flames in Fig. 3. In microgravity, the Froude number is large and hence, its effect on the flame structure may be negligible. For instantaneous reactions, negligible soot and radiation, the Re is the primary parameter to characterize flames in microgravity [4]. Accordingly, the contour plots of microgravity flames in Figs. 2 and 3 are expected to match with each other. The difference between these figures raises the possibility that the flame in Fig. 2 may not have reached the *true* steady state in the drop tower.

An understanding of the temporal evolution of flame in the drop tower is obtained from Fig. 4(a), which shows the temperature profiles at z/d =4 during the drop for d=1.19mm, and Re=70 and 40. The 300 K profile corresponds to the outer boundary of the temperature field (schlieren boundary) and the 2400 K profile corresponds to the reaction zone (flame boundary). We notice that the flame surface approaches steady state earlier than the schlieren boundary, with the time to achieve the *near* steady state at 0.4s and 1.0s, respectively. However, note the minor increase in the schlieren boundary throughout the drop, particularly for the flame at Re=40 in Fig 4(b). In this case, the flame surface reached near steady state in 0.8s. The time for the flame surface to reach near steady state was smaller (0.2s to 0.5s) for momentum-dominated flames from the smaller burner. These results demonstrate that the steady state of the flame surface is not a true measure of the steady state of the surrounding flow field.

The shape of normal and microgravity flames from different size burners are compared in Fig. 5(a) for Re=70 and in Fig. 5(b) for Re=40. The flame shape was determined from the location of the minimum refractive index (or maximum temperature) and hence, it represents the reaction zone. Several interesting results are revealed: i) the normalized flame length is independent of the burner diameter or gravity, ii) the flame length decreases with Re, iii) for a given Re, the buoyancy effects are significant with the larger burner, iv) the flame shape in microgravity is nearly independent of the burner diameter, and v) the flame anchoring distance upstream of the burner exit increases in microgravity. Finally, Figs. 6(a) and 6(b) show temperature profiles at z/d=4, respectively, for Re=70 and 40. These results show that the reaction zone temperature (2400K) is not affected by the gravity.

ACKNOWLEDGEMENTS

This work was supported by NASA Microgravity Science and Application Division, grant NAG3-1594.

REFERENCES

1. A.K. Agrawal, S.R. Gollahalli, and D. Griffin, 1997, "Study of Buoyancy Effects in Diffusion Flames using Rainbow Schlieren Deflectometry," *4th Int. μg Comb. Workshop*, NASA-CP10194, pp. 117-122.
2. K. Al-Ammar, A.K. Agrawal, S.R. Gollahalli, and D. Griffin, 1998, "Application of Rainbow Schlieren Deflectometry for Concentration Measurements in an Axisymmetric Helium Jet," *Experiments in Fluids*, vol. 25, pp. 89-95.
3. A.K. Agrawal, N. Butuk, S.R. Gollahalli, and D. Griffin, 1998, "Three-Dimensional Rainbow Schlieren Tomography of Temperature Field in Gas Flows," *Applied Optics*, vol. 37, pp. 479-485.
4. A.K. Agrawal, S.M. Cherry, and S.R. Gollahalli, 1999, "Effects of Buoyancy on Steady Gas Jet Diffusion Flames," *Combustion Science and Technology*. In press.
5. A.K. Shenoy, A.K. Agrawal, and S.R. Gollahalli, 1998, "Quantitative Evaluation of Flow Computations by Rainbow Schlieren Deflectometry," *AIAA Journal*, vol. 36, pp. 1953-1960.
6. Al-Ammar, K.N., 1999, "Scalar Measurements and Analysis of Hydrogen Gas-Jet Diffusion Flames in Normal and Microgravity," *PhD Dissertation*, University of Oklahoma.

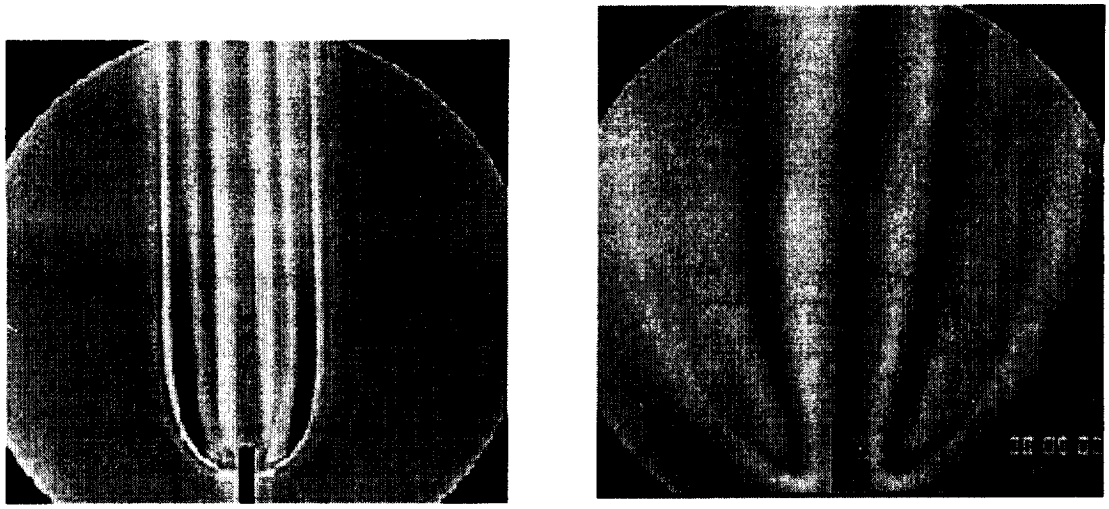

Figure 1. Color Schlieren Images in Normal (Left) and Microgravity (Right); d=1.19 mm, Re=70

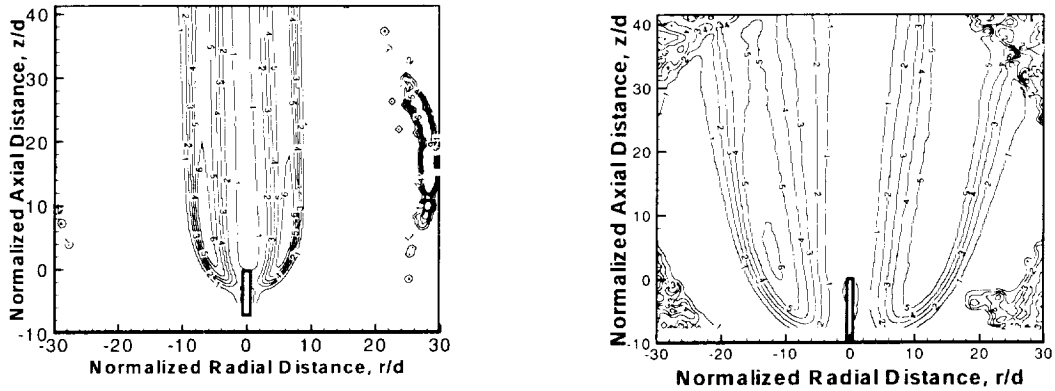

Figure 2. Contour Plots of Angular Deflection in Normal (Left) and Microgravity (Right); d=1.19 mm, Re=70

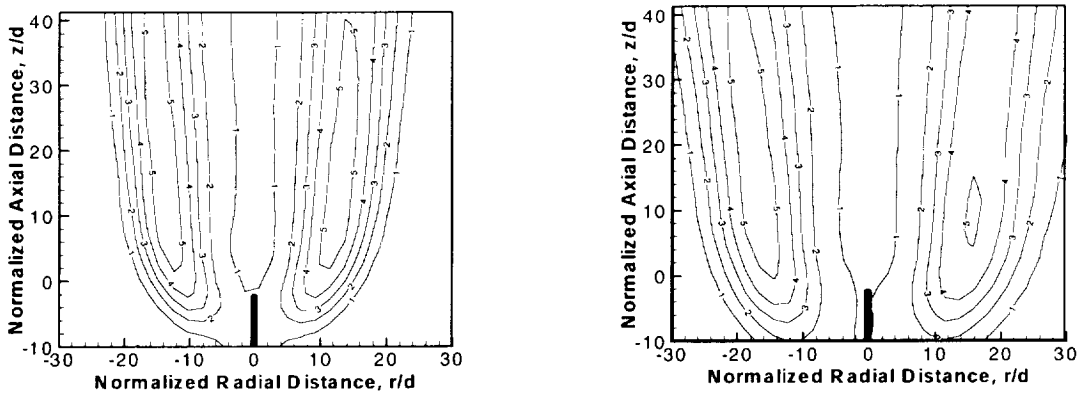

Figure 3. Contour Plots of Angular Deflection in Normal (Left) and Microgravity (Right); d=0.3 mm, Re=70

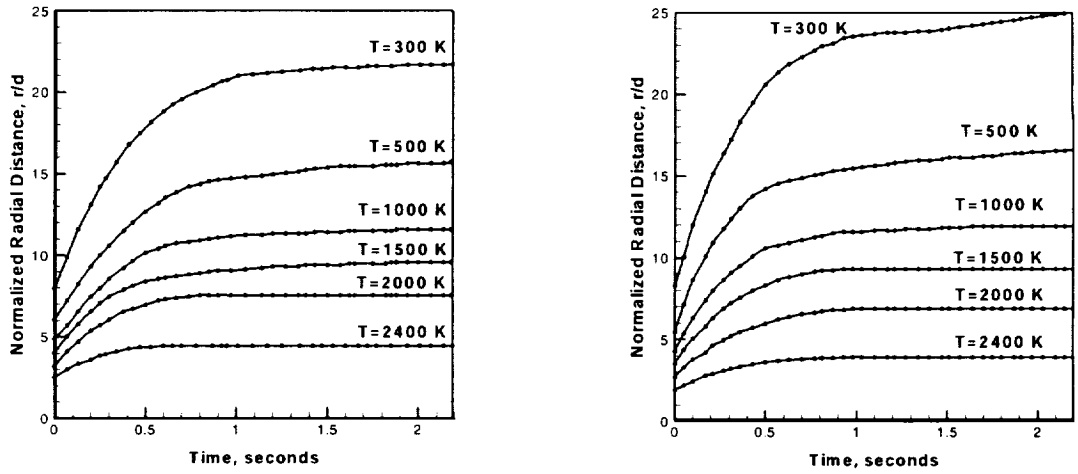

Figure 4. Temporal Evolution of Temperature Field in Drop Tower for d=1.19 mm; (a) Re=70, (b) Re=40

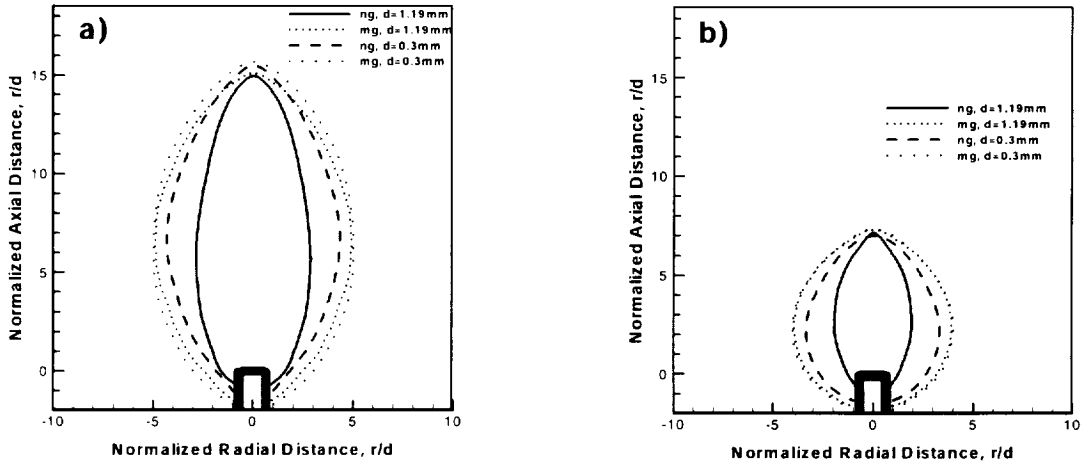

Figure 5. Flame Shape in Normal and Microgravity; (a) Re=70, (b) Re=40

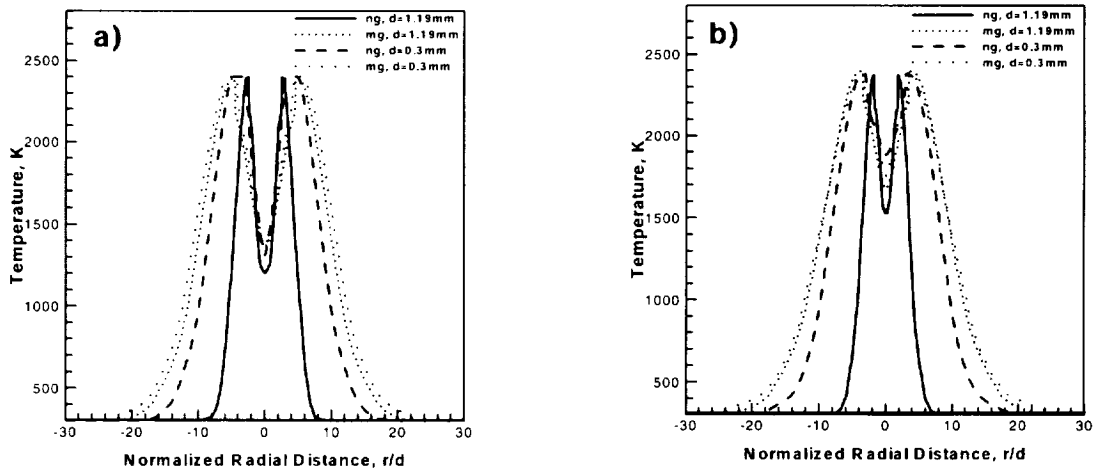

Figure 6. Temperature Profiles in Normal and Microgravity; (a) Re=70, (b) Re=40

Particle Clouds/Dusts

227-27

DETAILED STUDIES ON THE STRUCTURE AND DYNAMICS OF REACTING DUSTY FLOWS AT NORMAL AND MICROGRAVITY

M. GURHAN ANDAC, BRAD CRACCHIOLA, FOKION N. EGOLFOPOULOS & CHARLES S. CAMPBELL ,Department of Aerospace & Mechanical Engineering, University of Southern California, Los Angeles, California 90089-1453

INTRODUCTION

Dusty reacting flows are of particular interest for a wide range of applications. Inert particles can alter the flammability and extinction limits of a combustible mixture. Reacting particles can release substantial amount of heat and can be used either for power generation or propulsion. Accumulation of combustible particles in air can result in explosions which, for example, can occur in grain elevators, during lumber milling and in mine galleries [1]. Furthermore, inert particles are used as flow velocity markers in reacting flows, and their velocity is measured by non-intrusive laser diagnostic techniques. Despite their importance, dusty reacting flows have been less studied and understood compared to gas phase as well as sprays.

The addition of solid particles in a flowing gas stream can lead to strong couplings between the two phases, which can be of dynamic, thermal, and chemical nature. The dynamic coupling between the two phases is caused by the inertia that causes the phases to move with different velocities. Furthermore, gravitational, thermophoretic, photophoretic, electrophoretic, diffusiophoretic, centrifugal, and magnetic forces can be exerted on the particles. In general, magnetic, electrophoretic, centrifugal, photophoretic, and diffusiophoretic can be neglected [2,3]. On the other hand, thermophoretic forces, caused by steep temperature gradients, can be important. The gravitational forces are almost always present and can affect the dynamic response of large particles.

Understanding and quantifying the chemical coupling between two phases is a challenging task. However, all reacting particles begin this process as inert particles, and they must be heated before they participate in the combustion process. Thus, one must first understand the interactions of inert particles in a combustion environment.

The in-detail understanding of the dynamics and structure of dusty flows can be only advanced by considering simple flow geometries such as the opposed-jet, stagnation-type. In such configurations the imposed strain rate is well characterized, and the in-depth understanding of the details of the physico-chemical processes can be systematically obtained.

A number of computational and experimental studies on spray and particle flows (e.g. 2, 4-8) have been conducted in stagnation-type configurations. Numerically, the need for a hybrid Eulerian-Lagrangian approach has been identified by Continillo and Sirignano [4], and the use of such approach has allowed for the prediction of the phenomenon of droplet flow reversal [5,6]. Gomez and Rosner [2] have conducted a detailed study on the particle response in the opposed-jet configuration, and the particle thermophoretic diffusivities were determined experimentally. Sung, Law and co-workers [7,8] have conducted numerical studies on the effect of strain rate and temperature gradients on the dynamics of inert particles, as a way of understanding potential errors in experimental LDV data that may arise from thermophoretic forces.

OBJECTIVES

This investigation is a combined experimental and numerical study on the details of reacting dusty flows. The specific tasks are:

1. Experimental determination of laminar flame speeds, and extinction strain rates of dusty flows at normal- and micro-gravity as functions of the particle type, particle initial diameter, particle initial number density, and gas phase chemical composition.
2. Detailed numerical simulation of the experiments. Results are compared with experiments and the adequacy of theoretical models is assessed.
3. Provision of enhanced insight into the thermo-chemical coupling between the two phases.

EXPERIMENTAL APPROACH

The opposed-jet counterflow technique is used and is illustrated in Fig. 1. The burners are straight tubes with 22 mm diameter and 35 cm length. Honeycombs and steel screens are used in order to laminarize the flow. A cooling coil is wrapped around the top burner.

The particle seeder is the most important part of the experiment. It uses a piston technique similar to the one of Goroshin and co-workers [9]. Attached beneath the bottom burner is a piston shaft, and an electrically-driven linear actuator drives the piston. The piston shaft is filled with particles that are carried by the gas flow that enters at the top of the piston shaft through eight 1 mm diameter, equally-spaced holes. Dry particles are used so that agglomeration is reduced. In the present study inert aluminum oxide (Al_2O_3) particles are considered.

The particle seeding rate is calibrated by having air flowing for 30 seconds at three different piston speeds: 0.44, 0.87, and 1.30 mm/s. The air and particles are blown into a bag that is subsequently sealed. The mass of the bag is measured on a mass balance, accurate to 10 mg. This measurement is taken both before and after the particles are blown into the bag, so that the total mass of the particles is measured. The particle mass delivery and seeding rate for given piston speed and gas flow rate is then determined. This process is repeated 5 times and an average seeding rate is determined. The repeatability of the calibration was found to be approximately within 8%.

Experiments were conducted on the effect of inert particles on premixed flame extinction. Al_2O_3 particles of 1 and 25 micron average diameter were tested, in order to assess the effects of particle size. Lean methane/air and propane/air flames were first stabilized and subsequently the particles were seeded to the point of extinction. The extinction strain rate was determined through LDV.

NUMERICAL APPROACH

In this investigation, the particle number density is considered small enough so that there are no particle interactions. By assuming that there is no property variation in the radial direction, a quasi-one-dimensional set of equations was derived for the gas phase similarly to the traditional gas-phase formulation [10]. The particle equations were formulated for each particle independently, as particles are not allowed to interact.

For inert particles, the gas phase continuity and species equations are identical to the ones of Ref. 10, while the momentum equation was modified by adding a term which represents the force exerted by the particles on the gas phase. The energy equation for the gas phase was also modified by including a term describing the conductive/convective heat exchange between the two phases. The axial particle momentum equation includes the Stokes drag, thermophoretic, and gravitational contributions; the system configuration is assumed vertical (i.e., gravity points downwards). As the action of gravity and temperature gradients (and thus thermophoretic forces) only exists in the axial direction, the radial particle momentum equation includes only the contribution of the Stokes drag. The particle energy equation allows for the detailed heat diffusion within the particle and includes the contributions of conductive/convective heat exchange between the two phases, the radiative energy from the particle, and the energy that is radiated by the gas phase and is absorbed by the particles. Finally, a conservation equation for the particle number density was formulated.

Solutions are obtained by simultaneously integrating the entire system of equations for both phases. The gas phase equations are integrated in a Eulerian frame of reference while the particle equations are integrated in a Lagrangian frame of reference. Details on the equations formulation and solution procedure can be found in Ref. 3.

SUMMARY OF RESEARCH

The numerical simulations were conducted for opposed-jet, atmospheric, fuel-lean, laminar premixed H_2/air and CH_4/air flames seeded with inert Al_2O_3 particles. The nozzle exit velocities, u_{exit}, of the gas phase are identical for both nozzles. The particles are injected from one nozzle only with a velocity equal to the gas phase velocity, u_{exit}. The twin-burner assembly

is considered to be vertical so that the gravitational forces would act along the direction of the system centerline. Given the unidirectional nature of gravity, its effect on the particle dynamics is considered for three cases. The first case is that of (+g), in which the particles are injected from the bottom nozzle with the gravity opposing the particle axial motion. The second case is that of (-g), in which the particles are injected from the top nozzle with gravity favoring the particle axial motion. The third case is that of zero gravity (0-g).

Results show that the dynamic behavior of the particles depends on the relative magnitude of the drag, thermophoretic, and gravitational forces [3]. Figure 2 depicts results for heavy particles at (+g), (-g) and (0-g) which can also undergo flow reversal after crossing the gas phase stagnation plane (GSP). While gravity can have a nearly-obvious effect on the particle velocity, its effect on the mass flux and the thermal state of the particles is more subtle. Figure 3 depicts the spatial variation of the particle flux normalized by its injection value. It can be seen that the magnitude and direction of gravity can modify the rate of solid phase supply rate into the reaction zone. The effect of gravity on the particle thermal state is shown in Fig. 4. Again, it can be seen that the direction and magnitude of gravity has a noticeable effect on the particle temperature. The thermal effects on the gas phase was found to be significant as n_p increases. Figure 5 depicts the flame cooling and the eventual global extinction for a value of n_p about 25,000/cm^3. It is of interest to note the large discrepancy between the gas and particle temperature, a result of the large thermal inertia of the particles. It can be also seen that the cold jet that emerges from the right nozzle undergoes an early preheating by the particles as they penetrate deep into the right side of the GSP.

Extinction experiments have been conducted at normal gravity for lean CH_4/air and C_3H_8/air flames by seeding them with 1 and 25 micron particles. Representative results for C_3H_8/air flames are shown in Fig. 6. As expected, it can be seen that for larger particle mass flow rate flames of higher equivalence ratio can be extinguished. Furthermore, results show that the 1 micron particles cool the flame more effectively and facilitate extinction, compared to the larger 25 micron particles. This is a result of the larger surface to volume ratio that the 1 micron particle possess compared to the 25 micron particle.

REFERENCES

1. Faraday, M. & Lyell, C.: Report to the Home Secretary on the Explosion at the Haswell Colliery on 28 Sept. 1844; also Phil. Mag. 26, p. 16, (1845).
2. Gomez, A. & Rosner, D.E.: *Combust. Sci. Tech.* 89, pp. 335-362, (1993).
3. Egolfopoulos, F.N. & Campbell, C.S.: *Combust. Flame.* 117, pp. 206-226, (1999).
4. Continillo, G. & Sirignano, W.A.: *Combust. Flame* 81, pp. 325-340 (1990).
5. Chen, N.-H., Rogg, B. & Bray, K.N.C.: *Twenty-Fourth Symposium (International) on Combustion*, Combustion Institute, Pittsburgh, 1992, pp. 1513-1521.
6. Chen, G. & Gomez, A.: *Twenty-Fourth Symposium (International) on Combustion*, Combustion Institute, Pittsburgh, 1992, pp. 1531-1539.
7. Sung, C.J., Law, C.K. & Axelbaum, R.L.: *Combust. Sci. Tech.* 99, pp. 119-132 (1994).
8. Sung, C.J., Kistler, J.S., Nishioka, M., & Law, C.K.: *Combust. Flame* 105, pp. 189-201 (1996).
9. Goroshin, S., Kleine, H., Lee, J.H.S. & Frost, D. Microgravity Combustion of Dust Clouds. Quenching Distance Measurements. *Third International Microgravity Combustion Symposium*, NASA Lewis Research Center, Cleveland, Ohio, Apri, 1995.
10. Egolfopoulos, F.N. & Campbell, C.S.: *J. Fluid Mech.* 318, pp 1-29 (1996).

ACKNOWLEDGEMENTS

This work is supported by NASA under Grant NAG3-1877 under the technical supervision of Drs. Randall Vander Wal and Ming-Shin Wu of the Lewis Research Center.

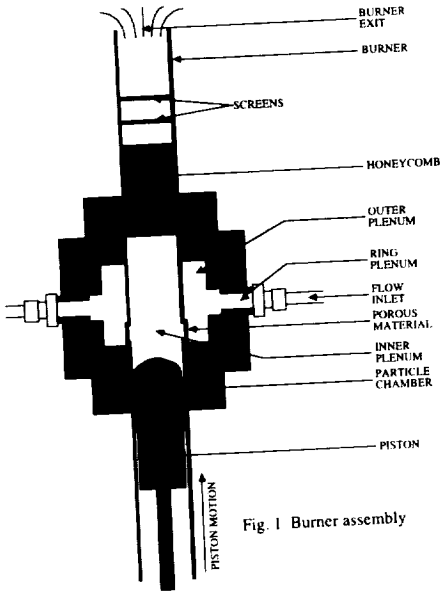

Fig. 1 Burner assembly

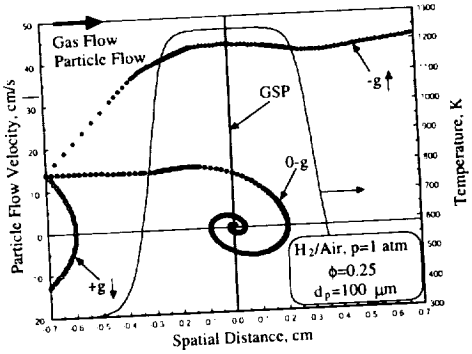

Fig. 2 Effect of gravity on particle velocity

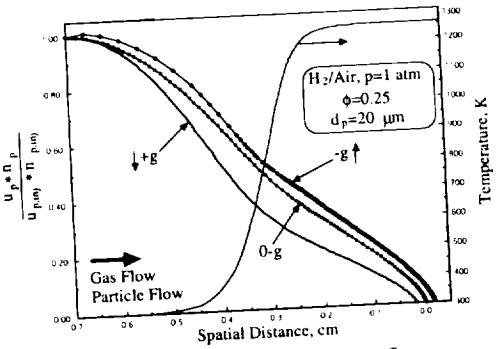

Fig. 3 Effect of gravity on particle mass flux

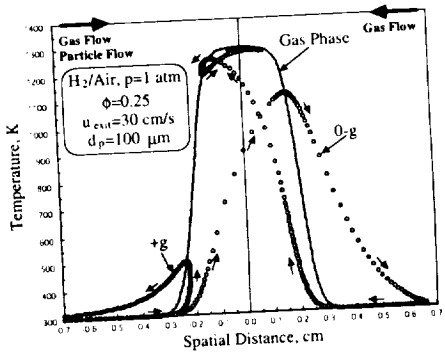

Fig. 4 Effect of gravity on particle temperature

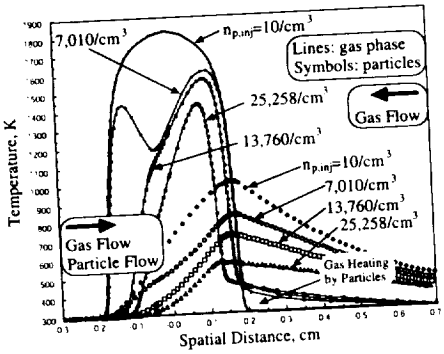

Fig. 5 Numerical results on flame extinction through particle addition

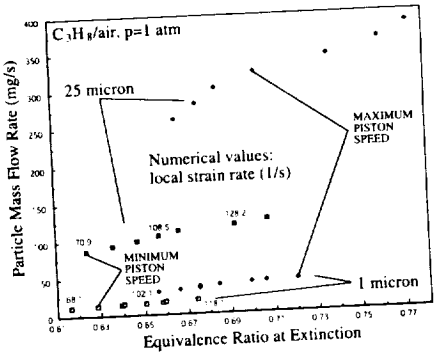

Fig. 6 Experimental results on flame extinction through particle addition

528-29

COMBUSTION MECHANISM OF DUST CLOUDS IN MICROGRAVITY

Jozef Jarosinski and Jerzy Podfilipski, Department of Heat Technology and Refrigeration
Technical University of Lodz, Stefanowskiego 12/16, 90-924 Lodz, Poland,
E-mail: jarosin@ck-sg.p.lodz.pl

INTRODUCTION

Combustion of suspended solid particles in air is important from the point of view of explosion hazards and several areas of modern combustion technology (various combustion systems of coal, propulsion systems etc). However, the physical mechanism of dust cloud combustion is still not well understood in comparison with a similar mechanism related to combustion of homogeneous gas mixtures.

For a long time various closed vessel bombs were used to study combustion of dust mixtures, mainly by simulating the explosion conditions in accidents and by classifying the relative level of hazards of different dusts. Cognitive value of closed vessel bomb experiments was very limited and resolved itself into collection of various empirical coefficients and indexes. Empirical knowledge from closed vessel bomb experiments was compiled in a number of monographs (book of W. Baknecht [1] is a good example).

Apart from closed vessel bomb experiments, parallel investigations were carried out in search of reliable fundamental data on dust combustion. These data imitated parameters typical for homogenous gas flames, such as laminar burning velocity [2, 3, 4], minimum ignition energy [5, 6], quenching distance [7, 8, 9] and flame thickness [3, 7, 9]. It was found in these experiments that values of measured parameters were comparable with experimental data for gas flames. Because the order of magnitude of measured dust flame parameters was the same as in gas flames, the processes controlling flame propagation in these flames should be similar. All these data support the opinion of Smoot and co-workers, who reported series parametric predictions to identify the controlling processes in premixed fine coal dust-air flame [3]. It has been found as a result of these predictions, that the rate of flame propagation is controlled by the rate of streamwise molecular diffusion of oxygen and volatiles, together with heat conduction from the hot gas to the particles.

On the other hand dust flames are very different from gas flames propagating in homogenous mixtures. Basic differences between combustion of dust clouds and homogenous gas mixtures result mainly from differences in properties of those mixtures. Dust cloud is heterogeneous mixture. None method of dust formation can secure uniform dust concentration. Turbulence usually present in dust cloud combustion, differentiates local dust concentration, due to its vortical structure (centrifugal effect). Non-uniformity of dust concentration results in more diffusional combustion regime. In gas flames the entire heat is released at the flame front. In dust flames, only small part of heat is released at the front, the remaining part being released far behind it. In other words, propagation of the flame front through the dust mixture is not equivalent to release of the entire heat contained in the dust fuel.

Most of the experiments on dust combustion are carried out in vessels with pneumatic dispersion systems, where turbulent mixing creates a dust-air mixture. In experiments carried out in microgravity conditions turbulent pulsations decay very fast (in similar experiments carried out in [10] RMS velocity decreased from 10 m/s to 0,5 m/s in 0,2 s), while dust particles continue to be in suspension. In such conditions flame propagates in quiescent mixture with very different local concentration. This would result in different local burning velocities and in diffusional combustion behind the flame front.

The objective of the present work is to report an experimental comparative study on the effect of turbulence and ignition system on dust combustion in the constant volume vessel and in open tube, provided both in ground conditions and in microgravity environment (created by falling assembly in the drop tower).

EXPERIMENTAL FACILITY

The schematic of the combustion vessel used for experiments is shown in Fig. 1. The vessel has volume of 8.4 liter. The side walls of the vessel, in the shape of a cylindrical tube, are made of transparent organic glass (0.172 m inner diameter and 0.36 m length; L/D = 2.1). The experiments were carried out in a closed (constant volume) or vented (constant pressure) vessel.

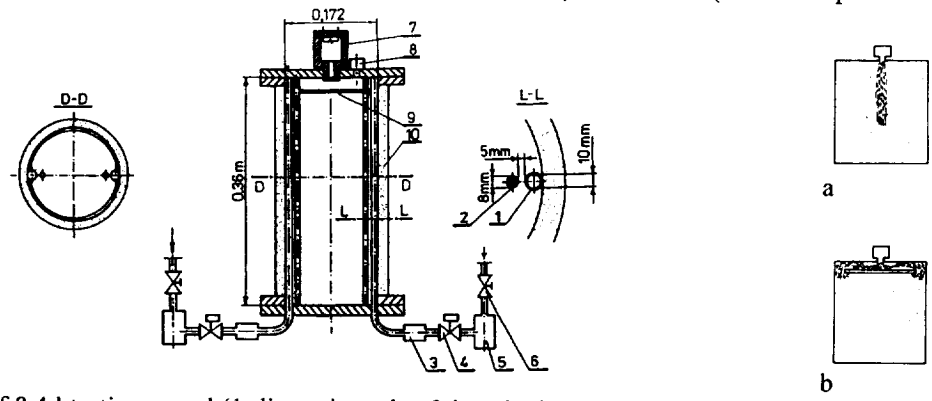

Fig.1. Structure of 8.4 l testing vessel (1-dispersion tube; 2-bar; 3- dust vessel; 4-magnetic valve; 5-air reservoir; 6-mechanical valve; 7-ignitor; 8-pressure transducer; 9-disc; 10-transparent wall); a-center ignition; b-top ignition.

The dispersion system, characterized by a small scale of turbulence is described in detail in [10]. A gas igniter, with an energy of 0.2 kJ, was used to ignite the mixture by a stream of hot combustion gases flowing from its reservoir of capacity 60 cm^3. Combustion gases could ignite the dust mixture in the central part of the vessel (volume ignition - Fig. 1a) or in the top part of the vessel (surface ignition - Fig. 1b). The pressure history was measured by the transducer FTSV 2100 and recorded by an AD card installed in a PC.

Cornstarch ($C_6H_{10}O_5$) was used as a fuel. The particles were nearly spherical in shape with a mean diameter of 11 μm.

Microgravity experiments were conducted in the Department of Heat Technology and Refrigeration of the Technical University of Lodz, in a drop tower, which could provide 10^{-2}g conditions for 1,2 seconds.

RESULTS AND DISCUSSION

It was found before [10], that dust suspension was almost stationary under microgravity conditions. This makes possible, for a long ignition delay time, to study dust explosion in microgravity environments, practically without influence of turbulence. To diminish the effect of turbulence on the combustion process, the ignition delay time 500 ms was used in the experiments. The experiments were carried out under normal gravity and microgravity conditions. The curves obtained under normal gravity conditions decrease their peak values and the rate of pressure rise in comparison with the gravity curves due to gravity sedimentation. The pressure curves as a function of time, for the constant volume combustion of cornstarch dust-air mixture, are shown in Fig. 2.

Direct photography was used to visualize the combustion process (Figs.3 and 4). Development of combustion was recorded by a high-speed video camera. Intensity of light during the initial and final stages of combustion varied by several orders of magnitude. The light from the flame front was week, but from the reburning regions very bright.

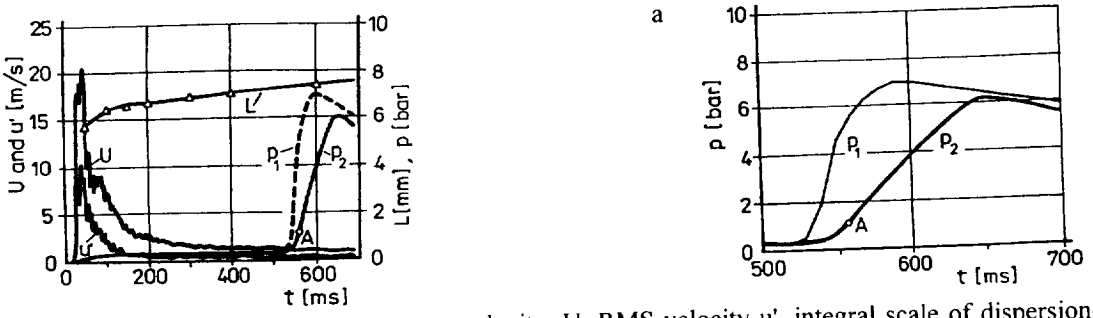

Fig.2. Variation of the ensemble instantaneous velocity, U, RMS velocity u', integral scale of dispersion-induced turbulence, L, measured in similar vessel [10] and explosion pressure in present experiments (p_1-center ignition, p_2-top ignition) -as functions of time for cornstarch (d_p=11 m, ϱ_d=500g/m^3, t_i=500ms). a) Fragments of pressure curves with extended time scale.

Visualization of combustion process under microgravity conditions, for ignition delay time 500 ms, showed irregular flame front and irregular distribution of the regions with local chemical reactions at the early stage of combustion (Fig. 3). Random distribution of the flame front and reburning regions shows, that despite the use of the carefully selected dispersion system, the distribution of the dust in the dust-air mixture was not uniform.

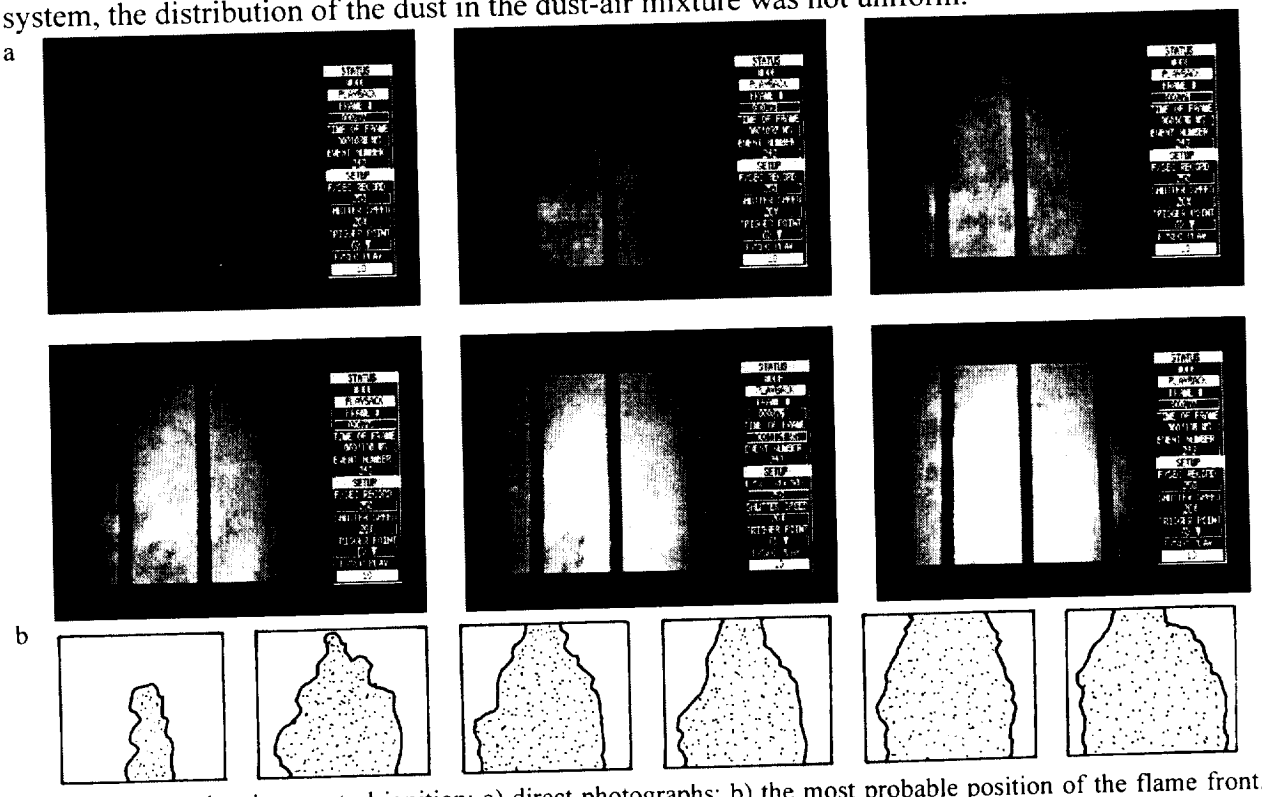

Fig.3a. Dust combustion, central ignition; a) direct photographs; b) the most probable position of the flame front. Framing rate 250 frames/s.

Mixture ignited by a stream of hot gases in the center of the vessel burns faster than that ignited at the upper part of the vessel (see Figs. 2 and 4). The maximum pressure is also higher for central ignition. This means that the heat release rate is higher for the central ignition (volume combustion) than for the top ignition (surface combustion in the flame front). Bend on the pressure curve, related to combustion with central ignition, indicates onset of heat transfer to the walls. Non-uniform dust concentration distributed random within the vessel volume does not change much during the combustion process. This conclusion can be deduced from the analysis of the video records, which indicate that bright regions representing fast reactions are quiescent.

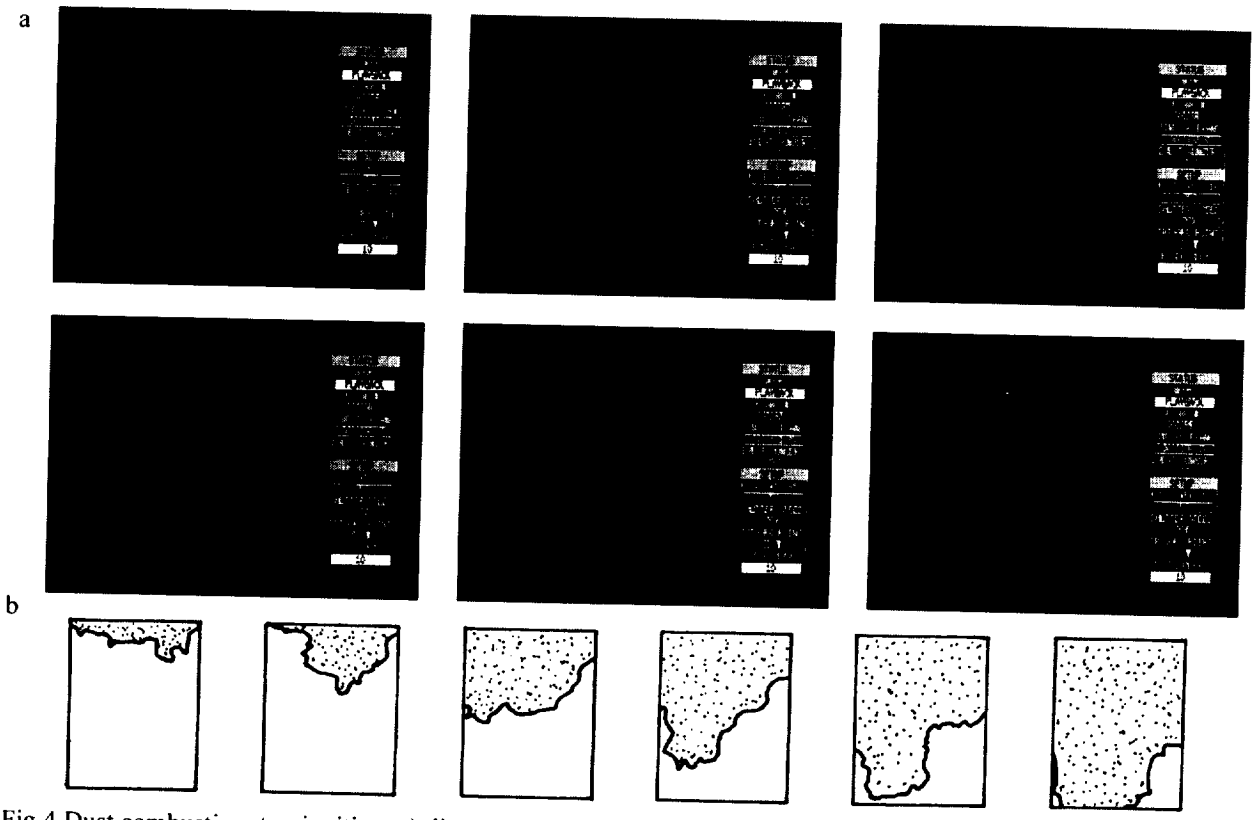

Fig.4 Dust combustion, top ignition; a) direct photographs; b) the most probable position of the flame front. Framing rate 250 frames/s.

During flame propagation from the top to the bottom of the vessel (after top ignition) only small part of the entire heat is released (point A in Fig. 2), the other part being released far behind the flame front, in the reburning regime. From the beginning of the combustion process, in this case, the flame front and the hot combustion gases are in direct contact with the walls transferring heat, which results in relatively gentle slope of the pressure curve. Video records show that at the final combustion stage the hot regions generate turbulence.

ACKNOWLEDGEMENTS

The State Committee for Scientific Research (KBN) sponsored this work, grant No. 9T12A02711.

REFERENCES

1. Barknecht W., Explosion –Course, Prevention and Protection, Springer Verlag, New York, 1980.
2. Cassel H. M., Gupta A. K. and Gumswamy S., Third Symposium on Combustion and Explosion Phenomena, Baltimore pp. 185-190, 1949.
3. Smoot L.D., Hedman P.O. and Smith P.J., Prog. Energy Combust. Sci., **10**: 359-441,1984.
4. Goroshin S., Fomienko I. and Lee J.H.S., Twenty Sixth Symposium (International) on Combustion, The Combustion Institute, 1996
5. Eckhof R.K., Combust. Flame, **24**: 53-64, 1975.
6. Hertzberg M., Conti R.S. and Cashdoller K.L., Twentieth Symposium (International) on Combustion, The Combustion Institute, pp. 1681-1690, 1984.
7. Jarosinski J., Lee J.H.S., Knystautas R. and Crowley J.D., Twenty First Symposium (International) on Combustion, pp. 1917-1924, 1986.
8. Proust Ch., Veyssiere B., Combust. Sci. Technol., **62**: 149-172, 1988.
9. Goroshin S., Bidabadi M. and Lee J.H.S., Combust. Flame, **105**: 147-160, 1996.
10. Pu Y., Podfilipski J. and Jarosinski J., Combust. Sci. Technol., **135**: 255-267, 1998.

LAMINAR DUST FLAMES: A PROGRAM OF MICROGRAVITY AND GROUND BASED STUDIES AT McGILL.

Sam Goroshin and John Lee
McGill University, Department of Mechanical Engineering, 817 Sherbrooke St. West, Montreal, Quebec, Canada H3A 2K6, e-mail: goroshin@mecheng.lan.mcgill.ca

Dust combustion and microgravity. Fundamental knowledge of heterogeneous combustion mechanisms is required to improve utilization of solid fuels (e.g. coal), safe handling of combustible dusts in industry, and solid propulsion systems. The objective of the McGill University research program on dust combustion (sponsored by the Canadian Space Agency and NASA) is to obtain a reliable set of data on basic combustion parameters for dust suspensions (i.e. laminar burning velocity, flame structure, quenching distance, flammability limits, etc.) over a range of particle sizes, dust concentrations, and types of fuel. This set of data then permits theoretical models to be validated and, when necessary, new models to be developed to describe the detailed reaction mechanisms and transport processes.

Microgravity is essential to the generation of a uniform dust suspension of arbitrary particle size and concentration. When particles with a characteristic size on the order of tens of microns are suspended, they rapidly settle in a gravitational field. To maintain a particulate in suspension for time duration adequate to carry out combustion experiments invariably requires continuous convective flow in excess of the gravitational settling velocity (which is comparable with and can even exceed the dust laminar burning velocity). This makes the experiments turbulent in nature and thus renders it impossible to study laminar dust flames. Even for small particle sizes on the order of microns, a stable laminar dust flow can be maintained only for relatively low dust concentrations at normal gravity conditions. High dust loading leads to gravitational instability of the dust cloud and to the formation of recirculation cells in the dust suspension in a confined volume [1], or to the rapid sedimentation of the dense dust cloud, as a whole, in an unconfined volume [2]. Many important solid fuels such as carbon and boron also have low laminar flame speeds (of the order of several centimeters per second [3,4]). Convection that occurs in combustion products due to buoyancy disrupts the low speed dust flames and makes observation of such flames at normal gravity difficult.

Ground-based experimental equipment. Due to the limited number of experiments that can be carried out in a microgravity environment, it is essential that ground-based studies supplement microgravity experiments, even if only in the narrow range of dust parameters that are not severely effected by gravitational sedimentation. Two ground-based apparatuses were developed at McGill permitting observation of dust flames in tubes [5] and also burner-stabilized [6] dust flames in the particle size range 1-10 μm with dust concentrations up to 500 g/m^3 (aluminum). The design of both apparatuses is based on a dispersion system (described elsewhere [5]) that permits continuous generation of the uniform, controllable laminar dust flows. These two apparatuses are used to study different aspects of the flame propagation. Flames in tubes can be observed in a wider range of dust concentrations than stabilized flames and are used to study flame propagation limits and quenching distances [5]. It was found that to deduce an accurate data on burning velocity from the tube experiments is difficult due to the complex flow field ahead of the flame front and difficulties in accurately measuring the flame surface area. Furthermore, the

acoustic instability that develops for the dust flames in tubes with small particle sizes [7] considerably shortens the laminar stage of the flame propagation. Bunsen-type dust flames were found to be a more accurate means for the measurement of the burning velocity as they show well defined flame cones in micron-size dust suspensions. Thus stabilized flames are used to study the effects of the dust and oxygen concentration and the molecular transport properties of the carrier gas on laminar flame burning velocity [6].

Microgravity dust combustion apparatus. The longest microgravity duration available in ground-based facilities is about 22 seconds on board parabolic flight aircraft. A relatively long time is required for the stabilization of a dust flame in a burner. Since it is difficult to operate a dust burner in parabolic flight, our current microgravity experiments are based on observation of the dust flames propagating in semi-opened tubes with free expansion and overboard venting of the combustion products. The detailed design of the microgravity apparatus is described in [8]. It employs the same type of dust dispersion system as our ground-based facilities. Conical nozzles installed at the ends of the tubes help to suppress acoustic excitation of the flame. The apparatus was tested by measuring flame quenching distances in aluminum dust clouds over a wider range of dust concentrations and particle sizes than in the ground-based experiments. Experimental data for dust concentrations as high as 1200 g/m^3 and particle sizes 18 μm were obtained in KC-135 parabolic flights [8]. These tests have also highlighted the need to develop reliable diagnostics for the measurement of local and average dust concentration as well as particle size distribution. At present, a laser light attenuation probe is used to monitor the dust concentration. For small particle sizes and low dust concentrations it can be calibrated on the ground by using a sampling method for the average dust concentration measurement (i.e. by aspiration of a known volume of the dust suspension through a filter). For high dust loading and larger particle sizes this calibration procedure has to be performed in situ (i.e. in parabolic flight), as microgravity is needed to maintain a stable dust suspension for these cases. An effort is now underway at McGill to develop a β-radiation absorption probe to measure and monitor the dust concentration. The absorption of β-radiation is directly related to the mass of the solid material between a radiation source and the detector, and is largely independent of the particular dust particle size and shape. Sheets of material of known thickness inserted between the source and detector can be used to calibrate the probe, eliminating the need of in-situ calibration in microgravity environment. Microgravity experiments have also indicated a considerable secondary (after dispersion) agglomeration of the particles in dense dust flows. Due to such agglomeration, the actual particle size distribution differs considerably from the particle size distribution in the initial dust. A laser light scattering probe [9] has to be developed to monitor particle sizes and the agglomeration process.

Dusts. The properties of the dust fuel can range from highly volatile organic solids to refractory metals that hardly produce any gaseous products during combustion. We chose the latter for the present study as they yield nearly pure heterogeneous combustion. Metallic dusts with the boiling points above flame temperatures are perhaps the most suitable for fundamental study since they are pure substances with well-defined phase transitions. It is also important that the metal powders are commercially available in spherical shape and in a variety of different sizes. Refractory metals such as zirconium and hafnium, which we are planning to employ in the future, are especially attractive. They do not form protective oxide films, thus their ignition temperatures are low. Their flame temperatures (in diluted oxygen mixtures) are below the boiling points both

of the metal and the combustion products, and they also do not form intermediate gaseous oxides (as, for example, aluminum, boron, and carbon) [10]. Therefore, their reaction fronts are completely free of continuous gas flames.

Theoretical approach. Due to the complexity of the mechanisms of heterogeneous dust combustion, the field is relatively underdeveloped (compare to homogeneous flames). Thus, it is necessary to isolate and examine each specific aspect of dust flame at first separately using simple (preferably analytical) models. These models should provide a clear and unambiguous prediction that can be readily verified in a specifically designated experiment. Examples of such theoretical problems are given below.

Effect of the discrete nature of heat sources in dust suspensions. In spite of the clearly discrete nature of the heat sources in a burning dust suspension, the source term in the energy conservation equation of most flame propagation models is considered to be a continuous function of spatial coordinates. The validity of this assumption has been recently examined in [11] by comparing dust flame speeds predicted by a continuous and by a discrete heat source model. The flame speeds obtained from continuous and discrete models coincide if the particle combustion time is much longer than the characteristic time of heat transfer between particles. In the opposite case, for fast (compared with the time of heat transfer between particles) burning fuels, the flame speed in the discrete system is a weak function of the particle combustion rate and is an explicit function of the distance between particles. Compared to the continuum description, the discrete source model predicts much lower flame speeds and a weak dependence of the flame speed on oxygen concentration in lean aluminum-air and zirconium-air suspensions. In our current study, the model will be extended to investigate the effects of the discrete nature of combustion on flame propagation limits and quenching distance. Microgravity experiments with lean zirconium dust clouds are planned to verify these predictions.

Effect of the regime of particle combustion. The combustion rate of a solid fuel particle in a gaseous oxidizer can be limited either by reaction kinetics or by the molecular transport of the oxidizer to particle surface. Therefore, within the flame reaction zone, there are two competing rates, the usual kinetically-controlled rate, and the rate of oxygen diffusion to the particles' surface. Preliminary models [12] have indicated a significant dependence of the flame structure on the underlying rate-controlling mechanism. Our proposed theoretical model will examine the competition in order to detail the resulting flame structure and its dependence on key parameters, such as particle radius (already recognized to be a principal control parameter in the competition). Domination by one rate will not be uniform within a given flame configuration (as in our preliminary models), but instead, each mechanism will dominate in a different layer within a single reaction sheet. Numerical investigations have already indicated unexpected variations in the front speed when the two effects are comparable in significance [12]. The balance and interplay of the kinetic and diffusively controlled regimes will be experimentally verified using solid fuels known to have a considerable kinetic resistance such as carbon and boron [13]. Microgravity will allow flame propagation experiments to be performed over a wide range of particle sizes, and therefore the transition from the predominantly kinetic flame (small particle sizes) to the flame controlled by microdiffusion processes (large particle sizes) can be observed.

Effect of dust polydispersity. With the exception of a few special dusts (e.g. licopodium), most dusts used in experiments have a continuous spectrum of particle sizes in a specific size range. All known theoretical flame models consider dust suspension as monodisperse. The validity of such an approximation has not yet been analyzed and the rules for the "averaging" of particle sizes in application to dust flames have not been established. This makes it difficult to quantitatively compare experimental results from different sources as every particular dust has its unique particle size distribution. Theoretically, we will approach this problem by analyzing flames in a suspension of two monodisperse dusts of different particle size and, in general, of a different chemical nature. This analytical analysis will then be experimentally tested by observing the flame speed in a binary suspension of two dusts with a very narrow range of particle size distribution.

The problems described above are by no means complete for a comprehensive understanding of dust combustion. Questions such as the role of radiation, particle motion in the flame front, and non-premixed (diffusive) dust flames in a coaxial burner should also be investigated. It is also apparent that due to the complexity and practical importance of dust combustion, a coordinated international effort is imperative in the success of the program.

REFERENCES

1. Green, F.T., and O'Donnell, J.E., *US Bureau of Mines, Report of Investigation* OFR 4-83 (1981)
2. Fuchs, N.A., *The Mechanics of Aerosols*, The Macmillan Company, NY (1964)
3. King, M., *22nd JANAF Combustion Meeting*, CPIA Pub., V. 1, 361-376 (1985)
4. Goroshin, S., Ageyev, N., Shoshin, Yu, Shevchuk, V., *Combustion of Boron-Based Solid Propellants and Solid Fuels*, Ed. K.K. Kuo and R. Pein , CRC Press, Ann Arbor, 469-477 (1992)
5. Goroshin, S., Bidabadi, M., Lee, J.H.S., *Comb. and Flame* V.105, 147-160 (1995)
6. Goroshin, S., Fomenko, I., Lee, J.H.S., *Proceedings of the Twenty-Sixth International Symposium on Combustion*, Combustion Institute, Pittsburgh, 1961-1967 (1996)
7. Goroshin, S., Shevchuk, V., Ageyev N., *Combust., Expl. and Shock Waves*, 595- 600, May (1982)
8. Goroshin, S., Kleine, H., Lee, J., Frost, D., *NASA Conference Publication* 10174, 141-146 (1995)
9. Jones, A.R., *Progr. Energy and Comb. Sci.*, V. 25, No. 1, 1-55 (1999)
10. Gupta, S.K., Maloney, K.M., J., *Appl. Phys.*, V. 44, No. 7, 3339-3346 (1973)
11. Goroshin, S., Lee J., *Proceedings of the Twenty-Seven International Symposium on Combustion*, Combustion Institute, Pittsburgh, (1998) - in press
12. Goroshin, S., Shoshin, Yu., Zolotko, A., *Phys. Chem.*, 321, 816-819 (1992)
13. Zhou, W., Yetter, R.A., Dryer F.L., Rabitz, H., Brown, R.C., Kolb, C.E., *Comb. and Flame* V.117, 228-243 (1999)

PRELIMINARY ANALYSIS OF A HIGH PRESSURE SPRAY AND CLOUD COMBUSTION MODULE FOR THE ISS

I. Gökalp[1], C. Chauveau[1], D. Durox[2], F. Lacas[2], B. Legrand[1] and E. Shafirovich[1]

[1] Laboratoire de Combustion et Systèmes Réactifs,
Centre National de la Recherche Scientifique, 45071 Orléans cedex 2, France
gokalp@cnrs-orleans.fr
[2] Laboratoire EM2C, Centre National de la Recherche Scientifique, Ecole Centrale de Paris,
Grande Voie des Vignes, 92295 Chatenay-Malabry, France

Introduction

Combustion of droplet sprays and particle clouds is a very important area due to numerous applications to engines and power systems as well as to problems of industrial safety and clean environment. However, combustion of two-phase systems is not well understood yet.

The detailed characterization of single droplet and particle burning necessitates the determination of temperature and chemical species concentration fields. Such measurements necessitate spatial and temporal resolutions that are impossible to attain with small particles. Therefore, one is obliged to move to larger droplet or particle sizes, and this brings in natural convection effects, which are proportional to the third power of the system characteristic dimension. In addition, natural convection effects are strongly increased under high pressure as they scale with the square power of ambient pressure. Furthermore, under supercritical conditions, the classical experimental technique of fiber suspended droplets is no longer applicable because of the drastic reduction or even annihilation of the surface tension.

In the combustion of sprays or clouds gravitational effects add another difficulty due to the sedimentation of the particles and droplets. Indeed, stability of a spray or a cloud under normal gravity can only be achieved by stirring this two-phase mixture which produces a turbulent flow field. Therefore, under normal gravity conditions, the combustion characteristics of two-phase mixtures can only be obtained in turbulent flow. On the other hand, and namely for high-pressure conditions, these characteristics are in fact also strongly influenced by natural convection.

The advantage of performing such experiments under reduced gravity are therefore twofold. First, as for single droplet or single particle experiments, the effects of natural convection are removed. But, furthermore, by preventing natural sedimentation of droplets and particles, experiments can be done under non-turbulent conditions. Fundamental characteristics of two-phase combustion, such as ignition and stability limits and flame propagation rates, can be determined independently of flow and turbulence conditions and then used for model validation.

It is proposed to develop a combustion facility for the International Space Station, which would make it possible to study high pressure combustion of spray and clouds as well as of single droplets and particles under microgravity. In this paper we present results of our preliminary analysis of possibilities to develop a high pressure spray and cloud combustion module for the ISS. We analyzed previous experiments on combustion of clouds and sprays under conditions of both normal and reduced gravity from the standpoint of working out the optimum techniques for the use onboard the ISS. The reader can find more details of this analysis in Ref. 1. On the basis of this analysis, some promising methods were identified and tested experimentally in parabolic flights of A300 ZERO-G aircraft in December 1998 and March 1999.

Analysis of previous experiences in the spray and cloud combustion area

Methods of droplets spray formation

Several techniques are identified by literature survey in the field of liquid spray formation by atomization for small scale experiments. We have classified the techniques in different groups. Table 1 shows the characteristics of the atomizers. It clearly shows that there is no ideal solution and that some compromise has to be found. In many circumstances, it is important to consider the quality of the spray in terms of physical parameters as the droplet size distribution or the mean velocity field. For an application designed to study flame propagation in a droplet spray, these two parameters seem to be the most relevant. For a space based experiment at high pressures, technological complexity is also important. Therefore, surface instabilities and electrostatic atomizers seem to be good candidates. But microgravity experiments are necessary to check their ability to work under these conditions.

Table 1 *Main characteristics of the different atomizer types*

	Liquid Jet Atomizer	**Air Assisted Atomizer**	**Jet Instabilities**	**Surface Instabilities**	**Electro-Static Spray**	**Condensa-tion Spray**
Droplets size dispersion	Broad	Broad	Very narrow	Narrow	Very narrow	Narrow
Possible liquid flow rate	Small to large	Small to large	Very small	Small	Small	Very small
Initial kinetic energy of drops	Very high	High	High	Small	Small	Very small
Design and fabrication technology	Intermediate	Easy	Difficult	Intermediate	Intermediate	Difficult
Use at high pressure	Easy	Intermediate	Easy	Easy	Easy	Difficult

Methods of particle cloud formation

Several methods of particle cloud formation have been used previously in studies on combustion of particle clouds. Some of them have been employed in previous microgravity experiments. We propose to use the method of cloud generation by means of compressed air. In normal gravity researchers place a powder sample before the experiment either directly into a combustion chamber, or into a special small chamber for mixing with air and subsequent transport of the produced two-phase mixture into the combustion chamber. The latter method is suitable for experiments onboard the ISS.

Combustion chamber

Chambers of different volumes and shapes have been used previously for dust explosion testing and basic combustion research. Small chambers may not be suitable due to high heat loss to the walls. Moreover, radiation may play an important role in dust combustion, and in the possible case of long absorption length, a large size chamber is required. With consideration for the limited mass and volume of the ISS facilities as well as for comparison with results of numerous

studies in normal gravity, it appears reasonable to envisage a 20-l chamber. For optical diagnostics, the chamber must have 2 or 3 windows of sufficient surface area. The chamber should be designed for high pressure experiments: a preliminary target is 20 bar. Cloud and spray combustion is often accompanied by deposition of condensed products on the chamber walls and windows. Precautions must be taken to insure that the windows will be clear at least before a new experiment.

Methods of spray/cloud ignition

For experiments onboard the ISS, it would be desirable to have an ignition system without any mounting before each experiment. A wire heated by electric current and an electric spark seem to be suitable for the proposed experiments. Such igniters have been used in previous microgravity experiments on particle cloud combustion. A laser pulse seems to be a very convenient tool for the experiments onboard the ISS, since no element should be mounted inside the combustion chamber. The main problems are difficulties in the determination of the energy absorbed by particles/droplets, and small ratios of energy to mass for most of the available lasers.

Experiments with single droplets and particles

The facilities under development will be used also for studies on combustion of single droplets and particles. Recent experiments with free Al particles in parabolic flights [2] have shown that the burning particles move intensively in microgravity due to asymmetrical flame shapes, resulting in difficulties of observations and measurements. It is therefore rational to work with fixed, relatively large droplets or particles. Microgravity makes possible to work with relatively large drops and particles, when the heat transfer into a supporting fiber or wire is reduced to a minimum, without the complicating effect of convection. Laser heating or small wire igniters are the most suitable tools for ignition of single droplets and particles in microgravity.

Diagnostics

It would be highly desirable in the planned experiments to determine the three-dimensional velocity distribution of the gas phase, droplets and particles as well as distributions of gas temperature, density and chemical species concentrations. Present studies on spray and cloud combustion generally use qualitative methods, such as shadowgraphy, to visualize the development of the flame front. Holographic and interferometric methods could be also useful for this purpose. Direct emission spectroscopy may help determine different reactive species distribution, if axisymmetry is conserved, by using inversion methods. This technique has been employed to the study of laminar gaseous diffusion flames during parabolic flights [3]. One very promising technique for cloud and spray combustion studies is the particle imaging velocimetry (PIV), which is a 2-D measurement technique where a pulsed laser light sheet (or white light flash lamp source) is used to illuminate a flow field seeded with tracer particles small enough to accurately follow the flow. The positions of the particles are recorded on either photographic film or digital CCD cameras at each instant the light sheet is pulsed. The data processing consists of either determining the average displacement of the particles over a small interrogation region in the image or the individual particle displacements between pulses of the light sheet. Knowledge of the time interval between light sheet pulses then permits computation of the flow velocity. PIV captures the instantaneous flow field, permitting the study of unsteady flow phenomena. Mean flow statistics can be computed by acquiring several hundred images and averaging the results.

Preliminary tests in microgravity

Parabolic flights onboard A300 Zero-G aircraft provide a way for testing under microgravity the main units of the planned spray and particle cloud combustion module. The test of the particle cloud formation system by the LCSR team has started during the parabolic flight campaign organised by CNES in December 1998. Figure 1 shows a schematic diagram of the set-up to be tested. The process of cloud formation is observed visually and by means of a CCD-camera. Light extinction methods are used to monitor the dynamics of cloud formation in different sections of the chamber.

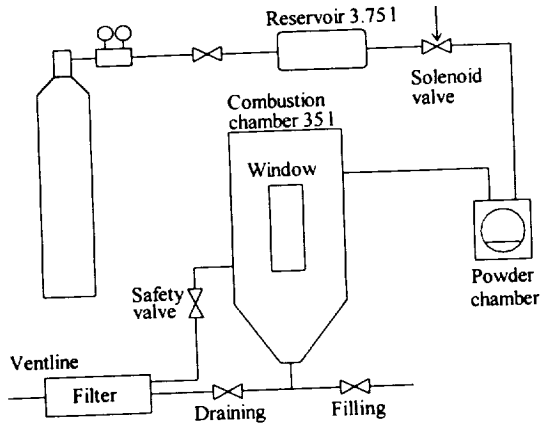

Figure 1 *Experimental set-up used in parabolic flight experiments in Dec. 1998*

A modified version of this set-up has been tested during the March 1999 CNES parabolic flight campaign. In these experiments a cleaning system and PIV diagnostics have been successfully employed. This version of the set-up includes a 70-l cylindrical steel chamber with several windows and a 4-l cylindrical glass chamber inside. The glass chamber is closed at the top by a piston, which can move down cleaning the chamber walls after the experiment. The piston is controlled with a pneumatic mechanism. The PIV system includes 2 pulsed Nd:YAG lasers, a CCD camera and a PC.

Conclusions

Analysis of experimental methods and facilities for studies in spray and particle cloud combustion areas has been made from the standpoint of their use in future experiments onboard the ISS. Suitable methods have been identified for spray and cloud formation and ignition. Some design solutions and methods of diagnostics have been tested in parabolic flight experiments.

Acknowledgements

The present wok is supported by ESA, CNES, CNRS and the Conseil Régional Centre. ES is also supported by the NATO research fellowships program. The authors wish to thank Novespace and Sogerma for their cooperation.

References

[1] I. Gökalp, C. Chauveau, D. Durox, F. Lacas, B. Legrand, and E. Shafirovich. *Proceedings of the 2nd European Symposium on the Utilisation of the International Space Station, 16-18 November 1998, ESTEC, Noordwijk, The Netherlands*, ESA SP-433, Feb. 1999, pp. 261-268.

[2] E. L. Dreizin. *Combust. Flame*, Vol. 116, 1999, pp. 323-333.

[3] H. Kato, S. Kunieda, H. Enomoto, K. Okai, T. Kaneko, C. Chauveau, I. Gökalp, J. Sato, M. Tsue and M. Kono. *Drop Tower Days 1998, Hokkaido, Japan*, paper 12-B-11.

Combustion Synthesis and Soot

LAMINAR SOOT PROCESSES

K. -C. Lin, Z. Dai and G. M. Faeth
The University of Michigan
Ann Arbor, Michigan

INTRODUCTION

Soot formation within hydrocarbon-fueled flames is an important unresolved problem of combustion science for several reasons: soot emissions are responsible for more deaths than any other combustion pollutant, thermal loads due to continuum radiation from soot limit the durability of combustors, thermal radiation from soot is mainly responsible for the growth and spread of unwanted fires, carbon monoxide associated with soot emissions is responsible for most fire deaths, and limited understanding of soot processes is a major impediment to the development of computational combustion. Thus, soot processes within laminar nonpremixed (diffusion) flames are being studied, emphasizing space-based experiments at microgravity. The study is limited to laminar flames due to their experimental and computational tractability, noting the relevance of these results to practical flames through laminar flamelet concepts. The microgravity environment is emphasized because buoyancy affects soot processes in laminar diffusion flames whereas effects of buoyancy are small for most practical flames (refs. 1-4).

Results discussed here were obtained from experiments carried out on two flights of the Space Shuttle Columbia. After a brief discussion of experimental methods, results found thus far are described, including soot concentration measurements, laminar flame shapes, laminar smoke points and flame structure. The present discussion is brief, more details can be found in refs. 5-7.

EXPERIMENTAL METHODS

Laminar jet diffusion flames in still air at the exit of a round fuel nozzle were observed within a windowed chamber (diameter and length of 400 and 740 mm). Measurements included visible flame shapes with a video camera, soot volume fractions by deconvoluted laser extinction imaging, soot temperatures by deconvoluted multiline emission imaging, soot structure by thermophoretic sampling and TEM analysis, and plume temperature distributions using a thermocouple rake.

A total of 21 flames were observed having properties as follows: ethylene and propane as fuels, ambient temperatures, T =300 K, ambient pressures, p =35-130 kPa, jet diameters, d =1.6 and 2.7mm, jet exit Reynolds numbers, Re =46-172, and luminous flame lengths, $L_f - L_o$ =15-63 mm). Measurements showed that 10-20s were required to reach steady flames after ignition, in accord with flame residence time estimates (ref. 5).

RESULTS AND DISCUSSION

Soot Concentration Measurements. The multiline emission measurements were used to check the laser extinction measurements of soot volume fractions, f_s , as illustrated in Fig. 1 (r and z denote radial and streamwise distances). The agreement between the two methods is excellent; in

addition, the multiline measurements reached soot volume fractions as small as 0.1 ppm, substantially expanding capabilities compared to extinction alone.

Luminous Flame Shapes. Flame shape predictions for nonbuoyant round laminar jet diffusion flames in still gases were developed based on the simple analysis of Spalding (ref. 9) with appropriate rules for selecting properties and handling soot luminosity (refs. 6 and 7). The resulting measurements and predictions of luminous flame lengths are illustrated in Fig. 2, where Sc =Schmidt number, L_o =length to virtual origin and Z_{st} =stoichiometric mixture fraction. The measurements (all near laminar smoke point conditions) are in excellent agreement with predictions, establishing an empirical factor to handle soot luminosity by the correlation. Notably, the present flames are 40% longer than similar flames observed in the KC-135 facility due to reduced g-jitter, 100% longer than soot-free flames measured in drop towers (ref. 9) due to soot luminosity and increased steadiness, and 100% longer than luminous buoyant flames at normal gravity due to the absence of buoyant mixing. Remarkably, the simple theory also provides excellent predictions of flame shapes, as illustrated in Fig. 3, except near the end of open tip flames where unmodeled effects of radiative quenching are encountered.

Laminar Smoke Points. Measurements of laminar smoke points were completed, similar to earlier measurements using the KC-135 facility (ref. 1). Results for ethylene /air flames are illustrated in Fig. 4. The laminar smoke point flame lengths (LSPFL) are seen to be relatively independent of burner diameter but are affected by buoyancy, disturbances and pressure: LSPFL of buoyant flames are five times longer than present values to due to buoyant mixing and smaller residence times, LSPFL measured using the KC-135 facility are 50% longer than present values due to disturbances and present LSPFL are roughly inversely proportional to pressure. The findings highlight the importance of tests at microgravity to find the fundamental soot emission properties of nonbuoyant flames.

Flame Structure. Insight about LSPFL behavior for present flames could be obtained from the temperature and soot volume fraction measurements of Fig. 5. These results are for a soot-emitting flame that has an open-tip shape characteristic of these conditions for nonbuoyant flames (ref. 5 and 6). The soot is mainly emitted through an annular region with temperatures at the flame tip reaching 1000K so that reactions quench and soot and unburned fuel escape from the end of the flame. Predictions show that reduced temperatures follow due to progressively smaller rates of reaction and progressively larger rates of radiation from soot with increasing streamwise distance, when flame residence times are large (refs. 5 and 6).

Flame structure is very different when residence times are reduced to values more typical of practical flames. An example of soot concentration distributions for such conditions is illustrated in Fig. 6. There is no evidence of tip opening and most paths from the burner exit to the surroundings exhibit nearly the same maximum soot concentration. This behavior agrees with the findings of theory for nonbuoyant laminar jet diffusion flames where variations of flame properties with *time* become independent of both the path and the jet exit velocity, suggesting universal reaction rate behavior (except near the jet exit). This behavior is representative of practical nonbuoyant flames where emitted soot has remarkably universal properties (ref. 5). In view of these observations, future measurements and analysis of data during the present

investigation will concentrate on corresponding conditions where flame residence times, and thus effects of radiative quenching, are small.

ACKNOWLEDGMENTS

This research is sponsored by NASA Grants NAG3-1245 and -2048 under the technical management of D.L. Urban of the Microgravity Science Division, NASA Glenn Research Center, Cleveland, Ohio.

REFERENCES

1. Sunderland, P.B., Mortazavi, S., Faeth, G.M. and Urban, D.L., Combust. Flame 96:97 (1994).
2. Sunderland, P.B., Köylü, Ü. Ö. and Faeth, G.M., Combust. Flame 100:310 (1995).
3. Sunderland, P.B., and Faeth, G.M., Combust. Flame 105:132 (1996).
4. Lin, K.-C., Sunderland, P.B. and Faeth, G.M., Combust. Flame 104:369 (1996).
5. Urban, D.L. et al., AIAA J. 36:1346 (1998)
6. Lin, K.-C. et al., Combust. Flame 116:415 (1999).
7. Lin, K.-C. and Faeth, G.M., AIAA J. 37:641 (1999).
8. Spalding, D.B., Combustion and Mass Transfer, Pergamon Press, New York, 1979, p. 185.
9. Sunderland, P.B., Mendelson, B.J., Yuan, Z.-G. and Urban, D.L., Combust. Flame 116:376 (1999).

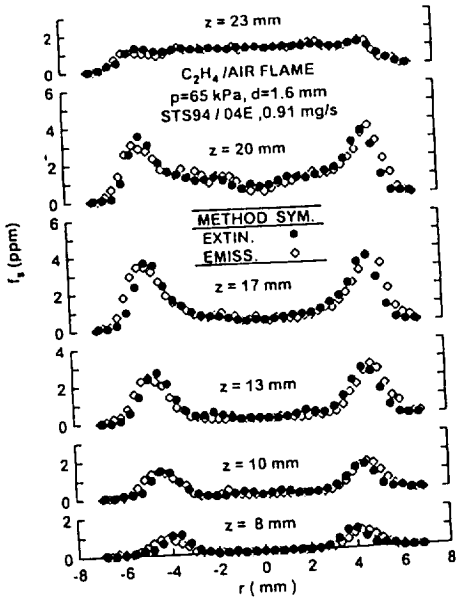

Fig. 1. Soot concentration measurements.

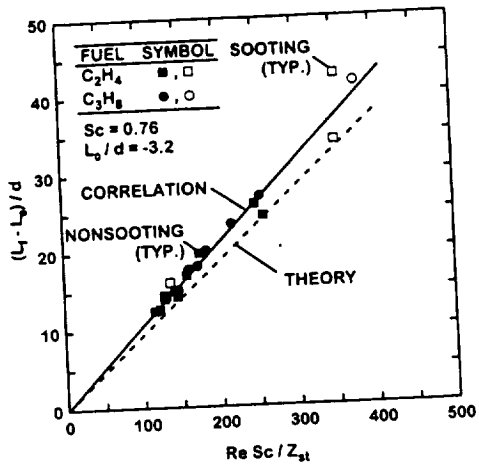

Fig. 2. Flame lengths.

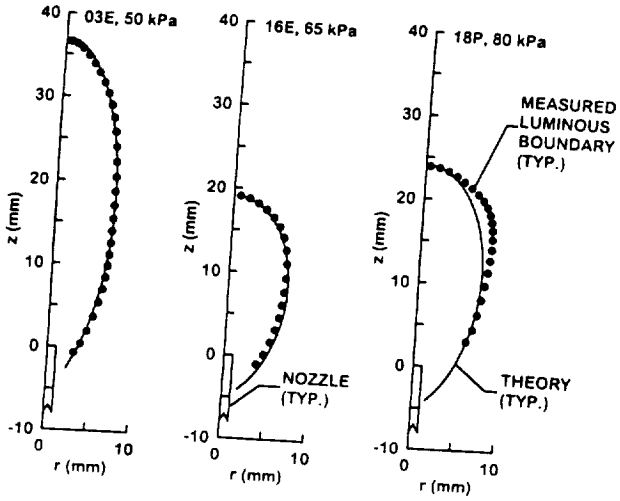

Fig. 3. Flame shapes.

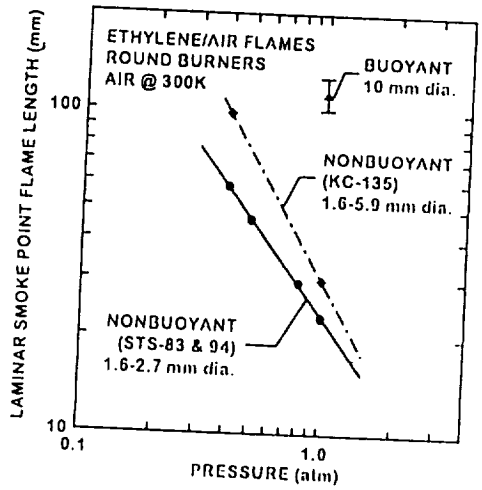

Fig. 4. Laminar smoke points.

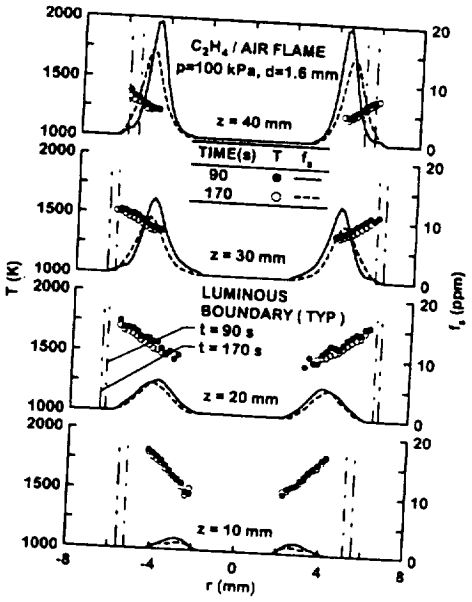

Fig. 5. Structure of open-tip flames.

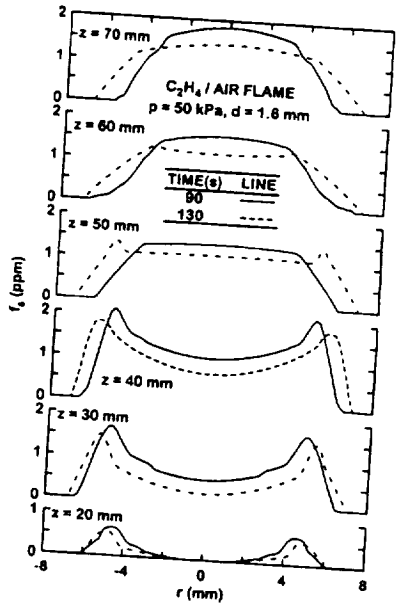

Fig. 6. Structure of closed-tip flames.

Synthesis of Fullerenes in Low Pressure Benzene/Oxygen Diffusion Flames

Peter Hebgen[1] and Jack B. Howard[2],
Department of Chemical Engineering, Massachusetts Institute of Technology, 77 Massachusetts Avenue, Cambridge, MA 02139, USA, e-mail: [1]phebgen@mit.edu [2]jbhoward@mit.edu

INTRODUCTION

The interest in fullerenes is strongly increasing since their discovery by Kroto et al. [1] in 1985 as products of the evaporation of carbon into inert gas at low pressure. Due to their all carbon closed-shell structure, fullerenes have many exceptional physical and chemical properties and a large potential for applications such as superconductors, sensors, catalysts, optical and electronic devices, polymers, high energy fuels, and biological and medical materials. This list is still growing, because the research on fullerenes is still at an early stage. Fullerenes can be formed not only in a system containing only carbon and an inert gas, but also in premixed hydrocarbon flames under reduced pressure and fuel rich conditions [2, 3]. The highest yields of fullerenes in flames are obtained under conditions of substantial soot formation. There a need for more information on the yields of fullerenes under different conditions in order to understand the mechanisms of their formation and to enable the design of practical combustion systems for large-scale fullerene production. Little work has been reported on the formation of fullerenes in diffusion flames. In order to explore the yields of fullerenes and the effect of low pressure in diffusion flames, therefore we constructed and used a low pressure diffusion flame burner in this study.

EXPERIMENTAL

The experimental system is a low pressure benzene/oxygen/argon diffusion flame (Fig. 1). Benzene diluted with argon is fed through a fuel port of 10 mm diameter surrounded by a stream of oxygen fed through a porous plate with a diameter of 30.5 cm. The cold gas velocity of the unburned benzene/argon mixture was varied from 433 to 840 cm/s with a cold gas velocity of the oxygen of 3.65 cm/s. The pressure in the burning chamber was varied from 12 to 40 Torr. Samples of condensable material including PAH, fullerenes and soot were collected using a quartz probe with an orifice of 1.5 to 2 mm, held in a water-cooled jacket and operated at 2 Torr. (Sampling times were from 1 to 5 minutes, limited by the clogging of the probe with soot. More heavily sooting conditions than those studied here couldn't be measured.) All condensable material was collected on a preweighed filter system, consisting of a glass wool plug in an aluminum foil sleeve in the region of the probe surrounded by the cooling jacket. The filter was submerged in toluene and ultrasonicated. After filtering, the solution was concentrated and analyzed using HPLC. The HPLC system was equipped with a diode array detector (DAD) and a variable wavelength detector (VWD). The stationary phase (Cosmosil Buckprep column, 4.6 x 250 mm) was used with a flow rate of 1.0 ml/min toluene. For the quantification of C_{60} and C_{70} the VWD detector was calibrated using a wavelength of 330 nm.

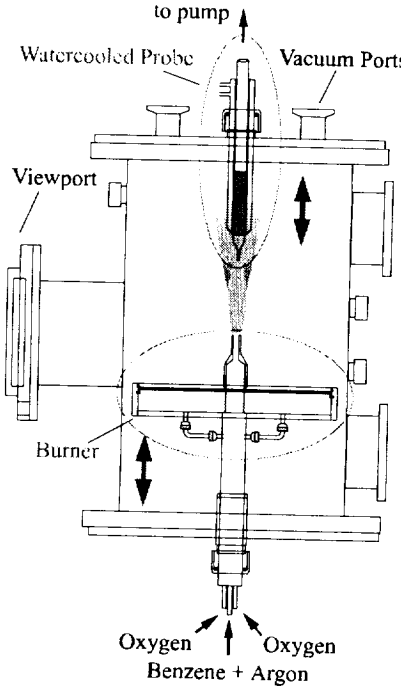

Fig. 1: Experimental setup.

Samples from different heights above the burner in the axial center of the flame were taken by changing the vertical position of the burner and the probe. To characterize the fullerene production in the flames, the ratio of the total mass of fullerenes to the total mass of condensable material and to the total volume of the noncondensable gas are used as parameters.

RESULTS AND DISUSSION

Figure 2 shows the mass of fullerenes C_{60} and C_{70} from a flame at 20 Torr as a percentage of the total mass of condensable material at different heights above the burner in different flames. The graph is also an indicator of the stoichiometric lengths of the different flames studied, because the highest concentration of fullerenes is detected just above the visible stoichiometric surface of the flame.

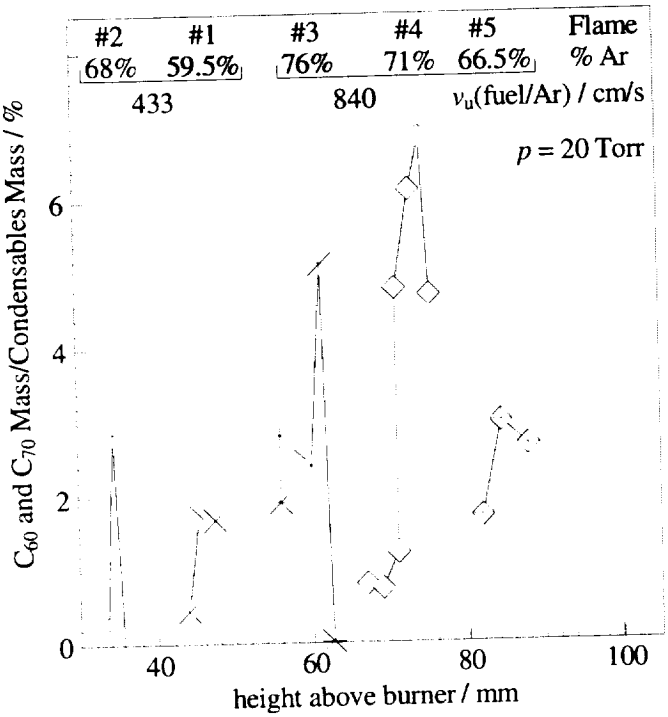

Fig. 2: Amount of fullerenes C_{60} and C_{70} in the condensable material from different heights above the burner at 20 Torr in different flames at different levels of argon dilution and different cold gas velocities of the unburned benzene/argon mixture.

Increasing the cold gas velocity of the benzene/argon mixture at the burner outlet v_u(fuel/Ar) increases the temperature and the length of the flame. A visible indicator for the increase of temperature was the change of the orange soot radiation to a bright white emission. The effect of the dilution of the fuel with argon at a constant fuel/argon velocity results in a shorter flame, but not necessarily in a lower temperature. Each flame was only studied at certain distances from the burner, because the intention was to find the maximum of the fullerene concentration.

A maximum for the percentage of fullerenes in the condensable material was detectable in the flames shown in Fig. 2. This behavior indicates that higher temperatures enhance the formation of the fullerenes, because the maximum fullerene percentage is observed in the flame region where temperature is highest. That the temperature maximum is located at the stoichiometric surface is well known for diffusion flames. In addition to the temperature effect there might also be an effect of the presence of oxygen. The elimination of CO from oxidized PAH is thought to be a source of five membered rings in the structure of combustion generated PAH, which are the precursors of fullerenes in flames. However, oxidation reactions are also responsible for the decomposition of the fullerenes with higher distances from the burner.

It is not yet clear if oxidation is the only process contributing to the reaction of fullerenes, PAH, and soot in the flame region of net condensable consumption, or if there is also a formation of fullerenes from PAH and soot in the hot zone of the flame, as in the formation of fullerenes from vaporized graphite in an electrical discharge.

That the maximum fullerene percentage is at such high dilutions of the fuel as those seen here (Fig. 2, flame #4) is surprising. The overall concentration of carbon in the flame and the soot formation go down with increasing dilution. The lower amount of soot at higher dilution decreases the heat loss from the flame due to radiation, thereby giving a higher temperature, which favors fullerene formation. The lower amount of soot might also decrease the consumption of fullerenes by reaction with soot, but on the other hand it would decrease the generation of fullerenes from soot if such a reaction occurs. The lower concentration of carbon would lower the concentration of fullerene precursors. Therefore opposing effects, and hence the potential for the occurrence of a maximum rate of fullerene formation at a particular dilution, can be suggested qualitatively, but quantitative prediction of the amount of dilution for maximum fullerene formation is not yet possible.

The next graph (Fig. 3, left) shows the mass of fullerenes as a percentage of the total mass of condensable material for a set of flames at a pressure of 40 Torr. As in Fig. 2 the flames are shorter with increasing dilution. Comparing Figs. 2 and 3 it can be seen that flames with the same dilution get longer with increasing pressure.

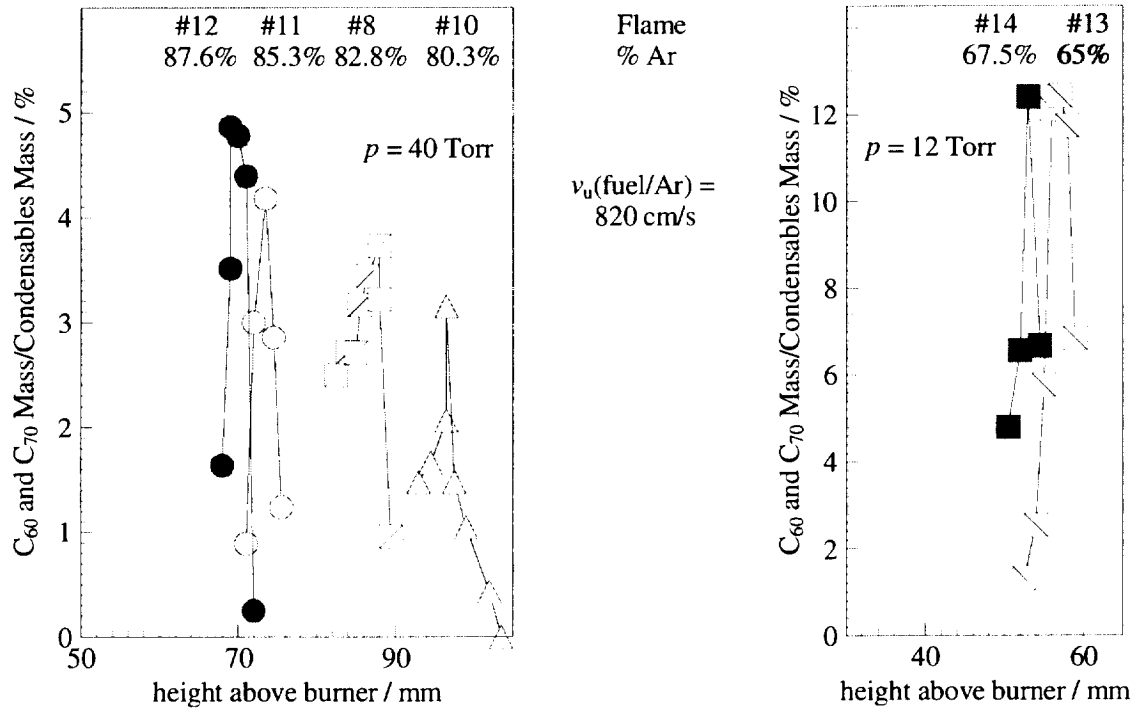

Fig. 3: Amount of fullerenes C_{60} and C_{70} in the condensable material from different heights above the burner in different flames.

Flames at 40 Torr are much more sooting than flames at 20 Torr. For that reason the dilutions with Argon are much higher at the higher pressure. For lower dilutions than those shown in the figures, the amount of soot in the flame was so high that the probe clogged very fast. All the flames show an increase in the maximum percentage of fullerenes with increasing dilution. The point where the percentage goes down again was not observed even though the measurements were done at dilutions up to 87.6 %. The percentage of fullerenes is lower at 40 Torr than at 20 Torr.

Two flames were studied at 12 Torr (Fig. 3, right), the lowest pressure that is manageable with the experimental setup. Consistent with the other results, the flames are shorter and the percentage of the fullerenes is higher then at 20 Torr.

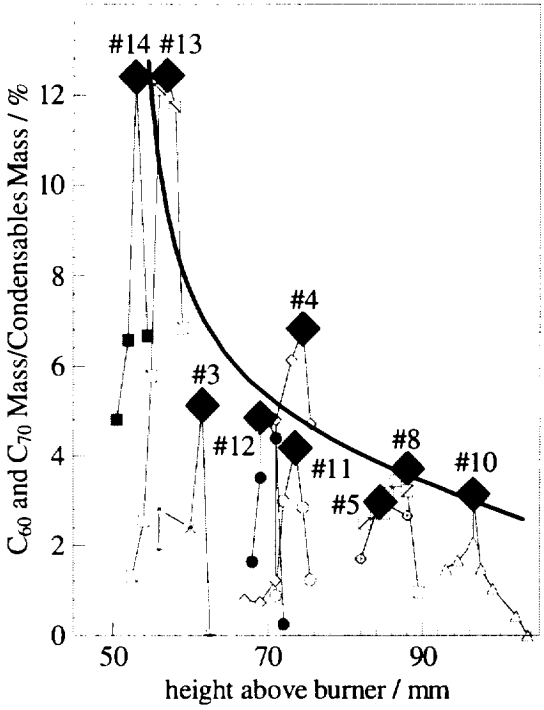

Fig. 4: Amount of fullerenes C_{60} and C_{70} in the condensable material from different heights above the burner in different flames at different pressures. Maximum for each flame is indicated by enlarged diamonds. Cold gas velocity of benzene/ argon mixture, 820 to 840 cm/s.

A plot of the percentage of fullerenes of all flames with almost the same cold gas velocity (Fig. 4) gives a better opportunity to see an overall effect. A closer look at the marked maxima indicates a strong relation of the percentage of fullerenes to the flame length if the measurements are done in the region of the maximum of fullerene formation for the different pressures. A shorter flame, which means a higher dilution or a lower pressure, favors the formation of fullerenes compared to the formation of soot. This behavior could indicate a strong correlation of fullerene formation to temperature, which may be higher for the lower pressures and higher dilutions, and not so much to the concentration of precursors, which goes down with decreasing pressure. An alternative explanation may be that a lower concentration of soot could provide a smaller source of consumption reactions for fullerenes.

An overall effect due to or strongly related to flame length on the formation of fullerenes in diffusion flames is that a shorter flame yields a higher percentage of fullerenes in the condensable material. However, the concentration of fullerenes in the flame seems not to be affected in the same way.

ACKNOWLEDGEMENTS

We are grateful to the National Aeronautics and Space Administration for financial support under Grant # NAG3 – 1879.

REFERENCES

[1] Kroto, H. W., Heath, J. R., O'Brien, S.C., Curl, R. E., Smalley, R. E., *Nature*, **318**, 162-164 (1985).

[2] Gerhard , P., Loeffler, S., and Homann, K.-H., *Chem. Phys. Lett.*, **137**, 306-310 (1987).

[3] Howard, J. B. McKinnon, J. T., Makarovsky, Y., Lafleur, A. L., and Johnson, E. M., *Nature*, **353**, 139-141 (1991).

S33-25

MONTE CARLO SIMULATION OF NANOPARTICLE ENCAPSULATION IN FLAMES

Z. Sun [1], J.I. Huertas [2], and R.L. Axelbaum [1],
[1] Department of Mechanical Engineering, Washington University, St. Louis, MO
[2] Department of Mechanical Engineering, Los Andes University, Colombia, SA

INTRODUCTION

Two critical challenges facing the application of flames for synthesis of nanopowder materials are: (1) overcoming formation of agglomerates and (2) ensuring that the highly reactive nanopowders that are synthesized in flames can be produced in such a manner that their purity is maintained during subsequent processing (Brezinsky, 1997). Agglomerates are produced in flames because particle formation occurs in a high temperature and high number density environment. They are undesirable in most advanced applications of powders. For example, agglomerates have a deleterious effect on compaction density, leading to voids when nanopowders are consolidated. Efforts to avoid agglomeration in flames without substantially reducing particle number density and, consequently, production rate, have had limited success. Powder purity must also be maintained during subsequent handling of nanopowders and this poses a significant challenge for any synthesis route because nanopowders, particularly metals and non-oxide ceramic powders, are inherently reactive. Impurities acquired during handling of nanopowders have slowed the advancement of the nanostructured materials industry.

One promising approach that has been proposed to address these problems is nano-encapsulation (DuFaux and Axelbaum, 1995; Axelbaum, *et al.*, 1997a,b). In this approach, the *core* particles are encapsulated in a removable material while they are within the flame but before excessive agglomeration has occurred. Condensation can be very rapid so that core particles are trapped within the condensed material and agglomeration is limited. Figure 1 shows transmission electron microscope (TEM) micrographs of powders produced with a nano-encapsulation process in sodium-halide flames: titanium (Figs. 1a,b) and aluminum nitride (Fig. 1c). These results demonstrate nano-encapsulation and they show that the size of the core particles can be varied by controlling process conditions (compare Figs. 1 a and b.)

For synthesis of titanium metal the relevant stoichiometry (Calcote and Felder, 1993; Glassman, *et al.*, 1993) is

$$TiCl_4 + 4Na + aAr \rightarrow Ti(s) + 4NaCl + aAr \quad (1)$$

For these flames the NaCl by-product, the lighter material in the micrographs, acted as the encapsulation material and argon was added to control encapsulation, as will be discussed.

Nano-encapsulation also addresses the handling concerns for post-synthesis processing. Results have shown that when nano-encapsulated powders are exposed to atmosphere the core particles are protected from oxidation and/or hydrolysis. Thus, handling of the powders does not require extreme care. If, for example, at the time of consolidation the encapsulation material is removed by vacuum annealing, the resulting powder remains unagglomerated and free of impurities.

In this work, we described a novel aerosol model that has been developed to simulate particle encapsulation in flames. The model will ultimately be coupled to a one-dimensional spherical flame code and compared to results from microgravity flame experiments.

MODELING

The need to model aerosols such as those in sodium halide flames where core particles are encapsulated by rapid condensation of a second component, requires a new multicomponent aerosol model. The model must predict both the final particle size and the size of the core particles under conditions of simultaneous coagulation and condensation. The sectional method is an established technique for modeling coagulation alone and some efforts have been made to extend this technique to allow for condensation (Gelbard, 1990.) However, the sectional method when applied to condensation suffers from numerical diffusion or dispersion because condensed mass is distributed over the entire section and there is a flux of mass across the section (bin)

boundaries. Furthermore, the sectional method yields integrated quantities describing the composition of particles in a given section. For this work we require not only composition but also the size and number of core particles in the particle, i.e., we require the size distribution of core particles within a section. To this end, a Monte Carlo scheme has been developed which affords a statistical treatment of coagulation coupled with a deterministic treatment of condensation and evaporation. Numerical diffusion and dispersion are avoided because the method solves for both mass and number, and by employing moving bins the flux of condensable mass across the bin boundary is avoided. The Monte Carlo approach is ideally suited to a moving bin approach and the addition of moving bins does not entail significant complexity.

For a given size distribution the probability of collision is determined for a discrete size interval (bin) and the Monte Carlo method is used to statistically solve for the evolution due to collisions. Condensation and evaporation on the other hand, are solved classically by integrating appropriate rate equations. This input is coupled to the Monte Carlo scheme by calculating the time between collision events.

Only binary collisions are considered and the collision frequency between particles of size i and j is given by $Z_{ij} = \beta_{ij} N_i N_j$, where β_{ij} is the collision frequency factor and N is the number density. The probability that a collision of type i-j occurs is $q_{ij} = \beta_{ij} N_i N_j / \Sigma \beta_{ij} N_i N_j$. In time step δt there are a total of $p = \Sigma \beta_{ij} N_i N_j \, \delta t$ collisions. To update a size distribution over a time step δt, p collisions are randomly chosen based on their probabilities and the distribution is updated accordingly. Since the aerosol under consideration has two components and we require not only the composition of the particles but also the distribution of core particles within the particle, we retain $N(d_i, Y_i)$, $m_1(d_i, Y_i)$ and $m_2 \, N(d_i, Y_i)$, where m_k is the mass distribution function of component k. For example, if component 1 is NaCl and 2 is AlN we seek the size distribution of AlN particles encapsulated within salt particles.

With the Monte Carlo method the particle size associated with bin i is not prescribed, but rather a mass mean diameter is determined based on the mass and number of particles within bin i. Condensation will cause the mass mean diameter of bin i to grow to a defined larger value and, from this perspective, numerical diffusion is avoided. Nonetheless, if the bins are fixed, the growth of the mass mean diameter beyond the boundaries of a bin would lead to numerical dispersion which would result in peaks and valleys in the number density distribution. This difficulty is avoided by employing a moving bin approach wherein the bin boundaries grow in accordance with growth of a particle of the same size. Thus, condensation does not result in mass transfer across bin boundaries and the common difficulty of modeling condensation in coagulating aerosols is avoided.

RESULTS

For simplicity, the particle encapsulation process relevant to the sodium-halide combustion of Eq. 1 is modeled assuming a homogeneous closed system. The actual flame is a complex process involving diffusive and convective transport and reaction. Nonetheless, the salient features of encapsulation in flames can be understood without detailed modeling of the flame and the usefulness of the Monte Carlo method can be demonstrated in this way as well.

From the chemistry of Eq. 1, it is clear that one component, in this case Ti, has a low vapor pressure (10^{-7} mm Hg at 1473 K) and will rapidly condense out at the flame front. The other component, the encapsulation material, NaCl, has a higher vapor pressure (84 mm Hg at 1473 K) and can be in either the vapor or condensed phase, depending on temperature and a, the stoichiometric coefficient for the inert in Eq. 1. Flame temperature can be controlled by heat loss and reactant dilution and is typically around 1400 K, which is sufficiently high that the NaCl is initially in the vapor phase. As particles are convected away from the flame, they rapidly cool due to radiation and entrainment. This decrease in temperature forces the salt to condense onto the Ti particles. A heat loss of 1-2 W/cm^3 is possible in these particle-laden flames and for the purposes of illustration we have assumed 2 W/cm^3.

Figure 2 shows the particle evolution of the aerosol at times just prior to salt condensation (t = 0 ms) and 50 and 400 ms later (Figs. 2a - c, respectively.) The particle size distribution shown in Fig. 2a, which is for Ti particles, was found to be independent of initial size distribution. The total

mass of Ti in the aerosol was prescribed by Eq. 1 with a = 50 and at a pressure of 1 atm. As seen from Fig. 2, the aerosol quickly evolves to a bimodal size distribution following the onset of condensation. The smaller particles are Ti and the larger particles are primarily NaCl. The size distribution of the NaCl particles is effectively frozen in time while that of Ti rapidly decays as the Ti particles collide with the large salt particles.

In Fig. 3 we see the early stages of the evolution that lead to the bimodal size distribution. Prior to condensation the critical size d^* (Seinfeld, 1986) for the NaCl is effectively infinite but with high heat loss it rapidly decreases (Fig. 4), reaching the tail of the Ti size distribution. As d^* reduces further condensation begins and since this is a closed system the amount of NaCl in the vapor phase decreases. Initially the heat loss is able to continue reducing d^* and smaller particles are coated, but as the vapor phase NaCl is depleted, d^* reaches a minimum and then increases.

The encapsulation process can be summarized as follows. The core or primary particles (Ti in this example) form in the flame and evolve normally as they would without a second phase. At the onset of condensation a small fraction of the particles in the tail of the distribution act as heterogeneous nucleation sites for the condensable vapor (NaCl) and are coated. These coated particles rapidly consume the NaCl and, due to the Kelvin effect, they are the only particles that receive additional condensate. These "salt" particles grow very large because of the large amount of NaCl in the products (see Eq. 1) and they act to scavenge the remaining Ti particles.

Three possible structures of core particles can be formed *within* the scavenging particles. First, the core particles can remain separate, as would occur if times prior to salt solidification are short (the melting point of NaCl is 1073 K), and this we term the frozen solution. If the core particles collide within liquid NaCl droplets they can form either small aggregates or fully coalesced particles. Referring back to Fig. 1, we see indications of all three structures. The powder produced with cool reactor walls (Fig. 1a) shows ca. 10 nm particles embedded in NaCl, indicating a frozen case. At flame conditions that lead to higher temperatures and with heated walls the particles are larger (Fig. 1b) presumably due to collision in the NaCl droplet and subsequent coalescence. The AlN particles in Fig. 1c appear to be small aggregates of rod shaped AlN particles.

An important aspect of the Monte Carlo model is that it retains a record of collisions. Thus, not only can the composition be obtained as a function of size, but the size of the core particles within a scavenging particle can be obtained. Thus for the limits of the frozen solution and the fully coalesced solution we can obtain size distribution of core particles and these are shown in Fig. 5. The frozen solution shows that in this limit the encapsulation process clips the tail of the size distribution, leading to a narrower size distribution. The fully coalesced solution shows the important result that nearly monodispersed particles can be formed with nano-encapsulation.

ACKNOWLEDGMENTS

This work was supported under NASA Grant NAG3-1910.

REFERENCES

Axelbaum, R.L., DuFaux, D.P., Frey, C.A.. and Sastry, S.M.L., (1997a) *Metallurgical and Materials Transactions B*, 28B: 1199-1211.

Axelbaum, R.L., Lottes, C.R., Huertas, J.I and Rosen L.J. (1997b) *Twenty-Sixth Symposium (International) on Combustion*, The Combustion Institute, pp. 1891-1897.

Brezinsky, K. (1997) *Twenty-Sixth Symposium (International) on Combustion*, The Combustion Institute, pp. 1805-1816.

Calcote, H.F. and Felder, W. (1993) *Twenty-Fourth Symposium (International) on Combustion*, The Combustion Institute, pp.1869-1876.

DuFaux, D.P. and Axelbaum, R.L. (1995) *Combustion and Flame.* 100:350-358.

Gelbard, F. (1990) *Aerosol Science and Technology*, 12: 399-412.

Glassman, I., Davis, K.A. and Brezinsky, K. (1993) *Twenty-Fourth Symposium (International) on Combustion*, The Combustion Institute, pp. 1-14.

Seinfeld, J.H. (1986) *Atmospheric Chemistry and Physics of Air Pollution*, John Wiley, NY.

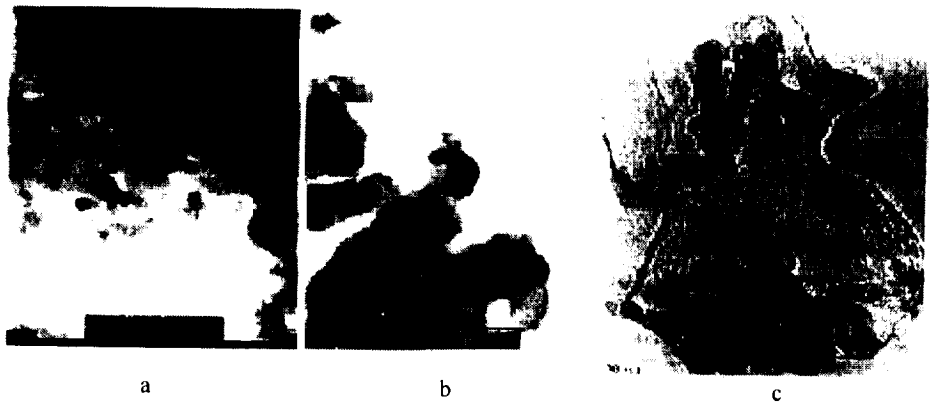

a b c

Figure 1. NaCl encapsulated particles produced in sodium/halide flames: (a) titanium produced in an open flame (b) titanium produced with reaction walls heated to 700 °C and (c) aluminum nitride. The dark particles are the core particles and the lighter material is the NaCl encapsulation.

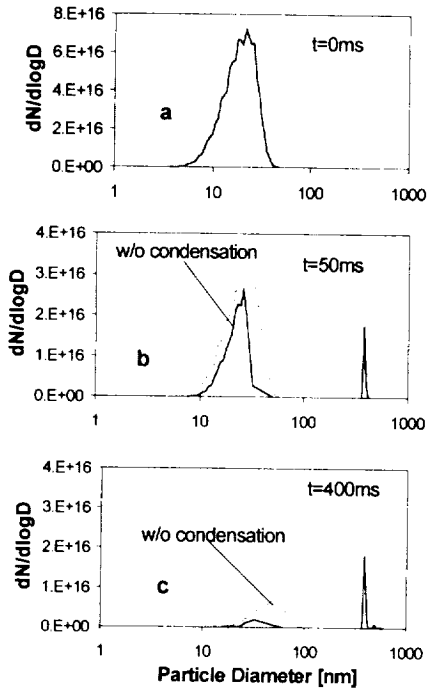

Figure 2. Evolution of aerosol undergoing rapid condensation of a second phase. The dashed line shows the evolution of the distribution without condensation.

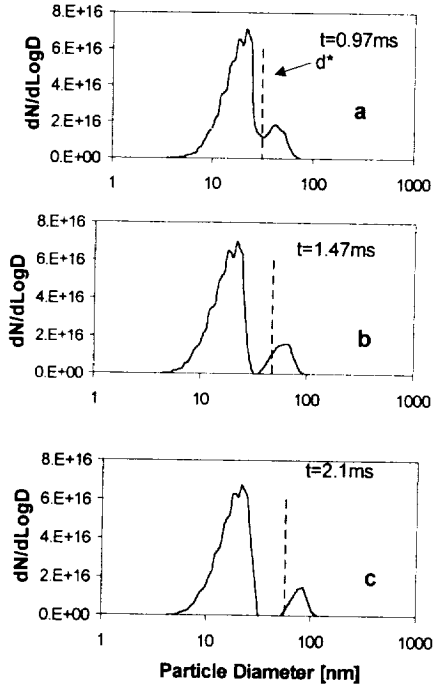

Figure 3. The early stages of condensation for the aerosol of Fig. 2 showing the development of a bimodal size distribution.

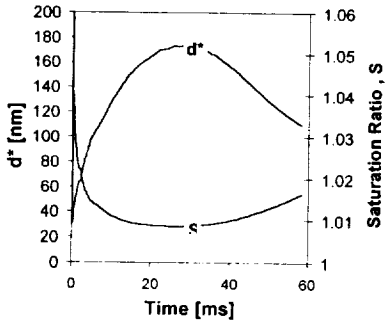

Figure 4. Evolution of d* and S for the aerosol of Fig. 2.

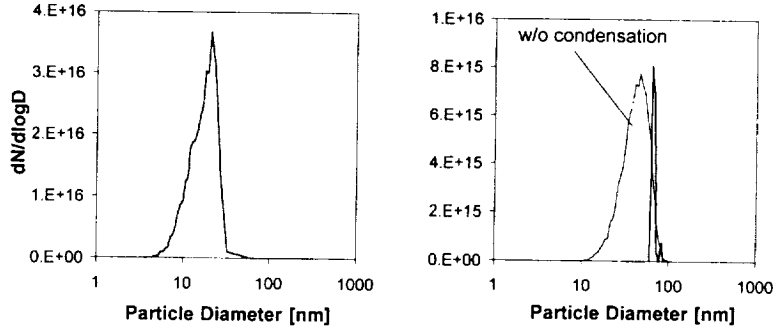

Figure 5. Core particle distribution: (a) frozen solution where core particles do not collide and (b) fully coalesced solution where core particles collide and coalesce.

34-27

COMBUSTION SYNTHESIS OF ADVANCED POROUS MATERIALS IN MICROGRAVITY ENVIRONMENT

X. Zhang (Colorado School of Mines, Golden, CO 80401, USA, E-mail: xzhang@mines.edu), J.J. Moore, F. D. Schowengerdt and D.P. Johnson.

INTRODUCTION

Combustion synthesis, otherwise known as self-propagating high temperature synthesis (SHS), can be used to produce engineered advanced porous material implants which offer the possibility for bone ingrowth as well as a permanent structure framework for the long-term replacement of bone defects. The primary advantage of SHS is based on its rapid kinetics and favorable energetics. The structure and properties of materials produced by SHS are strongly dependent on the combustion reaction conditions. Combustion reaction conditions such as reaction stoichiometry, particle size, green density, the presence and use of diluents or inert reactants, and pre-heating of the reactants, will affect the exothermicity of the reaction. A number of conditions must be satisfied in order to obtain high porosity materials: an optimal amount of liquid, gas and solid phases must be present in the combustion front (Moore, 1994). Therefore, a balance among these phases at the combustion front must be created by the SHS reaction to successfully engineer a bone replacement material system. Microgravity testing has extended the ability to form porous products (Pacas, 1996). The convective heat transfer mechanisms which operate in normal gravity, 1g, constrain the combustion synthesis reactions. Gravity also acts to limit the porosity which may be formed as the force of gravity serves to restrict the gas expansion and the liquid movement during reaction. Infiltration of the porous product with other phases can modify both the extent of porosity and the mechanical properties.

EXPERIMENTAL PROCEDURE AND RESULTS

Two combustion synthesis reaction systems have been examied:

$$2B_2O_3 + (4+x)Al + C = B_4C + 2Al_2O_3 + xAl\,. \quad (1)$$

$$(y+z)\,Ti + xz\,B = y\,Ti + z\,TiB_x\,. \quad (2)$$

The green pellets were ignited at the bottom surface of the sample by means of a horizontal tungsten coil heated by electrical current in an argon atmosphere, and the reactant reaction zone of the combustion wave propagated through the bulk of the sample. Semi-stable oscillatory reactions are observed in the B_4C-Al_2O_3-xAl and Ti-TiB_x reaction systems, leading to a layered structure visible on the exterior surfaces of the pellet and growth was observed to occur only in the axial direction. Research conducted in the SHS of porous ceramic-matrix composites at CSM has been concerned with reactions based on the B_4C-Al_2O_3-xAl system. B_2O_3, which melts at 723 K and volatilizes at approximately 2123 K, acts as a reactant and gassifying agent. Since the combustion temperatures for these reactions varies between 2173 K to 2773 K, this oxide acts as an ideal gassifying agent as well as a required reactant, i.e., an in-situ gassifying agent. This reaction system resulted in porosities of up to 85% and a two-dimensional expansion of up to 300% in the axial direction (Figure 1) when reacted in the propagating mode. This reaction uses xAl as both a diluent and an in-situ infiltrant to control (decrease) porosity and expansion. Increasing xAl decreases the porosity and the degree of expansion, decreases the maximum combustion temperature achieved in the reaction, and increases the compressive strength. The use of ex-situ infiltration with polymethyl methacrylate, PMMA, further controls the composite porosity and strength and provides a biocompatible interface.

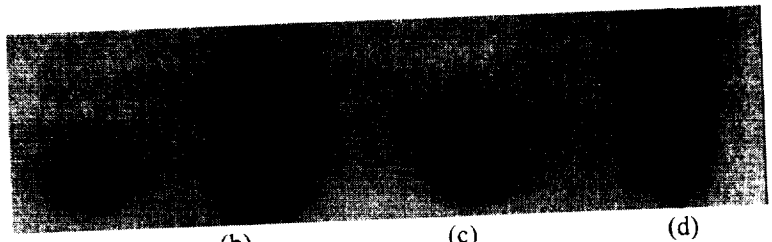

(a) (b) (c) (d)

FIGURE 1. Photographs showing the (a) green pellet and products obtained under (b) 1g, (c) 2g, and (d) microgravity conditions.

The combustion synthesis of a porous cermet composite has been concerned with reactions based on the Ti-TiB_x system in which part of Ti acts as reactant and the remainder acts act as a diluent. Increasing the amount of B in the reactant mix significantly increases the combustion temperature. In addition, the reaction stoichiometry also affects the product porosity as product phases are varied. The results presented in Figure 2 indicate that the product containing TiB_2 is more porous than that containing TiB. The formation of Ti_3B_4 decreases the porosity of products in both TiB_2+Ti_3B_4 and TiB+Ti_3B_4 phase regions. Since this system is a cermet composite material, all the metal components are thermally conducting, and heat can be transported throughout the pellet very easily. As a result, more heat will be lost from the propagating combustion front. Therefore, green density significantly affects the combustion velocity, temperature and pore size. As the green density is decreased, the velocity significantly decreases, and the combustion temperature decreases to approximately 1973 K. Decreasing the green density, increases the apparent porosity (Figure 3), and increases the pore size from 50 m to 200-

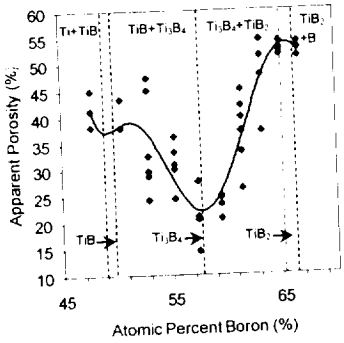

FIGURE 2. Effect of composition on porosity.

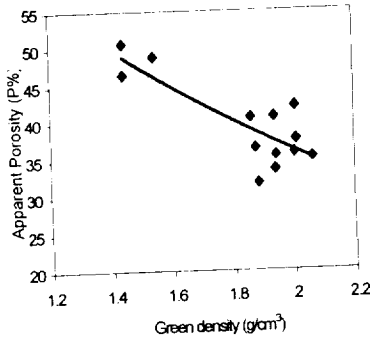

FIGURE 3. Effect of green density on porosity

300 m.

With incorporation of the gassifying agent, B_2O_3, which is released in the form of gas at the propagating combustion front, the pore size increases from 50μm to 300-800μm which is comparable to that of natural bone. Additionally, B_2O_3 helps to form a composite microstructure, which more closely resembles bone. Elevated pressures (2-3atm) effectively decrease the size and nature of the pores formed. This is thought to be due to two causes. Pressure initially acts as a limiting force on bubble expansion in the liquid phase resulting in increased closed pores. Secondly, the amount of heat convection present in a high pressure system is increased. Current research has confirmed that a minimum gas pressure is needed to sustain the reaction propagation. The B_4C-$2Al_2O_3$ system "quenches" out in low pressures (<1 atm). As expected, this effect is amplified with the addition of diluents.

Conducting these experiments under low gravity conditions has shown the following differences compared with reactions conducted under normal (1g) or slightly elevated (2g) gravity

conditions: (1) a decrease in segregation of components in metal matrix composites, (2) an increase in porosity in "foamed" or "expanded" ceramic composites, (3) an increase in pore size in ceramic and metal matrix composites, (4) greater control over the uniformity of pore size, and (5) greater control over combustion temperature and, therefore, microstructure. Conducting the B_4C-Al_2O_3 ceramic-matrix reaction systems in low gravity resulted in additional uniaxial expansions of at least a further 200%. At low gravity, the gas tends to remain in the reacting pellet, and the heat at the reaction front is less susceptible to convection, resulting in an increase in pore size (Figure 4). For the Ti-TiB_x metal-matrix composite system, the low gravity results also show that the degree of porosity and uniformity of pore size increases in low gravity (Figure 5).

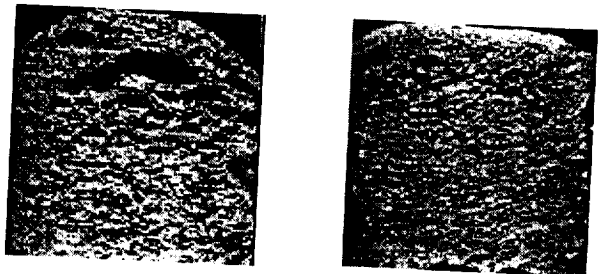

(a) Under low gravity (b) Under 2g

FIGURE 4. Macrostructures of B_4C-Al_2O_3-xAl system.

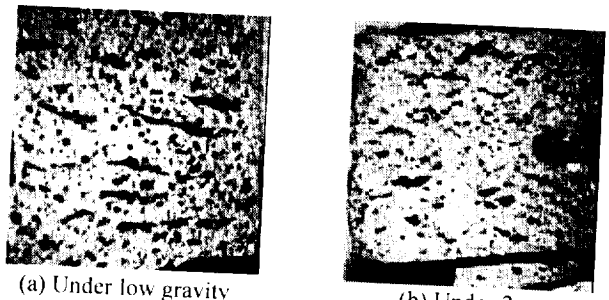

(a) Under low gravity (b) Under 2g

FIGURE 5. Photographs of Ti-TiB_x samples with the same green pellet

Recent research (Simske, 1995) indicates that bone replacement materials should exhibit 50-80% porosity with pore sizes of 200 to 500 microns and the elastic modulus of natural bone, 20GPa. Examples of the SHS porous materials compared with natural bone are presented in Figure 6.

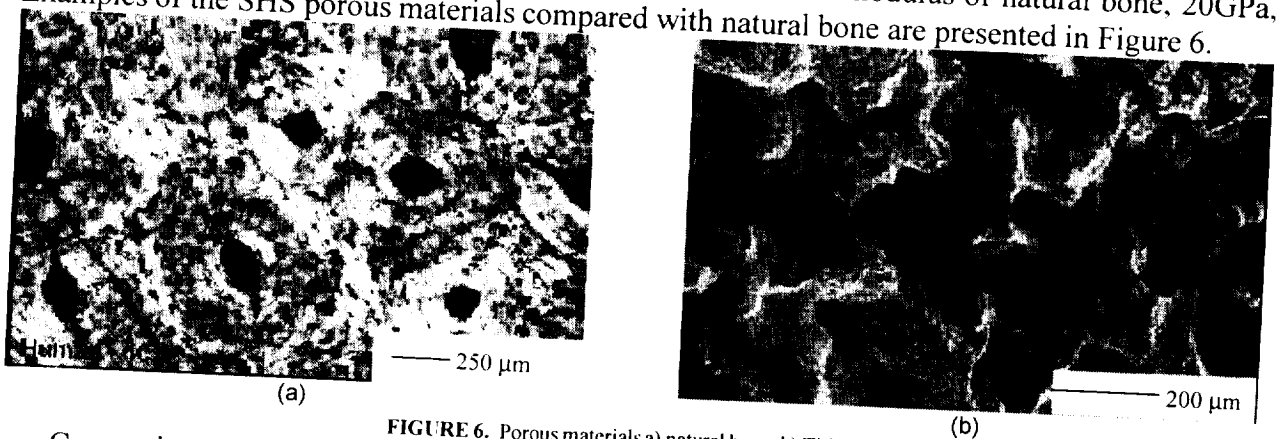

(a) (b)

FIGURE 6. Porous materials a) natural bone, b) Ti-TiB_x

Composites of B_4C-$2Al_2O_3$-xAl, 45atom% B composition in Ti-TiB_x system, and B_4C-Al_2O_3 infiltrated with polymethylmethacrylate were tested in compression to determine their mechanical behavior. The tests indicated, that within the range of testing, the materials show little evidence of elastic behavior. In fact, the polymer infiltration of the B_4C-Al_2O_3 sample causes the materials to behave in a non-linear viscoelastic manner. Due to the variety of materials involved in the composite, a moderate range of test values were obtained. The porous nature of the composite also complicates the issue of defining the mechanical properties of the material. However, from the compression tests several features were found to occur frequently. Each test contained a nearly linear portion at the beginning of the stress-strain curve. The polymer infiltrated samples exhibited a smooth curve with a slight overshoot, while the uninfiltrated samples exhibited rough

curves with evidence of multiple small failures. The polymer infiltrated samples proved to have much higher strength characteristics than the uninfiltrated samples, as can be seen in Figure 7.

A recent test has implanted three porous B_4C-Al_2O_3 samples into a rat for bone ingrowth trial. The resulting bone growth rates were determined to be sufficiently high and competitive with currently used materials to expand the trial to sixty further samples. The implantation of the samples into the rats and the bone growth rate measurements were conducted by Sulzer Medica, Inc., a commercial company that synthesizes bone growth proteins to accelerate the bone growth rate in these porous materials. After 30 days study, the skull onlay implant had 13% bone ingrowth, the mean pore size of implant is close to that of natural bone. The samples were thought to be bioactive and there was no apparent immune response.

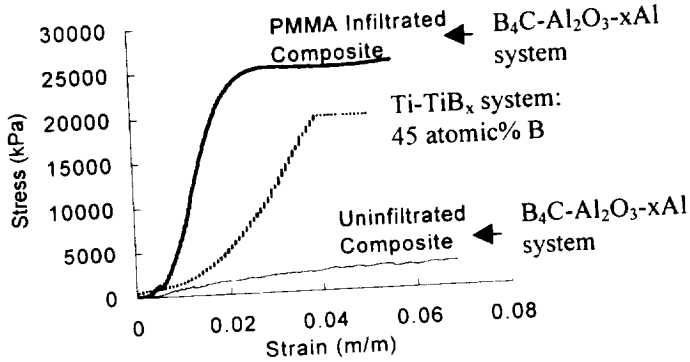

FIGURE 7. Stress-Strain Curves of both mechanical testing values for composites in both B_4C-Al_2O_3-xAl and Ti-TiB_x.

CONCLUSIONS

Evidence presented in this paper illustrates that gravity affects the overall expansion of the product and the phase distribution within the resulting product. Increased gravity was shown to decrease pellet expansion due to the gravitational force on the gases expanding within the reacting pellet. Low gravity conditions caused an increase in expansion due to less heat loss and decreased gravitational forces acting on the pellet. Utilizing the controlling parameters, porous bodies of a variety of matrix combinations can be formed with a reproducible amount of porosity and microstructural features. These composites can be further altered by ex-situ polymer infiltration to meet consumer needs.

ACKNOWLEDGMENT

The authors are grateful for the support by NASA Space Product Development Division, NASA Microgravity Science Division, CATI, GIL., Sulzer Medica.

REFERENCES

Moore, J. J., "An Examination of the Thermochemistry of Combustion Synthesis Reactions," in *Processing and Fabrication of Advanced Materials III*, edited by V. A. Ravi, T. S. Srivatsan and J. J. Moore, The Minerals, Metals, and Materials Society, 1994, pp. 817-831.

Pacas, D. A., Moore, J. J., Schowengerdt, F.D., "Effect of Gravity on the Combustion Synthesis of Porous *STAIF-98*, 1996, pp. 755-760.

Simske, S. J., Sachdeva, R., " Cranial Bone Apposition and Ingrowth in a Porous Nickel-Titanium Implant," in *Journal of Biomedical Materials Research* **29**, 527-533 (1995).

FILTRATION COMBUSTION IN SMOLDERING AND SHS [1]

BERNARD J. MATKOWSKY
Northwestern University
Evanston, Illinois

INTRODUCTION

Smolder waves and SHS (self-propagating high-temperature synthesis) waves are both examples of filtration combustion waves propagating in porous media. Smoldering combustion is important for the study of fire safety. Smoldering itself can cause damage, its products are toxic and it can also lead to the more dangerous gas phase combustion which corresponds to faster propagation at higher temperatures. In SHS, a porous solid sample, consisting of a finely ground powder mixture of reactants, is ignited at one end. A high temperature thermal wave, having a frontal structure, then propagates through the sample converting reactants to products. The SHS technology appears to enjoy a number of advantages over the conventional technology, in which the sample is placed in a furnace and "baked" until it is "well done". The advantages include shorter synthesis times, greater economy, in that the internal energy of the reactions is employed rather than the costly external energy of the furnace, purer products, simpler equipment and no intrinsic limitation on the size of the sample to be synthesized, as exists in the conventional technology.

When delivery of reactants through the pores to the reaction site is an important aspect of the combustion process, it is referred to as filtration combustion. The two types of filtration combustion have a similar mathematical formulation, describing the ignition, propagation and extinction of combustion waves in porous media. The goal in each case, however, is different. In smoldering the desired goal is to prevent propagation, whereas in SHS the goal is to insure propagation of the combustion wave, leading to the synthesis of desired products. In addition, the scales in the two areas of application differ. Smoldering generally occurs at lower temperatures and propagation velocities than in SHS. Nevertheless, the two applications have much in common, so that what is learned in one application can be used to advantage in the other.

We have considered a number of problems involving filtration combustion. Here we describe two such studies: (A) **fingering instabilities in filtration combustion**, (B) **rapid filtration combustion waves driven by convection**.

A. FINGERING INSTABILITIES IN FILTRATION COMBUSTION

Our investigation describes the possibility of a fingering instability in filtration combustion (FC) in microgravity conditions [1], in which the interface between the burned and unburned portions of the sample takes the shape of a propagating finger or a number of such fingers, which occupy only the interior of the sample and not its surface. Such a combustion wave is more dangerous, from the point of view of fire safety, in that (i) its combustion velocity exceeds that of the flat interface and (ii) the burning that occurs is hidden from view, and therefore not easily detected, as it occurs

[1]Work funded under NASA Grant NAG3-2209.

in the interior of the sample and not on its surface.

We consider planar, uniformly propagating combustion waves driven by the filtration of gas containing an oxidizer which reacts with the combustible porous medium through which it moves. We find that these waves are typically unstable with respect to hydrodynamic perturbations. For both forward (coflow) and reverse (counterflow) filtration combustion (FC), in which the direction of gas flow is the same as or opposite to the direction of propagation of the combustion wave, respectively, the basic mechanism leading to instability is the reduction of the resistance to flow in the region of the combustion products, due to an increase of the porosity in that region. Another destabilizing effect in forward FC is the production of gaseous products in the reaction. In reverse FC this effect is stabilizing. We also describe an alternative mode of propagation, in the form of a finger propagating with constant velocity. The finger region, occupied by the combustion products is separated from the unburned region by a front, in which chemical reactions and heat and mass transport occur. We show that the finger solution of the combustion problem can be characterized as a solution of a Saffman-Taylor (ST) problem, originally formulated to describe the displacement of one fluid by another having a smaller viscosity, in a porous medium or in a Hele-Shaw configuration. The ST problem is known to possess a family of finger solutions, with each member characterized by its own velocity and each occupying a different fraction of the porous channel through which it propagates. We propose a criterion to select the correct member of the family of solutions, based on consideration of the ST problem itself, rather than on modifications of the problem, e.g., by adding surface tension to the fluid displacement model and then taking the limit of vanishing surface tension.

In addition, we determine conditions for an instability driven by oxidizer diffusion, which leads to the formation of multiple fingers. Our theoretical results explain the recent experimental results in Zik, et. al. [2], and Olson, et. al. [3].

B. RAPID FILTRATION COMBUSTION WAVES DRIVEN BY CONVECTION

Another investigation describes a new type of FC wave, driven by convection rather than conduction of heat [4]. Such a wave arises due to the imbalance between the temperatures of the solid and gas phases. These waves can propagate much more rapidly than FC waves driven by diffusion of heat, and may be observed even in mixtures with very low thermal conductivity. Thus, it too poses a greater danger from the point of view of fire safety.

The propagation of filtration combustion (FC) waves in a porous solid which reacts with a gaseous oxidizer flowing through its pores may be significantly enhanced by increasing the infiltrating gas flux through the hot porous product region. For relatively small flux, enhancement occurs by the superadiabatic effect, i.e., by increasing the maximum temperature (T_b), and thus, the reaction rate $W(T_b)$ in the combustion front. Though convection of heat from the product region increases T_b, the mechanism of FC wave propagation is controlled by diffusion of the heat released in the reaction.

An alternative mechanism of enhancement, which occurs for relatively large gas fluxes, and corresponds to pronounced temperature nonequilibrium between the gas and solid phases, leads to an increase of the FC wave velocity without increasing the combustion temperature. The propagation

of such waves is controlled by the convection of heat stored in the products, rather than by diffusion of the heat released in the reaction. Such waves may propagate if diffusion is minimal or even absent altogether, due, e.g., to poor contact between the particles comprising the porous matrix.

Unlike conventional (driven by diffusion of heat) combustion waves, the combustion velocity of convection driven FC waves is not controlled by the maximum temperature T_b, but rather by an intermediate temperature T_i which launches the reaction. Here, T_i, the temperature at which the rate of heat release in the reaction equals the rate of heat exchange between the gas and solid phases, is the temperature at which the reaction begins to self-accelerate.

The structure of the convective FC wave is quite different than the structure of standard combustion waves. For the latter, the reaction typically occurs in a narrow temperature region in the vicinity of the maximum temperature. In other words, for a standard combustion wave the reaction occurs at essentially isothermal ($T \sim T_b$) conditions because all the energy released in the reaction diffuses into the fresh mixture. In contrast, for the convective mode of FC wave propagation the reaction is initiated at a certain "self-ignition" temperature T_i. The reaction occurs under essentially adiabatic conditions because the rate of heat release in the reaction significantly exceeds the rate of heat exchange between the solid and the gas. This results in a temperature jump in the reaction zone from T_i to T_b. In contrast to conventional combustion waves the processes in the reaction zone are not of such great importance for convective wave propagation. In a sense, convective FC waves are similar to detonation waves where the role of the reaction is to support the propagating shock wave by supplying it with energy.

An important characteristic of the convective FC wave is the self-ignition temperature T_i which initiates the reaction. The value of T_i is determined by equating the rates of interphase heat transfer and heat release in the reaction. The lower T_i the higher the velocity of the wave. Rapid propagation of the FC wave occurs due to the hot gas penetrating deeply into the medium, which initiates reaction in a thick layer ahead of the reaction front.

This investigation is for the case of forced FC. Other driving mechanisms are also possible, e.g., natural filtration in both gravity and microgravity environments. In a gravity environment buoyancy can serve as the driving mechanism, with hot gas rising and exiting the top of the sample, inducing the inflow of cold fresh gas through the bottom of the sample. We have studied buoyant filtration combustion [5, 6, 7] and determined the combustion characteristics. We are currently investigating the possibility of rapid buoyant convection driven FC, due to thermal nonequilibrium between the gas and solid phases. Of course, in microgravity the buoyant mechanism is not possible. However, a different natural mechanism is possible, namely oxidizer diffusion. To compare the combustion characteristics in gravity and microgravity environments, i.e., to determine whether tests of potential hazards, and of material properties, carried out on earth, can serve as a diagnostic for conditions in space, it is not sufficient to only compare forced FC in gravity and microgravity environments. Results for other driving mechanisms must also be considered, including the two natural mechanisms referred to above. These are currently under investigation.

References

[1] A.P. Aldushin, B.J. Matkowsky, *Instabilities, Fingering and the Saffman-Taylor Problem in Filtration Combustion*, Comb. Sci. & Tech. **133**, (1998), 293.

[2] O. Zik, Z. Olami, E. Moses, *Fingering Instability in Combustion*, Phys. Rev. Letters **81**, (1998), 3868.

[3] S.L. Olson, H.R. Baum, T. Kashiwagi, *Finger-like Smoldering Over Thin Cellulosic Sheets in Microgravity*, to appear, Proc. 27th Int'l. Symp. on Combustion, The Combustion Institute, Pittsburgh, PA, 1999.

[4] A.P. Aldushin, B.J. Matkowsky, *Rapid Filtration Combustion Waves Driven by Convection*, to appear, Comb. Sci. & Tech.

[5] A.P. Aldushin, B.J. Matkowsky, D.A. Schult, *Downward Buoyant Filtration Combustion*, Comb. and Flame **107** (1996), 151.

[6] A.P. Aldushin, B.J. Matkowsky, D.A. Schult, *Upward Buoyant Filtration Combustion*, J. Engineering Math. **31**, (1997), 205.

[7] A.P. Aldushin, B.J. Matkowsky, D.A. Schult, *Buoyancy Driven Filtration Combustion*, Comb. Sci. & Tech. **125**, (1997), 283.

536-29

GASLESS SHS IN PARTICLE CLOUDS UNDER MICROGRAVITY: EXPERIMENTS ABOARD THE MIR SPACE STATION

A. G. Merzhanov, A. S. Rogachev, and A. E. Sytschev, Institute of Structural Macrokinetics and Materials Science, Russian Academy of Sciences, Chernogolovka, Moscow, 142432 Russia, e-mail: isman@ism.ac.ru

INTRODUCTION

Self-propagating high-temperature synthesis (SHS) is some special kind of combustion in solid (powdered) mixtures that occurs in an autowave mode and yields valuable refractory compounds or materials as products [1,2]. SHS is known to involve numerous physical processes, such as melting of reagents and products, spreading of melt, droplet coalescence, diffusion and convection in liquid metals and nonmetals, buoyancy of solid particles and bubbles in the melt, nucleation of solid products, crystal growth, and sample deformation. Some of these processes are affected by gravity [3,4]. A few experimental works made up to date [5–8] have shown notable differences between SHS process conducted under microgravity and normal conditions.

For the most SHS systems, steady combustion is known to proceed even at the bulk density of charge (at normal gravity, minimum relative green density is normally about 30%). Therefore, we can also expect that combustion will continue at still lower charge density. In this work, we investigated SHS processes in the pressed samples as well as in the bulk (loose) powders. In microgravity, the bulk powder forms a cloud of free-moving suspended particles. The goals of our experiments are elucidation of the possibility of SHS in such clouds and comparative analysis of SHS products produced under normal and microgravity conditions.

EXPERIMENTAL

Our experiments were conducted both under terrestrial conditions and aboard the MIR Space Station in 1997–98. Experiments aboard the MIR Space Station were preceded by ground-based experiments. Experiments were performed in Optizon-1 apparatus primarily designed for zone melting [9] but then adapted to SHS. The design of the experimental set-up and experimental procedure were completely similar in the ground-based and microgravity experiments. Sealed reaction chamber was equipped with three halogen lamps that ensured sample heating up to 1300°C. Combustion was initiated by focused (to a spot of 1.5–2.0 mm in diameter) radiation from three halogen lamps located around the sample (Fig. 1).

In our experiments, we used spherical particles of Al cladded with Ni (d = 100–150 mm, T_m(Al) = 933 K, T_m (Ni)= 1728 K, T_m(NiAl) = 1911 K = T_c reaction product is partially melted at T_c, Q = 118.5 kJ/mol). The thickness of Ni coating corresponded to the ratio of Ni/Al=1/1 for each cladded particle. Cladded particles are convenient for these experiments because of reliable contact between reactants (Ni and Al), irrespective of separation between the particles. Two types of samples were used: (a) cylindrical pellets of cladded powder with a density of 3.45 g/cm^3 and porosity of 32 % and (b) loose powders with the bulk density of 2.37 g/cm^3 and porosity of 53 % (under normal g-conditions). In case (b), powders were placed in evacuated sealed quartz ampoules, the ratio of free space (pores + unoccupied ampoule volume) to powder volume being 70/30. The samples used in these experiments are shown in Fig. 2, a. Combustion was initiated at the bottom of the quartz ampoule. Gas evolution was insignificant since both Ni and Al were in their condensed (solid or liquid) state. At T_c = 1640°C, the pressure of Al vapor was about 2 mm

Hg. The pressure of impurity gases (largely water) was found (in ground experiments) to be below 0.00019 mol/g.

EXPERIMENTAL RESULTS

The effect of gravity on SHS in pressed samples

The pressed samples burnt in space and on the ground retained their cylindrical shape and size [8]. The surface of the space-burnt sample is smoother, exhibits a metallic glitter, and has no cracks and cavities found in the ground-burnt samples. At the top (initiation side), we found the drops of melt formed due to excessively high intensity of initiating light flux. Several rounded drops (1–3 mm in diameter) were found to run away from the top of the space-burnt sample. According to the data of electron probe microanalysis and X-ray diffraction, the chemical and phase compositions are identical (NiAl). Narrower (by a factor of 1.5) peaks were observed in the diffraction pattern of the space-burnt sample indicating more perfect crystal structure. As follows from Fig. 4, b the NiAl grains are larger in the space-produced material. For this material, the intercrystalline fracture is prevailing. Meanwhile, the ground-produced material exhibits marked transcrystalline fracture, which is evidenced by structures in the fractograms. The structure of the space-produced material is more uniform with lower fraction of large anisotropy pores. The open porosity is higher in the ground-produced material, while the closed porosity is higher in the space-produced material. Therefore, larger and more perfect crystals were found to form in microgravity. Apparently, microgravity affects the crystallization process due to the absence of convection.

The effect of gravity on SHS in loose powder and particle clouds

As we can see from Fig. 2, a, b, burning of the loose powder at normal gravity proceeds without volume change. The space-produced material (NiAl) exhibits higher porosity (density 1.51 g/cm^3, porosity 70%) and acquires the shape of the ampoule (Fig. 2, c). Combustion velocity in the loose powder (under terrestrial condition) is about 1.5 cm/s. At microgravity, for the first time we observed the propagation of gasless SHS wave in the particle cloud in vacuum. Some video-frames of this process are presented in Fig. 3. The combustion front propagates along the quartz ampoule with the average combustion velocity about 1.0 cm/s.

The microstructures of the samples are presented in Fig. 4, c, d. Prevailing are the globules of irregular shape forming a porous skeleton. In the space-produced material, this skeleton is more delicate and weaker linked: under pressure, the material easily disintegrates into powder. Since the expansion is absent, it can be assumed that the charge comprised of a powder suspension in vacuum, with the particles slowly moving in the cloud.

The space-produced material exhibits a high-porosity skeleton (bound) structure. This can be explained by the specific character of combustion of the cladded Ni–Al particles. Since the melting point of Ni is higher than that of Al, the latter tears up the Ni shell, thus forming shaggy pieces which, upon overlapping, form a skeleton structure.

DISCUSSION

The experimental results shown that space-produced pressed samples of NiAl possess more perfect microstructure with larger crystal grains. It is worth noting that in the most of previous experiments [e.g., 5–7] the finer microstructure was found for the microgravity-produced materials as compared to normal gravity. We may assume that increasing of the crystal

grains size in the microgravity conditions is a characteristic feature of Ni-Al system. It is also possible that this effect can be observed under conditions of long-term microgravity and becomes negligible when the period of weightlessness is short (as in the Drop Tower or Parabolic Flights experiments).

Gasless combustion of the vacuum particle clouds is the most interesting result of the present work. A mechanism of this process is to be studied. The observations and video recording of the initial powder inside ampoules aboard the MIR Space Station shown that the powder particles were uniformly distributed over the ampoule volume. After ignition, heat transfer from burnt to unburnet particles in microgravity and vacuum may occur by radiation and/or upon collisions. These mechanisms of the reaction front propagation differ significantly from the common mechanisms of combustion based on thermal conductivity and convection. High-porous continuous structure is formed due to change in the shape and size of particles during combustion. It can be used for preparation of high-porous materials and items with a desired configuration (corresponding to the shape of reaction ampoule).

ACKNOWLEDGMENTS

This work was supported by the ISMAN–RSC "Energy" Project (grant no. 6/97). We are grateful to Prof. V.P. Nikitskii for his support of and interest in this work, to astronauts V.V. Tsibliev and A.Ya. Solov'ev and T.A. Musabaev who performed the experiments aboard the MIR Space Station, and to A.I. Ivanov, S.F. Savin, E.V. Markov, V.Yu. Antropov for their help in this work.

REFERENCES

1. A.G. Merzhanov and I.P. Borovinskaya. Self-Propagating High-Temperature Synthesis of Inorganic Compounds. *Dokl. Akad. Nauk SSSR*, 204 (1972) 366–369.
2. A.G.Merzhanov. History of and New Developments in SHS. *Ceram. Trans.*, 56 (1995) 3–25.
3. A.S. Shteinberg, V.A. Shcherbakov, V.A. Martynov, M.Z. Mukhoyan, and A.G. Merzhanov. Self-Propagating High-Temperature Synthesis of High-Porous Materials under Zero-G Conditions. *Dokl. Akad. Nauk*, 318(2) (1991) 337–342.
4. A.G. Merzhanov. Gravity-Sensitive Phenomena in Self-Propagating High-Temperature Synthesis. *Proc. II European Symposium on Fluids in Space*, Naples, Italy, April 22–26, (1996) 57–64.
5. K.R. Hunter and J.J. Moore. The Effect of Gravity on the Combustion Synthesis of Ceramic and Ceramic-Metal Composites. *J. Mater. Synth. Process.*, 2(6) (1994) 355–365.
6. O. Odawara, N. Kanamaru, T. Okutani, H. Nagai, Y. Nakata, and M. Suzuki. Combustion Synthesis of GaP, InP, and (Ga,In)P under a Microgravity Environment. *Int. J. SHS*, 4(2) (1995) 117–122.
7. A. Mukasyan, A. Pelekh, A. Varma, A. Rogachev, and A. Jenkins. Effects of Gravity on Combustion Synthesis in Heterogeneous Gasless Systems. *AIAA J.*, 35(12) (1997), 1821–1828.
8. A.G. Merzhanov, A.S. Rogachev, V.N. Sanin, V.A. Scherbakov, A.E. Sytschev, and V.I. Yukhvid. Self-Propagating High-Temperature Synthesis (SHS) under Microgravity. *Joint 1st Pan-Pacific Basin Workshop and 4th Japan-China Workshop on Microgravity Sciences*, July 8–11, Tokyo, 1998, 119.
9. Yu.N.Dyakov, E.V.Markov, A.I.Loobushkyn, and S.N.Sulyghin. Automatic Equipment for

Semiconductor Production in Space. *Proc. AIAA/IKI Microgravity Science Symposium*, May 13–17, Moscow, USSR, 1991, 338–343.

Fig. 1. Astronaut A.Solov'ev is performing SHS experiments in the Optizon-1 facility aboard the MIR Space Station.

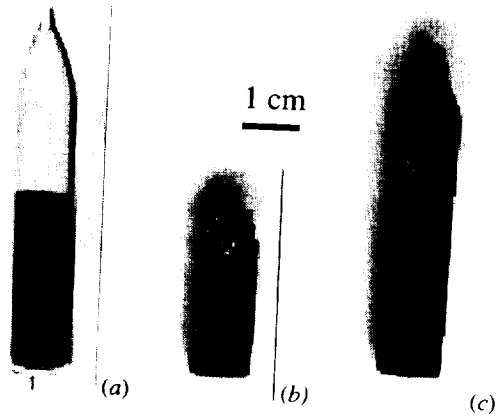

Fig. 2. Overall view of the starting ampoule (*a*) and the samples burnt under normal (*b*) and microgravity (*c*) conditions.

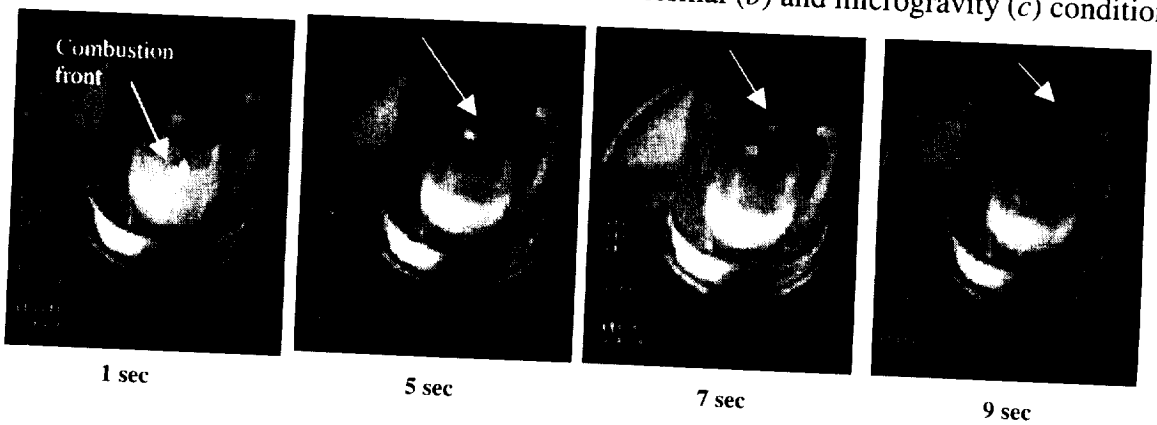

Fig. 3. Video-frame sequence showing gasless SHS in the Ni–Al particle cloud in microgravity.

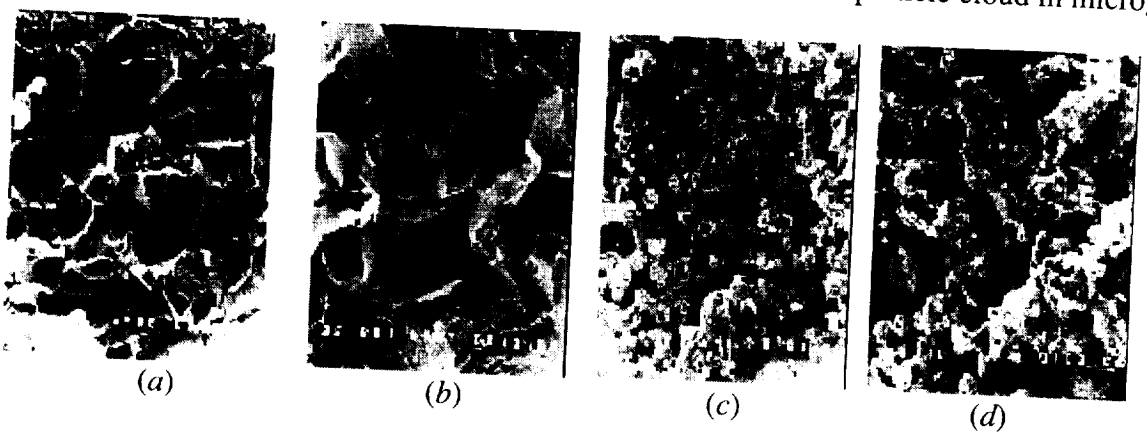

Fig. 4. Structure surfaces of the NiAl synthesized under normal ((*a*), (*c*)) and microgravity ((b), (*d*)) conditions: (*a*), (*b*) – pressed samples, (*c*) – loose powder, (*d*) – particle cloud.

Flame Stability

537-25

A THEORY OF OSCILLATING EDGE FLAMES

J. Buckmaster & Yi Zhang, University of Illinois at Urbana-Champaign,
Department of Aeronautical and Astronautical Engineering,
104 S.Wright St., Urbana IL 61801. limey@uiuc.edu

INTRODUCTION

It has been known for some years that when a near-limit flame spreads over a liquid pool of fuel, the edge of the flame can oscillate relative to a frame moving with the mean speed [9]. Each period of oscillation is characterized by long intervals of modest motion during which the edge gases radiate like those of a diffusion flame, punctuated by bursts of rapid advance during which the edge gases radiate like those in a deflagration [5]. Substantial resources have been brought to bear on this issue within the microgravity program, both experimental and numerical [10],[11].

It is also known that when a near-asphyxiated candle-flame burns at zero gravity, the edge of the (hemispherical) flame can oscillate violently prior to extinction. Thus a web-surfer, turning to the NASA web-site at http://microgravity.msfc.nasa.gov, and following the trail combustion science/experiments/experimental results/candle flame, will find photographs and a description of candle burning experiments carried out on board both the Space-shuttle and the Russian space station Mir. A brief report can also be found in the proceedings of the Fourth Workshop [4].

And recently, in a third microgravity program, the leading edge of the flame supported by injection of ethane through the porous surface of a plate over which air is blown has been found to oscillate when conditions are close to blow-off [1].

A number of important points can be made with respect to these observations: It is the edge itself which oscillates, advancing and retreating, not the diffusion flame that trails behind the edge; oscillations only occur under near limit conditions; in each case the Lewis number of the fuel is significantly larger than 1; and because of the edge curvature, the heat losses from the reacting edge structure are larger than those from the trailing diffusion flame.

We propose a general theory for these oscillations, invoking Occam's 'Law of Parsimony' in an expanded form, to wit: The same mechanism is responsible for the oscillations in all three experiments; and no new mechanism is invoked (Occam's original 'Razor'). Such a strategy eliminates Maringoni effects as the source [6], for these are absent in the second and third experiments. And it eliminates arguments that point to numerically predicted gas eddies as the source [10],[11], a new mechanism, unelucidated.

Indeed, we hypothesize that the essential driving mechanism for the instability is a combination of large Lewis number and heat losses from the reacting structure near the flame edge. Instabilities driven by these mechanisms are commonplace in 1D configurations. Chemical reactor theory, for example, leads to system responses which mimic the response of the candle flame - steady flame, oscillations,extinction [3]. In a combustion context, oscillating instabilities were first reported for diffusion flames in a theoretical study by Kirkby and Schmitz [8], and here also the instabilities are associated with near-extinction conditions, large Lewis numbers, and heat losses. And deflagrations

will oscillate if the Lewis number is large enough, oscillations that are exacerbated when heat losses are present, whether global or to a surface [7],[2].

THE MODEL

Our model is designed to capture only the most basic elements of a diffusion flame with an edge, within a framework that is consistent with the three experimental configurations. We confine the flame within two boundaries, a fuel-supply boundary at $y = 1/2$ and an oxygen-supply boundary at $y = -1/2$. The former plays the role of the wick/pool-surface/plate surface, the latter plays the role of the surrounding oxygen-laden atmosphere. Both X and Y, the reactant mass fractions, are specified at these boundaries. On the upper boundary X is zero everywhere, on the lower boundary Y is zero everywhere. We introduce an anchor point at $x = 0$ by setting $Y \equiv 0$ on the half-line $x < 0$ at the upper boundary, but otherwise $Y = Y_o$ there. On the lower boundary, $X = X_o$ everywhere. The point $x = 0, y = 1/2$ corresponds to the base of the wick, the transition point between fuel-laden wick and the solid wax. It also corresponds to the dividing point between the impermeable portion of the plate and the porous portion in the third experiment. The connection with the flame-spread configuration is less sharp, but ahead of the edge there is little evaporation, for the flame provides the heat for this. Both boundaries act as heat sinks, and we specify the temperature at each of them.

We adopt a constant density model, partly to avoid what we believe are unnecessary fluid-mechanical complications, and we seek unsteady two-dimensional solutions governed by the system of equations:

$$\frac{\partial}{\partial t}(X,Y,T) = \nabla^2(\frac{X}{Le_X}, \frac{Y}{Le_Y}, T) + (-\frac{1}{2}, -\frac{1}{2}, 1)DXYe^{-\theta/T}\,. \tag{1}$$

There are no convective fluxes between the flame and the boundaries for this model, but there is no reason to believe that the convective fluxes in the physical configurations play a role that is fundamentally different from that played by the diffusive fluxes, so that their omission should be of little qualitative consequence.

The equations are solved on the domain $[-5,5]\times[-1/2,1/2]$ with the supply conditions that we have described above applied at the boundaries $y = \pm 1/2$. At $x = \pm 5$ we assume that the solution is locally one-dimensional and apply Dirichlet data defined by the two appropriate 1D solutions. At the left boundary, this is the frozen solution. At the right boundary it is a strong flame solution, determined numerically but differing only a little from the asymptotic Burke-Schumann solution. A smooth interpolation is used to define the initial data in the interior. Solution is carried out using a sixth-order compact scheme to discretize the spatial variables, with time-advancement based on a low-storage, 5-stage, 4th-order accurate Runge-Kutta scheme.

RESULTS

We show here results when $Le_X = 1, Le_Y = 2$. When the Damköhler number D is assigned the value 2×10^7, a steady solution emerges for large values of t. On the other hand, for $D = 1.725\times10^7$, a time periodic solution emerges in which the edge advances and retreats without any y-motion of the trailing diffusion flame. Figures 1a,b are snap-shots of the temperature topography at $t = 2.61$ (withdrawn edge) and $t = 2.84$ (advanced edge).

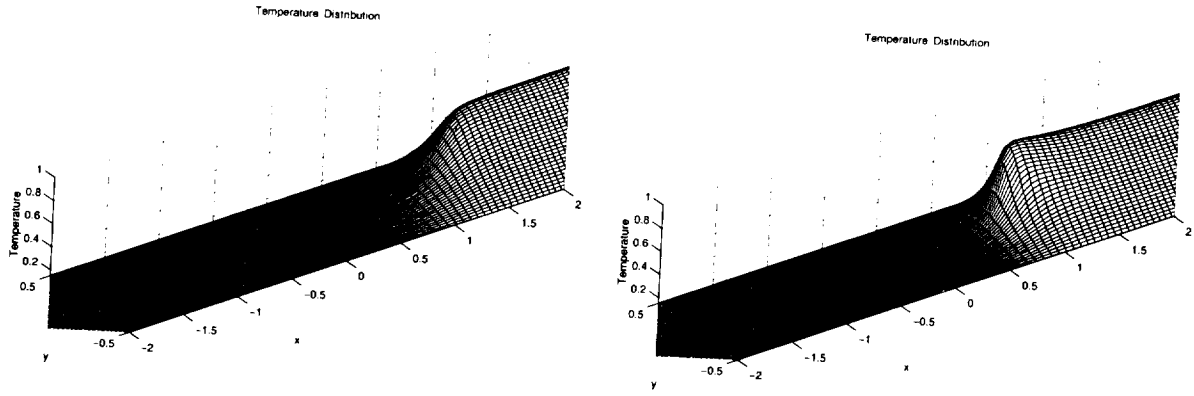

Figure 1: Temperature topography at times $t = 2.61, 2.84$; $D = 1.725 \times 10^7$.

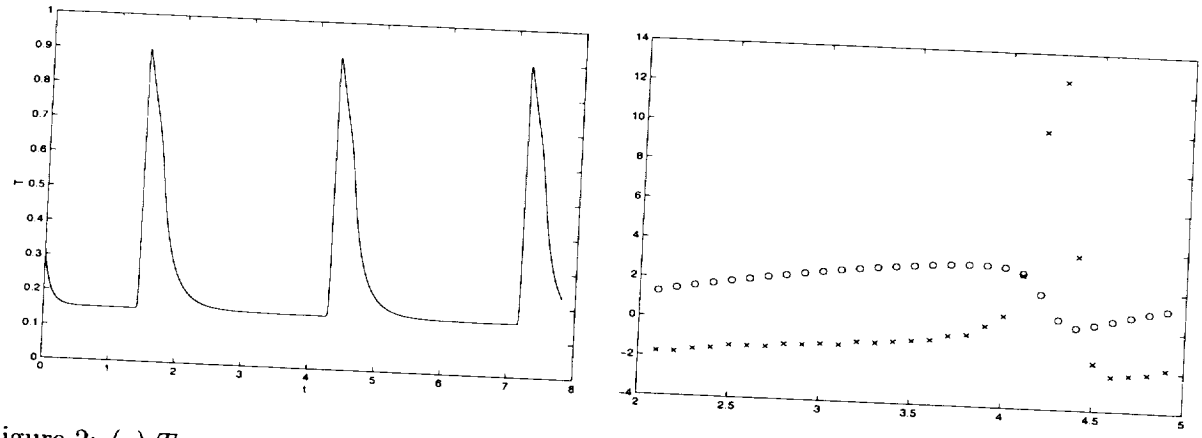

Figure 2: (a) T vs. t at $x = 0.45$, $y = 0.08$, $D = 1.6 \times 10^7$; (b) the front position (x) and speed(o).

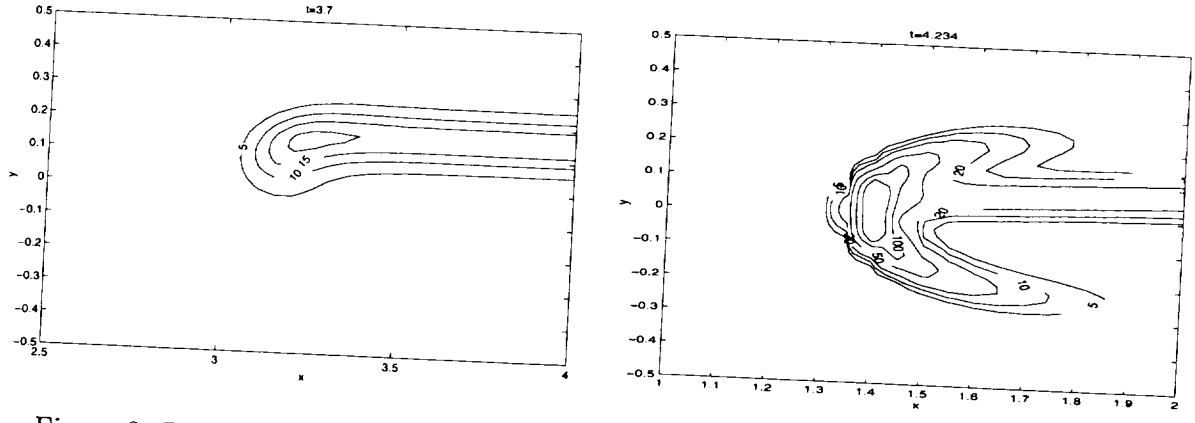

Figure 3: Reaction rate contours at $t = 3.7$ and $t = 4.234$ (cf. Figure 2b); $D = 1.6 \times 10^7$.

Reducing D to 1.6×10^7 generates oscillations with highly nonlinear features. This is apparent from Figure 2a which shows the temperature history at a fixed point. Figure 2b shows the position and speed of the front over a complete period. During most of this interval the edge slowly retreats or rests at its rearmost position, but in a brief sub-interval it shoots forwards at high speed. During the retreat the reaction rate contours reveal no significant premixed strutures, Figure 3a, but during the advance a vigorous tribrachial structure is seen, Figure 3b, characterized by strong premixed branches in addition to the trailing diffusion flame (cf. the remarks in the opening paragraph).

Oscillations are not observed when the Lewis number of the fuel is reduced to 1.5. In that case, reduction of the Damköhler number simply leads to 'detachment' of the edge from the anchor point and it retreats to the right as a failure wave (an edge flame with negative propagation speed). Finally, we have shown that a non-oscillating edge can be induced to oscillate by reducing the temperature to the boundary value at an internal rectangle of mesh points, thus simulating the insertion of a cold probe into the combustion field, a response observed in the Mir candle experiments.

ACKNOWLEDGEMENT

This work was supported by AFOSR and by the NASA-Lewis Research Center. We are indebted to T.L.Jackson for supplying computational modules and for his helpful advice. Our interest in edge-flames started some years ago with the viewing of Howard Ross's video of the space-flown candle flame.

References

[1] Brahmi,L., Vietoris,T., Joulain,P., David,L., Torero,J.L. *AIAA paper 99-0581*, 37th Aerospace Sciences Meeting (1999).

[2] Buckmaster,J. *SIAM J. on Appl. Math.* **43** 143 (1980).

[3] Cohen,D.S., Alexander,R. Article in *Reacting Flows, Combustion and Chemical Reactors*, ed. G.S.S.Ludford, North-Holland, Amsterdam, p.122, (1986).

[4] Dietrich,D.L., Ross,H.D., Frate,D.T., T'ien,J.S., Shu,Y. *NASA Conference Publication 10194* page 237 (1997).

[5] Glassman,I., Dryer,F. *Fire Safety Journal* **3** 132 (1981).

[6] Higuera,F.J., Garcia-Ybarra,P.L. *Combustion Theory & Modelling* **2** 43 (1998).

[7] Joulin,G., Clavin,P. *Combustion & Flame* **35** 139 (1979).

[8] Kirkby,L.L., Schmitz,R.A. *Combustion & Flame*, **10** 205 (1966).

[9] Ross,H.D. *Progress in Energy and Combustion Science* **20** 17 (1994).

[10] Ross,H.D., Miller,F.J., Sirignano,W.A., Schiller,D. *NASA Conference Publication 10194* page 375 (1997).

[11] Schiller,D.N., Sirignano,W.A. *AIAA paper 96-0216*, 34th Aerospace Sciences Meeting (1996).

INVESTIGATION OF DIFFUSION FLAME TIP THERMODIFFUSIVE AND HYDRODYNAMIC INSTABILITY UNDER MICROGRAVITY CONDITIONS

I. S. Wichman[1] and S. L. Olson[2]. [1]Department of Mechanical Engineering, Michigan State University, East Lansing, MI, 48824-1226, wichman@egr.msu.edu, [2]NASA Micro-gravity Combustion Division, Glenn Research Laboratories at Lewis Field, 21000 Brookpark Road, Cleveland, OH, 44135, sandra.olson@grc.nasa.gov.

INTRODUCTION

We employ the opposed flow flame-spread configuration in order to examine flame-front instability of diffusion flames near cold, solid boundaries. The thermo-diffusive and hydrodynamic instabilities can transform an initially planar flame front into an irregularly curved, corrugated, possibly fragmented front. Under ordinary 1-g conditions, the buoyancy-induced flow masks the thermo-diffusive and hydrodynamic instabilities and produces planar flames. Such stable spreading flames have been observed for decades in laboratory experiments.

Experiments in zero gravity are necessary to produce unstable flame fronts. The thermo-diffusive/hydrodynamic μ g instability appears in diffusion flames such as, for example: the candle flame oscillations observed by Dietrich et al. [1]; smolder instabilities on a recent Space Shuttle flight. Drs. T. Kashiwagi and S. Olson have attributed the latter to a lowered oxygen transport rate to the hot, reactive surface.

Consider a burning surface near the flame extinction limit. The flow, or stretch, induced by the diffusion flame is weak, hence buoyancy plays a small role, thereby enabling previously secondary mechanisms, such as differential thermo-diffusion, to become the most important mechanisms. The flame leading edge becomes unstable; and diffusion flame breakup, oscillation, and rejoining all occur at a measurable frequency of approximately O(1 Hz) [2].

This project has only begun in January of this year, 1999. To date, there have been no flight experiments on flame spread instabilities. However, we have made numerous experiments in the NASA 2.2 and 5 second drop towers on flame spread over very thin cellulosic fuels. We have been very fortunate through a combination of factors, to be explained below, to obtain some interesting, perhaps even compelling, results on diffusion flame instability in the presence of heat losses to cold surfaces.

PRELIMINARY EXPERIMENTS IN THE NASA 2.2 SECOND DROP TOWER

Experiments were conducted by dropping the Micro-gravity Combustion Tunnel Rig (CTR) in the NASA 2.2 second drop tower. The CTR is a wind tunnel that can provide an opposed flow of oxidizer for flame spread while being dropped in the test facility. The range of opposed flows used here was 1-5cm/s at atmospheric pressure. A rig gas reservoir, which is filled prior to the drop, supplies a plenum chamber that contains the sample with the premixed oxidizer, which may be air or some other Oxygen/Inert mixture. The flow is pre-set by a pressure regulator at the bottom of the rig and is controlled by a critical flow nozzle. The air flow is straightened by parallel plates, and a porous plate, before entering the combustion chamber. A T-vent at the top (i.e., downstream end) of the chamber is used to exhaust the flowing product gases.

Two video cameras showed a top and side view of the burning sample by recording through portholes in the CTR walls. These videos have been quantitatively analyzed by digitizing the frames using Tracker 3 Object Tracking and Image Processing software.

The fuel used was Kimberly Clark brand "kimwipes" 10.5 cm width. They were ignited under 1-g conditions at their topmost end using a Kanthall hot-wire wrapped around an alumina-ceramic rod. Care was taken to produce as flat or 1-D an ignition profile as possible. A metal backing placed at a small distance from the sample is employed in order to produce a heat sink to the flame spread. The metal was steel, 0.001 in. thick. The sample and the metal sheet did not touch, And the separation distance was approximately 1 cm. The purpose of the metal backing was to produce a heat sink to the spreading flame that would result in a near-extinction flame spread in air and with non-negligible inflow air velocities. If the backing were not used, weaker Oxygen/Inert mixtures would be needed and weaker inflow rates would be necessary. Under such additionally weakened conditions, measurements become increasingly difficult, as was determined in preliminary experiments with 17-20% Oxygen concentrations. Without the backing, no flame instabilities were observed. Hence, the "forcing" via heat loss was deemed necessary, even at a lowered Oxygen concentration. This flame spread/heat loss behavior is predicted from the Diffusion Flame Spread Map of S. L. Olson. We note that for thicker fuels such forcing is generally not necessary, for the sample is its own heat sink. Thus, the metal backing is a necessary artifice for the thin-fuel limiting case. We also note that higher flow velocities for the incoming Oxygen/Inert mixture are desired because they more quickly wash away the buoyant flow residual in the 1-to-zero-g transition of the drop.

We have, to date, not performed calculations on the detailed heat transfer to the metal backing. However, we plan to perform such calculations in the near future, in order to quantify as thoroughly as possible the influence of the backing on the flame spread heat transfer.

The sample is ignited at its downstream end. The flame spread is observed until it is nearly planar in 1-g. The rig is then dropped to produce zero-g spread. It has been established after many tests that the spreading flame fragments into flamelets. These flamelets usually number three, and they continue to spread in the streamwise direction. They are generally elliptical in shape (viewed from the top) with the larger dimension being perpendicular to the incoming flow. The principal flamelet oscillations occur in this plane. During the oscillations, the flamelet surface-covering area first increases, then decreases. Because of the limited time available in the 2.2 second drop tower, few full oscillations were in fact observed. There was ample time to observe the dramatic and definite breakup of the flame front once the drop commenced. The zero-g flame was very different from the 1-g flame.

Two different backings, steel and aluminum, were used in these tests. As expected, the range of conditions for which flamelets were observed was much broader for the steel backing. This had a much lower thermal conductivity (approximately factor of two smaller) than the aluminum, for which the range of conditions allowing flamelets was much narrower. With the steel backing, numerous tests were conducted in which a 2cm/s or 3cm/s flow produced three evenly spaced flamelets across the sample width. Their sizes were similar, and as noted above, no more than one or two oscillations could be observed. The leading edge of these flamelets was bright blue, tracing out the shape of a bowl. The middle and rear portions, however, were darker and more diffuse.

Generally, as these flamelets extinguished, they became more spherical in shape, interestingly in both the top and front view planes. This finding was confirmed by performing tests using lower flow speeds, such as 1 and t.5 cm/s. The flamelets formed upon dropping were unstable, spherical, and died away quickly.

A few flamelet interactions were observed. For one test at 4 cm/s, the elliptical flamelets combined to form the original flame front. Then this front fragmented once again into separate flamelets.

Our data analysis has been limited because of the preliminary nature of our work to visual examination by Tracker 3 software. We are attempting presently to produce images of the flame sheet, by filtering of extraneous wavelengths. In this we have been partially successful, but work is presently continuing. We have, to date made no detailed sample surface temperature measurements. These and other quantitative measurements are planned for future experiments.

PRELIMINARY EXPERIMENTS IN THE NASA 5-SECOND DROP TOWER

Because of the time limitations alluded to in Sec. 2, we began 5-second tests in the late Fall of 1998. A large preliminary effort was required to make the CTR comparable with the 5-second facility. This was caused chiefly by the difference between exhausting into a pressure of one atmosphere (2.2 sec. tower) and a vacuum (5 sec. tower). Once the proper adjustments were made, numerous drop tests were conducted in late 1998, early 1999. These tests were very successful, producing results largely in accord with those described above. The principal differences were the following: first, the flow speed did not have to be as large; second, the breakup and oscillations were easier to quantify and, in a sense, almost predictable. The reason for the former was apparently the decreased g-jitter associated with the much smoother drop in the 5-sec. Tower. Approximately one order of magnitude improvement is made in g-jitter. The reason for the latter is increased observation time. Once again, three flamelets are usually formed, in all respects similar to those described in Sec. 2. In some cases, the flamelets appeared to migrate partially off the sample onto the sample holder, which was made of an insulation ceramic. The reason was decreased heat losses, because the metal backing covered only the region directly behind the combustible sample. Hence, the flame segment that migrated over the edge had lower heat losses than the segment remaining over the sample.

PRELIMINARY PLANS FOR FLIGHT EXPERIMENTS

We discuss below some preliminary features of our anticipated flight experiments. These characterize our planning for the ground-based drop tests and any subsequent flight tests such as the sounding rocket or the KC-130. In other words, the anticipation of the flight tests described below will dictate, to a large degree, the approaches used in the preliminary research phase.

Our flight experiments shall focus on the following quantities:

- Wide samples --approximately 10 cm -- to promote non-planar front instability.
- Thick fuels to exaggerate the instability growth.
- Air environment. This is a near-limit O_2 level, which also promotes instability.
- Opposed flow rates of 0.1(quiescent) - 10 cm/s.

We list the experimental diagnostics for flight experiments. It is desirable for the ground based

testing to employ, subject to space limitations, as many of these diagnostic tools as possible.

- Multi-spectral UV-Vis intensified array camera(s) for OH*, CH*, and color flame images, for visualizing reaction zone for intensity variations indicating onset of instability. The views are from the top, looking down on the sample surface, and/or side.
- Narrow band-passed (3.8 mm filter) IR camera views the sample surface for non-uniform surface temperature measurement.
- Gas-phase IR camera with multi-spectral capability for visualizing fuel and product distributions (C-H compounds, CO_2, H_2O, CO, soot).
- Oblique-view 35mm camera for perspective. Despite slow framing rate, camera has excellent resolution, sensitivity, and dynamic range.
- Surface and subsurface TCs. Gas TCs.

THEORETICAL WORK

Our theoretical research will buildsupon knowledge gained on diffusion flame tips[3-5]. We refer to our theoretical solutions as the *basic state* [4,5]. The tips of diffusion flames are controlled by a complicated interaction between amplification of reaction, heat loss to the surface, and convection and diffusion of reactants [4,5]. The reaction rate is highest at or very near the point of flame tip extinction [4]. The heat losses to the fuel surface are highest at the quench point. Differential diffusion of the reactants strongly alters the flame-tip structure.

Our previous research demonstrated the evolution of the flame tip [4]. Far from the surface it was a pure, stereotypical gas-phase triple flame with full premixed-flame wings. Near the surface it became a flame nub, whose wings had now shrunk nearly to a point. *This is in complete agreement with computations.* This flame nub showed very different behavior from the trailing diffusion flame arc. In our work, we retained the complicated two-dimensionality of the flame-tip vicinity, producing theoretical results for elliptic conservation equations. We will continue to retain this inherent multidimensionality of the flame leading edge in our work on flame instability.

REFERENCES

1. Dietrich, D. L., Ross, H. D., Frate, D. T., T'ien, J. S. and Shu, T., "Candle Flames in Microgravity," 4th International Microgravity Combustion Workshop, NASA Conf. Pub. No. 10194, May 19-21, pp. 237-242 (1997).
2. Olson, S. L., "Buoyant Low Stretch Stagnation Point Diffusion Flames Over a Solid Fuel," Ph. D. Thesis, Case Western Reserve University, 1997.
3. Wichman, I. S., "Basic Features of Triple Flames in Combustion Science," 8th International Symposium on Transport Phenomena in Combustion, S. H. Chan, ed.Taylor and Francis, Washington, D. C., 1996, pp. 456-466.
4 Wichman, I. S., "On Diffusion Flame Attachment Near Cold Surfaces," Combustion and Flame, 117, pp. 384-393 (1999).
5 Wichman, I. S., Pavlova, Z., Ramadan, B. and Qin, G., "Heat Flux from a Diffusion Flame Tip to an Adjacent Surface," accepted for publication in Combustion and Flame, to appear, 1999.

DIFFUSION FLAMES: EXTINCTION AND STABILITY

Moshe Matalon, McCormick School of Engineering and Applied Science,
Northwestern University, Evanston, IL 60208-3125, matalon@nwu.edu

INTRODUCTION

Some of our recent results, [1-3, 9, 14-17], concerning extinction and stability properties of diffusion flames are summarized below.

EXTINCTION LIMITS

The spherical diffusion flame surrounding a fuel drop, burning in an oxidizing atmosphere is inherently unsteady; the droplet continuously shrinks as the fuel vapor is consumed. An alternative configuration that leads to steady flames is the burner-generated spherically symmetric diffusion flame. Current experiments carried out in microgravity ground facilities [1,13,18], which are of limited duration, show the flame in a transient state during the whole experiment. Nonetheless, a steady spherical flame is a solution of the conservation equations and may be attained under more appropriate experimental conditions. A detailed description of the steady flame structure was given in [16-17] for general non-unity Lewis numbers. The results identify the burning characteristics in terms of the mass flow rate parameter M, which is the rate at which fuel is supplied to the sphere in units of the diffusion length. It was found that extinction occurs at sufficiently low values of M, namely when the residence time in the reaction zone is too short. The extinction value M_{min} is found to depend strongly on the Lewis numbers (L_F and L_X for the fuel and oxidant, respectively) as illustrated in Figs. 8-9 of Ref. [16]. A diffusion flame can be sustained for sufficiently low injection velocities for hydrocarbon air flames, for which $L_F > 1$, but not for hydrogen-air flames, for which $L_F < 1$. The extinction value for a propane air flame, for example, is as low as 10^{-4} g/s.

At high injection velocity a Burke-Schumann flame sheet, with complete consumption of fuel and oxidant and with a temperature reaching the adiabatic limit is predicted. Experiments, however, have shown spherical flames that continue to decrease in luminosity and eventually extinguish as they grow in size. Evidence suggests that radiative loss may be a responsible mechanism; radiative heat loss from the flame scales with the volume of the radiating species and is therefore more pronounced for large flames. By incorporating the effects of thermal radiation from a finite shell, ignoring the chemical consequences, we obtained [17] an upper extinction limit for M. Typical response curves showing the flame temperature T_f as a function of the mass flow rate M are shown in Fig.1. The physically realizable states are those on the upper branch and these are limited to a finite range of mass flow rates, i.e. $M_{min} < M < M_{max}$. Note that the flammable region shrinks as the radiation intensity Ω increases; when radiative

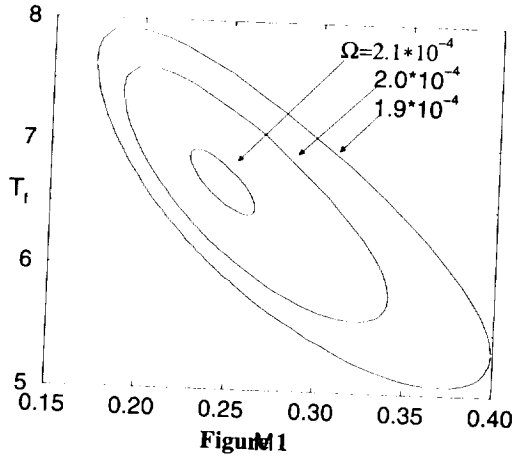

Figure 1

losses are too large a steady flame is no longer possible. We note that the flame temperature at the radiative-extinction limit is lower by nearly 500K, when compared to the flame temperature at M_{min}, as also noted in [19].

The effects of the Lewis numbers on the flammable region are shown in Fig.2. Here the allowable range of M is shown as a function of the oxidant Lewis number L_X for selected values of the fuel Lewis numbers L_F. Thus, it is expected that a methane-air flame for which $L_F \sim 0.96$ and $L_X \sim 1.01$ can be stabilized near the sphere for moderate values of the mass flow rate. However, when helium is added to the system as inert, the effective Lewis numbers become $L_F \sim 1.83$ and $L_X \sim 1.64$, and with these values steady burning is no longer possible. Diluents are often used in microgravity experiments in order to avoid unnecessary stratification of the initially separated fuel and oxidant, but this may produce different effective Lewis numbers with unwarranted consequences.

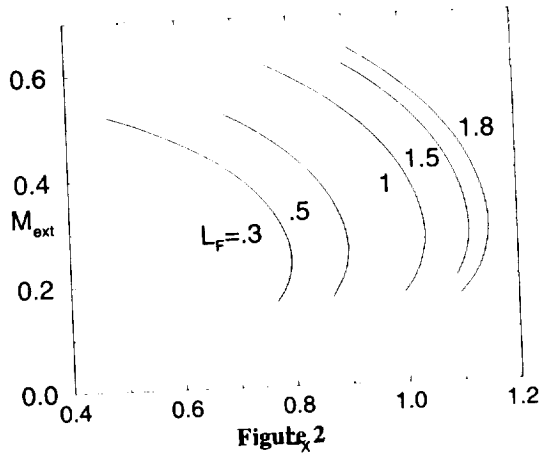

Figure 2

CELLULAR DIFFUSION FLAMES.

One form of an intrinsic instability in flames is the spontaneous development of cellular flames. Although studies of cellular flames have been predominantly carried out in premixed systems, there is experimental evidence of their occurrence in diffusion flames [5,7,8,11]. It is seen that, far from extinction, no mixture exhibited cellularity; cellular flames were formed at near-extinction conditions when the Lewis number of the more completely consumed reactant was sufficiently low. Based on a one-dimensional model [2,15], a stability study was performed in the limit of a large activation energy and general Lewis numbers distinct from one. The analysis reveals that a Burke-Schumann flame sheet, corresponding to complete reactant consumption (i.e. with the Damkohler number $D \to \infty$) is unconditionally stable. Cellular instability may only occur in the case of incomplete combustion when there is significant leakage of one of the reactants through the reaction zone; it is thus limited to $D_c < D < D^*$ where D_{ex} corresponds to extinction. The onset of instability occurs when D is reduced below D^*, and indeed, experiments indicate that the onset of cellular flames is usually associated with high flow rates conditions (i.e. low values of D), or with near-extinction conditions. Our predictions also show that no instability occur when both Lewis numbers equals to one; for cellular instability the reactants' Lewis numbers must be less then some critical value below one. The results in Fig.3 show regions of stability/instability in terms of the fuel and oxidant Lewis numbers, for different values of

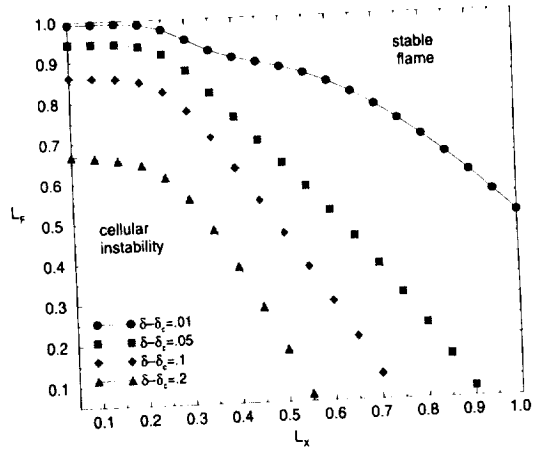

Figure 3

$\delta-\delta_c \sim D-D_c$. Note that as D increases the region of instability shrinks, as it should. Thus, in complete agreement with experiments, a hydrogen-oxygen flame will become cellular when hydrogen is diluted in nitrogen ($L_F \sim 0.35$) or in argon ($L_F \sim 0.33$), because L_F is then sufficiently low. Cellular flames will not be observed when the diluent is helium, for then $L_F \sim 1.02$ is much larger then the critical value. We also found that, at the onset of instability the maximum growth rate occurs at a wavelength $\sim 2\pi/k_{max}$ with $k_{max} \sim 1-2$ (see Fig.4; here $\Delta = \delta - \delta_c$ and σ is the growth rate). The predicted cell size is therefore several diffusion lengths wide, comparable in magnitude to the cell size observed experimentally ($0.7-1$ cm). When the onset of instability occurs near the extinction limit, i.e. when $D^* \approx D_c$, the maximum growth rate becomes very small, comparable to the reaction zone thickness, as found by Kim et al. (1996). In their analysis, which has been limited to the case $L_F = L_X < 1$, they only found instabilities with very short wavelengths, comparable to the thickness of reaction zone.

Another important parameter, besides the Lewis numbers, is the initial mixture strength. The flame appears more susceptible to cellular instability when the initial mixture was either lean or rich, depending on whether fuel or oxidant is the reactant supplied with the feeding stream. Figure 3, for example, corresponds to a lean system in which the net mass flux through the reaction zone is directed from the fuel side towards the oxidant side (i.e. the oxidant diffuses against the stream). In richer systems, the region of instability shrinks to lower values of L_F and L_X.

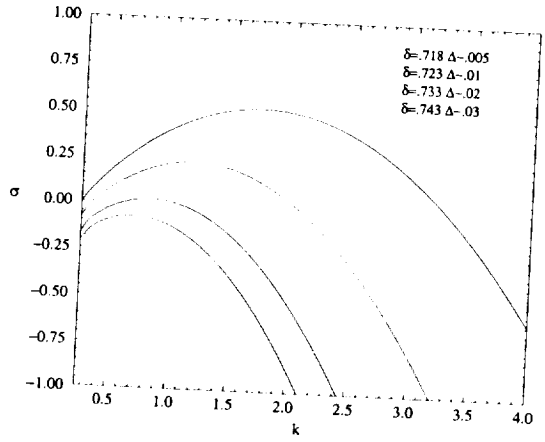

Figure 4

OSCILLATIONS IN DIFFUSION FLAMES

The onset of oscillations in diffusion flames, is another form of an intrinsic instability, which was the subject of our discussion in [3,4]. The problem we studied was that of a spherical diffusion flame surrounding a liquid fuel droplet. To minimize the stabilizing influences of curvature, and relate the findings to the microgravity candle flame experiments [6], we assumed that the burning occurs in a reduced oxidant ambient. We have also included in the analysis a volumetric heat loss term accounting, for example, for radiative losses. It was found again that the diffusion flame is stable for sufficiently large Damkohler numbers D; i.e. the Burke-Schumann flame sheet with complete consumption of fuel and oxidant is unconditionally stable. Oscillations were found for moderate values of D only. Also, for unity Lewis numbers and, in the absence of heat loss, the flame was always found stable. Oscillations develop only when the effective Lewis number is sufficiently larger than one. Thus, for example, when the ambient oxidant concentration is reduced, so as to lower D, critical conditions are reached beyond which spontaneous oscillations develop. By reducing the oxidant concentration further the amplitude of the oscillation increases; at first the growth in amplitude is moderate but eventually becomes sufficiently large leading to flame extinction. The marginally stable state, therefore, identifies a condition that promotes flame extinction. In the presence of heat loss, the flame was found more susceptible to

the instability. In general, increasing the heat loss lowers the critical Lewis number beyond which oscillations develop.

The onset of oscillations described here bears some similarity to the oscillations observed in the microgravity candle flame experiments. Candle wax is a mixture of paraffin and other hydrocarbons so that the Lewis number of the fuel vapor supporting the diffusion flame is typically much larger than unity. With the anticipated radiant heat loss, the conditions for the onset of oscillations are indeed accessible. The frequency of oscillations predicted by our model, ~ 1-2 Hz, matches those measured in the candle flame experiment.

The combination of heat loss and slowly diffusing fuels is also responsible to the onset of oscillations observed in spray flames. Using a co-flow configuration, it was observed [9] that when sufficient amount of fuel droplets were added to the fuel vapor inner stream, an oscillating flame occurs. Under the same operating conditions, but with no droplets present, the diffusion flame was steady. The observed oscillations were of low frequency ~ 1-5Hz. The operating conditions of the aforementioned experiments comply with those suggested earlier as responsible for spontaneous flame oscillations. The Lewis number corresponding to heptane vapor is sufficiently larger then one and there is an appreciable amount of heat loss from the flame used to vaporize the liquid droplets. Based on a simple one-dimensional model that appears to describe reasonably well the upper part of the spray flame [9,10], we were able to identify conditions for the onset of oscillations in terms of the loading parameter, the Lewis number and the structure of the spray. The frequency of the predicted oscillations was found to be of the same order of magnitude as in the experiment.

ACKNOWLEDGMENTS

This work was supported by the microgravity combustion program under NASA sponsorship; project NAG3-1604.

REFERENCES

1. Atreya A., Everest D.A., Agrawal S. & Anderson M.K. 1997, Proc. 4th Microgravity Comb. Workshop, p. 63.
2. Cheatham S. & Matalon M. 1999, submitted.
3. Cheatham S. & Matalon M. 1996, AIAA J., **34**(7), p. 1403.
4. Cheatham S. & Matalon M. 1996, 26th Symposium (Int.) on Combustion, p. 1063.
5. Chen, R., Mitchell, G.B. & Ronney, P.D. 1992, 24th Symposium (Int.) on Combustion, p. 213.
6. Dietrich D., Ross H. & Tien J.S. 1994, AIAA Paper 94-0429.
7. Dongworth, M.R. & Melvin, A. 1976, Combustion Science and Technology, **14,** 177-182.
8. Gardside, J.E. & Jackson, B. 1951, Nature, **168**, p. 1085.
9. Golovanevsky, B., Levy Y., Greenberg J.B. & Matalon, M. 1999 Combustion and Flame, **117**(1/2), p. 373.
10. Greenberg, J.B., Cheatham, S. & Matalon, M. 1998 Combustion Science and Technology, 131, p. 277.
11. Ishizuka, S. & Tsuji, H. 1981, 18th Symposium (Int.) on Combustion p. 695.
12. Kim, J.S., Williams, F.A. & Ronney, P.D. 1996, **327**, p. 273.
13. Law C.K., Sung C.J. & Zhu D.L. 1997, Proc. 4th Microgravity Comb. Workshop, p 69.
14. Matalon, M. & Greenberg J.B. 1998, AIAA Paper 98-0741.
15. Matalon, M. 1999, AIAA Paper 99-0584.
16. Mills, K. & Matalon, M. 1997, Combustion Science and Technology, **129**, 295.
17. Mills, K. & Matalon, M. 1998, 27th Symposium (Int.) on Combustion, to appear.
18. Struk P., Dietrich D. & Tien J.S. 1996 Microgravity Science and technology, IX/2, p.106.
19. Tien J.S. 1997 Proceedings of the Asian-Pacific Conference on Combustion, Osaka, Japan.

HYDRODYNAMIC INSTABILITY AND THERMAL COUPLING IN A DYNAMIC MODEL OF LIQUID-PROPELLANT COMBUSTION

S. B. Margolis, Combustion Research Facility, MS 9052, Sandia National Laboratories, Livermore, California 94551-0969 / margoli@sandia.gov

EXTENDED ABSTRACT

The notion of hydrodynamic instability in combustion originated with Landau's seminal study of premixed flame propagation.[1] In that work, it was postulated that a flame could be represented by a surface of discontinuity propagating normal to itself with constant speed. It was then determined that a premixed gaseous flame was intrinsically unstable to steady (cellular) disturbances. This specific form of hydrodynamic instability, generally referred to as Landau instability, also occurs in the combustion of liquids, and was briefly addressed at the end of Landau's original study. In that problem, the unburned mixture is a liquid propellant and the burned region consists of gaseous products. The physical existence of a liquid/gas interface led to the inclusion of additional physics in the model, namely surface tension and gravitational acceleration (downward propagation was assumed). Consequently, a stability criterion was derived such that the liquid/gas interface was either hydrodynamically stable or unstable in the Landau (cellular) sense, depending on the product of gravitational acceleration and surface-tension coefficient being greater or less than a critical value. This result was later extended by Levich,[2] who considered the effects of (liquid) viscosity in lieu of surface tension and obtained a similar result.

The assumption of a thin reaction region or sheet is often a valid and useful approximation, but the assumption of a constant normal burning rate is now regarded as an oversimplification when applied to the problem of combustion instability. Early attempts at modification postulated a linear relationship between burning rate and flame curvature,[3] while more recent approaches have employed asymptotic methods to analyze the flame structure and derive locally-dependent expressions for the burning rate.[4–7] In propellant combustion, on the other hand, it has long been customary to experimentally measure the pressure response, or pressure sensitivity, of the burning rate, as well as (to a lesser extent) its temperature sensitivity. Although asymptotic models that resolve the combustion-wave structure can be developed,[8–10] the representation of combustion as a surface that propagates according to a prescribed burning-rate law allows one to circumvent the intricacies of the combustion region and to impose fewer restrictions on the hydrodynamic model.

Thus, for liquid-propellant combustion, the Landau/Levich hydrodynamic models have been combined and extended to account for a dynamic dependence of the burning rate on the local pressure and temperature fields.[11,12] Analysis of these extended models is greatly facilitated by exploiting the realistic smallness of the gas-to-liquid density ratio ρ. Neglecting thermal coupling effects, an asymptotic expression was then derived for the cellular stability boundary $A_p(k)$, where A_p is the pressure sensitivity of the burning rate and k is the disturbance wavenumber.[13] The results explicitly indicate the stabilizing effects of gravity on long-wave disturbances, and those of viscosity and surface tension on short-wave perturbations, and the instability associated with intermediate wavenumbers for critical negative values of A_p. In the limit of weak gravity, hydrodynamic instability in liquid-propellant combustion becomes a long-wave instability phenomenon, whereas at normal gravity, this instability is first manifested through O(1) wavenumbers. In addition, surface tension and viscosity (both liquid and gas) each produce comparable stabilizing effects in the large-wavenumber regime, thereby providing important modifications to the previous analyses in which one or more of these effects was neglected. For $A_p = 0$, the Landau/Levich results are recovered in appropriate limiting cases, although this typically corresponds to a hydrodynamically unstable parameter regime for $\rho \ll 1$.[1,2,13]

In addition to the classical cellular form of hydrodynamic stability, there exists a pulsating form corresponding to the loss of stability of steady, planar burning to time-dependent perturbations.[14] This occurs for negative values of the parameter A_p, and is thus absent from the original Landau/Levich models. In the extended model, however, there exists a stable band of negative pressure sensitivities bounded above by the Landau type of instability, and below by this pulsating form of hydrodynamic instability. Indeed, nonsteady modes of combustion have been observed at low pressures in hydroxylammonium nitrate (HAN)-based liquid propellants, which often exhibit negative pressure sensitivities.[15] While nonsteady combustion may correspond to secondary and higher-order bifurcations above the cellular boundary,[16] it may also be a manifestation of this pulsating type of hydrodynamic instability.

In the present work, a nonzero temperature sensitivity is incorporated into our previous asymptotic analyses.[13,14] This entails a coupling of the energy equation to the previous purely hydrodynamic problem, and leads to a significant modification of the pulsating boundary such that, for sufficiently large values of the temperature-sensitivity parameter, liquid-propellant combustion can become intrinsically unstable to this alternative form of hydrodynamic instability. For simplicity, further attention is confined here to the inviscid version of the problem since, despite the fact that viscous and surface-tension effects are comparable,[13,14] the qualitative nature of the cellular boundary remains preserved in the zero-viscosity limit, as does the existence of the pulsating boundary.

The mathematical model[13] adopts the classical assumption that there is no distributed reaction in either the liquid or gas phases, but now the reaction sheet, representing either a pyrolysis reaction or an exothermic decomposition at the liquid/gas interface, is assumed to depend on local conditions there. Within the liquid and gas phases, the various physical properties are assumed constant, with appropriate jumps across the phase boundary. The downward-propagating liquid/gas interface is then sought as a function of space and time, with the steadily-propagating, planar state serving as the basic solution whose stability is to be investigated. The nondimensional mass burning rate A, and hence the motion of this interface, is assumed to be a local function of the nondimensional (gas) pressure p and temperature Θ. Consequently, two parameters $A_p = \partial A/\partial p$ and $A_\Theta = \partial A/\partial \Theta$ emerge in the linear stability analysis, representing the pressure and temperature sensitivity of the burning rate (evaluated at conditions that exist at the unperturbed gas/liquid interface). The governing equations then consist of conservation of mass, momentum and energy in each phase, subject to appropriate boundary and interface conditions.

Determination of the neutral stability boundaries that separate regions of steady, planar burning from regions of nonsteady (pulsating) and/or cellular instability is again facilitated by exploiting the limit $\rho \ll 1$. In particular, we introduce a bookkeeping parameter $\epsilon \ll 1$ and consider the realistic parameter regime $\rho = \rho^*\epsilon$, $\gamma \sim \mathrm{O}(1)$ and either $Fr^{-1} = g \sim \mathrm{O}(1)$ or $Fr^{-1} = g^*\epsilon \sim \mathrm{O}(\epsilon)$, where γ is the nondimensional surface tension of the liquid and Fr^{-1} is the inverse Froude number, taken to be O(1) for the case of normal gravity, and $\mathrm{O}(\epsilon)$ in the reduced-gravity regime. Realistic values for ϵ are on the order of 10^{-3} or 10^{-4}. In this parameter regime, it turns out that the appropriate scaling for A_p that describes the neutral stability region is $A_p = A_p^*\epsilon$, whereas the appropriate scale to describe the primary effects of thermal coupling turns out to be $A_\Theta = A_\Theta^*\epsilon^{1/4}$. Thus, $A_\Theta/A_p \sim \mathrm{O}(\epsilon^{-3/4})$ is at least as large as the nondimensional activation energy N, consistent with an Arrhenius dependence of the burning rate on temperature.

In the limit $A_\Theta = 0$, the results obtained from the dispersion relation are as follows.[13] First (see Figure 1), the pulsating hydrodynamic stability boundary is given, to leading order in ϵ, by $A_p^* = -\rho^*$, with instability occurring below this critical value. For the cellular stability boundary, the corresponding leading-order expression depends on the magnitude

of the wavenumber k. In particular, there are three wavenumber scales to be considered; the O(1), or outer, scale k, a far outer scale $k_f = k\epsilon$, and an inner scale defined by either $k_i = k/\epsilon$ if $Fr^{-1} \sim O(1)$ or $k_1 = k/\epsilon^2$ if $Fr^{-1} \sim \mathrm{O}(\epsilon)$. Obtaining expressions for the cellular stability boundary in each region and matching them to one another, a uniformly valid composite expansion $A_p^{*(c)}(k)$ may be constructed in the region $A_p^* < 0$ (the basic solution can be shown to be unstable for $A_p^* > 0$). The cellular boundary is thus given by

$$A_p^{*(c)} \sim -\frac{1}{2}\rho^* + \frac{1}{2}\epsilon\rho^{*2}\gamma k + \begin{cases} \epsilon\rho^{*2}g/2k, & Fr^{-1} \sim \mathrm{O}(1) \\ \epsilon^2\rho^{*2}g^*/2k, & Fr^{-1} \sim \mathrm{O}(\epsilon)\,, \end{cases} \tag{1}$$

where the definitions of k_i and k_f have been used to express the final result in terms of k.

It is seen from Figure 1 that there is a stable region between the pulsating and cellular stability boundaries for $A_\Theta = 0$, and this result is enhanced when viscous effects, which play a stabilizing role with respect to both boundaries for sufficiently large wavenumbers, are included in the analysis.[13,14] As for the Landau (cellular) form of hydrodynamic instability, gravity and surface tension are stabilizing for small and large wavenumber disturbances, respectively. The essential difference, as illustrated in Figure 1, between the normal and reduced gravity limits is that in the latter instance, gravity is only capable of stabilizing disturbances whose wavenumbers are $\mathrm{O}(\epsilon^2)$, whereas in the former case, gravity is sufficiently strong to stabilize disturbances whose wavenumbers are $\mathrm{O}(\epsilon)$. Consequently, hydrodynamic instability becomes a long-wave phenomenon in the reduced gravity regime, since, from Eq. (1), the most unstable wavenumbers are then $\mathrm{O}(\epsilon^{1/2})$, rather than O(1).

When the temperature-sensitivity parameter A_Θ is nonzero, significant modifications can occur, depending on the magnitude of A_Θ. In particular, for $A_\Theta = A_\Theta^*\epsilon^{1/4} \sim \mathrm{O}(\epsilon^{1/4})$, the pulsating stability boundary depicted in Figure 1 changes in the outer wavenumber region such that instead of $A_p^* = -\rho^*$, this boundary is determined implicitly by

$$A_p^* + \rho^* - \rho^{*3/2}(2k)^{-1/2}A_\Theta^*\left[-(2A_p^* + \rho^*)\right]^{-3/4} = 0\,. \tag{2}$$

Referring to the outer solution in Figure 2, it is seen that for $A_\Theta^* > 0$, the pulsating boundary becomes C-shaped, the upper branch approaching the cellular boundary as $k \to \infty$, and the lower branch approaching the original ($A_\Theta^* = 0$) pulsating boundary. These same limits are approached for any fixed value of k as $A_\Theta^* \to 0$. The region within the C-shaped curve is stable, and thus not only is steady, planar burning intrinsically unstable for sufficiently small wavenumbers, but also, for larger k, *any* crossing of the C-shaped boundary from the stable to the unstable region corresponds to the onset of a pulsating instability. As A_Θ^* increases, the turning point of the pulsating boundary shifts to the right; as A_Θ^* becomes small, the turning point shifts to small values of k that ultimately lie outside the O(1) wavenumber region. Thus, in the outer wavenumber regime, the original pulsating and cellular boundaries are recovered as A_Θ^* decreases, but for A_Θ^* sufficiently large, the original cellular boundary lies within the unstable region and the basic solution becomes intrinsically unstable to oscillatory disturbances.

A composite asymptotic representation of the neutral stability boundary for $A_\Theta \sim \mathrm{O}(\epsilon^{1/4})$ is obtained by matching the cellular and pulsating boundaries in the far outer wavenumber regime with the appropriate solution branch of Eq. (2) in the O(1) wavenumber region. The resulting leading-order composite stability boundary spans both the outer and far outer wavenumber regions as shown in Figure 2 (heavy curve). The lower branch of the composite boundary is a pulsating boundary for all wavenumbers, whereas the upper branch transitions from a pulsating boundary for O(1) wavenumbers to a cellular boundary for $\mathrm{O}(\epsilon^{-1})$ wavenumbers. Indeed, in the outer wavenumber regime, the size of the upper region of oscillatory instability, which is bounded below by the upper branch of the pulsating stability boundary and above by the region of nonoscillatory instability beyond the old cellular boundary $A_p^* \sim -\rho^*/2$, shrinks to zero as k becomes large.

The nature of the evolution, as A_Θ^* decreases, of the pulsating stability boundary depicted in Figure 2 to that shown in Figure 1 may be determined by analyzing the dispersion relation for smaller order-of-magnitude wavenumbers and appropriately rescaled values of A_Θ. In particular, it turns out that this transition occurs as A_Θ decreases through $O(\epsilon^{1/2})$ values,[17] thereby recovering the region of stability depicted in Figure 1.

ACKNOWLEDGEMENTS

This work was supported by the U.S. Dept. of Energy (contract DE-AC04-94AL85000) and by the NASA Microgravity Science Research Program (contract C-32031-E).

REFERENCES

[1] Landau, L. D., *Acta Physicochimica URSS* 19:77–85 (1944).
[2] Levich, V. G., *Dokl. Akad. Nauk SSSR* 109:975–978 (1956).
[3] Markstein, G. H., *Non-Steady Flame Propagation*, Pergamon Press, Oxford, 1964.
[4] Sivashinsky, G. I., *Combust. Sci. Tech.* 15:137–146 (1977).
[5] Pelcé, P., & Clavin, P., *J. Fluid Mech.* 124:219–238 (1982).
[6] Matalon, M., & Matkowsky, B. J., *J. Fluid Mech.* 124:239–259 (1982).
[7] Margolis, S. B., *Prog. Energy Combust. Sci.* 17:135–162 (1991).
[8] Margolis, S. B., & Williams, F. A., *Combust. Sci. Tech.* 59:27–84 (1988).
[9] Margolis, S. B., & Williams, F. A., *SIAM J. Appl. Math.* 49:1390–1420 (1989).
[10] Bechtold, J. K., & Margolis, S. B., *Combust. Sci. Tech.* 68:49-84 (1989).
[11] Armstrong, R., & Margolis, S., *22nd Symp. (Int'l) on Combustion*, 1807–1815 (1989).
[12] Armstrong, R. C., & Margolis, S. B., *Combust. Flame* 77:123–138, (1989).
[13] Margolis, S. B., *Combust. Flame* 113:406–423 (1998).
[14] Margolis, S. B., *Twenty-Seventh Symposium (Int'l) on Combustion*, to appear (1998).
[15] Vosen, S. R., *Twenty-Second Symposium (Int'l) on Combustion*, 1817–1825 (1989).
[16] Bechtold, J. K., & Margolis, S. B., *SIAM J. Appl. Math.* 51:1356–1379 (1991).
[17] Margolis, S. B., to appear (1999).

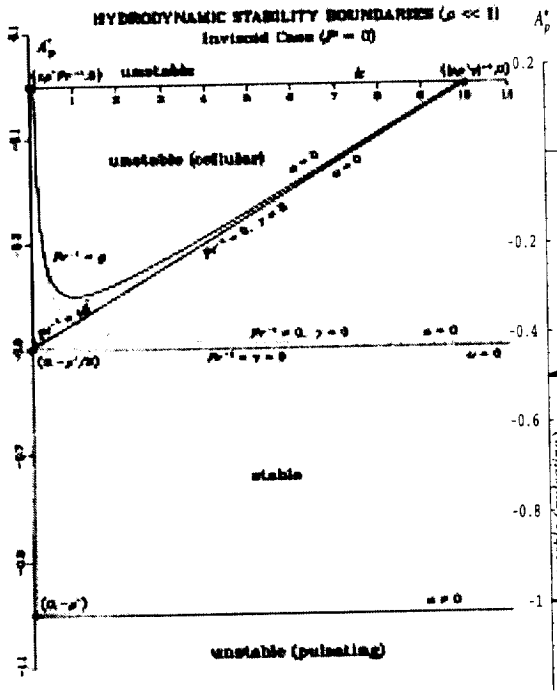

Figure 1

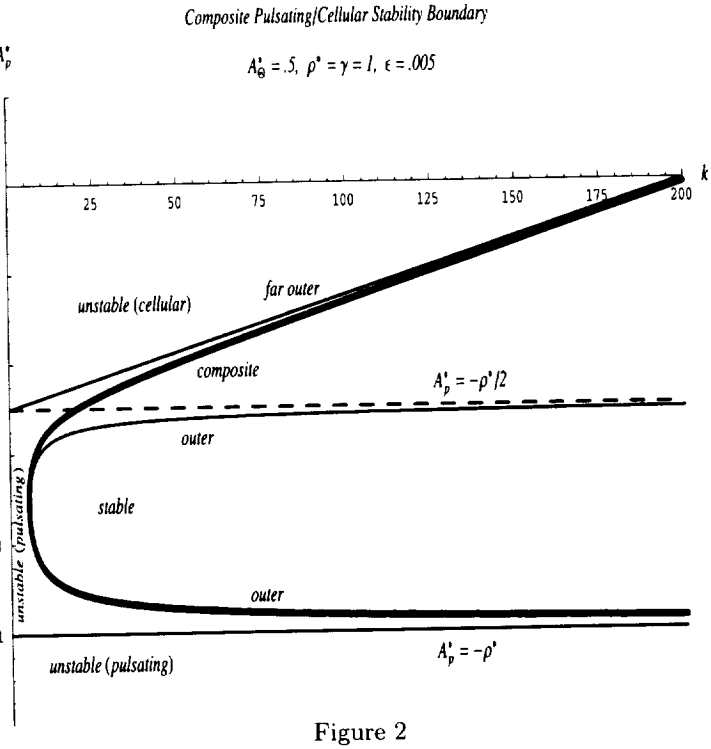

Figure 2

LOW-TEMPERATURE OXIDATION REACTIONS AND COOL FLAMES AT EARTH AND REDUCED GRAVITY

341-25

Howard Pearlman
University of Southern California
Department of Mechanical Engineering
Los Angeles, CA 90089

INTRODUCTION

Non-isothermal studies of cool flames and low temperature oxidation reactions in unstirred closed vessels are complicated by the perturbing effects of natural convection at earth gravity. Buoyant convection due to self-heating during the course of slow reaction produces spatio-temporal variations in the thermal and thus specie concentration fields due to the Arrhenius temperature dependence of the reaction rates. Such complexities have never been quantitatively modeled and were the primary impetus for the development of CSTR's (continuously stirred tank reactors) 30 years ago [1,2]. While CSTR's have been widely adopted since they offer the advantage of spatial uniformity in temperature and concentration, all gradients are necessarily destroyed along with any structure that may otherwise develop.

Microgravity offers a unique environment where buoyant convection can be effectively minimized and the need for stirring eliminated. Moreover, eliminating buoyancy and the need for stirring eliminates complications associated with the induced hydrodynamic field whose influence on heat transport and hot spot formation, hence explosion limits, is not fully realized [3].

OBJECTIVE

The objective of this research is to quantitatively determine and understand the fundamental mechanisms that control the onset and evolution of low temperature reactions and cool flames in both static and flow reactors. Microgravity experiments will be conducted to obtain benchmark data on the structure (spatio-temporal temperature, concentration, flow fields), the dynamics of the chemical fronts, and the ignition diagrams (pressure vs. temperature). Ground-based experiments will be conducted to ascertain the role of buoyancy. Numerical simulations including detailed kinetics will be conducted and compared to experiment.

STATIC TESTING

Static tests are experimentally conducted in the laboratory and aboard NASA's KC-135 aircraft using mixtures of H_2, "wet" CO and hydrocarbons diluted with oxygen and inert gases at elevated temperature, reduced pressure. To date, concentration has been on premixtures between 300-600°C at atmospheric pressure and below.

A "classical "apparatus consisting of an oven, a fused-silica spherical vessel of given diameter (d=5cm), and gas delivery system is used to conduct the 1g and μg tests. The oven employs resistive heating elements in the rear and top panels, a mixing fan to circulate the hot air, 7.5cm diameter quartz windows on both the top and side walls for viewing and a gas feedthrough

built into the door. Random spatial thermocouple measurements ensure temperature uniformity within the oven to ± 10°C throughout its operating range (20-600°C).

To minimize irreproducibility's resulting from wall affects, the vessel is either "baked out" prior to testing or chemically treated with Sylon™, a deactivating agent. Once baked or treated, exposure to the environment is minimized, typically by holding it under vacuum or filling it to atmospheric pressure with dry N_2 or He. The gases are premixed by partial pressure, prior to testing, and stored in 300 cc stainless steel sample cylinders. Each test is conducted by initially evacuating the vessel to 50 mTorr or below. An additional 50cc stainless steel sample cylinder is then filled with the premixture to given pressure; the outlet of the 50cc cylinder feeds directly into the vessel, isolated from it by pneumatic solenoids. One solenoid is situated as close to the vessel inlet as possible such that the vessel can be isolated immediately after it is filled. The filling process is driven by the pressure differential between the 50cc cylinder and the pre-evacuated flask. The dead volume between the sample cylinder and vessel inlet is minimized to shorten the fill time. There are two intensified Xybion cameras mounted on the oven. One on the top and the other on the side wall. Fig. 1 is a schematic of the apparatus.

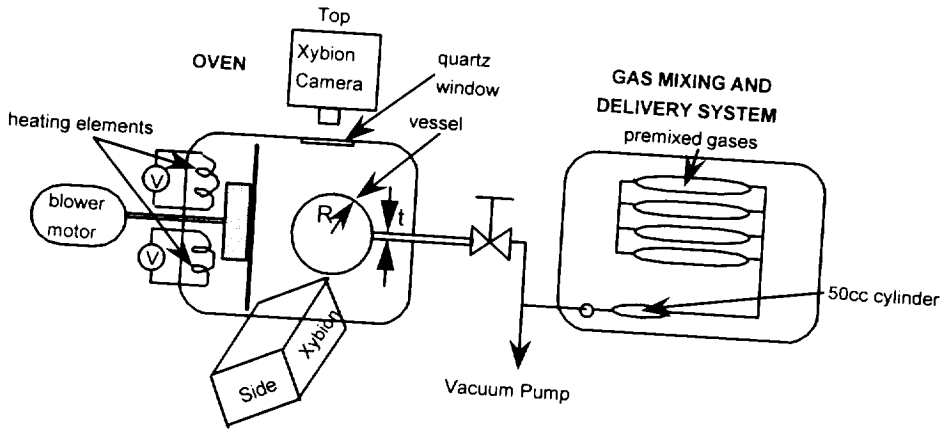

Fig. 1: Schematic of Static Reactor Apparatus for 1g and μg tests

To establish an isothermal initial condition, the gas is conductively preheated as it is introduced through the neck of the flask (151mm long, t = 6mm i.d.). The residence time, t_{res}, associated with the filling process is on the order of 1 sec measured from the pressure traces. Estimating a thermal preheat time as $t_{cond} \sim t^2/\alpha \sim (0.3cm)^2/0.32cm^2/s \sim 0.3s$ (e.g., taken for a $50\%C_3H_8$-$50\%O_2$ mixture, at T=310°C, P=0.5psia) suggests that the mixture should be at (or near) temperature as it enters the flask since $t_{cond} < t_{res}$.

The chemical time scale, t_{chem}, the buoyant rise time of the hot gas, t_{buoy}, and the diffusive time scales for heat (t_α)and mass (t_D) transport can be estimated as $t_{chem} \sim 1/rr \sim A\exp(E_a/RT)$, $t_{buoy} \sim R/V_{buoy}$, $t_\alpha \sim R^2/\alpha$, and $t_D \sim R^2/D$ where rr is the reaction rate, α is the thermal diffusivity, D is the binary diffusion coefficient, and V_{buoy} is the buoyant rise of the hot gas given as $V_{buoy} \sim \sqrt{\frac{\Delta\rho}{\rho} gR}$ (viscous solution) where ρ is density, g is gravitational acceleration and R is vessel size. Unlike hot flames where $\Delta\rho/\rho \sim 1$, the small temperature rises associated with cool flames (e.g., 10-200°C) result in $\Delta\rho/\rho \sim 0.2$-0.4. For a 5cm radius flask,

$V_{buoy}\sim\sqrt{0.2(981cm/s^2)(5cm)}$ ~30cm/s and t_{buoy}~5cm/30cm/s~0.17s. t_α and t_D are an order of magnitude (or more) longer estimated at T=310°C, P=0.5atm, for 50%C_3H_8-50%O_2 to be $t_\alpha\sim(5cm)^2/0.32cm^2/s\sim79s$ and $t_D\sim(5cm)^2/0.74cm^2/s\sim34s$. Since $t_{buoy} << t_\alpha$ or t_D, buoyancy dominates the transport of heat and species at 1g whereas diffusion controls transport at μg. t_{chem} spans several orders of magnitude depending on the temperature, pressure and stoichiometry; at low temperatures, reaction times can be on the order of hours or minutes, in many cases, much longer than either t_{buoy} or t_D, emphasizing the importance of buoyancy at 1g.

RESULTS

Representative 1g and μg data for a mixture of 66.7%C_4H_{10}-33.3%O_2 by volume (2:1) at T=310°C is shown in Figs 2-4 for different initial pressures. All tests are performed with the same batch of mixture in the same 10.2 cm i.d.. flask, initially chemically deactivated. To ensure repeatability, similar tests were performed approximately one month apart with little discrepancy.

Figure 2 shows the pressure trace as a function of time for initial pressures between 1.5 and 4.2 psia. The solid lines in all plots correspond to the KC-135 μg tests and the dashed lines correspond to 1g tests. At μg, all tests are performed (vessel filled, isolated and data acquired) during the 20s parabolic trajectory while at 1g, data is acquired for several minutes. All sampling rates are 100Hz. Based on the data, several features can be observed. Notably, the first induction time is always shorter at μg than at 1g and the difference decreases as the pressure increases. Since buoyant convection dominates diffusive transport at 1g, the heat (associated with the self-heating of the reaction) concentrates at the top of the vessel enhancing the conductive heat loss to the vessel wall thereby raising the explosion threshold (while this may be the conventional school of thought, ref. 3 suggests that the convective length scales may dictate enhancement/ suppression of the explosion limits). In addition, radicals/ wall reactions can occur more readily at 1g since the reaction is concentrated close to the top wall. Thus, at 1g, both conductive loss and perhaps enhanced wall reactions moderate the rate of temperature rise/ radical specie concentrations and thus delay the onset of cool flame generation. At μg, diffusive times are much longer than buoyant times, slowing the inhibiting effects of conductive loss (and perhaps, radical/ wall reactions), thus shortening the induction times.

As many have observed, cool flames originate at the top of the vessel at 1g. In contrast, they develop at the center of the vessel at μg. This tends to support the above conventional phenomenological arguments. The side camera view is shown in Fig.5 for identical initial conditions at 1g (Fig. 5a) and μg (Fig. 5b).

Fig. 3 demonstrates that the ignition diagrams at 1g and μg are different. As an example, at higher initial pressures, notably 4.4psia, cool flames are observed at both 1g and μg, yet at 4.7 psia, two-stage ignition is observed at μg while cool flames are observed at 1g. In effect, it appears that the transition from cool flame to 2-stage ignition as initial pressure increases is delayed at 1g perhaps due to the enhanced conductive losses and wall reactions.

Fig. 4 demonstrates that 1- and 2-stage ignitions also occur earlier at μg than at 1g. Note that the second induction time associated with the 2-stage ignition is also shorter at μg than at 1g.

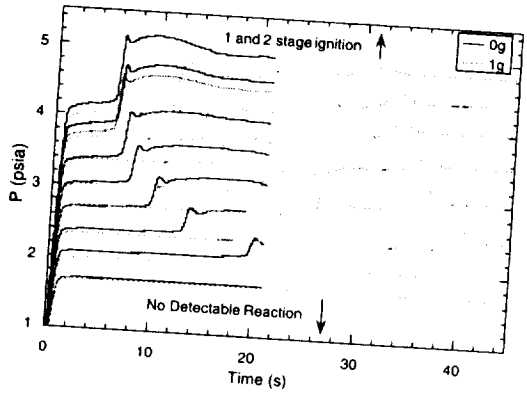

Fig. 2: Pressure vs. Time: $P_{initial}$<4.2psia

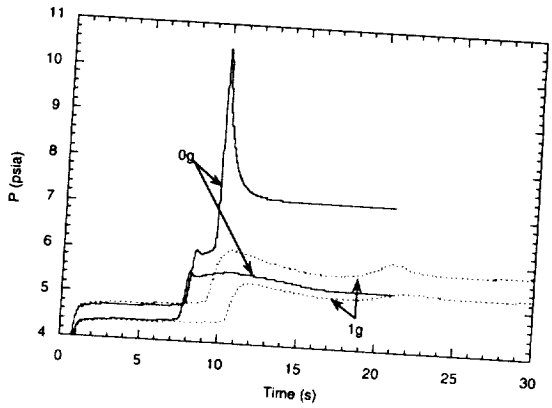

Fig. 3: Transition to 2-stage ignition

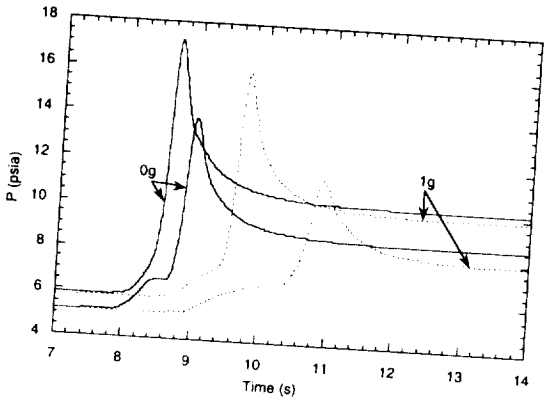

Fig. 4: 1- and 2-stage ignitions

ACKNOWLEDGMENTS

I wish to extend my gratitude to the cool flame team for all of their help and hard work. Special thanks are extended to Mr. Richard Chapek, Ms. Donna Neville, Dr. Ming-Shin Wu, and Dr. R. L. VanderWal. This work is dedicated to Mr. Thomas Kahoe for his encouragement, assistance and friendship over the years. This study is supported by NASA under contract NCC3-501.

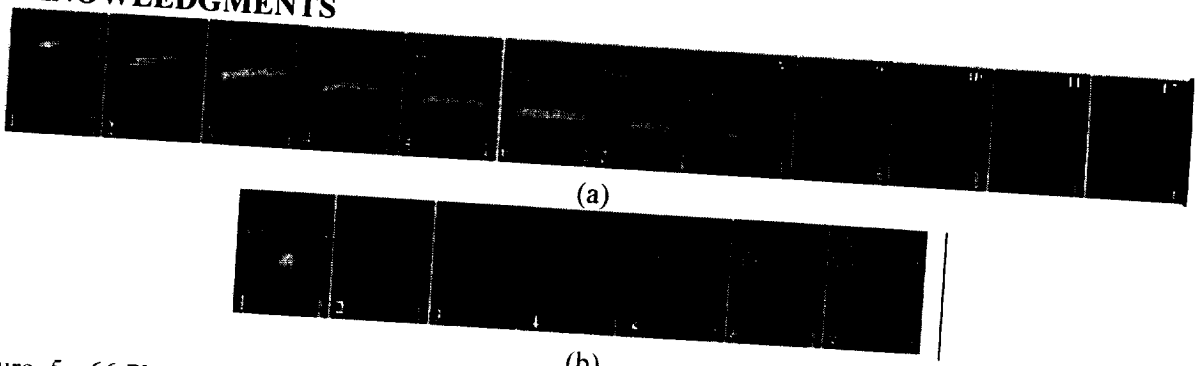

Figure 5: 66.7%C_4H_{10}-33.3%0_2 premixture, $P_{initial}$=4.4psia, T_{vessel}=310°C, Side Camera, (a) 1g (g is downward), (b) μg. Time between sequential images is 1/10s.

REFERENCES

1. Griffiths, J.F., Gray, B.F., and P. Gray, Thirteenth Symposium (International) on Combustion, (1971) 239-248.

2. Caprio, V., Insola, A. and P. Lignola, Flames as Reactions in Flow, 2o Simpsio Internazionale di Dinamica delle Reazioni Chimiche Su, Pudova, 1975, 47-51.

3. Kagan, L, Beresycki, H., Joulin, G. and Sivashinsky, G., Combustion Theory and Modeling, **1** (1997) 97-111.

DETAILED MULTIDIMENSIONAL SIMULATIONS OF THE STRUCTURE AND DYNAMICS OF FLAMES

K. Kailasanath and G. Patnaik
Laboratory for Computational Physics and Fluid Dynamics
Naval Research Laboratory, Washington, DC 20375

INTRODUCTION

Numerical simulations in which the various physical and chemical processes can be independently controlled can significantly advance our understanding of the structure, stability, dynamics and extinction of flames. Therefore, our approach has been to use detailed time-dependent, multidimensional, multispecies numerical models to perform carefully designed computational experiments of flames on Earth and in microgravity environments. Some of these computational experiments are complementary to physical experiments performed under the Microgravity Program while others provide a fundamental understanding that cannot be obtained from physical experiments alone. In this report, we provide a brief summary of our recent research highlighting the contributions since the previous microgravity combustion workshop.

There are a number of mechanisms that can cause flame instabilities and result in the formation of dynamic multidimensional structures. In the past, we have used numerical simulations to show that it is the thermo-diffusive instability rather than an instability due to preferential diffusion that is the dominant mechanism for the formation of cellular flames in lean hydrogen-air mixtures [1]. Other studies have explored the role of, gravity on flame dynamics and extinguishment [2,3], multi-step kinetics and radiative losses on flame instabilities in rich hydrogen-air flames [4,5], and heat losses on burner-stabilized flames in microgravity [6]. The recent emphasis of our work has been on exploring flame-vortex interactions [7,8] and further investigating the structure and dynamics of lean hydrogen-air flames in microgravity [9]. These topics are briefly discussed below after a brief discussion of our computational approach for solving these problems.

THE NUMERICAL MODEL

The results discussed here have been obtained from numerical simulations using the detailed, parallel, time-dependent flame code [10] either in its full three-dimensional form or in an axisymmetric version for problems in which three-dimensionality is of secondary importance. In all cases, in order to obtain definitive information about complex unsteady flames, a number of physical processes must be included and modeled to a sufficient level of detail. These processes include elementary chemical reactions, multi-species diffusion among various chemical species, thermal conduction, viscosity, radiation, and fluid convection. Body forces due to gravity are important for low speed flames and could also result in Rayleigh-Taylor instabilities. Both buoyancy and fluid expansion will drive flow in the fluid, so an accurate model of compressible fluid flow is needed. Therefore, the three-dimensional, time-dependent, Navier-Stokes, reactive-flow conservation equations are solved for density, momentum, energy, and the number densities of individual species. The numerical simulations of flames presented here include a detailed set of elementary reactions for hydrogen or methane combustion. Space restrictions do not allow the elaboration of the equations solved or the numerical solution procedure, but details can be found in previous reports [10,11].

FLAME-VORTEX INTERACTIONS

Many studies have been carried out on flame-vortex interactions as a means to improve our understanding of turbulent flames and for the development of better models of turbulent reactive flow. These studies include the work sponsored by the Microgravity Combustion Science Program focussing on the effects of buoyancy [12,13]. Our numerical experiments are complementary to these physical experiments, also reported elsewhere in these proceedings. In addition to showing results similar to those observed in their experiments, we have used the numerical simulations to explore the role of certain parameters in a controlled manner that is very difficult or impossible to achieve in a laboratory experiment in microgravity.

The calculations were initiated with a planar flame propagating upward, downward or in a zero-gravity environment in a premixed methane-air mixture. In all cases, a vortex ring with a Gaussian distribution of vorticity in its core was superimposed on the flow field in the unburned reactants upstream of the flame. The vortex travels towards the flame due to its self-induced velocity. The peak vorticity in the initial vortex is used to characterize the vortex strength. The vortex core diameter and the ring diameter can be varied more easily in the numerical simulations than in the laboratory experiments. By varying these parameters as well as the vortex strength and radiative losses in a controlled manner, these simulations have contributed to our fundamental understanding of flames.

In one series of simulations, the initial vortex core diameter and ring diameter were held fixed at 0.4 cm and 1.2 cm, respectively, and the initial vortex strength was increased from 90/s to 2400/s. These cases corresponded to "weak", "intermediate", and "strong" vortex regimes of interaction observed earlier in the microgravity experiments on propane-air flames [12]. As in the experiments, phenomena such as local flame extinguishment and the formation of pockets of unburned gases in the burnt region have been observed. In all these cases, gravity is very important in determining the final shape of the flame. In downward propagation, buoyancy stabilizes the flame and a planar flame is restored. In zero gravity, a wrinkled flame is left behind. In upward propagation, the destabilizing effect of gravity leads to some highly distorted flame shapes. The flame-vortex interaction itself is also influenced by gravity, though not very strongly for these cases.

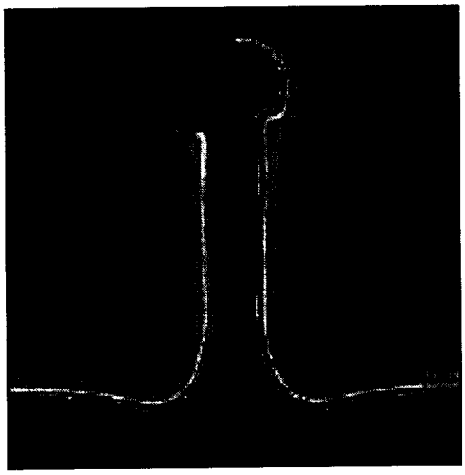

Different processes such as heat loss, strain and chemical kinetics have been reported to be responsible for the extinguishment of premixed flames. We have used the numerical simulations as a tool to understand the relative importance of heat loss and strain in the extinguishment observed during flame-vortex interactions. One of the advantages of numerical simulations is the ability to turn processes off and on and to control the magnitude of their contribution. For example, we performed simulations of flame interactions with strong vortices in which the radiation process was turned off. Unlike the "standard" case, the flame did not extinguish even when the initial vortex strength was increased to 2400/s (see Figure). In the

standard case, the flame extinguishes when the initial vortex strength is over 800/s, indicating the essential role played by radiative losses in extinguishing this flame. However, from this simulation, it was not clear if a small amount of heat loss will extinguish the flame or, for that matter, if a small change in the radiation will have a significant impact.

To investigate this matter, two series of simulations were carried out. In both series, the initial vortex strength was held constant at 850/s with a vortex core size of 0.2 cm radius and a ring diameter of 1.2 cm. The differences between the two series were the manner in which the radiative loss was controlled. Both approaches indicated that a significant amount of heat loss is required and that small changes in the overall heat loss does not drastically alter the results. This is fortunate since the uncertainties in the input parameters and the approximations used for estimating the radiative losses could result in some inaccuracies in the calculation of the effect of heat losses.

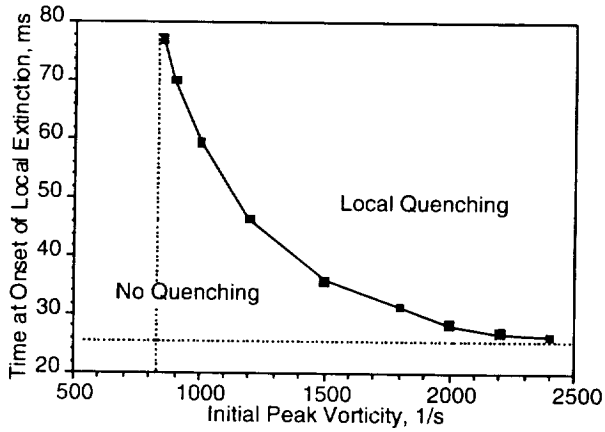

Another important observation from these studies is that the flame extinguishment is not an abrupt phenomenon but requires a finite amount of time. Furthermore, the time required for local flame extinguishment varies with the vortex strength as shown in the figure. That is, to extinguish the flame, a high enough strain rate needs to be present for a long enough time. This has important implications for turbulent flames since in many practical situations, high strain rates may be present only for short duration. Furthermore, the relevance of steady-state, opposed flow flame extinguishment studies for practical applications is questionable.

LEAN HYDROGEN-AIR FLAMES IN MICROGRAVITY

Experimental observations of flames in lean hydrogen-air mixtures in microgravity have shown that the structure and dynamics of these flames are quite complex, with the formation of multiple cells and the existence of a cell-split limit [14]. In mixtures below the cell-split limit, other complex phenomena such as flame balls and flame strings have been observed. Our previous two dimensional simulations [15] have been able to show the different regimes of cell splitting and had also predicted a cell-split limit. However, the predicted limit was higher than the observed limit. At that time, we speculated that the discrepancy could be due to the absence of three-dimensional modes in the simulations or uncertainties in the chemistry model. With the development of the three-dimensional flame code, this problem was re-examined.

Comparing 2-D and 3-D simulations of flames in a 9.5 % Hydrogen-air mixture shows that the flames do grow more rapidly and split in 3-D than in 2-D. Leaner mixtures that did not show cell-splitting in earlier simulations do indeed show splitting in the newer simulations which have also been carried out for much longer times. However, the time taken for the initial cell to grow and split is still longer than that observed experimentally. This suggests that in addition to three-dimensionality, uncertainties in the chemical parameters for these regimes could be a factor for the observed differences. Additional simulations were carried out with different chemistry

mechanisms but these again proved to be inconclusive. These observations are also in agreement with a one-dimensional study of flame balls that showed that different chemistry packages gave different results [16].

SUMMARY AND CONCLUSIONS

Recent numerical simulations of the structure and dynamics of flames in microgravity have been reported. Two topics have been highlighted. The first, on flame-vortex interactions, has brought out the complementary nature of numerical simulations to physical experiments and the additional insight that can be gained from controlled numerical experiments. The second topic, on flames in very lean hydrogen-air mixtures in microgravity, has exposed the need to have better chemistry models valid for these regimes. Since some of these mixtures are not flammable in Earth gravity, more basic studies of the chemistry and flame structure need to be done under microgravity conditions. It is hoped that this work will spur such new experiments.

ACKNOWLEDGMENTS

This work was sponsored by NASA Office of Life and Microgravity Sciences and Applications and the Office of Naval Research through the Naval Research Laboratory.

REFERENCES

1. Patnaik, G., Kailasanath, K., Laskey, K.J., and Oran, E.S., *Twenty-Second Symposium (International) on Combustion*, The Combustion Institute, Pittsburgh, PA, pp.1517-1526, 1988.
2. Patnaik, G. and Kailasanath, K., *Twenty-Third Symposium (International) on Combustion*, The Combustion Institute, Pittsburgh, PA, pp. 1641-1647, 1990.
3. Patnaik, G. and Kailasanath, K., *Twenty-Fourth Symposium (International) on Combustion*, The Combustion Institute, Pittsburgh, PA, pp.189-195, 1992.
4. Kailasanath, K., Patnaik, G. and Ganguly, K., *Prog. Astro.Aero.* v.151, pp. 247—262, 1993.
5. Kailasanath, K., Patnaik, G. and Oran, E.S., *Third International Microgravity Combustion Workshop*, NASA Conference Publications 10174, pp. 409-414, April 1995.
6. Patnaik, G., and Kailasanath, K., *Combust. Flame*, 99:247-253, 1994.
7. Patnaik, G., and Kailasanath, K., AIAA Paper 98-0742, Jan. 1998.
8. Patnaik, G., and Kailasanath, K., *Twenty-Seventh Symposium (International) on Combustion*, The Combustion Institute, Pittsburgh, PA., 1998.
9. Patnaik, G., and Kailasanath, K., Joint Meeting of the US Sections of the Combustion Institute, Washington, DC, March 1999.
10. Patnaik, G., Kailasanath, K., and Sinkovits, R.S., *Twenty-Sixth Symposium (International) on Combustion*, pp. 899-905, The Combustion Institute, Pittsburgh, PA., 1996.
11. Patnaik, G., Laskey, K.J., Kailasanath, K., Oran, E.S. and Brun, T.A., NRL Memorandum Report 6555, Naval Research Laboratory, Washington, D.C., 1989.
12. Sinibaldi, J.O., Driscoll, J.F., Mueller, C.J., and Tulkki, A.E., AIAA 97-0669, Jan.1997.
13. Sinibaldi, J.O., Mueller, C.J., Tulkki, A.E., and Driscoll, J.F., *AIAA J*, 36:1432-1439, 1998.
14. Ronney, P.D., *Combust. Flame* 82:1-14, 1990.
15. Patnaik, G., and Kailasanath, K., AIAA Paper 90-0041, Jan. 1990.
16. Wu, M-S, and Ronney, P.D., *Combust. Flame*, 116:387-397, 1999.

Combustion Diagnostics

QUANTITATIVE SPECIES MEASUREMENTS IN MICROGRAVITY COMBUSTION FLAMES USING NEAR-INFRARED DIODE LASERS

Joel A. Silver, Southwest Sciences, Inc., 1570 Pacheco Street, Suite E-11, Santa Fe, NM 87505
e-mail: jsilver@swsciences.com

INTRODUCTION

Understanding the physical phenomena controlling the ignition and spread of flames in microgravity has importance for space safety as well as for characterizing dynamical and chemical combustion processes which are normally masked by buoyancy and other gravity-related effects. Unfortunately, combustion is highly complicated by fluid mechanical and chemical kinetic processes, requiring the use of numerical modeling to compare with carefully designed experiments. More sophisticated diagnostic methods are needed to provide the kind of quantitative data necessary to characterize the properties of microgravity combustion as well as provide accurate feedback to improve the predictive capabilities of the models.

Diode lasers are a natural choice for use under the severe conditions of low gravity experiments. Reliable, simple solid state operation at low power satisfies the operational restrictions imposed by drop towers, aircraft and space-based studies. Modulation wavelength absorption spectroscopy (WMS) provides a means to make highly sensitive and quantitative measurements of local gas concentration and, in certain cases, temperature. With near-infrared diode lasers, detection of virtually all major combustion species with extremely rapid response time is possible in an inexpensive package. Details of WMS theory and its applications for combustion measurements can be found in Refs. [1-3].

Advancements in near-infrared diode laser fabrication technology and concurrent development of optical fibers for these lasers led to their use in drop towers [4]. Since near-infrared absorption line strengths for overtone and combination vibrational transitions are weaker than the mid-infrared fundamental bands, WMS techniques are applied to increase detection sensitivity and allow measurement of the major combustion gases.

In the first microgravity species measurement, Silver *et al.*[4] mounted a fiber-coupled laser at the top of the NASA 2.2-sec drop tower and piped the light through a single-mode fiber to the drop rig. A fiber splitter divided the light into eight channels that directed the laser beam across a methane or propane diffusion jet flame. The light beams were recaptured by a set of gradient index lenses, coupled back into separate fiber optic lines, and transmitted back to detectors and electronics in the instrument package. In these experiments a 6-mm od fiber cable (containing the nine optical fibers) fell with the drop rig. Using separate detection and demodulation channels, spatial and temporal (up to 20 Hz) maps of water vapor and methane concentrations were obtained at differing heights in the flames.

While this apparatus was useful from a demonstration standpoint, several drawbacks needed attention before useful scientific measurements could be obtained. First, eight lines of sight are somewhat insufficient for detailing the spatial profiles of the gas. Second, multiple detection channels operating in parallel are both expensive and present a challenge for accurate calibration.

As a result, a newer scanning system was developed in our first contract under this program. The primary characteristic of this system is that it contains a single detection channel and achieves "continuous" spatial resolution by scanning the laser beam across the flame region, then directing this beam onto a single detector. Thus spatial measurements are converted to a temporal series of data. The true spatial resolution is limited only by the beam diameter and width of the sweep. In these experiments the beam is focused to about 1-mm diameter and scans across a region up to 4-cm wide.

As compared to the fixed eight-channel instrument, the scanner approach requires a greatly increased detection bandwidth. Complete spectra must be obtained at each spatial position while acquiring a full spatial map at 10 Hz. This is achieved using high speed analog-to-digital converters coupled to digital signal processing (DSP) electronics, described in the next Section. These dedicated devices permit rapid acquisition of the data with good amplitude resolution. The results of preliminary experiments using this system for the measurement of molecular oxygen in candle and solid thin sheet flames are discussed below. Finally, current progress and future directions under our renewed contract for diode laser-based diagnostic systems are presented.

EXPERIMENTAL

The scanning WMS system is demonstrated by measuring molecular oxygen in candle and thin solid sheet flames. For the detection of oxygen at 760 nm (visible), a GaAlAs vertical cavity surface emitting laser (VCSEL) is used. In contrast to more expensive, conventional near-infrared InGaAsP distributed feedback lasers, VCSELs operate at much lower injection currents (3 and 10 mA), have circular, less diverging output beams, and can be continuously tuned over much larger ranges of wavelength, typically 10 cm^{-1}. This latter feature permits the acquisition of multiple-line spectra that could be used to determine local gas temperature.

Although vibrational bands of O_2 are infrared-*inactive*, the $v' = 0 \leftarrow v'' = 0$ vibrational transition in the $b^1\Sigma^+_g - X^3\Sigma^-_g$ electronic band near 760 nm can be used as the basis of an absorption diagnostic. The drawback for O_2 is that the absorption lines are quite weak (about 1000 times smaller than those of water, for example), making detection very difficult. The VCSEL accesses an oxygen line pair consisting of the RQ(13,14) and RR(15,15) + RQ(43,44) lines near 13,154 cm^{-1}. The ratio of the magnitudes of these lines varies near-linearly between 600 and 2000 K at about 7% per 100 K.

The experimental system comprises four components: 1) the optical scanning system containing the laser, scanner, mirrors, detector and preamplifier all mounted on a frame for which the absorption path can be varied; 2) stand-alone computer and DSP board; 3) an analog electronics box containing all laser control, WMS and signal processing circuitry; and 4) the dc computer power supply. The system is powered by the drop rig batteries. Power loading is relatively high, drawing ~200 W.

The laser beam is collimated by an anti-reflection coated aspheric lens to a diameter of <1 mm, and is pointed at a scanner mirror that is positioned at the focus of an off-axis paraboloidal mirror (OAP) so that all rays reflected by the OAP are parallel to one another. As the beam is swept by the scanner, it tracks in parallel lines across the flame. After traversing the flame, a second OAP refocuses the laser beam onto a photodiode detector.

The angle of the scanner is controlled by a programmable voltage ramp generated by the DSP. A second DSP waveform sweeps the laser wavelength across the spectral feature. A 280-bin spectrum is obtained during the time in which each 1-mm spatial element is traversed.

WMS detection is accomplished by modulating the laser wavelength at 500 kHz and detecting the $2f$ (1 MHz) component of the photodiode. Data are recorded using the analog inputs to the DSP and stored on a hard drive designed for use in a laptop computer. The electronic circuitry for modulation and demodulation is similar to that described in Ref. 6. The DSP board controls all timing, ramps, and triggering of the system, the computer board acts to load and start the DSP as well as control all data storage and communications functions. Numerical processing of the data and normalization to total laser intensity are made in post-drop analysis.

The solids combustion setup comprises a thin metal frame to which an 8.5-cm wide cellulose sheet (Kimwipe EX-L) is taped. A Kanthal ignitor coil is mounted in physical contact with the bottom of the sheet. A small fan below the frame provides a concurrent flow of air to promote migration of the flame front upwards from the ignition point. For candle measurements, a small birthday candle is inserted into the optical path.

OXYGEN MEASUREMENT RESULTS

Normal and zero-gravity experiments are performed in the 2.2-sec drop tower at the NASA Glenn Research Center. Spatial maps (30-mm wide with 1-mm resolution) are acquired at 8 Hz, processed, and stored. The effective detection bandwidth is about 70 kHz. A spectrum of two adjacent O_2 absorption lines near 760 nm is shown in Fig. 1. For comparison, a theoretical spectrum computed from known spectroscopic and physical constants is illustrated. The agreement between these spectra demonstrate the convergence of experiment and theory, with a 1Hz bandwidth noise level equivalent to 1×10^{-6} absorbance.

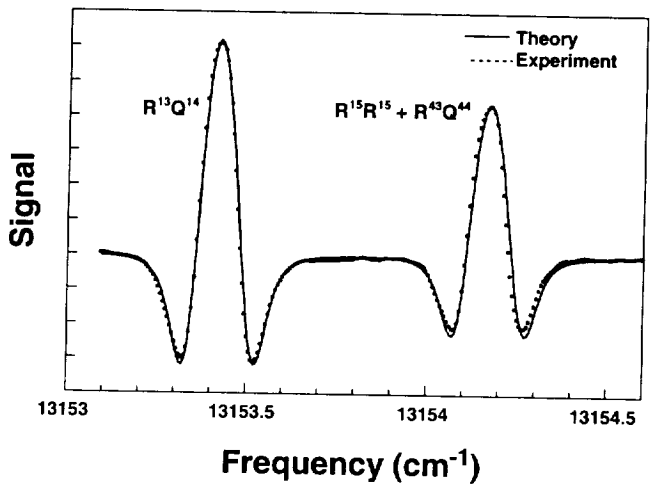

Figure 1 - Oxygen line pair spectrum.

One complication in the data analyses is that O_2 is present in the optical path external to the flame (*i.e.*, in the room air). This introduces a nearly overwhelming contribution to the observed signal that must be subtracted to determine the portion contributed only from the flame. Signals measured just prior to the drop (pre-ignition; scaled to the external path length) provide the external path contribution. Thus very large signal-to-noise ratios are required to be able to successfully subtract out the room temperature portion of the signal.

Candle Flames - Experiments on a small candle were carried out in normal gravity and microgravity. The long external path in these experiments (as compared with the flame diameter of only a few cm) results in flame region spectra having poor signal-to-noise. Thus spectra are co-averaged over all drop times beginning after the initial transient to zero gravity. Since the candle is axially symmetric, an Abel inversion [6] of the data converts the observed projections through the flame into radial absorbances. The reduced gravity data clearly show a wider flame than in normal gravity. The signals for the line pair are too noisy to extract exact temperatures, but qualitatively the line pair ratios that at the edge of the flame are near 300 K as expected. This line pair is optimized for temperatures of 1200-1500 K and in future work, a better range would be 600-1200 K, since O_2 disappears in the flame front and is not expected to be present in the hotter zones.

Solid Sheet Combustion - An 8.5-cm wide thin solid sheet is burned in zero gravity under a small concurrent flow of air. The laser beam traverses a path perpendicular to the sheet and the flame passes through this plane after ignition. Since the total laser intensity at the detector is recorded, partial obscuration of the laser beam by smoke is observed slightly ahead of the flame; this effect is strongest closer to the sheet. The absorbance map for O_2 remains fairly constant up to about 1.7 seconds, when a precipitous drop is observed due to the passage of the flame front. Future experiments will investigate these phenomena more closely and will measure local gas temperatures as well.

CURRENT RESEARCH

In our current program, the focus of research shifts toward further development of diode laser spectroscopy as a working tool aimed at space-borne applications and to perform detailed measurements of a suite of combustion species (H_2O, OH, O_2, CO_2, CH_4 and perhaps C_2H_6) in well-defined experiments that are concurrently being investigated from a theoretical standpoint.

From a hardware diagnostic perspective, the electronics used in our prior work will be reduced in size to approximately 5 cm ×10 cm ×15 cm in size; power requirements drop to below 30 W. This is possible by using a fully digital approach to WMS, where a modified square wave replaces the analog sine modulation waveform. A stand-alone DSP super-processor generates and processes all modulation, ramping and scanning waveforms, as well as analyzes and stores the data without the need of a separate computer board or other electronics. Laser modules (for different gases) will be interchangeable.

Two types of diffusion flames will be examined. The first type are laminar flames using a spherical or counterflow diffusion burner. These approximate an ideal one-dimensional flame and are well-suited to the line-of-sight laser absorption diagnostic approach. Measurements of the fuel/oxidizer interface provide information on the species locations and temperatures as a function of initial conditions. The simple dimensionality of these experiments allows direct comparison with theory.

In collaboration with Prof. W. Daum, we are investigating ring vortex diffusion flames. This flame exhibits many of the fundamental flow, transport and combustion properties of turbulent flames including vorticity, mixing, strain, diffusion, partial premixing and diluent effects, and heat release effects. Nevertheless, the elegant simplicity of the flame-vortex interaction permits the study of these complex interactions under relatively controllable experimental configurations, in contrast to direct measurements in turbulent flames. The ability to measure *and model* the fundamental phenomena that occur in a turbulent flame, but with time and spatial scales which are amenable to our diagnostics, will permit significant improvements in the understanding of turbulent combustion under both normal and reduced gravity conditions.

CONCLUSION

Diode laser-based absorption detection systems provide critical information on flame species concentrations and temperatures with fast response. Development of these sensors is important as quantitative gas diagnostics for combustion and other disciplines. The flexibility and interchangeability of diode lasers combined with the widespread capabilities of absorption measurements make this approach a strong candidate for use in the International Space Station, not only as compact, low cost sensors for the Modular Combustion Facility, but for air quality management and fire detection as well.

ACKNOWLEDGMENTS

This work was performed under NASA Contracts NAS3-26553, and NAS3-99140.

REFERENCES

1. Wilson G V H 1963 *J. Appl. Phys.* **34** 3276-3285.
2. Silver J A 1992 *Appl. Opt.* **31** 707-717.
3. Silver J A 1999 *Meas. Sci. Technol.* (Submitted).
4. Silver J A, Kane D J and Greenberg P A 1995 *Appl. Opt.* **34** 2787-2801.
5. Dasch C J 1992 *Appl. Opt.* **31** 1146-1152.

S44-25

FORMALDEHYDE-PLIF DETECTION OF COOL-FLAME REACTIONS DURING TWO STAGE IGNITION OF ALKANE DROPLETS

J. König, Chr. Eigenbrod, H.J.Rath, D. Grebner*, J.Hein*, W. Triebel* University of Bremen, Center of Applied Microgravity and Space Technology, ZARM; Hochschulring/ Am Fallturm, D-28359 Bremen, Germany, koenig@zarm.uni-bremen.de; *Institut für physikalische Hochtechnologie IPHT, Helmholtzweg 4, D-07743 Jena, Germany

INTRODUCTION

Whenever alkane fuels have to reside partially or fully mixed in an oxidizing atmosphere at high temperatures, ignition can occour in a multistage mode, subsequently following completely different schemes of oxidation. This behavior is experimentally well known for premixed gases [1] and for multiphase systems [2]. Moreover it is an apparent problem in prominent technical applications such as IC-combustion engines [3] as well as when designing continous flow reactors for high pressures and temperatures with large premixing zones.

If fuel is used in liquid phase, mixing, upheating and the subsequent ignition and combustion takes place in a transient field of temperature and concentration. This holds true, from the instant when the fuel is inserted as a spray up to beyond the time the liquid is completely vaporized. The understanding and modeling of the process requires a consequent coupling of the physical processes with a suitable chemical kinetic of the fuel covering the full range of temperatures encountered in the entire process. Numerical results are in reasonable good agreement with experiments for homogeneous gas phase ignition only. In particular the low temperature mechanism is very complex, and proceeds via different submechanisms sensibly governed by temperature. The frame of this mechanism is given by the subsequent oxidation of the parent fuel molecule, forming large alkylhydroperoxy-radicals. Exothermal "breakup" of these radicals is the major step to form a large amount of aldehydes and OH (and HO_2) -radicals, which promote the subsequent reaction by chain branching. Thermal runaway of the cool flame is inhibited by the second addition of oxygen to the alkylperoxy -radical, which is balanced by a backward reaction becoming important beyond a temperature of about 700K [4]. This balancing features the very important and characteristic negative temperature coefficient of the low temperature mechanism. Since the low temperature mechanism can proceed in a rather wide range of stochiometric mixtures, cool flame ignition can occur at very lean conditions, and is supposed to play a very important role favoring subsequent hot flame ignition.

In the presented work, the formaldehyde molecule HCOH has been selectively be detected as key species in the gas phase around a single, n-heptane drenched porous sphere during the process of two stage-selfignition by means of Planar Laser Induced Fluorescence PLIF. Currently the obtained concentration field yields qualitative data. Methods are under investigation to prepare the equipment for a quantitative interpretation of the images. To be able to gain the experimental data into a one dimensional numerical model, all experiments were carried out under microgravity at the Bremen Drop Tower.

EXPERIMENTAL

Fluorescence of Formaldehyde was induced by excitation of the $2^0_0 4^1_0$ -Line of the $A^1A_2 \leftarrow X^1A_1$ transition at 352,2nm [5-8] by means of a XeF- Excimer Laser (Lambda LPX 150T). Before entering the experimental section the laser light was shaped to a sheet of 30mm in height

and 0.5mm in width. High speed videos of the LIF-images were recorded with a two staged intensified FHG-Dalsa CCD- camera. Framing rate was 250sec-1 to resolve the site and instant of both ignition stages. To block Rayleigh- and Mie- scattering a WG1 filter was used in front of the UV-Nikkor. The outline of the high-pressure experiment chamber which is furnished with a furnace section that can be adjusted to temperatures of up to 1000K is displayed in Figure 1. Figure 2 shows the arrangement of the laser-lightsheet illuminating the gas phase adjacent to the fuel drenched porous sphere.

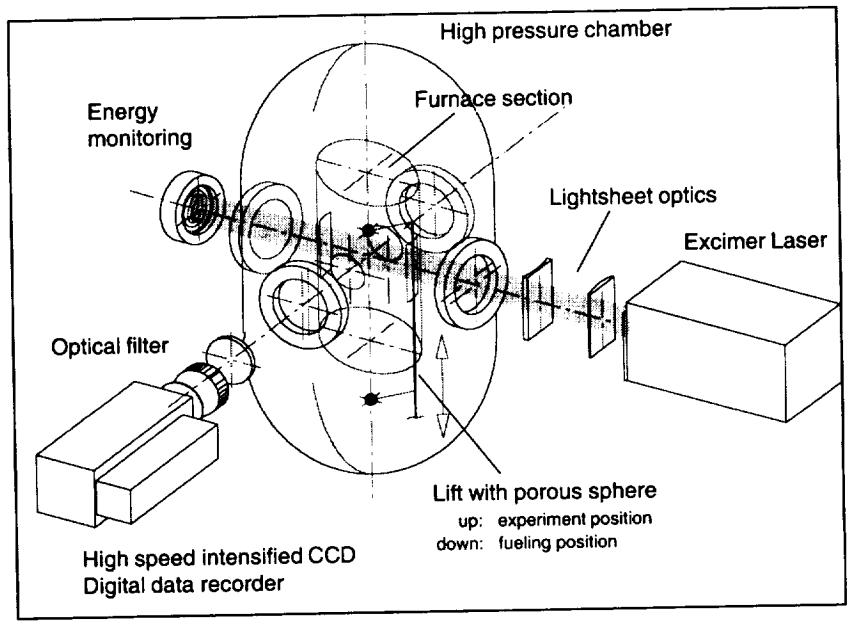

Figure 1:
Experimental Setup. For drop tower experiments, lightsheet optics, high-pressure chamber and high speed image-detection is mounted in the drop capsule.
The excitation laser is attached to the top of the tower, the laser light is mirrored into the top of the falling drop capsule.

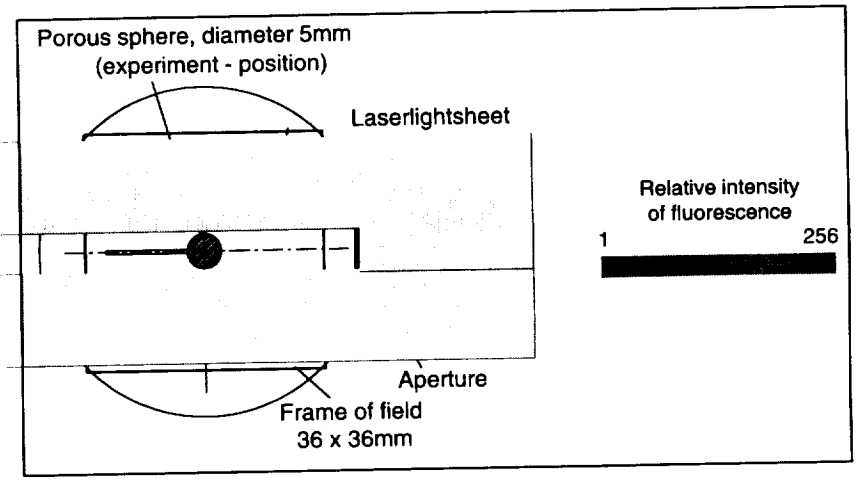

Figure 2:
Geometry of the frame of field for diagnostics.
The instant the experiment starts the fuel drenched sphere is rapidly lifted from the cold site of fueling to the displayed position within the furnace (See Fig.1).
The aperture shields the sphere from direct impact of laserlight.

RESULTS AND DISCUSSION

Sequences 1 to 5 show the temporal and spatial change of the formaldehyde concentration which visualizes the proceeding two stage ignition at selected typical conditions. The number of frame in each sequence corresponds to a distinct state in the ignition process: ***Frame 1*** marks the first appearance of a detectable amount of formaldehyde, which we refer to as "cool flame", cf-ignition here. The difficulty to identify the state of cool flame ignition is addressed in [9] e.g..

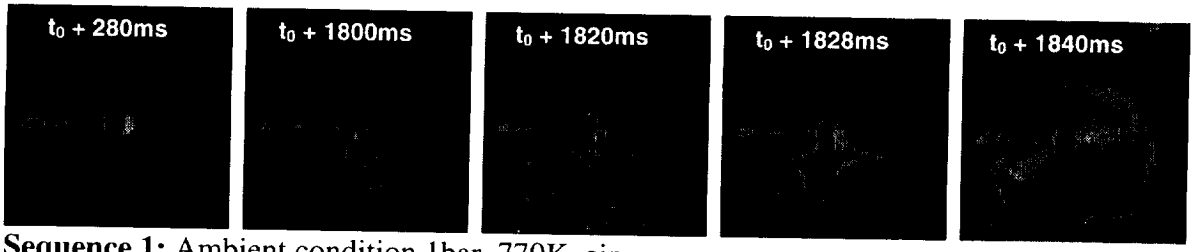

Sequence 1: Ambient condition 1bar, 770K, air

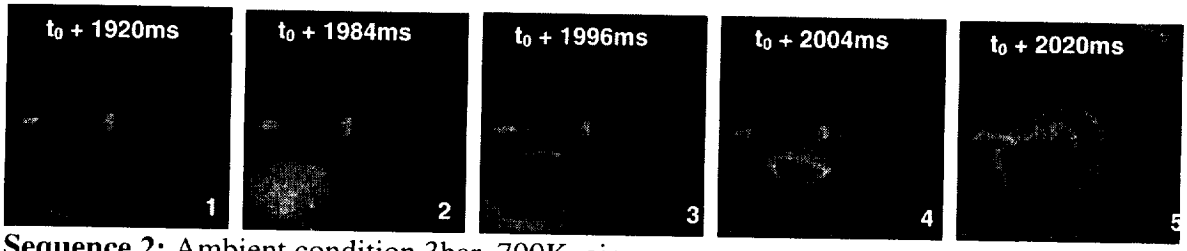

Sequence 2: Ambient condition 3bar, 700K, air

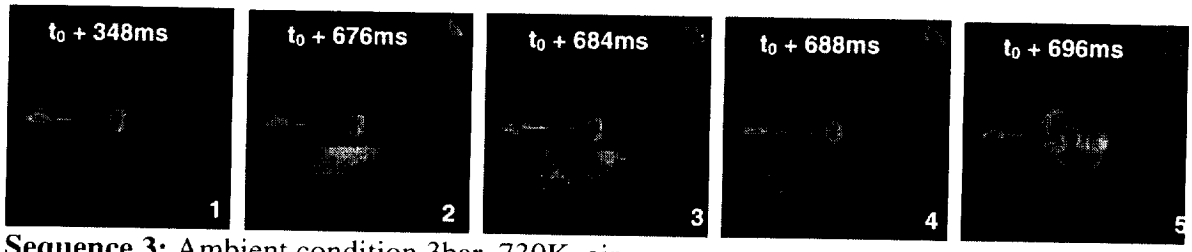

Sequence 3: Ambient condition 3bar, 730K, air

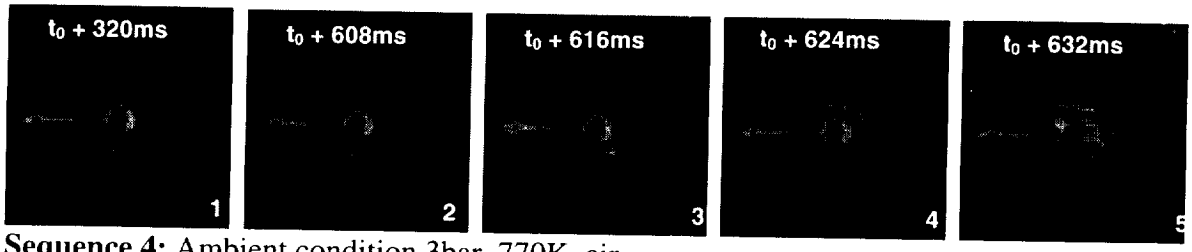

Sequence 4: Ambient condition 3bar, 770K, air

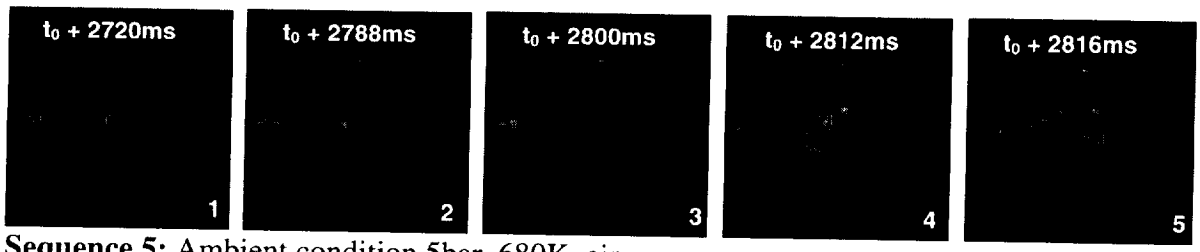

Sequence 5: Ambient condition 5bar, 680K, air

Frame 2 shows the concentration field of formaldehyde and thus the cool flame position just before the instant of high temperature, "hot flame" hf-ignition. ***Frame 3*** shows the instant of hf-ignition, which is, due to a sharp rise of temperature, accompanied by a rapid consumption of formaldehyde. ***Frame 4*** shows the residual structure of formaldehyde-concentration adjacent to the zone of high temperature reactions, when hf-ignition has surrounded the entire sphere. ***Frame 5*** shows the strong signal of scattering particles when the luminous flame body following hf-ignition is formed. The reaction zone is located close to the outer side of the luminous shell.

The images in all sequences show, that apart from the common expectation of a spherical behavior of the diffusion- driven processes in microgravity droplet combustion, ignition seem to be extremely sensitive against slightest disturbances. In case of the first ignition stage, the critical dependency of the low-temperature-chemistry on temperature [4, 9] is supposed to be responsible for that sensitivity. Exceptionally at ambient pressure of 1bar, for all temperatures investigated (but shown only as example for 770K in Sequence 1) the cool flame ignites and proceeds sperically. As the heat release of the cool-flame directly interferes with the "undisturbed" temperature field around the upheating, evaporating fuel drenched sphere, hot-flame ignition is affected by non-sphericity of cool flame -"burning" for all conditions shown in the sequences. Moreover, hf-ignition takes place where the formaldehyde concentration indicates the highest cool flame activity.

Another striking feature that could be drawn from the experiments, which have been done up to now for various temperatures and pressures ranging from 1 to 5 bar pressure, is that the maximum distance of cf-ignition site from the fuel source (at a given temperature) increases as pressure increases. Considering that either the size of the temperature and concentration field around the vaporizing sphere is strictly decreasing with increasing pressure, thus ruling the position of hf-ignition, cf-ignition can take place at very lean fuel-oxidizer ratios and is very sensitive against ambient temperature.

ACKNOWLEDGMENT

We hereby like to thank the DLR (Deutsches Zentrum für Luft- und Raumfahrttechnik) for funding the presented work (FKZ 50 WM 9448).

REFERENCES

1. Müller, U.C.: "Reduzierte Reaktionsmechanismen für die Zündung von n-Heptan und iso-Oktan unter motorrelevanten Bedingungen", *PHD-Thesis*, RWTH-Aachen, (1993)
2. Tanabe, M. Kono, M., Sato, J., König, J., Eigenbrod, C., Dinkelacker, F., Rath, H.J.,:"Two stage ignition of n-heptane isolated fuel droplets", *Combust. Sci tech. 108:103* (1995).
3. Bradley, D.:"Hot spots and engine knock", *J.Chem. Soc., 92(16), 2959* (1996)
4. Griffiths, J.F.:"Reduced kinetic models and their application to practical combustion systems", *Prog. Energy Combust. Sci., 22, 25,* (1995)
5. Strickler, S.J., Barnhart, R.J.:"Absolute vibronic intensitites in the $^1A_2 \leftarrow {}^1A_1$ absorption spectrum of formaldehyde", *J. Phys. Chem., 86, 448,* (1982)
6. Hanson, D.A., Lee, E.K.:"Radiative and non-radiative transitions in the first excited singlet state of symple linear aldehydes"; *J. Chem. Phys. 63, 3272,* (1975)
7. Wagner, V. "Untersuchungen zur Photophysik von Aldehyden, Ketonen und NO bei Anregung mit Ramankonvertierten Laserpulsen"; *Master Thesis*, Friedrich-Schiller Universität-Jena, 1997
8. Bäuerle, B., Warnatz, J., Behrendt, F.:"Time-resolved investigation of hot spots in the end gas of an S.I. Engine by means of 2-D Double pulse LIF of formaldehyde, *26th Symp. (Intl.) on Comb., 2619,* The Combustion Institute, Pittsburgh, (1996)
9. Walker, R.W., Morley, C.: "Basic chemistry of combustion", *Comp. Chem. Kin., Vol 35*, ed. Pilling M.J., Elsevier (1997)

OBSERVATIONS FROM THE MICROGRAVITY SMOLDERING COMBUSTION (MSC) ULTRASOUND IMAGING SYSTEM (UIS)

D.C. Walther[1], A.C. Fernandez-Pello[1], R.A. Anthenien[2], and D.L. Urban[3], [1]University of California, Berkeley, 94720, ferpello@newton.me.berkeley.edu, [2]Air Force Research Laboratory/ Propulsion Directorate, Wright-Patterson AFB, OH 45433, [3]NASA LeRC,Cleveland, OH 44135

INTRODUCTION

The Microgravity Smoldering Combustion (MSC) experiment is a study of the smolder characteristics of porous combustible materials in a microgravity environment. The objective of the study is to provide a better understanding of the controlling mechanisms of smolder, both in microgravity and normal earth gravity. Experiments have been conducted aboard the NASA Space Shuttle in the GAS-CAN, an apparatus requiring completely remote operation. Future GAS-CAN experiments will utilize an ultrasound imaging system (UIS). Thermocouples are currently used to measure temperature and reaction front velocities, but a less intrusive method is desirable, as smolder is affected by heat transfer along the thermocouple. It is expected that the UIS will eventually replace the existing array of thermocouples as a non-intrusive technique without compromising data acquisition.

Smoldering is defined as a non-flaming, self-sustaining, propagating, exothermic, surface reaction, deriving its principal heat from heterogeneous oxidation of the fuel [1]. Smolder of cable insulation is of particular concern in the space program; to date there have been a few minor incidents of overheated and charred cables and electrical components reported on Space Shuttle flights [2,3]. Recently, the establishment of the International Space Station and other space facilities has increased interest in the study of smoldering in microgravity because of the need to preempt the possibility, and/or to minimize the effect of a smolder initiated fire during the operation of these facilities [4].

The ignition and propagation of smolder are examined using both thermocouples and the UIS. The UIS has been implemented into the MSC flight hardware as shown in Figure 1&2. The system provides information about local permeability variations within a smoldering sample, which can, in turn, be interpreted to track the propagation of the smolder reaction. The method utilizes the observation that transmission of an ultrasonic signal through a porous material increases with increasing permeability [5]. Since a propagating smolder reaction leaves behind a char that is higher in permeability than the original (unburnt) material, ultrasonic transmission can be employed to monitor the progress of the primary reaction front, char evolution (i.e. material left by the smolder reaction), pyrolysis, and condensation fronts.

EXPERIMENTAL SET-UP

The tests are performed in a 21.7 L, semi-cylindrical, hermetically sealed, aluminum combustion chamber, identical to those used in the MSC flight assembly. The igniter consists of a Nichrome wire heater placed between two porous ceramic disks, one of which is in complete contact with the one end of the fuel sample. Gaseous oxidizer forced through the igniter and foam is controlled via mass flow controllers or choked flow nozzles. Reaction zone temperature and smolder propagation velocities are obtained from the temperature histories of thermocouples embedded at predetermined positions within the foam. Five speaker/microphone pairs are fixed at 25, 60, 80, 100 and 120 mm from the igniter surface. This placement coincides with several thermocouples, allowing for correlation of the temperature and permeability results.

The UIS system is thoroughly outlined in Tse et al. [5] and is therefore only shown here as Figure 3. Briefly, operation procedures for the ultrasonic imaging technique for a single set of speaker and microphone are as follows:

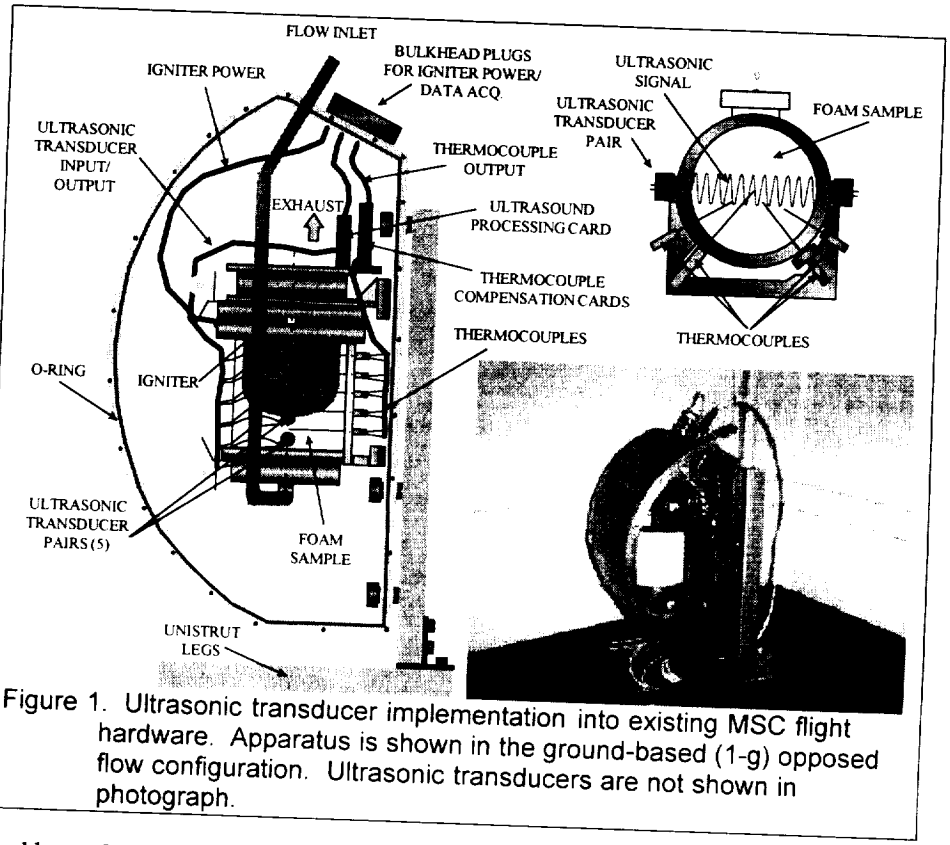

Figure 1. Ultrasonic transducer implementation into existing MSC flight hardware. Apparatus is shown in the ground-based (1-g) opposed flow configuration. Ultrasonic transducers are not shown in photograph.

1) A speaker emits a six (6) cycle, ultrasonic, sinusoidal, wave-train pulse through the porous medium. The pulsed ultrasound signals are amplified by a gain-selectable amplifier that is controlled by a feedback loop to optimize the received signal strength.
2) A microphone receives the wave-form, which is amplified and converted to a RMS signal. Based on the shortest path length through the sample, the first peak in the received waveform identifies the desired transmitted signal through the foam/char.
3) The received RMS waveform strength is digitally sampled and stored.
4) The next ultrasonic transmission data point is taken. The time between wave-train pulses must be longer than the time of flight for a single pulse and must also be long enough to prevent superposition effects from previously sent wave-trains reflected back into the propagation path of interest.

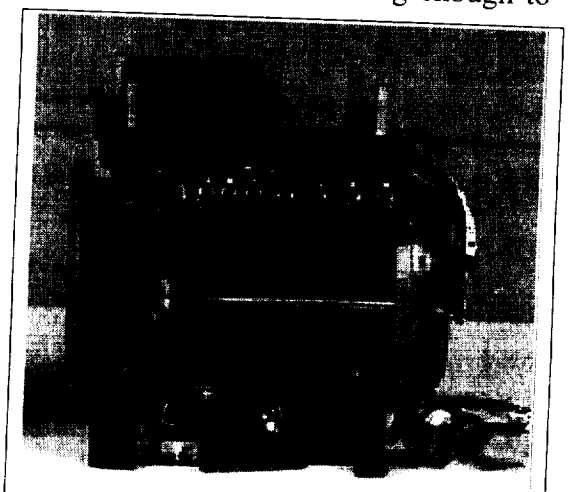

Figure 2. Photo of actual MSC test section with UIS hardware installed.

RESULTS / DISCUSSION

Figure 4 contains a plot of temperature and UIS received signal strength versus time. The test from which this data was taken was conducted in an upward burning, forward flow smolder with gas velocities (Darcy) of 0.1 mm/s during ignition and ≈2.5 mm/s during the propagation period. The UIS data shows an average smolder velocity of 0.118 mm/s. It was found from the temperature profiles that the smolder front propagated to a distance of 105 mm at an average velocity of

0.116 mm/s, confirming the findings of the UIS data.

It can be seen that the steep rise in transmission of the UIS signal at a given location correlates with a measured temperature of ~290-300°C, corresponding to the pyrolysis temperature of the polyurethane foam [6], further corroborating the UIS. The cause of the periodic nature of the UIS signal seen in Figure 4 is uncertain, however it is suspected that it may be the result of large-scale convection cells within the foam. The convection cells subtly effect the strength of reaction, causing it to produce more or less gaseous combustion products that are known to attenuate sound waves differently [7,8]. It is the fluctuations in gas concentration within these cells that may be attributed the received signal fluctuations. Future microgravity tests will confirm or refute these assertions.

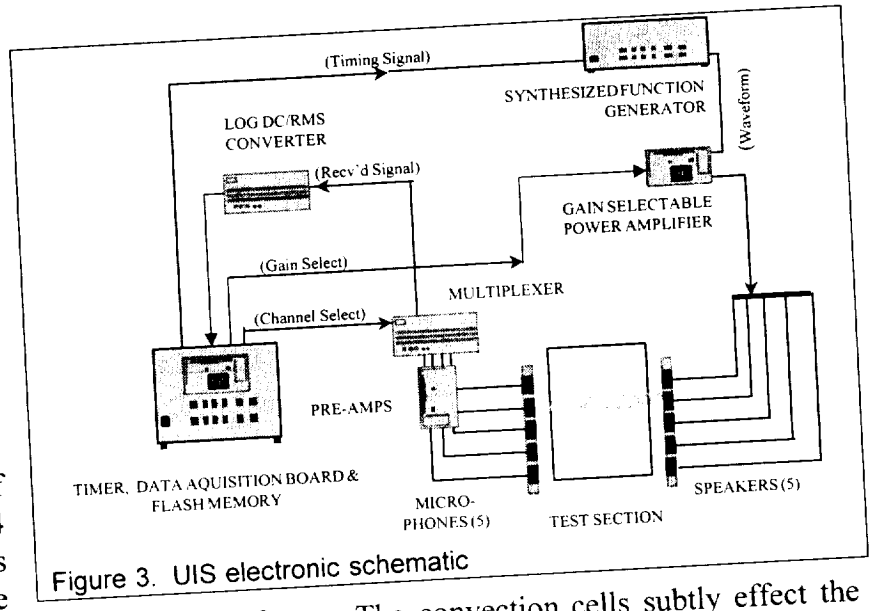

Figure 3. UIS electronic schematic

The sharp drop in signal transmission of Channel 1 between time t =400-600 s coincides with the switch from low to high oxidizer flow rate and the switching off of the igniter. This drop is caused by the passage of the water condensation front, which leads the reaction front [9]. In each channel, it may be seen from Figure 4 that the signal first undergoes a gradual decrease in

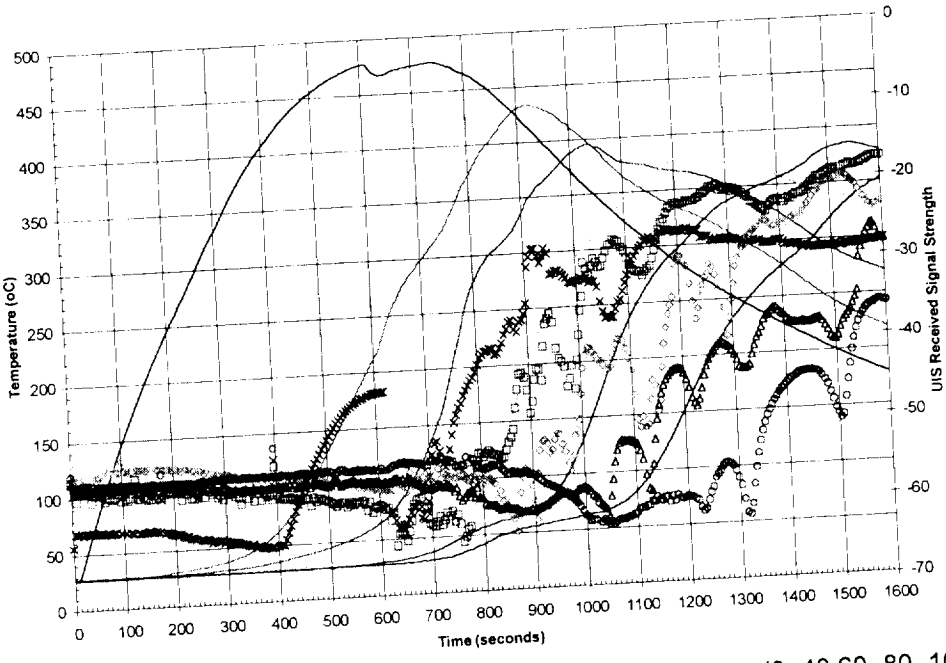

Figure 4. UIS T/C (solid lines) and signal (points) traces. T/C positions (0, 40,60, 80, 100, 120 mm). UIS transducer pairs (x-25mm, -60mm, ◊-80mm, ∇-100mm, o-120mm

transmission, then a sharp increase upon arrival of the actual reaction front. This gradual decrease is due to water from the reaction condensing in the cool foam ahead of the reaction. The water partially fills the pores of the foam, increasing the attenuation of the ultrasound signal. With the arrival of the reaction front, the water is evaporated from the pores and the permeability increases, increasing the UIS signal transmission. This is seen in every channel and is corroborated by the leveling off of the thermocouple traces at ~75°C (most notably TC's 4-6), an indication of an endothermic event such as water condensation. Peculiar to Channel 1, however is the sharp drop in signal after a short time of increasing signal. This is due to the large amount of preheated, unreacted fuel that is generated by the low oxidizer flow during the ignition phase of the test. When the oxidizer flow is switched to the higher rate, this fuel reacts quickly, generating large amounts of products, which rapidly fill the pores ahead of the reaction. This results in the sharp drop in signal transmission evidenced in Figure 4. Also coincident with the oxidizer flow rate switch, Channel 2 undergoes a sharp drop in signal transmission, although not as severe.

CONCLUDING REMARKS

An ultrasound imaging system has been developed and implemented into the ongoing Microgravity Smoldering Combustion experiments. The data collected will provide further insight into the smoldering process and provide a non-intrusive method for studying a smolder reaction propagating through a permeable material. The method has successfully imaged both the reaction front and the preceding water condensation front and has led to hypotheses regarding a transient flow and reaction pattern that will be corroborated with microgravity flight data.

ACKNOWLEDGMENTS

This work was supported by the National Aeronautics and Space Administration under NASA grants NAG3-1252 and NAG3-2026. The authors would like to acknowledge the work and support of Ms. S. Motil and the NASA Lewis engineering team.

REFERENCES

1. Ohlemiller, T.J., *Prog. Ener. & Comb. Sci.*, **11**:277, (1986).
2. Ross, H.D., "Invited Lecture," Natl. Fire Protection Assoc. Annual Meeting, May, 1996.
3. Friedman, R., NASA Technical Memorandum 106403, 1994.
4. Palmer, H., "Closing Address," International Microgravity Workshop, NASA LeRC, Cleveland, OH, January 25, 1989.
5. Tse, S.D., Anthenien, R.A., Fernandez-Pello A.C., and Miyasaka, K., *Comb & Flame* **116**:120 (1999).
6. Bilbao, R., Mastral, J.F., Ceamanos, J., and Aldea, M.F., *J. Macromolec. Sci. Chem.* **A15(1)**:169 (1996).
7. Herzfeld, K., and Litovitz, T., *Absorption of Ultrasonic Waves,* Academic Press, Inc., New York (1959).
8. Bhatia, A., *Ultrasonic Absorption,* Oxford University Press, New York (1967).
9. DeRis, J., *Comb. Sci. Tech.* **2**:239 (1970).

REAL TIME QUANTITATIVE 3-D IMAGING OF DIFFUSION FLAME SPECIES

D. J. Kane, J. S. Pilgrim, and J. S. Goldmeer, Southwest Sciences, Inc., 1570 Pacheco St., Suite E-11, Santa Fe, NM, 87505, djkane@swsciences.com

INTRODUCTION

Ideally, to bridge the gap between chemistry and fluid mechanics in microgravity combustion, species concentrations and temperature profiles are needed throughout the flame. However, restrictions associated with performing measurements in reduced gravity, especially size and weight considerations, have generally limited microgravity combustion studies to the capture of flame emissions on film or video[1-3] laser Schlieren imaging[4] and (intrusive) temperature measurements using thermocouples. Given the development of detailed theoretical models, more sophisticated studies are needed to provide the kind of quantitative data necessary to characterize the properties of microgravity combustion processes as well as provide accurate feedback to improve the predictive capabilities of the computational models.

Over the past ten years, Southwest Sciences has focused its research on the high sensitivity, quantitative detection of gas phase species using diode lasers. Our research approach combines three innovations in an experimental system resulting in a new capability for nonintrusive measurement of major combustion species. FM spectroscopy or high frequency wavelength modulation spectroscopy (WMS) have recently been applied to sensitive absorption measurements at Southwest Sciences and in other laboratories using GaAlAs or InGaAsP diode lasers in the visible or near-infrared[5] as well as lead-salt lasers in the mid-infrared spectral region.[6] Because these lasers exhibit essentially no source noise at the high detection frequencies employed with this technique, the achievement of sensitivity approaching the detector shot noise limit is possible. Such high sensitivity permits the *in situ* detection of chemical species of interest such as water, methane, O_2, CO, CO_2, OH, *etc.*

OBJECTIVES

The first quantitative measurements of species concentrations in microgravity flames focused on detection of water vapor and methane in nonpremixed diffusion jets.[7] A near-infrared diode laser operating at 1.341 μm was used in most of the experiments to detect water vapor in propane and methane flames. The instrument utilized fiber optics to direct the diode laser radiation into eight detection channels for simultaneous measurements along multiple lines of sight. Experiments conducted with this instrument lead us to believe that higher resolutions would be desirable. Thus, we have developed imaging high-frequency Wavelength Modulation Spectroscopy (WMS). With this new technique, we will be able to monitor strong absorbers such as water, methane, and possibly hydroxyl radicals. Ultimately, we will have the capability to take several seconds of video-rate images (i.e., "movies) of strong absorbers in flames under 1-g and μ–g environments. By coupling the imaging of water vapor with the imaging of methane in diffusion flames, we will be able to localize reaction zones in the flame leading to a better understanding of the roles of diffusion and buoyancy.

We will start our project by obtaining time-dependent water vapor concentration profiles of combustion in microgravity conditions using WMS and a near-infrared diode laser. The strong absorption line strengths of water make detection by optical means attractive and will allow 2-D

absorption images to be obtained in real time. By taking advantage of flame symmetry, these absorption images should be readily transformable to 3-D concentration profiles. By using two closely spaced water lines with different temperature dependencies, flame temperature profiles can be determined. This technique has the advantage over other laser-based methods as being simple and inexpensive to implement, provides signals which are directly linear in concentration, and is easily calibrated to provide accurate quantitative results. To test the system, we will obtain water vapor concentration profiles in an air diffusion flame (Wolfhard-Parker slot burner[8]). This type of burner creates a two-dimensional diffusion flame, so that we will not have to apply any transforms to obtain 3-D species and temperature profiles. Hence, we will be able to examine the reaction zone in this flame at virtually any resolution. Any changes in the reaction zone will be observed when the transition is made from 1-g to μ-g or flow rates are changed. Our previous microgravity water vapor absorption experiments of gas jet diffusion flames showed high concentrations of water at much greater radii than theoretical models predicted. We believe this to be a result of ignition. This will be another problem we will address in this project. These measurements of water vapor, temperature and methane in diffusion flames and candle flames will provide time and spatial resolutions sufficient to answer many outstanding questions concerning the relative effects of diffusion and kinetic limitations on observed combustion properties. Finally, we will investigate the effects of different ignition sources on flame properties as well as the transition of pre-ignited, 1-g flames to microgravity.

HIGH FREQUENCY WAVELENGTH MODULATION SPECTROSCOPY

High frequency laser wavelength modulation spectroscopy (WMS) is a technique used to measure the weak absorption signals or strong absorption signals very quickly. The usefulness of this method is that the WMS signals are linearly proportional to the absorber gas concentration. Unlike direct absorption, the detection sensitivity is limited by detector quantum noise and not by laser $1/f$ noise. This can improve the detection sensitivity by 3-4 orders of magnitude. We have described this technique in considerable detail in two recent publications, including comparisons with other high frequency diode laser detection methods (e.g. one- and two-tone frequency modulation spectroscopy)[6] In addition, these methods were recently applied to the measurement of water vapor in microgravity diffusion jet flames.[7]

Briefly, this method, which is an extension of diode laser "derivative spectroscopy" techniques widely used at kHz frequencies involves superposition of a small sinusoidal modulation at frequency f on the diode laser injection current In the small modulation limit, the WMS lineshape is the n^{th} derivative of the original molecular absorption lineshape. In practice, the modulation index is set at a value to maximize the signal level and, in this regime, lineshapes are only derivative-like but can be readily calculated. By implementing wavelength modulation at sufficiently high frequencies, laser noise is minimal and detector-limited (ideally, shot noise-limited) sensitivity can be achieved.

EXPERIMENTAL HARDWARE

The optical layout is fairly simple. The laser is collimated by an anti-reflection coated aspheric lens to a diameter of ~1 mm and is pointed onto an X-Y optical scanner placed at the focus of an off-axis paraboloid. This combination rasters the laser beam across the flame. A second off-axis paraboloid focuses the beam onto a single detector. We expect this device to have an image rate of about 200,000 pixels per second allowing 100×100 arrays to be obtained at a rate of 20 Hz. This high data rate is attainable because of the large signal-to-noise obtained when using WMS. (The high bandwidth requirements of imaging will force a modulation frequency of 5 MHz and a detection frequency of 10 MHz.) Raster scanning also allows the amount and position of the scan to be controlled so that different parts of the flame may be analyzed at varying temporal and spatial resolutions. For example, in some of the experiments we plan to use a Wolfhard-Parker slot burner to provide axial symmetry. Since no transform will be needed, we can increase the resolution to concentrate on only the portions of the flame of interest such as the reaction zone. Ultimately, we hope to obtain the water and methane concentration over this region along with the temperatures.

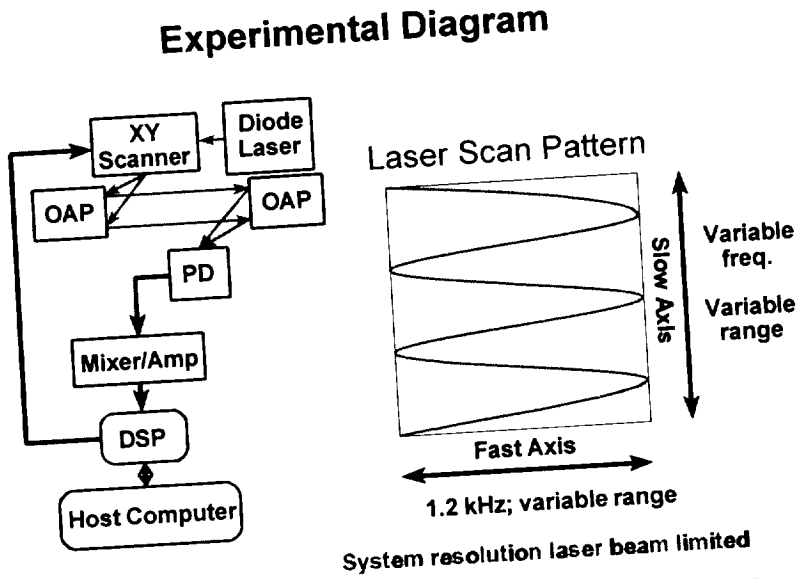

Figure 1. Schematic diagram of the Imaging WMS system developed. A wavelength modulated diode laser is raster scanned across a flame using an XY scanner and an off-axis paraboloid (OAP) mirror. Another OAP focuses the scanning diode laser onto a photodiode detector (PD). The data is read via a fast A/D and recorded on the host computer.

Preliminary results have indicated that we have obtained a signal-to-noise of 60 with a bandwidth of 184 kHz for absorbances of ~2-3% due to the water transition (7,6,2)↗(7,6,1) at 7179.8 cm^{-1} of the $\nu_1+\nu_3$ combination band. Figure 2 shows an absorption image of hot water vapor we have obtained in a Wolfhard-Parker diffusion flame using this line (one 100×100 pixel frame, 4.2 ms acquisition time). The figure is slightly distorted because the scan is actually trapezoidal and the resonant scanner scans as a sine wave rather than a triangle wave. The horizontal scan covers the entire flame; the red (dark) areas on each side of the flame show that there is little hot water vapor present. The yellow (gray) region in the lower central region of the scan indicate large amounts of hot water vapor. This diffusion flame has a slot of fuel (CH_4) in the center with oxidizer (air) on either side. There are two regions clearly visible, just to the left and right of center, where there is slightly less absorption due to water vapor.

CONCLUSIONS

The goal of this project is to take video frame rate images of water vapor, methane and possible OH in flames. The preliminary results are very positive, demonstrating the ability to image hot water vapor in the required bandwidth. While a few changes remain to be completed such as synchronization of the X and Y scanning and compensation for distortions imposed by the scanners, we are confident that we will be able to make "movies" of water vapor and methane in diffusion flames. After we have completed the instrument development, we will obtain methane concentrations, water vapor concentrations, and temperature profiles of the reaction zone in a laminar methane-air diffusion flame using a Wolfhard-Parker slot burner (methane measurements may not require WMS in these experiments), and map out 3-D methane concentrations, water vapor concentrations, and temperature profiles of gas jet diffusion flames using an Abel transform. We will also examine ignition effects, various flow rates, and transitions from 1-g to μ-g flames.

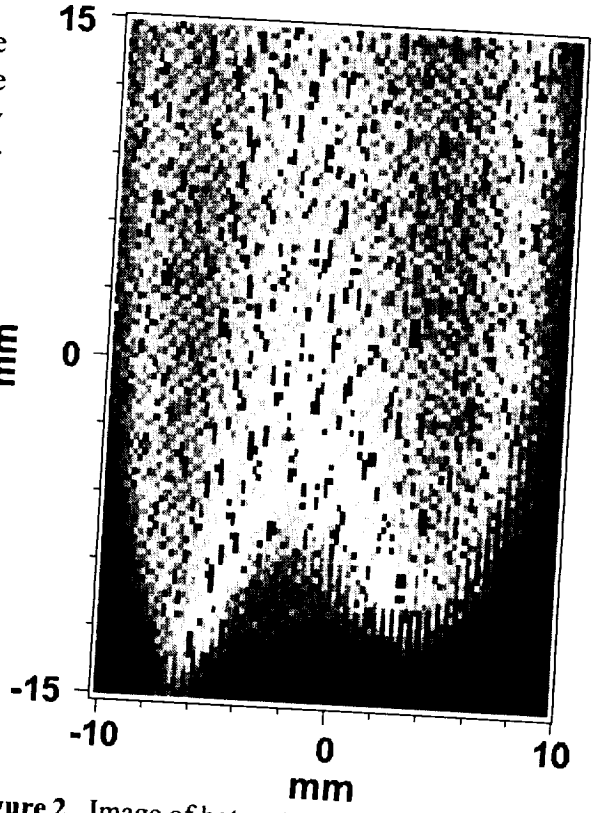

Figure 2. Image of hot water vapor in a flame. Red (black) areas indicate little hot water vapor; yellow (gray) areas indicate the presence of large amounts a hot water vapor.

REFERENCES

1. M. Y. Bahadori, R. B. Edelman, D. P. Stocker, and S. L. Olsen, AIAA Journal **28**, 236 (1990).
2. T. H. Cochran and W. J. Mascia, "An Investigation of Gravity Effects on Laminar Gas-Jet Diffusion Flames," NASA TN D-5872 (1970).
3. R. B. Edelman and M. Y. Bahadori, Acta Astronautica **13**, 681 (1986).
4. Proc. Second International Microgravity Combustion Workshop, NASA Conference Pub. 10113, Cleveland, OH (1992.).
5. D.B. Oh, A.C. Stanton and J.A. Silver, J. Phys. Chem. **97**, 2246 (1993).
6. J.A. Silver, Appl. Opt. **31**, 707 (1992); D. S. Bomse, A. C. Stanton and J. A. Silver, Appl. Opt. **31**, 718 (1992).
7. J.A. Silver, D.J. Kane and P.J. Greenberg, Appl Opt. **34**, 2787 (1995).
8. K. C. Smyth, J. H. Miller, R. C. Dorfman, W. G. Mallard, and R. J. Santoro, Combustion and Flame **62**, 157 (1985).

54 7-39

OPTICAL DIAGNOSTIC OF DROPLETS IN MICROGRAVITY

P. Massoli, Istituto Motori - C.N.R., Via Marconi 8, 80125 Napoli, Italy
massoli@motori.im.na.cnr.it

INTRODUCTION

The study of vaporizing/burning droplets is essential for understanding the mass and heat transfer processes in combustion systems. More and more sophisticated models have been developed to describe the transport phenomena inside droplets and in the outer environment. Despite their large use, especially in complex codes, up to now their experimental validation has been extremely scarce. A severe verification of droplet models is obtained by measuring droplet properties (size, temperature, and composition) during heating-vaporization-burning process.

Microgravity represents one of the most powerful tools when detailed combustion studies have to be performed. In microgravity environments the absence of buoyancy permits in many cases the reduction of three-dimensional problems to mono-dimensional ones with remarkable simplification of phenomenon complexity and thus of modeling. Droplets, in this view, represent one of the most emblematic cases.

In this contribution the application of light scattering methods to study droplets in vaporizing/burning regime will be discussed. The proposed techniques are particularly suitable to develop simple and compact equipment to study droplets in microgravity environments.

LIGHT SCATTERING BY UNSTEADY VAPORIZING-BURNING DROPLETS

Light scattering techniques represent the best candidates to study reactive droplets, being sensitive to size, shape and composition of the scatterers. In recent years many optical systems, based on the measure of the properties of elastically scattered light, have been developed to determine *in situ* and non-intrusively velocity, size and optical properties of single droplets inside sprays /1/. The Lorenz-Mie theory, which is strictly valid for homogeneous spheres, is generally used as basis of these techniques.

However, homogeneous droplets represent a limit case in practical combustors, being the typical droplet lifetime of the same order of magnitude of the transient heating period. Thus, normally droplets vaporize and burn in an unsteady state regime /2-4/. In case of monocomponent fuels a gradient of temperature and consequently of density is established inside the droplets. This implies a gradient of the real part, n, of the refractive index. In case of multicomponent fuels, the preferential vaporization of lighter compounds will generate species concentration profiles and, hence, of both the real and imaginary part of the refractive index. The situation is ulteriorly complicated if liquid phase pyrolysis of the parent fuel occurs, this resulting in a strong increase of the imaginary part of the refractive index, k /5/. Thus, vaporizing-burning-reactive droplets will typically present internal variations of both the real and imaginary part of the refractive index.

Here the case of reactive-unsteady vaporizing-burning droplets in quiescent microgravity environment is treated. Thus, droplets are expected to present radial symmetric refractive index profiles. In that case the Lorenz-Mie theory is not adequate, being valid solely for homogenous droplets, and more sophisticated models to interpret light scattering by inhomogeneous sphere have to be used. To compute the scattering by radially inhomogeneous droplets the Finely Stratified Sphere Scattering Model, FSSSM, was used /6/. This approach allows the computation

of the scattering by stratified spheres with a high number of layers. By using the FSSSM with a sufficient number of layers (namely, few thousands) the scattering by spheres with any continuous internal refractive index profile can be calculated with good accuracy /6/. Different shapes of the internal refractive index profile, $m(r) = n(r) - ik(r)$, were considered in the present study. $n(r)$ and $k(r)$ were varied in the ranges 1.3-1.6 and 10^{-6} to 10^{-1}, respectively. These profiles should cover the majority of cases expected during droplet vaporization, combustion, and liquid phase pyrolysis or chemical transformation processes. Droplets with size lower then 100 μm are treated here; that is the maximum droplet size encountered in practical combustors.

SIZING OF DROPLETS BY LIGHT SCATTERING MEASUREMENT IN FORWARD

In this section a very simple inexpensive technique to measure the size of both homogeneous and radially inhomogeneous droplets will be discussed.

A careful analysis of theoretical light scattering angular patterns highlighted that the cross sections relative to homogeneous and radially inhomogeneous droplets with the same diameter D but different refractive indices were almost identical at a scattering angle near 30° /7,8/. At this angle, ϑ_{ind}, the scattering intensities crossed together, especially for horizontally polarized light (Fig.1). Depending on the total variation and shape of the refractive index, slightly different angles can be chosen, but ϑ_{ind}=30°-33° represents the best compromise for liquid droplets with n or $n(r)$ ranging between 1.3 and 1.6. The identification of ϑ_{ind} posed the basis for a very simple inexpensive technique to measure droplet size. In fact in forward the light is mainly scattered by reflection and refraction, effects that depend on the square of the scatterers diameter. Thus:

$$I_{HH}(n(r), D, \vartheta) = K D^2 \text{ at } \vartheta = \vartheta_{ind}$$

where H stands for horizontal polarization of the light and K is the experimental calibration factor. Therefore the measurement of light scattered at ϑ_{ind} permits of inferring the size of homogeneous and radially inhomogeneous droplets even if n or $n(r)$ are unknown. The residual slight dependence of the cross sections on n or $n(r)$ gives a size uncertainty of about 2.5% in case of vaporizing droplets. Experimental tests carried out on droplets heated in a drop tube furnace were in good agreement with theoretical expectations /8/.

SIZING OF DROPLETS BY MIE SCATTERING IMAGING

Light scattered by droplets shows a complex angular structure characterized by large intensity oscillations along the entire pattern. In case of homogeneous droplets the oscillations have an almost uniform periodicity $\Delta\vartheta \cong 180°/\alpha$ (where α is the size parameter $\alpha = \pi D/\lambda$ and λ represents the radiation wavelength in the vacuum) /9/. Relevant feature is the almost total independence of $\Delta\vartheta$ on the droplet refractive index. On this basis, an optical technique to measure the size of homogeneous droplets was developed /10/. A new optical set-up, based on a planar imaging of the scattered light, permitted the extension of the technique to 2D-spray analysis. Sideward out-focus images of droplets in a spray were captured. The size of droplets was measured by counting the number of fringes present in each defocused drop image /11/. This approach, that we could call *Mie Scattering Imaging*, *MSI*, was subsequently improved /12/ and applied with good results to estimate the fuel droplets diameter distribution in a spark gasoline engine /13/. However, the application of the *MSI* technique has been limited to homogeneous droplets till now.

By using the FSSSM, the angular oscillations periodicity $\Delta\vartheta$ was computed in the case of transparent radially inhomogeneous droplets. The imaginary part of the refractive index was kept fixed to 10^{-6} (transparent droplets) while $n(r)$ ranged between 1.3 and 1.6. Different shapes of $n(r)$ were considered. The results relative to homogeneous and radially inhomogeneous droplets show that the periodicity of oscillations is not constant along the angular pattern and some dependence on refractive index is observed. However, in the sideward, between ϑ=40° and ϑ =80°, $\Delta\vartheta$ is practically constant and the dependence on the refractive index reduces to a minimum at ϑ=60°. At this angle the oscillation periodicity scales with droplet diameter according to the relation:

$$\Delta\vartheta(\vartheta, n(r), D) = 1.12\ (180° / \alpha) \text{ at } \vartheta=60°.$$

The residual dependence of $\Delta\vartheta$ on the refractive index results in a diameter uncertainty of about 4%.

In a second series of tests, the FSSSM was used to compute the scattering by absorbing radially inhomogeneous droplets. In this case n was kept fixed to 1.5 while $k(r)$ was varied between 10^{-6} and 10^{-2}. Generally speaking, the increase of droplet absorption results in a diminution of scattered light (at least until k is not very high). Thus the increase of droplet absorption should have no influence on $\Delta\vartheta$, being the intensity oscillations due to the interference between refracted and reflected light. As a matter of fact, no difference in $\Delta\vartheta$ was observed when absorbing droplets were studied. On the contrary the increase of droplet absorption has a strong influence on the experimental observation of the intensity fringes, namely on their visibility. The visibility of a signal oscillating between a maximum I_{max} and a minimum I_{min} can be defined as $\eta = (I_{max}-I_{min})/(I_{max}+I_{min})$ and runs between 0 and 1. A visibility near 1 indicates a strong fringe contrast and thus an easy recognition of oscillations. FSSSM calculations show that in case of light vertically polarized, visibility is typically higher than 0.8 up to an optical droplet depth, $\tau = \kappa D$, lower than 0.1. For $\tau > 0.1$, visibility collapses very rapidly to zero. On the contrary, visibility of horizontally polarized fringes is low and almost constant up to $\tau \approx 0.1$; after shows a sharp peak around $\tau \approx 0.4$ and then finally goes to very low values ($\eta \leq 0.1$) (Fig.2). The dependence of τ on the polarization state of light is characteristic of both homogeneous and radially inhomogeneous droplets. In case of homogeneous droplets $\kappa=k$. In case of radially inhomogeneous droplets, the optical thickness τ is function of both the total variation and shape of $k(r)$. However, for small droplets and for smooth profiles τ is mainly sensitive to the higher value, k_{max}, of $k(r)$; thus $\kappa \approx k_{max}$.

In conclusion the angular spacing of intensity oscillations in the sideward (in particular at ϑ=60°) is almost independent of the refractive index and scales inversely with the droplet diameter. On these bases the *Mie Scattering Imaging* technique can be applied to measure the size of transparent or absorbing homogenous and radially inhomogeneous droplets.

FINAL REMARKS

In this contribution light scattering methods able to infer the size of droplets of unknown optical properties have been discussed. These techniques should result appropriate to study unsteady droplet evaporation-combustion and whenever internal droplet radial symmetry is expected. Thus the discussed optical methods could represent very useful tools in order to test

evaporation-burning droplet models especially in microgravity, in high-pressure conditions, and when complex fuels have to be studied. In addition they are simple and prone to be applied in experiments where requirements of compactness, low energy consumption and facility of use are recommended. Besides size and composition, temperature is the other relevant property of droplets that should be measured. A recent paper showed that existent light scattering techniques are not able to measure temperature of radially inhomogeneous droplets /1/. Thus such techniques are not applicable in the more interesting cases of unsteady droplet processes. Efforts will be expended in the next future to cover this relevant lack.

REFERENCES

1. P. Massoli, Appl. Opt. **37**, 3227-3235 (1998).
2. C. K. Law, Prog. Energy Combust. Sci. **8**, 171-201 (1982).
3. W. A. Sirignano, Prog. Energy Combust. Sci. **9**, 291-322 (1983).
4. R. Kneer, M. Schneider, B. Noll and S. Wittig, Int. J. Heat Mass Transfer **36**, 2403-2415 (1993).
5. P. Massoli, F. Beretta, and A. D'Alessio, A., Combust. Sci. and Tech. **72**, 271-282 (1990).
6. Li Kai, P. Massoli, Appl. Opt. **33**, 501-511 (1994).
7. P. Massoli, F. Beretta, A. D'Alessio, and M.Lazzaro, Appl. Opt. **32**, 3295-3301 (1993).
8. P. Massoli, M.Lazzaro, 7th Europ. Symp. Particle Charact., pag. 527-536, Nürnberg, (1998).
9. M. Kerker, *The Scattering of Light and Other Electromagnetic Radiation.* (Academic Press, New York, 1969), p.175.
10. G. König, K. Anders, A. Frohn, J. Aerosol Sci., **17**, 157-167 (1986).
11. R. Ragucci, A. Cavaliere, P. Massoli, Part. Part. Syst. Charact. **7**, 221-225 (1990).
12. A.R. Glover, S.M. Skippon, R.D. Doyle, Appl. Opt. **34**, 8409-8421 (1995).
13. O. Pajot, C. Mounaïm-Rousselle, 9th Int. Symp. on Applications of Laser Techniques to Fluid Mechanics, paper 18.2, Lisbon, (1998)

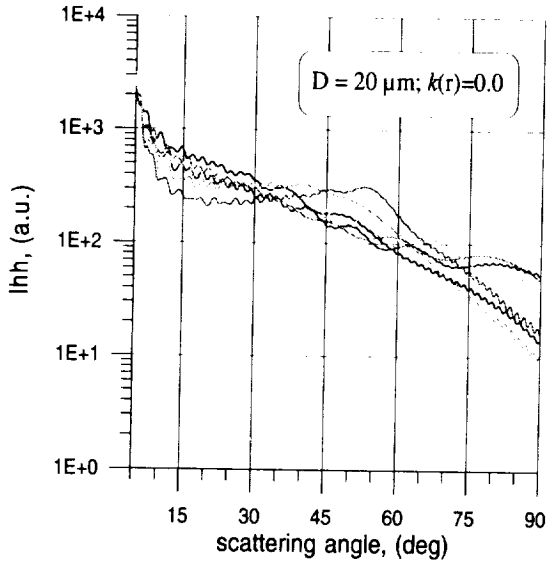

Fig.1 Angular patterns of 20 µm radially inhomogeneous transparent droplets (k(r)=0) with different refractive index profiles n(r). n(r) ranged between 1.3 and 1.6.

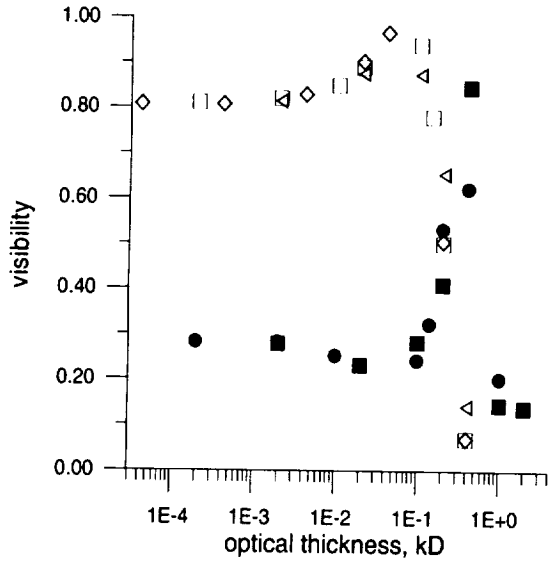

Fig.2 Visibility of vertically (empty symbols) and horizontally (full symbols) polarized oscillations fringes for radially inhomogeneous absorbing droplets with different refractive index profiles k(r). k(r) ranged between 10^{-6}-10^{-2} ; n(r) was kept fix to 1.5.

LASER OPTOGALVANIC SPECTROSCOPY OF NEON AND ARGON IN A DISCHARGE PLASMA AND ITS SIGNIFICANCE FOR MICROGRAVITY COMBUSTION

PRABHAKAR MISRA*, C. Haridass and H. Major, *Laser Spectroscopy Laboratory*, Department of Physics and Astronomy, Howard University, Washington, D.C. 20059

Introduction

A detailed study of combustion mechanisms in flames, employing laser-based diagnostics, has provided good knowledge and understanding of the physical phenomena, and led to better characterization of the dynamical and chemical combustion processes, both under low-gravity (in space) and normal gravity (in ground based facilities, e.g. drop towers). Laser induced fluorescence (LIF) (refs.1-2), laser-induced incandescence (LII) (ref. 3) and LIF thermometry (ref. 4) have been widely used to perform nonintrusive measurements and to better understand combustion phenomena. Laser optogalvanic (LOG) spectroscopy has well-established applications in ion mobility measurements, atomic and molecular spectroscopy, ionization rates, recombination rates, velocity measurements and as a combustion probe for trace element detection. Absorption spectra of atomic and molecular species in flames can be obtained via LOG spectroscopy by measuring the voltage and current changes induced by laser irradiation. There are different kinds of processes (ref.5) that contribute to a discharge current, namely: (i) electron impact ionization, (ii) collisions among the excited atoms of the discharge species and (iii) Penning ionization. In general, at higher discharge currents, the mechanism of electron impact ionization dominates over Penning ionization, whereby the latter is hardly noticeable. In a plasma, whenever the wavelength of a laser coincides with the absorption of an atomic or molecular species, the rate of ionization of the species momentarily increases or decreases due to laser-assisted acceleration of collisional ionization. Such a rate of change in the ionization is monitored as a variation in the transient current by inserting a high voltage electrode into the plasma. Optogalvanic spectroscopy in discharges has been useful for characterizing laser line-widths and for providing convenient calibration lines for tunable dye lasers in the ultraviolet, visible and infrared wavelength regions. Different kinds of quantitative information, such as the electron collisional ionization rate, can be extracted from the complex processes occurring within the discharge. In the optogalvanic effect (OGE), there is no problem of overlap from background emissions, and hence even weak signals can be detected with a high signal-to-noise ratio, which makes the optogalvanic effect sensitive enough to resolve vibrational changes in molecular bonds and differences in energy levels brought about by different electron spins. For calibration purposes, neon and argon gaseous discharges have been employed most extensively, because these gases are commonly used as buffer gases within hollow-cathode lamps and provide an acceptable density of calibration lines. In the present work, our main aim has been to understand the dominant physical processes responsible for the production of the OGE signal, based on the extensive time resolved optogalvanic waveforms recorded, and also to extract quantitative information on the rates of excited state collisional processes.

* Corresponding author; pmisra@fac.howard.edu

Experimental

The experimental arrangement used for recording the optogalvanic spectra is shown in Fig. 1. In this figure, a dye laser (DL) is pumped by the second harmonic of a Nd:YAG-laser (YL) running at 10 Hz. The output beam had a pulse duration of about 20 ns and a nominal line width of 0.07 cm^{-1} (without any intra cavity etalon). An uncoated quartz wedge (QW) was inserted in the optical path of the primary beam to pick off two weak beams (each about 5% of the primary pulse energy). One of the beams entered through a 1 mm diameter aperture to the cathode of either a commercial iron-neon hollow cathode lamp (Perkin Elmer) (HCL) or an Ar-containing commercial Laser Galvatron (L2783-26NE-FE, Hamamastu Co.) containing argon (2 Torr), neon (3 Torr) and trace amounts of iron vapor. The second beam traversed a negative lens (NL) and illuminated an uncoated, parallel-faced 6 mm quartz disk at a small angle of incidence (1-2 deg), which served as a low-finesse etalon (ET). An interference pattern (generated by the reflection beams from the front and rear surfaces of the disk) is recorded after passage through a pinhole aperture (AP) by a photodiode (PD). The third beam is directed to record the LIF-spectrum of the OH-free radical in a propane-air flame for calibration of the optogalvanic spectrum of argon. A high voltage power supply (PS) and a ballast resistor (R) of 20 KΩ for the iron-neon lamp (and 30 KΩ for the Ar-containing commercial Laser Galvatron) were used. When the laser pulse is resonantly absorbed by the discharge medium, the voltage across the lamp varies, and these variations are coupled via a capacitor (C) to a boxcar (BC) integrator. Temporal evolution of the signal was recorded by a digital oscilloscope (OSC). Outputs of the boxcar and the photodiode were recorded with a microcomputer-aided (PC) data acquisition system.

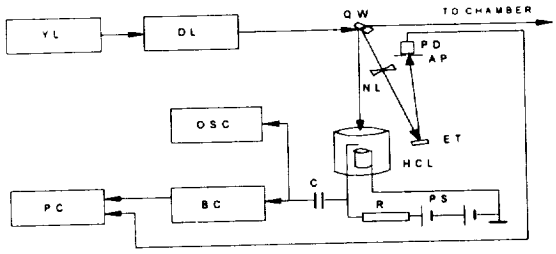

Fig. 1. A schematic experimental arrangement for laser optogalvanic spectroscopy. YL: Nd YAG Laser, DL: Dye Laser, QW: Quartz Wedge, PD: Photodiode, AP: Aperture, NL: Negative Lens, OSC: Oscilloscope, HCL: Hollow Cathode Discharge Lamp, PS: Power Supply, R: Resistor, C: Capacitance, BC: Boxcar, OSC: Oscilloscope, PC: Personal Computer

Results and Discussion

To quantitatively characterize the dominant physical processes contributing to the optogalvanic effect signal in a discharge plasma, it is desirable to analyze the optogalvanic signal associated with a particular transition. The observed intensity of the OGE signal as a function of time (when the laser is tuned to a transition, in the present case, neon/argon) is given by the sum of the signals originating from all the energy states involved, and is given by (Ref. 6)

$$S(t) = S_i(t) + S_k(t) + \sum S_j(t) \quad (1)$$

where S_i and S_k are the contributions from the lower state $|i\rangle$ and the upper state $|k\rangle$ associated with the laser excitation, respectively. In addition to $|i\rangle$ and $|k\rangle$ states that are directly involved in optical excitation, contributions to the OGE signal may also arise from another lower state $|j\rangle$ that the state $|k\rangle$ can relax to. The third term in Eq. (1) is due to this contribution. The shape

and intensity of the OGE waveform is dependent on $N_i I\sigma_i$ and $N_k I\sigma_k$, where N_i and N_k are the neon/argon populations of the states $|i\rangle$ and $|k\rangle$ involved, and the electron collisional ionization rate parameters are σ_i and σ_k. It must be remembered that the collisional ionization parameters are proportional to the electron collisional ionization cross sections associated with the $|i\rangle$ and $|k\rangle$ states. The observed waveform was fitted to the expression given by where a and c are the

$$s(t) = \frac{a}{1 - b\tau}(e^{-bt} - e^{-t/\tau}) + \frac{c}{1 - d\tau}(e^{-dt} - e^{-t/\tau}) \qquad (2)$$

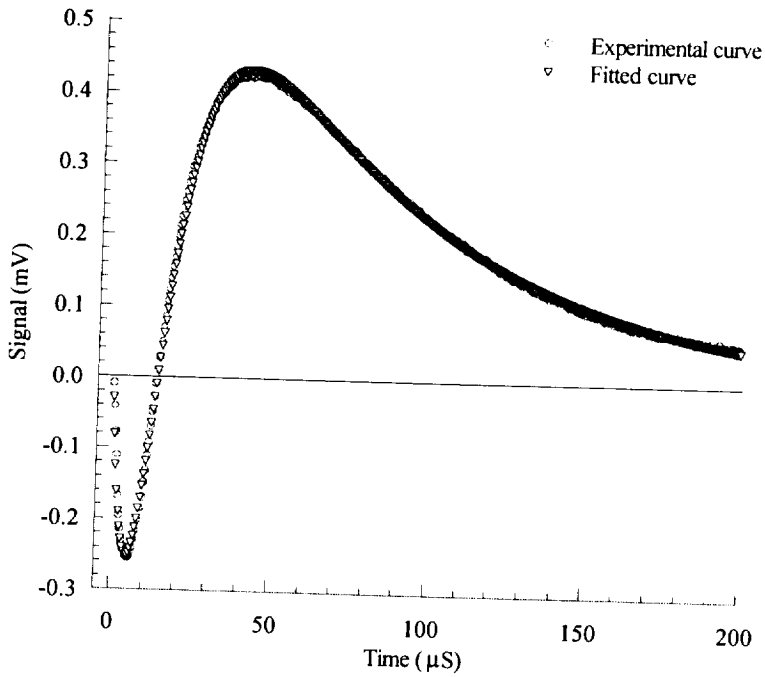

Fig. 2. Fitted and observed signal of neon transition at 640.299 nm for a discharge current of 0.5 mA

amplitudes and b and d are the decay rates for the two states involved in a transition. τ is the instrumental time constant of the waveform for the OGE signal. The time constant is crucial in determining the fast time region of the OGE signal and cannot be neglected. It can be determined by fitting Eq. (2) to the experimental waveform. A non-linear least-squares program was used to fit Eq. (2) to obtain parameters that determine the amplitudes and decay rates of the transitions. In the present work, the experimentally observed time-resolved OGE waveform associated with the neon 640.299 nm transition ($3s[3/2] - 3p[5/2]_3$) was chosen to understand the collisional ionization of the excited state of neon atoms in a gas discharge plasma. A typical time resolved OGE waveform extending from 0 μS to 200 μS together with the fitted curve for a current of 0.5 mA is shown in Fig. 2. Similarly, to understand the collisional ionization of the excited state of argon atoms in a discharge plasma a time-resolved OGE waveform of the 320. 366 nm transition ($4s[3/2]-8p[5/2]_3$), shown in Fig. 3. was chosen. The fitted parameters of both neon and argon OGE signals are given in Table. 1. The discrepancy in the positive part of the signal in Fig. 3. is probably an artifact. In fitting the OGE signal, the values of c and d are fixed, and only three parameters τ, a and b were estimated.

Conclusions

The analysis of the time resolved OGE waveforms has given quantitative information about the dominant physical processes in a discharge plasma that were described in the introduction.

Extending the analysis to signals produced with different currents will help understand the behavior of the effective decay rates of the states involved in the transitions and thereby determine the effective collisional ionization rates. Based on the present analysis, we conclude that the electron collisional ionization of neon and argon atoms is the main determining factor for the time-dependent OGE signals for both the neon (640.299 nm) and argon (320.366 nm) transitions. It is hoped that the LOG characterization and quantification of the significant physical processes in a discharge plasma will help refine laser-based diagnostics of both 1-g and μg combustion processes.

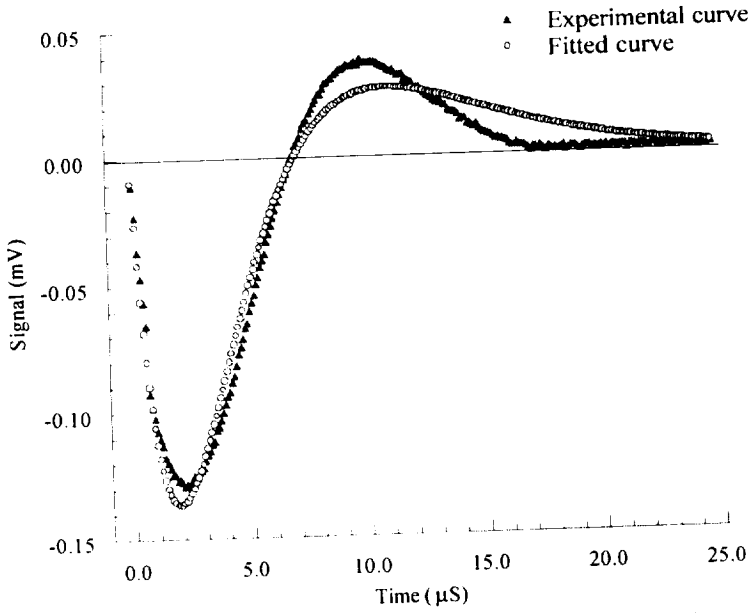

Fig. 3. Fitted and observed signal of argon at 320.366 nm for a discharge current of 5.0 mA

Table 1. Fitted parameters obtained from a non-linear least-squares fit of the observed optogalvanic signal of the neon and argon transitions at 0.5 mA and 5.0 mA, respectively.

Parameter	Neon	Argon
τ	4.893(28) μS	2.510 (77) μS
a	-1.6093(15) mV	-7.7384(50) mV
b	$7.692(32) \times 10^{-2}$ μS	$3.2747(37) \times 10^{-1}$ μS
c	$9.262(25) \times 10^{-1}$ mV	7.26097* mV
d	$1.5030(24) \times 10^{-2}$ μS	3.10886×10^{-1}* μS

*Value fixed in the fit.

Acknowledgments

The authors would like to acknowledge the financial support received from the the NASA Glenn Research Center (grant# NAG3-1677) and the *Center for the Study of Terrestrial and Extraterrestrial Atmospheres* (CSTEA) (NASA grant # NAGW-2950). The encouragement and support provided by the technical monitor for the NASA Glenn project, Dr. Nancy Piltch, is especially appreciated.

References

1.P. Misra, Y. -B. She, X. Zhu and K. King, *Proceedings of the Fourth International Microgravity Combustion Workshop*, NASA Lewis Research Center, Cleveland, OH, 287 (1997).
2.M. Winter, J. Wegge and K. T. Kang, *Proceedings of the Fourth International Microgravity Combustion Workshop*, NASA Lewis Research Center, Cleveland, OH, 299 (1997).
3.R. L. VanderWal, *Proceedings of the Fourth International Microgravity Combustion Workshop*, NASA Lewis Research Center, Cleveland, OH, 305 (1997).
4.T. Kadota, K. Suzuki, T. Fuji and D. Segawa, *Proceedings of the Fourth International Microgravity Combustion Workshop*, NASA Lewis Research Center, Cleveland, OH, 311 (1997).
5.K. C. Smyth, B. L. Bentz, C.G. Bruhn and W. W. Harrison, *J. Am. Chem. Soc.* **101**, 797 (1979).
6.X. L. Han, V. Wisehart, S. E. Conner, M. -C. Su and D. L. Monts, *Contrib. Plasma Phys.* **34**, 439(1995).

Metals Combustion

COMBUSTION OF METALS IN REDUCED-GRAVITY AND EXTRATERRESTRIAL ENVIRONMENTS

A. Abbud-Madrid, P. Omaly, M. C. Branch, and J. W. Daily
Center for Combustion and Environmental Research
Department of Mechanical Engineering
University of Colorado at Boulder
Boulder, CO 80309-0427

INTRODUCTION

As a result of the ongoing exploration of Mars and the several unmanned and manned missions planned for the future, increased attention has been given to the use of the natural resources of the planet for rocket propellant production and energy generation. Since the atmosphere of Mars consists of approximately 95% carbon dioxide (CO_2), this gas is the resource of choice to be employed for these purposes. Unfortunately, CO_2 is also a final product in most combustion reactions, requiring further processing to extract useful reactants such as carbon monoxide (CO), oxygen (O_2), and hydrocarbons. An exception is the use of CO_2 as an oxidizer reacting directly with metal fuel. Since many metals burn vigorously with CO_2, these may be used as an energy source and as propellants for an ascent/descent vehicle in sample-collection missions on Mars.

In response to NASA's Human Exploration and Development of Space (HEDS) Enterprise to search for appropriate in-situ resource utilization techniques, this investigation will study the burning characteristics of promising metal/CO_2 combinations. The use of reduced gravity is essential to eliminate the intrusive buoyant flows that plague the high-temperature metal reactions, to remove the destructive effect of gravity on the shape of molten metal samples, and to study the influence of radiative heat transfer from solid oxides undisturbed by natural convection. In studies with large metal specimens, the burning process is invariably influenced by strong convective currents that accelerate the reaction and shorten the burning times. Although these currents are nearly absent from small burning particles, the high emissivity of the flames, rapid reaction, small length scales, and intermittent explosions make the gathering of any useful information on burning rates and flame structure very difficult. This investigation has the ultimate goal of providing a careful probing of flame structure and dynamics by taking advantage of large, free-floating spherical metal samples and their corresponding long burning times available in reduced gravity.

The first set of experiments has been conducted with magnesium (Mg) samples burning in the low-gravity environment generated by an aircraft flying parabolic trajectories. Owing to its high adiabatic flame temperature, oxidizer/fuel ratio, and heat per unit mass of fuel, as well as its low toxicity and low ignition temperature, Mg has been identified as a promising metal fuel with CO_2 as oxidizer. The experimental effort is complemented by the development of a numerical model combining gas-phase chemical kinetics and transport mechanisms.

EXPERIMENTAL APPARATUS AND NUMERICAL MODELING TOOLS

The apparatus and experimental procedures used in this investigation have been described previously [1] hence only a brief description will be given here. The ignition source consists of a 1000-W xenon lamp that generates a collimated beam with broadband radiation. An aspheric lens focuses the beam to provide a 2-MW/m^2 power density on the top surface of the metal specimen.

A cylindrical metal sample, with equal diameter and length (2, 3, and 4 mm) is supported in the center of a 4.5-L chamber by a 0.13-mm-diameter, type-*R* thermocouple whose junction is placed in the center of the specimen. The thermocouple measures the temperature during heat-up and ignition and is eventually destroyed by the flame formed around the sample. This supporting technique allows the formation of a spherical flame around a free-floating specimen in the absence of gravity. The nearly spherical shape of the sample is achieved after its melting prior to ignition.

Magnesium specimens (99.95% purity) are burned in a pure CO_2 or pure CO environment (99.6% min.) at a 1-atm pressure. A high-speed, 16-mm movie camera provides surface and flame visualization; the images are also used for measurement of burning times. In addition to visible light imaging, time- and space-resolved spectral information on gas-phase reactants and products is obtained with an imaging spectrograph and a diode array detector. The reduced-gravity experiments were conducted onboard the NASA KC-135 research aircraft in Houston, Texas. Up to 20 s of reduced gravity (± 0.01 *g*) were available in a single parabolic maneuver.

The chemical-kinetic numerical modeling of the Mg-CO/CO_2 flames is performed using the CHEMKIN computer code. In the case of metal combustion experiments conducted in microgravity, a spherical flame is nearly achieved. Under these conditions, the burning can be modeled as a one-dimensional, spherically symmetric analogue to the CHEMKIN-based OPPDIF code that models the opposed flow of fuel and oxidizer in a diffusion flame configuration.

RESULTS

The main objectives of the present experiments are to evaluate the burning of a spherical sample in a free-floating configuration in low gravity and to obtain a correlation of burning time with sample size. A spherical shape of the metal sample is achieved during low gravity after melting and while the specimen is suspended from the thermocouple wire. A smooth surface is not generated due to the oxide film coating formed during the heat-up phase. Nonetheless, a spherical flame forms around the sample after ignition (around 1100 K), which immediately melts the thermocouple wire in both sides permitting the unsupported burning of the metal. Steady-state burning is achieved with the visible flame edge at a radius twice the diameter of the original specimen. The burning sample remains at its central position, which is perturbed only by initial explosions and the *g*-jitter present in the airplane. The explosions are a result of the superheating of the metal vapor inside its protective oxide shell. This phenomenon is also observed in Mg-O_2 flames [1] and has been reported previously in Mg-CO_2 reactions [2]. Slow, steady burning follows the initial explosions with the increasing accumulation of solid products in an outer shell. The inner sample remains black with some solid white oxide forming in the surface.

Figure 1a shows the correlation of burning times with initial sample diameter for the low-*g* experiments along with the results from normal-*g* tests conducted by Legrand et al. [3] with particles in the 50 μm to 2.5 mm range. These results correlate well with the $t_b = Kd_0^2$ expression for the burning time, t_b, of Mg particles with initial diameter, d_0, although the burning times in low-*g* are twice as long as the ones obtained in normal-*g*. Previous experiments [1] with Mg in O_2 showed the same trend in burning times between normal and low gravity. It appears that the slower combustion at low gravity is due to the reduced transport of oxidizer to the metal surface. This behavior is expected from a diffusion controlled reaction.

Several tests were conducted with Mg in pure CO with different sample sizes. The purpose of these experiments was to observe the possible role of the heterogeneous reaction Mg+CO = MgO(s)+C(s) in the combustion of Mg with CO_2. Shafirovich and Goldshleger [4] first proposed

a mechanism for the Mg/CO_2 reaction based on the gas-phase reaction, $Mg+CO_2 = MgO(s)+CO$ and the heterogeneous reaction $Mg+CO = MgO(s)+C(s)$ occurring on the sample surface. In all tests, a dim, slow flame developed around the sample after ignition. The condensed particles of MgO slowly moved outwards due to their initial momentum. The reaction continued while the external radiation from the lamp was present but immediately stopped after the lamp was turned off. The unburned sample retained its original shape prior to ignition with a thick black coating around it. This coating appears to be solid carbon C(s) that is formed during surface reactions. From the above results it is concluded that continuous reaction of Mg with pure CO is only possible as long as Mg vapor is continuously extruded through the increasingly thicker carbon coating. This situation may require a CO environment at a temperature above the ignition value.

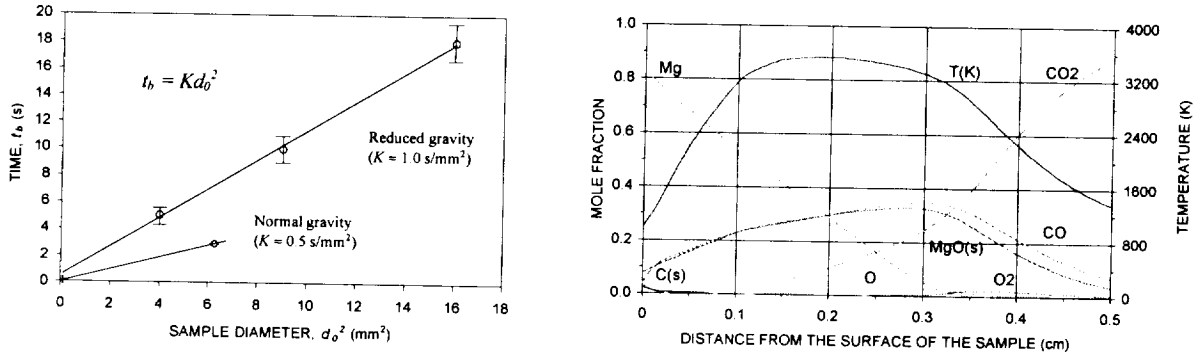

(a) (b)

Figure 1. (a) Burning time vs. initial sample diameter of Mg samples burning in CO_2 at 1 atm in reduced gravity (this investigation) and normal gravity (from [3]). (b) Temperature and concentration profiles from the OPPDIF model of the reaction zone near the surface of a Mg sample where Mg is vaporizing (left boundary) and burning in CO_2 that is diffusing from the surroundings (right boundary).

A simplified numerical model of the one-dimensional, spherically symmetric Mg/CO_2 flame was performed using the analogue opposed-flow diffusion flame configuration available from the OPPDIF code. The combustion process is modeled as a metal surface at the boiling point of Mg (1366 K) from which the metal is vaporizing. A counter flow of CO_2 is imposed to provide a stoichiometric mixture. The temperature in the CO_2 boundary is held at 1200 K. The vaporization rate is calculated from the experimental value of the burning rate of Mg. This value is also used for the velocity of CO_2 to ensure that the stoichiometric surface occurs within the defined computational domain of the model. The pressure throughout the reaction zone is 1 atm. The 12-step reaction mechanism and rate constants are determined from the literature. Since the rates for the Mg reactions with CO_2 and CO are not well known, a sensitivity analysis was performed to obtain the best fit with experimental results. Figure 1b shows the results obtained from the OPPDIF code for temperature and species concentration. The temperature in the reaction zone remains relatively constant near the value of the vaporization-decomposition of MgO (3430 K). The temperature profile drops rapidly near the CO_2 boundary probably due to the dissociation of CO_2 at high temperatures and to the low exothermicity of the Mg-CO_2 and Mg-CO reactions. There is an indication that MgO(s) and C(s) form in the surface of the sample where Mg reacts with CO as observed in the experiments. There is also close agreement in the

thickness of the reaction zone obtained numerically and the one observed experimentally. The observed location of the outer shell of MgO(s) coincides with the concentration peak of this element in Fig. 1b. Several OPPDIF runs were attempted with Mg reacting with different CO_2/CO ratios. No convergence was found for mixtures with more than 65% CO. In this way, the model predicts the absence of significant gas-phase reactions observed in the Mg-CO tests.

CONCLUSIONS

This investigation studies the burning behavior and flame structure of Mg in a CO_2 atmosphere to assess the feasibility of using metal-CO_2 reactions as an in situ resource utilization technology for rocket propulsion and energy generation on other planets. Suspended metal samples ignited in reduced gravity are used to generate free-floating, burning bulk metal samples exhibiting a spherical flame. Burning times twice as long as in normal gravity and five times longer than in Mg-O_2 flames are observed. The burning time is proportional to the square of the metal sample diameter. In tests conducted with pure CO, combustion is not possible without constant heating of the sample. It appears that surface reactions dominate in this case leaving behind a thick carbon coating around the molten Mg sample. It was found that free-floating metal samples burning in low gravity are very sensitive to *g*-jitter. The spherical shape of the flame tends to be distorted and the sample changes location in the direction of the gravity level experienced during the flight. Undoubtedly, this experiment could benefit greatly from the long-duration, high-quality microgravity environment provided by orbiting spacecraft.

The numerical modeling of the Mg-CO_2 flame structure using gas-phase chemical kinetics and transport mechanisms produced concentration profiles and a reaction zone thickness similar to the ones observed experimentally and a temperature profile close to the measured value. Currently, the model does not give a complete picture of the metal-oxidizer reaction since relevant physical and chemical mechanisms such as product condensation, radiation heat loss, and surface reactions are not included. There is also a lack of information on reaction rates of the most basic elementary reactions. Nevertheless, this initial modeling effort represents an encouraging first step towards the development of a realistic numerical simulation of metal combustion.

ACKNOWLEDGMENTS

This work is supported by the National Aeronautics and Space Administration under Grant NASA-NAG3-2220. The authors gratefully acknowledge the technical supervision of Robert Friedman from the NASA Lewis Research Center.

REFERENCES

1. Abbud-Madrid, A., Branch, M. C., and Daily, J. W., *Twenty-Sixth Symposium (International) on Combustion,* The Combustion Institute, 1929-1936, Pittsburgh, 1996.

2. Shafirovich, E. Ya. and Goldshleger, U. I., *Combustion and Flame*, **88**, 425-432 (1992).

3. Legrand, B., Shafirovich, E. Ya., Marion, M., Chauveau, C., and Gökalp, I., *Twenty-Seventh Symposium (International) on Combustion,* The Combustion Institute, 1998, in press.

4. Shafirovich, E. Ya. and Goldshleger, U. I., *Combust., Sci., and Technol.*, **84**, 33-43 (1992).

350-29

COMBUSTION OF AEROSOLIZED METAL PARTICLES IN MICROGRAVITY

E. L. Dreizin[1], C.H. Berman[1], V.K. Hoffman[1], and E.P. Vicenzi[2]
[1]AeroChem Research Laboratory, The Titan Corp., P.O. Box 2229, Princeton, NJ 08543-2229,
[2]Princeton Materials Institute, 70 Prospect Ave, Princeton, NJ 08540-5211

INTRODUCTION

The combustion behavior and interaction effects of multiple metal particles are addressed in this project. The microgravity environment presents a unique opportunity to create an "aerosol" consisting of relatively large, 50-300 μm diameter particles, so that both cloud flame structure and individual particle combustion behavior can be characterized simultaneously. The microgravity experiments are conducted using the 2.2 s NASA Lewis Research Center drop tower. Each test includes aerosolizing metal particles under microgravity, a delay required to produce a steady aerosol, and igniting such an "aerosol" at constant pressure using a hot wire igniter. The flame structure and details of individual particle combustion are visualized using both high speed movie and regular speed video cameras. Combustion products are collected and analyzed after the experiment. A detailed description of the experimental apparatus is given elsewhere [1,2].

Microgravity experiments with magnesium particle aerosols have been conducted and experiments with zirconium particles are currently in progress. A numerical, time dependent model of the flame propagation in magnesium aerosol is being developed.

MAGNESIUM AEROSOL COMBUSTION

Magnesium particles in the 150-220 μm size range were aerosolized and ignited in microgravity [1,2]. The magnesium aerosol flame was observed to consist of pre-heat and combustion zones whose radiation differed in both intensity and spectrum. The observed flame structure is typical of "volatile" aerosol flames, but is not usually anticipated for a coarse metal particle aerosol. The velocity of propagation of the pre-heat zone into the unburnt mixture was found to be in the range of 0.15-0.30 m/s, consistent with the microgravity flame speed measurements reported in the literature [3,4]. The combustion zone propagated significantly slower than the pre-heat zone, at a rate of less than 0.1 m/s. It was observed that the width of the pre-heat zone increased and the width of the combustion zone decreased during the flame propagation. It was also observed that the rates of propagation of both the pre-heat and combustion zones oscillated with periods of several tens of milliseconds.

Individual particles could be seen in the unburnt gas and in the pre-heat zone. They were observed to move primarily away from the flame front; however, in several experiments groups of particles in the pre-heat zone moved towards the flame front. A detailed description of the magnesium combustion experiments is presented elsewhere [2].

Analyses of the experimental results showed the importance of the inertial lag between the particles and the expanding gas (depending on particle size and gas temperature) in the development of an aerosol flame. The phenomena caused by this lag may be generic for many burning aerosols and need further investigation.

A numerical model of magnesium aerosol flame propagation has been developed. The model does not assume a steady-state flame speed but computes the time-dependent flame parameters considering the heat and mass transfer processes occurring in the burning aerosol. Several test computations for magnesium particle cloud combustion have been performed and the results are

being analyzed. The model predicts many of the effects observed in the microgravity experiments, such as an extended pre-heat zone, reversed gas and particle flows in the pre-heat and combustion zones, and changes in local equivalence ratio developing during the flame propagation. Currently, the model is being adjusted to include effects of oxide radiation affecting the heat transfer in the burning cloud.

ZIRCONIUM AEROSOL COMBUSTION

Aerosol of coarse zirconium particles (+50 Mesh, diameters greater than 297 μm) could not be ignited and finer particles (-375 Mesh, less than 44 μm diameter) were used in the first series of microgravity experiments. In each experiment, a flame started to propagate from the igniter wire and was observed to consist of multiple bright spots, likely individual particle flames. A view of the flame structure from the high-speed movie images is shown in Fig. 1. Large agglomerates are seen to form in the wake of the flame. These large, luminous agglomerates are observed to move around the chamber for a long time (~0.5 s) after the flame front vanishes.

Threshold tracking (Tracker software) was employed to follow the position of the flame front and estimate flame velocities for each experiment. These measurements used both regular video (30 frames per second) and high-speed (270 frames per second) movie images. Average flame velocities estimated using linear fits for the flame position in time are summarized in Table 1.

TABLE 1. Summary of zirconium powder combustion experiments

Run #	Mass loaded, g	Average distance between particles		Equivalence ratio	Average flame velocity m/s
		μm	particle diameters		
73	0.53	269	18.6	1.38	0.15
71	0.61	257	17.7	1.59	0.42
72	0.61	257	17.7	1.59	0.16
74	0.61	257	17.7	1.59	0.55
75	0.65	252	17.4	1.69	0.20
70	1.14	209	14.4	2.97	0.46
68	4.9	128	8.9	12.75	2.12
67	5	101	7.0	13.01	1.02

SEM images of unburnt and burnt zirconium powders are shown in Fig. 2. Large agglomerates are observed to form in the flame (cf Fig. 1) and multiple spherical particles of various sizes are strikingly different from the original zirconium powder. One possible mechanism for the formation of large agglomerates is due to the Stefan flow directed towards the particle surface. This flow is produced to compensate for the gas mass imbalance created by the inward oxygen diffusion to the burning particle surface that acts as an oxygen sink [1]. The significance of this effect was evaluated by comparison of the burning time of a zirconium particle versus the time required for a particle entrained in the Stefan flow to reach the adjacent particle surface. It was found that a 12 μm diameter particle (the average diameter used in these experiments) would capture all the neighboring particles

of 5.5 μm diameter and smaller during its burning time when particle separation is 120 μm, as was in the experiments. The expected effect is, therefore, significant and can indeed cause strong particle agglomeration. It can further be amplified if unignited particles are captured by a burning particle and ignite upon collision (e.g., because of contact with the hot burning surface). In this case, the burning time of the growing particle-"attractor" becomes longer and its "sphere of influence" expands further.

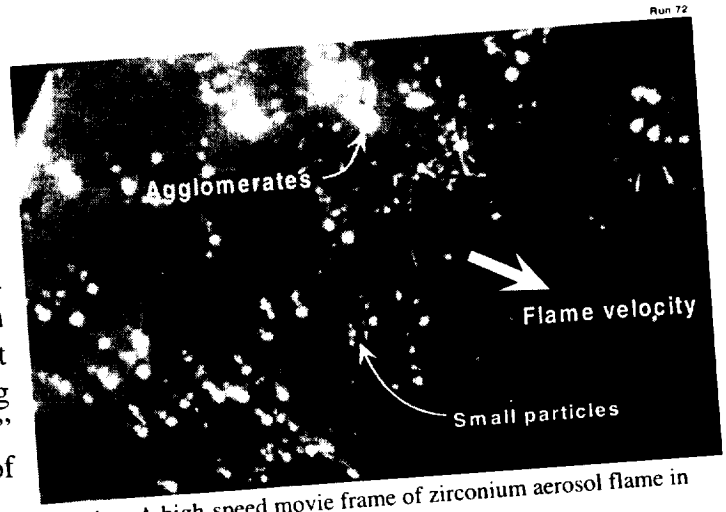

Fig. 1. A high-speed movie frame of zirconium aerosol flame in microgravity

Cross-sections of zirconium combustion products were examined using a Cameca SX50 x-ray microanalyzer. A typical example of a cross-sectioned agglomerate imaged using backscattered electrons is shown in Fig. 3. The contrast in this image is a sensitive function of the average atomic number and, thus, for the Zr-O-N system, the zirconium-rich phases appear brighter and the phases rich with the dissolved gas (or stoichiometric oxide or nitride phases) appear darker. All the results of the elemental compositions measurements made using several cross-sectioned particles are plotted on a ternary diagram, Fig. 4. As indicated on the diagram, most of the light-colored inclusions contain only small amounts of oxygen and some of them are rich with

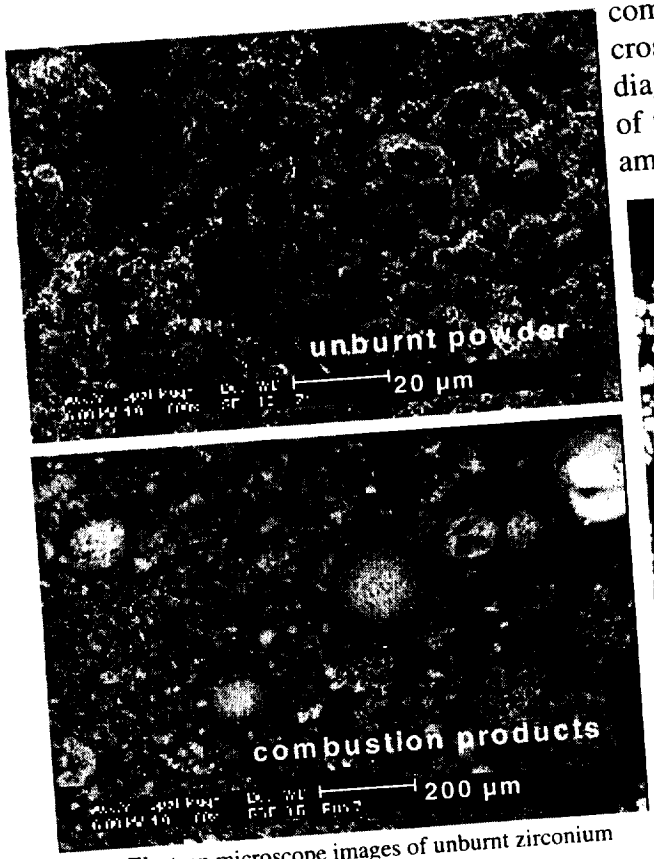

Fig. 2. Electron microscope images of unburnt zirconium particles and combustion products

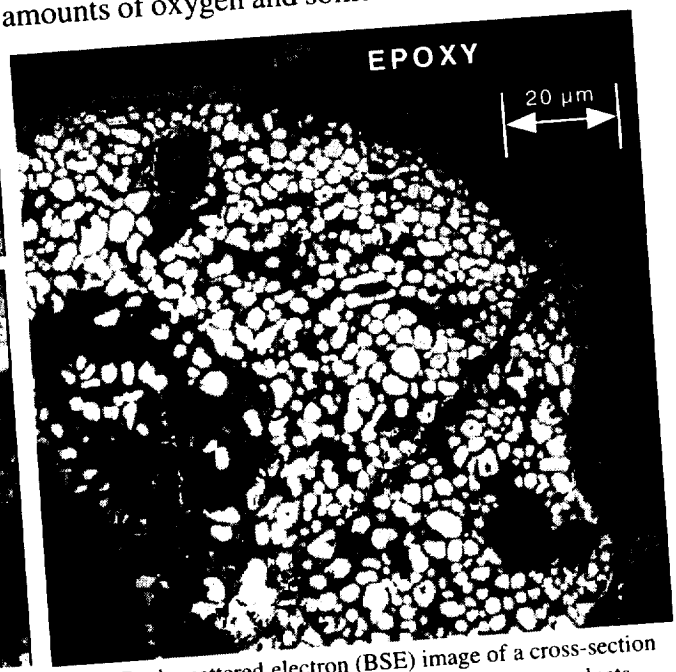

Fig. 3. Back-scattered electron (BSE) image of a cross-section of an agglomerate found in zirconium combustion products

nitrogen. The more uniformly gray, "matrix" phase is, in general, closer to the stoichiometric oxide. The observed phase composition appears to be consistent with the results of the single Zr particle combustion experiments in air [5] where a nitrogen-rich phase was detected in the particles quenched at early times, but ZrO_2 formed as the final combustion product.

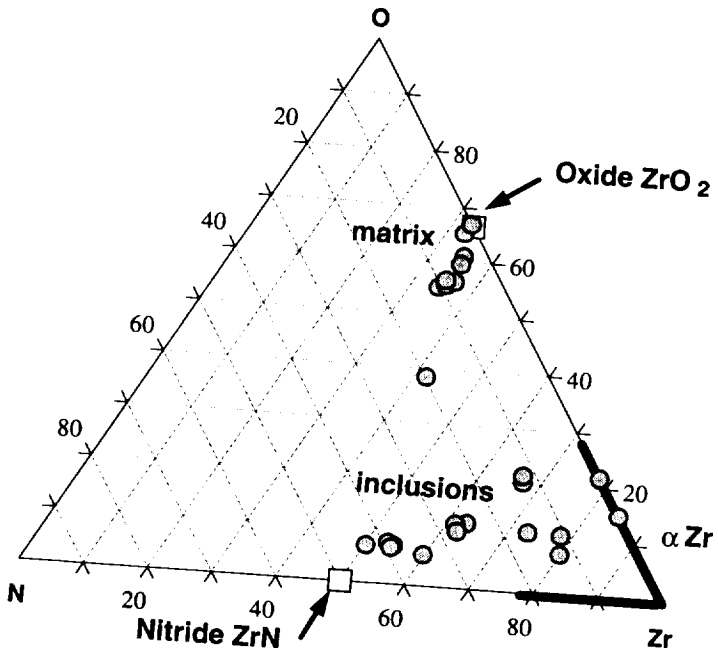

Fig. 4. Results of the elemental composition measurements in the cross-sectioned products of zirconium combustion

ACKNOWLEDGMENTS

This work has been supported by the NASA Lewis Research Center under Contract No. NAS3-96017. The support and encouragement of Mr. R. Friedman, the Contract Technical Monitor, are greatly appreciated.

REFERENCES

1. Dreizin, E.L., *NASA CP 10194*, Fourth International Microgravity Combustion Workshop, Cleveland OH 1997, pp. 55-60.
2. Dreizin, E.L., and Hoffman, V.K., *Combustion and Flame* (1999, in press)
3. Shevchuk, V.G., Goroshin, S.A., Klyachko, L.A., Ageyev, N.D., Kondratyev, E.N., and Zolotko, A.N., *Fizika Gorenia i Vzryva* No 1, pp. 57-63 (1980) (in Russian).
4. Ballal, D.R., *Proc. R. Soc. Lond.* A 385, pp. 21-51 (1983).
5. Molodetsky, I.E., Dreizin, E.L., and Law, C.K., *Twenty-Sixth Symposium (Int'l) on Combustion*, The Combustion Institute, Pittsburgh, 1996, pp. 1919-1927.

S51-25

Oxide Layer Effects in Metal Particle Combustion

Dirk Meinköhn
German Aerospace Center DLR
74239 Hardthausen, Germany

1 Deficiencies of Current Models

By and large, all current combustion modelling for metal particles may be traced back to a common origin. This is the original formulation by Law[1] which in essence is based on the concept of a vapour-phase flame enveloping the particle. The Law model is set up in close analogy with the combustion model for a hydrocarbon fuel droplet where gaseous oxides CO_2 and H_2O are produced.

The elements grouped as 'metals' for combustion applications are distinguished by a heat of combustion which is large[2] in comparison to that of hydrocarbons[3]. A convenient physical argument shows that the large heat of combustion entails a strong preference of the metal oxides for the condensed state of aggregation, so that the physics of metal combustion must differ from that of hydrocarbon combustion. It is an essential shortcoming of the Law model that the condensed-phase nature of the reaction products is not properly recognized. Typically, the surface of metal particles in combustion is covered by a condensed-phase oxide layer. Some of its evolutions result in ignition, extinction or oxide cap formation which designate important combustion characteristics. These are outside the Law model since it doesn't properly provide for the presence and the evolution of the oxide layer.

With respect to a flame envelope, the metal oxide may be grouped in two fractions. Metal oxide which is outside the flame envelope condenses into μ-size smoke particles which eventually escape with the gaseous exhaust. The other fraction of the oxide is in between the flame envelope and the particle and mostly condenses on the particle surface where it forms a uniform or nonuniform surface layer. The Law model makes the indiscriminate assumption of a uniform surface layer of negligible transport resistance, but ignition, extinction and cap formation arise from surface layers of strong nonuniformity and strong transport resistance. The importance of these effects, for instance in rocket propulsion with metallized fuels and propellants, is well documented[4,5]. Boron and aluminium represent primary examples of metals which are used as high-energy additives. For boron, a thick oxide layer is found to prevent ignition and effective combustion[6]. In contrast with boron, aluminium ignites easily but has the tendency to form oxide caps which are seen as causing major problems in propulsion applications[4]. Ignition, extinction and the onset of cap formation are associated with critical states of the particle where a sudden change in the reaction mode occurs. Such branching phenomena are easily disturbed by even small perturbations, so that their experimental investigation is expected to be much easier under reduced gravity.

2 Ignition/Extinction for Critical Marangoni Numbers

In order to treat effects not covered by Law[1], an alternative model is formulated, based on the primary assumption that the physics of the oxide surface layer is of importance to metal particle combustion. For this model to remain simple, the layer is assumed to be thin but nevertheless of significant transport resistance. The layer is seen as a barrier which separates the metal from the oxidizing atmosphere. Transverse transport of heat and molecular species (e.g. oxygen or metal suboxides) traversing the layer is of primary importance since it drives the reaction process by supplying oxygen or metal fuel to the reaction site. Transport resistance is a function of the layer thickness h, such that for an increase in h there is an increase in resistance[7-9]. The model includes the following transport processes: (1) transport of oxygen towards the metal surface, (2) transport of heat towards or away from the metal surface, (3) transport of oxide in the ambient atmosphere away from the particle. In order to demonstrate the capabilities of the model, the surface of the metallic core of the particle is to be the reaction site, which assumption corresponds to a modelling of ignition.

The model proposes to treat longitudinal flow in a liquid oxide layer. Ignition, particularly, is to be brought about by a rupture spreading in the layer, this leading to a surface cover of much reduced thickness. A changeover from a thick layer to a thinner one amounts to a transition from a slow oxidation mode to fast combustion, which is what ignition designates.

The model assumes that longitudinal film flow is hydrodynamic, but that conditions of strong transverse transport resistance prevail. Consequently, the well-established thin film hydrodynamics[10] are inapplicable, since they are based on neglect of dissipation. While ordinary thin-film hydrodynamics are nonlinear-dispersive, the present model needs to be nonlinear-dissipative. In fact, the evolution of the film thickness h, which is the primary variable of the combustion process, is determined by the following parabolic evolution equation[9]:

$$\partial_t h + \nabla_s \left[\left(\frac{1}{3} h^3 \sigma (\nabla_s \nabla_s) - \frac{1}{2} h^2 Ma \frac{\partial T_h}{\partial h} \right) \nabla_s h \right] = A_{form}/h - J_{vap}. \tag{1}$$

In Eq.(1) the following parameters occur: h = oxide layer thickness, t = time, ∇_s = surface nabla (in longitudinal coordinates), σ = surface tension, Ma = (thermal) Marangoni number, T_h = layer temperature, A_{form}/h = formation of layer oxide, J_{vap} = vaporization of layer oxide.

The Marangoni Ma number turns out to be of primary importance as to ignition, extinction and the onset of oxide cap formation. It is defined as follows:

$$Ma - \left(\frac{\partial \sigma}{\partial T} \right) \Big|_{T=T_h}. \tag{2}$$

Eq.(2) defines the thermal Marangoni number. There is also a solutal Marangoni effect which is usually weaker than the thermal one. For the present model it has been neglected, along with the effects of gravity.

In order to investigate ignition, an initial state is assumed in which the particle is covered by an oxide layer of uniform thickness, i.e. without variations in h. This gives:

$$\nabla_s h - 0. \tag{3}$$

Ignition is associated with a critical state of a uniform stationary layer. Such states therefore result as roots of the following equation:

$$\frac{A_{form}}{h} - J_{vap} = 0. \tag{4}$$

For the particular case of boron the solutions of Eq.(4) may be represented as functions of an independent parameter of the model, which is chosen to be the temperature T_∞ of the ambient atmosphere. Fig.1 shows the layer thickness h and the layer temperature T_h as functions of the ambient temperature T_∞, each function consisting of two branches. Branches emerging from the origin are stable whereas the other branches designate stationary uniform layers which are unstable. Ignition is associated with with the critical point at $T_\infty = 1810\ K$ where there is a merger for each pair of stable and unstable branches. This value of the critical ambient temperature was obtained earlier by a number of authors (see e.g. [11]).

The result for ignition with uniform oxide layers may now be improved by admission of symmetry-

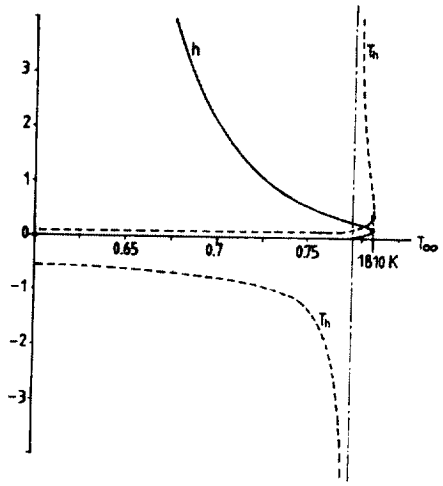

Fig.1: Critical State and Ignition

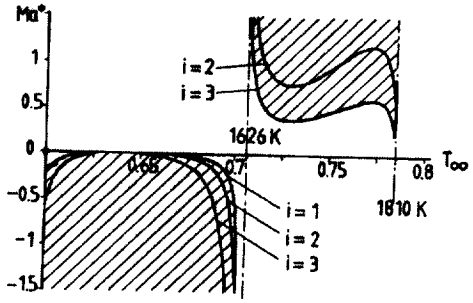

Fig.2: Critical Marangoni Number for Rupturing

breaking, which is brought about by layer rupturing. For this purpose the thickness h is scaled with respect to the thickness h_0 of the initial uniform layer. A small perturbation then gives:

$$h = 1 + h_1 \,. \tag{5}$$

The nonuniform thickness perturbation is designated by h_1. For a demonstration of the fact that symmetry-breaking leads to an improvement as to ignition, the initial state of the particle is assumed to be spherically symmetric, while h_1 is to be axially symmetric. This gives:

$$h_1 = h_1(\theta) \,. \tag{6}$$

θ designates the polar angle of a set of spherical coordinates, with the particle center at the origin. The left-hand side of Eq.(1) is given in terms of the surface Laplacian L which for axial symmetry results as:

$$L - \nabla_s \cdot \nabla_s - \frac{1}{\sin(\theta)} \frac{\partial}{\partial\theta} \left(\sin(\theta) \frac{\partial}{\partial\theta} \right) . \tag{7}$$

L as given by Eq.(7) has the eigenfunctions $P_k(\cos(\theta))$ which represent the Legendre polynomials. Since $\{P_k(\cos(\theta))\}$ form a complete function set, any arbitrary perturbation $h_1(\theta)$ may be expanded in a series of Legendre polynomials. For a solution to be stable, it needs to stable with respect to any perturbation. Therefore, improved critical states are obtained if the perturbation h_1 is expressed as:

$$h_1 = \exp(\mu t) P_k(\cos(\theta)) \,, \quad k = 1, 2, 3, \ldots \tag{8}$$

A negative sign of the parameter μ designates a stable uniform solution. μ is obtained if Eq.(8) is used in Eq.(1). Critical states then arise for a change of sign of the real part $\mathcal{R}(\mu)$ of μ. Therefore, the so-called *stability diagram* is given as:

$$\mathcal{R}(\mu) = 0 \quad \rightarrow \quad Ma^* = Ma^*(T_\infty) \,. \tag{9}$$

Ma^* designates the critical Marangoni number. For boron, Fig.2 shows Ma^* in the stability diagram corresponding to Eq.(9). The shaded regions in Fig.2 indicate instability with respect to rupturing.

The sign of Ma depends on the substance, but also on the direction of the transverse temperature gradient. There is therefore a difference between the case of self-heating for which heat is transported away from the particle, and the case of thermal heating, for which heat is transported towards the particle. For boron oxide, $\partial\sigma/\partial T > 0$ (cf.[12]) , so that self-heating gives $Ma > 0$, whereas $Ma < 0$ for external heating. Fig.(2) shows that for perturbations given by Legendre polynomials of the lowest orders (cf. Eq.(8)) there is only a slight improvement of about 200 K in the case of self-heating, whereas for external heating critical states are obtained for much lower ambient temperatures T_∞. Such an observation is of considerable importance when an improved ignition readiness needs to be achieved for propulsion applications.

In terms of Fig.(2) a comparison with aluminium is also possible. For aluminium oxide, $\partial\sigma/\partial T < 0$ (cf.[13]). In contrast with boron, ignition due to self-heating is therefore easily possible, with infinitesimal nonuniform perturbations driving the oxide layer to rupture. But rupture of an oxide layer does not lead to its disappearance from the particle surface. Rather, an agglomeration in the form of an oxide cap is formed.

References:

1 C.K.Law, Combust.Sci.Technol. **7** (1973) 197-212
2 T.A.Steinberg,D.B.Wilson,F.Benz, Combust.Flame **91** (1992) 200-208
3 G.W.Burdette,H.R.Lander,J.R.McCoy, J.Energy **2** (1978) 289-292
4 M.Salita, J.Propuls.Power **11** (1995) 10-23
5 R.Bhatia,W.A.Sirignano, Combust.Sci.Technol. **54** (1984) 299-318
6 M.K.King, J.Spacecraft **19** (1982) 294-306
7 A.Atkinson, Rev.Mod.Phys. **57** (1985) 437-470
8 D.Meinköhn, Combust.Sci.Technol. **105** (1995) 86-116
9 D.Meinköhn,H.Sprengel, J.Eng.Math. **31** (1997) 235-257
10 G.B.Whitham: *Linear and Nonlinear Waves*, Wiley, New York 1974
11 D.Meinköhn,Combust.Flame **59** (1985) 225-232
12 E.E.Shpilrain,K.A.Yakimovich,A.F.Tsitsarkin, High Temp.(USSR) **12** (1974) 77-82
13 E.E.Shpilrain,K.A.Yakimovich,A.F.Tsitsarkin, Teplofiz.Vys.Temp. **11** (1973) 1001

GRAVITY EFFECT IN ALUMINUM DROPLET IGNITION AND COMBUSTION

I. G. Assovskiy, O. M. Zhigalina, G. P. Kuzhnetsov, and V. I. Kolesnikov-Svinarev, Semenov Institute of Chemical Physics, RAS, Kosygin St. 4, Moscow 117977 Russia;
e-mail: iga@icp.msk.ru.

INTRODUCTION

A distinguish feature of aluminum combustion is formation of condensed products. Despite of great significance of this process for many applications (from ceramic to dust formation in cosmos), there is not any commonly accepted theoretical model of this process [1]. First, it is due to the difficulties of experimental investigation. These difficulties are associated with high values of temperature and concentrations gradients around burning particle that restricts application of the standard methods for diagnostics of chemical reactions. Additional difficulties are associated with free and induced convection complicating the streamline flow around the burning particle. To overcome these problems, an advanced experimental technique was used in this study. It allows one to determine the thermal structure of reaction zones and the products morphology at various moments of particle's ignition and combustion. This technique uses a special installation for multi-parametrical study of single particle combustion in low gravity environment [2,3].

There are several reasons to investigate droplet's ignition and combustion in the low- or micro-gravity environment. First, the microgravity gives a unique opportunity to avoid non-regular disturbances introduced in the combustion process by free convection. Such conditions, assumed in many theories [1], could provide a correct comparison of theoretical and experimental data. Second, preliminary experiments [3] have shown that morphology of condensed phase of combustion products depends significantly on gravity level and other characteristics of oxidizing gas-mixture. That is why the emphasis in this study is on morphology of combustion products and their dependence on combustion conditions

The morphology characteristics of condensed phase of combustion products have been determined in normal and low gravity environment using the scanning and transmission electron microscopy. Peculiar clusters and longitudinal macro-aggregates of spherical microparticles have been found in the products of low-gravity combustion under high-pressure. Correlation between geometrical characteristics of these aggregates and pressure of oxidizing environment has been found.

EXPERIMENTAL SET-UP

A laboratory-scale installation has been used to provide a low gravity environment for a single droplet combustion. The installation, Fig. 1, includes a dropping platform (6) equipped for optical and thermal registration of droplet ignition and combustion. The dropping platform provides decreasing of gravity level to 0.01 g. A high-pressure combustion- chamber (7) and equipment for high-speed photo and cinema-filming are placed on the dropping platform. The chamber keeps pressure up to 60 at. The ignition of particles is executed using the ruby-laser GOR-300 (the wave length is 0.69 micron, the laser-pulse duration is 6-7 ms). The dropping platform provides decreasing of gravity level to 0.01 g. Maximum duration of low gravity conditions is equal to 0.65 s that is enough to study ignition and combustion of small droplet.

The combustion chamber (7) has a set of micro-thermocouples (W+5%Re)/(W+ 20% Re),

diameter 10-20 microns). The purpose of this set is to record the temperature distribution around the burning particle during its slow drift through the set in low-gravity conditions. A special unit is used in some experiments to fix a metallic droplet on micro- thermocouple during ignition and subsequent combustion. The thickness of that wolfram-rhenium thermocouple is equal to 10 microns. The droplet temperature was recorded during the life-time of droplet.

The effect of gravity level on the condensed products formation is tested by catching of burning particle on metallic plate at different instants of combustion process. The condensed products morphology is investigated using scanning and transmission electron microscopy. The Philips microscopes SEM 515, and EM-430ST (operated at 200 kV) have been used for this purpose.

The ignition and subsequent combustion of aluminum particles of 0.2 up to 0.8 mm have been studied in oxygen mixtures: 20% oxygen and 80% argon (or helium, nitrogen, CO2), under pressures from 1 at up to 60 at in normal and low-gravity environment.

RESULTS AND DISCUSSION

Thermal characteristics of droplet ignition and combustion

The temperature-time curves of droplet indicate that temperature in the ignition instant is about 2300 +/-100 K for all tested conditions, that correlates with melting temperature of Al_2O_3 (2320) coating the tested particles. The droplet temperature during combustion in 20%O_2+ 80%Ar environment is equal to 2390 +/-50K. It is less than boiling temperature of aluminum (2790 K) or its alloy Al+Al_2O_3.(<3250 K). The droplet temperature during the combustion in 20%O_2+80%N_2 environment under 1 ata is equal to 2240 +/-50K. It is close to the ignition temperature of aluminum droplet: 2300 +/-100K, but less than aluminum boiling temperature.

The ignition and combustion temperatures of particle do not significantly depend on the gravity level. Meanwhile, in low-gravity environment (in contrast to the normal gravity) the temperature distribution around the particle is characterized by wide spatial scale. In addition, there are observed pulsations of the thermal radiation of particle during combustion in low gravity environment. It is more expressed if gas pressure is higher than a critical one (5 at for 20% O_2+80%N_2). These clearly defined pulsations are (most probably) associated with the thermal hysteresis [4] of heterogeneous oxidation of aluminum.

Microparticles Aggregates in Combustion Products

Reduction of gravity level influences most significantly the morphology of condensed phase (c-phase) of combustion products. Figs. 2-4 illustrate this gravity effect on products of droplet-combustion. The scanning electron microscopy have shown that c-phase of products in low-gravity conditions constitutes aggregates of spherical microparticles (sizes from tens nanometer to 3 microns), Fig. 2. These microparticles form chains (length up to 10 microns), Fig. 2, looking like fine fibers at low magnification. Aggregates of such fibers can form peculiar space-structures around a large nuclear particle (about 3 microns). This structure (size up to 5 microns) can look like a dandelion in one case or like a cellular frame in other case. Altogether these frames form a longitudinal (a snake-like) macro aggregate (length up to 1-2 cm), Fig. 3. Such a structure is probably due to a drift of the burning particle through its own cloud of combustion products.

The indicated space structures are not observed in normal-gravity conditions. In such a case the sediment of products of droplet combustion is uniformly distributed as separate particles or small aggregates (consisting from several particles) size from 0.1 up to 1-2 microns, see Fig. 4. In

these aggregates sizes of contact surfaces are comparable with sizes of contacting microparti les. The linear aggregates are not observed.

The snake-like macroaggregates are observed only in low gravity conditions if the gas pressure is high enough. It is found a correlation of geometrical characteristics of microparticles, chains, and aggregates with pressure of oxidizing gas. The mean size of spherical microparticles at 60 at (0.6-0.7 micron) is three times higher than that one at 20 at. The size distribution of microparticles is more uniform at 60 and 20 at than that one at 40 at.

In all cases the investigated structures are quite stable against the long effect of electron beam of scanning microscope, which results, for example, to heating of tested sample. The chains of microparticles are strongly connected among themselves, in spite of the fact that the square of particles' contact is rather small. The transmission electron microscopy of these aggregates indicates that microparticles can have different nature: crystalline (Al or Al_2O_3) and amorphous spherical particles covered by thin layer of Al_2O_3-crystals.

CONCLUSION

Formation of chains, clusters and macro-aggregates of microparticles are observed in products of Al-droplet combustion in low-gravity environment. This phenomenon is significantly expressed if gas pressure is high enough (20-60 atm). The content and pressure of oxidizing environment influence sizes and shape of macro-aggregate, as the size-distribution of spherical microparticles. These microparticles can have different nature.

ACKNOWLEDGMENTS

This work has been supported by the Russian Foundation for Basic Research, Grant No 96-03-33775 and partially by the INTAS, Grant No 93-2560-EXT.

REFERENCES

1. K.P. Brooks, M. W. Beckstead, J. of Propulsion and Power, **11**, 4, 769 (1995).
2. I.G. Assovskiy, V.I. Kolesnikov-Svinarev, G.P. Kuznetsov, in *Proceedings. of the Int. Conference on Combustion (ICOC'96)*, Published by IPM UrD of RAS, Izhevsk, Russia, 1997, vol. I, p: 84.
3. I.G. Assovskiy, Kim Yoo, V.I. Kolesnikov-Svinarev, G.P. Kuznetsov, in *Proceedings of the 7th Int. Conference on Liquid Atomization and Spray Systems*, Seoul, 1997, p. 1023.
4. I.G. Assovskiy, Doklady Chemistry, Proc. of the Russian Academy of Sciences, **352**, 3, 1 (1997).

FIGURES

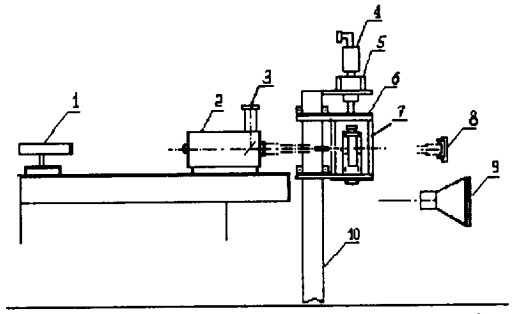

Fig. 1. Schematic diagram of the experimental setup: 1-alignment laser; 2-ruby laser; 3-radiation energy meter; 4-electromagnetic launching device; 5-lock; 6-dropping platform; 7- combustion chamber; 8-reflector; 9-control camera; 10-rail.

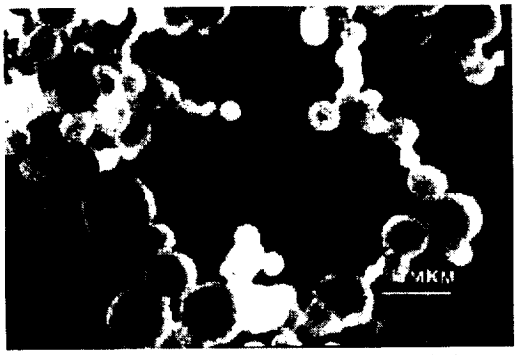

Fig. 2. The chains of microparticles. P=60 atm., O2+Ar

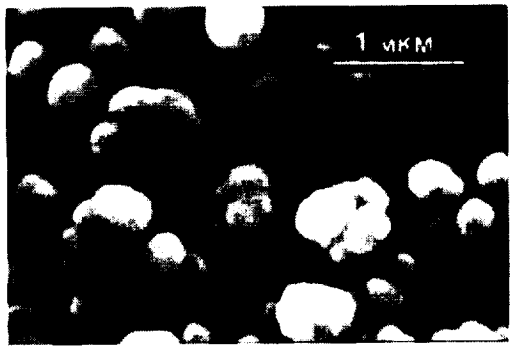

Fig. 4. Products of droplet combustion in normal gravity environment

Fig. 3. A snake-like macro aggregate of spherical microparticles. Low gravity, P=60 at., O_2+Ar.

Droplet and Particle Combustion

FLAME HISTORIES IN HEPTANE DROPLET COMBUSTION

Forman A. Williams[1], [1] Center for Energy & Combustion Research, Applied Mechanics & Engineering Sciences, University of California, San Diego, La Jolla, CA, 92093-0411

INTRODUCTION

In a joint program, among in particular Prof. F.L. Dryer of Princeton University and Dr. V. Nayagam of the National Center for Microgravity Research on Combustion and Fluid Dynamics at the NASA Lewis Research Center, combustion of liquid fuel droplets having initial diameters between about 1 mm and 5 mm is being studied, with the objective of improving fundamental knowledge of droplet combustion through microgravity experiments and theoretical analyses. This research has involved many experiments in both of the drop towers at Lewis and experiments in Spacelab during three different flights of the Space Shuttle. The Spacelab experiments concerned 1) fiber-supported droplet combustion (FSDC), a Glovebox experiment performed first (FSDC1) on the USML-2 mission in October, 1995 (STS-73) [1] and next (FSDC-2) on the second flight of the MSL-1 mission in July, 1997 (STS-94), and 2) the droplet combustion experiment (DCE), a two-rack experiment performed on the MSL-1 mission in both the April, 1997 flight (STS-83) [2] and STS-94. The DCE studies, thus far employing only heptane as the fuel, addressed mainly the combustion of free droplets, although some DCE tests also were made with fiber support for comparison with FSDC results. All of the FSDC experiments involved combustion in normal Spacelab cabin air, while in the DCE tests the combustion occurred mainly in oxygen-helium atmospheres at pressures of 1.00 atm, 0.50 atm and (for 2 droplets) 0.25 atm, although 4 DCE data points from STS-94 involved combustion in normal Spacelab cabin air, 2 for free droplets and 2 for fiber-supported droplets; flame-diameter results for one of these free-droplet tests are shown below. The FSDC experiments covered a number of different fuels, including methanol, methanol-water mixtures, ethanol, ethanol-water mixtures, methanol-dodecanol mixtures, n-heptane, n-decane and heptane-hexadecane mixtures; in addition to studying single droplets in quiescent atmospheres, the FSDC work investigated single droplets in forced convective flow and droplet pairs. In total, in Spacelab there have now been more than 160 successful FSDC burns and 44 successful DCE burns.

The principal types of data obtained in these experiments are histories of droplet and flame diameters, as well as extinction diameters, as functions of atmospheric composition and pressure. In addition, information was acquired on soot-particle behavior, on droplet interactions, on flame elongation through convection, on droplet and flame oscillation phenomena, on staged combustion and on ignition and extinction characteristics. The main focus in the analysis of the results thus far has been on burning rates and flame-diameter histories, including identifying conditions and mechanisms of flame extinction. Efforts to explain the experimental results include computational investigations at Princeton and theoretical studies at UCSD. The Princeton contributions are described by F.L. Dryer in a companion communication in this volume. The present communication reports recent theoretical studies at UCSD focused on predicting flame histories and extinction conditions. An asymptotic analysis, treating the gas-liquid density ratio and the stoichiometric air-fuel ratio as small parameters [3], is outlined, and some comparisons with experimental results are made. First, and identification of different regimes of droplet combustion will be introduced.

REGIMES OF DROPLET COMBUSTION

The first FSDC results showed the existence of two different regimes of droplet combustion. It has long been known from experiments with initial droplets small enough to be studied in drop towers that the ratio of flame to droplet diameter often approaches a constant quasisteady value, and flame extinction occurs (for combustion in cool atmospheres) by diffusive heat loss after the flame diameter becomes sufficiently small. The FSDC experiments for methanol droplet combustion revealed a different flame-extinction mode for sufficiently large initial droplet diameters, in which the flame diameter increased with time, and the flame then extinguished through radiative heat loss. It is thus now known that there are two different regimes in the combustion of droplets in atmospheres of temperatures sufficiently below the adiabatic flame temperature, the regime of radiative flame extinction and the regime of diffusive flame extinction. One objective of theoretical studies now is to determine the location of the boundary between these two regimes.

The DCE measurements, first run on STS-83 , demonstrated the existence of these same two regimes for heptane droplet combustion. The first observations of radiative extinction for heptane droplets were made on this April, 1997 flight. The DCE results enable a rough sketch of the boundary between radiative and diffusive extinction for heptane droplet combustion in oxygen-helium atmospheres to be drawn in a plane of oxygen percentage in the atmosphere and initial droplet diameter, for both 1.00 atm and 0.50 atm total pressure. Figure 1 is a preliminary approximation to these results; further analysis of the data may refine this figure. One objective of continuing theoretical analyses is to explain these results, predicting the location of the boundary curve. This objective has not yet been achieved; there are preliminary indications that without the effect of energy overdrive by the igniter, the boundary would be vertical, independent of initial droplet diameter, and the larger influence of the ignition energy on the smaller droplets enables them to burn longer, into a regime of diffusive extinction. This qualitative suggestion, however, currently is unsubstantiated, and much more theoretical study and better data analysis are needed.

The DCE results apparently established an additional boundary of regimes, also shown in figure 1. For sufficiently small droplets burning in atmospheres of sufficiently large oxygen mole fractions, the droplet disappears completely, vaporizing to zero diameter prior to flame extinction, while the flame contracts rapidly but extinguishes at an apparently measurable small diameter, slightly after droplet disappearance. The lower curves in figure 1 are rough estimates of the upper experimental boundary of this regime of droplet disappearance. Theoretical work is needed to address the location of this boundary as well and also to describe the flame motion and (diffusive) extinction following complete droplet vaporization. Work is in progress to obtain flame diameters at extinction in this regime, as accurately as possible, from the DCE data, for comparison with future theoretical predictions; theories for this final stage of droplet combustion, after droplet disappearance, have not yet been worked out. It may again be felt that this boundary may be vertical, independent of initial droplet diameter, in the absence of ignition-energy overdrive, and possibly heptane kinetics are robust enough that with diffusive extinction the droplet always disappears in these atmospheres, that is, the two sets of boundaries indicated in figure 1 effectively coincide. Continuing improvement in accuracies of both data reduction and theoretical prediction are needed to resolve these questions.

Flame Histories in Droplet Combustion at Small Stoichiometric Air-Fuel Ratios

In droplet burning, for small ratios ε of gas to liquid density there are two different regions of the gas-phase flow [4], an inner region in which, after a short initial stage and prior to a short final stage, the flow and scalar fields are quasisteady, and an outer region in which they are perpetually time-dependent (transient). The flame may be in either of these regions; at sufficiently large values of the stoichiometric air-fuel ratio s it is in the quasisteady region and at sufficiently small values in the transient region. Although for small s flame-history analyses that account for the initial and final stages predict qualitatively similar Burke-Schumann flame-surface histories for flames in the quasisteady and transient regions, it could be helpful to have flame-history results (as yet unavailable) that are uniformly valid in s for small ε. With the flame in the quasisteady region, to leading order in ε, unless flame extinction occurs in the initial stage, radiative extinction is impossible; the continual decrease in quasisteady flame diameter with decreasing droplet diameter reduces the possibility of radiative extinction and increases the tendency towards diffusive extinction. Most existing analyses of flame extinction in droplet combustion are quasisteady and predict the droplet diameter at (diffusive) flame extinction, the extinction diameter. Since much of the DCE data sits well into the regime of radiative extinction in figure 1, flame-history and extinction analyses were performed for the flame in the transient region [3]. Previous asymptotic analyses [4] of this case had addressed only conditions under which temperature changes are small in the transient region, so that extensions to account for the large experimental temperature variations in the outer zone were needed. Those extensions turn out [3] to convert the transient-diffusive character of the outer zone into a transient-convective-diffusive character, that is, convection no longer is everywhere negligible in the outer region at leading order. This complication forces use of numerical solution of partial differential equations in the outer zone, a program that was completed so that accurate comparisons could be made with results of DCE measurements.

Representative results [3] for nondimensional flame-location histories $X_f(\tau)$ in the Burke-Schumann limit are shown in figures 2 and 3 and are discussed, along with many other results, in the publication [3]. Figure 4 is a preliminary comparison of the predicted flame history with DCE data for a droplet initially 3 mm in diameter, burning in air. The data have been smoothed, and not shown is the initial rapid growth in flame diameter, probably associated with flame propagation from a fuel-rich ignition point, not addressed in the theory. Immediately evident is that initially the flame diameter is larger than predicted. The flame diameter appears to approach the theoretical prediction with increasing time. This behavior can be attributed to the initial conditions imposed. It was assumed that the ignition impulse was applied only in the inner zone near the droplet, excess energy was excluded from this zone, and the initial conditions for the outer-zone analysis were taken to be those of the ambient, unheated atmosphere [3]. Although this choice is helpful, in that it produces predictions independent of the initial ignition impulse, it clearly leads to an underestimate of the experimental flame diameter during a significant portion of the flame history, for the experiments that have been performed. It is straightforward to perform the integration with a different selection of initial conditions, accounting for excess energy delivered by the igniter. It would be of interest to complete such calculations and then to make further comparisons with the experimental results of figure 4. Extinction, which occurs at the end of the experimental curve in figure 4, also was addressed in the theory [3].

CONCLUSIONS

Much more theoretical work is needed on flame histories in droplet combustion if full understanding and quantitative prediction of experimental results such as those of FSDC and DCE are to be obtained. There are a number of qualitative agreements between prediction and observation, such as flame extinction subsequent to achievement of maximum flame diameter and the prevalence of non-quasisteady flame-diameter histories. There are, however, entire regimes in which no theory yet exists, such as the regime of flame extinction after droplet disappearance. It may be concluded that many outstanding research opportunities remain in this subject.

ACKNOWLEDGMENT

Among many who deserve thanks is Malissa Ackerman, a UCSD graduate student whose research includes this data reduction and interpretation.

REFERENCES

1. Dietrich, D.L., Haggard, J.B., Jr., Dryer, F.L., Nayagam, V., Shaw, B.D., and Williams, F.A., "Droplet Combustion Experiments in Spacelab," *Twenty-Sixth Symposium (International) on Combustion*, The Combustion Institute, Pittsburgh, PA, 1996, pp. 1201-1207.
2. Nayagam, V., Haggard, J.B., Jr., Colantonio, R.O., Marchese, A.J., Dryer, F.L., Zhang, B.L., and Williams, F.A., "Microgravity N-Heptane Droplet Combustion in Oxygen-Helium Mixtures at Atmospheric Pressure", *AIAA Journal*, Vol. 26, 1998, pp. 1369-1378.
3. Fachini, F.F., Liñán, A. and Williams, F.A., "Theory of Flame Histories in Droplet Combustion at Small Stoichiometric Air-Fuel Ratios," AIAA Paper No. 99-0586, *AIAA Journal*, to appear, 1998.
4. Crespo, A. and Liñán, A., "Unsteady Effects in Droplet Evaporation and Combustion," *Combustion Science and Technology*, Vol. 11, 1975, pp. 9-18.

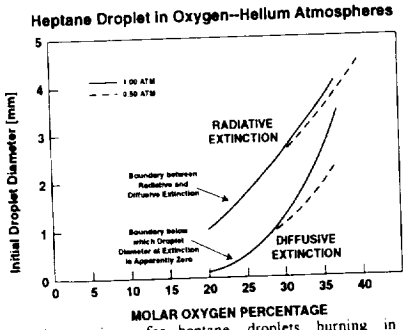

Figure 1: Combustion regimes for heptane droplets burning in oxygen-helium atmospheres, in a plane of oxygen mole percentage and initial droplet diameter, inferred from DCE results

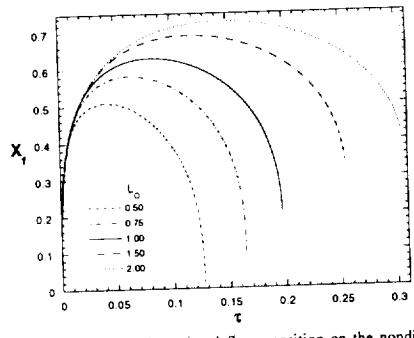

Figure 2: Dependence of the nondimensional flame position on the nondimensional time for different values of the oxidizer Lewis number, without radiation and with a fuel Lewis number of unity, for a representative stoichiometry and heat release

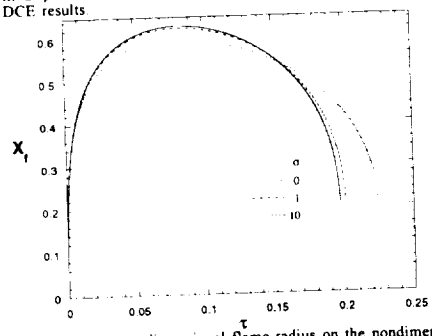

Figure 3: Dependence of the nondimensional flame radius on the nondimensional time τ for different values of the ratio σ of radiative to conductive energy flux, with Lewis numbers unity and a representative stoichiometry and heat release, in the Burke-Schumann limit

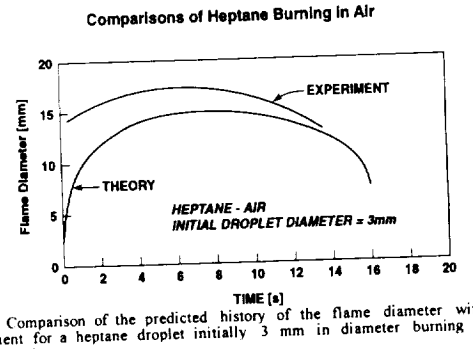

Figure 4: Comparison of the predicted history of the flame diameter with a DCE measurement for a heptane droplet initially 3 mm in diameter burning in normal atmospheric air

HETEROGENEOUS COMBUSTION OF POROUS GRAPHITE PARTICLES IN NORMAL AND MICROGRAVITY [1]

Harsha Chelliah,[†] Fletcher Miller,[‡] David Pantano, [†] and Aslan Kasimov[†]
[†]Mechanical and Aerospace Engineering, University of Virginia, Charlottesville, VA 22903
[‡] National Center for Microgravity Research, MS 110-3, Cleveland, OH 44135-3191

OBJECTIVES: Combustion of solid fuel particles has many important applications, including power generation and space propulsion systems. The current models available for describing the combustion process of these particles, especially porous solid particles, include various simplifying approximations. One of the most limiting approximations is the lumping of the physical properties of the porous fuel with the heterogeneous chemical reaction rate constants [1]. The primary objective of the present work is to develop a rigorous model that could decouple such physical and chemical effects from the global heterogeneous reaction rates. For the purpose of validating this model, experiments with porous graphite particles of varying sizes and porosity are being performed at NASA Lewis Research Center. The details of this experimental and theoretical model development effort are described below.

EXPERIMENTAL APPROACH: As reported in the last Microgravity Workshop [2], experimental work on this project is focused on particle deployment, ignition, and obtaining regression rate and surface temperature data for 200-2000 μm graphite particles burning in normal and microgravity. Four types of porous particles were used; glassy carbons with two porosities, experimental carbons, and spherocarbs.

(i) Particle Deployment: Considerable effort was expended on trying to meet the challenge of keeping the particle in the camera field-of-view (FOV) during oxidation. Initially it was thought that mounting the particles on small fibers would accomplish this, similar to droplets, but this proved exceedingly difficult. Although 12.5 μm holes could be drilled into the 200 μm particles, allowing them to be glued to SiC fibers, the glue melted upon heating and the particles fell off. It was hoped that in microgravity the particles, if they left the fiber end, would float in place, but instead the vaporizing glue acted like a small jet and propelled them out of the camera FOV. Due to these problems, and others associated with particle ignition, the drop experiments were temporarily suspended and 1g tests were undertaken. After trying several concepts, we finally settled on merely placing the particles on the top of a small, stainless steel tube 800 μm OD and 300 μm ID to support them during oxidation. While the physical presence of the tube negatively effects the heat losses and the formation of the flame, this technique allows for quick repetition of tests.

(ii) Ignition: For one type of particle tested, the spherocarbs, a hot wire could successfully be used to ignite the particles. However, the spherocarbs could only be used in microgravity since they were too small to perch atop the 300 μm ID support tube used in 1g. To ignite and sustain combustion of other particles in 1g, we used a 5W CO2 laser. The laser was focussed to a spot of about 200 μm and the beam shape was measured with a beam profiler; it was approximately Gaussian. The total beam power was also measured. It was found that the laser had to remain on during the entire period of combustion or the oxidation would cease.

[1]Work funded under NASA Grant NAG3-1928

(iii) Regression Rate Measurements: Upon imaging the combusting particles it was found that they were self-luminous to a degree that they could be seen in the camera directly, rather than requiring a backlight to image their silhouettes. A Cohu monochrome camera with an Optem microscope lens, together with a VCR was used to record the particle size and shape during oxidation. The initial particle shape was almost spherical, but when it got small part of it began to sink into the support tube and changed its shape. Since the particle appeared as a bright object against a dark background, image processing software was used on the digitized images to calculate the particle projected area, from which the equivalent diameter was determined.

(iv) Surface Temperature Measurements: The particle surface temperature during oxidation was obtained by recording the spectral emission from the particle with an Ocean Optics S2000 Spectrometer in the range from 767 to 937 nm and fitting the resulting intensity vs. wavelength data to a blackbody curve to obtain the temperature. Note that this method requires only that the particle emissivity be constant over the spectral region measured, but not necessarily unity. From the curve fits, it appears that this condition is fulfilled. To obtain the spectrometer sensitivity function, we measured a calibrated blackbody source at 1000°C.

(v) Experimental Results: All of the results presented here are for normal gravity tests using the CO2 laser as the ignition and heat source. Two main sets of tests were conducted. In one, the laser power was held constant and the particle type was varied; in the other a single particle type was chosen and the laser power was changed. The particle temperature and regression rate were measured in both cases. Figure 1 shows some selected data for the normalized equivalent diameter square vs. time for large glassy spheres with a porosity of 37.2% being heated and oxidized at various laser power levels. Except at the lowest power level, a linear decrease in D^2 is observed, from which a constant surface regression rate could be calculated. Figure 2 shows the variation of measured particle temperature vs. time for conditions identical to those in Fig. 1. For the same laser power, different particle temperatures were achieved if the initial particle sizes were somewhat different within the same particle group. Smaller particles get hotter since the power input remains the same, but the surface area for convective and radiative losses decreases. Thus, different tests with particles of the same group and the same laser power level have indicated a noticeable spread in the oxidation rate data because of temperature variations from test to test. Figure 3 presents a graph for three types of graphite particle at a single power level. For the two types of glassy spheres, no conclusive difference in oxidation rate can be seen. However, for the experimental carbon (porosity = 75%), the oxidation rate is much higher. It is not known at this time if that is due to increased porosity, or due to the smaller initial particle sizes.

NUMERICAL APPROACH: Mitchell et al. [3] and Chelliah [4] have previously reported numerical models that can predict the burning rate of graphite particles, subject to the assumptions of spherical symmetry and quasi-steady surface regression. Dryer and co-workers [5,6] have relaxed the latter approximation and investigated the effects of unsteady combustion. In all these studies, the internal and external heterogeneous reactions have been lumped as a set of *ad hoc* semi-global reactions occurring at the external surface of the particle. For quasi-steady combustion conditions, a method of decoupling the physical effects associated with the particle porosity from the intrinsic heterogeneous chemistry was described by Kasimov and

Chelliah [7], however, here only the details of *unsteady* solid particle combustion model that is being developed is presented. The final goal is to couple the internal pore combustion model [7] with the unsteady combustion model described here.

(i) Formulation: Under the assumption of spherical symmetry and isobaric condition, the system of partial differential equations for conservation of mass, species and energy as a function of time and radial coordinate is well known. However, the interface conditions employed in various articles are not consistent with the approximations introduced. For example, for a non-porous particle with internal temperature variations, the general interface condition for energy is given by

$$(-\lambda \partial T/\partial r)_- = (-\lambda \partial T/\partial r)_+ - \sum h_k s_k + \sigma\epsilon(T_s^4 - T_\infty^4), \tag{1}$$

where the subscript (-) identifies conditions within the solid phase and (+) in the gas phase. In the conduction limit, i.e. $\lambda_- \gg \lambda_+$, although the temperature within the particle is uniform, transient effects associated with particle heating can introduce significant errors to the particle ignition process. Under such conditions, the above interface condition must be modified appropriately. To simplify the integration of this moving boundary problem, a coordinate system attached to the interface and described by the transformation $x = r - r_s(t)$, $\tau = t$ is employed. Under this transformation, a grid reconstruction may be necessary after significant changes in particle radius, however, no singularities arise as the particle radius approach zero.

(ii) Numerical Algorithm: The method employed to integrate the above system of equations is a time-splitting algorithm, in which the transport processes are treated separately from the chemical reactions. On the first half of the time step the governing equations are integrated without chemical reactions, while on the second half the chemical reactions are calculated using Gear's BDF method with no transport. The integration of the convection-diffusion terms is performed using an implicit mass-operator Crank-Nicholson scheme.

(iii) Numerical Predictions: Unlike the previous quasi-steady calculations [4], the present fully unsteady code allows for simulating the particle heating, ignition and oxidation phenomena. Figure 4 shows the onset of the detached flame front for a 900 μm diameter particle in an quiescent environment containing moist air at 1400K. The initial gas-phase composition is assumed to contain only O_2, N_2 and H_2O. The code developed is currently being extended to the experimental conditions described above with external heat flux with the CO_2 laser. The major uncertainty here is the heat loss to the support tube.

REFERENCES:

[1] Laurendeau, N.M., *Prog. Energy Comb. Sci.* **4**:221 (1978).
[2] Chelliah, H.K. and Miller, F.J., *Fourth Int. Microgravity Combustion Workshop*, Cleveland, OH, May 1997
[3] Mitchell, R.E., Kee, R.J., Glarborg, P., and Coltrin, M.E., *Twenty-third Symposium (International) on Combustion*, The Combustion Institute, p.1169 (1991).
[4] Chelliah, H.K., *Comb. and Flame* **104**:81-94 (1996).
[5] Cho, S.Y., Yetter, R. and Dryer, F.L., *J. Comp. Phys.* **102**:160, 1992.
[6] Lee, J.C., Yetter, R.A., and Dryer, F.L., *Comb. and Flame* **101**:387-398 (1995).
[7] Kasimov, A. and Chelliah, H.K., *Eastern States Section Meeting of the Combustion Institute*, Hartford, CT, November 1997.

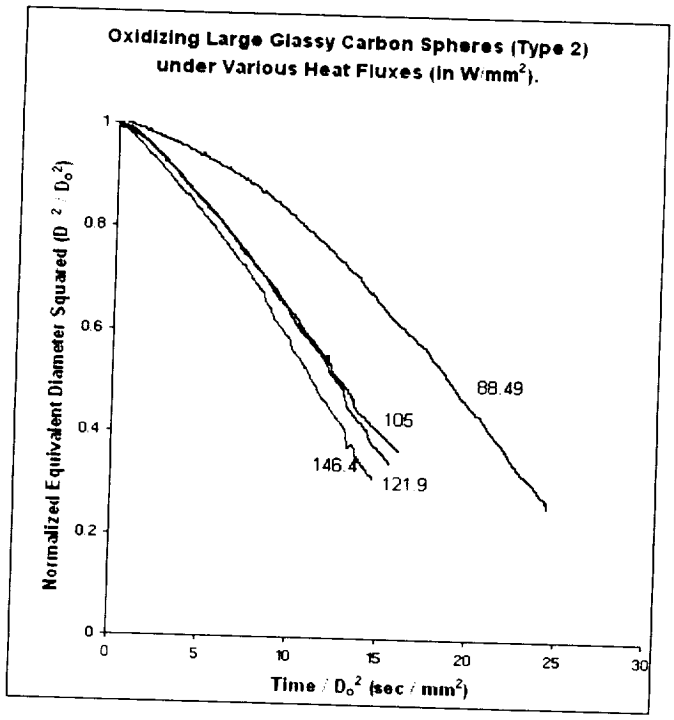

Figure 1: Measured normalized equivalent diameter square vs. time, for glassy carbon spheres under several heat flux rates from a CO_2 laser.

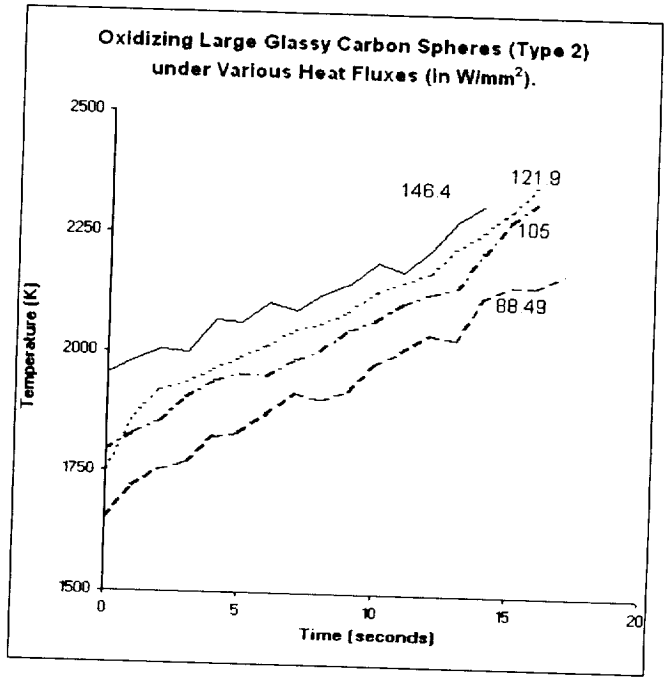

Figure 2: Measured surface temperature variations vs. time, for a glassy carbon spheres under several heat flux rates from a CO_2 laser.

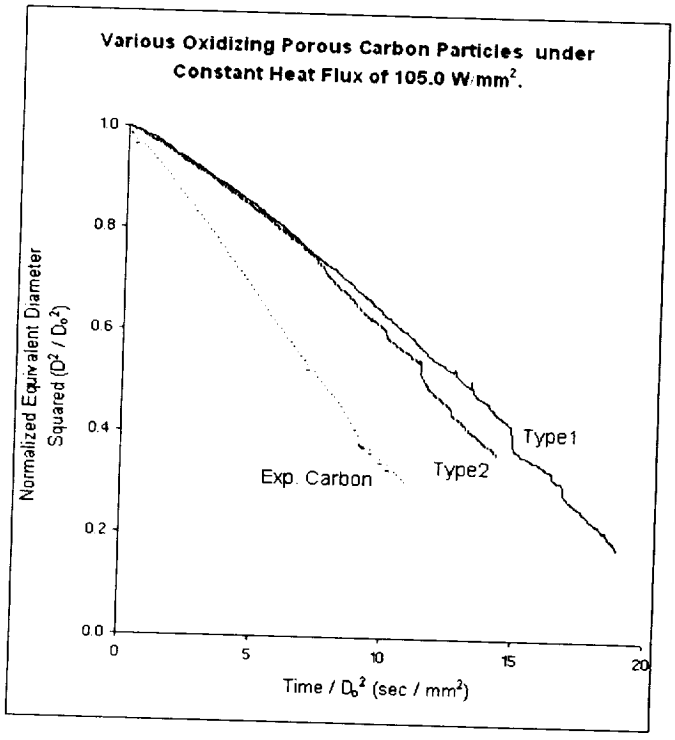

Figure 3: Measured normalized equivalent diameter square vs. time, for different graphite spheres with the same heat flux rates from a CO_2 laser.

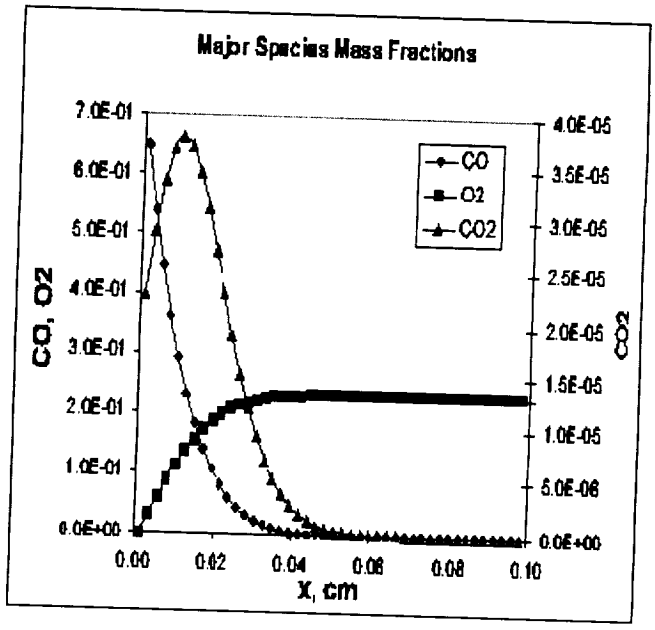

Figure 4: Predicted gas-phase flame structure after 5.0 msec, for a 900 μm particle in moist air at 1400 K.

COMBUSTION OF TWO-COMPONENT MISCIBLE DROPLETS IN REDUCED GRAVITY

B. D. Shaw, MAE Department, University of California, Davis, CA 95616

INTRODUCTION

This paper presents recent theoretical and experimental results from an ongoing research program that deals with reduced-gravity combustion of bi-component droplets initially in the mm size range or larger. The primary objectives of the research are to study the effects of droplet internal flows, thermal and solutal Marangoni stresses, and species volatility differences on liquid species transport and overall combustion phenomena (e.g., gas-phase unsteadiness, burning rates, sooting, radiation, and extinction). The research program utilizes a reduced-gravity environment so that buoyancy effects are rendered negligible. Use of large droplets also facilitates visualization of droplet internal flows, which is important to this research.

This program is a continuation of extensive ground based experimental and theoretical research on bi-component droplet combustion which has been ongoing for several years. The focal point of this research program is a flight experiment (Bi-Component Droplet Combustion Experiment, BCDCE). This flight experiment is still under development. However, supporting ground studies have been performed, and preliminary data have been obtained from flight experiments (Fiber Supported Droplet Combustion Experiment, FSDC-1 and FSDC-2). These flight experiments were performed during the STS-73/USML-2 and STS-94/MSL-1 missions.

In the experiments, droplets composed of low- and high-volatility species are burned. The low-volatility components are initially present in small amounts. As combustion of a droplet proceeds, the liquid surface mass fraction of the low-volatility component will increase with time, resulting in a sudden and temporary decrease in droplet burning rates as the droplet rapidly heats to temperatures close to the boiling point of the low-volatility component. This decrease in burning rates causes a sudden and temporary contraction of the flame. The decrease in burning rates and the flame contraction can be observed experimentally. Measurements of burning rates as well as the onset time for flame contraction allow effective liquid-phase species diffusivities to be calculated, e.g., using asymptotic theory [1]. A goal of the research is to relate effective liquid species diffusivities to droplet internal flow characteristics. Droplet internal flows will be visualized in future flight and ground-based experiments.

FSDC-2 FLIGHT EXPERIMENT RESULTS

Experimental results for the combustion characteristics of fiber-supported liquid droplets in ambient Shuttle cabin air were obtained from the Glove Box Facility aboard the STS-94/MSL-1 mission using the FSDC-2 apparatus. Each test occurred in an ambient of Spacelab air. The FSDC-2 experiments complement previous FSDC-1 experiments [2] that were performed during the STS-73/USML-2 flight in 1995. The FSDC-2 experiments utilized different initial droplet compositions than FSDC-1, and also employed radiometers to measure radiant fluxes from the flame zone as a function of burning time. One radiometer (denoted as Radiometer 1) was used to detect radiant fluxes in the wavelength range 0.6 - 40 microns. The other radiometer (denoted as Radiometer 2) was used to detect radiant fluxes in the wavelength range 5.1 - 7.5 microns. Results from the FSDC-2 experiments have been submitted for publication [3].

Twenty-two droplets were deployed, ignited and burned in the FSDC-2 heptane-hexadecane experiments, with 11 droplets having an initial hexadecane mass fraction Y = 0.05 and the remainder Y = 0.2. Initial droplet sizes ranged from about 1.8 mm to about 6 mm. In both the

FSDC-1 and FSDC-2 experiments, flames were detected by the video cameras only for times shortly after ignition, after which the flame luminosity was too low to record. Even glowing of the support fiber was typically not evident in the video images after the initial ignition transients. These factors suggest that flame temperatures were very low for the mixture fractions and droplet sizes studied. Burning rates were observed to decrease as droplets became larger, with the largest droplet exhibiting burning-rate constants roughly 30 % lower than smaller droplets.

The initially larger droplets extinguished at large diameters (a few mm), while smaller droplets could burn to very small sizes. Figure 1 shows the square of the droplet diameter (d) and radiometer data as a function of burning time for a droplet (Y = 0.05) initially about 4.9 mm in diameter. The radiometer data in Fig. 1 show increases after the igniter was turned on, with very sharp increases after droplet ignition. Following ignition, the radiant heat fluxes slowly grow, and then rapidly decrease to low but nonzero values about 7 s after ignition. These decreases in radiometer outputs appeared to coincide with decreases in radiation from soot particles, i.e., soot particles were observed to stop glowing about 7 s after ignition. This droplet continued to burn until about 48 s after ignition. Following this, radiometer outputs rapidly decreased to small values, indicating the flame extinguished.

The d^2-t data in Fig. 1 are essentially linear until a plateau occurs about 48 s after ignition. This plateau occurs at about the time that a flame contraction was expected, indicating that the flame contraction induced extinction, as evidenced by the radiometer data. The burning-rate constant prior to the flame contraction is about 0.41 mm^2/s. This value, in conjunction with asymptotic theory [1] yields the effective liquid-phase species diffusivity $D \approx 12 \times 10^{-9}$ m^2/s.

SOOTING OF HEPTANE AND HEPTANE/HEXADECANE DROPLETS

Laser attenuation methods were used [4] to gain information on average soot volume fractions around heptane/hexadecane droplets (which displayed flame contractions) and heptane droplets (which did not exhibit flame contractions). The experiments made use of a drop rig that was constructed as part of earlier studies [1]. The experiments were performed at the NASA Lewis Research Center 2.2 Sec Drop Tower. A beam from a diode laser was directed across the flame zones of heptane and heptane/hexadecane droplets burning in reduced gravity. Measurements of beam intensities provided information on average soot volume fractions (f_{ave}) between droplets and flames. In the experiments, laser beams passed close to droplet surfaces such that the beams passed through most of the flame zone and through soot shells that were present. The laser beam diameter was about 0.7 mm, and droplets were initially about 1 mm in size.

It was found that flame contractions influenced soot fields significantly. Representative data are shown in Fig. 2, where it is shown that f_{ave} is in the 0.1 – 1 ppm range. In order to estimate peak soot volume fractions from the present data, the effective path length to be used in calculating f_{ave} should be a representative thickness of the soot shell. Based upon visual observations of soot shells from the present film records, as well as data from Ref. [5], it is evident that an effective path length for laser attenuation is roughly 1/10 to 1/2 of the droplet diameter. Using effective path lengths of this magnitude provides estimates for peak soot volume fractions as being in the range 10 - 50 ppm, which is in reasonable agreement with Ref. [5].

EFFECTS OF SUPPORT FIBERS ON DROPLET SHAPES

This research presents asymptotic analyses and experimental results on how droplet shapes are influenced by support fibers that extend through droplets. Previous researchers have analyzed

how shapes of droplets are affected by support fibers, yielding exact results that are difficult to interpret physically [6]. Computational analyses of effects of fibers on droplet shapes have also been presented [7].

This present work provides asymptotic analyses that illustrate major features of interest. It is assumed that droplet shapes are dominated by surface tension and that droplets are symmetric about the fiber. Asymptotic analyses are performed assuming that support fibers are thin relative to droplet dimensions normal to the fibers, which corresponds to typical droplet combustion experiments. The following asymptotic solution, which is uniformly valid, is obtained [8].

$$w \approx (1 - z^2)^{1/2} + \varepsilon \, \mathrm{Cos}\theta \, \ln[2 \, (1 + (1 - z^2)^{1/2}) \, / \, (z + (z^2 - \varepsilon^2 \mathrm{Cos}^2\theta)^{1/2})] \qquad (1)$$

In. Eq. (1), ε is the ratio of the fiber radius to the maximum droplet radius normal to the fiber, and θ is the contact angle between the droplet and the fiber. The variables w and z are shown in Fig. 3. (w and z are made dimensionless using the maximum droplet radius normal to the fiber), where experimental data are presented on the normalized shape of a fiber-supported droplet burning in reduced gravity. Also shown are plots of Eq. (1) and, for comparison, the outline of a circle. Figure 3 shows that Eq. (1) provides a good description of the droplet outline and that droplets are spherical away from the fiber, with deviations from a spherical shape near the fiber.

FUTURE PLANS

More flight experiments are planned with the FSDC apparatus. These experiments, which are termed FSDC-3, will investigate decane-hexadecane droplets and will also make use of a thermocouple rake. Development of the BCDCE flight experiment will continue.

Future ground-based research will include drop tower experiments on reduced-gravity combustion of bi-component droplets initially about 0.8 - 1 mm in diameter. Experiments at UC Davis will include measuring local droplet interior compositions using absorption spectroscopy. Theoretical and computational studies will include development of a 2-dim computational model of fiber-supported droplet combustion, as well as development of theory to predict effects of solutalcapillary stresses on droplet interior flows.

ACKNOWLEDGEMENTS

The financial support of NASA is gratefully acknowledged. Drs. V. Nayagam and D. Dietrich are acknowledged for providing project supervision and technical support. Special thanks are extended to the MSL-1 crewmembers, in particular to R. Crouch and D. Thomas, who conducted the FSDC-2 experiments. Thanks are expressed to the many individuals at the Payload Operation Control Center, Marshall Spaceflight Center. Without the dedicated efforts of the Engineering Team at the NASA Lewis Research Center, particularly S. Motil, the FSDC-2 experiments would not have been possible. The contributions of B. Clark and J. Rankin to data reduction and analysis efforts are gratefully acknowledged. Drs. M. King and H. Ross provided valuable suggestions and support during the MSL-1 mission. Thanks are expressed to the FSDC-2 Science Team (Dr. R. Colantonio, Dr. D. L. Dietrich, Prof. F. L. Dryer, J. B. Haggard, Jr., Dr. V. Nayagam, and Prof. F. A. Williams) for valuable discussions.

REFERENCES

1. Aharon, I. and Shaw, B. D., *Combust. Flame* **113**, 507 (1998).
2. Dietrich, D. L., Haggard, J. B., Jr., Dryer, F. L., Nayagam, V., Shaw, B. D., and Williams, F. A., *26th Symp. (Int'l.) on Comb.*, p. 1201 (1996).

3. Shaw, B. D., and Clark, B. D., *AIAA J.* (submitted).
4. Chen, A. G., and Shaw, B. D., *Comb. Sci. Tech.* (accepted).
5. Choi, M. Y. and Lee, K.- O., *26th Symp. (Int'l.) on Comb.*, p. 789 (1996).
6. Carroll, B. J., *J. Coll. Int. Sci.***57**, 488 (1976).
7. Struk, P. M., Ackerman, M., Nayagam, V., and Dietrich D. L., *Micro. Sci. Tech.* (accepted).
8. Shaw, B. D. *SIAM J. Appl. Math.* (in preparation).

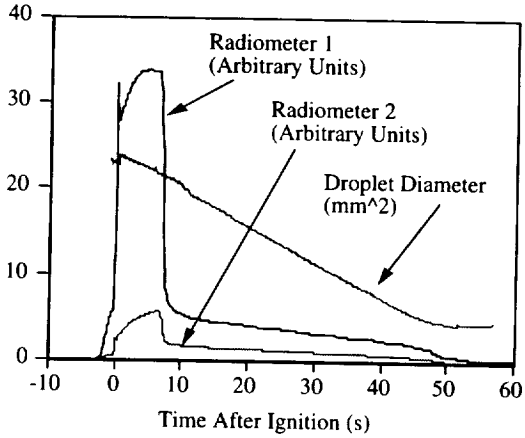

Figure 1. FSDC-2 data (Y = 0.05).

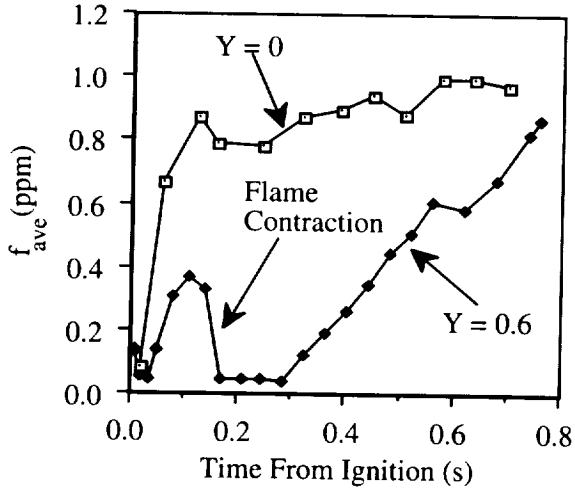

Figure 2 Average soot volume fractions for heptane (Y = 0) and heptane/hexadecane (Y = 0.6) droplets.

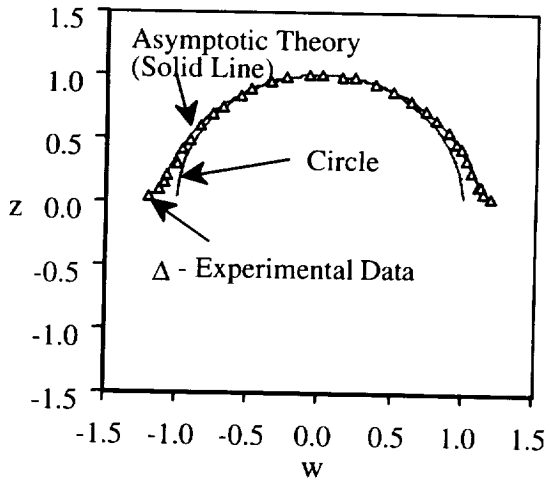

Figure 3. Normalized droplet outline data, asymptotic theory, and a circle.

Experiments and Model Development for the Investigation of Sooting and Radiation Effects in Microgravity Droplet Combustion

Samuel L. Manzello, Ming Hua and MUN Y. CHOI
Department of Mechanical Engineering
University of Illinois at Chicago, Chicago, IL 60607

Frederick L. Dryer
Mechanical and Aerospace Engineering
Princeton University, Princeton, NJ 08544

Introduction

Combustion of fossil fuels represents a significant portion of the energy consumption in the world. For example, in 1997, the equivalent of 1,800 million tons of oil was consumed in the United States. This staggering number, which represents 25% of the total world consumption, illustrates the need not only for conservation, but for promoting efficiency in required uses. Another consideration of equal importance is the impact of combustion on the environment. Most practical energy conversion processes involve introduction of liquid fuels into an oxidizing environment in the form of sprays that are comprised of droplets burning in isolation or in groups. Empirical engineering approaches to advancing combustion system design must be computationally assisted if we are to make significant improvements while meeting more demanding emissions constraints in the future. However, theoretical/computationaldevelopments and experimental validation of spray combustion remains a daunting task due to the complex coupling of a turbulent, two-phase flow with phase change and chemical reactions. Individual droplet behavior (including ignition, evaporation and combustion) has long been recognized as an important component for developing a better understanding of the more complex spray combustion processes [Faeth, 1977; Williams, 1981; Law, 1982; Law and Faeth, 1994]. Since the early 1950's, the burning of an isolated droplet has been theoretically analyzed in a spherically-symmetric configuration involving coupling of chemical reactions and two-phase flow with phase change. Since then, the simple 'd^2-law' analysis using an infinite reaction rate producing a thin flame has been superceded by fully-transient computational models that describe the evolution of 50 chemical species using nearly 300 reversible reactions in the gas-phase and detailed transport coupling in the liquid-phase. This level of description is required since new generations of time-dependent computational tools must embody compact, but realistic sub-models that accurately represent the properties and coupling of fluid dynamics, diffusive processes, heat transfer, and combustion. New computational tools based upon direct numerical simulation and other methods hold promise for modeling multi-dimensional reacting systems. Computational resource limitations and a desire to perform parametric calculations require that these tools utilize reduced representations of parameters including degree of asymmetry and the scope of the description of chemical kinetics and other sub-model components. Unidimensional, time-dependent, laminar, non-premixed combustion problems are critical to developing, testing, validating and systematically reducing sub-models to produce descriptions that can be used in more applied computations.

Objectives of Study

The scientific objectives of this effort are to elucidate the unresolved issues related to sooting

and accompanying radiation effects in the simple, spherically-symmetric configuration of isolated droplet burning in microgravity. Spherically-symmetric droplet combustion is an ideal, uni-dimensional configuration for advancing understanding of diffusion flames in general and those involving soot in particular, especially for hydrocarbon fuels that are typical of those used in internal combustion engines and gas turbines. Based on recent observations in microgravity experiments performed in support of the current effort, it appears that the formation and lingering presence of soot within the fuel-rich region of isolated droplets can modify the burning rate, flame structure and extinction. The study of the burning characteristics of larger liquid droplets in microgravity, combined with spherically-symmetric numerical modeling provide opportunities to advance our understanding of the fundamentals of transient diffusion flames, as well as to test and validate the chemical kinetic, transport, sooting and radiation sub-models for a realistic system. Refinements of these models through comparison against well-characterized experiments can yield new and important understanding as well as sub-models which can be further simplified for implementation in more complex geometries. The specific objectives of our work include:

- Determine the influence of sooting and radiation on the droplet burning rate. Investigate the influence of initial droplet diameter on sooting behavior in droplet combustion configuration for a wide range of conditions;
- Define the influence of sooting and radiation on flame dynamics and structure;
- Further elucidate through both experiments and modeling the mechanisms through which sooting affects the extinction of droplet flames;
- Develop and validate numerical models (inclusive of sooting and radiation effects) using accurate and reliable experimental measurements. The numerical model will serve not only as a useful predictive and analytical tool, but as a skeletal model against which simplifications of various sub-models can be evaluated;
- Determine the effects of parameter adjustments (pressure, oxygen, inert, etc.) on sooting and burning behavior;
- Study the influence of flame residence time on the morphology of soot.

Microgravity droplet combustion is an ideal platform for advancing our understanding of the influence of sooting and radiation on combustion behavior. Isolated droplet combustion in microgravity provides the flexibility to vary the residence time over a wide range (residence time is an important and desirable parameter adjustment for studying soot processes) by changing the droplet size and/or environmental parameters (pressure, inert, oxygen index). Chemical composition, temperature, convection, soot particle drag, diffusion and thermophoresis are all radially oriented. Because of the geometric simplicity, particle temperature and spatial history are well defined, and robust models of each of the processes can be developed in great detail without overwhelming computational resources.

The effort that is just beginning will be comprised of three equally-important components: ground-based experiments (for 1 to 2 mm droplets); flight experiments (for 2 to 5 mm droplets) and model development and validation. We plan to continue earlier successful ground-based experiments at the NASA 2.2 sec and 5.2 sec facilities and pursue collaborative work with Professor T. Hirano at the 10 sec. JAMIC dropshaft. The ground-based studies can be used to provide important data for smaller droplets (2.0 mm in diameter or less). Larger initial droplet size studies improve the spatial resolution of measurement techniques. Experiments using large droplets are also required to

explain unexpected behaviors observed in recent isolated droplet studies conducted during the MSL-1 mission aboard the Shuttle (STS-83, STS-94). Contrary to more generally offered hypotheses, experiments using n-heptane droplets burning in air showed that sooting does not monotonically increase with initial droplet size, but eventually is reduced for larger droplets [Dryer et al., 1998]. The principal reason for the reduced sooting appears to be increasing radiative heat loss from the diffusion flame with increased initial droplet size, eventually leading to flame temperatures too low to induce sooting. These experiments identify the important potential for using large droplet experiments to determine secondary sooting threshold conditions. Extending microgravity combustion times (up to 50 seconds) beyond the capabilities of ground-based facilities is required to fully investigate the influence of sooting/radiation on droplet combustion, including extinction.

Experimental Approach

The proposed experiments will consider two fuels: n-heptane, and ethanol. N-heptane has received considerable attention in ground-based experiments and was recently flown on STS-83 and 94 as a fuel for both DCE and FSDC-2 (Fiber Supported Droplet Combustion) experiments. N-heptane is the simplest of liquid alkanes with properties similar to those found for conventional liquid fuels such as gasoline and distillates. Ethanol has been initially studied in both droptowers and in FSDC-2 experiments. Although the sooting tendency for n-heptane is greater than that for ethanol, both fuels are considered to be mildly sooting. Furthermore, the magnitude of sooting can be controlled over a wide range by varying inert, droplet size, oxygen concentration and pressure.

Soot volume fraction will be measured using full-field light extinction at 635 nm. In this method, line of sight extinction measurements are deconvoluted using tomographic inversion [Dasch, 1992]. Soot temperature will be measured using line of sight flame emission data at two separate wavelengths (700 nm and 900 nm) with subsequent tomographic inversion. The ratio of the spectral emission intensity at each radial position will then be used for the application of two-wavelength pyrometry. This technique is similar to that used successfully in Laminar Soot Processes (LSP) space-shuttle experiments. As in the LSP experiments, it is expected that due to the small soot particle sizes, the difference between the gas-temperature and the soot temperature will be small as reported by Köylü and Faeth [1993]. Radiation from the flame will be measured using a broadband radiometer (detection spectrum ranging from 1 to 50 microns). Soot aggregates will be sampled using a thermophoretic technique and analyzed using transmission electron microscopy.

Ultraviolet emission due to hydroxyl radical chemiluminescence (and the interference from soot emission) occurring within the flame is to be imaged using a Xybion intensified array CCD camera with a narrowband filter with central wavelength of 310 nm and a FWHM of 10 nm. This approach yields the instantaneous location of maximum OH^* emission which, in conjunction with detailed numerical modeling will be used to define the transient flame structure.

Modeling Approach

At present, fully-transient droplet combustion models that incorporate detailed gas-phase chemical kinetics and sooting/radiation mechanisms are lacking. However, 2-D axi-symmetric [Kaplan et al., 1994] and spherically-symmetric [Ezekoye and Zhang, 1997] gaseous diffusion flames produced in microgravity have been modeled using semi-empirical soot mechanisms including inception, growth, agglomeration and oxidation. In these formulations, the source terms for the soot number density and soot mass fractions are dependent on the C_2H_2 concentration. The prediction of Ezekoye and Zhang [1997] for bulk properties (such as soot mass and mass averaged soot

temperature) provided favorable agreement with measurements performed in microgravity using an acetylene diffusion flame supported on a large porous sphere. Similar sub-models to describe the formation, oxidation, and radiation of soot will be incorporated into the Princeton Droplet Combustion Model [Marchese and Dryer, 1997; 1999]. This fully-transient model considers detailed, multi-component molecular transport and a complex chemical kinetic mechanism to solve the gas phase energy (including gas-phase radiative transport) and species equations. In addition, the conservation of energy and species are solved within the droplet interior. The gas phase chemical kinetics for n-heptane experiments will be developed as an extension of the semi-empirical mechanism of Held et al. [1997] used in prior studies. A comprehensive mechanism for ethanol experiments will be based on modifications of the works of Norton and Dryer [1992] and Marinov [1999].

Progress Since Award

- The 2.2 sec experimental rig was completely overhauled for operation in the JAMIC 10 sec. microgravity facility.
- Eleven experiments were performed in February 1999 at the JAMIC facility to study the initial sooting behavior of large droplets. Preliminary results suggest that sooting does not monotonically increase with droplet size (as suggested by current understanding based on small droplet diameter experiments). Additional experiments are planned for the summer of 1999.

References

1. Dasch, C.J., Applied Optics, 31:1146, 1992.
2. Dryer, F.L., Nayagam, V., and Williams, F. A., The DCE on MSL-1, L+1 Meeting, Marshall Space Flight Center, Huntsville AL, August 25-26, 1998. Published in Proceedings.
3. Ezekoye, O.A., and Zhang, Z., Combustion and Flame, 110:127, 1997.
4. Faeth, G.M., Prog. Energy and Comb. Sci., 3:191, 1977.
5. Held, T.J., Marchese, A.J. and Dryer, F.L., Combust. Sci. Tech., 123:197, 1997.
6. Kaplan, C.R., Baek, S.W., Oran, E.S. and Ellzey, J.L., Combust. and Flame, 96:1, 1994.
7. Law, C.K., Prog. Energy Combust. Sci., 8:171, 1982.
8. Law, C.K., Law, H.K. and Lee, C.H., Energy, 4:329, 1979.
9. Law, C.K. and Faeth, G.M., Prog. Energy Combust. Sci, 20:65, 1994.
10. Marchese, A.J. and Dryer, F.L., Combust. Sci. Tech., 124:373, 1997.
11. Marchese, A.J., Dryer, F.L. and Colantonio, R. O., 27th Symposium (Int'l) on Combustion, The Combustion Institute, Pittsburgh, PA, p. 2627-2634, 1999.
12. Marinov, N., "A Detailed Chemical Kinetic Model for High Temperature Ethanol Oxidation", Int. J. Chem Kin., In Press, 1999.
13. Norton, T.S., and Dryer, F.L. (1992). I.J. Chem. Kin., 24, 319.
14. Williams, F.A., Droplet Burning, Combustion Experiments in Zero-Gravity Laboratory (ed. By T.H. Cochran), Vol. 73 of Progress in Astronautics and Aeronautics, AIAA, N.Y. p.31, 1981.

Acknowledgments: The authors to wish to thank Dr. Paul Ferkul, project scientist, for helpful comments and suggestions. We would like to acknowledge NASA GRC Staff including Art Birchenough, Eric Baumann, Mike Johnston, Ron Mileto, Chris Hampton and Joe Corion for their excellent work in converting our NASA rig for JAMIC operation.

EXPERIMENTAL STUDY OF NONANE AND NONANE/HEXANOL FUEL DROPLET COMBUSTION IN MICROGRAVITY

C.T. Avedisian and B.J. Callahan
Cornell University
Ithaca, New York

357-29

Introduction

In this presentation we review experiments carried out on nonane droplets, and a nonane/hexanol droplet, burning in microgravity to promote spherical symmetry. The nonane/hexanol combination was selected for the following reasons: 1) the spherically symmetric burning history of nonane and nonane/hexanol mixtures has not been previously studied; 2) measurements of the burning history of pure nonane droplets in air extend the existing data base of spherical droplet flames of soot-producing fuels which are useful for testing detailed chemical kinetic models of the spherically symmetric droplet burning process; 3) nonane and hexanol have almost identical boiling points so heterogeneous nucleation on a support fiber is unlikely; 4) hexanol does not have a strong propensity for water vapor absorption; 5) hexanol produces less soot than nonane so that mixtures of nonane and hexanol should show an effect of composition on soot formation. The far-field gas was atmospheric pressure air at room temperature. The evolution of droplet diameter was measured using high speed cine photography of spark-ignited droplets within a confined volume in a drop tower.

The importance of soot formation during droplet combustion is derived from the fact that soot is the basic component of the particulate emission process that occurs in spray combustion. The complexity of soot formation motivates a one-dimensional transport condition which is advantageous for modeling. Recent numerical studies of droplet combustion have assumed spherical symmetry when incorporating such aspects as detailed chemistry and radiation (e.g., Cho et al. 1992; Jackson and Avedisian 1996; Marchese and Dryer 1996), though soot formation itself has not yet been included in any droplet combustion modeling effort. If radiation is not important as would be the case for 'small' droplets (i.e., droplets with initial diameters less than about 1mm), soot formation can lead to a nonlinear burning process and a time-varying burning rate, (non-linear burning of a non-sooting fuel like methanol is due to water vapor absorption on the droplet (Marchese and Dryer 1996)). The classical quasi-steady droplet burning theory predicts a linear evolution of droplet diameter in scaled coordinates for any fuel type (Glassman 1987).

Experiment

Both free-floating and fiber supported droplets were studied. Unsupported droplets in microgravity were studied using a variation of a method reported in previously (Avedisian et al. 1988; Jackson et al. 1992; Jackson and Avedisian 1994, 1998; Callahan and Avedisian 1999). A fuel droplet is projected into a vertical trajectory in a chamber attached to a support package. At the apex of the droplet's trajectory, the package which houses the combustion chamber and surrounding instrumentation is released into free-fall. A short time later, the droplet is ignited by two sparks positioned on opposite sides of the droplet. The electrodes are then quickly retracted. New and more powerful electrode retraction solenoids were fabricated with non-brushing contact to improve the reliability of retraction and re-positioning of the electrodes. The burning process was recorded by a high speed cine camera. The difficulty of keeping a free-floating (unsupported) droplet stationary makes it difficult to use laser-based diagnostics for quantifying soot. However, photographic images are still quite useful for qualitatively assessing sooting tendencies. A drag shield around the support package provided a gravity level of about 10^{-4} that of the Earth's normal gravity.

Fiber supported experiments were carried out for nonane/hexanol droplets due to the difficulty of producing a steady droplet stream for hexanol concentrations above 10%. Small silica fibers 12μm diameter were used to reduce the effect of the fiber on the burning process, which for a sooting fuel includes the effect of the fiber on the soot shell dynamics (Avedisian and Jackson 1999). Two fibers were mounted in a crossing pattern in the free-droplet apparatus. The fibers were placed at the apex of the trajectory produced by the droplet generator. Fuel was deposited on the fibers by impinging droplets produced by the generator on the crossed fibers. In this way, reliable droplet deposition on these small fibers was achieved.

The high speed movie camera was operated at 200 frames/sec. The film images were digitized on a Microtek slide scanner at 3900 dpi, then imported into an image analysis software package. The software finds the edge of the droplet by means of categorizing the pixels according to a threshold brightness. The lighting and magnification are the same for all results presented in this study. The resolution in the droplet diameter measurement was estimated to be 25μm. The backlighting was adjusted to show the translucent droplet and granular soot shell as a shadow at the expense of observing the outer luminous zone of the flame. A video camera was mounted perpendicularly to the movie camera to record the droplet position along the view axis of the movie camera. A 40W halogen light mounted outside the package back-lit the droplet in the initial stages of free fall while the video camera automatic intensity gain control remained off. In this fashion, the lighting illuminated the droplet before ignition, and the camera could view the droplet and the flame after ignition using the visible flame radiation.

Results

Nonane

Figure 1 shows photographs of a free nonane droplet and figure 2 shows a fiber supported nonane/hexanol droplet. The stretched support fibers are visible as the blurred lines on either side of the droplet in figure 2. The time after ignition is shown beneath each photo. The luminous region of the flame is barely visible in figure 2a while the photos for the nonane droplets were enlarged to show only the soot shell, and the flame is not visible in fig. 1. The soot shell is the black 'ring' structure surrounding the droplet for both the nonane droplet (fig. 1) and the nonane/hexanol mixture (fig. 2). The droplet and soot shell are spherical and reasonably concentric. The fiber supported droplet is spherical throughout nearly the entire burning history showing a minimal fiber affect on droplet shape. The fiber glows where it is contacted by the flame. Some evidence of soot accumulation on the fiber is shown in fig. 2c by the large aggregate attached to the fiber in the first quadrant. The pure nonane soot shell shows reasonable sphericity except for a 'tail' that is created by a very small convection component. This tail has been observed for other fuel types as reviewed in Avedisian (1997). No 'tail' exists fo the fiber supported nonane/hexanol droplet.

The evolution of nonane droplet diameter is shown in fig. 3 for three data sets in scaled coordinates of the classical 'd^2' law (Glassman 1987). Several points to note about fig. 3 are the following: 1) the burning histories of the three separate runs are close to each other, are very repeatable, and show the same trends; 2) the droplet diameter decreases almost from ignition and shows no effect of droplet heating; 3) the variation of droplet diameter with time is not linear; and 4) the droplets burned to completion. The solid line in fig. 3 is included to better show the non-linear nature of the burning process. Figure 4 shows the evolution of burning rate for the data in figure 3. Two curve-fits were tried (parabolic and cubic) but the linear variation is probably more reasonable for the data in figure 3. The continual increase in burning rate evidences increased heat transfer to the droplet. We here suggest that this effect is due to the influence of soot formation.

As burning proceeds the droplet produces less soot per mass of fuel evaporated due to the effect of droplet size on soot formation (Jackson and Avedisian 1994, 1996 ; Jackson et al. 1992; Lee et al. 1998), as well as the effect of droplet size on radiative losses from the flame (Easton et al. 1999). The droplet burns faster as time prrogresses because less soot is produced relative to the instantaneous droplet diameter. By this argument, if no soot at all is produced the burning process should be linear. (There are, of course, other reasons that could lead to a nonlinear burning process: the aforementioned question of water absorption which does not occur of the fuel types studied here; property variations with temperature; and droplet heating. If droplet heating occurs, curvature in the evolution of diameter could extend well into the burning process. Because of the small droplet diameters studied here, we do not expect droplet heating to be significant. Indeed, 0.45mm heptane droplets studied previously show no evidence of the droplet heating effect (Jackson et al. 1992; Jackson and Avedisian 1994).) Re-examination of published unsupported heptane diameter data obtained in microgravity (Jackson et al. 1992; Jackson and Avedisian 1994) do show a linear burning process for small heptane droplets for which no prominent soot shells were seen. Larger heptane droplets with visible soot shells showed a time varying burning rate. For these latter data, a single burning rate value was taken over the region where the evolution of droplet diameter in scaled coordinates is most linear.

Mixtures of Nonane (0.9) and Hexanol (0.1)

Fig. 5 shows the evolution of droplet diameter of a 10% hexanol mixture with an initial diameter of 0.65mm. Three points to note are that 1) there is no strong evidence for droplet heating; 2) two stages of burning occur; and 2) there is no plateau between the stages. The latter two effects are due to the differing heats of vaporization between hexanol and nonane coupled with their almost identical boiling points. The solid lines in figure 5 are meant to enhance the visibility of the staged burning process. The heat of vaporization of nonane is 25% less than hexanol (Lide 1993) so that the first stage is dominated by nonane combustion. At the junction of the two stages, there is no period of constant diameter or plateau because the droplet temperature remains essentially the same as burning changes from nonane to hexanol domination due to the almost identical boiling points of these two fuels.

Conclusions

The data presented here for nonane and a nonane-hexanol mixture show a nonlinear droplet burning process. This effect is due to changes in soot formation as burning progresses. The decrease of droplet diameter during burning results in a greater fraction of the evaporated fuel being converted into energy by oxidation at the flame which enhances heat transfer to the droplet and the burning rate. For the nonane/hexanol mixture, a staged burning process without a plateau is observed. In each stage the burning rate is nonlinear. A definitive explanation for a non-linear burning process for sooting fuels will emerge when numerical analyses are developed that include all of the effects that soot can have on the droplet burning process.

Acknowledgments

The authors are pleased to acknowledge the support provided by NASA grant NAG 3-1791 (Dr. Merril King, Program Director, and Dr. Daniel Dietrich, Project Monitor). The authors would also like to acknowledge the advice and assistance of Prof. Francis Mcleod and Ms. Nadia Bishai, and Dr. Dietrich for providing the silica fibers.

References

Avedisian, C.T. and Jackson, G.S. 1999 *AIAA J. Propulsion and Power*, to be published.
Avedisian, C.T., Yang, J.C. and Wang, C.H. 1988 *Proc. R. Soc. Lond.* A 420, 183-200.
Avedisian, C.T. 1997 in *Physical and Chemical Aspects of Combustion*, Chapter 6, pp. 135-160, Gordon and Breach Publ..
Callahan, B.J. and Avedisian, C.T. 1999 AIAA Paper no. 99-1077.
Cho, S.Y., Yetter, R.A. and Dryer, F.L. 1992 *J.* Comp. Phys. 102, 160.
Easton,. J., T'ien, F., and Dietrich, D. 1999 *Proceedings of the Combined Eastern, Central and Western States Section Meeting of the Combustion Institute*, pp. 665-668, March 15-17, 1999, Washington, D.C.
Glassman, I. 1987 *Combustion*, 2nd Edition, p. 275, Academic Press
Jackson, G.S. and Avedisian, C.T. 1996 *Comb. Sci. Tech.* 115, 127-147.
Jackson, G.S., Avedisian, C.T., and Yang, J.C. 1992 *Int. J. Heat Mass. Trans.*, 35(8), 2017-2033 (1992).
Jackson, G.S. and Avedisian, C.T., 1994 *Proc. R. Soc. Lond.* A 446, 255-276.
Jackson and Avedisian, C.T. 1998 *Int. J. Heat Mass Transf.* 41(16), 2503-2515.
Lee, K.Y., Manzello, S.L. and Choi, M.Y. 1998 *Comb. Sci. Tech.* in press.
Lide, D.R. 1993 "Basic Laboratory and Industrial Chemicals," pp. 160, 229, CRC Press, Boca Raton.
Marchese, A.J. and Dryer, F.L. 1996 *Comb. Flame.* 105, 104 (1996).

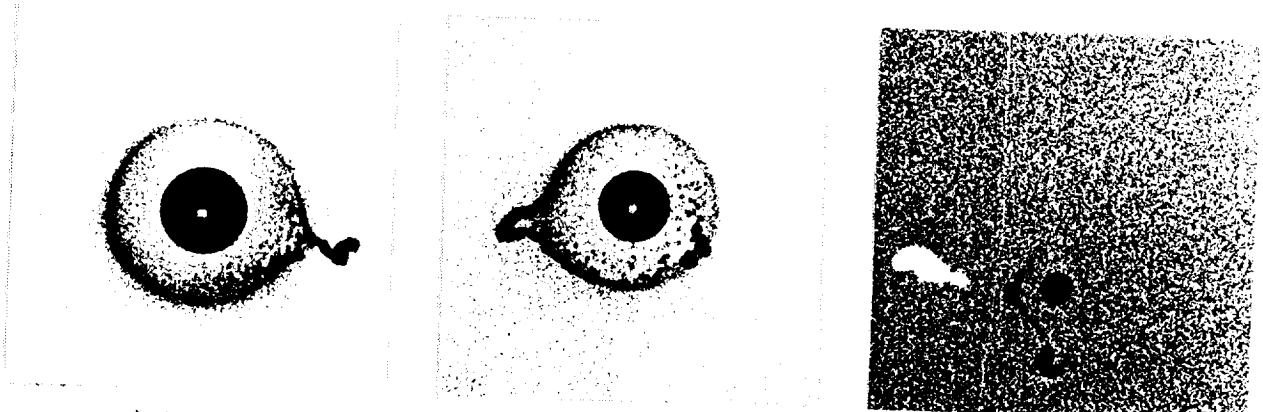

a) 220ms b) 325ms c) 490ms

Figure 1; d=0.47mm in a)

a) 200ms b) 370ms c) 720ms

Figure 2; d=0.59mm in a)

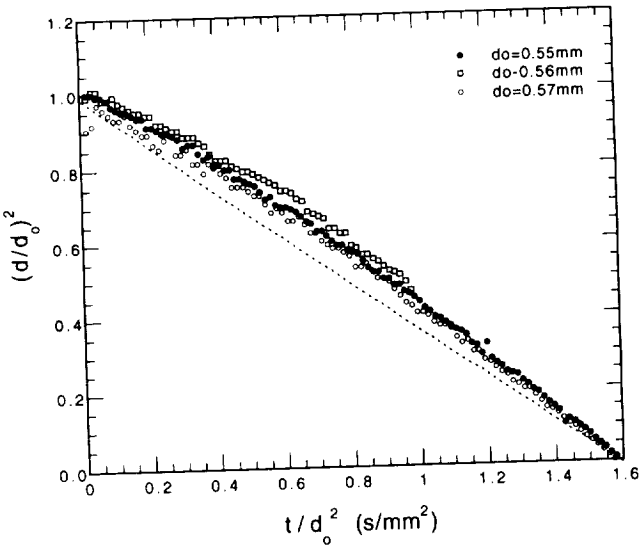

Figure 3

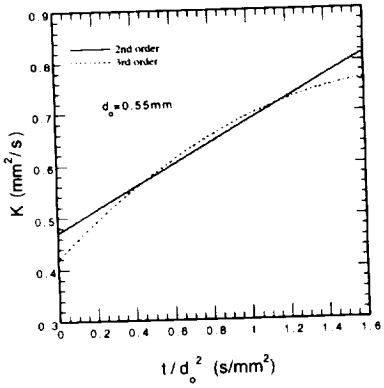

Figure 4a

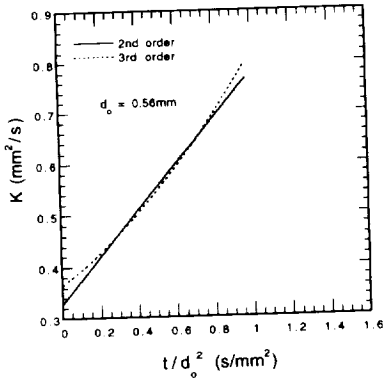

Figure 4b

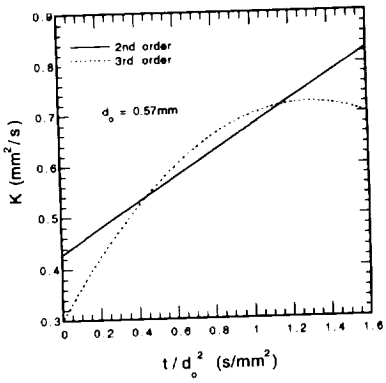

Figure 4c

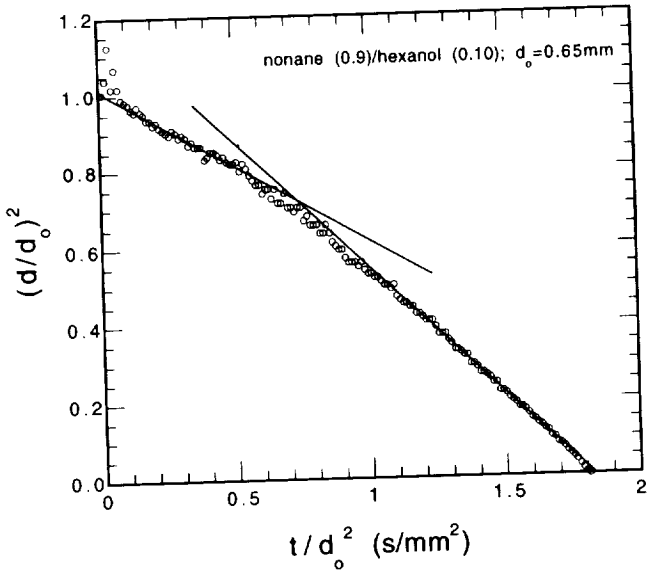

Figure 5

INFLUENCE OF ACOUSTIC FIELD ON DROPLET COMBUSTION IN MICROGRAVITY

M. Tanabe[1], K. Aoki[2], K. Sato[3] and T. Fujimori[4]

[1,2]Department of Aerospace Engineering,
College of Science and Technology, Nihon University
7-24-1 Narashinodai, Funabashi, Chiba 274-8501, Japan

[3,4]Research Institute, Ishikawajima-Harima Heavy Industries, co. Ltd.
3-1-15 Toyosu, Koto-ku, Tokyo 135-8732, Japan

e-mail: [1]tanabe@aero.cst.nihon-u.ac.jp

Abstract

Combustion of an isolated fuel droplet in an acoustic field is investigated by microgravity experiments. The influence of acoustic field is examined by varying sound pressure level and frequency of sound. Configuration of Flames and soot and burning rate is determined. As a result, hemispheric and conical flames are observed under the presence of sound depending on the sound pressure level. Ring-shaped soot coagulation (soot-ring) is observed as well for a moderate loudness of sound. Burning rate is significantly enhanced by sound and this is clarified to be able to explain by the enhancement mass/heat transfer by convection induced by the sound.

INTRODUCTION

A strong acoustic vibration often induces instability in combustion[1,2]. Stable combustion requires better understanding of the influence of acoustic field on combustion. Droplet is one of the simplest models of spray system, including the most characteristic processes such as heat transfer from gas to liquid phase, vaporization and diffusion controlled combustion. Many investigations have been done on the combustion characteristics of single droplets under the presence of sound. Enhancement in burning is reported as the influence of acoustic field and the reason is determined to be the enhanced heat- and mass- transfer due to the convection induced by sound wave. These past works are done on ground and the burning droplets are exposed to natural convection. They failed to detect the influence of acoustic field alone. Microgravity experiments, on the contrary, have an advantage, for it provides natural convection free conditions. The small velocity fluctuations of sound wave need not to be coupled with relatively high velocity of natural convection. By performing droptower experiments, we try to determine the influence of acoustic field in a clearer way than ever.

EXPERIMENTAL SETUP AND PROCEDURE

The employed experimental apparatus is shown in Fig. 1. A duct, whose size is 80*80(cross section)*160(length) [mm], is placed in the center of a pressure chamber. Sound is generated by a loudspeaker at the bottom of the chamber. The frequency of the sound is carefully chosen so as to form a standing wave in the duct. A microphone detects sound pressure on the duct wall. *n*-

earlier occurrence of extinction. Even the 125 [dB] case could not sustain a flame till droplet burns out. Although these general trend is true for all the data, there is a slight disagreement between the data of different frequency. Frequency, as well as velocity, seems to be a controlling factor probably through coupling with response time of vaporization.

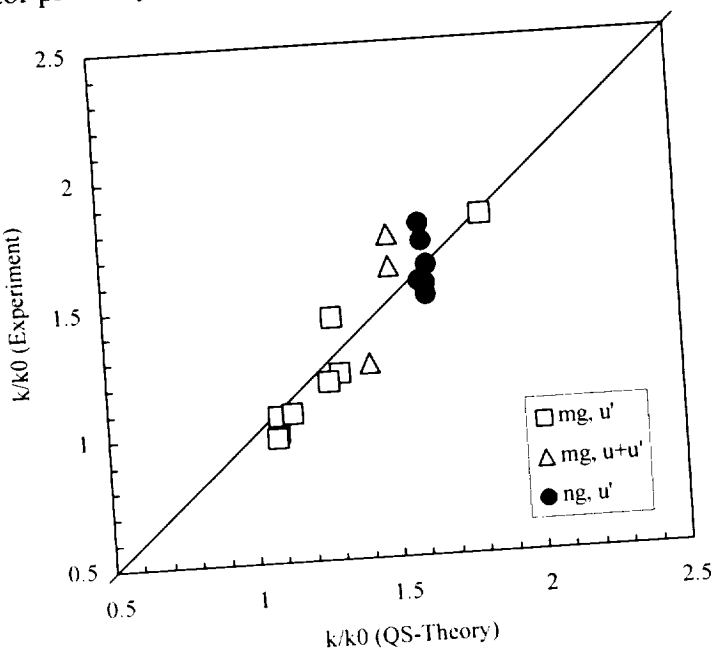

Fig. 5 Comparison of reduced burning rate constants

The simple analysis of the role of convection due to sound can be done in a quasi-steady manner. Instantaneous Nusselt number is calculated from velocity due to sound, that is measured by the hot wire anemometer. Averaging this over a cycle time, the average transfer coefficients is determined and burning rate constant can be calculated. Comparison between experiments and this evaluation is shown in Fig. 5. Agreement is good and the principal cause for the elevated burning rate is proven to be the enhanced transfer due to the sound-induced alternating convection.

The solid symbols show normal gravity data. As is seen in this figure, the data are not spread as widely as the microgravity ones. Natural convection also is a kind of convection and hence normal gravity data is only for relatively high speed of convection. It is impossible to unveil clearly the influence of sound from normal gravity experiments.

SUMMARY

Hemispherical and conical flame is observed in acoustic fields of different sound pressure levels. Soot ring is formed for these flames. Burning rate is elevated in acoustic fields. An enhanced transfer, that is due to the sound-induced alternating convection, realize it.

Further research is required to clarify the followings; 1: Roles of sound on flame and soot configuration around droplets. 2: The frequency dependence of burning rate. 3: Extinction characteristics. 4: High-pressure effect.

ACKNOWLEDGEMENTS

This study is funded by a part of "Ground Research for Space Utilization" promoted by NASDA and Japan Space Forum. The authors wish to thank Mrs. Hanada and Mr. Morita for experimental assistance.

REFERENCES

1. A. Duvvur, C. H. Chiang and W. A. Sirignano, J. Propulsion and Power, vol. 12, No. 2 ('96)
2. M. S. Ondas and D. A. Santavicca, Proceedings of the ASME Fluid Engineering Div. ('97)

Turbulent Combustion

VORTEX/FLAME INTERACTIONS IN MICROGRAVITY PULSED JET DIFFUSION FLAMES

M. Y. Bahadori[1], Science and Technology Development Corporation, U. Hegde, National Center for Microgravity Research, and D. P. Stocker, NASA Glenn Research Center

INTRODUCTION

The problem of vortex/flame interaction is of fundamental importance to turbulent combustion. These interactions have been studied in normal gravity.[1,2] It was found that due to the interactions between the imposed disturbances and buoyancy induced instabilities, several overall length scales dominated the flame. The problem of multiple scales does not exist in microgravity for a pulsed laminar flame, since there are no buoyancy induced instabilities. The absence of buoyant convection therefore provides an environment to study the role of vortices interacting with flames in a controlled manner. There are strong similarities between imposed and naturally occurring perturbations, since both can be described by the same spatial instability theory.[3,4] Hence, imposing a harmonic disturbance on a microgravity laminar flame creates effects similar to those occurring naturally in transitional/turbulent diffusion flames observed in microgravity.[5,6]

In this study, controlled, large-scale, axisymmetric vortices are imposed on a microgravity laminar diffusion flame. The experimental results and predictions from a numerical model of transient jet diffusion flames are presented and the characteristics of pulsed flame are described.

APPROACH

Turbulent Gas-jet Diffusion Flames (TGDF) experiment was a self-contained, autonomous payload flown in the bay of Space Shuttle *Columbia*. The combustion chamber (with free volume of 53 liters) contained the fuel supply system, igniter system, a vortex generation mechanism, and science instrumentation. The fuel nozzle had an internal diameter of 1.65 mm. Propane was injected at a flow rate of 3.6 mg/sec (Re $\cong$ 400). A vortex-generation mechanism, using an iris assembly located near the flame base, provided axisymmetric vortices for interaction with the flame front. Temperature measurements in and near the flame were made at 50 Hz by a rake of type-K thermocouples. Three thermopile radiometers were used at a sampling rate of 50 Hz. Two provided the radiation from narrow slices of the flame. The third radiometer was a wide-view unit for global radiation measurement. Following ignition, the flame was allowed to develop for 25 seconds to reach a quasi-steady state. Four periods of pulsing (with frequencies in the range of 1.5-5.0 Hz) followed this phase. The pulsing periods were each of a duration of 15 seconds, and each was separated by six seconds. Following the final period of pulsing, the flame continued to burn until extinction due to the decay in fuel bottle pressure. More details on the experiment hardware and procedure are presented elsewhere.[7]

The transient numerical model of the pulsed laminar flame provides the capability of calculating the flame characteristics under imposed, oscillatory disturbances. The model provides solutions for velocity, pressure, temperature, and species fields, and is described in detail in another publication.[8] In the computations, the iris is modeled as a thin boundary within the domain with no-slip condition imposed on both its upper and lower surfaces. Suitable modification to the coordinates of the grid at each time-step accomplishes the desired sinusoidal motion.

[1] Science and Technology Development Corporation, 11661 San Vicente Boulevard, Suite 500, Los Angeles, CA 90049; e-mail: bahadori@earthlink.net

RESULTS

The comparisons between data and predictions for the steady-state flame (i.e., for the first 25 seconds of the experiment) are presented in other publications[9] and will not be discussed here.

Figure 1 shows the phase relationship between the centerline temperature and flame surface radiation (from narrow-angle radiometer) near the flame base for 1.5 Hz. The phase of the iris maximum open position is also shown. It is seen that the temperature and radiation oscillations are in phase (i.e., phase difference < 90°) near the flame base. Also, the maximum amplitudes of the oscillations occur approximately one quarter of a cycle after phase of maximum iris opening. This corresponds to iris maximum inward velocity, which results in increased local combustion rate during the inward iris motion causing enhanced entrainment and mixing (see radiation behavior in Fig. 1). The predicted phase of the oscillation phase angle near the flames base from the numerical model is shown in Fig. 2. The phase difference between radially separated oscillations at this location is less than 90°, which agrees with the measurements of Fig. 1.

The phase relationships between centerline temperature and flame surface radiation (from the upper narrow-angle radiometer) at an axial location beyond the flame half-height are shown in Fig. 3. In contrast to the in-phase characteristics of the oscillations near the flame base (see Figs. 1 and 2), the signals are out of phase (i.e., phase difference > 90°). The predicted radial variation of the oscillation phase angle in the downstream region obtained from the numerical model is shown in Fig. 4. Consistent with the measurements, the predicted oscillations close to the flame surface ($3 < r/d < 7$) are out of phase compared to the oscillations at the centerline ($r/d = 0$).

The vortex dynamics in the flame core region can be assessed from the amplitude variation of the centerline temperature oscillations by comparing their decay rates with that of the mean velocity. If the oscillations do not interact significantly with each other or the mean flow, then they may be viewed as passive contaminants which are merely convected and dispersed by the mean flow. Hence, their decay rate will be the same as that of the mean velocity. On the other hand, if their decay rate is different from that of the mean velocity, then their deviation provides significant insight into the characteristics of vortex dynamics in the flame. Figure 5 plots as functions of x/d: (i) the computed variation of the normalized centerline velocity from the numerical model, which has an inverse relationship with x/d; (ii) the measured values of the normalized temperature amplitudes at the pulsed frequency of 3 Hz; and (iii) the measured values of the temperature amplitude at 3 Hz when it occurs at the first harmonic in the 1.5-Hz pulse case. Three zones are identified in Fig. 5, as: linear oscillation/mean-flow interaction zone (Zone I), non-linear oscillation/mean-flow interaction zone (Zone II), and oscillation decay zone (Zone III).

In the lower third of the flame to approximately $x/d = 30$ (Zone I), it is seen from Fig. 5 that: (a) the decay rate of the oscillations is lower than that of the mean velocity, i.e., both the primary and harmonic grow in strength; (b) the decay rate of the 3-Hz oscillations is the same whether it occurs as primary or harmonic, indicating that the dynamics is linear, i.e., non-linear interactions between the oscillations are not significant; and (c) since the oscillations grow in strength, and interactions between the oscillations are not significant, the energy transfer must be from the mean field to the oscillations. This behavior is consistent with the measurements of the temperature field which show that the mean temperature in the lower part of the flame decreases upon pulsing.

In the central region of the flame between $x/d = 30$ and $x/d = 55$ (Zone II), Fig. 5 shows that: (a) the decay rate of the oscillations for the primary is greater than that of the mean velocity, i.e., the primary vortex loses strength; (b) the decay rate of the oscillations at 3 Hz is different depending upon whether it is the primary or harmonic, and can only occur if interactions exist

between oscillations, i.e., the dynamics is no longer linear; and (c) since the oscillations at the primary decrease in strength, the energy transfer must be from the primary (e.g., 3 Hz) to the mean field and/or its harmonic (i.e., 6 Hz). Measurements also show that in the downstream locations (x/d = 55 and higher), the mean temperatures increase upon commencement of pulsing. This clearly indicates energy transfer from the primary vortex to the mean flow in this zone.

In the downstream region of the flame, i.e., x/d > 55 (Zone III) in Fig. 5, the decay rate for both the primary and harmonic approach that of the mean velocity. This indicates that energy transfer between the mean flow and oscillations as well as non-linear interactions between the oscillations are no longer significant, and the balance is simply between convection and diffusion. This is the first time that the decay of vorticity by dissipative (i.e., viscous) effects has been demonstrated in flames. It may be noted that this phenomenon has not been documented in normal-gravity studies due to the effects of buoyant acceleration.

Figure 6 plots as functions of x/d: (a) the predicted variation of the amplitude of the normalized temperature oscillations; (b) the experimentally measured variation of the amplitude of the normalized temperature oscillations; and (c) the predicted variation of the amplitude of the normalized axial velocity oscillations. The predictions are in good agreement with measurements and further show that the behavior of the axial velocity oscillations and the temperature oscillations are similar. The amplitude of the oscillations grows in the lower part of the flame as the oscillations extract energy from the mean flow. Further downstream, the oscillations decay returning energy back to the mean flow. Finally, the decay rate of the oscillations approaches the 1/x decay behavior of the mean velocity. The numerical computations also show, as is clear from the amplitude variation of the velocity oscillations, that the kinetic energy, k, of the oscillations peaks in the lower part of the flame. Energy balance considerations then show that the vortex dissipation rate, ε, also peaks in the lower parts of the flame. This behavior is completely different from buoyancy dominated flame characteristics where the dissipation rate continues to increase with axial distance.

ACKNOWLEDGMENTS

The authors would like to thank NASA for supporting this space experiment under Contracts NAS3-98031 with Science and Technology Development Corporation and NCC3-544 with National Center for Microgravity Research. The efforts of the project manager, Mr. Franklin Vergilii, and the project team are gratefully acknowledged.

REFERENCES

1. Strawa, A. W. and Cantwell, B. J. (1985), *Phys. Fluids*, vol. 28, pp. 2317-2320.
2. Roberts, W. L., Driscoll, J. F., Drake, M. C., and Ratcliffe, J. W. (1992), *Twenty-Fourth Symposium (International) on Combustion*, pp. 169-176, The Combustion Institute, Pittsburgh, PA.
3. Huerre, P. and Monkewitz, P. A. (1985), *J. Fluid Mech.*, vol. 159, pp. 151-168.
4. Morris, P. J. (1976), *J. Fluid Mech.*, vol. 77, pp. 511-529.
5. Bahadori, M. Y., Stocker, D. P., Vaughan, D. F., Zhou, L., and Edelman, R. B. (1993), *Modern Developments in Energy, Combustion, and Spectroscopy*, (F. A. Williams, A. K. Oppenheim, D. B. Olfe, and M. Lapp, eds.), pp. 49-66, Pergamon Press, New York.
6. Hegde, U. G., Zhou, L., and Bahadori, M. Y. (1994), *Combust. Sci. Tech.*, vol. 102, pp. 95-113.
7. Hegde, U., Bahadori, M. Y., and Stocker, D. P. (1999), *AIAA Journal*, in press.
8. Bahadori, M. Y., Hegde, U., and Stocker, D. P. (1999), *AIAA Journal*, submitted.
9. Bahadori, M. Y., Hegde, U., and Stocker, D. P. (1999), *Combust. Sci. Tech.*, submitted.

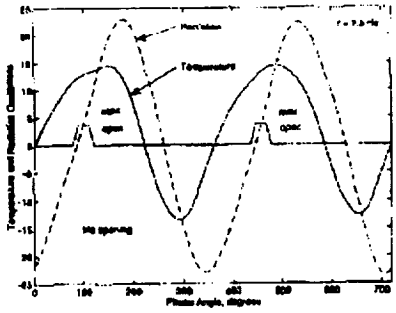

Fig. 1. Phase variation of centerline temperature oscillations (x = 1.5 cm) and radiation from lower radiometer, f = 1.5 Hz.

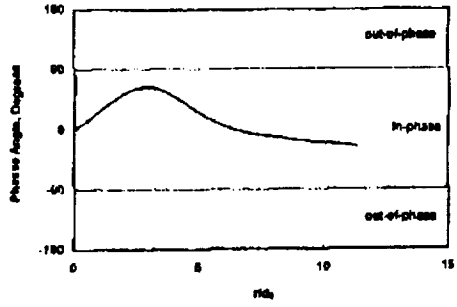

Fig. 2. Predicted phase angle (relative to centerline value) of the axial velocity oscillations near the iris.

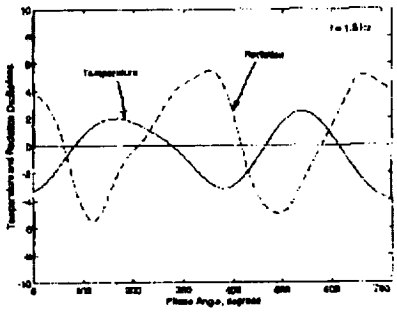

Fig. 3. Phase variation of centerline temperature oscillations (x = 9 cm) and radiation from upper radiometer, f = 1.5 Hz.

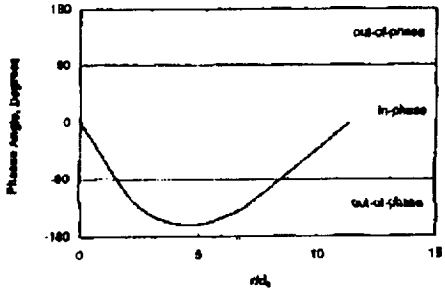

Fig. 4. Predicted phase angle (relative to centerline value) of the axial velocity oscillations near the flame half-height

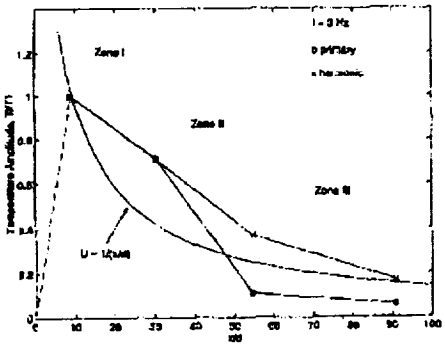

Fig. 5. Axial variation of normalized measured centerline temperature amplitude (3 Hz primary and 3 Hz harmonic) and computed axial velocity

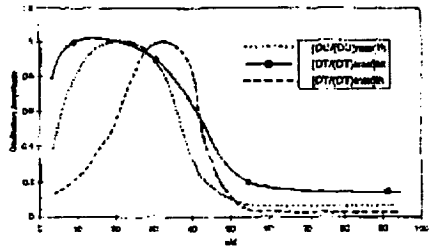

Fig. 6. Oscillation amplitude of predicted normalized temperature, measured normalized temperature oscillations, and predicted normalized axial velocity oscillations.

S2-27

CHARACTERISTICS OF NON-PREMIXED TURBULENT FLAMES IN MICROGRAVITY

U. Hegde[1] and Z. G. Yuan, National Center for Microgravity Research, D. P. Stocker, NASA Glenn Research Center, and M. Y. Bahadori, Science and Technology Development Corporation

INTRODUCTION

The momentum of the fuel (and/or air) jet is important in classifying gas-jet diffusion flame behavior. Normal-gravity data on gas-jet flames show that the flame height (non-dimensionalized with respect to an effective diameter) can be correlated to a density weighted Froude number in the buoyancy-dominated limit[1,2]. In the momentum-dominated limit this non-dimensional flame height asymptotes to a constant value. The momentum-dominated limit under normal gravity conditions is usually obtained for very high injection velocities which in turn results in high values of the injection Reynolds number. This results in a complicated flame structure because of the large number of turbulence scales involved. In order to gain better insight into the structure of these flames it would be useful to reduce the injection Reynolds number while still maintaining turbulent conditions. This can be done in microgravity where momentum-dominated turbulent flames are obtained at much smaller velocities than in normal gravity.

In this paper, experimental results on the effects of nozzle diameter and fuel dilution on flame height are discussed. The experimental values are compared with predictions from a numerical procedure utilizing the standard k-ε turbulence model. Flame height scaling with nozzle size and dilution is established. Differences between model predictions and measurements are presented. In order to explain these differences, evolutions of turbulent spectra and Taylor microscale along the flame axis are considered.

APPROACH

The microgravity experiments in this study were conducted at the 5.18-second Zero-Gravity Facility and the 2.2 -second Drop Tower at NASA Glenn. Fuel-nitrogen mixtures are injected into quiescent air through a nozzle made of stainless steel tubing. For the tests to be described, propane was used as fuel. The flame is ignited just after the drop commences by means of a hot wire. Side views of the flame are imaged by means of video cameras at 30 frames per second. Type K thermocouples with bead diameters in the range of 150-200 microns are strung across the flame at various axial locations above the nozzle tip. The measured signals from the thermocouples have to be compensated for their time response in order to measure the temperature spectrum. The technique for obtaining the time constant has been described before[3]. The acoustic pressure generated by the flames have been measured utilizing a condenser microphone assembly mounted near the chamber side wall. The microphone has a flat frequency response to about 10,000 Hz. A 16-bit data acquisition system is utilized for the temperature and pressure measurements. Sampling rates for the thermocouples are 1000 Hz while the pressure measurements are sampled at up to 5000 Hz.

The numerical model utilizes standard turbulent models in conjunction with state relationships for chemistry for predicting the time-averaged flow field. A single step chemical reaction between fuel and oxidizer is assumed. The model solves for pressure, velocity,

[1] National Center for Microgravity Research on Fluids and Combustion, MS 110-3, 21000 Brookpark Road, Cleveland, OH 44135; e-mail: uday.hegde@grc.nasa.gov

temperatures, species concentrations, and turbulent kinetic energy and dissipation rate. The code utilizes a discrete transfer radiation model[4] for CO2 and H2O emissions for radiative transport.

RESULTS

Fig. 1 plots three sets of measured flame heights as function of the injection Reynolds number. The turbulent regime exists for Re > 3000[5]. These sets are:

(i) 0.8 mm nozzle diameter, no fuel dilution, normal gravity and microgravity

(ii) 1.6 mm nozzle diameter, 60% (by volume) propane-40% (by volume) nitrogen, normal gravity and microgravity, and

(iii) 1.6 mm nozzle diameter, 50% (by volume) propane-50% (by volume) nitrogen, microgravity

Several observations can be made. First, the microgravity flames are about two times taller than the normal gravity flames. Second, flame height is relatively insensitive to Reynolds number in the turbulent regime for both normal gravity and microgravity flames. Third, blow-off Reynolds number for the microgravity flame is larger than for the normal gravity flames. It is also found that blow-off Reynolds number decreases with increase in percentage of diluent. It is observed that by doubling the nozzle diameter and reducing the fuel percentage by half, the flame height is not affected. This suggests the scaling that $L \alpha d\phi$,where L is flame height, d is nozzle diameter and ϕ is the fuel mole fraction of the injected mixture.

The computational model recovers the experimentally observed dependence on nozzle diameter, fuel dilution and Reynolds number. For example, the computed temperature profiles and fuel and oxygen mass fractions are shown for two nozzle diameters for zero-gravity conditions in Fig. 2. In this case, the injection Reynolds number is 5000 for both cases and $\phi = 1$ (pure fuel). One way to define the flame height is the location of peak temperature along the axis. The computed average flame height for the 1.6 mm dia nozzle is 20 cm whereas that for the 0.8 mm dia nozzle is around 10 cm. This recovers the observed dependence of flame height on flow rate and nozzle diameter. However, the predicted flame heights are less by a factor of approximately two for the microgravity flames. It may be noted that for the normal gravity flames, the discrepancy is found to be much less, on the order of 10%-20% overprediction.

A possible reason for the discrepancy between measured and computed flame heights is obtained from consideration of the turbulent viscosity. As noted, the microgravity turbulent flames are observed to be taller (see Fig. 1) at the moderate injection Reynolds numbers of interest. Utilizing the argument of the equality between the characteristic time for diffusion and the travel time from the nozzle exit to the flame tip[6], it was shown[5] that the effective (or turbulent) diffusivity of the normal-gravity flame was two to three times that of the microgravity flame at the moderate Reynolds numbers. The effective diffusivity and the turbulent viscosity are related by the turbulent Schmidt number which should be near unity. Thus, the computed turbulent viscosity profile can provide insight into the discrepancy in computed and experimental flame heights. Figure 3 plots the computed turbulent viscosity profile along the flame centerline for different gravitational levels. Note that it peaks downstream of the nozzle, levels off and then begins to increase again. It would be useful to compare this behavior with estimates obtained from experiment. In order to do this, measurements of temperature fluctuations as described next were made. However, it may be noted that the computed values of the turbulent viscosities are very close in magnitude for the different gravitational levels until the computed tips (~ 0.2 m) of the flame.

Thermocouple measurements have been utilized to measure temperature on the flame centerline and obtain the corresponding spectra. Figure 4 shows typical obtained spectra. These spectra show that at the downstream locations (x/d = 70 and x/d =100) the temperature fluctuations have higher amplitudes with spectral levels about 10-15 dB greater than at the lower level (x/d = 9). In addition, the fall off in spectral level with frequency is steeper at the lower location. This indicates that the flame becomes more turbulent with increasing axial distance in the lower half of the flame.

The autocorrelation of these signals can be related to the Taylor microscale and the turbulent viscosity[7]. Figure 5 plots the axial variation of the Taylor microscale obtained from the autocorrelation function along the flame axis. Note that it decreases consistent with the increase in turbulence levels but then as the turbulence levels flatten out, its value also flattens out in the central portion of the flame. In future work, variations in the downstream regions of the flame will be obtained. However, it is expected that for the microgravity flame, turbulence levels will begin to decrease downstream with corresponding increase in the microscale. This would indicate[8] a reduction in the value of the turbulent viscosity in the downstream regions which is opposite to the behavior in the computations.

Pressure spectra of the acoustic field radiated from the flames have also been obtained. The radiated sound field is related to the time-dependent volumetric heat release rate of the flame[9]. In the absence of chamber resonant excitation, the frequency content of the pressure spectrum provides a good estimate of the frequency content of the fluctuations in the flame region and an estimate of the turbulent spectrum frequency bandwidth. Figure 6 plots measured pressure spectra of the microgravity propane flame considered above. The pressure measurements were made near the chamber side wall. No chamber resonant frequency effects are observed in the spectra suggesting that the frequency range of the spectra is indicative of the corresponding frequency range of the flame region fluctuations. It is observed that the dissipation regime is approached for frequency around 100 Hz which is a time scale of the order of 0.01 seconds. This is smaller than the Taylor microscale values noted earlier which is expected.

ACKNOWLEDGEMENTS

The assistance of Dennis Thompson, Zero-G Facility manager, in the conduct of the tests is greatly appreciated. Jonathan Sakai, an intern with the National Center for Microgravity Research, assisted with the numerical code computations and drop testing in the 2.2 Second Drop Tower.

REFERENCES

1. Blake, T. R. and McDonald, M. [1995] *Combustion and Flame*, vol. 101, pp. 175-184.
2. Delichatsios, M. A. [1993], *Combustion and Flame*, vol. 92, pp. 349-364.
3. Hegde, U., Stocker, D. P., and Bahadori, M. Y. [1996] AIAA Paper No. 96-0621.
4. Siegel, R., and Howell, J. [1981]*Thermal Radiation Heat Transfer*, Second Edition, McGraw-Hill.
5. Hegde, U., Zhou, L., and Bahadori, M. Y. [1994] *Combustion Science and Technology*, vol. 102, pp. 95-113.
6. Glassman, I.[1987] *Combustion*. Second Edition, Academic Press, New York.
7. Tennekes, H. and Lumley, J. L. [1977] *A First Course in Turbulence*, The MIT Press, Cambridge, MA.
8. Hegde, U., Yuan, Z. G., Stocker, D. P., and Bahadori, M. Y.[1998] Characteristics of Turbulent Diffusion Flames in Microgravity. Fall Meeting of the Western States Section of the Combustion Institute, Seattle, WA.
9. Strahle, W. C. [1985] A More Modern Theory of Combustion Noise, in *Recent Advances in the Aerospace Sciences* (C. Casci, Ed.), Plenum Press, New York.

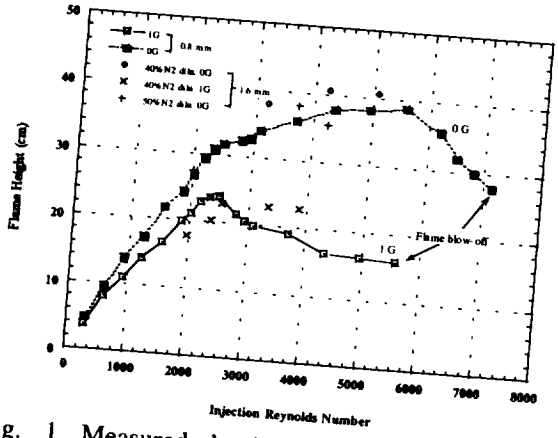

Fig. 1 Measured luminous flame heights of propane-nitrogen flames as function of injection Reynolds number.

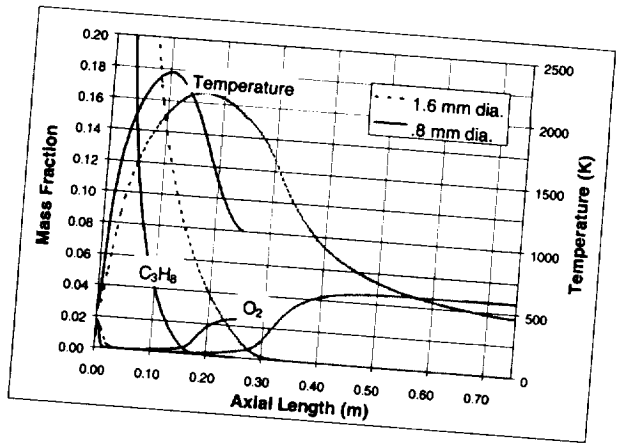

Fig. 2 Computed centerline distributions of fuel and oxygen mass fractions and temperature for propane flames for two nozzle diameters.

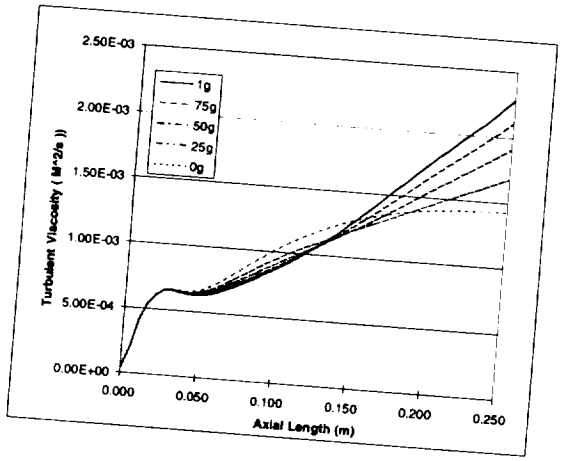

Fig. 3 Computed centerline distributions of turbulent viscosity for propane flames under different gravitational levels.

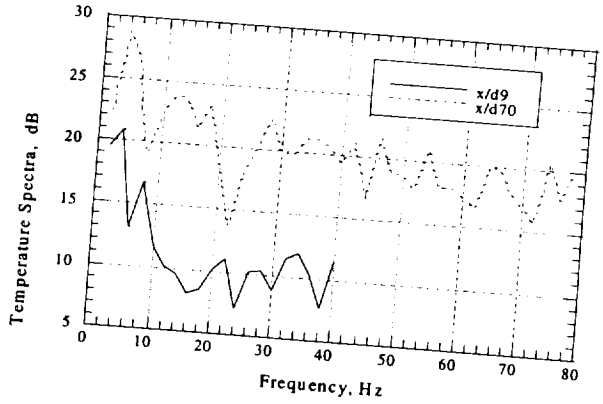

Fig. 4 Measured centerline temperature spectra at two axial locations

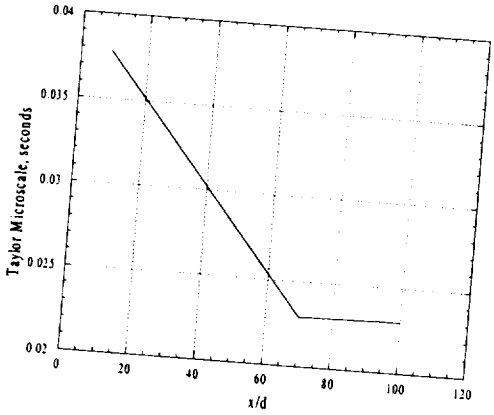

Fig. 5 Measured Taylor microscale along the flame centerline

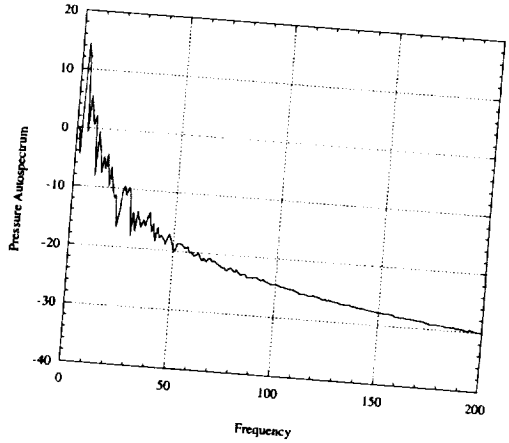

Fig. 6 Measured flame pressure spectrum in microgravity

EFFECTS OF BUOYANCY ON THE FLOWFIELDS OF LEAN PREMIXED TURBUENT V-FLAMES

R. K. Cheng[1], B. Bédat[1], D. T. Yegian[1], P. Greenberg[2],
[1]Lawrence Berkeley National Laboratory, Berkeley, CA
[2] NASA John H.Glenn Research Center at Lewis Field, Cleveland OH

INTRODUCTION

Open laboratory turbulent flames used for investigating fundament flame turbulence interactions are greatly affected by buoyancy. Though much of our current knowledge is based on observations made in open flames, buoyancy effects are usually not considered in data interpretation, numerical analysis or theories. This inconsistency remains an obstacle to merging experimental observations and theoretical predictions. To better understanding the effects of buoyancy, our research focuses on steady lean premixed flames propagating in fully developed turbulence. We hypothesize that the most significant role of buoyancy forces on these flames is to influence their flowfields through a coupling with the mean and the fluctuating pressure fields. This coupling relates to the elliptical problem that emphasizes the importance of the upstream, wall and downstream boundary conditions in determining all aspects of flame propagation. Therefore, buoyancy has the same significance as other parameters such as flow configuration, and flame geometry.

BACKGROUND

To characterize the field effects of buoyancy, our approach is to compare flames in normal gravity (+1g), reversed gravity (-1g) and in microgravity (μg). μg flames experiments provide key information to reconcile the observations made in +1g and –1g flames. Thus far, we have conducted laboratory studies of the field effect of buoyancy on stabilization limits, flame wrinkle structures, and mean and rms velocities in several flame configurations. Exploration of these phenomena helps to gain an overview and to build the scientific foundation needed for defining an appropriate configuration and conditions for microgravity flight experiments. Our investigation of rod-stabilized v-flames subjected to +1g and –1g have lead to the observation of a buoyancy stabilized flame [Bedat and Cheng, 1996].

We also found that the effects of buoyancy persist beyond the limit predicted by current scaling laws [Bedat, Cheng and Kostiuk, 1999]. This interesting phenomenon was first shown by the mean v-flame angles. Simple scaling suggests that the +g, -g and μg flame angles should converge with increasing flow momentum. For laminar flames, this convergence was found for Re > 2000. For turbulent flames, convergence was not found. The use of 2D Planar Laser Induced Fluorescence technique for OH radicals revealed that the difference is due to the fact that the -1g turbulent flame is more wrinkled than the +1g flame. Therefore, buoyancy has a direct effect on the development of turbulent flame wrinkle structures and these effects are present even at high flow momentum.

LDA SYSTEMS FOR 1g AND μg EXPERIMENTS

To further understand how the differences in flame wrinkling relate to the flowfield, we use laser Dopper anemometry (LDA) to measure the velocity statistics in +1g, -1g and μg flames. In the laboratory we use a two-component frequency-shifted four-beam LDA with a 4 watt Argon-Ion laser source. It is interfaced to a PC that also controls a three-axis traverse table to scan the flame automatically. Obviously, this system is too complex for reduced gravity aircraft experiments. To develop a LDA system for parabolic flights, we took a two step approach.

Starting with a compact one-component LDA, the first goal was to demonstrate the feasibility of deploying LDA in aircraft. The main challenge was to develop a system that can withstand varying g forces and vibration during the airplane pull-ups and parabolas. There were other issues such as seeding device and suitable experimental protocol for scanning the flowfield. Based on the 1D LDA experience, a 2D-LDA system has been designed and tested.

The experimental package for reduced gravity experiment is fully computerized. The burner is mounted on a two-axis translating stage for automatic scanning. Fuel and air are metered by flow controllers and mixed prior to entering the burner. The 1D LDA system for reduced-gravity experiment is designed in a forward scattering configuration. The laser source is a 14 mW (532 nm) external cavity-doubled diode pumped Nd:YAG laser (Adlas DPY 205C). An equal-path BK-7 splitting prism is utilized, so that additional pathlength compensation elements are not required. The beams are brought to a focus by a 160 mm achromat lens, yielding a $1/e^2$ transverse probe volume dimension of approximately 150 microns. Scattered light is collected at 15° off the forward scattered direction by a 55 mm, F/2.8 commercial camera lens. The probe volume is focused onto a 100 micron diameter multimode optical fiber. The signal is digitized by a burst spectral processor (QSP M240S).

The 2D-LDA system uses a pair of semiconductor diode lasers each emitting 15 mW at 676 and 780 nm respectively. The two beam paths are arranged coaxially employing two equal-path BK-7 beam splitters. Separate mode matching optics for each channel render probe volume of 90 μm. Scattered light is collected at 15° off the forward scattered direction and a dichroic filter is used to separate the scattered signal into its component wavelengths. The twin images of the probe volume are filtered and focused onto the input facets of two 100 micron diameter optical fibers. The signals are digitized by a burst spectral processor (QSP M240S). The two velocity components (angularly separated by 90°) are arranged at +/- 45° relative to vertical. The algebraic combination of the ouputs directionally resolves the radial velocity providing that there are no flow reversals in the axial direction.

Measurements of velocity statistics in μg flames involve rather complex protocol. Fortunately, the LDA systems were sufficiently robust such that re-alignment was not necessary between parabola. During the short time of each parabola (about 30 sec pullup, 15 sec. reduced-gravity), the follow steps were executed : 1) purge the burner, 2) set the fuel and air flow rates, 3) ignite the flame, 4) traverse the burner to a pre-assigned position, 5) trigger the LDA measurements, 6) record gravitational levels, 7) turn off the flame and 8) return the burner to its park position. Consequently, each parabola produced measurements at only one position.

RESULTS

The experiments include both laminar and turbulent flames all using research grade methane as fuel. The experimental matrix covers flow velocities from 0.8 to 2 m/s, equivalence ratio ϕ from 0.6 to 0.8. The μg flame experiments have been conducted in three campaigns using DC9 and KC135 aircraft. Figure 1 compares the 2D velocity vectors obtained in a +1g and a −1g laminar flames at Re = 1250, ϕ = 0.7. Under this low velocity condition, there are significant differences in the flame shapes and in their flowfields. In +1g, flow acceleration is observed in the products but in -1g constant deceleration is found. The stagnation point and the outer flow circulation zone of the −1g flame are also apparent.

Though the outline of the turbulent flame brushes of Figure 2 indicate that the -g turbulent flame is broader and shorter than the corresponding +g flame, differences in the velocity vectors are much less noticeable. Compared to the +1g case, the −1g velocity vectors show a more

divergent flow in the reactants. This is consistent with the change in mean radial pressure gradient due to the mean products flow circulating upstream due to buoyancy. Whether or not this slight change can be responsible for the drastic change in flame wrinkle structure needs to be investigated more thoroughly.

Figure 3 compares centerline profiles obtained in laminar +1g, -1g and μg v-flames (Re = 2500 and $\phi = 0.7$). Each point on the μg velocity profile was collected during separate parabolas to ensure that a sufficient number of LDA validations can be collected to produce stable velocity statistics. A lack of significant scatter in the mean and rms velocities is a good indication that the experiments were highly reproducible. As expected, the mean profile of the +1g flame shows continuous acceleration. In contrast, the −1g mean profile shows deceleration after an initial acceleration in the near field ($x > 12$ mm). The most interesting feature of the μg flame mean profile is that the peak velocity occurs father downstream at $x = 30$ followed by a slight deceleration. This indicates that without buoyancy, the velocity in the products plum decelerates because of divergence. Due to the use of frequency shifting in our laboratory LDA system, the rms velocities of the +1g and −1g flame are slightly higher than the levels measured in μg. However, the trend shown by the profiles can still be compared. In 1g and −1g, the fluctuations in the far field increases because of buoyancy induced instabilities. For the μg flames, the rms velocity also increases in the far field, this shows that some instabilities exist even without buoyancy.

Figure 4 shows the centerline profiles of turbulent +g, -1g and μg flames with Re = 2506 and $\phi = 0.65$. Due to the higher flow momentum and turbulence, the differences in the mean velocity profiles are not obvious. In the nearfield, the mean velocities have the same trend up to $x = 30$ mm. For $x > 30$ mm, mean velocity increases in the +1g flame and decreases in the −1g flame. The mean profile of the μg flame drops slightly and then levels off. At $x = 40$m, the differences in the +1g, -1g, and μg mean velocity are less than 0.5 m/s. The corresponding rms velocity profiles show that buoyancy effects on velocity fluctuations also occur mainly in the farfield. At $x > 30$ mm rms velocities in +1g and −1g flames increase and those in μg flame decrease.

SUMMARY

The velocity results show that the effects of buoyancy on the flame flowfields can be quite subtle. To better understand how these velocity changes relate to the development of flame wrinkles requires a more complete comparison. Of particular importance is the measurement of the transverse velocity component. We are planning to use the two-component LDA system to measure transverse velocity profiles in μg flames.

ACKNOWLEDGEMENT

This work is supported by NASA Headquarters Microgravity Research Division, Microgravity Combustion Science Discipline Working Group under contract No. C-32000-R through the U. S. Department of Energy Contract No. DE-AC03-76F00098.

REFERENCES

Bédat, B. and Cheng, R. K., (1996) "Effects of Buoyancy on Premixed Flame Stabilization" *Combustion and Flame, 107,* 13-26.

Cheng, R. K., Bédat, B., Kostiuk, L. W.(1999) "Effects of Buoyancy on Lean Premixed V-Flames: Part I: Laminar and Turbulent Flame Structures, *Combustion and Flame, 116.*

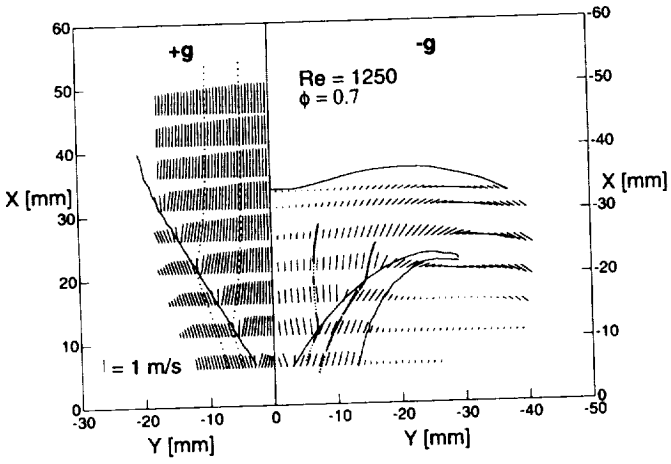

Figure 1 Comparison of 2D velocity vectors measured in a +1g (left) and a -1g (right) laminar v-flame

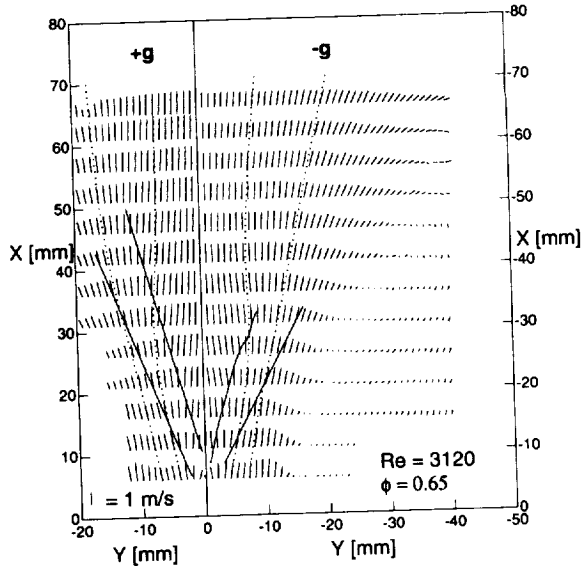

Figure 2 Comparison of 2D velocity vectors measured in a +1g (left) and a -1g (right) turbulent v-flame

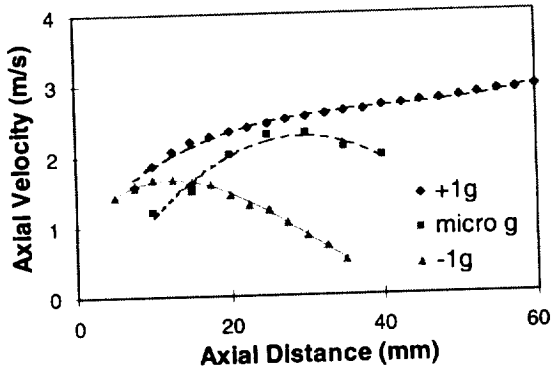

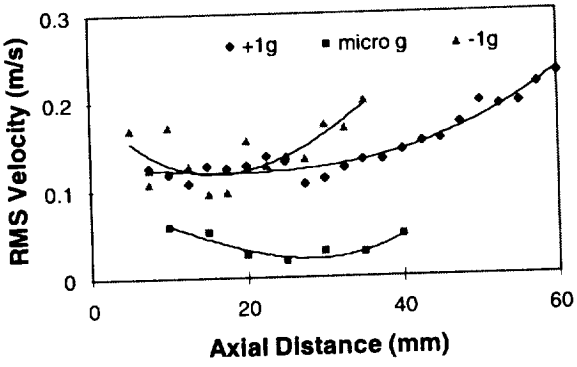

Figure 3 Mean and rms centerline profiles of +1g, -1g and μg laminar v-flame at Re = 1880 and ϕ = 0.7

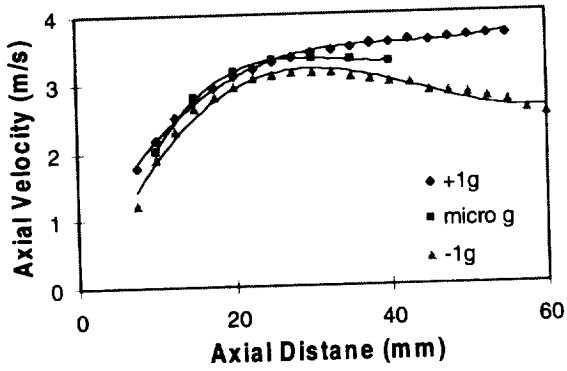

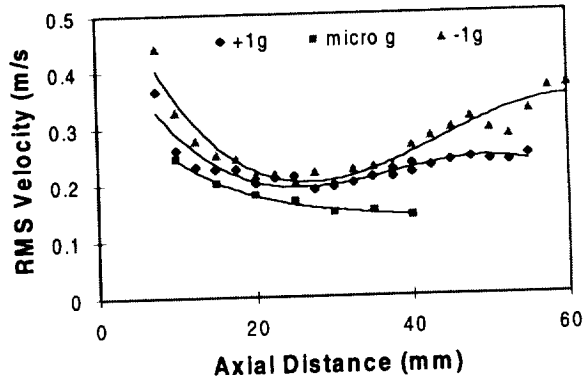

Figure 4 Mean and rms centerline profiles of +1g, -1g and μg turbulent v-flame at Re = 2506 and ϕ = 0.65

Flame-Vortex Interactions in Microgravity to Improve Models of Turbulent Combustion

562-29

James F. Driscoll
Department of Aerospace Engineering
University of Michigan
NASA Contract NAG 3 - 1639

A unique flame-vortex interaction experiment is being operated in microgravity in order to obtain fundamental data to assess the Theory of Flame Stretch which will be used to improve models of turbulent combustion. The experiment provides visual images of the physical process by which an individual eddy in a turbulent flow increases the flame surface area, changes the local flame propagation speed, and can extinguish the reaction. The high quality microgravity images provide benchmark data that are free from buoyancy effects. Results are used to assess Direct Numerical Simulations of Dr. K. Kailasanath at NRL, which were run for the same conditions.

The Michigan drop tower experiment (Fig. 1) is unique because: (a) it is a simple but general "canonical" problem of an eddy interacting with a flame - researchers developing DNS simulations recognize that their codes must correctly simulate this type of simple problem before they attempt to simulate fully turbulent flames, (b) it provides the only measurements of all components of the local stretch rate, the strain rate, vorticity field, and local propagation speed because of its axisymmetric geometry, and (c) it allows control of the Froude number and buoyancy forces. Previously, high quality digitized images of the flame-vortex interaction were obtained in microgravity at the NASA Lewis 2.2 Second Drop Tower. Results showed that:

a) Flame wrinkle amplitude and shape in microgravity compared favorably with the DNS of Dr. Kailasanath at NRL for the same vortex strengths, sizes, fuel type (methane).
b) "Flame generated vorticity" (turbulence) was conclusively identified experimentally for the first time - it is created by buoyancy forces in our one-g experiment. A Baroclinic Stabilizing Mechanism also was identified from PIV data at one-g which reduces flame wrinkling and should be included in models of turbulent combustion.
c) PIV images were obtained at four different Froude numbers (at one-g) to provide the first images showing how vorticity is attenuated by the flame.
d) The PIV images also provide the first strain rate data for freely propagating wrinkled flames, at four Froude numbers at one-g.

Six journal articles [1-6] describe the results. The goals of the next phase are:

(1) To develop microgravity PIV diagnostics to measure simultaneously the two most important quantities in the field of premixed turbulent combustion, namely the local flame propagation speed and local stretch rate.

(2) To continue to compare measured local propagation speed and stretch rate to the Direct Numerical Simulations of Kailasanath [7].

(3) To look at two aspects of the flame-vortex interaction in more detail -the formation of a "cusp" in the flame by the vortex and the "spherically inward propagating flame" that occurs as the vortex creates a pocket of reactant.

(4) To measure radical species CH and OH at four different Froude numbers. CH and OH radical concentrations have been made (at one-g) with PLIF diagnostics and will be compared to the DNS simulations of Kailasanath [7].

PIV and high speed shadowgraph movies will be made in the NASA Lewis 2.2 Second Drop Tower using the existing experiment. The local displacement speed (S_d) and stretch rate (K), will be measured to assess the Theory of Flame Stretch, [8-10], which states that:

$$S_d / S_{L,o} = 1 - Ma\ K / (S_{L,o}^2/D)$$

At one-g, we have used PIV data shown in Fig. 2 to measure the displacement speed: the difference between the flame speed in lab coordinates and the speed of the reactants ahead of the flame: $S_d = \mathbf{V_f \cdot n - V_r \cdot n}$. Our measured displacement speed and stretch rates at one-g are plotted in Ref. 5. Stretch rate (K) is:

$$K = \nabla \cdot \mathbf{V_r} - (\mathbf{n} \cdot \nabla) \cdot \mathbf{V_r} + S_L/R$$

a) Direct Numerical Simulations of Flame-Vortex Interactions by Kailasanath at NRL, [7] use the Michigan data for comparisons. He includes complex methane chemistry and realistic heat losses. It is planned to publish a joint paper to compare results.

b) Microgravity studies of Dr. Robert Cheng at LBL, also have shown that microgravity increases the wrinkling of turbulent flames [11], in agreement with our findings.

c) Markstein numbers measured by G.M. Faeth for spherical flames
Markstein numbers of the present work are being compared to those of Faeth [10].

References

1. Sinibaldi, J.O., Driscoll, J.F., Mueller, C.J. "Suppression of Flame Wrinkling by Buoyancy: The Baroclinic Stabilization Mechanism", AIAA Journal, 36, 8,1432, 1998.

2. Mueller, C., Driscoll, J. F., Reuss, D. and Drake, M., "Vorticity Generation as Vortices Convect Through a Premixed Flame", Combust. Flame, 112, 342-356, 1998.

3. Mueller, C., Driscoll, J.F., Roberts, W.L., Drake, M.C., and Smooke, M.D., "Effect of Stretch Rate on Flame Chemistry During a Transient Flame-Vortex Interaction - to Assess Flamelet Models", Combustion and Flame 100, 323-331, 1995.

4. Driscoll, J.F., Sutkus, D., Roberts, W., Post, M. and Goss, L. "The Strain Exerted by a Vortex on a Flame", Comb. Sci. and Technol., 96, 213, 1994.

5. Sinibaldi, J.O., Mueller, C. J., and Driscoll, J. F., "Local Flame Propagation Speeds Along Wrinkled Unsteady Stretched Premixed Flames, Twenty-Seventh Symposium (International) on Combustion, Boulder CO, 1998.

6. Mueller, C., Driscoll, J. F., Reuss, D. and Drake, M. "Effect of Unsteady Stretch on the Strength of a Flame Wrinkled by a Vortex", Twenty-Sixth Combust. Symp., 1996

7. Patniak, G., and Kailasanath, K., "Computational Study of Quenching in Flame-Vortex Interactions", Twenty Seventh Symp. on Combustion, 1998.

8. Clavin, P. and Williams, F.A., J. Fluid Mech. 116, 251, 1982.
9. Law, C.K., Twenty Second Symp. on Combustion, The Comb. Inst., 1988, p. 1381.
10. Tzeng, L.K., Ismail, M. and Faeth, G.M., Combust. Flame 95: 410, 1993.
11. Bedat, B. and Cheng, R.K., Combust. Flame 107: 13, 1996.

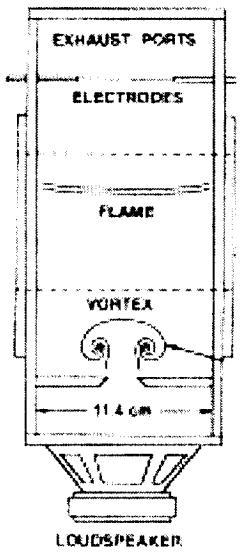

University of Michigan
Flame-Vortex Experiment

and Images of Flame Wrinkled
by the Vortex in Microgravity

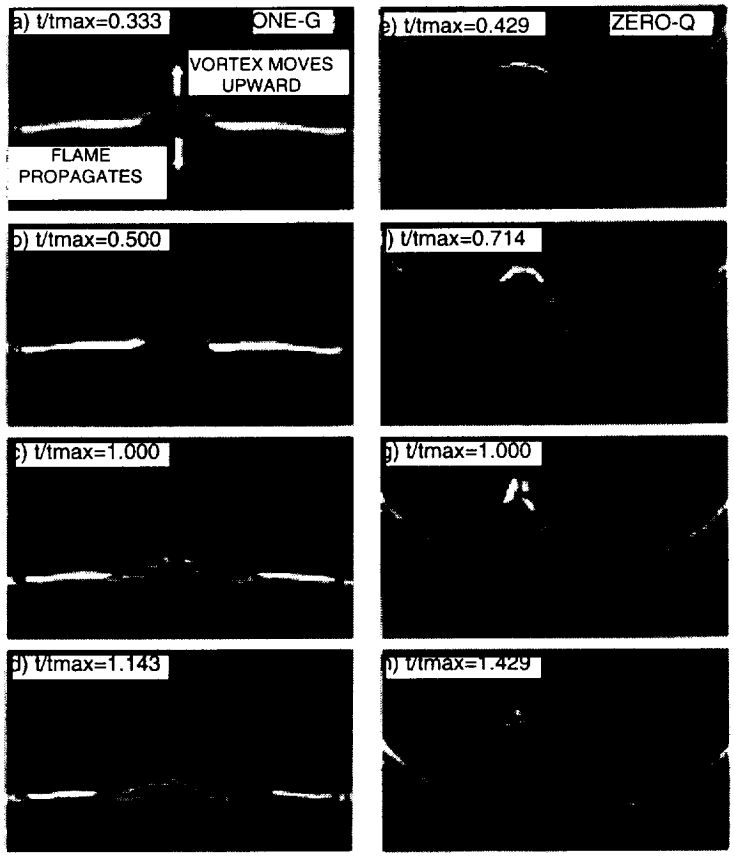

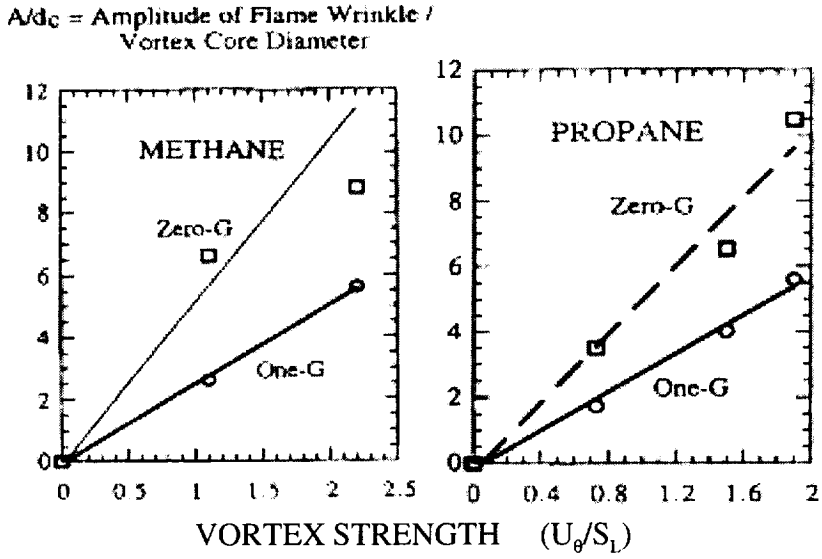

Fig. 1. Microgravity Flame-Vortex Interaction Results Showing that Buoyancy Reduces Flame Wrinkling, in part due to the Baroclinic Stabilization Mechanism. Results have been compared to the DNS simulations of Kailasanath, et al.

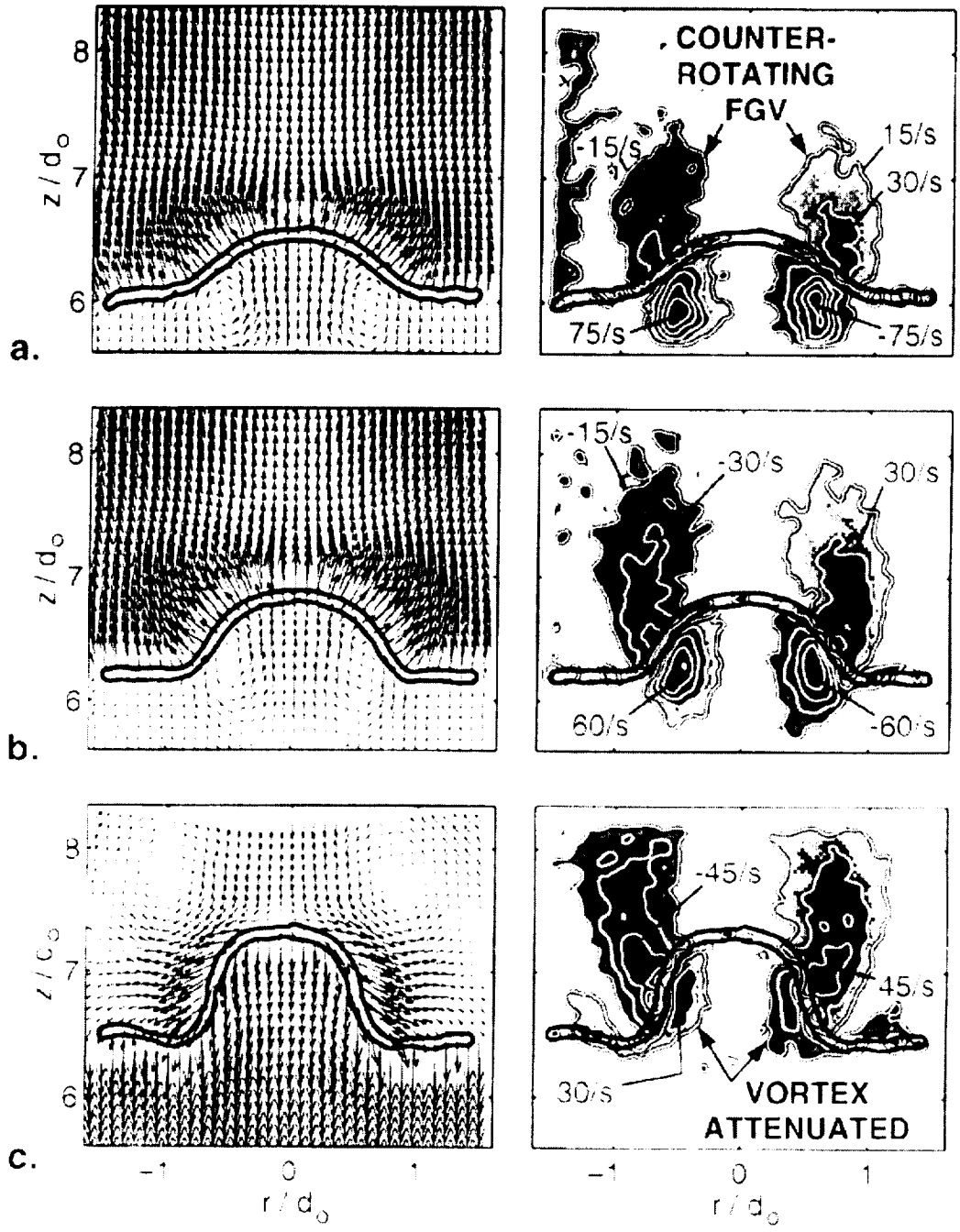

Figure 2. One-g PIV Images of Velocity Field (only every ninth vector shown) and the Vorticity Field ((blue = clockwise rotation, red = counterclockwise). Note that flame causes the initial vortex to be completely attenuated but that it also creates new "flame-generated" vorticity that is opposite in sign to the initial vortex.

THE INTERACTION OF A VORTEX RING WITH A DIFFUSION FLAME UNDER MICROGRAVITY CONDITIONS

Shin-Juh Chen[1] and **Werner J. A. Dahm**[2]
Laboratory for Turbulence and Combustion (LTC), Department of Aerospace Engineering
The University of Michigan, Ann Arbor, MI 48109-2140
[1]sjchen@engin.umich.edu, [2]wdahm@engin.umich.edu

INTRODUCTION

Turbulent diffusion flames represent by far the largest class of combustion problems, with applications ranging from aerospace propulsion systems, to industrial combustion processes, and to utility power generation systems. Direct investigation of turbulent flame processes to identify the fundamental effects of elementary flow, transport, and combustion phenomena can be difficult. Flame-vortex interactions provide a way to isolate these fundamental elements and study them under carefully controllable conditions. The flame-vortex configuration used in this study allows direct study of many of these phenomena, but has not previously been accessible to experiments owing to the fact that such investigations can only be conducted under microgravity conditions as shown by Chen & Dahm (1996, 1997). Limiting theoretical analyses by Karagozian & Manda (1986) and Manda & Karagozian (1988) for the corresponding two-dimensional problem allow comparisons, as do recent direct numerical simulations by James & Madnia (1996). Here we present results revealing effects of heat release and radiation on the combustion process.

EXPERIMENTAL RESULTS

A vortex ring is generated by issuing pressurized gaseous fuel into a plenum and axisymmetric nozzle. The interaction with a diffusion flame occurs as the ring exits the nozzle. A detailed description of the experiments, conducted in the NASA LeRC 2.2 sec drop tower, can be found in Chen & Dahm (1998). The fuel volume and ring circulation are set independently, and cover a wide range of conditions. A CCD camera records the visible luminosity of the resulting flame-vortex interaction, shown in inverse grayscale format in the attached figures.

Time sequences of reacting vortex rings in air are shown in Figs. 1-4. The reduced luminosity of Fig. 1 compared to Fig. 2 with similar ring circulation and fuel volume is due to the higher sooting propensity of propane than ethane. By doubling the circulation and fuel volume, both ethane and propane begin to soot heavily (Figs. 3-4). However, propane cases appear to soot much heavily which results in a more spherical shape compared to the more elongated shape of ethane cases. Heat loss from soot radiation must be accounted for the shape discrepancy. With more heat release going into heating the reactants, the ring's shape becomes more elongated and streamlines are more open (Manda & Karagozian, 1988).

Fuel consumption time is defined as the time when all the fuel injected have been consumed by the reaction. Theoretical fuel consumption time based on the simple spherical diffusion flame model used by Chen & Dahm (1998, 1999) agreed well with the observed burnout time (time when no visible luminosity is seen) for cases of propane, diluted propane with nitrogen, and ethane. In addition, there is also good agreement with methane cases as shown in Fig. 5.

The burning ring trajectories for a few cases are shown in Fig. 6, and it is evident that the inviscid theory of ring translational speed failed to follow the trajectories. Effects of heat release, which is to increase viscosity, must be incorporated into the model. Viscous model with constant viscosity (at ambient temperature and adiabatic temperature) also failed; this suggests that a model with time varying viscosity may be appropriate to capture the salient features of the

burning ring trajectories.

Subsequent work will include the measurements of soot number density using laser induced incandescence, and the measurements of major and minor species concentrations and temperatures using wave modulation spectroscopy with diode lasers. These measurements will allow the investigation of some of the key aspects of the diffusion flame/vortex ring interactions.

Chen, S.-J. & Dahm, W.J.A. (1996) Bull. Am. Phys. Soc. **41**, 1726 (abstract only).
Chen, S.-J. & Dahm, W.J.A. (1997) Proc. 4th Int'l. Microgravity Comb. Wkshp., NASA Publ. 10191, 191-196.
Chen, S.-J. & Dahm, W.J.A. (1998) Proc. 27th Int'l. Symp. Comb., The Combustion Institute, Pittsburgh.
Chen, S.-J. & Dahm, W.J.A. (1999) Proc. Joint Sections of U.S. Sections, The Combustion Institute, Pittsburgh.
James, S. & Madnia, C.K. (1996) Phys. Fluids **8**, 2400-2414.
Karagozian, A.R. & Manda, B.V.S. (1986) Combust. Sci. Tech. **49**, 185-200.
Manda, B.V.S. & Karagozian, A.R. (1988) Combust. Sci. Tech. **61**, 101-119.

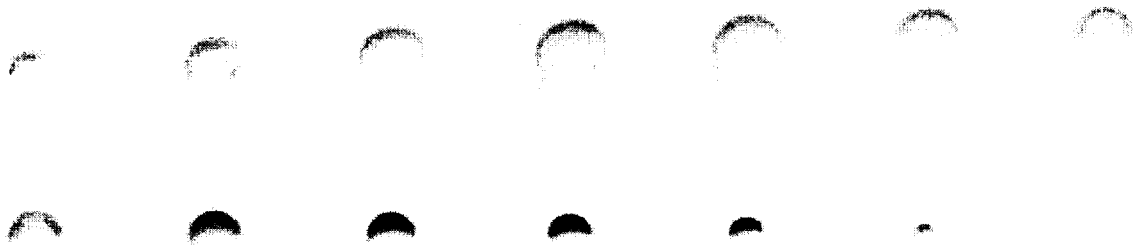

Fig. 1 Flame/vortex interaction using ethane as fuel, V = 15 cc and Γ = 117 cm^2/sec. The observed burnout time is 400 msec. Compare to Fig. 2.

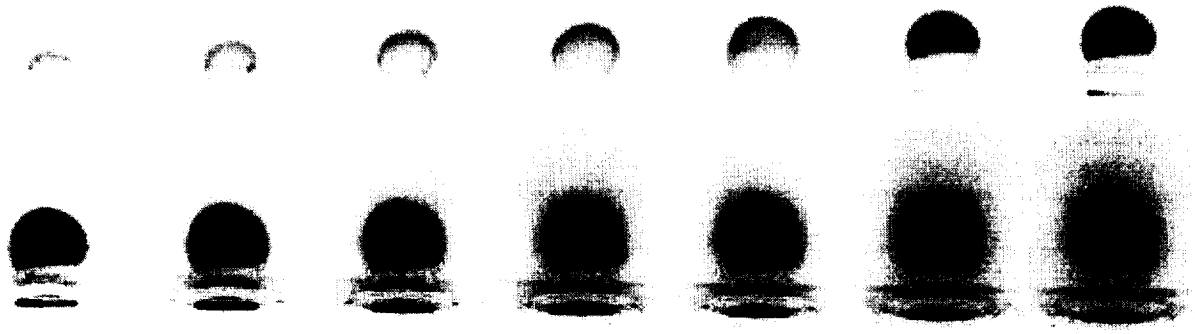

Fig. 2 Flame/vortex interaction using propane as fuel, V = 17 cc and Γ = 137 cm^2/sec. The observed burnout time is 1100 msec. Since Figs. 1 & 2 have the same fuel volume and circulation, they should have the same burnout time. Due to the heavy sooting in the propane case, the burnout time will be longer to accommodate the soot burnout. In addition, because of heat loss due to soot radiation in the propane case, the burning ring translated farther than the ethane case. Note that heat release has the effect of increasing viscosity thereby slowing down the vortex ring.

Fig. 3 Flame/vortex interaction using ethane as fuel, V = 26 cc and Γ = 282 cm^2/sec. The observed burnout time is 633 msec. Compare to Figs. 1 & 4.

Fig. 4 Flame/vortex interaction using propane as fuel, V = 26 cc and Γ = 273 cm^2/sec. The observed burnout time is 1267 msec. Compare to Figs. 2 & 3. Note that there is a gap of 17 frames between the second and third row of pictures. Since propane is sooting more heavily than ethane, Fig. 3 has an elongated shape because of higher heat release than Fig. 4. The difference in observed burnout time between Figs. 3 and 4, even though both have similar fuel volume and circulation, can be attributed to soot burnout. Furthermore, the burning ring in Fig. 4 has moved farther downstream than that in Fig. 3.

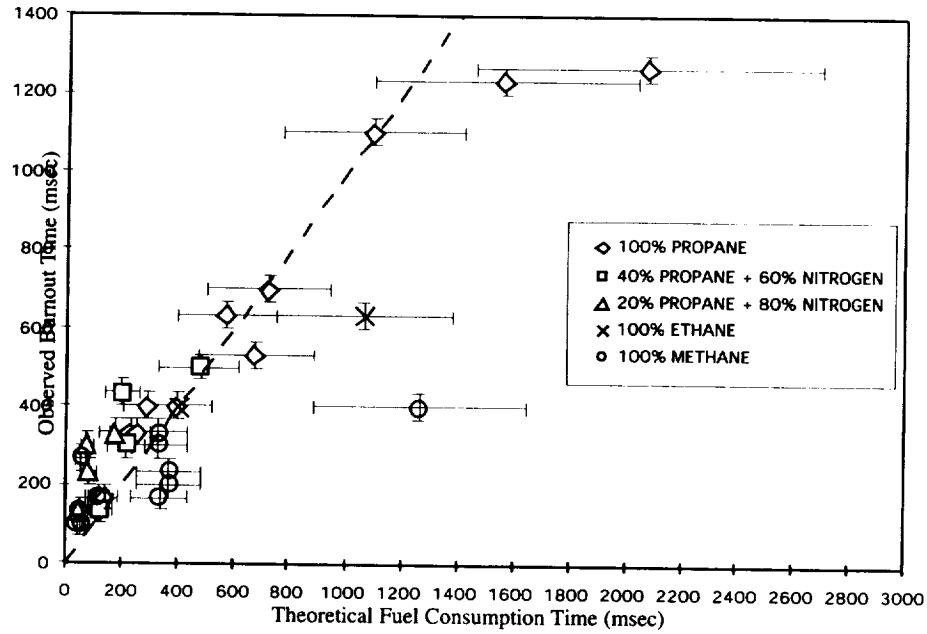

Fig. 5 Comparison of theoretical fuel consumption time, obtained via simple spherical diffusion flame estimate, with observed burnout time. This simple model agrees generally well with the experimental data, considering that the observed burnout times span by more than an order of magnitude. This model will need to incorporate the effects of soot burnout and circulation.

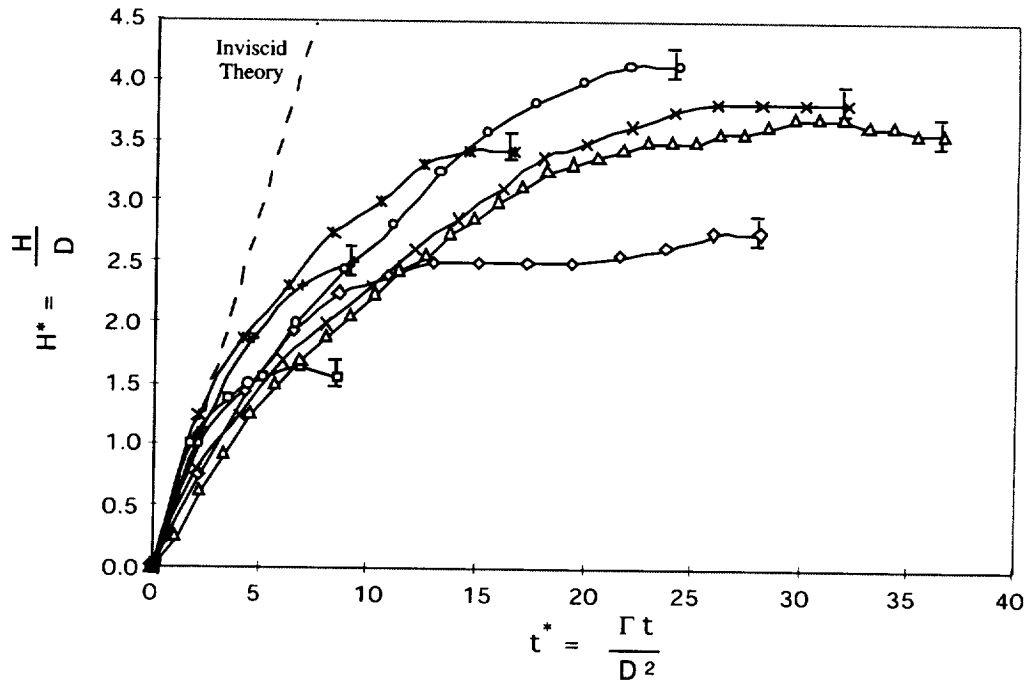

Fig. 6 Burning vortex ring trajectories for a few cases. The inviscid theory is only useful in capturing the early stage of translation where it is dominated by momentum. Effects of heat release and heat loss due to soot radiation must be incorporated in a model for the translation of burning vortex rings.

EFFECTS OF GRAVITY ON SHEARED TURBULENT NONPREMIXED FLAMES

S. E. Elghobashi and R. Zhong, Mechanical and Aerospace Engineering Department, University of California, Irvine, CA 92697.

Introduction

In the present study, we use the method of direct numerical simulation (DNS) to obtain the instantaneous, three-dimensional flow field of a turbulent nonpremixed flame subjected to uniform shear. The fuel and oxidant initially exist as two separate parallel streams. As the reactants mix, chemical reaction takes place and the resulting exothermic energy creates density gradients. In the presence of a gravity field, the spatial and temporal distributions of the induced buoyancy forces depend on the local density gradients, the magnitude and direction of the gravitational acceleration. Our objective is to gain an understanding of the multi-way interaction between turbulence, chemical reaction, imposed shear and buoyancy in nonpremixed flames.

Fig. 1 shows the imposed uniform velocity gradient along z direction where the mean velocity in $x-$direction is $U_1(z) = S\ (z - 0.5)$. S is the non-dimensional shear parameter. The instantaneous velocity is the sum of the prescribed mean velocity and the deviation from the mean. Thus, only the velocity deviation needs to be determined. The governing equations and numerical procedure are provided in Ref. [1] & [2]. The value of the non-dimensional shear parameter S is prescribed equal to 1 in all simulations, which results in a strain number $St = (v_{rms}/l)/S = 0.4$ at the initial time $t = 1.5$. St represents the ratio of the strain rate of the energy-containing eddies (large-scale strain rate) to that of the mean flow. The shear flow simulations require a parallelpiped computational domain instead of a cube. The longer side length in the $x-$direction allows the large vortical structures to develop in time without violating the periodic boundary condition imposed in the streamwise direction. This boundary condition is satisfied by insuring that the two-point Eulerian velocity correlations vanish within an axial distance smaller or equal to half the domain length in the $x-$direction. Periodic boundary conditions are also imposed in the spanwise (y) direction. Outflow boundary conditions are imposed at the top and bottom z planes of the domain. The grid used for the computations consists of 192x96x96 mesh points in the x, y and z directions respectively.

Results

In the Fourth Microgravity Workshop we presented the results of our DNS of unsheared buoyant nonpremixed flames. Here we present some of the results of the sheared nonpremixed flames. In the presence of shear and exothermic reaction, we observe that the fluctuating velocity u is typically negative in the upper half region above $z = 0.5$, while positive in the lower half region below $z = 0.5$. This pattern does not exist in the flames *without* imposed mean shear. Fig. 1 shows the mean velocity profile $U_1(z)$ (thick solid line) associated with the imposed uniform mean shear where $U_1(z)$ is zero at $z = 0.5$. The flow expands along the vertical z direction due to the exothermic chemical reaction, in the presence of periodic boundary conditions in the x and y directions. The center of expansion is located around

$z = 0.5$. The fluid particles above $z = 0.5$ are always carried upwards by the expansion velocity w, while the fluid particles below $z = 0.5$ move downwards. Since these fluid particles are transported from the smaller to larger mean velocity layer, a deficit of the host streamwise velocity, u, is generated. The planar average of the fluctuating velocity u is depicted by the hollow arrowheads. The profile of $< u >$ is denoted by the dashed line. The correlation $< uw >$ is negative (not shown), thus demonstrating that the kinetic energy is transferred from the mean motion to the fluctuating field.

Fig. 2 shows the contours of the spanwise vorticity component ω_y, in the central vertical $x-z$ plane at time $t = 5$ for nonbuoyant (Froude number $Fr = \infty$) and buoyant ($Fr = 10.6$) flames. Well-organized coherent structures of high-vorticity are observed as elongated vortex filaments. A vorticity transport equation, for a variable density flow *subjected to a uniform shear*, can be written as:

$$\begin{aligned}\frac{D\omega_i}{Dt} &= -U_1(x_3)\,\frac{\partial \omega_i}{\partial x_1} + \omega_m\,\frac{\partial u_i}{\partial x_m} + S\,\frac{\partial u_i}{\partial x_2} + S\,\omega_3\,\delta i1 - (\omega_i + S\,\delta_{i2})\,\frac{\partial u_m}{\partial x_m} \\ &+ \frac{\varepsilon_{ijk}\,\rho_{,j}\,p_{,k}}{\rho^2} + \frac{1}{Re}\left[\frac{1}{\rho}\frac{\partial^2 \omega_i}{\partial x_m \partial x_m} - \frac{1}{\rho^2}\,\varepsilon_{ijk}\,\rho_{,j}\left(\frac{\partial u_k}{\partial x_m \partial x_m} + \frac{1}{3}\,\frac{\partial}{\partial x_k}\left(\frac{\partial u_m}{\partial x_m}\right)\right)\right] \quad (1)\end{aligned}$$

The first r.h.s. term represents the advection of vorticity by the mean shear which causes the spatial structure of vorticity to incline towards the streamwise (x) direction *without* changing the direction of vorticity vector. The second describes vortex stretching. The third term represents either a conversion of vorticity from the mean vorticity to the i-th component ($i \neq 2$) or a change in intensity of the spanwise vorticity ($i = 2$) [3]. The fourth term describes a conversion of vorticity from the vertical to the streamwise component by the mean shear. This term enhances the inclination of vortical structure towards the streamwise direction *with* changing the direction of vorticity vector. The fifth term is the vorticity sink due to velocity divergence. The sixth and seventh term are the baroclinic torque and viscous diffusion, respectively.

The mean advection by the shear flow is mainly responsible for the vortex tubes' inclination toward the x axis. These vortex tubes are also elongated and intensified by stretching and deformed into hairpin shapes. From our spectral analysis (not shown), the mean shear strongly dominates other mechanisms outside the central reaction zone. Thus, we observe quite similar flow fields outside the reaction zone in both the nonbuoyant and buoyant flows, as shown in Fig. 2a & 2b. In the central reaction zone of the nonbuoyant flame, the vorticity is suppressed by the heat release (fifth term in Eqn. (1)). While in the buoyant flame, the counter rotating vortices still exist. These vortices are generated by the baroclinic torque (sixth term in Eqn. (1)). In contrast with nonsheared flames, the counter rotating vortices here are being squashed in the z direction and stretched in the x direction.

Fig. 3 shows the temporal development of the root-mean-square vorticity $< \omega^2 >^{1/2}$ and its directional components $< \omega_1^2 >^{1/2}, < \omega_2^2 >^{1/2}, < \omega_3^2 >^{1/2}$, sampled over the mixture fraction range $0.5 \leq F \leq 0.9$, for the nonbuoyant and buoyant flames. By sampling over the mixture fraction field, the initial homogeneous unmixed scalar regions are thereby eliminated from the statistics, thus the characteristics of the central reaction zone can be investigated. Both flows have equal r.m.s. vorticity components at time $t = 1.5$, due to the initial isotropic flow condition. Between $t = 1.5$ and 2.5, a reduction of r.m.s. of vorticity is observed due

to the large heat release during that initial period. A finite period of time is required for the enstrophy production by mean shear to counteract the effects of viscous dissipation and heat release. The effects of mean shear appear to be well established at time $t = 2.5$.

In the absence of gravity, the flow is symmetrical around the stoichiometric F_{st} surface. Thus, the temporal development sampled over $0.1 \leq F \leq 0.5$ are nearly identical to those of $0.5 \leq F \leq 0.9$. In contrast to the flow behavior outside the reaction zone (not shown), the streamwise component $< \omega_1^2 >^{1/2}$ is smaller than $< \omega_2^2 >^{1/2}$ and $< \omega_3^2 >^{1/2}$. The heat release suppresses the enstrophy in the reaction zone, thus the effect of stretching by mean shear is minimized. In the buoyant flow, the temporal behavior of $< \omega^2 >^{1/2}$ depends on the region of the flow. In Fig. 3(b), the streamwise component $< \omega_1^2 >^{1/2}$ exceeds other two for $t \geq 4$. The vorticity is enhanced by the buoyancy in the upper region of the reaction zone. Thus, the effect of stretching by mean shear greatly increases the streamwise component ω_1.

References

[1] S. Elghobashi, R. Zhong, and O. Boratav. Effects of gravity on turbulent nonpremixed flames. *Phys. Fluids, Submitted*, 1998.

[2] R. Zhong. Direct numerical simulation of gravity effects on turbulent nonpremixed reacting flows. *Ph.D. dissertation, Univ. of California, Irvine*, 1999.

[3] S. Kida and M. Tanaka. Dynamics of vortical structures in a homogeneous shear flow. *J. Fluid Mech.*, 274:43-68, 1994.

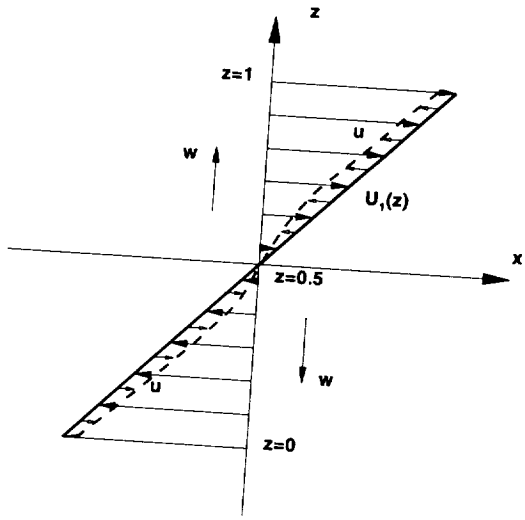

Figure 1: The imposed mean velocity profile $U_1(z)$ is illustrated by thick solid line. The fluctuating velocity u is depicted by the hollow arrowheads. The profile of the planar average $< u >$, measured from the solid line, is denoted by the dashed line.

(a) (b)

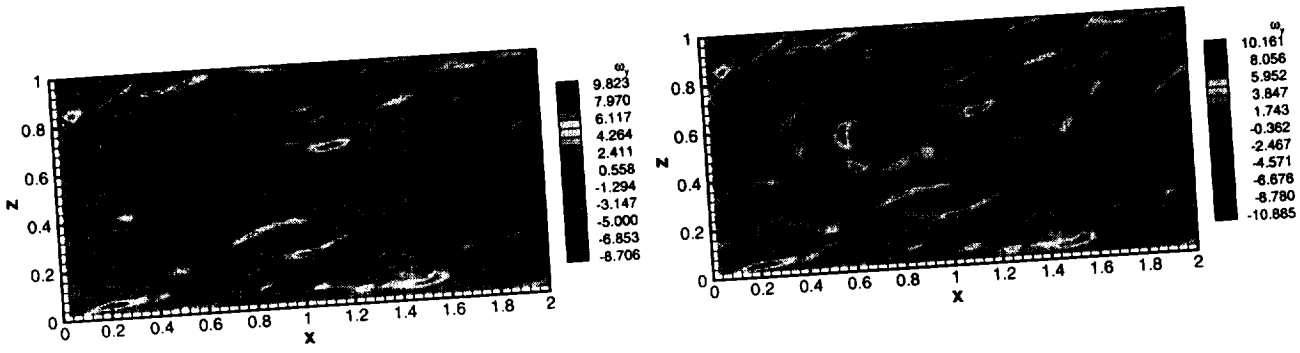

Figure 2: The contours of spanwise vorticity component ω_y in the central $x - z$ plane, at time $t = 5$, in (a) nonbuoyant and (b) buoyant flames subjected to imposed shear.

(a) (b)

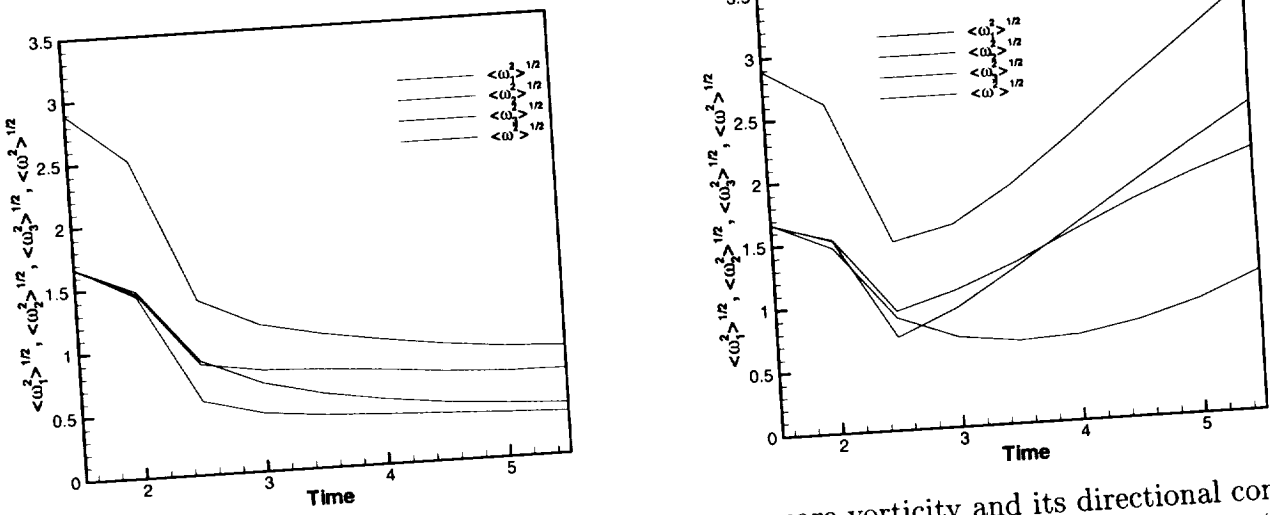

Figure 3: Temporal development of the root-mean-square vorticity and its directional components, sampled over the mixture fraction range $0.5 \leq F \leq 0.9$, for (a) nonbuoyant and (b) buoyant flames subjected to imposed shear.

Sprays and Droplet Arrays

COMBUSTION OF INTERACTING DROPLET ARRAYS IN A MICROGRAVITY ENVIRONMENT

D.L. Dietrich[1], P.M. Struk, [2], K. Kitano[3] and M. Ikegami[3]; [1] NASA Glenn Research Center, Cleveland, Ohio 44135 (Daniel.Dietrich@grc.nasa.gov), [2] National Center for Microgravity Research, [3] Hokkaido National Industrial Research Institute.

INTRODUCTION

Investigations into droplet interactions date back to Rex et al.[1]. Recently, Annamalai and Ryan[2] and Annamalai[3] published extensive reviews of droplet array and cloud combustion studies. The authors studied the change in the burning rate constant, k, (relative to that of the single droplet) that results from interactions. Under certain conditions, there exists a separation distance where the droplet lifetime reaches a minimum, or average burning rate constant is a maximum[1,4-8]. Additionally, since inter-droplet separation distance, L, increases relative to the droplet size, D, as the burning proceeds, the burning rate is not constant throughout the burn, but changes continuously with time[7-10].

Only Law and co-workers[7,8] and Mikami et al.[11] studied interactions under conditions where buoyant forces were negligible. Comparing their results with existing theory, Law and co-workers found that theory over predicted the persistency and intensity of droplet interactions. The droplet interactions also depended on the initial array configuration as well as the instantaneous array configuration. They also concluded that droplet heating was retarded due to interactions and that the burning process did not follow the "D-squared" law. Mikami et al.[11] studied the combustion of a two-droplet array of heptane burning in air at one atm pressure in microgravity. They showed that the instantaneous burning rate constant increases throughout the droplet lifetime, even for a single droplet. Also, the burn time of the array reached a minimum at a critical inter-droplet spacing.

In this article, we examine droplet interactions in normal and microgravity environments. The microgravity experiments were in the NASA GRC 2.2 and 5.2 second drop towers, and the JAMIC (Japan Microgravity Center) 10 second drop tower. Special emphasis is directed to combustion under conditions that yield finite extinction diameters, and to determine how droplet interactions affect the extinction process.

EXPERIMENTAL HARDWARE AND DATA ANALYSIS

The experiments utilized the classical fiber-supported droplet combustion technique. A 125 or 230 μm (depending on the initial droplet size) fiber with a small bead (approximately 1.5-2.0 times the fiber diameter) supported the droplets. The fuel was n-decane for all of the tests. A small coiled hot-wire, withdrawn immediately after ignition, ignited the droplets.

The data for all of the experiments was from two orthogonally located video cameras. The first camera provided a magnified, backlit view of the droplet to obtain the droplet regression history. The second was an orthogonal view of the flame. The droplet diameter reported herein is an equivalent size obtained by equating the measured volume or the projected area of the droplet to that of the equivalent sphere or circle, respectively[12]. For the data herein, we report both an average and an instantaneous k. The average k comes from a linear fit of the data between t = $0.1*t_b$ and $0.9*t_b$, where t_b is the total burn time. We use this in cases where the deviation from linear behavior is small. The instantaneous k comes from a modified cubic spline fit to the experimental data[13].

EXPERIMENTAL RESULTS

Figure 1 shows the average burning rate constant as a function of separation distance normalized by the initial diameter, L/D_o, for three different pressures in normal gravity. This figure clearly shows that the average burning rate constant is not significantly affected by interactions. This, at first review, may seem in conflict with existing studies. We note that, however, in the work of Mikami et al.[11], even though the instantaneous burning rate for an array may differ from the single droplet burning rate by as much as 70%, the droplet lifetime, or average burning rate constant varies less than 10% for L/D_o greater than or equal to 6. The greatest change occurs early in the droplet lifetime, during the droplet heating period. After this period is over, interaction effects on the burning rate constant are small.

At pressures below 90 torr in normal gravity, the flame surrounding the droplet(s) extinguished at a finite droplet diameter. Figure 2 shows the extinction droplet diameter as a function of pressure for single droplets and two droplet arrays at two different inter-droplet spacings. The single droplet results compare favorably with the work of Chung and Law[14], with the extinction droplet diameter increasing with decreasing pressure. Figure 2 clearly shows that interaction effects have a significant influence on the extinction droplet diameter.

There are three other important points that are not represented in Figure 2. First, at inter-droplet spacings below 12 mm (8 mm was the next smallest size), the flame did not extinguish at a finite droplet diameter. Or, more specifically, the extinction droplet diameter was smaller than the supporting fiber and bead and thus was not measurable. Second, the interaction effect on flame extinction was present whether there was an envelope flame surrounding both droplets or individual flames around each droplet. Finally, the array results in Figure 2 are for identically sized droplets. There were a large number of tests (not shown here) where there was a significant difference in the initial droplet size, at pressures that yielded finite extinction droplet diameters. In these cases, the flame around the larger droplet extinguished immediately (within 0.033 second or 1 video frame) after the smaller droplet disappeared. This occurred for cases where a single envelope flame surrounded both droplets and where individual flames surrounded each droplet.

The first series of microgravity tests were of two binary-droplet arrays and a single droplet in a 0.17 oxygen mole fraction, 380 torr ambient in the JAMIC facility. Figure 3 shows the results for a single droplet and two, two-droplet arrays. The behavior was as expected, with burn time and instantaneous k increasing slightly with decreasing separation distance. The burning behavior, however, was very non-linear. Figure 3 also shows the change in the instantaneous burning rate constant for the single droplet test.

We are currently analyzing microgravity data from the JAMIC facility for droplet interactions under conditions of extinction.

DISCUSSION

The effect of interactions during droplet burning occurs as a result of two competing mechanisms. The droplets compete for oxidizer, and this effect tends to weaken the burning of each individual droplet. The heat loss between the droplets is reduced, however, and this tends to strengthen the flame. At large separation distances, neither effect is significant, and there is no interaction effect. The results in this work show that for burning in the diffusion dominated regime (negligible chemical kinetic effects), the net effect of these two competing mechanisms averaged over the lifetime of the droplet is quite small. Thus, the average burning rate constant varies only slightly with inter-droplet separation distance.

Near extinction, however, the effects of interaction are significant. In this case, the diffusive and chemical kinetic time-scales are comparable. Extinction occurs when the characteristic

residence time is smaller than the characteristic chemical reaction time. The residence time is not significantly affected by interactions since both the burning rate constant and flame standoff ratio distance (for individual flames) are nearly the same (Figure 4). Thus, interactions primarily affect the characteristic chemical reaction time. Diminished oxygen transport to the flame tends to weaken the flame, but the reduced heat loss tends to strengthen the flame. The characteristic chemical time is exponentially dependent on temperature, and linearly dependent on the local oxygen concentration (assuming first order dependence in oxidizer concentration). The reduced heat loss thus dominates near extinction.

We are currently developing a numerical model for the binary droplet array. The model is based on an existing model of the candle flame[15]. It includes the effects of finite rate chemistry (single step currently) and gas-phase radiative energy loss.

ACKNOWLEDGEMENTS

The authors would like to acknowledge S. Honma and K. Ikeda of the Hokkaido National Industrial Research Institute for their help with the JAMIC experiments, and C. Sims and B. Picot for their help with the normal gravity experiments.

REFERENCES

1. Rex, J.F., Fuhs, A.E. and Penner, S.S. *Jet Propulsion* **26**, 179 (1956).
2. Annamalai, K. and Ryan, W. *Progress in Energy and Combustion Science* **18**, 221-295 (1992).
3. Annamalai, K. *Mechanics and Combustion of Droplets and Sprays* , ed. H.H. Chiu and N. Chigier, Begell House Inc., New York, New York, 116-160 (1995).
4. Sangiovanni, J.J. and A.S. Kesten *Sixteenth Symposium (International) on Combustion* / The Combustion Institute, 577-592 (1976).
5. Fedoseeva, N.V. *Advances in Aerosol Physics* **2**, 110-117 (1972).
6. Fedoseeva, N.V. *Advances in Aerosol Physics* **3**, 27-38 (1973).
7. Miyasaka, K. and C.K. Law *Eighteenth Symposium (International) on Combustion* / The Combustion Institute, 283-292 (1981).
8. Xiong, T.Y., C.K. Law, C.K. and K. Miyasaka *Twentieth Symposium (International) on Combustion* / The Combustion Institute, 1781-1787 (1984).
9. Labowsky, M. *Combustion Science and Technology* **18**, 145-151 (1978).
10. Labowsky, M. *Combustion Science and Technology* **22**, 217-226 (1980).
11. Mikami, M., Kato, H., Kono, M. and Sato, J. *Twenty-Fifth Symposium (International) on Combustion* / The Combustion Institute, 423-428 (1995).
12. Struk, P., Ackerman, M., Nayagam, V. and Dietrich, D. "Fiber Effects in Droplet Combustion," to appear in Microgravity Science and Technology (1999).
13. Struk, P.M., Dietrich, D.L., Sims, C., Picot, B., Kitano, K., Honma, S., Ikeda, K., Ikegami, M. "Interacting Droplet Combustion Under Conditions of Extinction," Joint Meeting of the United States Sections of the Combustion Institute (1999).
14. Chung, S. and Law, C.K. *Combustion and Flame* **64**, 237-241 (1986).
15. Dietrich, D.L., Ross, H.D., Shu, Y. and T'ien, J.S. "Candle Flames in Non-Buoyant Atmospheres," submitted.

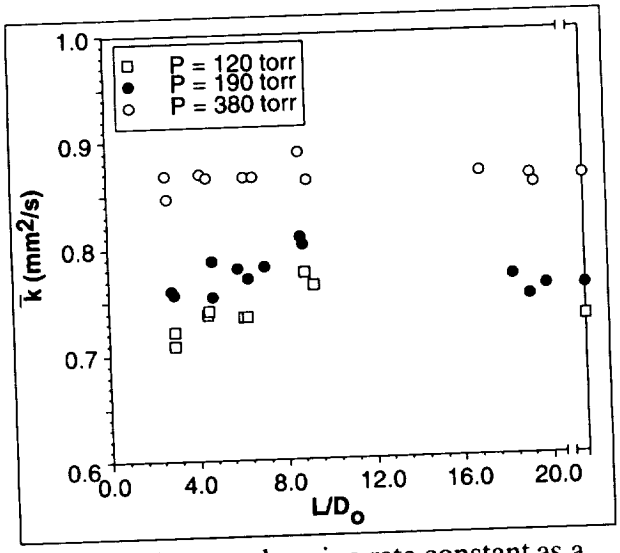

Figure 1. Average burning rate constant as a function of inter-droplet spacing for three pressures in normal gravity.

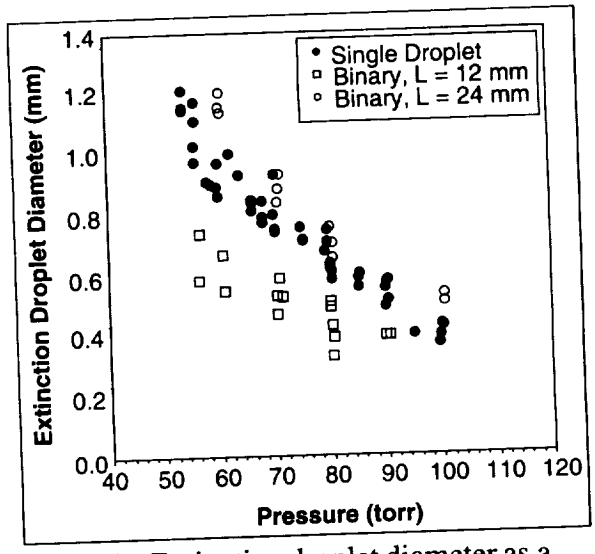

Figure 2. Extinction droplet diameter as a function of pressure for a single droplet and two droplet arrays in normal gravity.

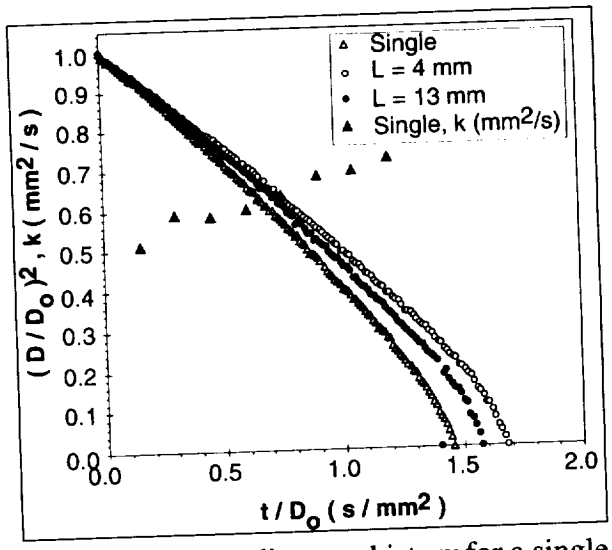

Figure 3. Droplet diameter history for a single droplet and two binary droplet arrays in a 0.17 oxygen mole fraction, 380 torr ambient. The burning rate constant for the single droplet is also shown. Do ~ 1.7 mm.

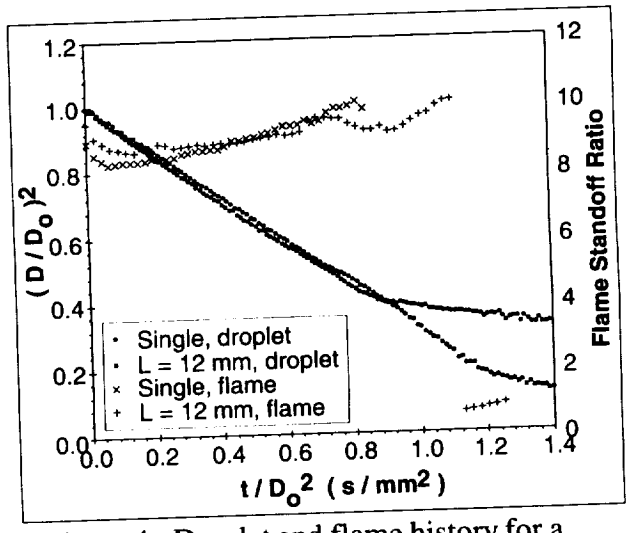

Figure 4. Droplet and flame history for a single droplet and binary droplet array (L = 12 mm). The initial droplet size was 1.2 mm. The ambient pressure was 70 torr. (normal gravity)

Formation and Levitation of Unconfined Droplet Clusters

S. Liu[1] and G. A. Ruff[2]
[1]Graduate Research Assistant (sg95x4sj@post.drexel.edu)
[2]Associate Professor (gruff@coe.drexel.edu)
Mechanical Engineering and Mechanics Department
Drexel University
Philadelphia, PA 19104

INTRODUCTION

Combustion experiments using arrays of droplets seek to provide a link between single droplet combustion phenomena and the behavior of complex spray combustion systems. Both single droplet and droplet array studies have been conducted in microgravity to better isolate the droplet interaction phenomena [1-4] and eliminate or reduce the confounding effects of buoyancy-induced convection. In most experiments involving droplet arrays, the droplets are supported on fibers to keep them stationary and close together before the combustion event. The presence of the fiber, however, disturbs the combustion process by introducing a source of heat transfer and asymmetry into the configuration. As the number of drops in a droplet array increases, supporting the drops on fibers becomes less practical because of the cumulative effect of the fibers on the combustion process.

The overall objective of this research is to study the combustion of well-characterized drop clusters in a microgravity environment. Direct experimental observations and measurements of the combustion of droplet clusters would fill a large gap in our current understanding of droplet and spray combustion and provide unique experimental data for the verification and improvement of spray combustion models. This paper describes current work on the design and performance of an apparatus to generate and stabilize droplet clusters using acoustic and electrostatic forces.

EXPERIMENTAL APPROACH

The difficulty in producing an unconfined cluster of liquid drops in ground-based experiments is that drops begin to settle or disperse before a cluster of drops can be formed and stabilized. The experimental apparatus developed in this study is unique because it allows a well-characterized drop cluster to be formed and stabilized in a resonant acoustic field. Experiments can then be conducted in a drop tower by forming the drops, stabilizing them in the acoustic field, and then *turning off the field* immediately prior to the combustion event. Figure 1 shows a sketch of the experimental apparatus developed in this work. It consists of an acoustic levitator assembly, an electrostatic charging unit and a droplet generator. The droplet cluster is formed by introducing drops into the antinode of a resonant acoustic field developed between the acoustic horn and reflector. An electrostatic charge placed on the drops during their formation prevents them from coalescing into a single large drop in the antinode. The acoustic field not only supports the droplets against gravity but also exerts a lateral positioning force that helps maintain the shape of the cluster. In the following sections, details of the experimental apparatus, operating procedure, and performance characteristics are presented.

Acoustic Levitator

The single-axis acoustic driver assembly consists of two piezoelectric transducers in a sandwich configuration similar to that developed by Cao *et al.* [5]. Aluminum transmitter blocks are placed on both sides of the sandwich transducer and sized to create a plane standing wave in the material when oscillating at 20 kHz. A titanium stepped acoustic horn is tightly coupled to the forward transmitter to amplify the transducer displacement. The tip of the horn is 29 mm in diameter and directs the acoustic wave towards the reflector (50-mm diameter). For these conditions, an acoustic pressure well 8.5-mm high and 11 mm in diameter can be obtained. A sound pressure level of approximately 180 dB provides a sufficient force to levitate drops up to 5 mm in diameter.

Droplet Generator

An on-demand droplet generator was developed to introduce droplets into the acoustic levitator. The liquid fuel is placed in a 0.1-ml syringe having a 90-micron hypodermic needle attached at its end. The syringe assembly is mounted on a traversing stage controlled by a stepping motor. A piezoelectric screw positioner depresses the plunger of the syringe to form drops as small as 300 microns on the end of the needle. The liquid is charged to help break up the drop placed on the end of the hypodermic needle and to prevent the drops that are produced from coalescing in the antinode of the acoustic field. An induction charging system consisting of a copper ring mounted on the syringe and an adjustable 0 – 10 kV high voltage power supply charges the liquid as it passes through the needle.

Imaging system

An imaging system consisting of a fiber-optic light sheet illuminator, a 45-deg reflecting mirror and a CCD video camera allows the formation, stabilization, and ultimately, the combustion of the droplet cluster to be clearly observed. The light sheet produced by the fiber optic illuminator is directed towards the plane of the droplet cluster. The 45-deg mirror is mounted above the acoustic reflector and allows the cluster to be viewed from the top through a window in the reflector. The CCD camera and microscope lens is positioned to view the cluster. The image is transmitted to the computer to monitor the experiment and to a video recorder.

EVALUATION OF SYSTEM PERFORMANCE

The sound pressure level between the driver and reflector was mapped using a 3-mm diameter microphone. As shown in Fig. 2a, two antinodes are produced when the driver and reflector are 20 mm apart. The radial sound pressure measurements in Fig. 2b show that a pressure well having a radius of approximately 4-mm is also formed.

Formation of Droplet Clusters

Because methanol has been used in previous microgravity investigations [1,2] and can be easily charged, it was used in the initial tests of the acoustic levitator system. Figures 3 and 4 show images of droplet clusters, viewed from above, having 3 and 13 droplets, respectively. Table 1 shows the average drop sizes, drop spacing, and cluster sizes from these images, as well as for a cluster containing 8 drops. The group combustion number for these configurations is also

shown in Table 1. Based on the criteria given by Annamalai and Ryan [6], these clusters lie in the group combustion regime. More specifically, these conditions are between the internal and external group combustion regimes, where the flame front lies within the droplet cluster and both isolated drop and group combustion occurs. Therefore, using this apparatus, we will be able to perform a detailed experimental analysis of group combustion phenomena. Current work is focusing on developing methods to introduce a greater number of droplets into the cluster and installing apparatus to conduct combustion experiments.

SUMMARY

In the current work, a single axis acoustic levitator has been designed and constructed. Droplets are introduced into the field by using the acoustic field itself to break up a charged droplet on the end of a hypodermic needle. The design of the acoustic levitator provides both a vertical and lateral positioning force on the droplet cluster. By specifying the charge placed on the initial drop, stable clusters containing between 2 and 15 drops have been generated. Current work focuses on installing an ignition system so that the drops can be ignited. The entire apparatus will be incorporated into a drop tower test rig so that experiments can be conducted under microgravity.

ACKNOWLEDGEMENT

This work is supported by the NASA Office of Life and Microgravity Sciences and Applications, Microgravity Combustion Science Program (NASA Grant NAG3-1884, Dr. Randy Vander Wal, Technical Monitor.)

REFERENCES

1. D. L. Dietrich, P. M. Struk, K. Kitano, K. Ikeda, and S. Honma "Combustion of Interacting Droplet Arrays in a Microgravity Environment," Proceedings of the Fourth International Microgravity Combustion Workshop (NASA Conference Publication 10194), Cleveland, Ohio, May 19-21, 1997.
2. I. Gokalp, C. Chauveau, B. Vieille, T. Kadota, and D. Segawa, "High Pressure Burning of Methanol Droplets: A Comparison between Parabolic Flight and Drop Tower Experiments," Proceedings of the Fourth International Microgravity Combustion Workshop (NASA Conference Publication 10194), Cleveland, Ohio, May 19-21, 1997.
3. B. D. Shaw, "Combustion of Two-Component Miscible Droplets in Reduced Gravity," Proceedings of the Fourth International Microgravity Combustion Workshop (NASA Conference Publication 10194), Cleveland, Ohio, May 19-21, 1997.
4. C. H. Wang and G. J. Ueng, "An Experimental Investigation of Fuel Droplet Combustion Under Micro-Gravity," *Int. Comm. Heat Mass Transfer*, Vol. 24, No. 7, pp. 931-944, 1997.
5. Z. Cao, S. Liu, Z. Li, and M. Gong "Development of an Acoustic Levitation Reactor," *Powder Technology*, Vol. 69, pp. 125-131, 1992.
6. K. Annamalai and W. Ryan, "Interactive Processes in Gasification and Combustion. Part I: Liquid Drop Arrays and Clouds," *Progress in Energy and Combustion Science* Vol. 18, pp. 221, 1992.

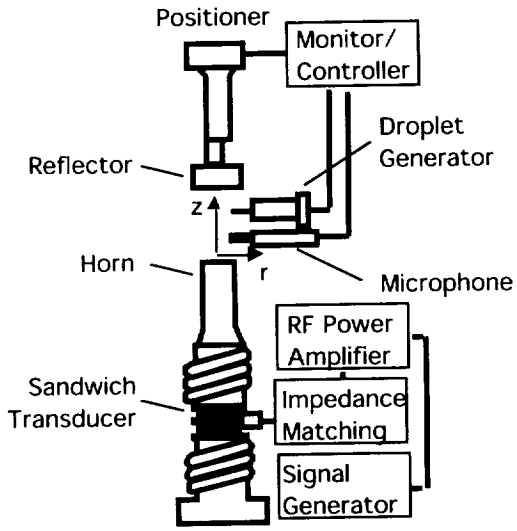

Figure 1. Acoustic levitation and drop generation apparatus

Table 1. Characteristics of Droplet Clusters

Number of Drops	Cluster Diameter (mm)	Drop Diameter (mm)	Drop Spacing (mm)	G
3	3.18	0.34	2.58	0.96
8	4.88	0.20	1.96	0.98
13	7.43	0.19	2.22	1.00

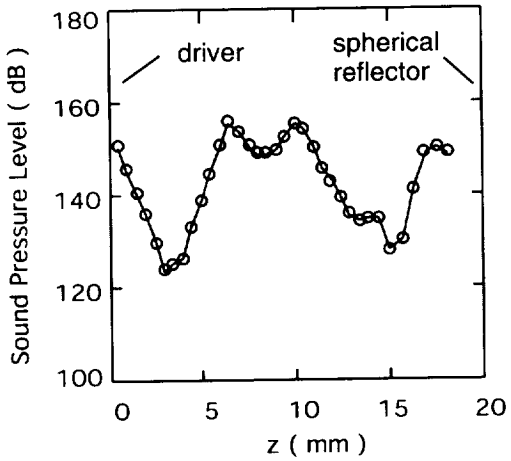

(a) axial sound pressure on r = 0

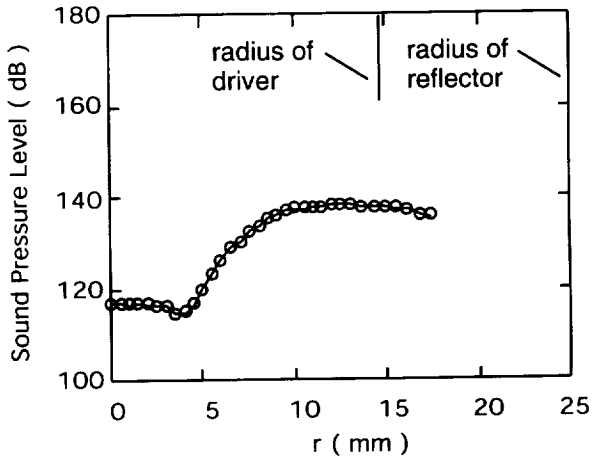

(b) radial sound pressure at z = 3 mm

Figure 2. Sound pressure level between the acoustic driver and reflector

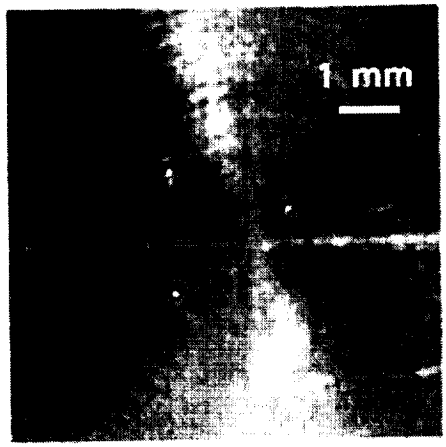

Figure 3. Droplet cluster containing 3 drops

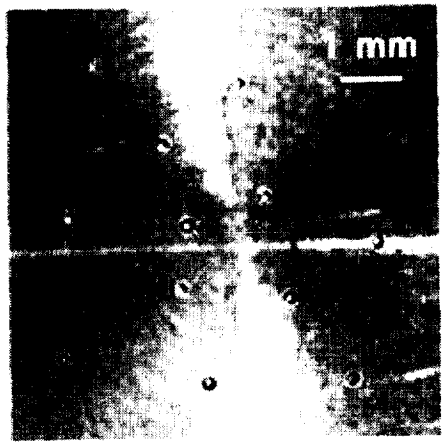

Figure 4. Droplet cluster containing 13 drops

MICROGRAVITY EXPERIMENTS ON COMBUSTION OF MONODISPERSED AND MONO-SIZED FUEL DROPLET CLOUDS

H. Nomura[1], M. Koyama[1], Y. Ujiie[1], J. Sato[2], M. Kono[3] and S. Yoda[4]

[1] College of Industrial Technology, Nihon University, 1-2-1 Izumi-cho, Narashino-shi, Chiba 275-8575, Japan, nomura@me.cit.nihon-u.ac.jp, [2] Research Institute, Ishikawajima-Harima Heavy Industry Co., Ltd., 3-1-15 Toyosu, Koto-ku, Tokyo 135-8732, Japan, [3] Department of Aeronautics and Astronautics, University of Tokyo, 7-3-1 Hongo, Bunkyo-ku, Tokyo 133-8656, Japan, [4] Space Utilization Research Center, National Space Development Agency of Japan, 2-1-1 Sengen, Tsukuba, Ibaraki 305-8505, Japan

INTRODUCTION

Monodispersed and mono-sized droplet clouds as a simple model of sprays have been applied to fundamental studies on spray combustion by some researchers [1-4]. Burgoyne and Cohen [1], Mizutani and Ogasawara [2] and Hayashi and coworkers [4] investigated mainly flammability limits of droplet clouds. They used droplet clouds falling down in a combustion tube. Hayashi and Kumagai [3] investigated flame propagation in stationary droplet clouds. To realize uniform and stationary droplet clouds, they developed a rapid expansion apparatus, which was based on the principle of Wilson's cloud chamber. They used small droplet clouds for experiments because large droplets fell down during the generation process of droplet clouds. In the present work, flame propagation in fuel droplet clouds was studied experimentally with a rapid expansion apparatus. To prevent droplets from falling down by gravity, for large droplet clouds, experiments were performed under microgravity conditions. A new type of rapid expansion apparatus was developed for microgravity experiments.

EXPERIMENTAL APPARATUS AND PROCEDURE

Monodispersed and mono-sized droplet clouds were generated by rapid and uniform temperature drop of saturated fuel vapor-air mixtures. The principle of the generation of droplet clouds is the same as that of Wilson's cloud chamber. The rapid and uniform temperature drop was realized by rapid pressure reduction of fuel vapor - air mixtures as Hayashi and Kumagai [3] employed. Figure 1 shows a schematic diagram of the experimental apparatus. A rapid expansion device consisted of a high pressure chamber, main valve, flow control valve and exhaust gas reservoir. Rapid expansion started when the main valve was opened and ended when the pressure of the high pressure chamber balanced with the pressure of the exhaust gas reservoir. Since there were few movable parts, this rapid expansion device made only little vibration and was suitable for microgravity experiments.

A combustion chamber was installed in the high pressure chamber. An electric heater and a cooling jacket were equipped in the combustion chamber wall. In the test section of the combustion chamber, there were an ignition wire, a fuel injection nozzle and two thermocouples. The ignition wire was a platinum rhodium wire (50 μm in diameter, 5 mm in length), and located at the center of the test section. The temperature of the ignition wire was kept constant automatically during the ignition procedure by a power supply system which included a Wheatstone bridge. This function of the power supply system prevented the ignition wire from snapping due to the heat from a flame. The required time for the ignition wire to reach a constant temperature was about 10 ms. Temperature of the fuel vapor-air mixture was measured with a platinum-platinum rhodium thermocouple and a chromel-alumelthermocouple 4 mm away from the center of the combustion chamber. The ignition wire and thermocouples were coated with silica to suppress catalytic combustion on their surfaces.

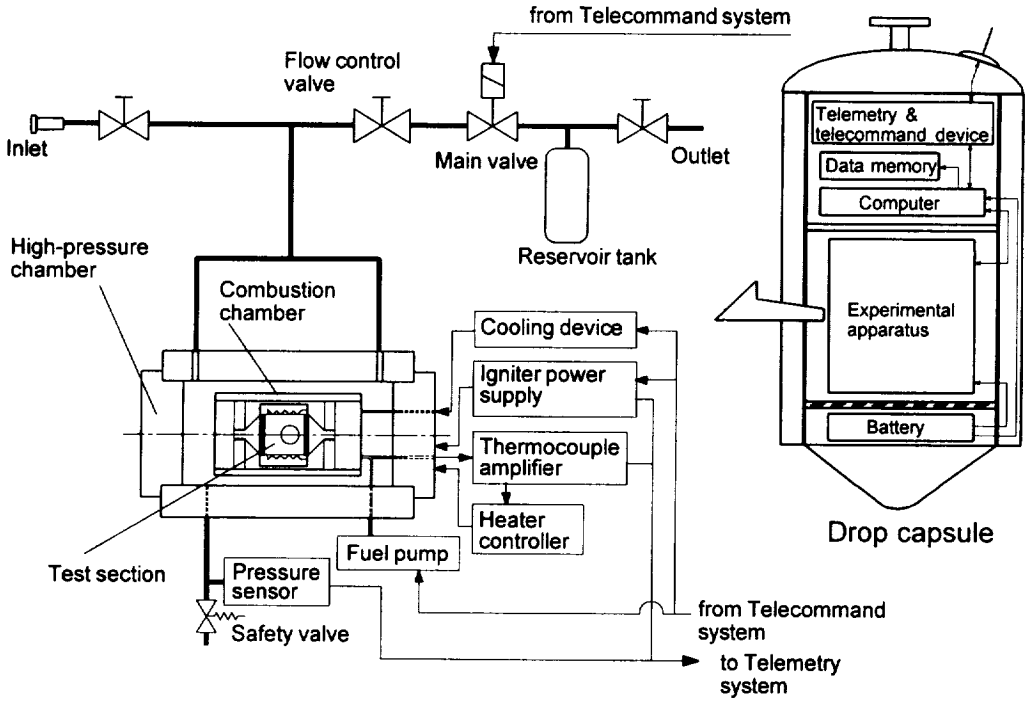

Fig. 1 Experimental apparatus.

Droplet diameter was measured with a laser droplet size analyzer (LDSA), which calculated droplet diameter distributions from the angle and intensity of the laser lights scattered by droplets. The Sauter mean diameter was used as mean droplet diameter. Shadowgraphy was applied to observe flame propagation. Images of a flame were recorded with a high speed video camera (frame speed: 2000 fps, exposure time: 1/3000-1/6000 s).

The drop shaft operated by the Micro-Gravity Laboratory of Japan (MGLAB) was used in order to produce microgravity conditions. Duration of microgravity conditions was about 4.5 s.

Ethanol and pure air were used as fuel and ambient gas, respectively. In the previous work [5], dry air which was made from liquid oxygen and nitrogen was used as ambient gas. However, flame speed differed with the dry air makers even though the oxygen concentrations were the same. This may be attributed to some minor component which was taken into dry air during the production process. Pure air which was made by removing water vapor and dusts from atmospheric air was used in the present work.

After charging air into the high pressure chamber, air in the combustion chamber was heated up by the electric heater and liquid ethanol was injected into the test section. Saturated fuel vapor-air mixtures were used as an initial mixture for all experiments. Therefore, total equivalence ratio can be determined from the temperature and pressure of the initial mixture. After an onset of microgravity, the main valve was opened by an air actuator. The combustion chamber wall was cooled during the expansion process to suppress heat transfer from the chamber wall to the mixture.

Due to the temperature drop caused by rapid expansion, a part of fuel vapor was condensed into a droplet cloud. The ignition wire was heated rapidly 0.5-1.5 s after the end of the pressure reduction process. At that moment, droplet speed was less than 1.5 mm/s. Temperature and pressure of fuel droplet clouds were defined as those values just before the ignition wire was heated up. The pressure in the test section was nearly constant during combustion. Total equivalence ratio ϕ_t and pressure P_{ig} of droplet clouds were set 0.8 and 0.2 MPa, respectively. Gas equivalence ratio ϕ_g was obtained from the temperature and pressure of fuel droplet clouds and was varied in the range of 0.35-0.8 by change of the temperature and pressure of the initial mixtures. Liquid equivalence ratio ϕ_ℓ was defined as $(\phi_t - \phi_g)$. Mean droplet diameter of fuel droplet clouds d_{ig} was varied in the range of 9-45 μm with varying pressure reduction speed.

EXPERIMENTAL RESULTS AND DISCURSION

Figure 3 shows the relationship between the flame speed and the mean droplet diameter of droplet cloud. The flame speed at 20 mm in flame diameter was used as a characteristic flame speed of fuel droplet clouds. The flame speed decreases throughout the mean droplet diameter range of the present experiments for both conditions of ϕ_ℓ. The decrease in the flame speed is supposed to be due to increased evaporation lifetime of fuel droplets. The droplets which do not evaporate completely in the preheat zone make flame temperature lower and the existence of droplets in the reaction zone leads to the decrease in the equivalence ratio of the gas phase. In the range of $d_{ig} < 30$ μm for $\phi_\ell = 0.30$ and $d_{ig} < 25$ μm for $\phi_\ell = 0.41$, the flame speed is larger than that of the premixed gas of the same total equivalence ratio. In the case that fuel droplets exist in the reaction zone of a lean mixture flame, the mixture of the maximum burning velocity exists locally around droplets. It is supposed that flames propagate selectively through such mixtures.

Figure 4 shows the flame speed as a function of ϕ_ℓ. Small droplet clouds of $\phi_\ell > 0.15$ were not able to be generated. Therefore, data for the droplet clouds of $d_{ig} = 23$ and 28 μm were plotted only in the region of $\phi_\ell > 0.15$. In all cases of d_{ig}, the flame speed decreases in the range of $\phi_\ell > 0.2$. In the case of $d_{ig} = 11$ μm, with the increase in ϕ_ℓ, the flame speed increases, takes the maximum value around $\phi_\ell = 0.2$, and then decreases. Since d_{ig} is restricted in the narrow range, the number of droplets in unit volume increases proportionally to ϕ_ℓ. In the case of droplet clouds of $d_{ig} = 11$ μm, with the increase in ϕ_ℓ, the flame speed

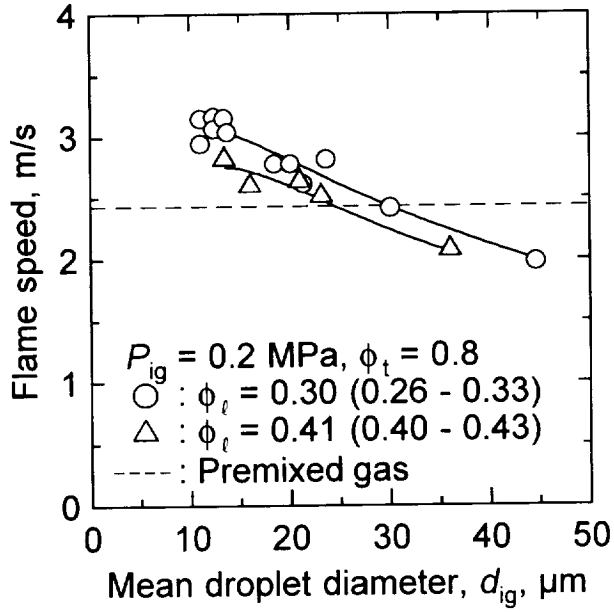

Fig. 2 Effect of mean droplet diameter on flame speed of ethanol droplet clouds.

increases in the range of $\phi_\ell < 0.2$ because of the increase in the total volume of the mixture which has large burning velocity. On the other hand, flame speed decreases in the range of $\phi_\ell > 0.2$ because the number density of droplets in the reaction zone increases proportionally to ϕ_ℓ and the rate of the increase in the total volume of the mixture which has large burning velocity deceases.

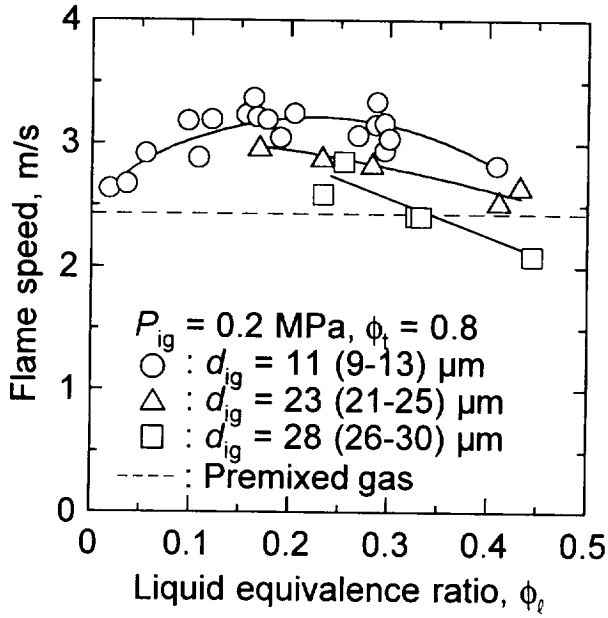

Fig. 3 Effect of liquid equivalence ratio on flame speed of ethanol droplet clouds.

CONCLUSIONS

An experimental study on the flame propagation in uniform ethanol droplet clouds has been made by using microgravity conditions. The total equivalence ratio and pressure were set 0.8 and 0.2 MPa, respectively. Mean droplet diameter of the fuel droplet clouds was varied in the range of 9 - 45 μm. The following conclusions were obtained:

(1) The flame speed of fuel droplet clouds decreases with the increase in the mean droplet diameter of droplet clouds. In the case of small mean droplet diameters, a flame propagates faster in a droplet cloud than in a premixed gas of the same total equivalence ratio.

(2) For fuel droplet clouds of 11 μm in mean droplet diameter, with the increase in the liquid equivalence ratio ϕ_ℓ, the flame speed increases, takes the maximum value around $\phi_\ell = 0.2$, and then decreases. For fuel droplet clouds of 23 and 28 μm in mean droplet diameter, the flame speed decreases monotonically in the range of $\phi_\ell > 0.2$.

ACKNOWLEDGMENTS

This study was carried out as a part of "Research Projects by Using TR-1A Rocket" promoted by NASDA.

REFERENCES

[1] Burgoyne, J. H. and Choen, L., *Proc. Roy. Soc.* A225:375-392(1954).

[2] Mizutani, Y. and Ogasawara, M., *Int. J. Heat Mass Transfer* 8:921-935(1965).

[3] Hayashi, S. and Kumagai, S., *Fifteenth Symposium (International) on Combustion*, The Combustion Institute, 1975, pp. 445 - 452.

[4] Hayashi, S., Ohtani, T., Iinuma, K. and Kumagai, S., *Eighteenth Symposium (International) on Combustion*, The Combustion Institute, 1981, pp. 361 - 367.

[5] Nomura, H., Izawa, K., Ujiie, Y., Sato, J., Marutani, Y., Kono, M. and Kawasaki, H., *Twenty-Seventh Symposium (International) on Combustion*, The Combustion Institute, 1998.

FLAME PROPAGATION OF SPRAY COMPOUND MIXTURE IN A CONSTANT VOLUME VESSEL

T. Yoshizaki[1], M. Yamaguchi[2], K. Nishida[3], H. Hiroyasu[4], H. Yoshida[5], and T. Sakuraya[6], [1]Dept. of Mech. Eng., Hiroshima University, 1-4-1 Kagamiyama, Higashi Hiroshima, 739-8527 Japan, yoshi@mec.hiroshima-u.ac.jp, [2]Dept. of Mech. Eng., Hiroshima University, [3]Dept. of Mech. Eng., Hiroshima University, [4]Dept. of Mech. Sys. Eng., Kinki University, [5]Dept. of Power. Eng., Maritime Safety Academy, [6]Japan Space Utilization Promotion Center.

INTRODUCTION

Flames that are sustained in a spray compound mixture are considered to be similar to the start of flame kernels and the subsequent flame development in the evaporating gasoline spray in spark ignition engines. This is especially so in the case of direct injection stratified charge (DISC) engine, in which a gasoline spray is injected directly into the cylinder and ignited by an electric spark before evaporation of the spray drops is completed. The gasoline spray is heated and evaporated by the hot spark discharge plasma, after which the flame kernel develops and the flame propagates in the gaseous mixture containing the droplets. Moreover, an investigation into the flame propagation of the spray compound mixture leads to a further understanding of spray combustion, such as diesel combustion and gas turbine combustion.

Many various studies have been conducted on the ignition characteristics of spray flows [1)-5)]. The effects of the droplet diameter, fuel concentration and flow condition in the spray on the ignition characteristics were investigated in these studies. Mainly their interest was focused on the minimum ignition energy necessary to maintain successful ignition of the spray flow. Some of these studies [1),5)] tried to estimate the gaseous fuel concentration in the spray flow, but did not adopt the gaseous fuel concentration as the main variable parameter in the experiment. The flame propagation characteristics have been studied in spray flows and spray compound mixtures [6)-13)]. The effects of the droplet diameter, fuel concentration and flow condition of the spray flow and the mixture on the flame propagation velocity (flame speed) and the lean limit of the flame propagation were examined in these studies. However, detailed analyses of the effects of the gaseous fuel (vaporized fuel) fraction in the spray compound mixture on the flame propagation characteristics were not made, except for a few studies [6)-8)]. Even in these studies, the compounded spray drops had a velocity relative to the ambient gas, and were not distributed homogeneously because these experiments were performed under conditions of normal gravity. Moreover, the effect of buoyancy reflected in the results is not negligible under normal gravity. Thus, fundamental information of the ignition and flame propagation characteristics in the spray compound mixture is required from an experiment in which fractions of the gaseous fuel and droplets are independently and widely changed under microgravity.

EXPERIMENTAL SET-UP AND PROCEDURE

Fig.1 shows a schematic diagram of the experimental apparatus. The experimental apparatus size was 870mm in length, 870mm in width and 918mm in height. It consisted of a combustion chamber, a liquid fuel injection system, a spark ignition system, a high-speed video camera system and a timing control system. Experiments were performed under normal gravity and microgravity with changing experimental parameters, such as ambient pressure, total equivalence ratio ϕt (Total of Gaseous Fuel Equivalence Ratio

and Kerosene Equivalence Ratio, $\phi t = \phi g + \phi l$).

The combustion chamber was filled with a propane-air mixture at a known equivalence ratio before the capsule was dropped. The kerosene spray was injected into the combustion chamber using a D.I. gasoline injector at a certain timing from the start of the fall. The fuel drops lost their velocity by the air resistance, and floated almost homogeneously in the combustion chamber. After the fuel drops lost their velocity, the spray compound mixture was ignited by the spark plug, and the flame propagated. The ignition and propagation processes were recorded by the high-speed video camera.

The Sauter's mean diameters of the sprays injected by the gasoline injector were measured using a LDSA equipment around the center of the vessel under normal gravity. The number of density of the liquid droplets around the spark electrode was calculated using the Sauter's mean diameter and the attenuation of the laser beam. By using the Sauter's mean diameter and the number of density, the equivalence ratio for the kerosene fuel droplets could be estimated as shown in Fig. 2 for an ambient pressure of 0.1 MPa, and in Fig. 3 for an ambient pressure of 1.0 MPa.

At this stage, the number of data obtained under microgravity conditions is very few. Therefore, mainly experimental results under normal gravity will be presented in the next section.

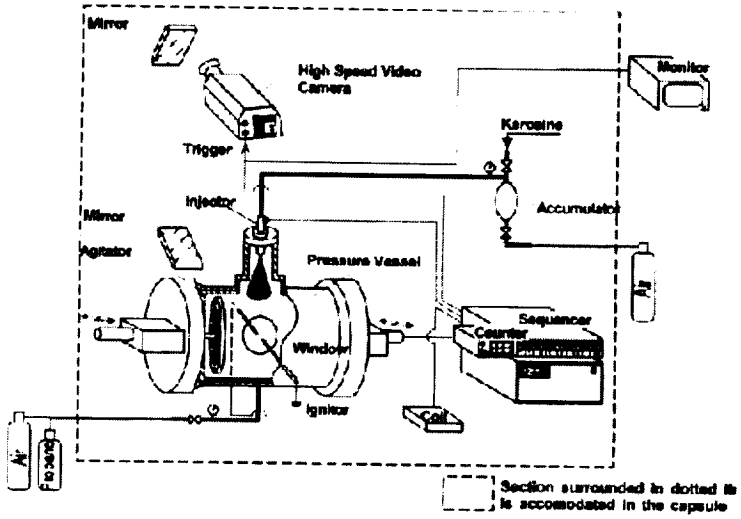

Fig. 1 Schematic diagram of the experimental apparatus

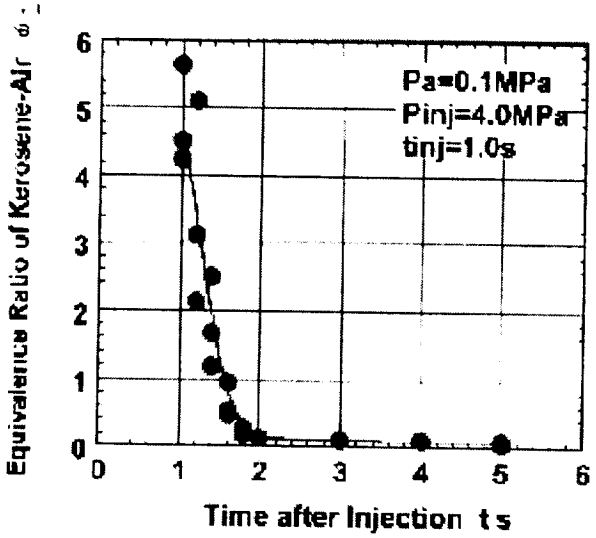

Fig. 2 Temporal variation of the equivalence ratio for the liquid droplets under atmospheric pressure

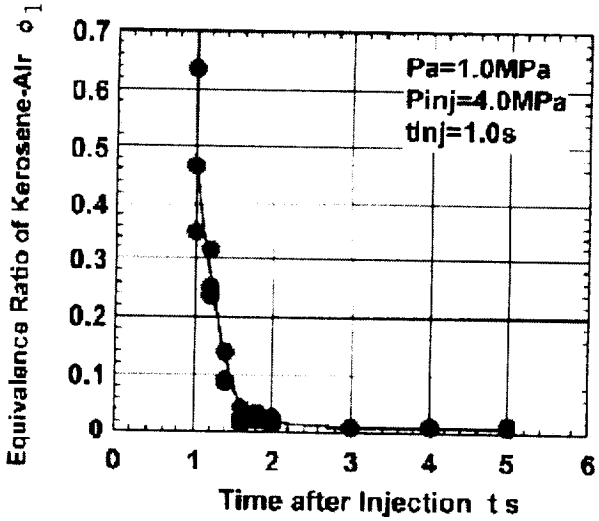

Fig. 3 Temporal variation of the equivalence ratio for the liquid droplets under ambient pressure of 1.0MPa

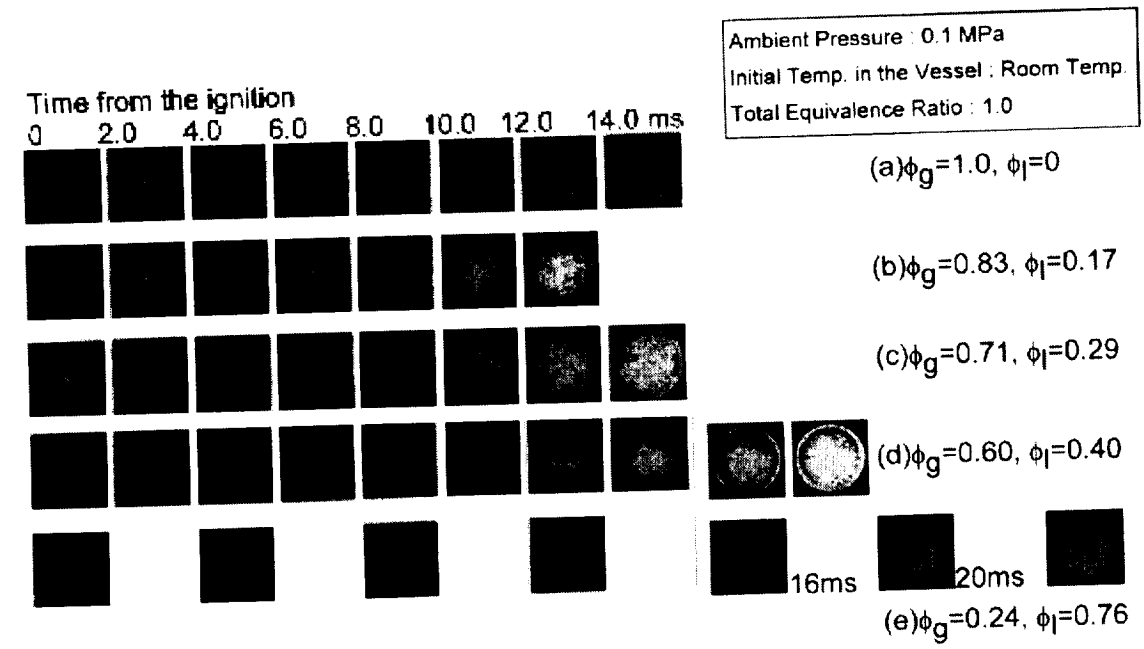

Fig. 4 Flame propagation process of the spray compound mixture

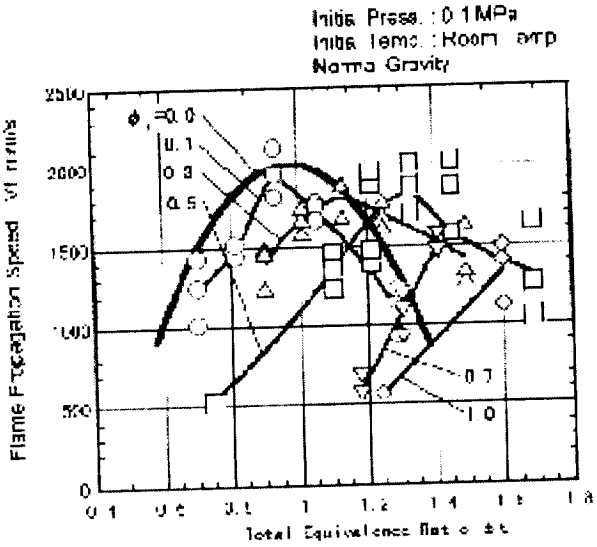

Fig. 5 Flame propagation speed of spray compound mixture for the initial pressure of 0.1MPa

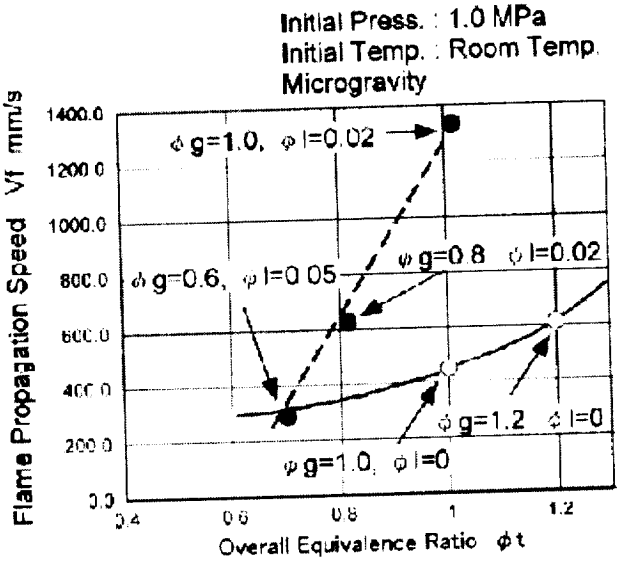

Fig. 6 Flame propagation speed of spray compound mixture for the initial pressure of 1.0MPa

EXPERIMENTAL RESULTS

Figure 4 shows the photographs of the flame propagation process of the spray compound mixtures under normal gravity conditions. The total equivalence ratio was fixed to 1.0, and the propane equivalence ratio was changed from 1.0 to 0.24 as shown in Fig. 4 (a) to Fig.4 (e).

Figure 5 and Fig. 6 show the flame propagation speed of the spray compound

mixture as a function of the total equivalence ratio, ft. The result for an initial pressure of 0.1 MPa and the normal gravity conditions is shown in Fig. 5. The X-ordinates show the total equivalence ratio. The liquid fuel equivalence ratio was changed from 1.0 to 0.0. The results for initial pressure of 1.0MPa under microgravity conditions are indicated in Fig. 6. In the microgravity experiments, the liquid fuel equivalence ratio was changed from 0.0 to 0.05.

SUMMARY

(1) In the case of the ambient pressure of 0.1MPa under normal gravity conditions, the flame propagation speeds of the spray compound mixture show lower values than the flame speeds of the gaseous fuel mixture for the lean equivalence ratio conditions. However, the flame speeds of the spray compound mixture are higher than those of the gaseous fuel mixture for rich conditions.

(2) In the case of an ambient pressure of 1.0MPa under microgravity conditions, the flame speeds drastically increase compared to the gaseous fuel flame speeds at the same total equivalence ratio around the total equivalence ratio of 1.0. However, around the total equivalence ratio of 0.6, the flame propagation speed of the spray compound mixture shows almost the same value as the gaseous flame speed.

(3) Fig.5 and Fig.6 cannot be compared easily because of the difference of gravity conditions, however, the flame propagation speed of the gaseous fuel mixture is drastically affected by the ambient pressure. The effects of the ambient pressure seem to be smaller for the flame propagation speed of the spray compound mixture. For example, in the case of a total equivalence ratio around 1.0, the flame speed of the gaseous fuel is about 2000mm/s under atmospheric pressure, but decreases to about 450mm/s under an ambient pressure of 1.0MPa. The flame speed of the spray compound mixture is about 1800mm/s under the atmospheric pressure (ϕl=0.1), and is about 1350mm/s under the higher pressure condition.

ACKNOWLEDGEMENT

This work was performed under the management of the Japan Space Utilization Promotion Center (JSUP) as a part of the Advanced Combustion Science Utilizing Microgravity, supported by the New Energy and Industrial Technology Development Organization (NEDO).

REFERENCES

1) Ballal, D. R. and Lefebvre, A. H. : Combust. Flame, 31, pp.115-126 (1978).
2) Rao, H. N. S. and Lefebvre, A. H. : Combust. Sci. Technol., 8, pp.95-100 (1973).
3) Rao, K. V. L. and Lefebvre, A. H. : Combust. Flame, 27, pp.1-20 (1976).
4) Singh, A. K. and Polymeropoulos, C. E. : 21st Symp. (Int.) Combust., pp.513-519 (1986).
5) Danis, A. M. Namer, I. and Cernansky, N. P. : Combust. Flame, 74, 285-294 (1988).
6) Mizutani, Y. and Nakajima, A. : Trans. Jpn. Soc. Mech. Engrs., 39-325, pp.2872-2878 (1973). (in Japanese).
7) Cekalin, E. K. : 8th Symp. (Int.) Combust., pp.1125-1129 (1962).
8) Richards, G. A., Sojka, P. E. and Lefebvre, A. H. : Trans. ASME, 111, pp.84-89 (1989).
9) Myers, G. D. and Lefebvre, A. H. : Combust. Flame, 66, pp.193-210 (1986).
10) Bulewicz, E. M. and Kucnerowicz-Polak, B. J. : Combust. Flame, 70, pp.127-135 (1987).
11) Richards, G. A., Sojka, P. E. and Lefebvre, A. H. : Trans. ASME, 111, pp.84-89 (1989).
12) Polymeropoulos, C. E. and Das, S. : Combust. Flame, 25, pp.247-257 (1975).
13) Ballal, D. R. and Lefebvre, A. H. : 18th Symp. (Int.) Combust., pp.321-328 (1981).

OMIT THIS PAGE

High Pressure

569-25

PRESSURE EFFECTS ON COMBUSTION OF METHANOL AND METHANOL-DOCECANOL DROPLETS

K. Okai, Y. Ono, O. Muriue, M. Tsue, M. Kono[1], J. Sato[2], D.L. Dietrich[3] and F.A. Williams[4], [1]The University of Tokyo, Tokyo 113-8656, Japan, [2]Ishikawajima-Harima Heavy Industries, Tokyo 135-0061, Japan, [3]NASA Lewis Research Center, Cleveland, OH 44135, [4]University of California, San Diego, La Jolla, CA, 92093-0411

INTRODUCTION

The objective of this research is to improve understanding of the combustion of binary fuel mixtures in the vicinity of the critical point. Fiber-supported single droplets and two-droplet arrays of methanol and of mixtures of methanol and 1-dodecanol, initially 0.9 mm in diameter, were burned in room-temperature air at pressures from 0.1 MPa to 9.0 MPa in the NASA Lewis 2.2-second drop tower. The work is a continuation of a collaborative Japan-US research effort designed to increase knowledge of high-pressure combustion of fuel sprays, relevant to application in propulsive and power-production devices such as Diesel engines. Some previous publications from this cooperative program may be cited [1,2]. All of the previous experiments concerned alkanes and alkane mixtures. The new research reported here addresses alcohols and alcohol mixtures, to ascertain the degree to which previous results for alkanes extend to alcohols. There have been many previous experimental studies of methanol droplet combustion [3,4] and a few of alcohol mixtures [5,6], but not at the high pressures of interest here. There is some experimental information on methanol droplet combustion at elevated pressure [7] but none on the alcohol mixtures extending to critical pressures, as in the present study.

EXPERIMENTAL APPARATUS AND PROCEDURE

The experimental apparatus consists of a combustion chamber, a fuel-supply system, a hot-wire igniter, two CCD cameras, a lamp, a timer unit, a motor driver, and related equipment described previously [2]. Since the apparatus resembles that described previously, only essential differences are mentioned here. The critical temperature T_c and pressure P_c for the two pure alcohols are (T_{c1}=512.6K, P_{c1}=8.1MPa for methanol and T_{c2}= 679K, P_{c2}=1.9MPa for dodecanol. Two almost identical droplets were dispensed in air at the end of two identical 0.125 mm quartz fibers (with small beads on the end) in normal gravity just prior to the start of the test. The droplets then were simultaneously ignited by two hot wires shortly after release of the experimental package to microgravity. The igniter duration was minimized subject to reliable ignition for each condition rather than employing a constant duration as in earlier experiments; this reduces effects of the ignition impulse. After ignition the hot-wires were quickly retracted. Two orthogonal views of the combustion process were secured by two black-and-white CCD cameras directed through the windows of the chamber. One view is backlit for accuracy in determining the droplet cross-sectioned area, while the other provides a direct photograph of the flame. The images from the cameras were entered into a computer by a black-and-white frame grabber for analysis.

RESULTS FOR PURE METHANOL

Extinction Diameters

Pure-methanol tests were performed for both single droplets and droplet pairs for various pressures between atmospheric and slightly above the critical pressure of the fuel. Extinction

was observed only at 0.1MPa. Figure 1 shows the dependence of droplet lifetime t_d and extinction diameter d_{ext} on initial separation ratio (ℓ/d_0). Here ℓ is the distance between the centers of the two droplets and d_0 the initial droplet diameter. Single-droplet results are plotted as $\ell/d_0=\infty$. The methanol flame was very dim, almost invisible, for all pressures (even at 9MPa), but flame existence was indicated by a glowing fiber. The extinction diameter was determined from the last record that exhibited fiber glow. Though Vieille and coworkers [7] did not report extinction of fiber-supported methanol isolated-droplet combustion, extinction was clearly seen both for single droplets and droplet pairs at atmospheric pressure, in agreement with earlier free-droplet work [3,4] and explained previously [4]. For the droplet pairs, unlike isolated droplets, the concentration and temperature fields of the gas phase in the vicinity of the liquid surfaces are asymmetric, which may cause liquid-phase internal flow beyond diffusocapillarity, but the extinction diameter was found to be almost independent of droplet spacing (Fig. 1). At 1MPa and above, extinction was no longer observed for either single droplets or droplet pairs.

Interaction Effects

Droplet-array combustion experiments in normal gravity have demonstrated that the burning lifetime has a minimum at a certain spacing for many fuels [8,9]. The increase in lifetime with spacing for large spacing is explained by buoyancy for normal-gravity tests. It has been demonstrated [2,8] that those minima in lifetime can also be seen for heptane and heptane-hexadecane droplet pairs in microgravity for atmospheric pressure and at high pressures, respectively. The minimum in microgravity tests was explained by effects of radiative heat transfer, enhanced by soot emissions for these fuels. For the present experiments, Fig. 1 shows that droplet lifetime monotonically decreases with increasing spacing, explained by the lower radiation from the non-sooty methanol. At higher pressures, the interaction effects decrease, as shown in Fig. 2. Previous investigators [2,9] found that interaction effects still exists until pressures exceed the critical pressures of both components. The earlier disappearance of the pressure effects in the present experiments may be due to the smaller flame diameters for methanol and the weaker radiative heat-transfer effects. The decrease in lifetime of the isolated droplets with increasing pressure, seen in Fig. 2, is consistent with literature results [7].

RESULTS FOR METHANOL-DODECANOL MIXTURES

Droplet-Diameter and Flame-Diameter Histories

Mixtures of methanol and dodecanol are known to exhibit strong disruption phenomena during droplet combustion. Figure 3 shows that those disruption phenomena occur both for single droplets and droplet pairs even in the presence of fiber supports. In this figure, it is seen that burning-rate constants of single droplets and droplet pairs ($\ell/d_0=3.9$) for an initial dodecanol volume fraction of 0.1 at atmospheric pressure are still different until midway through combustion and that disruption then occurs both for single droplets and droplet pairs. The variety of disruption-like phenomena observed in the present experiments were classified as:

1. Disruption, as in the disruptive burning described by Lasheras et al. [10], Yap et al. [11] and Niioka and Sato [12]. In the disruption regime, the droplet diameter is observed to suddenly decrease in the middle of the burn, leaving droplet fragments that continue to burn. Often the sudden reduction of droplet diameter is associated with a small oscillation or swelling.
2. Puffing, during which the droplet vibrates, and the oscillation induces open shapes that puff gas or trap gas but do not produce a sudden diameter decrease.

3. Boiling, in which droplet oscillation is clearly seen but no puffing nor disruption is observed. In a sense, this behavior resembles a weak 'puffing' regime, but sometimes the oscillation or deformation is so strong that the equivalent diameter cannot be estimated.
4. Stable burning, during which no disruption, puffing or boiling phenomena ever occur. Staged burning, observed for all mixtures tested here, is consistent with stable burning.

Figure 3 shows conditions exhibiting boiling and disruption. Puffing, not shown in Fig. 3, typically occurs for conditions between those of boiling and disruption. Some of flame diameter D_f histories also are plotted in Fig. 3; at earlier times the flame could not be discerned in these tests. Although this was a common occurrence, flame contraction could still be inferred from the shapes of the later flame histories. Figure 4 shows that boiling occurs even for single pure methanol droplets at high pressures. Maps (not shown) have been generated indicating where the different combustion regimes occur. Results also were obtained on the onset of instability and correlated on the basis of published theoretical estimates [13,14].

CONCLUSIONS

These results provide both qualitative and quantitative information on the combustion of methanol droplets and of droplets of methanol-dodecanol mixtures, both single droplets and droplet pairs, at pressures from atmospheric to above the critical pressures of the pure constituents. The results are comprehensible qualitatively on the basis of previous knowledge. The quantitative results, as well as the identification of regimes of boiling, puffing and full disruption, extend understanding of droplet combustion and droplet interaction effects at high pressures. In particular, the tendency for droplet interactions to reduce disruptive effects was identified and explained.

ACKNOWLEDGMENT

This work was performed under the management of the Japan Space Utilization Promotion Center (JSUP) as a part of the R&D project of Advanced Combustion Science Utilizing Microgravity, supported by the New Energy and Industrial Technology Development Organization (NEDO). FAW acknowledges support from grant No. NAG-1689. The helpful advice of M. Mikami of Yamaguchi University in gratefully acknowledged.

REFERENCES

1. Mikami, M., Habara, O., Kono, M., Sato, J., Dietrich, D.L. and Williams, F.A., *Combustion Science and Technology*, Vol. 124, 1997, pp. 295-309.
2. Okai, K., Tsue, M., Kono, M., Mikami, M., Sato, J., Dietrich, D.L. and Williams, F.A., *Twenty-seventh Symposium (International) on Combustion*, The Combustion Institute, Pittsburgh, PA, 1998, to appear.
3. Cho, S.Y., Choi, M.Y. and Dryer, *Twenty-third Symposium (International) on Combustion*, 1990, pp. 1611-1617.
4. Dietrich, D.L., Dryer, F.L., Haggard, J.B., Jr., Nayagam, V., Shaw, B.D. and Williams, F.A., *Twenty-sixth Symposium (International) on Combustion*, The Combustion Institute, Pittsburgh, PA, 1996, pp. 1201-1207.
5. Wang, C.H. and Law, C.K., *Combustion and Flame*, Vol. 59, 1985, pp. 53-62.
6. Yang, J.C., Jackson, G.S. and Avedisian, C.T., *Twenty-third Symposium (International) on Combustion*, The Combustion Institute, Pittsburgh, PA, 1990, pp. 1619-1625.

7. Vieille, B., Chauveau, C., Chesneau, X., Odeide, A. and Goakalp, I., *Twenty-sixth Symposium (International) on Combustion*, The Combustion Institute, Pittsburgh, PA, 1996, pp. 1259-1265.
8. Fedoseeva, N.V., *Advances in Aerosol Physics*, Vol. 2, 1972, pg. 110-118.
9. Mikami, M., Kato, H., Sato, J. and Kono, M., *Twenty-fifth Symposium (International) on Combustion*, The Combustion Institute, Pittsburgh, PA, 1994, pp. 431-438.
10. Lasheras, J.C., Fernandez-Pello, A.C. and Dryer, F.L., *Combustion Science and Technology*, Vol. 22, 1980, pp. 195-209.
11. Yap, L.T., Kennedy, I.M. and Dryer, F.L., *Combustion Science and Technology*, Vol. 41, 1984, pp. 291-313.
12. Niioka, T. and Sato, J., *Twenty-first Symposium (International) on Combustion*, The Combustion Institute, Pittsburgh, PA, 1986, pp. 625-631.
13. Shaw, B.D. and Williams, F.A., *International Journal of Heat Mass Transfer*, Vol. 33, 1990, pp. 301-317.
14. Shaw, B.D., *Combustion and Flame*, Vol. 81, 1990, pp. 277-288.

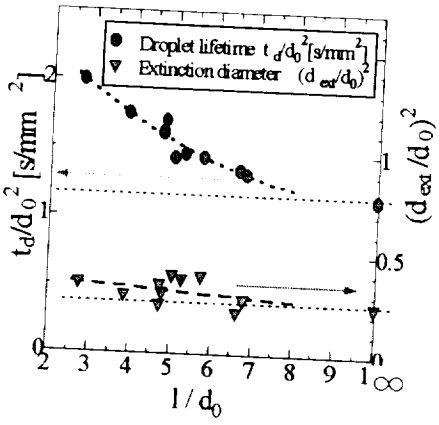

Fig. 1

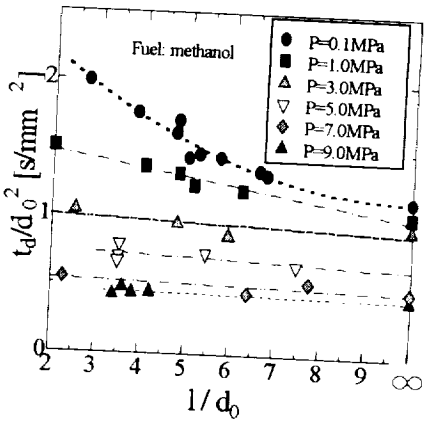

Fig. 2

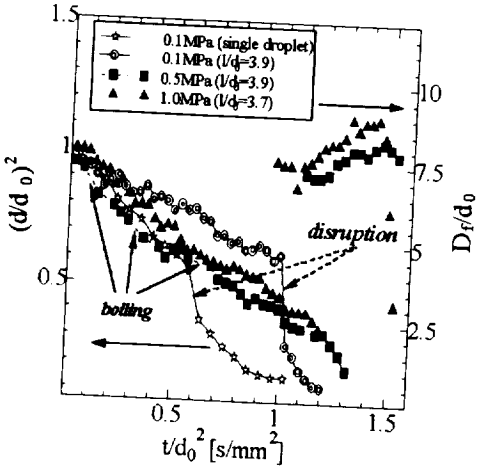

Fig. 3

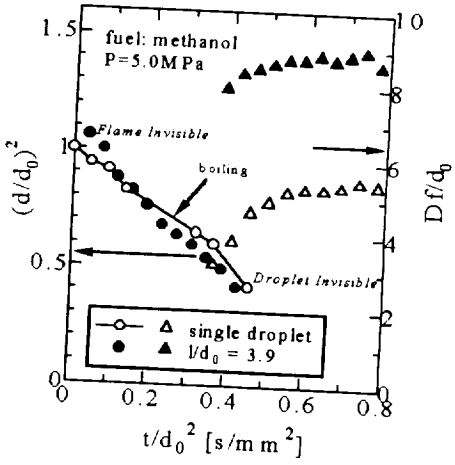

Fig. 4

S70-29

AUTOIGNITION OF A FUEL DROPLET IN SUPERCRITICAL GASEOUS ENVIRONMENTS UNDER MICROGRAVITY IN A DROP SHAFT

Toshikazu Kadota, Akira Nakainkyo, Shuichi Hirota and Daisuke Segawa
Osaka Prefecture University
1-1 Gakuen-cho, Sakai, Osaka, 599-8531, Japan, e-mail: kadota@ava.osakafu-u.ac.jp.

INTRODUCTION

The operating pressure in the combustion chamber of internal combustion engines which use liquid fuel spray has increased, and often exceeded the thermodynamic critical pressure of the liquid fuel of frequent utilization for the higher thermal efficiency and higher rate of heat release. In such conditions, the liquid fuel droplets are allowed to burn in the gaseous environments of which temperature and pressure exceed the critical conditions of the liquid fuel. In spite of the extensive efforts [1-8], there is still lack of knowledge on the combustion of a fuel droplet in supercritical gaseous environments.

This has caused us to be involved in a series of a research program designed for obtaining the detailed information leading to the deep understanding of the combustion phenomena of fuel droplets in supercritical gaseous environments under microgravity. The first phase of the experimental study [9] has been done on the combustion of a fuel droplet under microgravity during the parabolic flight of aircraft. Photographic observation was made of a fuel droplet evaporating inside a luminous sooting flame which was subjected to the backward irradiation of an intensive laser light. This resulted in the determination of the time histories of the droplet diameter and hence the burning rate constant. Also measured were the ignition delay, the burning life time and the flame diameter.

EXPERIMENTAL PROCEDURE

Figure 1 shows the schematic diagram of the experimental apparatus provided in the present study. It consists of a high pressure combustion chamber in which a fuel droplet is allowed to burn, a pressure gauge, a thermometer, a temperature controller, a sequence controller which enables the automatic operation of the measurements and a high speed video camera which is available for taking an image of the luminous envelope flame formed around a fuel droplet. The indications of the pressure gauge and the thermometer were recorded by using a video camera aboard the capsule of which signal is transmitted to a video monitor in the control room.

Figure 2 shows the cylindrical high pressure combustion chamber made of duralumin which has the dimension of the inner diameter 100 mm and the inner height 250 mm. For the optical access, two pairs of circular glass windows are equipped on the side wall of the combustion chamber. The upper portion of the combustion chamber is occupied by an electric furnace with quartz glass windows. The furnace is surrounded by a heat insulator. A thermocouple is available to measure and to control the temperature of the gas inside the furnace. The fuel supply system is installed below the furnace inside the combustion chamber. Thin aluminum plates are inserted between the furnace and the fuel supply system for shielding the thermal radiation from the furnace. This kept the fuel supply system near the room temperature during the experiments. The cylindrical fuel supply system has eight cylindrical holes of the inner diameter 10 mm. Each hole contains a fine quartz fiber supported by a metal rod and a spring. A fuel droplet is suspended at the spheroidal portion of the tip of a quartz fiber of the diameter 125 μm. The fuel tested is

octadecanol which solidifies at 331 K. Its critical pressure and temperature are 1.4 MPa and 747 K, respectively.

As the microgravity environment is attained in the capsule right after the start of its free fall, an electric signal is generated to actuate a stepping motor installed outside the combustion chamber. This results in the translation of a spindle to push a metal rod up inside a small hole of the fuel supply system. A spherical solid fuel at the tip of the quartz fiber supported by the metal rod is allowed to move through a small hole on the bottom of the furnace and is subjected to the high temperature gas. This causes rapid phase change, evaporation, autoignition and combustion of the fuel droplet. As the spindle is pulled down after the end of burning of the fuel droplet, the spring pushes the metal rod down and lets the quartz fiber out of the furnace. This is followed by rotation of the fuel supply system. A new fuel droplet is ready for the measurement in the next drop.

The experiments were done under microgravity in the drop shaft at the Microgravity Laboratory of Japan (MGLAB). The duration and the level of microgravity were 4.5 seconds and less than 10^{-5} G. The ambient gas consists of oxygen and carbon dioxide. The ambient pressure ranged from 0.56 to 1.72 times of the critical pressure of the fuel. The oxygen concentration in the ambient gas was varied from 20% to 40%. The ambient temperature and the initial droplet diameter were kept constant at 870 K and at 1.0 mm.

RESULTS AND DISCUSSION

Figure 3 shows the time histories of the diameter of the visible flame formed around a fuel droplet at various reduced ambient pressures (ratio of the ambient pressure to the critical pressure of the fuel tested). The oxygen concentration is kept constant at 25% in carbon dioxide and oxygen environment. A thin sheet of visible flame appears around the fuel droplet at the onset of autoignition and it moves away from the droplet surface with the lapse of time.

It is evident that the flame diameter increases fairly rapidly at the early stage of the burning

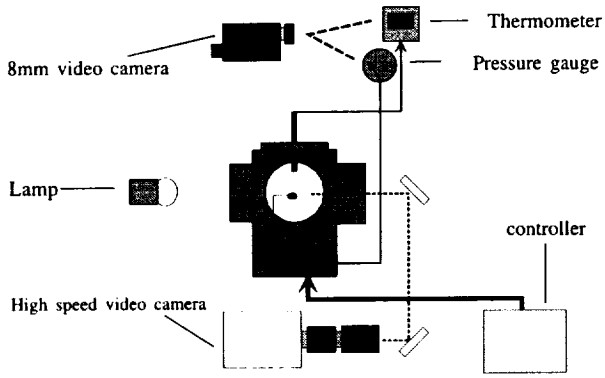

Fig.1 Experimental apparatus

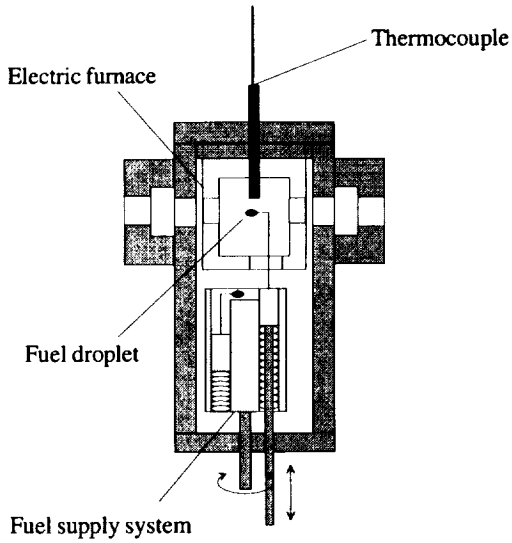

Fig.2 High pressure combustion chamber

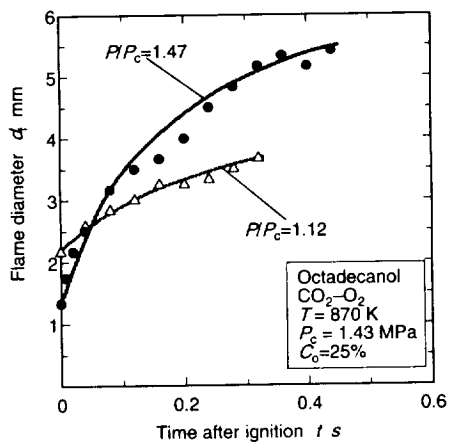

Fig.3 Time histories of flame diameter at various ambient pressures

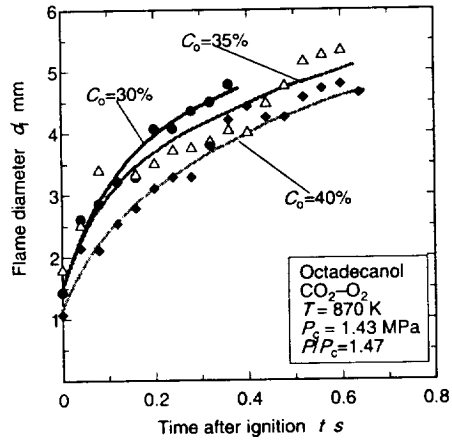

Fig.4 Time histories of flame diameter at various oxygen concentration

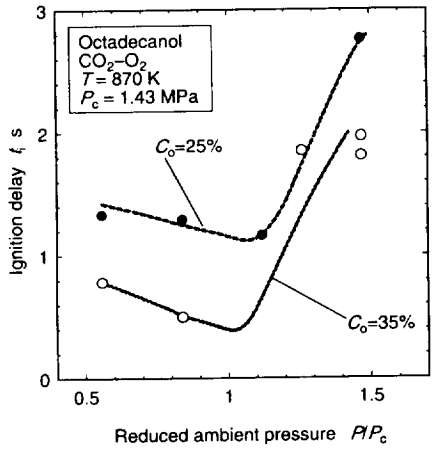

Fig.5 Ignition delay as a function of ambient pressure

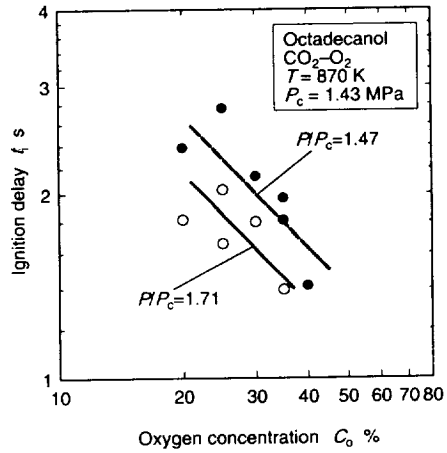

Fig 6 Ignition delay as a function of oxygen concentration

and its growth rate decreases gradually with the lapse of time. The flame diameter right after autoignition is smaller in the reduced ambient pressure of 1.47 than 1.12. However, higher ambient pressure causes higher rate of flame growth and larger flame diameter afterward. This is consistent with the evidence [9] revealed in the experiments of a fuel droplet burning in nitrogen and oxygen environment under microgravity by using a parabolic flight of aircraft.

Figure 4 shows the time histories of a flame diameter at various oxygen concentrations at ambient pressure of 1.47. It is evident that higher oxygen concentration in the ambient gas results in higher rate of flame growth and larger flame diameter.

Figure 5 shows the ignition delay as a function of the reduced ambient pressure at two different oxygen concentrations. It is evident that the ignition delay decreases and reaches a minimum at reduced ambient pressure approximately unity. Further increase in the ambient pressure causes the increase in the ignition delay. It has been widely recognized that the inert ambient gas absorbed in the liquid fuel modifies the thermodynamic critical conditions of pure

fuel. It has been predicted that the critical concentration and temperature in the mixture of fuel and ambient gas decrease and the ignition delay increases with an increase in the ambient pressure for a spherical symmetric processes of droplet combustion in supercritical gaseous environments [8]. It has also been reported [9] that higher ambient pressure in supercritical region causes longer ignition delay in nitrogen and oxygen environment.

Figure 6 shows the ignition delay as a function of the oxygen concentration in the ambient gas at two different reduced ambient pressures. The ignition delay decreases linearly with an increase in the oxygen concentration in the logarithmic diagram. It is probable that the higher concentration of oxygen in the ambient gas enhances the rate of chemical reaction in the gaseous mixture of fuel vapor and ambient gas formed around an evaporating fuel droplet during the induction period prior to the autoignition. This causes short ignition delay in the ambient gas at higher oxygen concentration.

CONCLUSIONS

An experimental study was performed to obtain the detailed information needed for the deep understanding of the combustion phenomena of a fuel droplet in supercritical gaseous environments under microgravity in a drop shaft.

The primary conclusions reached in the present study are as follows.

(1) The increase in the ambient pressure causes smaller flame diameter at the onset of autoignition and higher rate of flame growth and larger flame diameter at late stage of burning in supercritical gaseous environments.
(2) Flame diameter decreases with an increase in the oxygen concentration in the ambient gas.
(3) The ignition delay shows a minimum at ambient pressure near the critical pressure of the fuel tested.
(4) Higher oxygen concentration in the ambient gas causes shorter ignition delay.

ACKNOWLEDGMENTS

This study is carried out as a part of Ground Research Announcement for the Space Utilization promoted by NASDA and Japan Space Forum.

REFERENCES

(1) Faeth,G.M., Dominics,D.P, Tulpinsky,J.F. and Olson,D.R., Twelfth Symp. (Int.) on Combustion, 1969, 9-18.
(2) Kadota,T. and Hiroyasu,H., Eighteenth Symp. (Int.) on Combustion, 1981, 275-282.
(3) Umemura, A., Twenty-First Symp. (Int.) on Combustion, 1988, 463-471.
(4) Niioka,T. and Sato,J., Twenty-First Symp. (Int.) on Combustion, 1988, 625-631.
(5) Sato,J., Tsue,M., Niwa,M. and Kono,M., Combust. Flame 82: 142-150(1990).
(6) Mikami,M., Kono,M., Sato,J., Dietrich,D.L. and Williams,F.A., Combust. Sci. Technol., 90:111-123(1993).
(7) Li,Y.Q. and Umemura,A., Japan Soc. Mech. Engrs., 59: 3639-3644(1993).
(8) Vieille,B., Chauveau,C., Chesneau,X., Odeide,A. and Gokalp,I.., Twenty-Sixth Symp. (Int.) on Combustion, 1996, 1259-1265.
(9) Kadota,T., Satoh,K., Segawa,D., Marutani, Y. and Sato,J., Twenty-Seventh Symp. (Int.) on Combustion, 1998.

MICROGRAVITY EXPERIMENT ON FLAME SPREAD OF A FUEL DROPLET ARRAY IN A HIGH-PRESSURE ENVIRONMENT

J. Park[1], T. Iwahashi[2], H. Kobayashi[2], and T. Niioka[2]
[1] Korea Advanced Institute of Science and Technology
373-1 Kusong-dong, Yusong-gu, TaeJeon 305-701, Korea
[2]Institute of Fluid Science, Tohoku University
2-1-1 Katahira, Aoba-ku, Sendai, Miyagi 980-8577, Japan

S71-29

INTRODUCTION

The researches on flame spread of a droplet array are useful for understanding the fundamental mechanism of spray combustion. However, the flame size of a suspended single droplet is more than 1.0 mm and a spreading flame of a fuel droplet array is much larger than the single droplet flame, so that natural convection extensively affects the flame spread phenomenon especially in a high-pressure environment. In this study, flame spread experiments of a n-decane droplet array were conducted over the wide pressure range from ordinary pressure to supercritical pressures of the fuel in microgravity to eliminate the natural convection. Flame spread rates were measured by OH emission images recorded by an intensified high-speed video. A high-speed Schlieren observations were also conducted and flame spread characteristics around the critical pressure without natural convection were discussed.

EXPERIMENTAL SETUP

Figure 1 shows schematics of the experimental setup [1]. In total fourteen silica fibers are arranged in a high-pressure chamber and fuel droplets are suspended at the end of the fibers using a micro syringe controlled by a personal computer. The droplet diameter, D, is 1.0 mm and the droplet spacing, S, and the ambient pressure, P, were varied. The fuel used is n-decane (n-$C_{10}H_{22}$, T_b=447.3 K, T_c=617.6 K, P_c=2.11 MPa, where T_b, T_c, and P_c are boiling temperature, critical temperature, and critical pressure, respectively). The droplet array is ignited at the end of the array by an electrically heated platinum wire and the flame spread is observed using a high-speed video (max. 600 fps) with an image-intensifier and an OH band-pass filter. The flame spread rate is determined as a gradient of a linearly fitted line of flame spread distance and time taken from the OH image forefront. Several droplets influenced by the igniter and the last droplet flame with less symmetry were omitted from the calculation. Microgravity experiments were performed using the 4.5 sec drop-shaft facility of the Japan Microgravity Laboratory (MGLAB) in Toki, Japan.

RESULTS AND DISCUSSION

Figure 2 shows typical OH emission images of spreading flames for the droplet spacing of 2.0 at various pressures. At pressures close to the ordinary pressure, the flame spreads continuously and has a smooth OH emission region (Fig.2a). However, with the increase in pressure, the flame spread gradually becomes intermittent (Fig.2b). Around the critical pressure or over the critical pressure, the OH emission region is corrugated and the flame spread becomes quite intermittent (Fig.2c). In this case, the global shape of spreading flame tends to be zigzag.

Figure 3 shows variations of flame spread rate with pressures for 3 kinds of spacing (i.e., 1.5 mm, 2.0 mm, and 3.0 mm). The data in normal gravity are also shown for comparison. In normal

gravity, the flame spread rate decreases quickly with increase in pressure and there exists a limit ambient pressure above which the flame does not spread anymore. Flame spread does not occur over the critical pressure. This is because natural convection induces a strong upward flow of burned gas, decreasing the flame diameter and weakening lateral heat transfer to the unburned droplet.

In contrast to this, as shown in Fig.3, flame spread occurs even at 5.0 MPa for every spacing in microgravity, which is the maximum pressure of this experiment. The flame spread rate decreases with pressure then increases after having a minimum value at about 1.0 MPa. The spread rate has a maximum near the critical pressure (2.11 MPa) and then decreases again with pressure. These characteristics are common to every spacing, but the pressure at which the spread rate has a maximum for small spacing is a little larger than that for large spacing.

It is reasonable to assume that the flame spread time, which is inversely proportional to the flame spread rate, is determined by competition between the transfer time of flame zone (i.e., the outer edge of high-temperature region) and the ignition time of a fuel droplet. The transfer time of flame zone is smaller for larger flame diameter. For a single droplet, it is known that flame diameter decreases monotonously with the ambient pressure [2,3], meaning that transfer time of flame zone increases and the flame spread rate decreases with pressure in the low pressure region. It is also known that the ignition time mainly consists of the time of fuel evaporations in the case of less volatile fuels like n-decane [4,5]. As for the droplet evaporation, the evaporation constant increases with ambient pressure and has a maximum around the critical pressure [6], so that the ignition time decreases with pressure. This is basically because the latent heat can reach to zero at the critical pressure. Therefore the time for evaporation decreases and the flame spread rate increases again when the pressure approaches the critical pressure.

However, we should consider the difference in the heating process between the flame spread and droplet ignition in a heated furnace. The major heating process of the former is through the approaching of the flame zone to the unburned droplet but that of the latter is uniform heating of the unburned droplet through radiation and conduction in the furnace. Because the diffusion coefficient and thermal diffusivity are inversely proportional to the pressure, the approaching of the flame zone becomes difficult unless any mechanism of flame zone transfer when the pressure increases very much.

As mentioned above, the flame spread is very intermittent and the flame shape is irregular near the critical pressure. From the observation of flame spread using a color CCD video camera, images like small clouds were found at the forefront of the spreading flame at high-pressure. In order to know what they are and how the irregularity of the flame spread is caused, high-speed Schlieren observations were performed in microgravity.

Figure 4 shows time history of Schlieren images. We can see that, as the flame zone approaches the unburned droplet, evaporated fuel gas is issued from the unburned droplet to the other side of the flame zone and form a vortex ring like structure. The flame often propagated though the issued fuel gas. Because issued fuel gas is not always axisymmetric to the array axis, the spreading flame is not axisymmetric. Consequently, the flame spread becomes irregularly intermittent and zigzag as shown in Fig.2c. We can say that this phenomenon plays an important role in increasing the flame spread rate around the critical pressure, as shown in Fig.3, because the flame can propagate though the issued fuel gas between the droplets. This decreases the transfer time of flame zone to the unburned droplet and increases the flame spread rate.

To clarify possible mechanism of the generation of fuel gas flow from an unburned droplet,

we have observed droplet motions and flows around the droplet near the critical pressure precisely in normal gravity. As a result, it was found that, when the flame zone reaches the unburned droplet, the surface of the unburned droplet on the other side of the approaching flame sticks out and pushes the evaporated fuel gas layer quickly, forming the vortex ring structure of the evaporated fuel gas and mist. The velocity of the sticking out is around 17 cm/s and was equivalent to the velocity of the issued fuel gas shown in Fig.4. It is presumed that this sticking out of the droplet surface is caused by ill-balanced surface tension between the heated side by the flame and the opposite side near the room temperature because the surface tension becomes zero when the surface of droplet is inhomogeneously heated and a part of the droplet surface becomes close to the supercritical condition. Preliminary estimation of the sticking out velocity based on the ill-balanced surface tension was 45 cm/s and the order of magnitude was agreed with the experimental results.

CONCLUDING REMARKS

Microgravity experiments on flame spread of a n-decane droplet array over the wide range of pressure were performed. It was found that flame spread rate has a minimum at about 1.0 MPa and a maximum around the critical pressure (2.11 MPa). The fuel gas issued from the unburned droplet was observed at supercritical pressure. This fuel gas flow plays an important role in increasing the flame spread rate around the critical pressure.

ACKNOWLEDGMENTS

The authors would like to express thanks to Prof. K.Maruta, Mr. S.Kato, and Mr. S.Hasegawa for their assistance of experiments and helpful discussions. This study is funded by a part of "Ground Research for Space Utilization" promoted by NASDA and Japan Space Forum.

REFERENCES

1. Kato,S., Mizuno,H., Kobayashi,H., and Niioka,T., JSME Int. Journal. Ser.B, 41: 322 (1998).
2. Faeth,G.M., Dominics,D.P., Tulpinsky,J.F., and Olson,D.R., 12th Symp.(*Int.*) on Combust., The Combustion Institute, 1969, p.9.
3. Sato,J., Tsue,M., Niwa,M., and Kono,M., Combust. Flame 82 :142 (1990).
4. Law,C.K., Combust. Flame 24: 89 (1975).
5. Nakanishi,R., Kobayashi,H., Kato,S., and Niioka,T., 25th Symp.(*Int.*) on Combust., The Combustion Institute, 1994, p.447.
6. Tsukamoto,T. and Niioka,T., Prog. Aeronaut. Astronaut.152: 263 (1993).

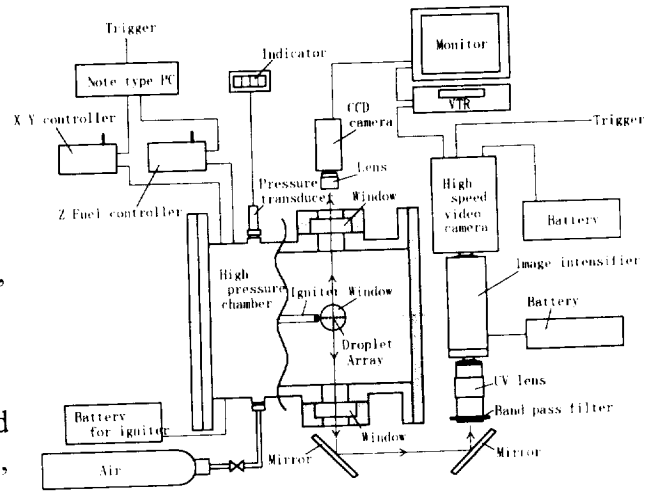

Fig.1. Schematics of the experimental setup.

(a) (b) (c)

Fig.2. OH emission images of spreading flame at various pressures: (a) 0.5 MPa; (b) 1.5 MPa; (c) 2.5 MPa (S=2.0 mm).

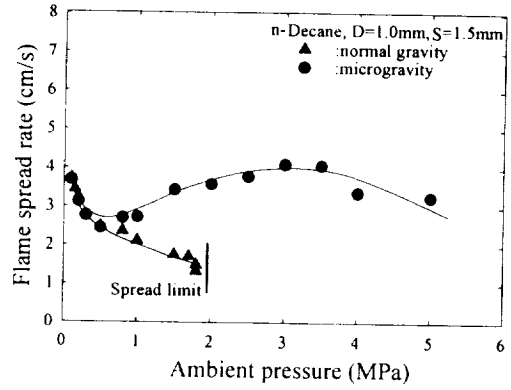

(a)

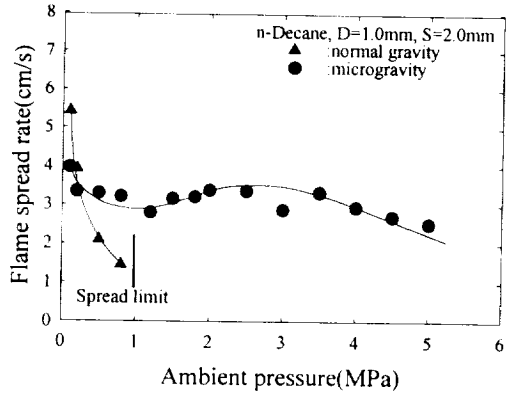

(b)

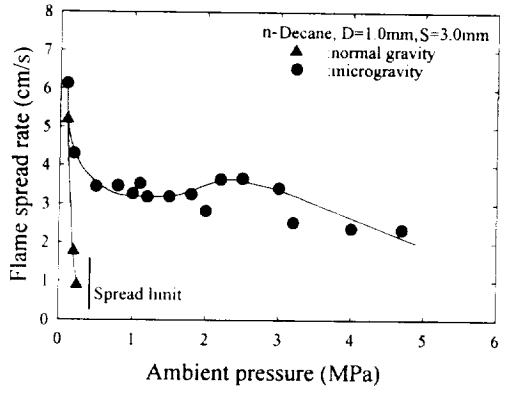

(c)

Fig.3. Variation of flame spread rate with pressure:(a) S=1.5 mm; (b) S=2.0 mm; (c) S=3.0 mm.

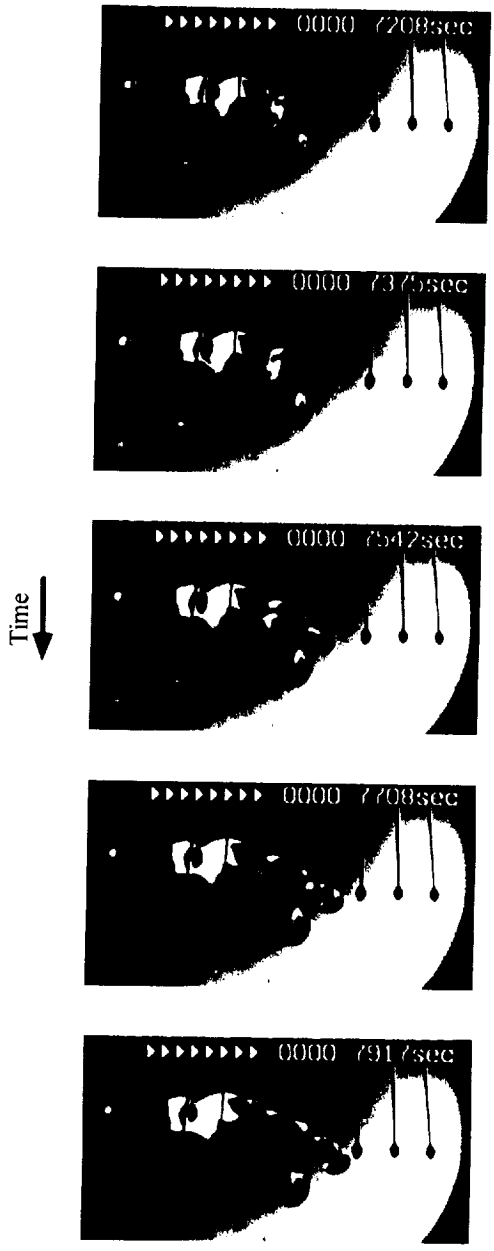

Fig.4. High-speed Schlieren images of spreading flame (P=3.0 MPa, S=3.0 mm).

EFFECTS OF GRAVITATIONAL ACCELERATION ON HIGH PRESSURE COMBUSTION OF METHANOL DROPLETS

C. Chauveau, B. Vieille, I. Gökalp
Laboratoire de Combustion et Systèmes Réactifs
Centre National de la Recherche Scientifique
45071 Orléans Cedex 2, France
e-mail: gokalp@cnrs-orleans.fr

572-29

and

D. Segawa, T. Kadota, A. Nakainkyo
Department of Mechanical Engineering, Osaka Prefecture University
1-1, Gakuen-cho, Sakai, Osaka 599-8531, Japan

Introduction

A Franco-Japanese cooperative research program on microgravity combustion has been initiated since 1996; part of this program is devoted to understand the combustion processes of methanol droplets under high pressure conditions. Methanol is considered to be one of the most promising candidates as alternative fuel for several applications. Also, the operating pressures in the combustion chamber of liquid fueled internal combustion engines are increasing for higher thermal efficiency. Liquid fuel droplets burn therefore in high pressure gaseous environments and the ambient pressure often exceeds the critical pressure of the fuel. A review of the literature indicates that the combustion characteristics of fuel droplets burning in high-pressure gaseous environments remain largely unexplored [1]. For example, it was found experimentally under microgravity conditions [2, 3] and theoretically [4, 5] that the burning rate of various fuels shows a maximum around the critical pressure. However, the burning rates obtained in a recent experiment under microgravity conditions did not show a peak around the critical pressure [6]. The difficulty in the experiments on droplet combustion arises from the combustion generated buoyant flow in normal gravity, which is enhanced in high-pressure gaseous environments. The reduced surface tension of the droplet burning in high-pressure gaseous environments does not allow the use of the well-known suspended droplet technique in normal gravity. Microgravity conditions offer therefore the opportunity to perform droplet combustion experiments in an environment free from the effect of gravity induced natural convection. The primary objective of our study is to obtain the detailed information needed for the understanding of the combustion process of a single methanol droplet in high-pressure gaseous environments. The present paper describes recent results on the combustion of a methanol droplet under variable ambient pressures and gravitational accelerations. The experiments were conducted under normal gravity, and under microgravity with the use of the parabolic flights of the CNES A300 airplane in France and the drop shaft at JAMIC in Japan.

Experimental apparatus and procedure

Different experimental facilities are used in Japan and in France. The global concept of the apparatus is the same, however. The two different apparatus have been fully described previously [7, 8]. The well-known suspended droplet technique is adopted. A methanol droplet is suspended at the center of a high-pressure combustion chamber and is ignited with an electrically heated kanthal coil. The initial diameters of the droplet d_i range from 1 to 2 mm. The test chamber is filled with dried air at 298 K. Experiments are conducted in normal gravity, and microgravity with the use of the parabolic flights of the CNES A300 airplane (where the gravitational acceleration is of the order of 10^{-2} g_0) in France and the drop shaft at JAMIC (where the gravitational acceleration is of the order of 10^{-4} g_0) in Japan. The backlighted images of the droplet is recorded on a high-speed video camera (500 fps). The droplet surface area is measured by using image processing. The droplet diameter d is defined as the diameter of the sphere that has the same surface area. The obtained time histories of the squared droplet diameter are used to determine the droplet burning rate. Degassed and dehydrated methanol is used in all experiments. The critical pressure (P_{cr}) and the critical temperature of methanol are 8.09 MPa and 513K, respectively.

Results and discussion

Normal Gravity

The time variation of the burning methanol droplet diameter d is determined from backlighted images. Figure 1 shows the time histories of the squared droplet diameter at different ambient pressures. The abscissa is the time after ignition divided by the square of the initial droplet diameter d_i. The ordinate is the square of the instantaneous diameter normalized by the square of the initial droplet diameter. It is evident that the squared droplet diameter decreases quasi-linearly with time at all the ambient pressures; the d^2 law is therefore valid for methanol droplet burning in high pressure air under normal gravity conditions. The slope of the fitted straight line to the data, i.e., the burning rate constant $K_b = -d(d^2)/dt$ increases with increasing ambient pressure.

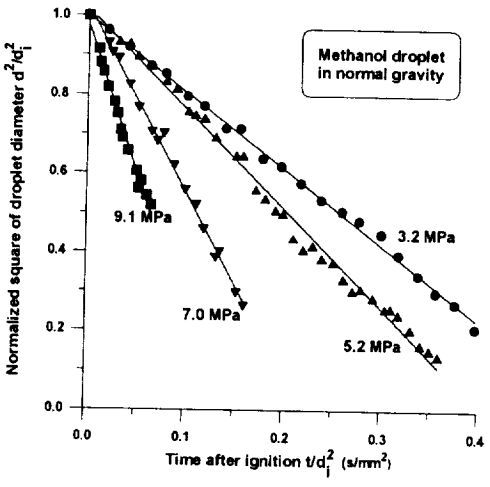

Figure 1 : Time histories of the squared droplet diameter under normal gravity.

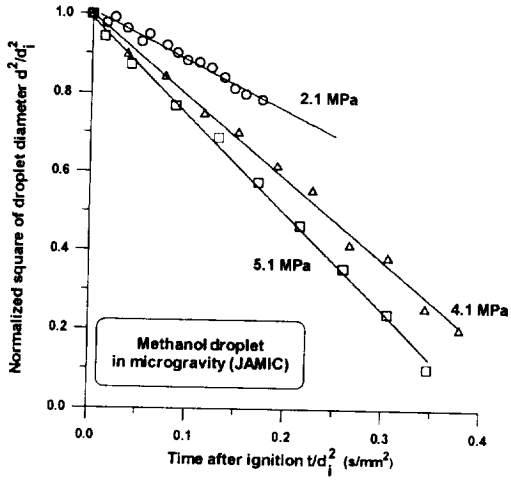

Figure 2: Time histories of the squared droplet diameter under microgravity.

Microgravity

The combustion experiments of methanol droplets on board the CNES A300 airplane were carried out at ambient pressures up to 11.1 MPa. Weak natural convection remains around the burning droplet at high ambient pressures. The droplet surface appears to be smooth even at 11.1 MPa, which is higher than the critical pressure of methanol. This indicates that the droplet has not reached its critical state. In the combustion experiments of methanol droplets in the JAMIC drop shaft, the ambient pressure was increased up to 14.0 MPa; at these highest pressures, the droplet image became blurred and the determination of the droplet diameter more difficult. Figure 2 shows the time histories of the squared droplet diameter under microgravity in the drop shaft. As in the parabolic flight experiments, the d^2 law is valid and the slope of the fitted straight line to the data increases with an increase in the ambient pressure.

Figure 3 shows the dependence of the burning rate on the ambient pressure in normal gravity and in microgravity. The abscissa is the ambient pressure P_a normalized by the critical pressure of methanol, P_{cr}. The normal gravity curves show a good agreement between results obtained in France and in Japan by using different facilities. It is evident that the burning rate increases monotonically with the ambient pressure up to 1.25 times the critical pressure of methanol. The two other curves show the dependence of the burning rate on the ambient pressure in microgravity. The results obtained during the parabolic flights indicate that the burning rate constant increases monotonically with the ambient pressure up to 1.4 times the critical pressure of methanol. We can observe for all these experiments, that the burning rate is unlikely to show a peak near the ambient pressure equal to the critical pressure of methanol. It is in fact likely that the actual critical pressure of the methanol droplet exceeds that of pure methanol due to absorption of inert gases into the droplet. It can be noted however that the dependence of the burning rate constant on the ambient pressure becomes weaker with increasing ambient pressure above the critical pressure. The burning rates derived from the drop shaft experiments increase monotonically with the ambient pressure up to 0.6 times the critical pressure. At each pressure, the burning rate constant of methanol droplets obtained in drop shaft experiments are lower than those obtained in parabolic flight experiments.

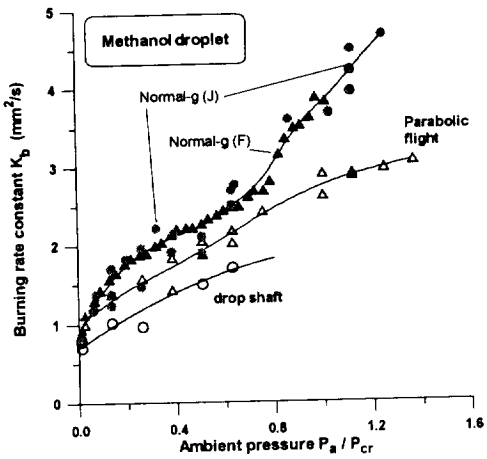

Figure 3 : Dependence of the burning rate constant on ambient pressure

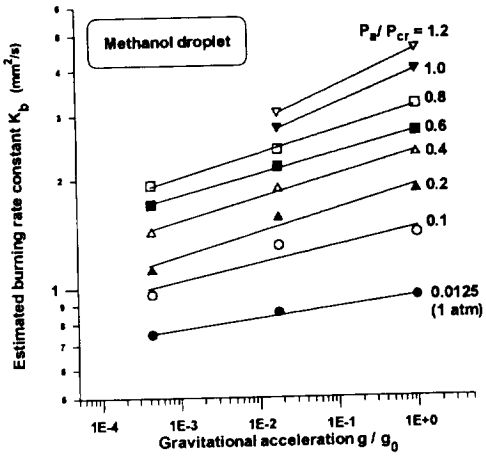

Figure 4 : Estimation of the dependence of the burning rate versus pressure for different gravitational acceleration.

The data on methanol droplet burning rate constant vs. ambient pressure are fitted with curves as shown in Figure 3, and the burning rate constants at eight arbitrary pressures are estimated for normal gravity and the two microgravity conditions. The estimated burning rate constants at each ambient pressure are plotted against gravitational acceleration in Figure 4. The burning rate constant increases with an increase in gravitational acceleration as expected. The increase in gravitational acceleration enhances the influence of the combustion generated natural convection, resulting in the increasing burning rate constant, especially for the highest pressures. When all the experimental data for the burning rate constant, for all pressures and gravitational accelerations, are plotted versus the Grashof number estimated for each experiment, a power lower in the form of $K_b \propto Gr^{0.25}$ is obtained as in Ref. 6.

Conclusions

An experimental study was carried out on the burning of methanol droplets in high-pressure air under microgravity conditions by using the parabolic flights of an airplane and a drop shaft, and under normal gravity. The primary conclusions reached in the present study are as follows.

1. The d^2 law is valid for different ambient pressures and gravitational accelerations within the range of experimental conditions of the present study.
2. The burning rate constant increases monotonically with the ambient pressure up to 1.4 times the critical pressure of methanol.
3. In reduced gravity, dependence of the burning rate constant on the ambient pressure becomes weak above the critical pressure.
4. The burning rate constant decreases with a decrease in gravitational acceleration.
5. The variation of the burning rate constant as $Gr^{0.25}$ is confirmed for the first time by varying the Grashof number both by varying the gravitaional accelaration and the ambient pressure.

Acknowledgments

The Memorandum of Understanding signed between CNRS, CNES and NEDO has made this international collaboration possible. The authors wish to thank Novespace, Sogerma, JSUP and JAMIC for their cooperation.

References

1. Williams, A., (1973) Combust. Flame, **21**, 1-31.
2. Faeth, G. M., Dominicis, D. P., Tulpinsky, J. F. and Olson, D. R., (1969) 12th Int. Symp. on Combustion, 9-18.
3. Sato, J., Tsue, M.,Niwa, M. and Kono, M., (1990) Combust. Flame,**82**, 142-150.
4. Spalding, D. B., (1959) ARS J. **29**, 828-835.
5. Tsukamoto, T. and Niioka, T., (1993) Microgravity Sci. Technol., **4**, 219-222.
6. Vieille, B., Chauveau, C., Chesneau, X., Odeïde, A. and Gökalp, I., (1996) 26th Int. Symp. on Combustion, 1259-1265.
7. Chauveau, C., Chesneau, X. and Gökalp, I., (1993) AIAA Paper**No. 93-0824.**
8. Segawa, D., Kadota, T., Nakainkyo, A., Chauveau, C., Gökalp, I., and Vieille, B., (1998) 27th Int. Symp. on Combustion, poster presentation.

OMIT THIS PAGE

Flame Spread

573-25

DIFFUSIVE AND RADIATIVE TRANSPORT IN FIRES (DARTFire): OPPOSED-FLOW FLAME SPREAD IN LOW-VELOCITY FLOWS

R.A. Altenkirch[1], S.L. Olson[2], J.L. Deering[3], L. Tang[1], S. Bhattacharjee[4], and Uday Hegde[2],
[1]Mississippi State University, Office of Research, NSF Engineering Research Center for Computational Field Simulation, 617 Allen Hall, Mississippi State, MS 39762, altenkirch@research.msstate.edu, [2]NASA Lewis Research Center, 21000 Brookpark Road, Cleveland, OH 44135, sandra.olson@lerc.nasa.gov, [3]Washington State University, School of Mechanical and Materials Engineering, Pullman, WA 99164, deering@mme.wsu.edu, [4]San Diego State University, Department of Mechanical Engineering, San Diego, CA 92182, subrata@voyager5.sdsu.edu

INTRODUCTION

For flames spreading into a low-velocity flow that can only be obtained in microgravity, we have observed behavior that is different from that which is obtained at higher velocities where radiative effects are unimportant and species transport is relatively fast. Unfortunately, lack of a large body of low-gravity flame spread experimental data inhibits progress in developing an understanding of the physics of low-velocity, opposed-flow flame spread phenomena. Recent DARTFire sounding rocket experimental studies though, coupled with developing theory and modelling, have allowed some strides in understanding to be made, on which we report here.

Four launches to date have resulted in six experiments for opposed-flow flame spread over a thick PMMA sample. During the 6 min microgravity period, the PMMA samples were ignited, and steady flame spread was studied under varied flow velocity, oxidizer atmospheric conditions, and, because radiative heat transfer is so important in these slowly spreading flames, external radiant flux. These were the first attempts at such experimental control and measurement in microgravity.

A recent reflight of the Solid Surface Combustion Experiment (SSCE) has demonstrated, as modelling predicts, that for the thick fuel of the DARTFire experiment, flame spread in a quiescent environment is a transient process evolving from ignition to extinction on the order of 600 s (Altenkirch *et al.*, 1999). Further study then of the effects of radiation in the very low-velocity opposing flows is of interest in understanding the transition from steady, sustained spread to the unsteady evolution to extinction as the opposing flow is reduced further and eventually removed.

EXPERIMENTAL

DARTFire sounding rocket hardware is shown in Fig. 1. Two experiments are conducted simultaneously during the 6-min experiment in mirror twin flow tunnels that support from 1-20 cm/s flow through each 10 cm x 10 cm tunnel. Black PMMA samples, 2 cm long x 2 cm thick x 0.635 cm wide, are mounted in the floor of the duct 4 cm from the inlet flow straighteners.

A laser diode and associated lenses provide a uniform external radiant flux of up to 2 W/cm^2 onto one of the sample surfaces. The controlled external radiant flux, which is turned on with the ignitor, turned off when the flame has spread half the length of the sample, turned on again when the flame has reached the end of the sample, and then later tuned off at around 6 min, allows the surface energy balance to be adjusted to compensate for radiant loss from the surface and gaseous species.

A multispectral intensified array video camera with a resolution of 0.1 mm is used to image the

flame. Color images are obtained by combining red, green, and blue filtered images to obtain a 24-bit color composite image. The chemiluminescence of OH and CH radicals in the reaction zone is imaged through 20 nm bandwidth OH and CH filters at 310 nm and 430 nm.

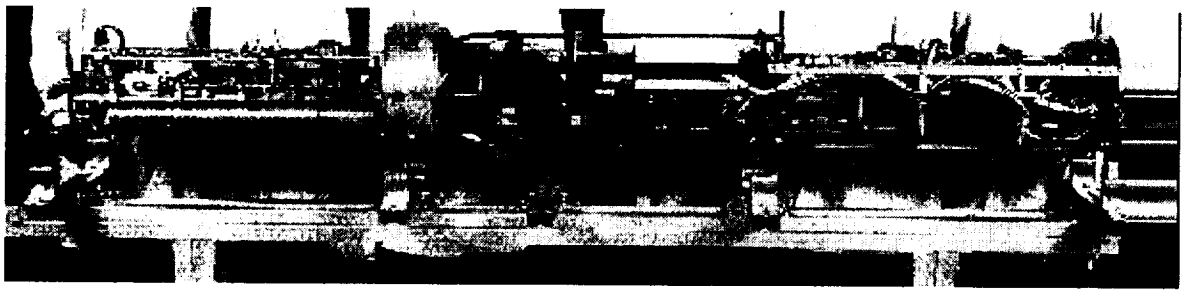

Fig. 1 DARTFire Hardware

Infrared emissions from the gaseous combustion products are also recorded. A multispectral PtSi detector camera (Inframetrics, Inc. Model Infra-Cam PtSi FPA (256x256 pixel array)) was modified to include a 6-filter internal wheel. Filters include 1.87 μm (H_2O), 2.7 and 4.3 μm (CO_2), 3.4 μm (MMA vapor), 4.8 μm (CO), and soot at 1.6 μm.

The test matrix consists 50% O_2, 1, 5, and 10 cm/s with no irradiation, 50% O_2 at 1 cm/s with 1 and 2 W/cm^2 irradiation, and 70% O_2 at 1 cm/s with no irradiation.

MODELLING

The spreading flame is modelled by solving the unsteady, two-dimensional forms of the continuity, momentum, species and energy equations in the gas for a single-step Arrhenius reaction and the unsteady energy equation in the solid that incorporates finite-rate surface pyrolysis (Altenkirch *et al.*, 1999). Surface reradiation and gas-phase radiation, both the loss to the environment and feedback to the surface are included (Bhattacharjee and Altenkirch, 1991).

INFRARED IMAGING

Infrared emission from the flame imaged as described above has been used to determine flame temperature and CO_2 distributions using a hybrid, two-color emission pyrometry scheme in which the ratio of the measured intensities is expressed as the product of the ratio of the Planck functions and the equivalent bandwidth ratio, A_r (Bhattacharjee *et al.*, 1999). For suitable band pairs and their bandwidths, the equivalent A_r is approximately constant, which can be approximated from modelling results.

Temperatures extracted from the IR images with this hybrid approach tend to be lower than what is expected from simulation due, most likely, to the fact that the image in the hottest part of the flame is saturated, and, in application of the technique, uniform properties along the line of sight across the width of the sample are employed. The extracted CO_2 field in the outer, cooler reaches of the flame agrees qualitatively with the simulated field (King *et al.*, 1999).

UV-VISIBLE IMAGING

An example of OHchemiluminescence in the reaction zone is shown in Fig. 2. The dark notch in the flame is a shadow of a thermocouple post.

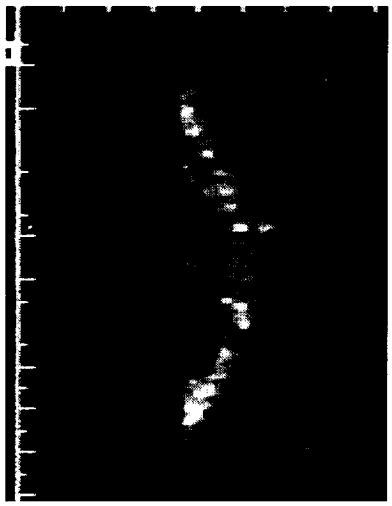

Fig. 2 OH Chemiluminescence

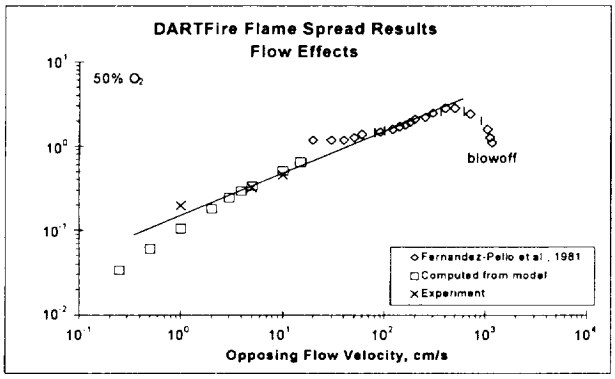

Fig. 3 Spread Rates

FLOW EFFECTS ON SPREAD RATE

Fig. 3 shows the flame spread rate as a function of flow for the experiments without imposed radiation compared to higher flow data obtained on earth (Fernandez-Pello *et al.*, 1981). Flame spread rates show an approximate power law dependencies on flow with an exponent of about 0.5 down to about 5 cm/s. The earth-bound data are for fully developed flow in a channel, whereas the DARTFire data are for developing flow in a channel, approximating a boundary layer flow, so the power law dependence on flow for the earth bound and DARTFire data are not identical.

The model results match well with experimental results down to about 5 cm/s, at which point the model predicts a faster decrease in spread rate than experiment as radiation comes in to play. Eventually as the opposing flow in flame fixed coordinates approaches zero, the spread process becomes unsteady, and flame evolution from ignition leads to extinction (Altenkirch *et al.*, 1999).

EXTERNAL RADIANT FLUX

The laser flux levels were selected in this experiment to offset roughly the surface radiative loss at 1 W/cm^2, and roughly offset the surface plus flame radiative loss in the 2W/cm^2 case. Surprisingly, the spread rate from the no flux case, plotted above in Fig. 3, and for the 1 W/cm^2 flux case with the laser on, were the same, which might not be expected because the added energy input from the laser would be thought to increase the spread rate, which is the case for 2 W/cm^2. When the laser was deactivated, the flame slowed, to well below the no flux case, which indicates that the flame was weakened considerably by the sudden removal of the heat flux. Whether the no-flux and 1 W/cm^2 flux case results are experimentally consistent is unclear; modelling predicts an increase in spread rate for the laser on contrary to experiment.

For the no flux case, the flame standoff reaches a steady value of about 0.6 mm. It takes 40 s to reach this value, but then it is steady within the error of the measurement for the rest of the spread. For the 1W/cm^2 case, the flame standoff distance is just under 0.9 mm during irradiation.

The flame moves out to about 1.05 mm after the laser shuts off. It stays there for about 20 s before moving back in. The standoff distance approaches the 0.6 mm of the no flux case when the laser turns back on. The flame moves out again after a lag of about 10 s.

To interpret the laser effects fully, it is important to take into consideration the conduction-radiation balance at the fuel surface. Using the thermocouple data, conductive flux to the surface was estimated in each case. The absorbed flux from the laser, estimated by assuming an emissivity of 0.8 based on radiometer and surface thermocouple data for an experiment with flux only (no flame), is then added to that to determine the total flux from the gas to the surface in each case

The flame spread process appears to be approximately linearly dependent on the net heat flux from the flame to the surface. The laser flux is part of that, but because the flame responds to the laser by moving the flame away from the surface, the effect of the laser is muted.

CONCLUSIONS

The DARTFire sounding rocket hardware has provided new information on opposed flow flame spread over thermally-thick solids using multispectral visible and infrared imaging systems. The effect of flow velocity on flame spread over the 1-15 cm/s range extends data previously reported at high opposing flows almost two decades lower in flow. Stable flames are found down to 1 cm/s flow, even though previous experiments have shown that quiescent conditions are not flammable (Altenkirch *et al.*, 1999). This demonstrates that even a flow on the order of diffusive velocities (0-2 cm/s) is sufficient to sustain combustion where in a perfectly quiescent environment, the flame would not be viable. Laser effects are unexpectedly complex and muted. The flame moves away from the surface with increased radiant flux, thereby reducing the conductive feedback from the flame to the surface.

ACKNOWLEDGEMENTS

The authors gratefully acknowledge support for this work through NASA Grant NCC3-221.

REFERENCES

Altenkirch, R.A., Tang, L., Sacksteder, K., Bhattacharjee, S., and Delichatsios, M.A. (1999). Inherently Unsteady Flame Spread to Extinction over Thick Fuels in Microgravity, *Twenty-Seventh Symposium (International) on Combustion*, The Combustion Institute, Pittsburgh, in press.

Bhattacharjee, S., King, M., Cobb, W., Altenkirch, R.A., and Wakai, K. (1999). Approximate *Journal of Heat Transfer*, submitted.

Bhattacharjee, S. and Altenkirch, R.A. (1991). *Twenty-Third Symposium (International) on Combustion*, The Combustion Institute, Pittsburgh, pp. 1627-1633.

Fernandez-Pello, A.C., Ray, S.R., and Glassman, I. (1981). *Eighteenth Symposium (International) on Combustion*, The Combustion Institute, Pittsburgh, pp. 579-589.

King, M., Bhattacharjee, S., Altenkirch, R.A., Olson, S., Hedge, U., and Horowitz, J. (1999). Application of Hybrid Emission Pyrometry in Flame Spread Experiments in Microgravity, in preparation.

S74-25

FLAME SPREAD ACROSS LIQUIDS – EXPERIMENTAL RESULTS

H. D. Ross[1] and F. J. Miller[2], [1]NASA Glenn Research Center; MS 500-115, 21000 Brookpark Road, Cleveland, OH 44135; Howard.D.Ross@grc.nasa.gov; [2]National Center for Microgravity Research; MS 110-3, 21000 Brookpark Road, Cleveland, OH 44135; fletcher@rosebud.grc.nasa.gov

INTRODUCTION

The goal of our research on flame spread across a pool of liquid fuel is the quantitative identification of the mechanisms that control the rate and nature of flame spread when the initial temperature of the liquid pool is below the fuel's flash point temperature. Besides numerous experiments in drop towers and 1g laboratories, we have flown five microgravity (μg) experiments on sounding rockets. As described in earlier papers [1-3], the first three flights examined the effect of forced opposed airflow over a 2.5 cm deep x 2 cm wide x 30 cm long pool of 1-butanol in μg. It was found that the flame spread is much slower and steadier than in 1g where flame spread has a pulsating character. It was speculated that the flame spread in μg resembled the character of pseudo-uniform spread in 1g; Ito et al [4]later confirmed this conclusively in 1g experiments. Much of the μg flame is also farther from the surface, dimmer, and with less soot, when compared to the 1g flame. Three-dimensional liquid-phase flow patterns that control the liquid preheating were discovered in both 1g and μg.

Our numerical model, restricted to two dimensions, had predicted faster, pulsating flame spread [5] in μg for opposed airflow. In examining the differences in the dimensionality of the model and experiment, it was noted that the experiment allowed gas expansion in the lateral direction (across the width of the pool), for which the model could not account. Such lateral expansion could reduce the expansion in the forward and upward directions. Because only these latter directions could be modeled, it was decided to artificially reduce the gas thermal expansion in the predictions. When this was done, satisfactory agreement could be obtained between the predicted and observed spread rates and the steadiness of the spread in microgravity [2]. In 1g, however, the predicted flame spread character also changed to pseudo-uniform, which disagreed with our 1g experiments where the spread is pulsating. It was then speculated that gas-phase buoyant flow might oppose the lateral gas expansion, so that the 1g experiments retained their pulsating flame spread character. If this speculation was valid, a difference in lateral gas expansion should be observable when comparing 1g and μg experiments. Specifically, it was anticipated that greater flow divergence caused by lateral expansion would be measured in μg in the absence of a buoyant flow directed towards the flame.

RECENT EXPERIMENTAL RESULTS

Based on the above model-to-experiment comparison and related experiments, the 4th sounding rocket flight was used to visualize the extent of lateral thermal expansion and the gas-phase recirculation cell, which were both expected to be greater in μg than in 1g[6]. Smoke filaments flowing ahead of a flame spreading across 1-butanol into a 30 cm/s opposed air flow were illuminated with two orthogonal laser light sheets and showed clearly for the first time in μg the extent of the gas-phase recirculation cell in front of the flame and the lateral flow divergence due to thermal expansion (see [6] for the images). As predicted by numerical modeling, the gas-phase recirculation cell is larger in μg, but unlike predictions it was not cyclically destroyed and reformed because the flame spreads steadily. Experimentally the liquid-phase flow is both faster and extends further ahead of the flame in μg[2], so that the driving force for the gas-phase cell is larger. This larger cell may contribute to the slow flame spread in μg, since fuel vapor in the cell is distributed in a larger volume (presumably at a lower concentration) and dispersed more readily into the free stream by the larger cell. In both 1g and μg the top view shows lateral thermal expansion as the smoke approaches the flame front in μg is not dramatically different than in 1g.

The only observed gravitational effect is the smoke traces near the trailing μg flame do not rise nor turn inward in the absence of buoyancy, unlike those displayed in [3].

The flow patterns, found in this flight test to be approximately the same regardless of gravitational level, challenge the notion that thermal expansion should be reduced in the 2-D numerical model to account for 3-D effects. Two specific objectives were then established for the fifth sounding rocket flight, both of which revolved around an improved experimental ability to compare with the model: first a nearly 40:1 ratio of the width-to-depth for the tray pool was selected to minimize the finite-width effects in the experiment (the model effectively assumes infinitely wide pools and the previous tray had a width:depth aspect ratio of 0.8:1); and second, the tray width nearly reached the flow duct walls to physically hamper the lateral gas expansion. The tray dimensions for flight test 5 were 2 mm deep by 78 mm wide by 298 mm long.

Experiments prior to the flight revealed interesting and new phenomena related to fuel depth and aspect ratio. For the shallow tray with a 40:1 aspect ratio, the surface deformation was visualized by video-imaging the reflection in the pool surface of an illuminated grid placed above the tray. Immediately upon energizing the ignitor, the pattern of the grid warped, indicating surface deformation, likely due to thermocapillary flow away from the igniter. As shown in Fig. 1, a series of small waves progressed down the tray after ignition, then the grid reflection changed to a washed-out chaotic tangle when the flame spread. For the deep pool with a 0.8:1 aspect ratio tray, the grid deformation was much less pronounced, though a wave that traveled along the tray length was noted to accompany each flame pulsation. Current numerical models of flame spread assume a flat surface.

Tests were also conducted to measure the flame-spread rate and character across shallow pools in the presence of a forced airflow from 10 to 30 cm/s. Sample flame fronts are shown in Fig. 2 and a result of the flame position vs. time is shown in Fig. 3. One interesting feature of both the 1g and μg flames is that they no longer have simple curved fronts, but instead exhibit "fingering," whereby parts of the flame are convex and parts are concave to the direction of spread. This is unlike our results for pools that are the same depth but are only 20 mm wide, where flames have a consistently shaped, slightly convex flame front. The fingers in the wide tray are not steady in time, but may retreat and advance in what appears to be an erratic fashion. This highly wrinkled and erratic front makes it difficult to characterize the flames as pulsating or uniform. On a qualitative level, however, the μg flames are more unstable (frequency and amplitude of oscillations were larger) than their 1g counterparts, perhaps because of a sloshing liquid pool in μg or because of the presence in 1g of a stabilizing buoyant flow in addition to the imposed airflow. While the 1g flame front maintained the same brightness as it spread, the μg flame front alternated between bright and dim (see Fig. 2b) This unsteadiness is also manifested in the flame position graphs where the oscillations along the centerline are larger. Finally, perhaps the most unexpected feature of the flame spread is that it is as fast or *faster* in μg than in 1g for the same opposed airflow rate. In no previous tray geometry has this been found.

These tests required longer μg time and a clearly quiescent pool for this feature to be proven, so a flight test was planned where additional diagnostics could also be brought to bear. While the drop tower allowed the tray to be filled in 1g prior to release into μg, this could not be done in flight and filling of liquid into the new, wide-shallow tray while in flight required substantial hardware/software modifications. Filling was intended to be accomplished through three stages: a. mechanical pumping of fuel from a reservoir into one end of the tray, b. wicking at the corners of the bottom and two sidewalls of the tray to pull the liquid to the other end of the tray, and c. bulk liquid spreading toward an equilibrium surface shape. All stages were tested to the extent possible in 1g and μg, and were supported by calculation [7]. Unfortunately, problems were encountered in filling this tray in μg and no combustion results were obtained from the flight. While indications are that the tray would have completely filled eventually, it did not do so in the time available before the end of the μg period of the sounding rocket flight.

FUTURE WORK

Currently tests are being conducted to determine with certainty the cause of the filling failure aboard the last sounding rocket flight, and to determine the best test conditions for the remaining three flight tests. In addition, the previously found differences between model and experiment regarding the character and rate of spread are still being investigated; the following table shows various means that achieve transitions in flame spread character.

Means to Effect Transition	Uniform ⇒ Pulsating	Pulsating ⇒ Pseudo-Uniform
Lower Pool Temperature	Predicted and shown by experiments	Predicted and shown by experiments
Changed Pool Depth	Predicted and shown by experiments: decreases in pool depth can cause this transition	Predicted that increases in pool depth can cause this transition; not yet examined in expts.
Reduced Lateral Gas Expansion	Not yet examined	Predicted; no direct test, however, enhanced lateral gas expansion was not seen in μg experiments
Lower Oxygen Concentration	Predicted and shown by expts in 1g; predicted and shown by expts to go from Uniform ⇒Extinction in quiescent μg.	Predicted not to occur at any g level; not yet examined in 1g expts. Pulsating spread not yet observed in μg expts done to date.
Reduced Gravity	Not found for case with forced gas-flow; in quiescent μg, transition to flame extinction, rather than pulsating spread, is observed & predicted	Predicted not to occur, but observed in μg experiments with forced airflow
High diffusivity diluents	Found in experiments with He/O_2 Superflash spread predicted.	Not yet examined
Radiative Heat Loss	Not yet examined	Not yet examined

Radiative heat loss has been shown to weaken the μg flame proportionately more than the 1g flame in experiments with solid fuels. There is every expectation that the same behavior will be predicted in flame spread across liquid fuels. It is known from our experiments that the μg flames are weaker than in 1g, perhaps due to radiative heat loss. If so, the accounting for radiative loss in the model may enable the prediction of pseudo-uniform spread as is observed in μg while retaining the pulsating character of spread found in 1g. Experiments to validate this idea are being developed.

ACKNOWLEDGEMENTS

Special thanks to Michael Lewis, Rosemary Huang, and Kevin Magee for their assistance with these experiments.

REFERENCES

1. Ross, H. D., *et al.*, *Flame Spread Across Liquids*, in *3rd International Microgravity Combustion Workshop*. 1995, NASA Lewis Research CP 10174, p. 47-54.
2. Ross, H. D., and Miller, F. J., *Detailed Experiments of Flame Spread Across Butanol Pools*. Twenty-Sixth Symposium (International) on Combustion, 1996, p. 1327-1334.
3. Ross, H. D., Miller, F..J. and Sirignano, W. A. ,*Spread Across Liquids*, in *Flame Spread Across Liquids*. Fourth International Microgravity Combustion Workshop:. NASA Lewis Research CP 10194, 1997, p. 375-381.
4. Ito, A., Konoshi, T., Narumi, A., Tashtoush, G., Saito, K., and Cramers, C. J. *The Measurement of Surface Temperature and Vapor Concentration Profiles for a Spreading*

Flame Over Liquid Fuels. in *5th ASME/JSME Thermal Engineering Joint Conference*, 1999, San Diego, CA: ASME.

5. Schiller, D.N., Ross, H. D. and Sirignano, W. A., *Computational Analysis of Flame Spread Across Alcohol Pools.* Combust. Sci. Tech., 1997. **118**: p. 203-255.
6. Miller, F.J..and.Ross, H. D. *Smoke Visualization of the Gas-Phase Flow During Flame Spread Across a Liquid Pool.* in *27th International Symposium on Combustion.* 1998. Boulder, Colorado: The Combustion Institute.
7. Weislogel, M.M., *Fluid Interface Phenomena in a Low-Gravity Environment: Recent Results from Drop Tower Experimentation.* Space Forum, 1998. **3**: p. 59-86.

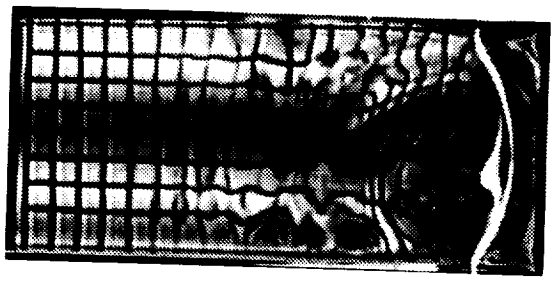

Figure 1. A reflected grid shows the surface deformation as a flame spreads across a 2 mm deep, 80 mm wide pool of 1-butanolin quiescent, 1g conditions The flame is spreading right to left and is about 1/3 of the way from the right side. The bright line on the right side is the ignitor. The grid squares are approximately 1 cm on a side.

(2a)

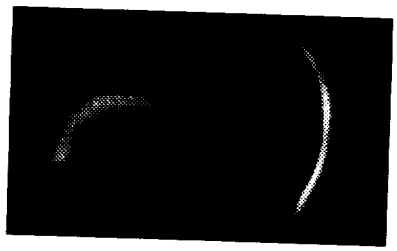

(2b)

Figure 2 Top view of flame spread across an 80 mm wide by 2 mm deep pool of 1-butanol. a) 1g. Smoke lines (red) indicate flow direction one 1 mm above surface 30 cm/s left to right. b) μg. Flame is more erratic in shape, direction, and brightness. Spread is again right to left against a 30 cm/s flow.

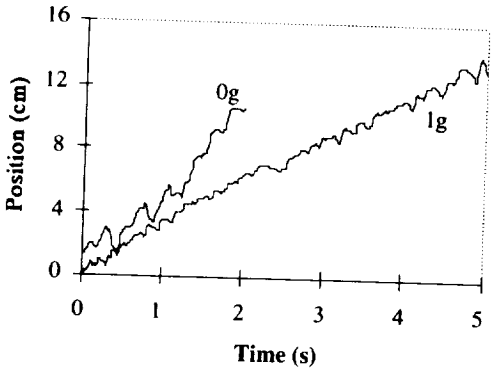

Figure 3. Flame position vs. time along the centerline of 2 mm deep by 80mm wide trays in 1g and μg. Both have opposed air flows of 30 cm/s.

FLAME SPREAD ACROSS LIQUIDS: NUMERICAL MODELLING

Inchul Kim, Huaidong Li, and William A. Sirignano
Department of Mechanical and Aerospace Engineering,
University of California, Irvine, Irvine, CA 92697

INTRODUCTION. The goals of our theoretical/computational program are to study flame spread over liquid fuel pools to guide and explain the microgravity experimental research of H. Ross and F. Miller and to provide fundamental insight for the flame spread phenomenon. The approach has involved the development and exercise of planar 2-D, axisymmetric, and 3-D codes for the unsteady two-phase flow. The gas-phase model accounts for multicomponent reacting flow. Thermocapillary and gravity flows are included in the models.

During the past year, we concentrated on comparisons of the model with existing axisymmetric experimental data in order to validate the model and to establish, to the extent possible, the appropriate global chemical kinetics to be used for n-propanol and n-butanol. We also examined the effect of liquid fuel depth on planar flame spread with and without forced, opposed airflow in order to support the sounding rocket flight tests. The depth of a liquid fuel pool affects the heating of the liquid fuel pool and thus the liquid fuel surface temperature ahead of the flame. A three-dimensional code has been developed and is being benchmarked: it will be used to explain the effects of fuel pool width and various edge effects.

VALIDATION OF AXISYMMETRIC ANALYSIS. In order to compare the model with existing axisymmetric experimental data, we investigated flame spread for a shallow (1.6 mm), 30 cm diameter pool filled with propanol as a function of oxygen concentration for 0-g_0 as well as 1-g_0 without forced gas-phase flow.

CASE	21% O_2		17.5% O_2	
	1-g	0-g	1-g	0-g
Present Result	14 cm/s	16 cm/s	3.8 cm/s (3.5 Hz)	extinction
Experiment by Ross & Sotos (1990)	15 cm/s	15 cm/s	3.5 cm/s (3.9 Hz)	extinction

Table 1 Comparison of the mean flame spread rate between present and experimental results

Flame spread is uniform for oxygen concentration ≥ 21% in normal and zero gravities at 21° C. As the concentration increases, the reaction rate and hence the flame spread increases. As the concentration is reduced to 17.5%, flame spread at 1-g_0 becomes pulsating; on the other hand, the flame at 0-g_0 extinguishes. The rate of flame spread and the frequency of pulsation are in good agreement with the results from the experimental study by Ross and Sotos (1990) in Table 1.

DEPTH EFFECT IN PLANAR FLAME SPREAD. This computational study examines the effect of liquid fuel depth on flame spread across propanol pools with and without forced, opposed air flow. The initial pool temperature is below its closed-cup flash point temperature T_{cc}, so the liquid fuel must be heated sufficiently to create a combustible mixture of fuel vapor before ignition and flame spread can occur. Furthermore, in order for the flame to spread, an approximate rule is that the liquid fuel surface temperature ahead of the flame must be heated above T_{cc} so that a flammable mixture just above the lean limit exists ahead of the flame. The depth affects the heating of the liquid fuel pool and thus the liquid fuel surface temperature ahead of the flame.

The liquid fuel (n-propanol) is in a tray of 30 cm length with an exit plate of 10 cm length. The height of the open computational domain in the gas phase is 10 cm. A weak dependence on the gas phase height was predicted (Schiller *et al.*, 1996). The igniter (2 mm length, 0.1 mm thickness) is modeled as a hot pocket of gas located x = 1 cm from the left edge of the liquid phase and 1 mm above the liquid surface with a temperature that increases linearly from T_0 at time t = 0 to 1300° C in 0.1 second following activation of the igniter. The igniter temperature remains constant until t = 1 to 2 second, after which time the igniter is deactivated.

Laboratory coordinates are used in the solution of the governing equations with variable density and thermophysical properties and a one-step chemical kinetics scheme is employed. The conditions at the gas/liquid interface are obtained from balances of energy and mass fluxes, balance of stresses, continuity of the temperature and tangential velocity, and the assumption of negligible recession of the liquid surface. (See Kim *et al.*, 1998.) The numerical method uses the SIMPLE algorithm with the SIMPLEC modification and the hybrid-differencing scheme. The gas phase and liquid phase are solved separately during a time step. Interface conditions are used for the solution of each phase. In order to determine the effect on flame spread of the initial profile of fuel vapor concentration before the igniter activation, we first solve the governing equations without chemical reaction as a function of time

The initial profile of fuel vapor concentration in the gas phase before the igniter is activated (and thus before the chemical reaction occurs) is important because it determines the chemical reaction rate soon after flame spread begins. This profile is investigated as a function of time after filling the fuel tray both for normal gravity (1-g_0) and zero-gravity (0-g_0). Kim *et al.* (1998) showed that, without forced air flow (U_{opp} = 0) at 1-g_0, the propanol evaporates into the gas phase, and then the mixture of propanol and air flows out of the tray since propanol (and the propanol/air mixture) is heavier than the air. The air flows down to the tray to satisfy mass conservation, and a steady vapor-concentration boundary layer is established at t = 10 s after filling the fuel tray. Unlike the 1-g_0 case, the 0-g_0 case shows that the propanol vapor diffuses continuously into the air, and no velocity boundary layer is established in the gas phase. With forced air flow U_{opp} = 30 cm/s, it is found that a steady vapor-concentration boundary layer is established quickly at t = 5 s both for 1-g_0 and 0-g_0.

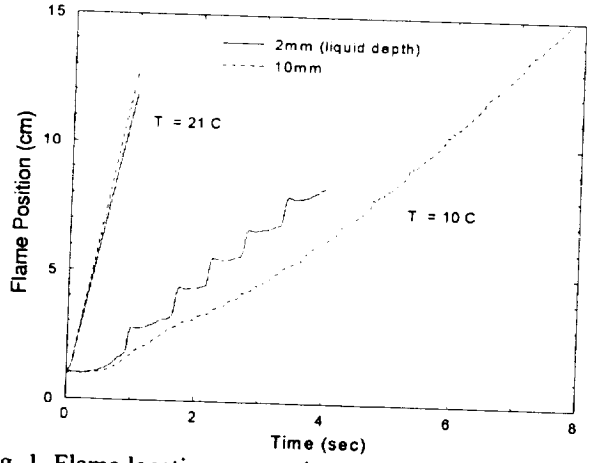

Fig. 1. Flame location versus time under U_{opp} = 30 m/s and 1-g_0 for two different H_l (2mm and 10mm) with two different T_0 (21° C and 10° C)

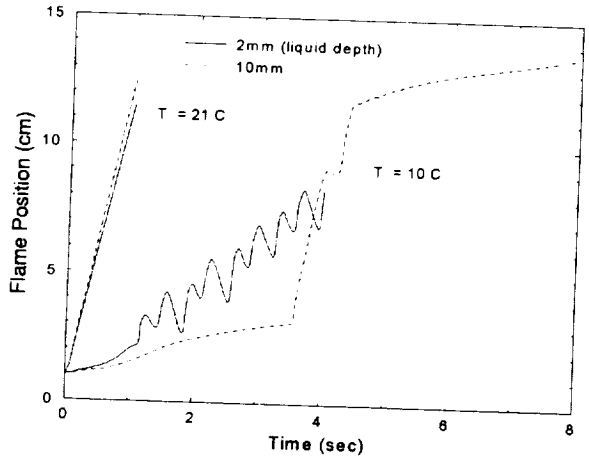

Fig. 2. Flame location versus time for the same parameters as in Fig 1 but for zero-gravity (0-g_0).

Consider the depth effects on the flame spread under forced air flow after the vapor concentration layer is established and the igniter is activated. Fig. 1 shows the flame location versus time under forced air flow (U_{opp} = 30 cm/s) and normal gravity (1-g_0) for two different liquid depths (H_l = 2 mm and 10mm) with two different initial liquid temperatures (T_0 = 21° C and 10° C). For T_0 = 21° C (uniform spread regime), the flame spread on the deeper pool of H_l = 10mm is a little faster than the flame spread on the shallow pool of H_l = 2mm. For T_0 = 10° C (pulsating regime), the flame spread rates of the shallow and deep pools are similar to each other. But the flame on the shallow pool spreads with much higher frequency than the flame on the deep pool. A long liquid preheating distance ahead of the flame occurs when the liquid fuel has an initial temperature in the pulsating regime (Kim *et al.*, 1998). For a shallow pool, the liquid vortex is restricted by the tray bottom. This lessens the recirculation time, so more of the surface heat, that is normally connected far from the flame, instead recirculates near the flame, causing the flame spread frequency to increase. Furthermore, the deeper pool requires more heat flux into the control volume in the liquid phase ahead of the flame.

Figure 2 illustrates the flame location versus time for the same parameters as in Fig. 1 but for zero-gravity (0-g_0). For T_0 = 21° C (uniform spread regime), the flame spreads are close to those at 1-g_0. On the other hand, for T_0 = 10° C (pulsating regime), the flame on the deeper pool of H_l = 10 mm spreads slowly for initial 3.6 sec, then spreads fast for the next 1 sec, and then spreads slowly again.

In summary, the effects of the depth of liquid fuel pool to flame spread under forced air flow have been examined for 1-g_0 and 0-g_0, where the initial pool temperature is below the closed-cup flash point temperature and the depth of the pool is 2mm and 10mm. For the uniform spread regime, the flame spread on the deeper pool is faster than the flame spread on the shallow pool. For the pulsating regime, the flame on the deep pool spreads with much slow frequency than does the flame on the shallow pool.

THREE-DIMENSIONAL CODE. We have expanded our 2-dimensional code, which was developed in the past to simulate flame spread across fuel pools, to a 3-dimensional code. This enables us to quantify the effects of tray aspect ratio, tray/flow duct geometry, lateral hot gas expansion, and the sideflow processes in the liquid and gas phases. Most assumptions made in the 2D model (for details, see Schiller *et al.*, 1996) are also adopted in the 3D model. The numerical method uses the SIMPLE algorithm (Patankar, 1980) with the SIMPLEC modification (Van Doormaal and Raithby, 1984) and the hybrid-differencing scheme. Non-uniform, partially adaptive grids are used for all three coordinates. A one-step chemical kinetics scheme is assumed. In order to assure that the 3D code performs well, we first attempted to reproduce the 2D planar results by assuming that the igniter is infinitely long and the properties are uniform in transverse direction. To reduce CPU time requirements, we used sparse grids.

Figures 3 and 4 show the contours of the flow field (a) and the temperature (b), which are calculated by the 2D and 3D codes, respectively. As can be seen, general distributions are consistent, except for the flame shapes (Figs. 3a & 4a). Comparison of the flame position and the maximum reaction rates between the 2D and 3D calculations are shown in Figs. 5 and 6, respectively. The difference can be partly attributed to the difference in grids used in the 2D and 3D calculations. The finer grids are used in the 2D simulation.

There are some convergence problems with each code at certain grid sizes. These must be corrected. The next step is to reproduce the axisymmetric calculation to further validate the 3D code. Then we will add the lateral side boundary conditions to the equations to examine the three-dimensional effects of tray aspect ratio.

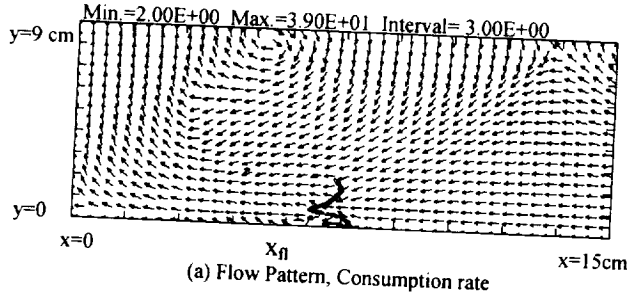

(a) Flow Pattern, Consumption rate

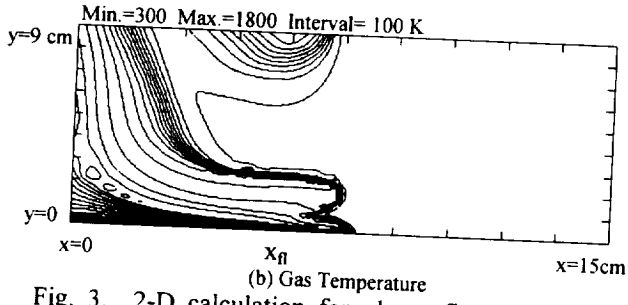

(b) Gas Temperature

Fig. 3. 2-D calculation for planar flame spread Propanol, T_0 =23° C, 1-*g*.

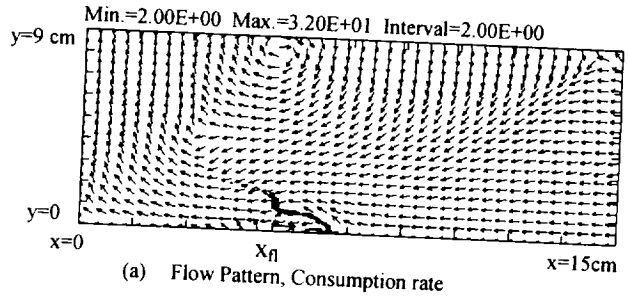

(a) Flow Pattern, Consumption rate

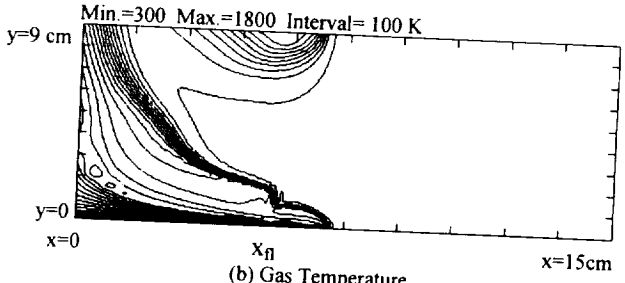

(b) Gas Temperature

Fig. 4. 3-D calculation for the same conditions as Fig. 3 at lateral distance z = 3 cm.

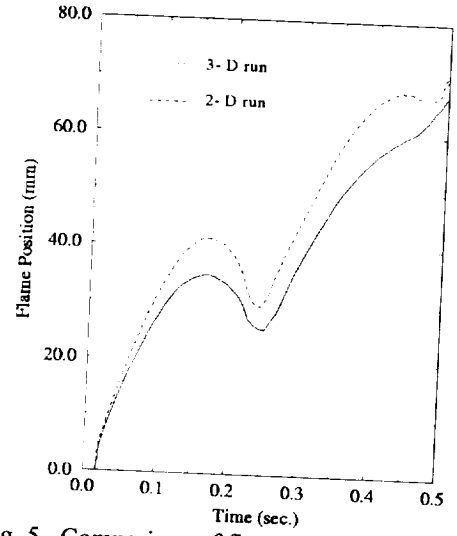

Fig. 5. Comparison of flame positions

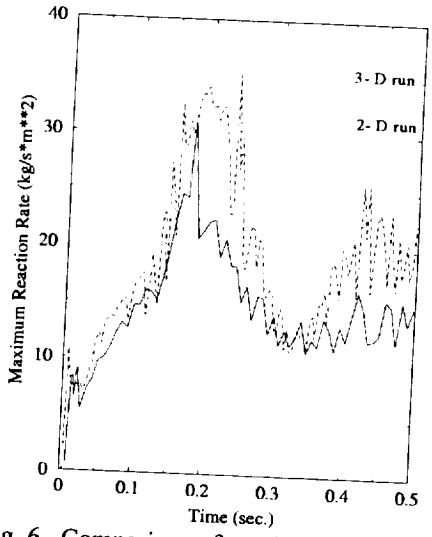

Fig. 6. Comparison of maximum reaction rates

REFERENCES

Kim, I., Schiller, D. N., and Sirignano, W. A. (1998), ``Axisymmetric Flame Spread over Propanol Pools in Normal and Zero Gravities," Comb. Sci. Tech., 139, pp. 249-275.

Patankar, S. V. (1980), Numerical Heat Transfer and Fluid Flow, McGraw-Hills, New York.

Ross, H. D. and Sotos, R. G. (1990), ``An Investigation of Flame Spread Over Shallow Liquid Pools in Microgravity and Nonair Environments," Twenty-Third Symp. (International) on Combustion, The Combustion Institute, Pittsburgh, PA, pp. 1649--1655.

Schiller, D. N., Ross, H. D. and Sirignano, W. A. (1996) "Computational Analysis of Flame Spread Across Alcohol Pools," Comb. Sci. Tech., 118, pp. 203-255.

Van Doormaal, J. P. and Raithby, G. D. (1984) "Enhancements of the SIMPLE Method for Predicting Incompressible Fluid Flows," Numerical Heat Transfer, 7, pp. 147-163.

S76-25

THE THREE-D FLOW STRUCTURES OF GAS AND LIQUID GENERATED BY A SPREADING FLAME OVER LIQUID FUEL

G. Tashtoush, A. Ito, T. Konishi, A. Narumi, K. Saito and C.J. Cremers
University of Kentucky, Department of Mechanical Engineering
Lexington, KY 40506-0108

ABSTARCT

We developed a new experimental technique called: Combined laser sheet particle tracking (LSPT) and laser holographic interferometry (HI), which is capable of measuring the transient behavior of three dimensional structures of temperature and flow both in liquid and gas phases. We applied this technique to a pulsating flame spread over n-butanol. We found a twin vortex flow both on the liquid surface and deep in the liquid a few mm below the surface and a twin vortex flow in the gas phase. The first twin vortex flow at the liquid surface was observed previously by NASA Lewis researchers, while the last two observations are new. These observations revealed that the convective flow structure ahead of the flame leading edge is three dimensional in nature and the pulsating spread is controlled by the convective flow of both liquid and gas.

INTRODUCTION

Flame spread over liquids is of our current interest because of the fundamental curiosity of its mechanisms and necessity of understanding the phenomenon and its impact on fire safety in liquid-storage tanks and accidental spills of flammable (e.g., crude oil and jet fuel) liquids. In the flame spread over liquids, liquid convection ahead of a flame spreading over liquids is unique and plays an important role in the spreading process [1-5]. Because of the presence of liquid convection, the flame spreading process is complex in comparison to the flame spread over solids. An extensive review by Ross [5] summarizes well the current progress on flame spread studies over liquids offering the list of future tasks.

Almost nine years ago, we started our experimental investigation of flame spread over liquids using a Pyrex narrow tray. We obtained many valuable discussions and comments from researchers who are knowledgeable in this subject including Forman Williams of UCSD, Irv Glassman of Princeton University, John DeRis of Factory Mutual, Toshi Hirano of U. of Tokyo, Howard Ross of NASA, Vedha Nayagam of NASA, and Castero's group in Spain. Based on knowledge gained through these discussions and our own literature survey, we found the transient measurement of flow (both liquid and gas), temperature (both liquid and gas) and gaseous fuel concentrations generated by the spreading flame is curtail. At that time we found none of already exiting techniques to be able to satisfy all the above requirements simultaneously. Thus, we decided to develop several different techniques, each of which can satisfy one of the above requirements, and eventually integrate them into one single technique of all the capability. First we developed a holographic interferometry that is capable of measuring transient two-D temperature map in liquids. Second, we developed a laser sheet particle tracking technique that is capable of measuring transient two-D map of the flame induced-flow both in liquid and gas. Third, we developed a dual wavelength holographic interferometry that is capable of measuring two-D profiles of transient fuel vapor concentration in the gas phase. The first and the second methods [1,2,7] proved our methods to be accurate enough to study the

detailed structure of flame spread phenomena. Since our publication details these results [7], further discussion is not provided here.

Three major experimental efforts made recently should be mentioned. (1) NASA researchers applied a rainbow Schlieren to visualize the liquid flow and an infrared camera to measure the liquid-surface temperature [4,5]. In addition, NASA group conducted a successful series of flame-spread experiments over n-butanol under microgravity and provided valuable experimental data [8] that revealed a twin vortex ahead of the flame's leading edge showing the 3-D nature of the spread phenomenon. (2) Castillo et al. [6] applied Schlieren technique and found theoretical predictions of the flame-spreading velocity to be larger than the measured values. (3) We applied a dual wavelength holographic interferometry to measure fuel concentrations in the gas phase [7].

Despite these findings, unfortunately the currently available (all the above mentioned) techniques are at best 2-D. Thus, we put together an international collaboration among the University of Kentucky, Oita University and Kanagawa Inst. of Technology to develop a 3-D measurement technique which can accurately and simultaneously measure the transient 3-D structures of flow, temperature and fuel concentration. As the first step toward this integrated multi-measurement technique, we upgraded our 2-D LSPT technique to 3-D capability of measuring a transient three-dimensional flow distribution of both gas and liquid phases simultaneously. We applied this technique to improve the current understanding of the twinning flow that was first reported by Ross et al. at the NASA Lewis Research Center [6] from their infrared imaging (IR) measurement data on the fuel-surface temperature. The NASA's IR image result revealed that the preheated distance ahead of the flame was much longer in microgravity than in normal gravity where no twin structure was observed. In this paper we attempt to explain why that happed by using our measured flow structure.

EXPERIMENTAL METHODS

A schematic illustration of the experimental apparatus and setup for the LSPT technique used in this study is the same as our previous studies [1,2] and is not shown here. Fuel trays of (5, 10, 20 mm wide) x 20 mm deep x 300 mm long were used; the two long sides of the fuel trays were made of Pyrex of 2-mm thickness. A 4-W Ar-ion laser was used as light source to form a 1-mm thick laser sheet by passing the beam through cylindrical lenses. Three positions of the laser sheet were chosen under the liquid surface at 2 mm, 4 mm and 6 mm and two positions over the liquid surface in the gas phase at 1 and 2 mm as will be seen. Talc particles were dispersed uniformly over the fuel surface for the measurement of gas phase convection. Aluminum particles of 15 ($\pm$ 5) μm diameter were mixed with the liquid for the measurement of liquid convection. A high-speed camera system with an ultraviolet lens and an image intensifier having a speed of 500 frames/s was used to obtain the velocity profiles. The trajectories of these particles were recorded by the high-speed video camera, which was connected to a video system and a TV monitor for the real time observation of both the flow field and spreading flame.

SOME RESULTS AND DISCUSSION

As the flame began to propagate, the preheated region extended ahead of the flame. It then developed two symmetric vortices that rolled up toward the sidewalls while the preheated liquid at the center continued to proceed upstream of the flame. Later, when the gaseous fuel-air

mixture over the liquid surface reaches the lean flammability limit, the flame accelerates forward in the premixed gas layer and covers the twin vortices. The existence of this side-flow structure was first reported by Ross [8] using a 20-mm wide tray. In this study using 5, 10 and 20 mm trays we confirmed that the preheated liquid extended ahead of the flame with twin vortices flow structure. It was found that the length of the preheated zone ahead of the flame is inversely proportional to tray width. Once the flame leading edge reaches the front of the liquid convection zone, it stops or decelerates to start another cycle. We also observed that the flame inclination angle defined in [8] is smaller in the acceleration step than in deceleration because the flame acceleration only occurs when the gaseous fuel-air mixture is within the flammability limit [9,10].

Figure 1 shows the velocity profiles ahead of the flame in the liquid phase using 10-mm wide tray at four different laser sheet positions on the liquid surface. Those images show clearly that the size of the twin vortices decrease as the laser sheet moves down from the liquid surface.

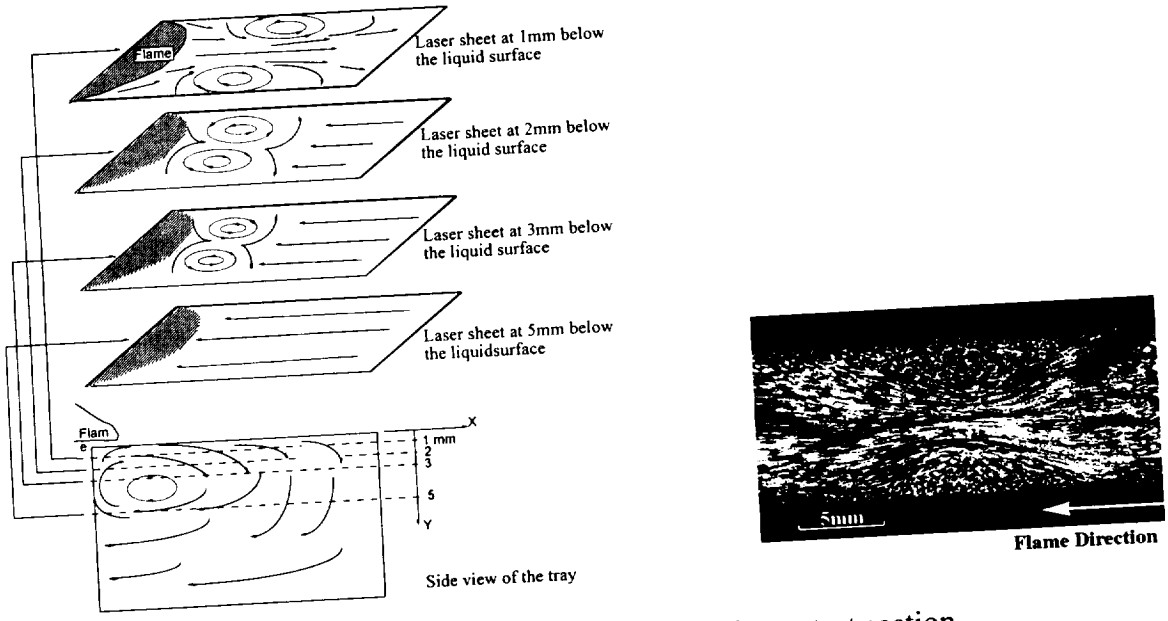

Figure 1 Flow visualization in the liquid phase using 20 mm test section.

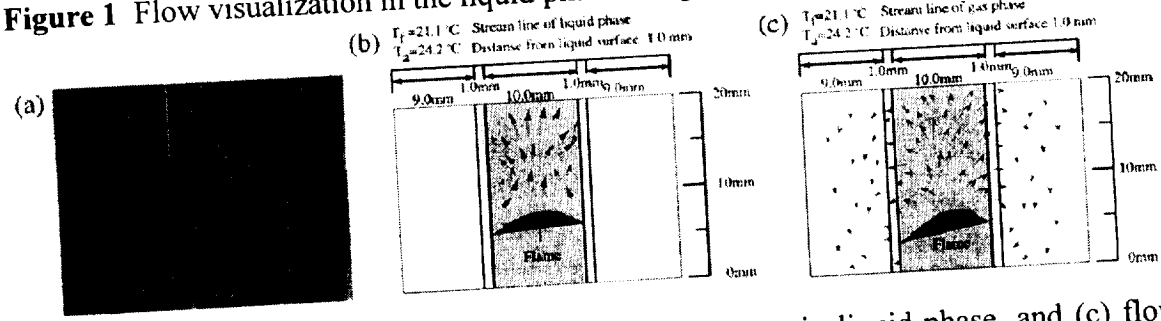

Figure 2 (a) A photographic picture, (b) flow vector map in liquid-phase, and (c) flow vector map in gas-phase at height of 2.0 mm above fuel surface in pulsating regime of n-Butanol.

Figure 2 show the gas flow ahead of the flame over a 10 mm tray where the twin vortices appear 1 and 2 mm above the liquid surface. It can be seen in these figures that the effect of the

thermocapillary force in the liquid on the airflow is within a height approximately 1.5 mm above the fuel surface. Any air movement above that distance is affected and controlled by the flame-front shape and the flame leading edge structure. Figure 3 is an illustration of the 3-D flow structure in both liquid and gas phases in the pulsating region.

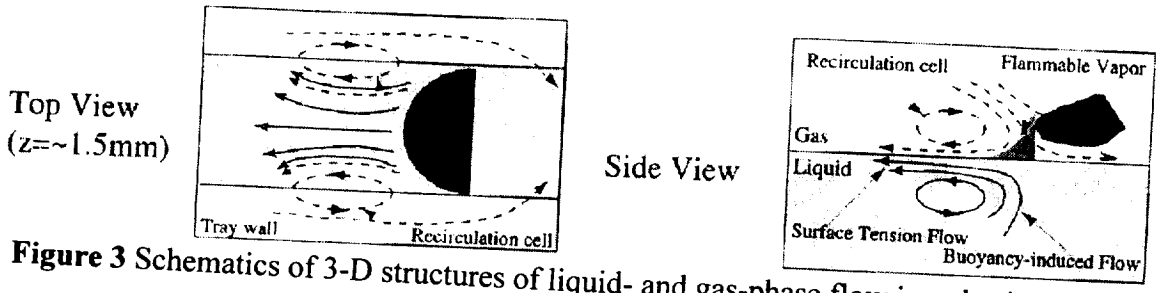

Figure 3 Schematics of 3-D structures of liquid- and gas-phase flow in pulsating regime.

SUMMARY AND CONCLUSIONS

We found twin circulation cells existed in the liquid as the mirror image of the gas-phase-flow structure. Our LSPT revealed the flow profiles both in gas and liquid ahead of the flame to have a 3-D structure. Under the microgravity, the liquid convection observed in this paper won't exist, thus a longer preheat length ahead of flame needs to keep the flame to spread.

ACKNOWLEDGMENTS

This study was supported in part by the Kentucky NASA EPSCoR Program (NCCW-60) and in part by the Center for Manufacturing Systems at the University of Kentucky. We wish to acknowledge H. Ross and F. Miller of NASA Lewis Research Center for valuable technical discussions on flame spread and the particle tracking system.

REFERENCES

1. Ito, T. Konishi, A. Narumi, G. Tashtoush, K. Saito and C. Cremers, *ASME International Mechanical Engineering Congress and Exposition*, J. Heat Transfer, to appear 1999.
2. G. Tashtoush, Experimental Investigation on Flame Spread Over Liquids Using Holographic Interferometry, Ph.D. Thesis, Mechanical Engineering Department, University of Kentucky, Lexington, KY (1997).
3. T. Hirano, *Combustion*, Kaibundo Pub., 1986, in Japanese.
4. F. Miller, and H. Ross, Temperature Field During Flame Spread over Alcohol Pools: Measurements and Modeling, *Eastern State Section, The Combustion Inst.*, Clearwater, FL (1994).
5. H. Ross, *Progress in Energy and Combustion Science*, 20:pp. 17 (1994).
6. P. Garcia-Ybarra, J. Castillo, J. Antoranz, V. Sankovitch, and J. San Martin, Study of the Thermocapillary Layer Preceding Slow, Steadily Spreading Flames Over Liquid Fuels, *26th Symposium (International) on combustion/ The Combustion Institute*, pp. 1469-1475 (1996).
7. Ito, D. Masuda, and K. Saito, *Combustion and Flame*, 83: pp. 375 (1991).
8. H. Ross, F. Miller, D. Schiller and W. Sirignano, Flame Spread Across Liquids, *3rd International Microgravity Combustion Workshop*, NASA Lewis Research Center, Cleveland, OH, (1995).
9. Glassman and F. L. Dryer, *Fire Safety Journal*, 3: pp. 123 (1980).
10. Williams, *Combustion Theory*, The Benjamin/Cummings, 1985.

577-29

IGNITION, TRANSITION, FLAME SPREAD IN MULTIDIMENSIONAL CONFIGURATIONS IN MICROGRAVITY

Takashi Kashiwagi[1], William E. Mell[1], Howard R. Baum[1], Sandra Olson[2]

[1]Mail Stop 8652, National Institute of Standards and Technology, Gaithersburg, MD 20899

[2]Mail Stop 500-115, NASA Lewis Research Center, Cleveland, OH 44135

INTRODUCTION

In the inhabited quarters of orbiting spacecraft, fire is a greatly feared hazard. Thus, the fire safety strategy in a spacecraft is (1) to keep any fire as small as possible, (2) to detect any fire as early as possible, and (3) to extinguish any fire as quickly as possible. This suggests that a material which undergoes a momentary ignition might be tolerable but a material which permits a transition from a localized ignition to flame spread would significantly increase the fire hazard in a spacecraft. If the transition does not take place, fire growth does not occur. Therefore, it is critical to understand what process controls the transition.

Many previous works have studied ignition and flame spread separately[1,2] or were limited to a two-dimensional configuration[3,4]. In this study, time-dependent phenomena of the transition over a thermally thin sample is studied experimentally and theoretically in two- and three-dimensional (2D, 3D) configurations. Furthermore, localized ignition can be initiated at the center portion of thermally thin paper sample instead of at one end of the sample. Thus, the transition to flame spread could occur either toward upstream or downstream or both directions simultaneously with an external flow. In this presentation, the difference in the transition between the 3D and 2D configurations is explained with the numerically calculated data. For sufficiently narrow samples edge effects exist. Some results on this issue are presented. New analysis of the surface smoldering experiments conducted in the space shuttle STS-75 flight is also described.

NUMERICAL RESULTS

The numerical model has been described in detail in our previous publication[5,6]. The theoretical prediction and the experimental data show that the transition from localized ignition to subsequent flame spread tends to occur more easily in the three-dimensional configuration than in the two-dimensional configuration in the oxygen supply limit regime such as a low external flow[7]. This trend is explained in Figure 1 (3D case) which shows the top down view of the stream lines and the mass flux vectors for both oxygen and fuel in the plane parallel to the sample surface. The colors used in the figures correspond to gas phase reaction rate. Pyrolysis and expansion from the gas phase reaction create an obstacle which the upstream originating flow circumvents. The upper and lower halves of the figure contain the fuel and oxygen mass flux vectors, respectively. Fuel gases flow radially from the center due to diffusion and expansion. Far from the flame, the oxygen mass flux vectors and streamlines point in the same direction (convective flux dominates). Oxygen mass flux along the outer regions of the flame is toward the centerline plane. The magnitude of the oxygen mass flux from the side (which is diffusion dominated) is as large or larger than the centerline flux in the upstream part of the flame (where it is most aided by the external flow). Diffusion in the 2D case can only occur within the centerline plane. Thus, it is clear that the curvature of the reaction zone of the 3D flame allows more oxygen to be supplied to the flame. The 3D flame is therefore less dependent on oxygen supply from an external flow and successfully undergoes transition to flame spread while the 2D flame is quenched (at this low external flow speed,

1 cm/s). More detail of this discussion can be found in our recent publication[8].

In the experimental apparatus, a paper sample is secured within a stainless steel card. This card acts as a heat sink. For samples of a small enough width heat loss to the steel will affect flame evolution – even in the centerline plane which is farthest from the sample/steel interface. In such cases, a 2D model of the flame will not be accurate. Three 3D cases are simulated: 2 cm and 9 cm wide samples in stainless steel cards; and a 2 cm wide sample in a card with thermal properties identical to the sample. Figure 2 shows that the 2 cm wide sample cases differ significantly from each other and from the 9 cm wide case. Thus, edge effects significantly influence flame behavior in the centerline plane for the 2 cm wide samples. Figure 3 shows color contours of temperature on a reaction isosurface for the cases with a stainless steel card. The 2 cm case has a flame in the centerline plane which is smaller (consistent with Fig. 2), lower, and cooler. This is due to stronger diffusive mixing of oxygen from the outer region of the 2 cm wide flame (a 3D effect) as was seen in Fig. 1.

EXPERIMENTAL RESULTS: SMOLDERING

The same type of the paper used for above flaming study was doped with potassium ions to enhance char formation and char oxidation and the experiments were conducted in air. Smoldering was initiated at the center of the sample by a lamp. Smolder patterns developing under two different gravity environments are shown in Figure 4. In normal gravity, as shown in Figures 4a-c, the glowing smolder front remained symmetric although segmented (horizontal sample in a quiescent condition). The smolder area pattern was nearly uniform and continuous. In microgravity, a very complex finger-shaped char pattern was observed from the onset of smoldering ignition. Discrete glowing smoldering fronts were localized at the finger tips as seen in Figures 4d-f (flow velocity of 0.5 cm/s). The direction of growth of the char fingers was almost solely upstream during the lowest flow velocity experiment. Normalized smolder area, a fraction of the upstream area available that smoldered, linearly increased with external flow, and approached unity (uniform front) at external flow velocities of 9 cm/s to 10 cm/s. Analysis of oxygen transport revealed that each smolder front cast an "oxygen shadow" which influenced the oxygen mass flux to adjacent smolder fronts. More detailed discussion can be seen in our recent publication[9]

ACKNOWLEDGMENTS

This study is supported by the NASA Microgravity Science Program under the Inter-Agency Agreement No.C-32001-R.

REFERENCES

1. Amos, B. and Fernandez-Pello, A.C., *Combust. Sci. Tech.* 62:331-343 (1988).
2. Ferkul, P.V. and Tien, J.S., *Combust. Sci. Tech.* 99:345-370 (1994).
3. West, J., Tang, L., Altenkirch, R.A., Bhattacharje, S., Sacksteder, K., and Delichatsios, M.A., Twenty-Sixth Symposium (International) on Combustion, The Combustion Institute, pp.1335-1343 (1996).
4. Di Blasi, C., *Fire & Materials,* 22:95-101 (1998).
5. McGrattan, K.B., Kashiwagi, T., Baum, H.R., and Olson, S.L., *Combust. Flame* 106:377-391 (1996).
6. Kashiwagi, T., McGrattan, K.B., Olson, S.L., Fujita, O., Kikuchi, M., and Ito, K., Twenty-Sixth Sympsoium (International) on Combustion, The Combustion Institute, pp.1345-1352 (1996).

7. Kashiwagi, T., Mell, W.E., McGrattan, K.B., Baum, H.R., Olson, S.L., Fujita, O., Kikuchi, M., and Ito, K., Fourth International Microgravity Combustion Workshop, NASA Conference Publication 10194, p. 411-416 (1997).
8. Mell, W.E. and Kashiwagi, T., "Dimensional Effects on the Transition from Ignition to Flame Spread in Microgravity" in press, Twenty-Seventh Symposium (International) on Combustion, The Combustion Institute.
9. Olson, S.L., Baum, H.R., and Kashiwagi, T., "Finger-Like Smoldering Over Thin Cellulosic Sheets in Microgravity", in press, Twenty-Seventh Symposium (International) on Combustion, The Combustion Institute.

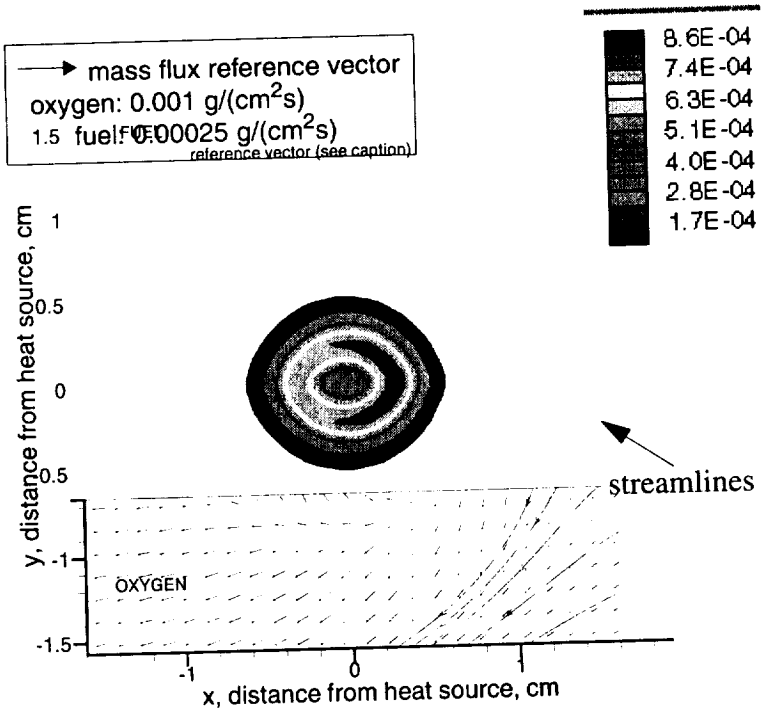

Figure 1: Various data on a horizontal plane 2.5 mm above the surface of a burning sample. Color contours of reaction rate (g/cm^3·s), mass flux vectors (fuel on upper half, oxygen on lower half), and streamlines. A 1 cm/s wind flows from right to left. The flame is ignited by applying a radiative flux for 3.5 s to the paper over a circular area. The data shown here are at t=1.5 s, shortly after ignition.

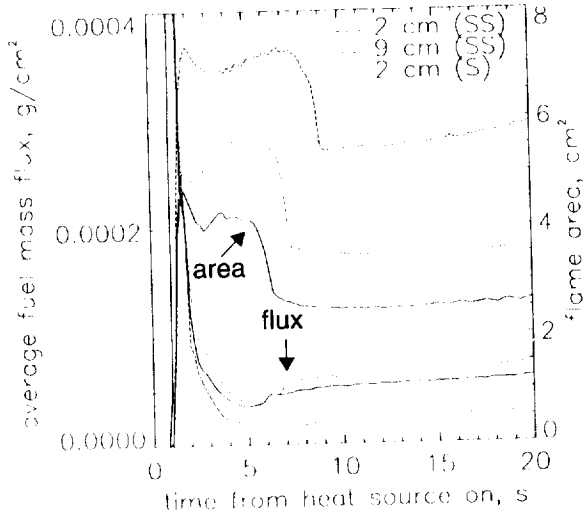

Figure 2: Average fuel mass flux from sample surface along the centerline and flame area in the centerline plane versus time. Three cases are shown: 2 cm and 9 cm wide samples bounded by stainless steel (denoted SS) and a 2 cm wide sample bounded by a non–degrading material with thermal properties identical to the sample (denoted S). Ignition occurs by applying a radiative flux across the width of the sample for 3.5 s (see Fig. 3). After approximately 10 s all flames are relatively quasi–steady. The fuel mass flux is directly related to the net heat flux on the sample. The flame area is largest in the 9 cm case but the fuel mass flux is smallest. This is because the 9 cm flame stands off the sample more – see Fig. 3. Flame area was computed by averaging all area elements in the centerline plane with reaction rates larger than 1 μg/(cm^{3}s).

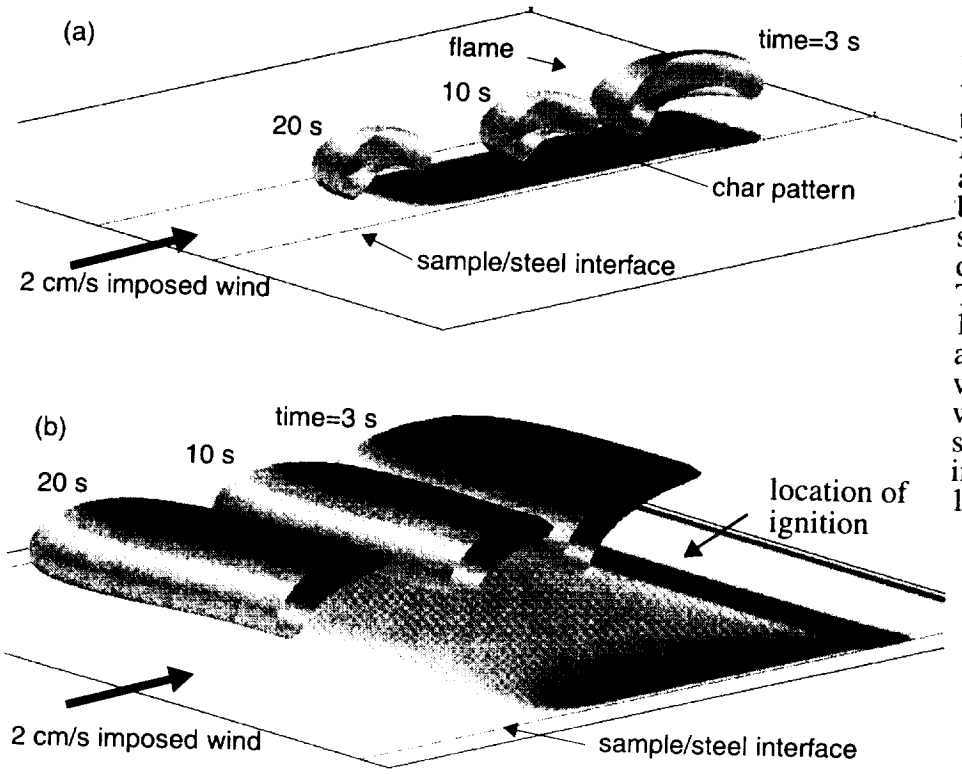

Figure 3: Color contours of temperature on the 50 μg/(cm^3·s) reaction rate isosurface. Highest temperatures are in red; lowest in blue. Charring of the sample at $t = 20$ s is denoted by greyscale. Three times t = 3 s, 10 s, 20 s for two cases are shown: (a) 2 cm wide sample; (b) 9 cm wide. Overall dimensions are 11 cm length in wind direction, 10 cm wide.

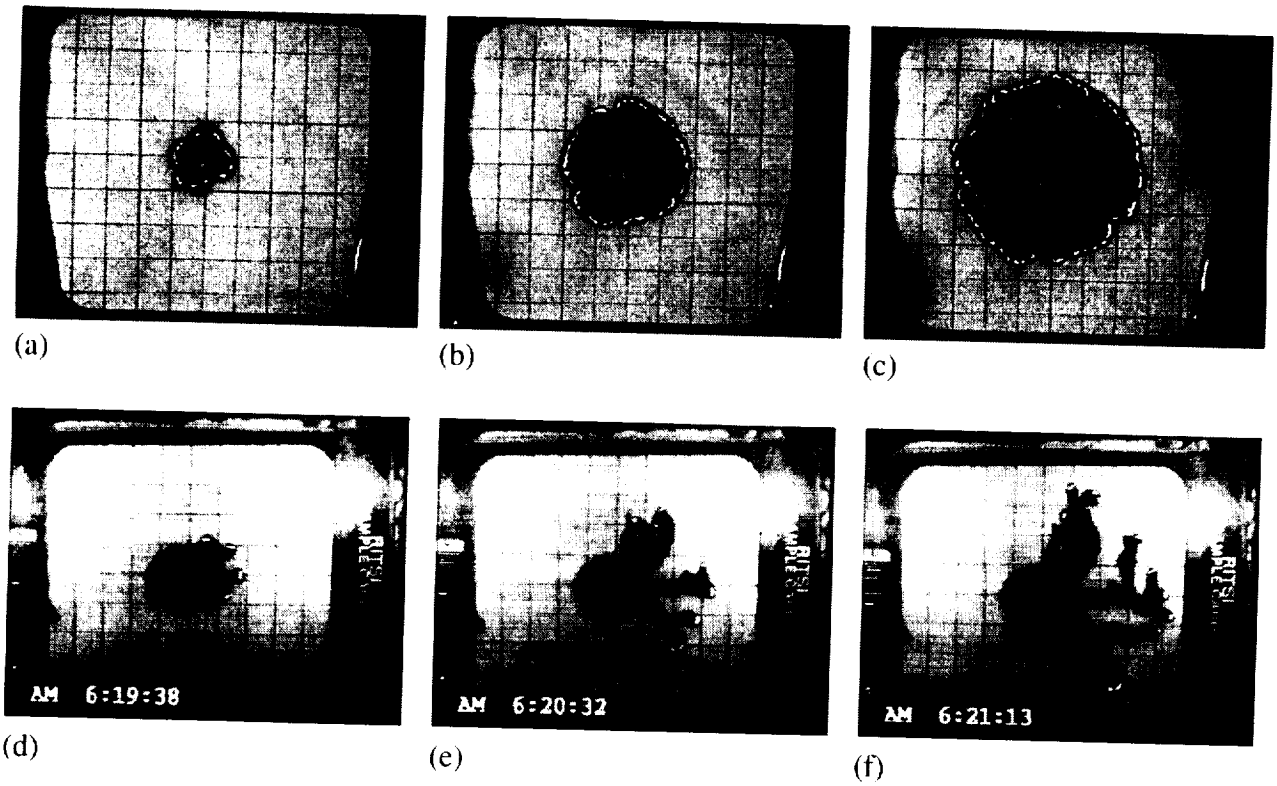

Smolder patterns developing under conditions of normal gravity (a) - (c) and microgravity (d) - (f). In the microgravity case a 0.5 cm/s wind flows from right to left.

578-29

TRANSPORT AND CHEMICAL EFFECTS ON CONCURRENT AND OPPOSED-FLOW FLAME SPREAD AT MICROGRAVITY (NASA Grant No. NCC3-671)

L. K. Honda and P. D. Ronney
Department of Aerospace and Mechanical Engineering
University of Southern California, Los Angeles, CA 90089-1453

INTRODUCTION

With support from a previous NASA grant, NAG3-1611, the PI studied the effects of diluent type, the addition of sub-flammability-limit concentrations of combustible gases, and the effects of concurrent buoyant flow on flame spread processes. The results of these studies are reported and directions for the current grant outlined.

Most experiments were conducted in a 20 liter combustion chamber (Fig. 1). Exactly the same apparatus was used for 1g and μg tests. The effect of inert gases He, Ar, N_2, CO_2 and SF_6 on flame spread were tested since they provide a variety of radiative properties and oxygen Lewis numbers. CO and CH_4 were used for the gaseous fuels in partially-premixed atmosphere tests, plus H_2, C_3H_8 and NH_3 for 1g tests only. In most experiments 5 cm wide Kimwipe samples 15 cm long were used and were held by aluminum quenching plates. The samples were ignited by an electrically-heated Kanthal wire. The flame spread process was imaged via three video cameras and a laser shearing interferometer.

EFFECT OF DILUENT TYPE

For He, N_2 and Ar diluents, the flame spread rates (S_f) at μg were always lower than the 1g values and the minimum oxygen concentrations that would support flame spread were lower at 1g than μg. These findings are consistent with prior studies in O_2-N_2 atmospheres and results from the greater radiative heat losses at μg due to the increased flame thickness (δ) at μg. In contrast, for CO_2 diluent, S_f was slightly higher at μg and the minimum O_2 concentration was lower (Fig. 2a). For SF_6 diluent, S_f was substantially higher at μg for all oxygen concentrations and the minimum O_2 concentration was significantly lower (Fig. 2b). These effects was attributed to changes in the character of radiative transfer for CO_2 and SF_6. He, Ar and N_2 diluents do not emit thermal radiation and thus only the H_2O and CO_2 combustion products radiate significantly. For our test conditions tested the Planck mean absorption length (L_P) of the combustion products in these diluents is typically 1 m, which is much larger than δ, consequently, radiative transport is optically thin. However, for CO_2 and especially SF_6 diluents, L_P is comparable to δ or smaller, thus reabsorption effects cannot be neglected. With reabsorption, radiation emitted near the flame is not lost to the surroundings and instead augments conventional thermal conduction to increase S_f above radiation-free values. Interferometer images (not shown) showed that δ increased at μg for all diluents but most dramatically for radiatively-active diluents, most likely due to these reabsorption effects.

Pressure (P) effects were investigated by employing, for each diluent, one value of O_2 mole fraction that was well above both the 1g and μg flammability limits. Figure 3 shows that for all diluents, at 1g S_f is nearly independent of P, which is consistent with the classical deRis prediction. For He and N_2 diluents, values of S_f at 1g and μg converge as P increases, which is expected for optically-thin radiative effects since δ decreases and thus the volume of radiant gas decreases. In contrast, for SF_6 the values of S_f at 1g and μg diverge as P increases, which is consistent with an increasing effect of optically-thick radiation, leading to reduction in radiative loss and augmentation of heat transport.

Tests were also conducted using thick polystyrene foam samples. It was found that *steady flame spread is possible over thick fuels at quiescent μg conditions when gas-phase radiation effects are significant*. This is also consistent with the classical deRis model. Figure 4 shows

that, as was also seen in the thin fuel tests (Figs. 2a, b), for thick fuels the quiescent μg S_f can be higher than its 1g (downward) counterpart. Moreover, the μg S_f becomes less dependent on thickness as thickness increases. This shows the approach to a thick fuel regime. Similar results can be anticipated for conventional model fuels, *e.g.* PMMA, but the much lower S_f dictate that space experiments are required. In the current flight definition study, this work will be extended to longer-duration μg experiments and other fuel types that are more readily characterized.

Cellular flame structures were observed in spreading flames at μg in O_2-CO_2 and O_2-SF_6 atmospheres near extinction limits. In conjunction with J.-S. Kim and F.A. Williams of UC San Diego, it was shown that the cell structures result from an instability similar to the diffusive-thermal instability of premixed flames, but for non-premixed flames this can occur only when (1) significant reactant leakage occurs through the front, which can only occur near extinction conditions and (2) the leaking reactant has a sufficiently low Lewis number. These predictions were in excellent qualitative and fair quantitative agreement with experiments.

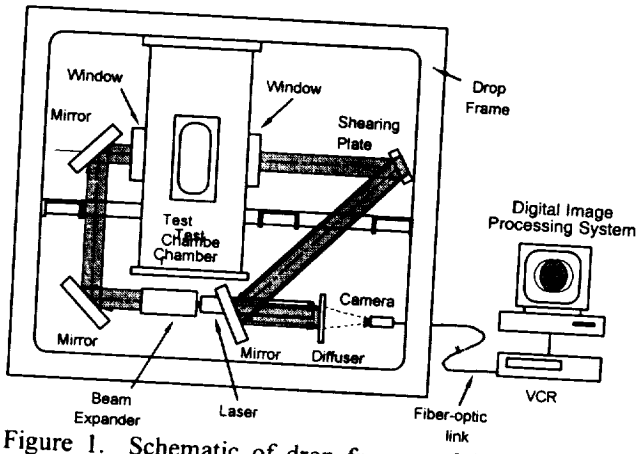

Figure 1. Schematic of drop frame and interferometer apparatus. The fuel bed is mounted inside the chamber parallel to the plane of the page.

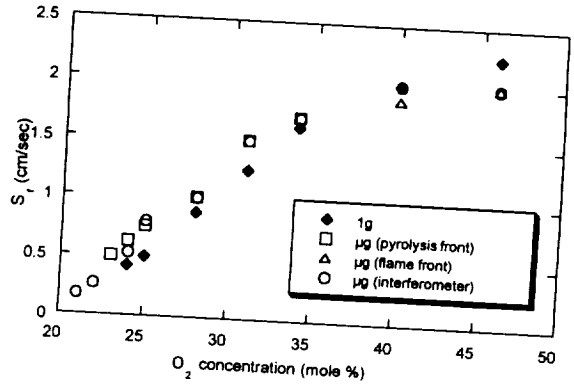

Figure 2. Flame spread rates vs. O_2 mole fraction at 1 atm. a) Carbon dioxide diluent.

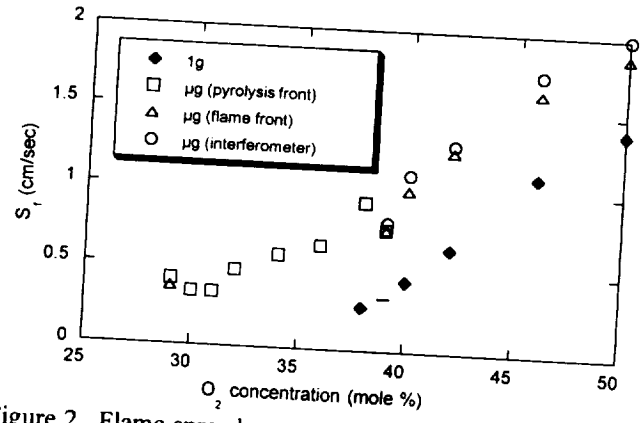

Figure 2. Flame spread rates vs. O_2 mole fraction at 1 atm. b) Sulfur hexafluoride diluent.

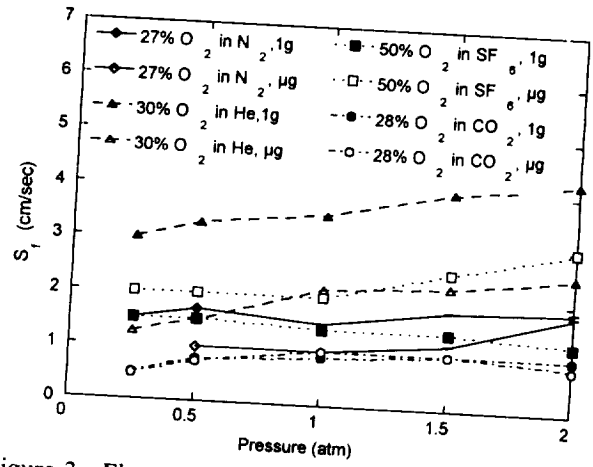

Figure 3. Flame spread rate vs. pressure for He, N_2, SF_6 and CO_2 diluents at fixed O_2 mole fractions.

FLAME SPREAD IN PARTIALLY-PREMIXED ATMOSPHERES

Fires in enclosures usually burn in under-ventilated conditions, leading to atmospheres containing unburned fuel or intermediates such as CO. With this motivation, thin-fuel flame spread experiments were conducted at 1g and μg in atmospheres containing sub-flammability-limit concentrations of gaseous fuels in O_2-N_2 atmospheres. 1g tests showed that that for some fuels

such as CO and H_2, there is a substantial effect of gaseous fuel on S_f, whereas for other fuels such as NH_3, there was practically no effect. Remarkably, for CO fuel (Fig. 5), a very important case for practical applications, S_f was higher and the minimum O_2 concentration was lower when a given number of oxygen atoms in the ambient atmosphere was present in the form of CO rather than O_2. Moreover, these data do not even account for the fact that in practical fires the vitiated air will be hotter than ambient due to the heat release associated with the partial oxidation. For all gaseous fuels enhancement of S_f correlated well with the characteristic chemical reaction rate of the premixed fuel and no correlation with the heating value or diffusive properties of the premixed fuel was observed. In the current flight definition study, this work will be extended to thick fuels using longer-duration μg experiments.

It was found that the effect of adding gaseous fuel to the ambient atmosphere was qualitatively similar at 1g and μg but the effect is stronger at μg than 1g, and in fact S_f is actually higher at μg than 1g at high premixed fuel concentrations (Fig. 6). Also, the effect of added gaseous fuel was found to be more substantial at higher oxygen concentration and with CO fuel. All of these results are consistent with the simple theoretical model proposed by the PI which shows the effect of the premixed fuel is to cause a partially-premixed flame sheet to occur upstream of the conventional non-premixed flame. This additional flame increases the total heat flux to the fuel bed and thus S_f. Finite-rate chemistry of the premixed flame was found to affect the additional heat flux, even when the nonpremixed flame is at the high Damköhler number (mixing-limited) condition.

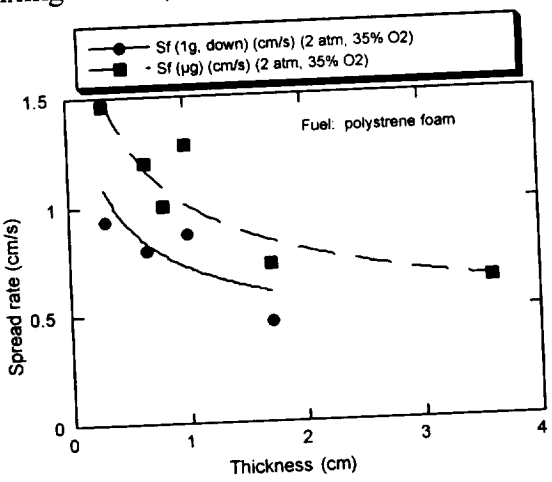

Figure 4. 1g and μg flame spread rates over polystyrene foam beds in a 35% O_2 - 65% CO_2 mixture at P = 2 atm.

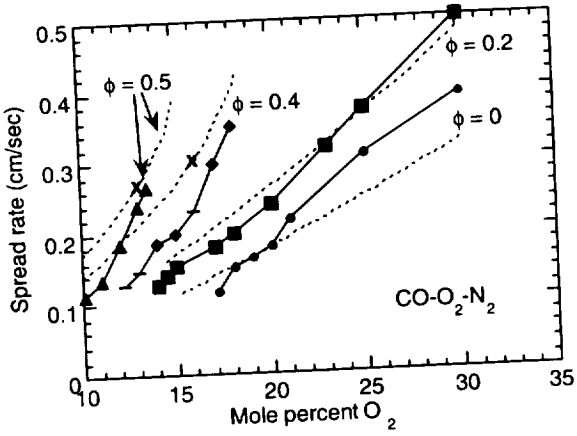

Figure 5. Effect of O_2 mole fraction and gaseous CO addition on S_f. Solid lines and data points: experiment; dashed lines: theoretical predictions. ϕ is the equivalence ratio of the premixed atmosphere.

CONCURRENT-FLOW FLAME SPREAD

A study of upward flame spread over solid fuels was conducted to clarify the mechanisms of spread rates for concurrent-flow flame spread and in particular, buoyancy effects on this process. It was proposed that, contrary to many prior theoretical predictions, upward flame spread could be steady because convective losses to the sides of the fuel samples and/or surface radiative losses prevent the flame length and thus spread rate from growing indefinitely. These losses were argued to be unavoidable because the flame length will grow until these losses balance the heat generation rate. Scaling relations for the spread rates in the presence of convective and radiative losses, laminar and turbulent flow, buoyant and forced convection, and thin and thick fuels were derived. Tests of some of these relations were conducted for upward-propagating flames over tall, thermally-thin fuel samples, subject to buoyant convection only, for a range of pressures,

oxygen mole fractions, diluents and fuel bed thicknesses. In this manner a seven-decade range of Grashof number, defined as gW^3/ν^2, where g is the gravitational acceleration, W the fuel bed width and ν the kinematic viscosity, was studied. Only conditions away from quenching were studied to minimize chemical influences. Flames were found to achieve steady values of both S_f and flame length when the sample was sufficient tall. Measured values of S_f, normalized by the opposed-flow (downward) spread rate with the same atmosphere and fuel bed ($S_{f,opp}$), are shown in Fig. 7. At low Gr_W, $S_f/S_{f,opp} \sim Gr_W^{1}$ with the value of the proportionality constant being slightly different for different atmospheres. At higher W, S_f is independent of Gr_W, indicating a transition to radiatively-stabilized flame spread. At intermediate Gr_W, there is some indication of a region where $S_f/S_{f,opp} \sim Gr_W^{4/7}$ as would be characteristic of turbulent buoyant regime. The data deviate from $S_f/S_{f,opp} \sim Gr_W^{1}$ behavior towards $S_f/S_{f,opp} \sim Gr_W^{4/7}$ near Gr_W = 20,000, which is close to where a predicted transition from laminar to turbulent behavior occurs. Furthermore, visually the flames were observed to change to a turbulent structure near this value of Gr_W. In the current flight definition study, this work will be extended to consider μg conditions, where gas-phase radiation effects will be important, as well as thick fuel beds.

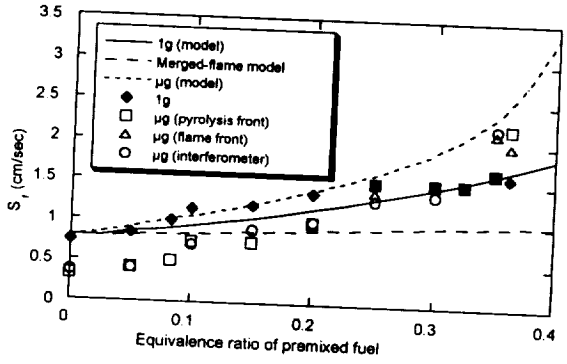

Figure 6. Measured and predicted flame spread rates vs. ϕ. Atmosphere: 18% O_2 in N_2 at 1 atm with CO as added gaseous fuel.

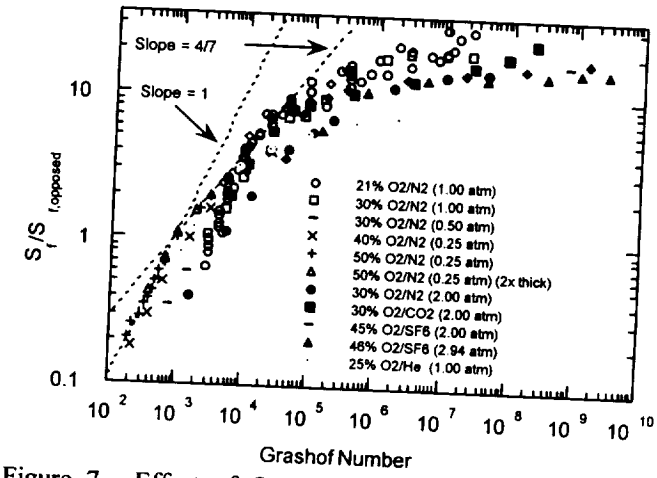

Figure 7. Effect of Grashof number (Gr_W) on upward flame spread rate, normalized by downward spread rate, over thin fuel samples. Gr_W = 20,000 corresponds to the estimated transition from laminar to turbulent flow.

PUBLICATIONS

Honda, L. and Ronney, P. D., "Concurrent-Flow Flame Spread Rates Over Thin Solid Fuel Beds," in preparation.

Honda, L. and Ronney, P. D., "Effects of Ambient Atmosphere on Flame Spread at Microgravity," *Combustion Science and Technology*, Vol. 133, pp. 267-291 (1998).

Shay, M. L. and Ronney, P. D., "Nonpremixed Flames in Spatially-Varying Straining Flows," *Combustion and Flame*, Vol. 112, pp. 171-180 (1998).

Liu, J. B., Ronney, P. D., "Modified Fourier Transform Method for Interferogram Fringe Pattern Analysis," *Applied Optics*, Vol. 36, pp. 6231 - 6241 (1997).

Kim, J. S., Williams, F. A., Ronney, P. D., "Diffusional-Thermal Instability of Diffusion Flames," *Journal of Fluid Mechanics* , Vol. 327, pp. 273-302 (1996).

Ronney, P. D., Greenberg, J. B., Zhang, Y., Roegner, E. V., "Flame Spread Over Thin Solid Fuels in Partially Premixed Atmospheres," *Combustion and Flame*, Vol. 100, pp. 474-484 (1995).

Observation of Flame Spread along Solid Fuel Particle Array in Microgravity -Effect of Surrounding Gas Condition-

5-19-27

Osamu Fujita, Kenichi Ito, and Manami Nogami,
Dept.of Mechanical Science, Hokkaido University, Kita-13 Nishi-8,
Kita-ku, Sapporo 060-8628, Japan, (E-mail: ofujita@eng.hokudai.ac.jp)

1. Introduction

In fuel particle cloud combustion such as spray or pulverized coal combustion individual particle burns with spherical flame because the particle size is small enough to neglect the effect of buoyancy. However, as the each particle is too small it is difficult to observe the combustion phenomena. Even if simulation of the fine particle combustion with larger size particle is tried, the effect of buoyancy becomes significant because of the larger Grashof number with larger size. Therefore, the use of microgravity environment is quite effective to do the simulation experiments.

For this reason many experiments on fuel droplet combustion have been performed in microgravity. Single droplet[1,2], interference of fuel particle flames[3], flame spreading over fuel droplet array[4-7]. However, experiment on flame spreading over solid particle array in microgravity is limited. The flame spread over solid particle array can be a simulation of flame spreading of spray combustion of high boiling point fuel or the pulverized coal combustion, in which the evolution process of volatile matter is dominant for the flame propagation.

In the previous research[8] the flame spreading over foamed polystyrene particle array have been investigated to know the effect of surrounding gas condition such as O2 concentration and inert dilution gas as well as particle spacing on the flame spreading phenomena. In the present work the effect of pressure in the range of 0.25 to 2.5atm have mainly been discussed in comparison with the effect of the parameters reported in the previous work.

2.Experimental

In the experiments flame spreading over foamed polystyrene particle array have been observed. Figure 1 shows the schematic description of the arrangement of the tested sample. The foamed polystyrene is held at the top of fine steel wire of 0.2 mm diameter. The spacing is changed in the range of 2.5 to 6.5mm. At the end of the array single nicrome wire is set to ignite the array. After the ignition the electric current supplied to the nicrome wire is stopped to prevent the radiative effect on the subsequent flame spreading. The flame started at the end of the array spreads with time and the spread rate have been measured. At a certain position from the end of the array thermocouples are set above the sample. The arrangement is set into a airtight rectangular chamber of 6.0 L in volume. By using the air tight chamber surrounding gas components and pressure can be changed. Flame spreading phenomena is recorded by a Hi-8 video camera to determined the flame spreading rate. The microgravity experiments were performed with Micro-Gravity Laboratory of Japan(MGLAB, around 100m drop distance) and aircraft parabolic flight(Diamond Air Service).

The tested sample is foamed polystyrene bead with initial diameter of 2.5mm. The general property of the foamed polystyrene are shown in table 1.

3.Experimental results and discussion

3.1 Observation of flame spreading

Figure 2 shows the typical flame spreading phenomena for various surrounding pressure. Ignition is performed at the right end of the array. Unburned particle ahead of the flame front shrinks by preheating prior to the ignition and then it is ignited. This preheating and ignition continuously occur. In this research the average speed of the flame front motion is determined as flame spread rate.

The effect of pressure is clearly observed in the figure. With higher pressure the width of the flame becomes narrower and brightness of the flame becomes higher. The number of particles shrinking prior to the flame front is more with lower pressure. This implies that the high temperature region becomes thicker with decrease in the surrounding pressure.

Figure 3 shows the effect of O2 concentration and particle spacing on flame spread rate. Flame spread rate shows a peak value at a certain particle spacing. This means closer particle spacing dose not always give an larger spread rate. This tendency is corresponding to that of combustion velocity of pulverized coal cloud[9]. It

is known that combustion velocity of pulverized coal cloud shows an peak value at certain coal density. The flame spread rate is much larger for higher O2 concentration at shorter particle spacing. However, its difference becomes smaller with increase in particle spacing. In this figure it is interesting to note that the maximum particle spacing where flame spreading is possible is larger for lower O2 concentration. This results implies that the minimum flammability limit (lean limit) in particle density is wider for lower oxygen concentration.

Figure 4 shows the effect of pressure on flame spread rate in various balance gas. Flame spread rate also has a peak value for a certain pressure except the case with CO2 balance. In the other researches on fuel droplets array [4,6,7] spread rate shows monotonous decrease with increase in pressure in the range except around critical pressure.

3.2Discussion on flame spread rate

Flame spreading is caused by continuous ignition of unburned particle ahead of the flame front as seen in Fig.2. The ignition of unburned particle is dominated by the heat transfer from the burning region. Especially, the solid fuel require higher temperature to release volatile matter than liquid fuel, so heat transfer process is more critical to determine the flame spread rate. The heat transfer to unburned fuel is strongly affected by the relative position between flame front and unburned particle[6,7,8]. Therefore, the change in flame diameter is important to discuss the flame spread rate.

Figure 5 shows the comparison of the flame diameter of single polystyrene particle for various pressure in microgravity. The size of the flame is apparently larger with less pressure. Figure 6 shows the example of the flame diameter change as a function of pressure. As seen in the figure it decreases with increase in pressure. Figure 7 shows the maximum width of the flame column measured from Fig.2. Assuming half of this width is the radius of the flame, the flame radius at around 1.0 atm is close to the spacing in the case of Fig.2, i.e. 3.5mm. The flame spread rate showed a maximum value at around the similar pressure where assumed flame radius is close to the spacing.

Figure 8 shows the conceptual description of the relative position of the flame front and unburned particle. In case of larger flame diameter flame front is further than the unburned fuel particle, which mean unburned fuel is included in the flame. This situation may leads to lower flame temperature and less flame spread rate. On the other hand, when flame radius is less than the spacing flame spread rate decrease with decrease in flame radius. Therefore, there must be a suitable flame radius for a given spacing. As flame diameter strongly depends on the pressure, peak value appears around the 1 atm as seen in Fig.4. As seen the fact that the flame radius is affected by pressure is very essential to determine the relation between flame spread rate and the experimental parameter.

4. Summary

Flame spreading of solid particle array has been investigated to know the dominant factors for flame spread rate. It is pointed out that the importance of the fact that the flame radius is changed by surrounding pressure as well as O2 concentration, balance gas. Through this fact the effect of each parameters on flame spread rate is determined.

Acknowledgement

This research was supported by NASDA and the Japan Space Forum, under Ground Research Announcement for Space Utilization.

References

1.Kumagai,S.,etal.13th Symp.(Int.)on Comb.,p779.,1971.
2.Okajima,S., and Kumagai,S.,15th Symp.(Int.) on Comb.,p.401,1974.
3.Mikami,M.,etal.25th Symp.(Int.)on Comb.,p.431.,1994.
4.Okajima,S.and Hara,H.,Vol.113 of Progress in Astronautics and Aeronautics, AIAA,(1988).
5.Brzustowski,T.A., Sobiesiak,A., and Wojcicki,S.,18th Symp.(Int.)on Comb.,p.265.,1994.
6.Kato,S.,et al., NASA 4th Int. Microgravity Comb. Workshop, p.491,(1997).
7.Park,J. et al.,36th Japan Comb. Symp.,p.426.
8.Fujita,O., etal., Proc.21st Int. Symp on Space Technology and Science, Vol.2,(1998), pp.1312- 1318.
9.Horton,M.D.,etal.,Comb.and Flame,28,187, (1977).

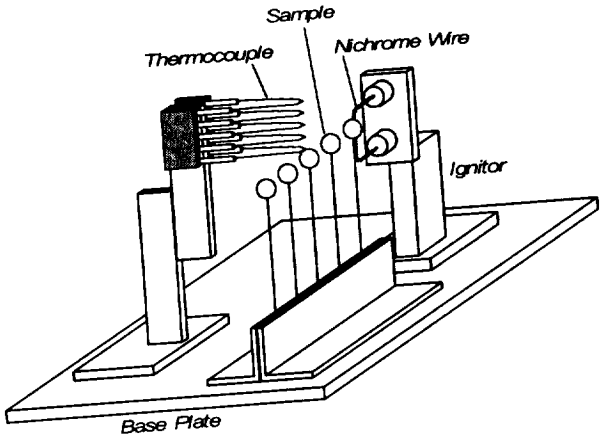

Fig.1 Arrangement of the polystyrene beads array and ignitor

Table 1 General properties of the foamed polystyrene

Chemical Fomula	(- $CH(C_6H_5)CH_2$ -) n
Molecular Weight	1,000,000
Specific Wehight	0.02 - 0.03
Specific Heat (kcal/kg*k)	0.29
Heat Release (kcal/kg)	10,000
Flush Temp (C)	295
Ignition Temp (C)	490

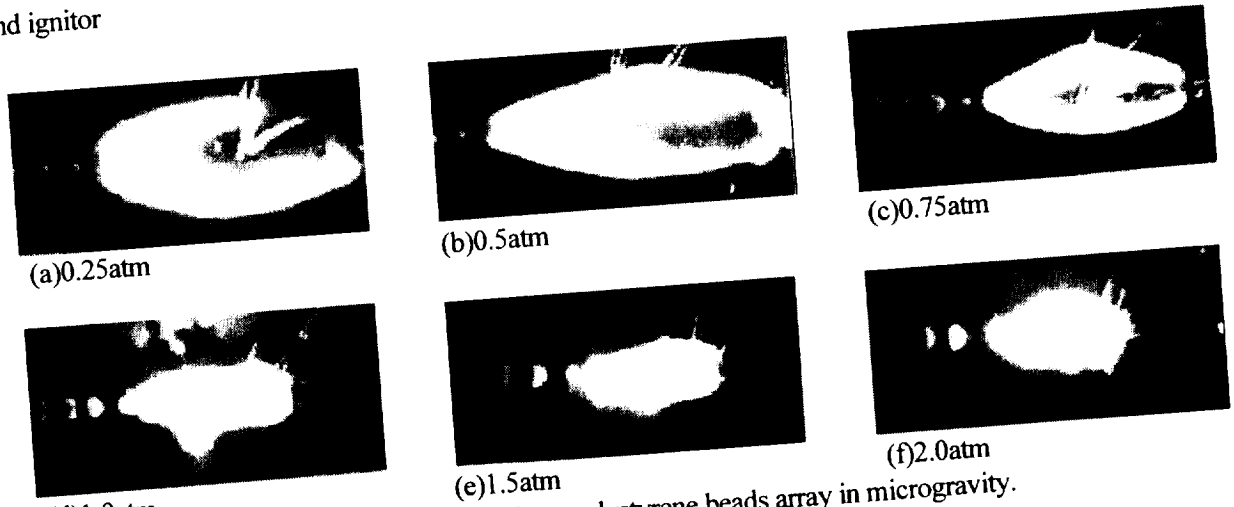

Fig.2 Typical example of flame spreading along polystyrene beads array in microgravity. (Spacing=3.5mm, O2=40%, N2 balance)

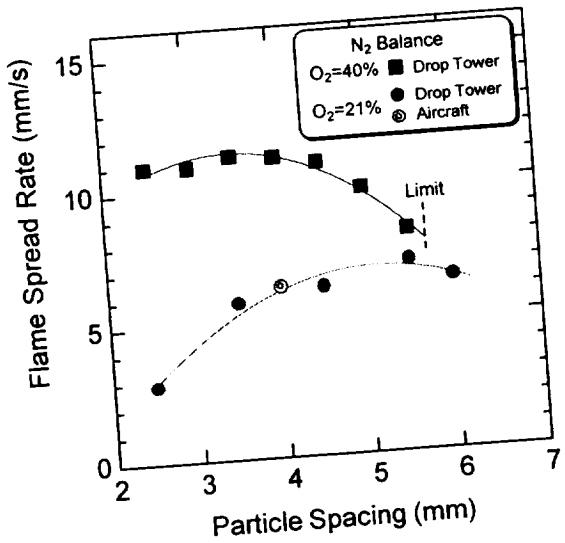

Fig.3 Flame spread rate as a function of particle spacing

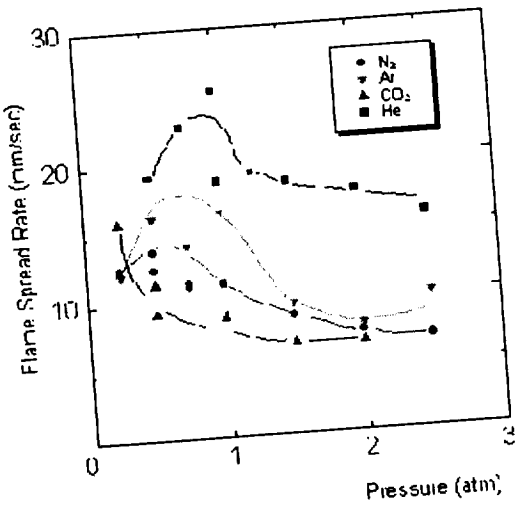

Fig.4 Effect of pressure on flame spread rate for various balance gases(O2=40%)

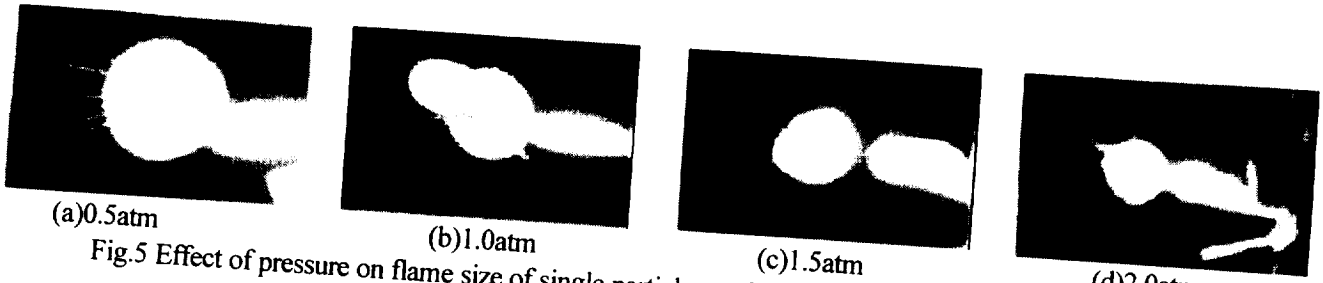

(a)0.5atm (b)1.0atm (c)1.5atm (d)2.0atm

Fig.5 Effect of pressure on flame size of single particle combustion(O2=21%)

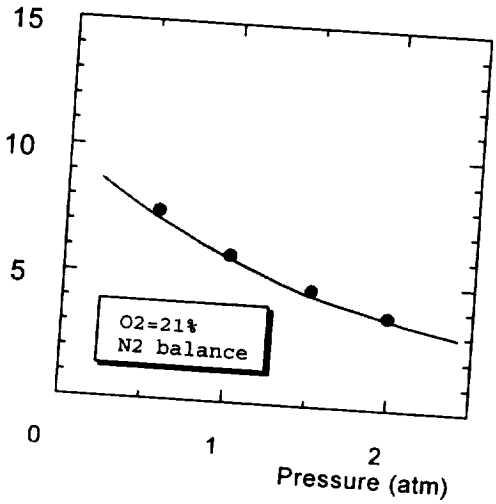

Fig.6 Effect of pressure on flame diameter of single particle combustion (O2=21%)

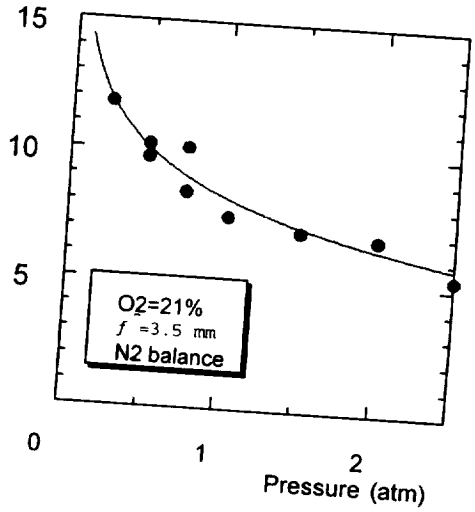

Fig.7 Effect of pressure on flame width of single particle combustion (O2=21%)

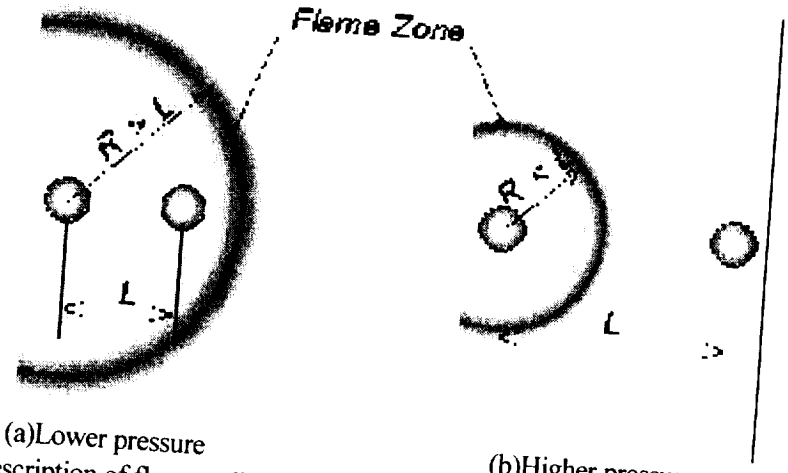

(a)Lower pressure (b)Higher pressure

Fig.8 Conceptual description of flame radius change and its effect of flame spreading

COMBUSTION OF 2-DIMENTIONALLY ARRANGED FUEL SAMPLES UNDER MICROGRAVITY CONDITIONS

H. Nagata[1], S. Nakamura[2], I. Kudo[3], K. Ito[3], Y. Takeshita[4],[1]Department of Mechanical Science, Hokkaido University, Sapporo 060-8628, Japan.E-mail: nagata@eng.hokudai.ac.jp [2]Graduate School of Engineering, Hokkaido University, Sapporo 060-8628, Japan.,[3]Department of Mechanical Science, Hokkaido University, Sapporo 060-8628, Japan., [4]Japan Space Utilization Promotion Center, Nishiwaseda, Shinjuku, Tokyo 169-8624, Japan.

INTRODUCTION

In the combustors of jet engines or rocket engines, fuel droplets burn in droplet clouds and their combustion mechanism is different from that of single droplets because of the interaction between the droplets. Two droplets combustion and droplets array combustion have been studied experimentally to investigate the basic mechanism of the interaction. These simple arrangements are effective to improve basic understandings of group combustion from the microscopic viewpoint. To understand the interaction from the macroscopic viewpoint, on the other hand, it is desirable to observe burning droplets which are arranged two or three dimensionally. It is a promising method to simulate group combustion by placing some spherical fuel samples that are large enough to afford easy arrangement and observation. When the fuel sample's size is large, however, the effect of natural convection increases, modifying the combustion field.

To eliminate the effect of natural convection, the authors employed microgravity environment. Butanol and hexanol are employed as fuels and they are mixed into polyethylene-glycol to make them solid state in room temperature. This treatment enables us easy set up of initial sample diameter and sample arrangement. Group combustion is simulated with large fuel samples arranged 2-dimensionally. Effects of sample space on flame shape and droplet life time are investigated experimentally.

EXPERIMENTAL APPARATUS

The experimental apparatus, which Fig. 1 shows schematically, mainly consists of a combustion chamber, an 8-mm VTR camera, a 35-mm single-lens reflex camera, controlling system, and battery units. Figure 2 shows the detail of the combustion chamber. Electrically heated nichrome wires ignite the fuel samples. To ignite all the samples simultaneously, the nichrome wires are flat and cover all of the fuel samples. Right after ignition the nichrome wires escape from the neighborhood of the fuel samples not to disturb the phenomena.

Fuels employed in this study are 1-butanol (C_4H_9OH) and 1-hexanol ($CH_3(CH_2)_5OH$). Butanol and hexanol are mixed into polyethylene glycol ($HOCH_2(CH_2OCH2)_nCH_2OH$) to make them solid state in room temperature. This treatment enables us easy set up of initial sample diameter and sample arrangement. Mean molecular weight of the polyethylene glycol employed in this study is 6,000 to 7,000 and the melting point is 333 to 336 K. In room temperature it is white powder. The procedure to prepare the sample is;

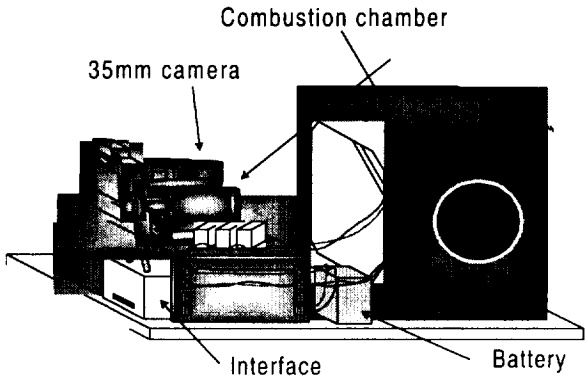

Fig. 1 Experimental apparatus.

(1) Melt the polyethylene glycol powder by warming it in hot water.
(2) Mix the polyethylene glycol and 1-butanol (or 1-hexanol) with the volumetric ratio of about 1:2.
(3) Soak a glass rod in the mixture and cool it in the room temperature to make it congeal.
(4) Repeat the above procedure until the sample grows to the prescribed size (about 2.5 mm in diameter).

Figure 3 shows the arrangement of fuel samples. The diameter of each grass rod is less than 0.5 mm. They have almost the same length, with errors less than 0.5 mm, to arrange samples in the same plane. The definition of sample space L is in the figure.

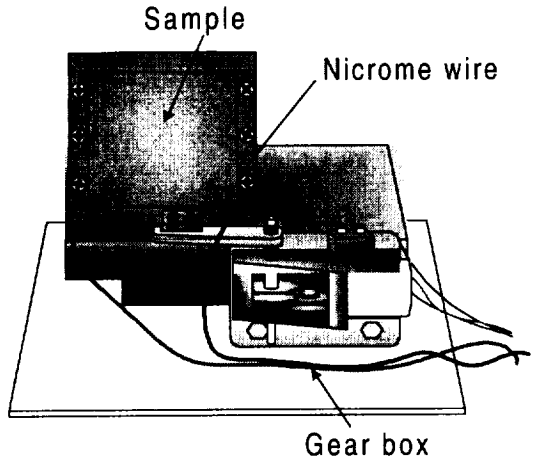

Fig. 2 Detail of the combustion chamber.

RESULTS AND DISCUSSION

Serial flame photographs after ignition are in figures 4 with the sample space of 30 mm. Time goes by from left to right. The fuel is hexanol. In the present study most of all flames are dim blue flames that are hard to see. To take clear photographs of these dim flames we employed high-speed films (ASA3200) and set the shutter speed 0.5 second. Without buoyancy effect under microgravity, the flame exists at the place where diffusion effect forms suitable fuel-air mixture. As time passes after the ignition, the temperature of the samples increases and each flame grows up. Flames merge with each other to be single flame that surrounds fuel samples. After the merger the single flame keeps glowing up because of the accumulation of fuel vapor around the samples.

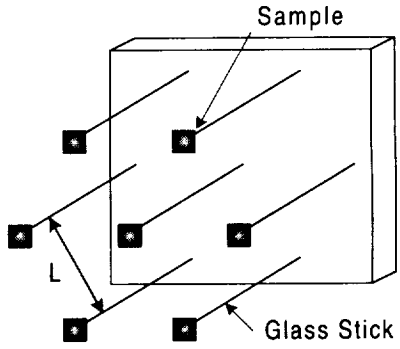

Fig. 3 Sample arrangement.

Figure 5 shows the effect of sample space on flame shape. When sample space is small, the flame is almost a circle. With the increase of sample space the flame shape approaches to the shape

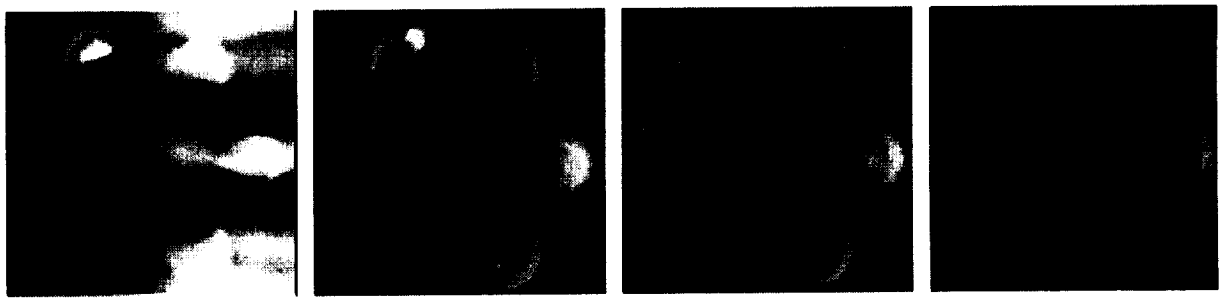

Fig. 4 History of the flame shape.

fuel samples form, i.e., hexagon. Further increase of sample space cause hollows on the flame edge. These hollows become deep with the increase of sample space. Chiu et al.[1] theoretically studied group combustion assuming quasi-steady state and reported that flame approaches to the edge of droplet cloud as droplet number density decreases. The critical state is defined to be the state at which the flame reaches the edge of the cloud. At the critical state the mode changes from the group combustion to the isolated one. The transformation of the flame shape in Fig. 5 shows the process of the mode change.

Figure 6 shows the history of flame distance, which is defined by the distance of the flame from the edge sample. The result with sample space of infinity is the flame radius history of a single fuel sample. According to the quasi steady model of single droplet combustion, the flame diameter depends on the droplet diameter. The flame diameter decreases with time because of the decrease of the droplet diameter. The actual flame diameter, on the other hand, is reported to increase with time at the early period of the combustion[2]. The increase is due to the heating up of the droplet and the accumulation of fuel vapor around the droplet. When the heating up and the fuel vapor accumulation are finished, the quasi steady state is realized and the flame diameter begins to decrease with time. As the result, the droplet flame diameter increases, takes optimum, and then decreases. The result obtained with the single fuel sample (with sample space of infinity) agrees with the

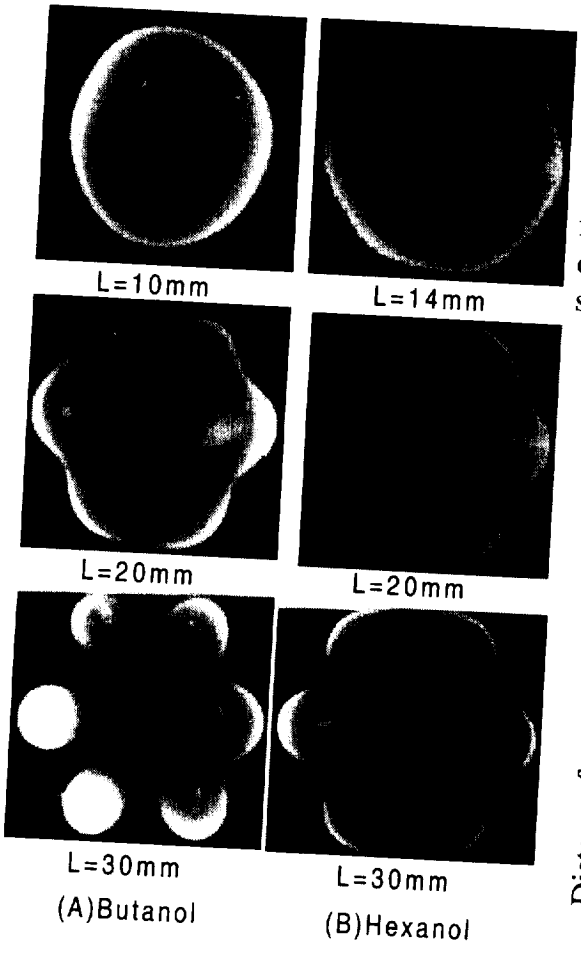

Fig. 5 Effect of sample space on flame shape.

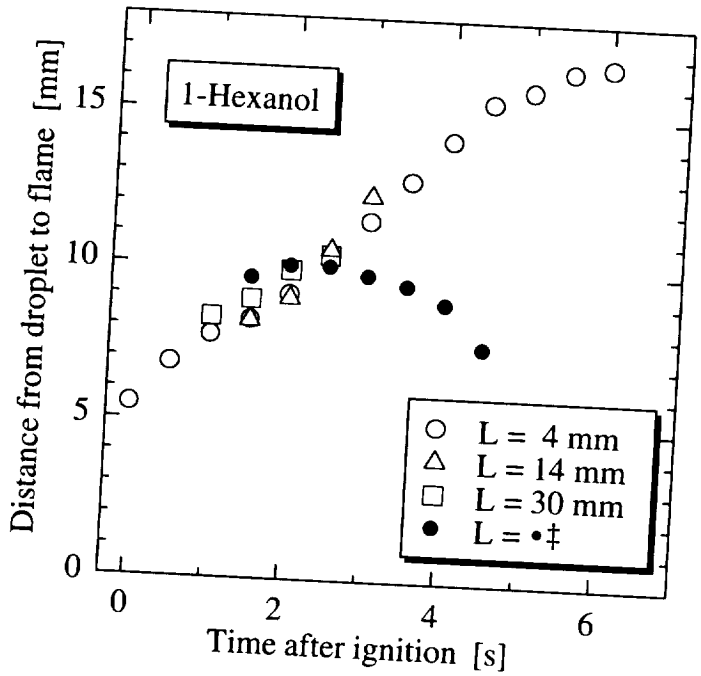

Fig. 6 The history of flame distance.

history mentioned above. The flame distance obtained with seven samples, on the other hand, keeps increasing until all fuel runs out. This result shows that all of the combustion belongs to the unsteady period. In other words, when the sample burns in a group, the fuel runs out before the fuel vapor accumulation finishes.

Figure 7 shows the effect of sample space on samples' life time. The vertical axis is the number of photographs which records the flame. Because the shooting interval is 0.5 second, the number of photographs n means that the life time is between n-0.5 and n+0.5 seconds. In both fuels' cases, the life time increases as sample space decreases. These results show the fact that the heat input rate from the flame to the fuel samples decreases with the decrease of the sample space.

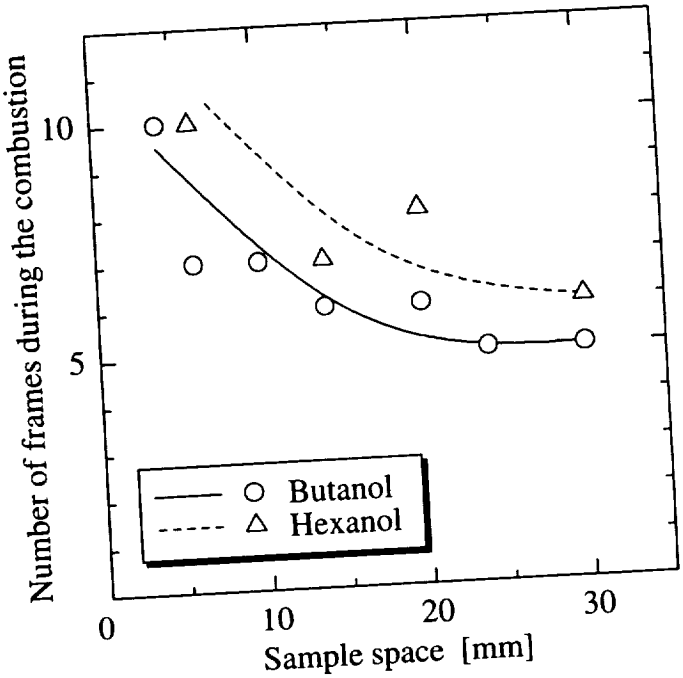

Fig. 7 The effect of sample space on the samples' life time.

CONCLUDING REMARKS

Main results obtained are in the followings: Sample space has a strong effect on the flame shape. With the increase of sample space, flame shape changes from circle to hexagon and then hollowed contour. This transformation shows the process of the change from the group combustion mode to the isolated combustion mode. Because of the interaction between samples, the unsteady combustion period, in which fuel vapor is accumulated around the droplets, becomes long. As the result, the steady state combustion is not observed in the combustion process and the flame size keeps increasing until it disappears.

ACKNOWLEDGMENT

This work was performed under the management of the Japan Space Utilization Promotion Center (JSUP) as a part of the R&D project of the 'Advanced Combustion Science Utilizing Microgravity' supported by the New Energy and Industrial Technology Development Organization (NEDO).

REFERENCES

(1) Chiu, H. H., Kim, H. Y., and Croke, E. J., 19th Symposium (International) on Combustion, The Combustion Institute, Pittsburgh, pp. 971-980, 1982.

(2) Kumagai, S. and Isoda, H., 13th Symposium (International) on Combustion, Reinhold, New York, pp. 726-731, 1957.

Poster Presentations

OMIT THIS PAGE

Flammability and Extinction

S81-25

THICKNESS EFFECTS ON FUEL FLAMMABILITY (TEOFF)

Paul Ferkul and Richard D. Pettegrew
National Center for Microgravity Research, Cleveland, OH 44135

INTRODUCTION

The U-shaped flammability boundary for thermally-thin fuels burning in low-speed flows is well-established [e.g. Olson et al., 1988; Ferkul and T'ien, 1994; T'ien and Bedir, 1997]. The importance of radiative loss is evident in leading to flame extinction when the flow velocity (or ambient oxygen concentration) is reduced sufficiently. This quenching extinction occurs when the flame power output decreases, and the radiative heat loss rate becomes a significant fraction of the total combustion heat release from the flame.

The existence of a similar boundary is hypothesized for fuels which are not thermally thin. For such fuels, heat conduction into the depth of the solid will become an increasingly important parameter as the solid thickness is increased. Thus, one can imagine that different materials will exhibit different burning characteristics as their thickness is increased away from the thermally-thin limit. When solid conductivity begins to become important, materials with different thermal diffusivities may have a different material flammability ranking, compared to their thermally-thin ranking. In effect, conduction heat loss in depth of the solid will manifest itself in different degrees for different materials. Hence, in order to determine an accurate and absolute material flammability ranking, the effect of solid thickness must be accounted for.

In addition, there are other related (secondary) effects which will be investigated. Some materials will form a char layer that tends to inhibit pyrolysis of fuel beneath it. This barrier will have implications for the flammability ranking as well. Other materials will tend to sputter when they burn, sending off flaming bits in many directions. Clearly, a material's ranking must consider the susceptibility of a burning section to ignite another section by such a mechanism.

OBJECTIVES

The primary goal of this research is to examine how microgravity flammability ranking may change with fuel thickness and whether a correlation can be developed to establish an absolute ranking which accounts for different thicknesses. Our secondary goal is to determine whether the well-known, U-shaped flammability boundary for thermally-thin fuels (with quenching and blowoff branches) exists for non-thermally-thin fuels, and how the parameters of interest (material properties, thickness, flow rate, oxygen percentage) affect the boundary.

The determination of the role of fuel thickness, preheating, and material effects is highly relevant to the study of the flammability of thick fuels, one of the fire research areas of interest relating to the Human Exploration and Development of Space (HEDS) Enterprise.

EXPERIMENT DESCRIPTION

The experimental aspects of the project will employ ground based facilities (normal gravity reduced pressure, drop tower, and airplane facilities) to develop baseline data on the flame spread characteristics of several fuels (e.g., wood, paper, textiles) in varying thicknesses. The effects of internal and external heat addition will be examined by systematically varying the preheat fuel temperature, as well as varying the external radiant heat flux to the fuel. Some efforts will be made to develop fuels with non-isotropic thermal conductivity (e.g. fuels with a grain-structure), to determine how flame propagation rates change with fuel orientation. This will help determine

how fuel thickness and conductivity combine to alter a material's flammability characteristics.

In the ground-based testing, we will utilize a drop tower microgravity environment to determine the:

1.) Thermally-thin flammability ranking of different materials based on ignitability and initial flame growth
2.) Thickness effects (if any) on this ranking
3.) Pre-heating effects (if any) on this ranking with
    a.) external radiant heater
    b.) internal conductive heater
    c.) nearby burning surface

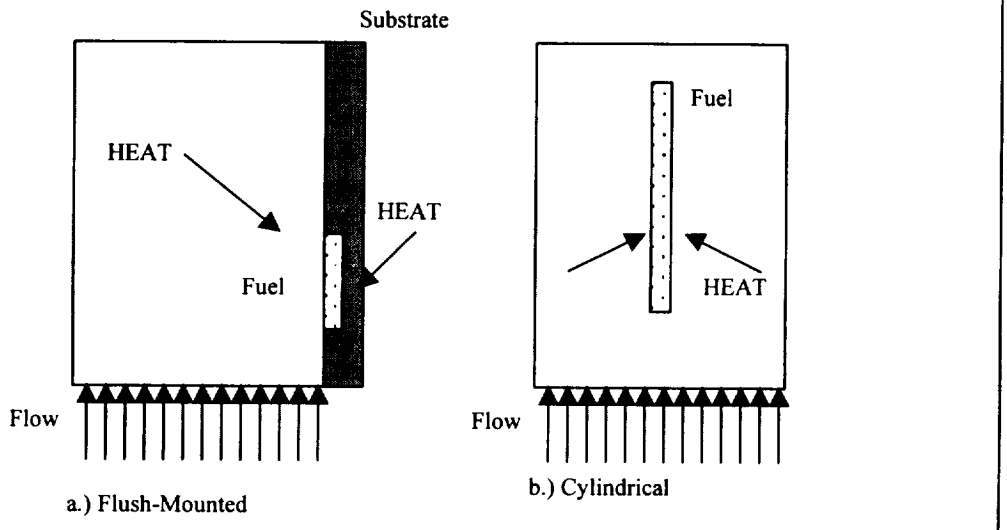

Figure 1. Schematic of Drop Tower Tests. The bottom of the sample will be ignited to establish concurrent-flow flame spread.

The experiment is shown schematically in fig. 1. Samples of various thicknesses and materials will be mounted in a low-speed concurrent-flow wind tunnel. There will be the capability to heat the samples either externally or internally. Two different geometries will be studied, a flush-mounted, flat sample holder consisting of an insulated substrate, and a cylindrical sample holder.

By varying the incoming flow velocity and oxygen concentration, we can map out an ignition boundary as a function of material thickness, for a given applied heat flux. By ranking different materials at different thicknesses, we will demonstrate whether the material flammability ranking may change as a function of thickness, based on the ignition behavior and in conjunction with the modeling effort.

MODELING

Our group has developed a formulation and solution method for studying concurrent-flow flame spread. The model contains all essential elements to capture the detailed structure of spreading flames, including the flame stabilization zone, and flame extinction behavior in low-speed flows.

We summarize the assumptions made to derive the governing equations of this model below. More details can be found elsewhere [Jiang, 1995].)

(1) The solid is both thermally thin (in the sense that the temperature gradient perpendicular to the solid surface is negligible) and aerodynamically thin (in the sense that the flame standoff distance is much greater than the thickness of the solid). The solid is allowed to burn out and using the flame-fixed coordinates system, a steady solution is sought (which implies a constant flame length).
(2) The flow is two-dimensional, steady and laminar.
(3) A one-step, second-order global gas-phase reaction, which obeys Arrhenius kinetics, applies.
(4) Specific heats as a function of temperature for each species are obtained from standard reference books. The multi-component transport properties are modeled in detail [Smooke and Giovangigli, 1991].
(5) Solid decomposition follows zeroth-order, one-step Arrhenius kinetics.
(6) Gas-phase flame radiation is from carbon dioxide and water vapor only (soot is absent). The assumed absence of soot is supported by available drop tower data in low oxygen concentrations and low-speed flow [Grayson et al., 1994]. Radiative absorption by gaseous fuel vapor is not included due to a lack of data (but can be added later).
(7) The solid radiation is assumed to be gray and diffuse.

The governing equations are written in finite difference form and solved numerically. The fluid mechanical treatment in the model is free of the conventional boundary layer approximation: the full elliptic Navier-Stokes momentum, energy, and species equations are used, providing a precise description of the flow field. The flow pattern affects the flame structure, especially for shorter flames in low-speed flows. The flame base region, which is important to stabilization and extinction, can be predicted and compared to experiments enabled by microgravity where larger flame scales can be probed to resolve structures.

The model is already able to examine concurrent-flow flame spread over a thin solid fuel in both low-speed buoyant and forced flows. However, in order to fully extend the model to cover this experiment, certain elements must be added.

The effect of fuel thickness on the flammability boundary will be explored. Initially, the solid phase equation will be modified to permit time variation (unsteady) as well as heat conduction in depth. We will assume 'quasi-steady' behavior, that is, that the gas phase responds instantaneously to the solid phase, permitting us to retain the steady gas-phase formulation. As part of the solution, however, we will be able to estimate an actual gas-phase response time, thus providing feedback on how appropriate the quasi-steady assumption is. In fact, we anticipate that in some situations, the assumption will break down, forcing us to re-formulate the gas-phase in unsteady terms. Fortunately, the current 'steady' algorithm can be systematically converted to 'unsteady' without the need to determine new finite difference expressions.

Our understanding of the gas-phase radiation treatment needed to accurately predict flame behavior has been improving. Using the simple case of a one-dimensional stagnation point flame, several different gas-phase radiation models with widely varying complexity have been examined [Bedir et al., 1996]. It was found that a spectral line weighted sum of gray gas model produced accurate results with only moderate computational complexity. Thus, we plan to incorporate this sub-model into the full 2-D model to continue the improvement of the gas-phase radiation aspects. The modeling effort and drop tower experiments will enable us to test our hypotheses.

APPLICATIONS

Spacecraft fire safety concerns are a strong motivation for reduced gravity combustion research. Currently, the flammability hazards of materials considered for use in manned spacecraft are evaluated using normal gravity, concurrent (buoyant) flow tests [Ohlemiller, 1992], on the premise that this configuration represents the most hazardous possible arrangement due to enhanced convective heat transfer. This viewpoint stems from quiescent tests conducted on Skylab [Kimzey, 1986], which suggested that some materials are less flammable in the absence of flow than they would be with buoyancy present, and implies that normal gravity, upward burning tests would be conservative tests that would adequately characterize the risk of combustion. However, recent studies have shown that low speed flows (such as that produced by the ventilation systems of spacecraft) can sustain flames under conditions where neither normal-gravity buoyant flows nor quiescent atmospheres allow combustion [e.g., Foutch, 1987].

A direct application of this work will be to bridge the gap between material flammability testing in normal gravity and practical material selection for microgravity.

REFERENCES

Bedir, H., T'ien, J. S., and Lee, H. S. (1996): Comparison of Different Radiation Treatments for One-Dimensional Diffusion Flame, Eastern States Section Meeting of the Combustion Institute.

Ferkul, P. V. and T'ien, J. S. (1994): A Model of Low-Speed Concurrent Flow Flame Spread Over a Thin Solid, Combustion Science and Technology, Vol. 99, pp. 345-370.

Foutch, D. W. (1987): Size and Shape of Solid Fuel Diffusion Flames in Very Low Speed Flows, NASA CR-179576.

Grayson, G. D., Sacksteder, K. R., Ferkul, P. V., and T'ien, J. S. (1994): Flame Spreading Over a Thin Solid in Low-Speed Concurrent Flow - Drop Tower Experimental Results and Comparison with Theory, Microgravity Science and Technology, VII/2, pp. 187-195.

Jiang, C.-B. (1995): A Model of Flame Spread Over a Thin Solid in Concurrent Flow with Flame Radiation, Ph.D. Thesis, Case Western Reserve University, Cleveland, Ohio.

Kimzey, J. H. (1986): Final Report: Skylab Experiment M-479, Zero Gravity Flammability, NASA Johnson Space Center, JSC 22293.

Ohlemiller, T. J. (1992): An Assessment of the NASA Flammability Screening Test and Related Aspects of Material Flammability, NASA CR-189226.

Olson, S. L., Ferkul, P. V., T'ien, J. S. (1988): Near-Limit Flame Spread Over a Thin Solid Fuel in Microgravity, 22nd Symposium (International) on Combustion, The Combustion Institute, pp. 1213-1222 and NASA TM 100871.

Smooke, M. D. and Giovangigli, V. (1991): Formulation of the Premixed and Nonpremixed Test Problem, Lecture Notes in Physics, Springer-Verlag, New York, Series 384, Chapter 1, pp. 1-28.

T'ien, J. S. and Bedir, H. (1997): Radiative Extinction of Diffusion Flames - A Review, Asia-Pacific Conference on Combustion, Osaka, Japan.

THE EXTINCTION OF LOW STRAIN RATE DIFFUSION FLAMES BY A SUPPRESSANT

A. Hamins[1], J. Yang[1], and I.K. Puri[2],[1]National Institute of Standards and Technology (100 Bureau Drive, Stop 8652, Gaithersburg, MD 20899), [2] The University of Illinois at Chicago (Department of Mechanical Engineering, M /C 251, Chicago, IL 60607-7022).

INTRODUCTION

This paper describes plans for an experimental and computational study on the structure and extinction of low strain rate diffusion flames by a suppressant added to the oxidizer stream. Stable low strain rate flames will be established through ground based reduced gravity experiments using the 2.2 s drop tower. A variety of agents will be investigated, including both physically and chemically acting agents (He, N_2, CO_2, and CF_3Br) for flames burning methane and propane. A computational model of flame structure and extinction will be modified to include radiative losses, which is thought to be a significant heat loss mechanism at low strain rates.

There have been few microgravity studies on the effect of suppressants on flames [Ronney, 1985; VanDerWege et al., 1995]. Recently, Maruta et al. [1998] reported measurements of the low strain rate (a=2 s^{-1} to 15 s^{-1}) extinction of methane/air diffusion flames with N_2 added to the fuel stream. The required N_2 concentration to achieve extinction increased as the strain rate decreased until a critical value (7 s^{-1}) was obtained, and then as the strain was further decreased the required N_2 concentration decreased. These results were explained in terms of enhanced radiative loss at low strain rates. The experiments discussed here are similar to that of Maruta et al. [1998], but various agents and fuels will be tested, agents will be added to the oxidizer side of the flame, and understanding the near-extinction structure of these flames will be emphasized through measurements and models.

Radiant energy losses are usually neglected in analyses of high and moderately strained near-extinction diffusion flames. This is because these flames are generally non-luminous and the hot gases are confined to a thin reaction zone. In a previous study, Lee et al. [1996] measured the radiative heat loss in moderately strained (a=100 s^{-1}) counterflowing methane/air nonpremixed flames with and without agent added to the oxidizer stream, i.e., near and far from extinction [Lee et al., 1996]. The results for constant strain rate showed that as nitrogen was added to the oxidizer stream, the radiative heat loss fraction decreased. This is consistent with the view that radiative heat loss should diminish as the peak flame temperature decreases and the reaction zone narrows [Vranos and Hall, 1993]. The radiative heat loss fraction was found to vary from approximately 2 to 4 percent depending on the type of agent and its concentration in the oxidizer stream. These results confirm the validity of the assumption of small radiative heat loss for moderately strained, thin, non-luminous diffusion flames. However, the importance of radiative losses at low strain rates (< 20 s^{-1}) and for luminous fuels is not known, nor is it known for a halogenated agent like CF_3Br, which promotes soot [Smyth and Everest, 1996].

A primary objective of this study is to measure the agent concentrations that are required to achieve extinction of counterflowing non-premixed flames at low strain rates, measurements that are not possible to perform in normal gravity due to flame instabilities. For this reason, there is a gap in knowledge regarding the suppression effectiveness of agents for strain rates below approximately 20 s^{-1}. A secondary objective of this study is to characterize the magnitude of the various chemical and transport processes that impact flame stability and lead to flame extinction.

PLANNED EXPERIMENTS

In the first series of experiments that are planned, the agent concentration in the oxidizer stream will be incrementally increased until extinction occurs. The experimental apparatus and procedure will be designed to minimize the experimental duration, such that experiments can be conducted using the 2.2 s or 5 s drop towers. A burner with a small dead volume is being designed. Preliminary experiments will be conducted in normal gravity. If short duration experiments (<2 s or 5 s) are not achievable, then free floating experiments on aircraft will be considered. Measurements will be conducted to insure that the rate of change in agent concentration does not influence the measured value of the critical agent concentration required to achieve extinction. As the temperature profile broadens at low strain rates, some conductive losses may occur. An attempt will be made to minimize these losses by establishing the location of the reaction zone away from the burner ducts through judicious selection of fuel and air flows. Temperature measurements in the flame will indicate the extent of conductive losses.

In the second series of experiments that are planned, the structure of near-extinction flames will be investigated. Specifically, the distributions of temperature, soot volume fraction, and radiative heat flux will be measured. Flame temperatures will be measured using thermocouples in flame regions where soot levels are not significant. For flame locations that are soot laden and have sufficient luminosity, the temperature and soot volume fraction distributions will be measured using two-wavelength emission pyrometry [Choi et al., 1994]. These two complementary techniques are expected to provide an adequate picture of the temperature and soot volume fraction distributions in the flame. The radiative heat flux emitted will be measured using a small (~1 mm diameter) water-cooled Schmidt-Boelter total heat flux gauge. The gauge has a flat spectral response and a view angle of 150°. Experimental details are described in an earlier study [Lee et al., 1996], also in a small counterflow burner. Measurements will be made at locations on a cylindrical control surface surrounding the flame. Using appropriate view factors [Howell, 1982], the measured heat fluxes will be integrated to determine the total radiative enthalpy emitted by the flame [Lee et al., 1996]. Determination of the fractional flame heat loss due to radiation requires knowledge of the flame heat release. This will be estimated by integrating the local net heat release for each of the chemical reactions in the model simulation. The flame area, which varies as a function of distance from the ducts, must also be carefully considered [Lee et al., 1996].

NUMERICAL MODEL

A flamelet code (Rogg, 1991) will be used to predict the structure and required suppressant concentration to achieve extinction for the flames of interest. The code solves the conservation equations using detailed models of molecular transport and chemical kinetics. Detailed transport and kinetic rate information are available for the fuel and agent systems of interest. The kinetic data for the C/H/O systems will be based on Miller and Bowman [1989]. The kinetic data for the F/Br system will be the same that was used in Noto et al. [1996] and Babushok et al. [1996]. Transport and thermodynamic data for the F/Br system is listed in Noto et al. [1998]. Details of the calculation methodology are described elsewhere [Yang et al., 1994]. A gravitational body force term will be added to the momentum equation for consideration of buoyancy effects in the normal gravity flames. The numerical simulations will be used as a tool to further the understanding of the differences between low and high strain rate flames near extinction. A

complete kinetic model will not be initially used for soot formation. Instead, the measured soot volume fractions will be used as input data for the simulation.

The code will be modified to include radiative losses by appropriate gas species and particulates. Currently, a simple model of gas phase thermal radiation is used (Chen et. al., 1993) and emission by only two gas phase species, CO_2 and H_2O, are considered. The code assumes the optically thin limit and adopts the gray–medium approximation. The code will be modified to include radiation by particulates as well as appropriate gas species. The mean absorption coefficients will be obtained from Abu-Romia and Tien [1967] and checked using RADCAL [Grosshandler, 1993]. For addition of CF_3Br to the flames, radiation by HBr and HF will be considered. Ground state spectral information is available for HBr and HF, although high temperature spectral data is lacking [Rothman et al., 1992]. The absorption-emission coefficients for these molecules will be estimated using a temperature correction to the ground state data assuming a non-rigid rotator, anharmonic oscillator model [Ludwig et al., 1973].

COMPARISON OF MODEL AND MEASUREMENTS

The computations will be validated by comparison with the measurements of (1) the measured agent concentrations required to achieve flame extinction, (2) the measured temperature profiles, and (3) the measured radiative heat flux at various locations about the flame. Observations and measurements will guide model development, in the sense that the radiative transfer model will be refined to include radiative transfer by particulates, if flames are observed to be luminous. It is anticipated that such a sub-model will be appropriate to simulate the near-extinction low strain rate flames.

Consideration of temperature profiles and the equation of radiative transfer will allow quantification of the effects of conductive and radiative heat loss on flame stability. The radiative heat flux will be estimated using appropriate view factors [Howell, 1982] and compared to the measurements. A reaction path analysis will be conducted to identify important chemical routes in the suppression process. In particular, the model will be used to seek answers to the following questions:

- To what extent do radiative losses impact the extinction of a diffusion flame by an agent?
- At what strain rate do radiative losses become significant?
- Are there certain chemical routes (associated with fuel pyrolysis, agent decomposition, inhibition, or oxidation) that play an enhanced or diminished role as the strain rate changes?

SUMMARY

An experimental and computational study has been initiated to investigate the extinction of low strain rate diffusion flames by an agent. To illuminate the mechanisms of flame suppression at low strain rates, the structure and radiative heat loss from near-extinction flames will be experimentally measured. Computational simulations that include radiative heat transfer will be compared with the measurements. The experimental apparatus is being designed and the computational model is under development. Initial low strain rate microgravity experiments using the 2.2 s drop tower are planned for the fall of 1999.

ACKNOWLEDGEMENTS

This research project started February 1999 and is supported by NASA under Contract No. C-32066-J. The support and guidance of Dr. Sandra Olson, NASA Technical Monitor, are greatly appreciated.

REFERENCES

Abu-Romia, M.M., and Tien, C.L., *J.Heat Transfer*, **11**, 321 (1967).

Babushok, V., Noto, T., Hamins, A., and Tsang, W., *Combust. and Flame*, **107**, 351 (1996).

Chen, J.-Y., Liu, Y., and Rogg, B., *Reduced Kinetic Mechanisms for Applications in Combustion Systems*, (N. Peters and B. Rogg, Eds.), pp. 196-223, Springer-Verlag, 1993.

Choi, M.Y., Hamins, A., Rushmeier, H., and Kashiwagi, T., *Twenty-Fifth Symp. (Int.) on Combustion*, The Combustion Institute, Pittsburgh, pp. 1471-1480, 1994.

Grosshandler, W.L., "RADCAL: A Narrow-Band Model for Radiation Calculations in a Combustion Environment," *NIST Technical Note 1402*, US Govt. Printing Office, Washington, DC, 1993.

Howell, J.R., A Catalog of Radiation Configuration Factors, McGraw Hill, NY, pp. 32-33, 1982.

Lee, K.Y., Cha, D.J., Hamins, A., and Puri, I.K., *Combust. Flame*, **104**, 27 (1996).

Ludwig, C.B. Malkmus, W., Reardon, J.E., Thompson, J.A.L., *Handbook of Infrared Radiation from Combustion Gases*, (Eds.: R. Goulard. and J.A.L. Thomson), NASA Report SP-3080, 1973.

Maruta, K., Massaharu, Y. Hongsheng, G., Ju, Y., Niioka, T, *Combust. Flame*, **112**, 181 (1998).

Miller, J.A., and Bowman, C.T., *Prog. Ener. Combust. Sci.*, **15,** 287 (1989).

Noto, T., Babushok, V., Burgess, D., Hamins, A., Tsang, W., and Miziolak, A., *Twenty-Sixth Symp. (Int.) on Combustion*, The Combustion Institute, Pittsburgh, pp. 1377-1385, 1996.

Noto, T., Babushok, V., Hamins, A., and Tsang, W., *Combust. Flame*, **112**, 147 (1998).

Rogg, B., University of Cambridge Report Number CUED/A-THERMO/TR39, April 1991.

Ronney, P.D., *Acta Astronautica,* **12**(11), 915 (1985).

Rothman, L., Gamache, R., Tipping, R., Rinsland, C., Smith, M., Benner, D., Malathy, D., Flaud, J.M., Peyret-Camy, C., Perrin, A., Goldman, A., Massie, S., Brown, L., and Toth, R., *J. Quant. Spectroc. Radiat. Transf.*, **48**, 469 (1992).

Smyth, K., and Everest, D., *Twenty-Sixth Symp. (Int.) on Combustion*, The Combustion Institute, Pittsburgh, pp. 1385-1392, 1996.

VanDerWege, B.A., Bush, M.T., Hochgreb, S., *Proceedings of the Fourth International Microgravity Combustion Workshop*, NASA Conference Publication 10174, 1995, pp. 369-374.

Vranos, A., and Hall, R.J., *Combust. Flame,* **93**, 230 (1993).

Yang, M.H., Hamins, A., and Puri, I.K., *Combust. Flame*, **98**, 107 (1994).

S33-29

The Study Of Polymer Material Combustion In Simulated Microgravity By Physical Modeling Method

A.S. Melikhov[1], I.A.Bolodyan[1], V.I.Potyakin[1], A.V.Ivanov[2], V.F.Alymov[2], A.B.Smirnov[2], D.Ye.Belov[2], Ye.V.Balashov[3], and T.V.Andreeva[3],

[1]All-Russia Institute For Fire Safety, Moscow, Russia, [2]Keldysh Research Center, Moscow, Russia, [3]RSC-Energia, Korolev, Russia

INTRODUCTION

The tendency in space-mission development is that as overall spacecraft mass decreases, the use of polymer material increases. These materials as a part of the structure and hardware present the primary flammable payload of the spacecraft. In the oxygen enhanced environment of spacecraft, the danger of a fire becomes real. In order to ensure fire safety, researchers in many countries are evaluating material flammability in microgravity [1]. Unique data were collected to describe material flammability in microgravity, and new flammability parameters were identified. The material combustion at its limit is characterized by the limiting flow velocity (V_{lim}), which is required to sustain a fire in microgravity, and by the level of microgravity (g_{lim}) itself. These parameters appeared to depend on oxygen concentration (C_{ox}) in the environment, and the quantitative dependency was recovered. The physical parameters described above are essential to characterize flammability of the material in space and thus to promote fire safety.

It is extremely difficult and expensive to conduct experiments in real microgravity (in the drop tower; in the airplane, flying along a parabolic trajectory; on the space station). Therefore, it became advantageous to develop new methods to evaluate material combustion and ignition in the ground environment with suppressed convection. A specific method was developed that makes it possible to create a physical model of polymer material ignition and combustion in simulated microgravity. This method is based on material flammability evaluation in the flat moving layer of gaseous media that contains oxygen (the Narrow Channel apparatus). The gaseous media flows between two parallel horizontal plates [2], that are closely spaced and heavy enough to maintain a uniform wall temperature. The sample of the evaluated material is positioned along the longitudinal axis of the apparatus on the end of the holder, which is operated by the drive mechanism. The gas mixture of prescribed C_{ox} is blended and then flows through the channel. Flow velocity setting for the test is based on previously obtained results of flow calibration using smoke visualization technique.

The work presents some of the results of Narrow Channel testing compared to the results of space experiment in Skorost test apparatus on Orbital Station Mir in 1998 [1].

RESULTS OF NARROW-CHANNEL TESTS

The following characteristics of polymer material combustion (PMMA, high-density polyethylene, and Delrin) were evaluated in the Narrow Channel apparatus: combustion-zone shape and size versus flow velocity, limiting velocity of the flow versus flow oxygen concentration, flame-spread rate along the sample length versus flow velocity.

The most significant results of ground testing were:

- combustion zone increased in size when gaseous flow velocity increased;
- flame extinguishment occurred at flow shutoff;

- limiting flow velocity V_{lim} for all materials decreased when the oxygen concentration in the environment increased;
- flame-spread rate along the sample surface increased when flow velocity and oxygen concentration C_{ox} increased.

LIMITING FLOW VELOCITY

The dependency of limiting flow velocity V_{lim} on oxygen concentration C_{ox} is presented in Figures 1-3. These data were obtained in the Narrow Channel apparatus for the materials tested in Skorost on OS Mir in 1998 [2]. Left branches of well-known U-shaped curves of material flammability diagrams are shown on these figures.

The oxygen index C_{lim} is on Fig. 1-3 as well. When C_{ox} is lower than C_{lim}, the combustion is not feasible at g=981 cm/sec^2 and at any other gasdynamic conditions in microgravity of different levels.

It is noticeable that values for V_{lim} obtained on Mir are lower than those obtained in the Narrow Channel. However, even though there was a discrepancy in the numerical value of the data obtained in space and on the ground, qualitatively the two models of combustion agreed very well, because in both cases the combustion on the front edge of the sample was sustained by forced convection with no or minimum (in the Narrow Channel) buoyancy. Therefore, the flame on the front edge of the sample was of the same shape at the combustion limit in both models (Fig. 4). Hence, the comparative analysis of material combustion in microgravity is possible without performing an expensive experiment in space.

However, these results indicate that the additional analysis is required to improve the ground-test technique to be able to obtain data, which correspond accurately to the data obtained in a microgravity experiment of long duration.

FLAME-SPREAD RATE

The Narrow Channel method was employed also to determine the flame-spread rate along the sample. Fig. 5 shows the data for Delrin obtained in the Narrow Channel experiment and in the space experiment on OS Mir. The flame-spread rate obtained in the Narrow Channel is lower than corresponding values from the space experiment on OS Mir.

The Narrow Channel method was also used for the smoldering study in simulated microgravity [2]. The limiting velocity of the flow for smoldering V_{lim} was determined. The limiting velocity V_{lim} vs. oxygen concentration C_{ox} function for cotton cord is shown on Fig.6.

Data shown on Fig. 6 and Figs. 1-3 indicate that limiting modes for smoldering in the oxygen-enhanced environment (C_{ox} > 21%) are associated with lower flow velocities compared to combustion of gaseous phase. This might be explained by the temperature difference in the reaction zone. Thermocouples measured the temperature of the smoldering cotton cord. For the limit mode, the temperature did not depend on the oxygen concentration, was constant, and was equal to 910 K.

OTHER EXPERIMENTAL RESULTS

The Narrow Channel method was also used to study material ignition by the electrical spike in simulated microgravity. The sample was ignited by the spike in the flow at various distance X from the front of the sample. The limiting flow velocity for the ignition was determined, which was minimal on the front surface of the sample and increased when X increased.

The limiting value of gravity (g_{lim}), the level at which the material combustion becomes stable without forced convection, is of great scientific interest. When g increases, buoyant movement of the gaseous media might sustain combustion by providing a flow equal to V_{lim}. Therefore, a limiting

level of gravity g_{lim} shall exist. Since spacecraft control is associated with the maneuvers in orbit induced by thruster operation, g_{lim} may also be flammability criteria for the materials that are used on spacecraft and space stations.

The g_{lim} experiments were conducted using a drop system with a centrifuge in the inner container. The centrifuge had a combustion chamber where the sample was mounted in radial orientation. The combustion occurred at g sustained by centrifuge rotation with the prescribed angular velocity. For a given material combustion, g_{lim} was determined accounting for both centripetal ($\omega^2_{lim} \times R$) and Coriolis ($2\omega_{lim} \omega \times V_{lim}$) accelerations.

The determination of g_{lim} is possible only if V_{lim} for the material is known. Fig.7 shows g_{lim} vs. C_{ox} for PMMA (curve 1) and for Getinax (curve 2). When $g=g_0$, (881 cm/sec^2 in these tests), the material is flammable at minimum oxygen concentration, given by C_{lim1} and C_{lim2}, in Fig. 7, which is the material oxygen index C_{lim}. For PMMA: C_{lim}=15.5%; for Getinax: C_{lim}=19%. For higher values of C_{ox}, upper and lower limits of gravity exist, similar to V_{lim} (Figs. 1 to 3 extrapolated). When $g<g_0$, to the left of the minimum, the lower C_{ox} is, the higher g_{lim} will be. When $g>g_0$, to the right of the minimum, the higher C_{ox} is, the higher g_{lim} will be.

Data presented on Fig. 7 support the selection of fire-safe materials for manned compartments of stations that will be built on other planets, accounting for the surface gravitational acceleration of the planets. For example, Getinax, which is flammable on Earth (C_{lim}-19%), will be a safe material for Moon application (g=162 cm/sec^2). On the Moon, C_{lim} of Getinax will be 32%. On Mars, where g=376 cm/sec^2, Getinax will not be flammable up to 23% of oxygen concentration.

REFERENCES

1. A.V.Ivanov et al. Preliminary Results of the Third Series of Nonmetal Material Flammability Evaluation in Skorost Apparatus on OS Mir. Proc. Fifth Inter. Microg. Comb. Workshop. Cleveland, Ohio, 1999.
2. A.S.Melikhov, V.I.Potyakin et al. On the Limiting Conditions of Polymer Combustion at the Lack of Buoyancy - *Physics of Combustion And Explosion*, 1982, No 4 (in Russian).
3. A.S.Melikhov, I.N.Nikitenko, A.V.Shtepa. Investigation of Material Smoldering Process. *Combustion Of Condensed Systems - Chemical Physics of Combustion and Explosion.* Proc. 11th All-Union Symp.on Comb. and Expl. Suzdal, Nov. 19-24, 1989, p. 110 (in Russian).

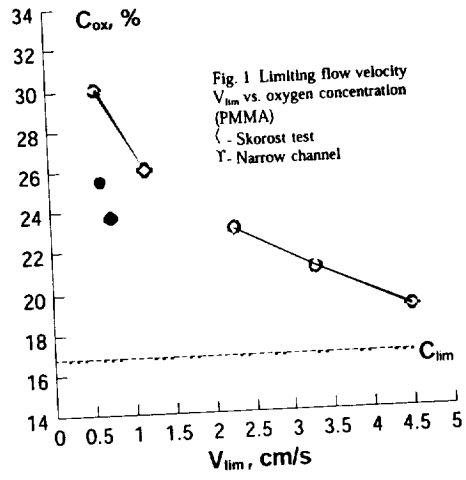

Fig. 1 Limiting flow velocity V_{lim} vs. oxygen concentration (PMMA)
(- Skorost test
Y- Narrow channel

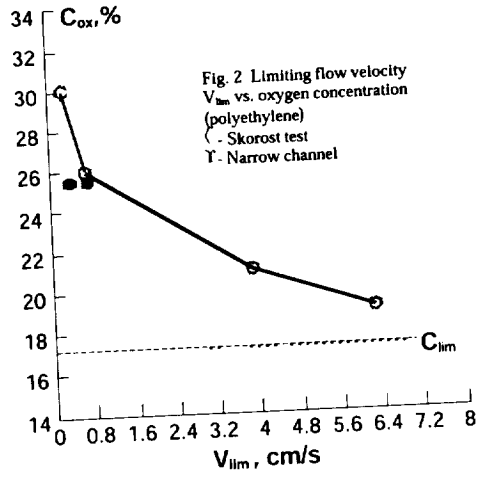

Fig. 2 Limiting flow velocity V_{lim} vs. oxygen concentration (polyethylene)
(- Skorost test
Y- Narrow channel

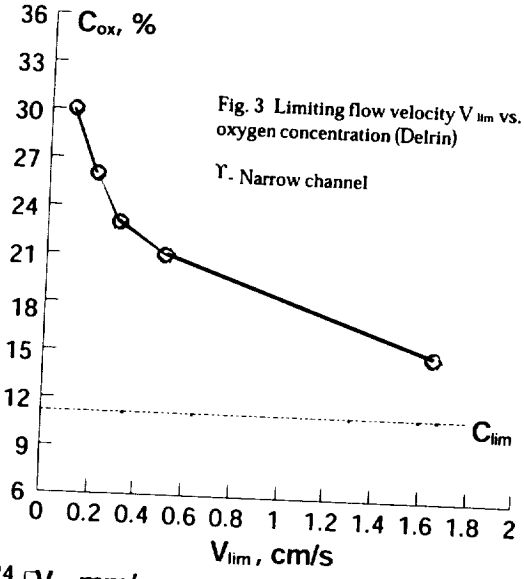

Fig. 3 Limiting flow velocity V_{lim} vs. oxygen concentration (Delrin)

Υ- Narrow channel

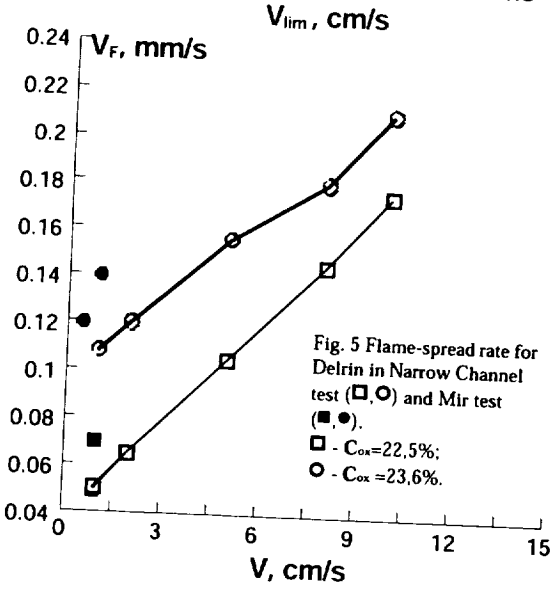

Fig. 5 Flame-spread rate for Delrin in Narrow Channel test (□,○) and Mir test (■,●).
□ - C_{ox}=22,5%;
○ - C_{ox} =23,6%.

Fig. 4 Delrin Combustion in Narrow Channel.
Flow velocity V=1.5 cm/sec; C_{ox}=21%

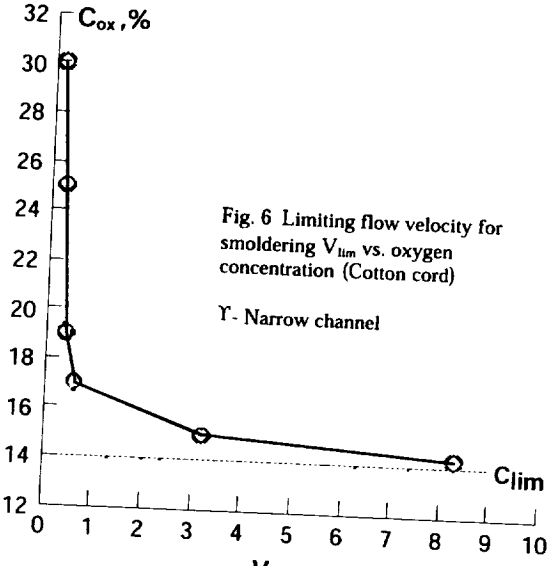

Fig. 6 Limiting flow velocity for smoldering V_{lim} vs. oxygen concentration (Cotton cord)

Υ- Narrow channel

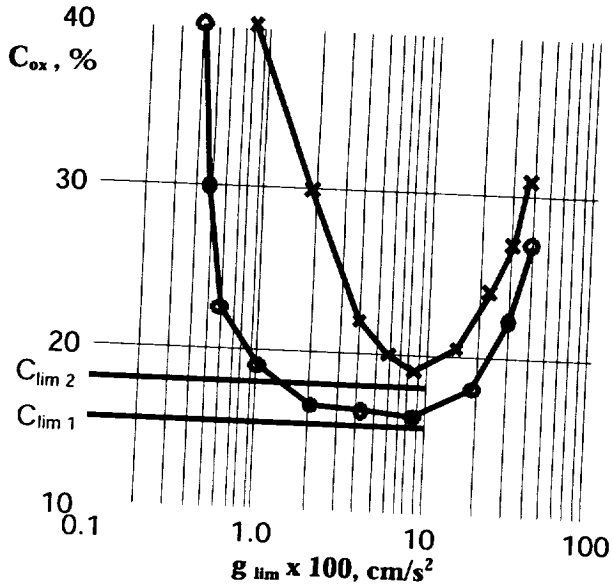

Fig. 7. g_{lim} vs. C_{ox}
1 - PMMA;
2 - Getinax

EFFECT OF LEWIS NUMBER ON RADIATIVE EXTINCTION AND FLAMELET MODELING

584-25

T. Shamim
Department of Mechanical Engineering
The University of Michigan-Dearborn
Dearborn, MI 48128-1491 (shamim@umich.edu).

INTRODUCTION

Lewis number, which relates the rates of heat and mass diffusion of various species, is an important parameter in combustion studies. Despite the early recognition of the importance of unequal rates of diffusion on the flame's structure and stability [1], the assumption of unity Lewis number has been common in many combustion modeling approaches. It is a convenient, and in many cases, a reasonable assumption which provides an ease in obtaining analytical and numerical solutions and helps simplifying the experimental data interpretations. However, in some applications, this assumption may lead to significantly erroneous conclusions. For example, in the turbulent flames, the effect of non-unity Lewis number may be responsible for the discrepancies between the measured and the predicted mass fraction of combustion intermediates [2]. This effect has also been reported to influence the flame's extinction limit [3] and to induce temperature oscillations in diffusion flame [4]. The present study is motivated by realizing the importance of Lewis number effects and its influence on a couple of combustion phenomena of recent interest, namely, transient effects in flamelet modeling [5,6] and radiative extinction [7-9]. Microgravity environment and hence the absence of buoyancy effect is essential for gaining better understanding of these effects.

In the present study, the influence of non-unity Lewis number due to unequal rates of heat and mass diffusion is considered. Transient effects are simulated by considering flames subjected to time dependent fluctuations in reactant concentrations, reactant temperatures, and partial premixing. The governing equations were reduced by using the assumptions of axisymmeteric, negligible body forces, negligible viscous dissipation, and negligible Dufour effect. The radiative heat flux is modeled by using the emission approximation. To focus on the physical understanding of the problem, the chemistry was kept simple by employing a single step overall reaction. The governing equations were solved by using the *Numerical Method of Lines* employing a second order 3-point central differencing for spatial discretization and an implicit backward differentiation formula (BDF) for temporal integration.

RESULTS AND DISCUSSION

To better understand the influence of Lewis number on unsteady flames, steady flames with different Lewis numbers are first considered. Figure 1 shows the temperature profiles of flames subjected to a strain rate of 10 s^{-1} with different Lewis numbers. The results show that the peak flame temperature decreases and the reaction zone thickness increases with an increase of Lewis number. The flame temperature decreases due to an increase of the thermal diffusivity, which increases the heat removal rate from the high temperature zone. This decrease of temperature is nearly exponential as shown in the insert of Figure 1. In this insert, the temperature is normalized by the peak flame temperature corresponding to a unity Lewis number. Due to high flame temperatures, the radiative heat losses are found to be maximum at low Lewis number.

Effect on Reactant Concentration and Temperature Fluctuations

These results were obtained by considering initially steady flames that were later subjected to sinusoidal variations in reactant concentrations or boundary temperatures. Figure 2 shows the variation of the maximum flame temperature (normalized with the steady state value) as a function of time period for flames with different Lewis numbers. These flames were subjected to a strain rate of 10 s^{-1} with the fuel concentration varied sinusoidally at 1 Hz and 50% amplitude. The results show that the flame temperature responds sinusoidally to sinusoidal fluctuations. Lewis number does not affect the flame response. The phase lag, asymmetry of the response and the normalized amplitude of the response remain unchanged for values of Lewis numbers ranging from 0.75 to 2. However, Lewis number greater than unity may cause extinction for flames subjected to the reactant concentration fluctuations at high strain rates. Figure 3 shows such extinction at a strain rate of 100 s^{-1}. An increase of Lewis number increases the amplitude of the flame response to the fluctuations in reactant temperatures as shown in Figure 4. The figure shows that the phase lag in the response decreases slightly with an increase of Lewis number, which is due to an increase of the thermal diffusivity.

Effect on Time Dependent Partial Premixing

These simulations were carried out by considering initially a steady partially premixed flame, which was later subjected to sinusoidal fluctuations in partial premixing. Figure 5 shows the variation of the maximum diffusion flame temperature (normalized with the steady state value) as a function of time period for flames with different Lewis numbers subjected to time dependent partial premixing. The results shown are for flames subjected to a strain rate of 10 s^{-1} with 5% oxidizer partially premixed on the fuel side. The concentration of the premixed oxidizer was varied sinusoidally at 1 Hz and 100% amplitude (i.e., ±5% O_2). The imposed fluctuations in this case also bring about sinusoidal flame response. The results show that the amplitude of the flame temperature response increases with an increase of Lewis number, i.e., the effect of fluctuations in partial premixing is greater on flames with large Lewis number. This may be explained by considering that with an increase of Lewis number, the diffusion flame becomes weaker and thus may be more extensively influenced by changes of partial premixing. The increase of Lewis number is found to have no effect on the phase lag and the asymmetry of the flame response. The distance between the premixed and the diffusion flames is found to increase with an increase of Lewis number (as shown in the insert of Figure 5). Results, not shown here, suggest that an increase of Lewis number in partially premixed flames improves the incomplete burning of the premixed flame.

Effect on Radiative Extinction

The simulations of radiative extinction of diffusion flames were carried out by utilizing the analytical solutions of non-radiating flames as the initial conditions. Emissions from the major combustion products were considered. Figure 6 shows the drop of the peak flame temperature due to gas radiation as a function of time for various values of strain rates with Lewis numbers of 1 and 2. The flame temperature drops for all strain rates and Lewis numbers. However, the temperature reduction is significant at low strain rates, which eventually leads to extinction. Recall that at low strain rates, the flame has a low heat release rate (due to slow burning rate) and hence its stability is greatly affected by the temperature drop due to radiation. Figure 6b shows that with an increase of Lewis number, flames become relatively "weak" and are more

susceptible to radiative losses. This is more clearly shown in Figure 7. The figure depicts that the flame at strain rate of 1 s^{-1} escapes radiative extinction (defined here as the disappearance of chemiluminescence ≈ 1550 K [7]) for Lewis numbers of 0.5 and 1.0 but not for 2. Hence, keeping all conditions similar, an increase of Lewis number pushes the radiative extinction limit toward higher values of strain rate.

CONCLUSIONS

The effect of Lewis number on radiative extinction and flamelet modeling is numerically investigated in this study. The results show that at large Lewis numbers, flames are relatively "weak" and become susceptible to radiative heat losses. With an increase of Lewis number, radiative extinction limit, which has been reported in recent studies to occur at low strain rates, is found to be pushed toward higher values of strain rates. The study also examines the influence of Lewis number and its interaction with transient effects on flamelet combustion modeling. The results clearly show the significance of including the influence of Lewis number in flamelet modeling as under some conditions large Lewis number may result in extinction.

REFERENCES

1. Lewis, B., and von Elbe, B., *Combustion, Flames, and Explosion of Gases,* Academic Press, NY, 1961.
2. Barlow, R. S., and Chen, J. Y., *Twenty-Fourth Symposium (International) on Combustion,* The Combustion Institute, Pittsburgh, 1992, pp. 231-237.
3. Cuenot, B., and Poinsot, T., *Comb. & Flame,* 104:111-137 (1996).
4. Katta, V. R., Goss, L. P., and Roquemore, W. M., *Comb. & Flame,* 96:60-74 (1994).
5. Rutland, C. J., and Ferziger, J. H., *Combust. Sc. Tech.,* 73:305-326 (1990).
6. Ghoniem, A. F., Soteriou, M. C., Knio, O. M., and Cetegen, B., *Twenty-Fourth Symposium (International) on Combustion,* The Combustion Institute, Pittsburgh, 1992, pp. 223-230.
7. Bonne, U., *Comb. & Flame,* 16:147-159 (1971).
8. Shamim, T., and Atreya, A., *Proceedings of the ASME Heat Transfer Division,* HTD Vol. 317-2, pp. 69-74 (1995).
9. Atreya, A., and Agrawal, S., *Comb. & Flame,* 115:372-382 (1998).

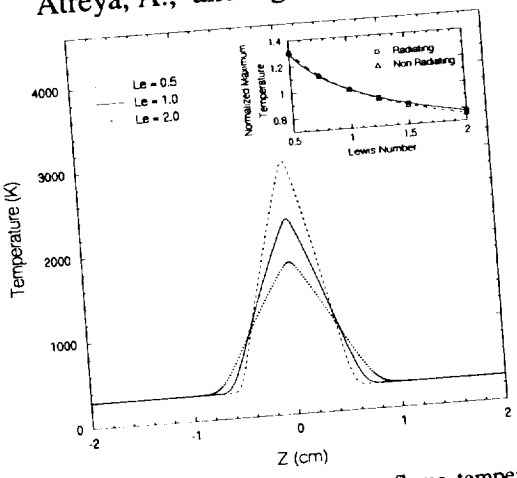

Figure 1 Effect of Lewis number on flame temperature (strain rate = 10 s^{-1}; boundary temperature = 295 K; reactant mass fractions = 12.5% CH_4 + 87.5% N_2 on the fuel side and 50% O_2 + 50% N_2 on the oxidizer side)

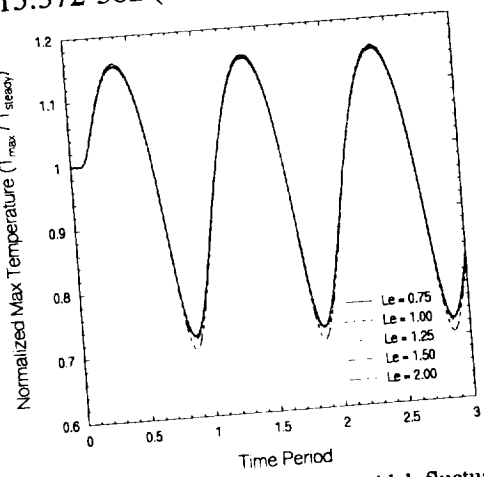

Figure 2 Flame response to sinusoidal fluctuations in reactant concentrations: variation of the normalized maximum flame temperature (amp = 50%; freq = 1 Hz; strain rate = 10 s^{-1}; time period = 2 π f t)

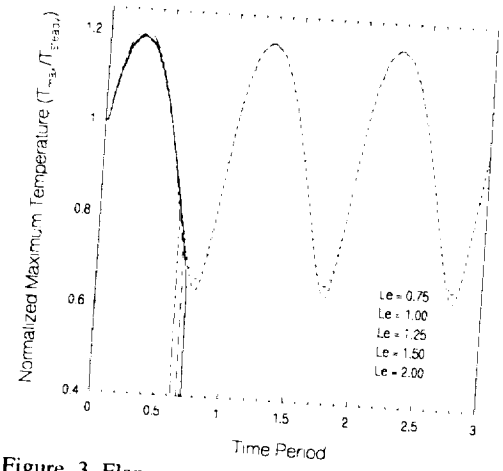

Figure 3 Flame response to sinusoidal fluctuations in reactant concentrations: variation of the normalized max flame temperature (amp = 50%; freq = 1 Hz; strain rate = 100 s^{-1}; time period = 2 π f t)

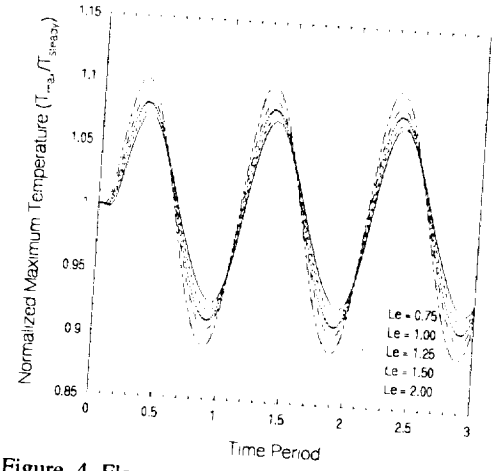

Figure 4 Flame response to sinusoidal fluctuations in reactant boundary temperatures: variation of the normalized max flame temperature (amp = 50%; freq = 1 Hz; strain rate = 10 s^{-1}; time period = 2 π f t)

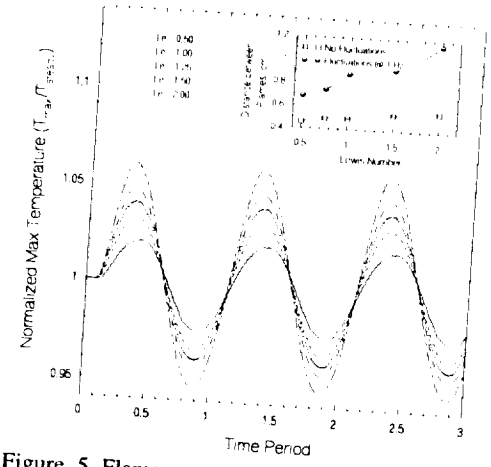

Figure 5 Flame response to sinusoidal fluctuations in partial premixing: variation of the normalized max flame temperature (amp = ±5% O_2; freq=1 Hz; strain rate = 10 s^{-1}; time period = 2 π f t)

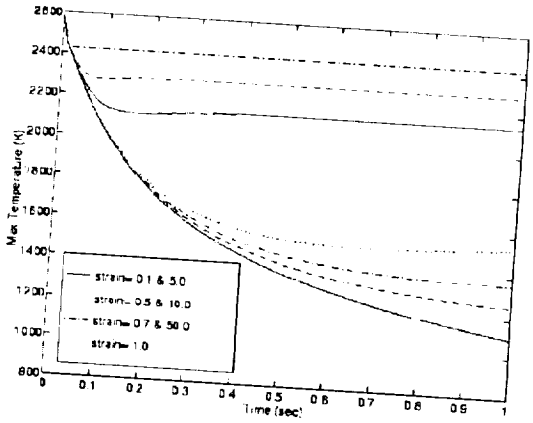

Figure 6a Effect of Lewis number on radiative extinction: variation of the peak flame temperature due to radiation for various strain rates (Le = 1)

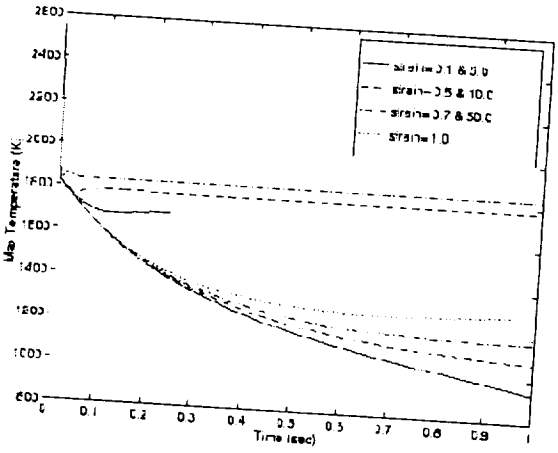

Figure 6b Effect of Lewis number on radiative extinction: variation of the peak flame temperature due to radiation for various strain rates (Le = 2)

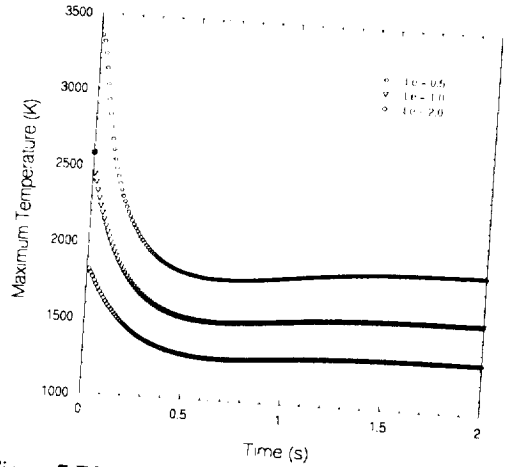

Figure 7 Effect of Lewis number on radiative extinction (strain rate = 1 s^{-1}; boundary temp = 295 K; 12.5% CH_4 + 87.5% N_2 on the fuel side and 50% O_2 + 50% N_2 on the oxidizer side)

Combustion Diagnostics

S85-35

QUANTITATIVE INTERPRETATION OF OPTICAL EMISSION SENSORS FOR MICROGRAVITY EXPERIMENTS

Jay B. Jeffries, Gregory P. Smith, and David R. Crosley, Molecular Physics Laboratory, SRI International, 333 Ravenswood Ave., Menlo Park, CA 94025, Jay.Jeffries@SRI.com

INTRODUCTION

Microgravity flight experiments uniquely test our knowledge and understanding of the coupling between chemistry and fluid mechanics. However, compared to ground based laboratory experiments the number of useful diagnostic tools suitable for microgravity environments is severely limited by the space, weight, power consumption, and operator complexity requirements. One of the available tools is the observation of optical emission, and total emission has already proven useful for observations of stable "flame balls" on the space shuttle.[1] wavelength resolved tomographic measurements of flame emission offer the promise of diagnostics to test our understanding of flame chemistry and structure. Individual emissions from electronically excited radicals, e.g., CH^*, OH^*, and C_2^*, can be identified in a methane/air flame. Spatially resolved measurements of the intensity of this resolved optical emission from a specific excited molecule enable chemically resolved flame structure studies. Wavelength resolved emission measurements to determine such structure in diffusion flames are being readied for flight experiments by a group at Yale headed by Profs. Smooke and Long.[2]

A quantitative relationship between emission intensity and flame properties, as expressed by a flame model, is needed for species specific optical emission measurements to fulfill its promise. The Yale group compared models and measurements of optical emission in laboratory tests at 1-g. Unfortunately, these experiments[2] show disagreement between measurement and state-of-the-art flame models by over a factor of 50. Therefore, an improved chemical mechanism for optical emission from flames is needed to enable quantitative tests of microgravity flame models. The connection between excited state emission and flame chemistry is not yet adequate.

PLANNED RESEARCH

We will develop an optimized chemical kinetic mechanism for optical emission from CH^*, OH^*, and C_2^* in flames using a series of ground-based, support experiments. These will be performed in close collaboration with the Yale group, which has moved from laboratory experiments to the design of flight measurements. The resulting mechanism will enable quantitative interpretations of optical emission measurements from microgravity combustion experiments, and thus be a quantitative tool in the quest to unravel the interaction between chemistry and fluid mechanics in flames.

Our proposed research involves laboratory measurements, the development of a model for chemiluminescent emission (within the framework of an existing combustion model), and carefully designed flame experiments to test that model. Note that optical emission in flames is primarily produced by chemiluminescent reactions, and therefore is described by finite rate chemistry not by equilibrium emission.[3] The products are electronically excited atoms or molecules that subsequently radiate to produce the flame emission. Developing a chemical mechanism for the optical emission consists of three parts. First, the chemical pathway must be identified to tell us which atoms and molecules are the precursor reactants that produce the excited state products.

Second, the temperature and pressure dependent rate coefficients for the chemical reactions in this pathway must be determined to allow us to model the rate at which the excited species are produced. Third, the collisional quenching of the electronically excited products must be determined to quantify the probability that an excited state species will radiate and contribute to the optical emission.

Our previous work on the development of the GRI-Mech chemical mechanism for natural gas combustion provides guidance for the work proposed here. We have already developed a protocol and instrument to test chemical mechanisms using laser-induced fluorescence in premixed, low-pressure flames.[4,5,6] Our model of the combustion chemistry has been validated by previous laser based measurements of the absolute concentration of CH and OH which agree well with the predictions of our chemical model.[4,5] We propose to add to this model the chemistry of optical emission and to optimize this chemical mechanism with respect to measured emissions from test flames. This approach will take advantage of our database by measuring the optical emission in the same flames we have successfully characterized and modeled, tomographically reconstructing the spatially resolved optical emission, and using this data to optimize the chemical mechanism for optical emission. In these flames, we already have empirical measurements of the electronic quenching which is needed to connect emission intensity with the concentration of electronically excited CH^* and OH^*.[7].

For electronically excited OH^*, the reaction $CH+O_2$ is the most likely chemical pathway.[3] However, for excited CH^* and C_2^* there are several chemical pathways possible. It may well be that more than one of these pathways are important in different regions of the flame or in flames of different stoichiometry. We will identify the chemical pathway, select reaction rate coefficients from the literature, add these chemical pathways into our chemical mechanism for combustion, and optimize the chemical reaction rate coefficients of the excited state formation reactions within their known uncertainties to match these target experiments. We will use modeling results to select additional target flames (different fuels, different stoichiometry) which minimize or maximize the optical emission from different proposed chemical pathways. For the OH^* example, trace amounts of CH_4 in an H_2/O_2 flame will maximize the influence of reactions involving CH but not reactions of molecules with two carbon atoms, whereas a C_2H_2 flame provides the reverse. This research will produce an optimized and validated chemical mechanism for quantitative optical emission diagnostics for methane/air flames.

ACKNOWLEDGEMENTS

The NASA Office of Life and Microgravity Sciences and Applications will support this work.

REFERENCES:

1. P. D. Ronney, M.-S. Wu, H. G. Pearlman, and K. J. Weiland, "Experimental Study of Flame Balls in Space: Preliminary Results from STS-83," AIAA Journal, Vol. 36, p. 1361-1368 (1998).
2. M. B. Long, K. T. Walsh, and M. D. Smooke, "Computational and Experimental Study of Laminar Diffusion Flames in a Microgravity Environment," 4th International Microgravity Combustion Workshop, Cleveland, OH, May, 1997; K. T. Walsh, M. B. Long, M. A. Tanoff,

and M. D. Smooke, "Experimental and Computational Study of CH, CH^*, and OH^*, in an Axi-symmetric Laminar Diffusion Flame," 27th Symposium (International) on Combustion, The Combustion Institute, Pittsburgh, PA, 1999, in press.

3. A. G. Gaydon, **The Spectroscopy of Flames,** Chapman and Hall, London, 1957, 2nd Edition, John Wiley and Sons, New York, 1974; A. G. Gaydon and H. G. Wolfhard, **Flames: Their Structure, Radiation, and Temperature,** Chapman and Hall, London, 1953, 4th Edition, John Wiley and Sons, New York, 1979.
4. J. Luque, G. P. Smith, and D. R. Crosley, "Quantitative CH Determinations in Low-Pressure Flames," Twenty-sixth Symposium (International) on Combustion, The Combustion Institute, Pittsburgh, PA, 1996, p. 959-966; J. Luque and D. R. Crosley, "Absolute CH Concentrations in Low-Pressure Flames Measured with Laser-Induced Fluorescence," Appl. Phys. **B63** (1996) 91-98.
5. P. A. Berg, D. A. Hill, A. R. Noble, G. P. Smith, J. B. Jeffries, and D. R. Crosley, "Absolute CH Concentration Measurements in Low-Pressure Hydrocarbon Flames: Comparisons with Model Results," AIAA 97-0905, 35th Aerospace Sciences Proceedings, 1997.
6. P. A. Berg, G. P. Smith, J. B. Jeffries, and D. R. Crosley, "Nitric Oxide Formation and Reburn in Low-Pressure Methane Flames," 27th Symposium (International) on Combustion, The Combustion Institute, Pittsburgh, PA, 1999, in press.
7. M. Tamura, P. A. Berg, J. E. Harrington, J. Luque, J. B. Jeffries, G. P. Smith, and D. R. Crosley, "Collisional Quenching of OH, CH, and NO in Low-Pressure Flames," Combustion and Flame, **114**, 502 (1998).

DETECTING THE ONSET OF FIRE IN AN AIRCRAFT BY EMPLOYING CORRELATION SPECTROSCOPY

Kisholoy Goswami[1], Indu Saxena[1], Claudio Egalon[1], Edgar Mendoza[1], Robert Lieberman[1] and Nancy D. Piltch[2], [1]Intelligent Optical Systems, Inc., 2520 West 237th Street, Torrance, CA 90505, Kisholoy@hotmail.com, [2]NASA Glenn Research Center, 21000 Brookpark Road, Mail Stop 110-3, Cleveland, OH 44135, Nancy.D.Piltch@grc.nasa.gov

INTRODUCTION

The cause of aircraft fire and locations of the fires are numerous. Worldwide, numerous in-flight fires have been passenger initiated, the prime location being the lavatory areas. Most in-flight fires in commercial carriers are of electrical origin and cigarettes. A cargo bay fire can be caused by a variety of reasons. The sheer number of different types of cargo makes it difficult to identify the origin, especially when the fire reaches the catastrophic level. The damage can be minimized, and fire can be suppressed effectively if a warning system for the onset of fire is available for onboard monitoring.

In general, in-flight cabin fires can be detected by monitoring the combustion by-products of aircraft materials. The first material available to any interior fire is the paneling, followed by epoxy and other polymers. Fires involving fuel and hydraulic fluid can also be detected by monitoring the combustion by-products of these fluids. The U.S. Federal Aviation Administration (FAA) has studied the combustion by-products of 141 different aircraft materials.[1] The most commonly occurring gaseous by-products of these materials are carbon dioxide (CO_2), carbon monoxide (CO), hydrogen chloride (HCl), hydrogen cyanide (HCN), oxides of nitrogen (NOx), ammonia (NH_3), chlorine (Cl_2), carbonyl chloride ($COCl_2$), hydrogen fluoride (HF) and sulfur dioxide (SO_2). Table 1 shows the average concentrations of marker compounds from various studies.

TABLE 1. Typical Concentrations of Aircraft Fire Byproducts[1]

Markers	CO_2	CO ppm	HCl ppm	HCN ppm	N_2O ppm	NO ppm	NH_3 ppm	Cl_2 ppm	$COCl_2$ ppm	HF ppm	SO_2 ppm
Maximum	60%	2200	2500	90	130	T	T	T	T	50	50
Typical	30%	400	600	40	T	T	T	T	T	5	5

T indicates insufficient data or trace quantities less than 10 ppm

An early warning device will detect these markers before a flame erupts, enabling the crew to take fire-suppressing measures before serious damage occurs. Carbon dioxide is a product of complete oxidation; thus, it is not a marker for the onset of fire. It is therefore important to monitor as many of the other markers as possible. By using correlation spectroscopy, this goal can be accomplished.

CORRELATION SPECTROSCOPY

Classic absorption spectroscopy has been used for remote monitoring and chemical detection for many decades, but the sensitivity of steady-state methods is often unsuitable for the detection of trace compounds at the low levels (parts per million to parts per billion) appropriate for scientific and regulatory purposes. This is particularly so for monitoring equipment, which must be compact and cost-effective, and which is often subject to shock, vibration, and other effects that can severely degrade the performance of high-sensitivity spectrometers in an aircraft.

In correlation spectroscopy, a dramatic increase in sensitivity is achieved by phase- or wavelength-modulation of a very narrow band optical source whose natural wavelength coincides with one of the absorbance lines of the target compound. Highly specific chemical detection is accomplished by using a sample of the target compound itself as an optical filter. The positions of the absorbance maxima in the filter sample are modulated via an external physical process, such as an electric field (Stark effect modulation) or pressure. This modulation, which brings the reference sample's absorbance bands periodically into and out of registry with the absorbance bands of the target gas in the substance under test, creates a modulated signal at the detector whose intensity is directly related to the concentration of the target. This technique can achieve one or two orders of magnitude better sensitivity than simple modulation of source intensity, and has the added benefit of rendering the detection system virtually insensitive to other gases. Because the detailed structure (e.g., the manifold of rotational states on infrared vibrational absorbance bands) is unique for each compound, the use of tunable filters matched to the spectral properties of the target compound makes correlation-spectroscopy systems extremely good at detecting trace quantities of target molecules in complex mixtures. During presentation we will demonstrate that correlation spectroscopy is well suited for monitoring the marker compounds to provide an early warning of fire.

ACKNOWLEDGMENTS

This work is funded by NASA Glenn Research Center under a Small Business Innovation Research Contract (Contract No. NAS3-99030). The authors wish to thank Mr. Douglas A. Rohn (Element Manager, Accident Mitigation and Aviation Safety Program at NASA Glenn Research Center) for his keen interest and support.

REFERENCE

1. Gross, D., and Loftus, J. J., "Smoke and gases produced by burning aircraft interior materials," FAA Report No. 510-001-11x, February 1969.

S87-36

MICROGRAVITY TESTED 38 W CO_2 LASER REACTOR PROTOTYPE FOR THE GAS-PHASE SYNTHESIS OF REFRACTORY MATERIALS

P. R. Buerki[1], U. Ott[2] and P. Roth[3]
[1]GIA Research, 5355 Armada Drive, Carlsbad, CA 92083, USA, pbuerki@gia.edu
[2]Max-Planck-Institut für Chemie, D-55020 Mainz, Germany
[3]Inst. for Combustion and Gas Dynamics,University of Duisburg, D-47048 Duisburg, Germany

INTRODUCTION

The use of CO_2 laser driven flow reactors for the gas-phase synthesis of high purity ceramic powders, including Si_3N_4, SiC, B_4C, TiO_2, TiB_2, and diamond, has become an established method during the past twenty years [1-4]. By matching an emission line of the CO_2 laser with a strong absorption band of at least one of the reactants, an efficient and rapid excitation and the initiation of chemical reactions is achieved. A wall-free compartment is created at the intersection of laser beam and reactant gas flow. Typical for laser driven gas-phase reactions are high temperature gradients (10^6 K/m), fast heating (10^5 K/s) and fast cooling rates (10^4 K/s), which cause strong gravity induced convection on ground. Consequently, the particle growth and particle properties depend strongly on the local conditions in the reaction zone. This results in broad and often multimodal particle size distributions, hard agglomerates, and large variations of particle characteristics within the same batch.

Until recently, the use of high power lasers in microgravity research had been rather limited, due to severe restrictions in terms of safety, weight, power consumption and cooling requirements. With the development of more compact and energy efficient CO_2 lasers and multiwatt laser diodes, laser induced gas-phase materials synthesis is now ready to be applied in microgravity research. Compared to crystal growth from the melt or from solution, microgravity experiments on gas-phase materials synthesis are still rare and suitable hardware is not widely available. The characteristics and performance of a first prototype of a CO_2 laser driven reactor for gas-phase materials synthesis and attempts to synthesize diamond particles in microgravity are the topic of the present report. Instead of using a flow reactor, the syntheses were performed in batches, i.e., the laser photolysis of reactant gas bubbles created in the center of a reaction chamber filled with nitrogen. The experiments were performed during the 25th ESA Parabolic Flight Campaign, October 20 - 30, 1998 in Bordeaux-Mérignac (France).

HARDWARE

The experiment hardware is shown schematically in figure 1 and in flight configuration in figure 2. The experiments were performed in a reaction chamber located inside the ESA Multi User Combustion Chamber, M.U.C.C. The latter was built by ESA in 1986 and had repeatedly participated in parabolic flights. It was used here as a second containment in order to prevent any combustible gases from leaking into the aircraft cabin. The M.U.C.C. was connected to the Airbus vent line and thus constantly evacuated during the flights. The reaction chamber viewports were coaxially aligned with the M.U.C.C. main viewports. One axis was used for the laser beam path, the other for the observation and documentation using Super-VHS video recording and a 24 x 36 mm reflex camera. A compact 38 W cw CO_2 laser (λ = 10.591 μm) model OPL-40 from Oerlikon Precision Laser, Crissier (Switzerland) was used for photolyzing

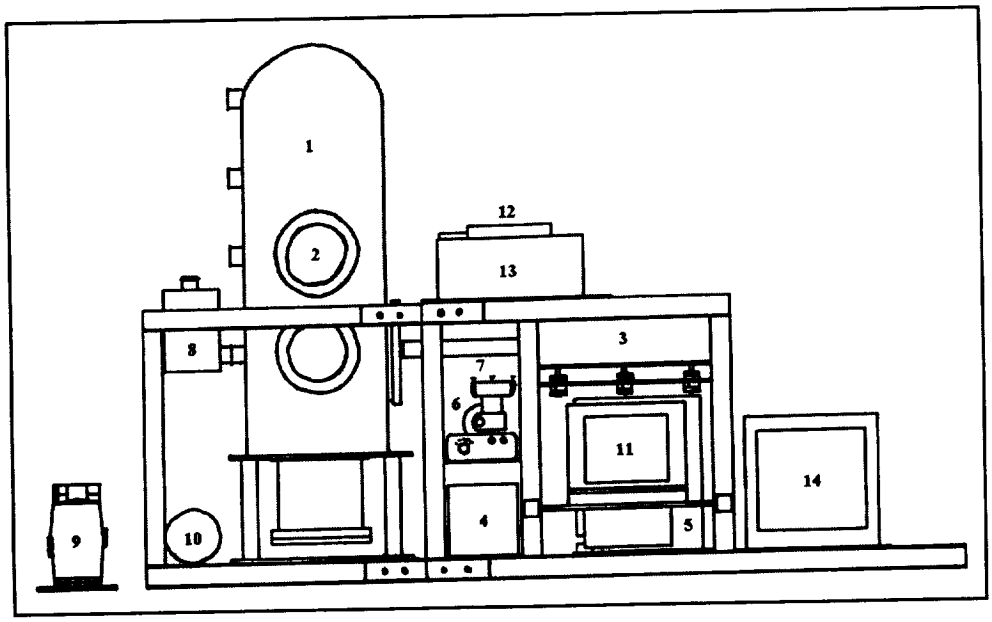

Figure 1: Prototype of a microgravity tested CO_2 laser reactor for the gas-phase synthesis of refractory materials. 1: ESA Multi User Combustion Chamber, M.U.C.C.; 2: gas lines and reaction chamber (inside M.U.C.C.); 3: 38 W cw CO_2 laser; 4: laser power supply; 5: 0.02 m^3 HDPE tank; 6: peristaltic pump with controller; 7: laser beam guide and focusing unit; 8: laser beam stop; 9: rotary vacuum pump; 10: 0.01 m^3 N_2 pressurized gas cylinder; 11: notebook computer; 12: SCXI data acquisition and relay boards; 13: Super-VHS video recorder; 14: video monitor.

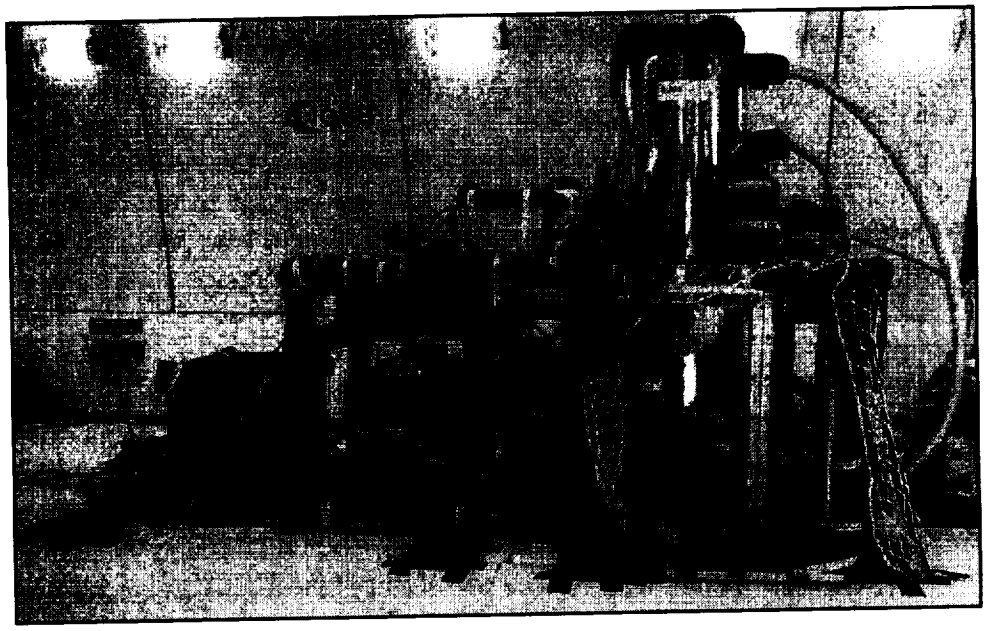

Figure 2: Prototype of CO_2 laser reactor shown in figure 1 in flight configuration. Note that the view depicted in figure 1 is facing the wall.

the reactant gases. The laser head measured 440x166x89 mm, weighed 7.7 kg and was connected to a Ferropac FP800DC 28VDC/28A power supply. Cooling water was circulated through the laser head from a 0.02 m^3 tank using a peristaltic pump. The laser beam was aimed into the M.U.C.C. and the reaction chamber through a stainless steel tube and focusing unit. The laser beam was stopped on the other side in a water-filled copper tank. The gas lines were located inside the M.U.C.C. Five reactant gas mixtures were stored in 50 ml pressurized gas cylinders (Whitey 304L-HDF4-50). The pressure was reduced from 74 bar down to 1.6 bar with compact stainless steel pressure regulators. Nitrogen was stored externally in a 0.01 m^3 pressurized gas cylinder. The connections to the reaction chamber, the filter units and the rotary vacuum pump were made of 1/4" copper tubing, 21 electromagnetic valves, SWAGELOK fittings and WHITEY valves. The pump was backed up by the Airbus vent line. The reaction chamber had a volume of 0.004 m^3 and was built from a stainless steel double cross and flange material according to DIN 28403. The experiments were semiautomatic and controlled by software written in Borland Pascal 7.0. The data acquisition and control hardware consisted of an 80486 notebook computer (Toshiba TI1900), National Instruments SCXI-1160 relay boards for operating the electromagnetic valves and a SCXI-1200 DAQ board for acquiring pressure data from two piezo-resistive pressure transmitters (Keller AG, Winterthur, Switzerland, series PA21).

EXPERIMENTS

The parabolic flight experiments focused on the synthesis of homogeneously nucleated diamond particles [5]. C_2H_4 and mixtures of C_2H_4 with H_2 and other reactants were photolyzed. Among the expected reaction products were polyaromates, graphite, soot, fullerenes and diamond. In an attempt to address some open questions concerning the formation of interstellar microdiamonds found in meteorites [6], mixtures of C_2H_4, H_2 and traces of noble gases were photolyzed in order to study the incorporation of noble gas atoms into the growing diamond particles. After purging the gas lines, the reaction chamber was filled with nitrogen to a background pressure between 0.8 and 2.0 bar. In microgravity, the piston was actuated pneumatically and a reactant gas bubble created in the center of the chamber. The bubble was then ignited with the CO_2 laser beam. The total pressure and the reactant gas composition were the parameters varied in the experiment program, while laser power and the amount of reactant gas were kept constant. After each parabola, the reaction chamber was evacuated through a filter unit, where any solid reaction products were trapped. TEM grids were installed in front of the filters in order to collect an unaltered fraction of the products. For increasing the yield, each parameter set was repeated during 6 to 8 parabolas.

Considerable technical problems were encountered during the parabolic flights. The notebook caused a number of false starts during the hypergravity phases, because its keys were actuated by their own weight. This was temporarily by-passed by changing the timing of certain operator interactions at the cost of some microgravity time. During the second flight day, the problem was permanently solved by implementing software routines that constantly read out the keyboard buffer during hypergravity. A loose contact in the video system and a constant loss of pump oil through the vent line did not negatively affect the experiments. The main difficulties were properly aligning the laser beam and insufficient focusing. Misalignment of the M.U.C.C. viewports during manufacturing and the requirement to divide the experiment into two separate modules for complying with the maximum loads specified for the Airbus were responsible for

this. The reassembly of the modules in the aircraft was difficult and the final alignment of the laser beam far from perfect. The infrared laser beam had to be traced by creating burn marks on pieces of MACROLON (a high-temperature resistant polycarbonate) attached to the viewports and placed in the center of the reaction chamber. Each laser shot created a small amount of black smoke, too, and thus caused a contamination of the reaction chamber we had to live with. Due to a poorly designed focusing unit, the laser could not be sufficiently focused. On ground, the obtained laser power density of ~1000 W/cm^2 would be by a factor of 3.5 too low to induce chemical reactions and visible light emission in C_2H_4 [2]. In microgravity, longer residence times of the reactants in the laser beam partially compensated for this. However, the compensation was insufficient and no visible light emission was observed.

The evaluation of the experiments is not terminated yet. A preliminary examination of the TEM grids with a cold cathode FE-TEM (Hitachi HF-2000) showed a number of globular aggregates about 1 μm in size and consisting of carbon and oxygen. These particles are suspected to represent pyrolysis products from the MACROLON. A number of carbon onion shells and carbon nanotubes with multiple walls was found, too. However, it is not clear at this moment, whether these fullerene-type structures represent reaction products or a contamination. The TEM grids contained very few particles and a first visual inspection of the filters did not show noticeable amounts of reaction products either. Thus, it is not clear yet whether the synthesis of diamond particles and other products was successful or not.

Future projects shall concentrate on the design on improved and less complex prototypes for laser reactors suited for microgravity research including CO_2 laser and laser diode reactors. Research topics will include the gas-phase synthesis of a larger range of suitable model materials, e.g., SiC, Si_3N_4, BC, BN, and diamond.

ACKNOWLEDGEMENTS

This study was funded under project no. 50WM9584 by the Bundesministerium für Bildung, Wissenschaft, Forschung und Technologie (BMBF), Bonn (Germany). Further support came from Intospace GmbH, Hannover (Germany) and the Swiss government. The authors are grateful to J. Steffen and Oerlikon Precision Laser, Crissier (Switzerland) the loan of a suitable CO_2 laser and to the European Space Agency for making the M.U.C.C. available to us. We would like to thank the staff of Novespace and the other participating research teams for their support during the assembly of the equipment in the aircraft and D. Tillmann for his assistance during the flight. The PI is grateful to Y. Sato (NIRIM, Tsukuba, Japan) and J. Schoonman (Institute for Applied Inorganic Chemistry, Technical University of Delft, The Netherlands) for their support during the proposal preparation. We further thank B. Tesche and J. Splithoff (Max-Planck-Institute for Coal Research, Mülheim, Germany) for the FE-TEM characterization of our samples.

REFERENCES

[1] J. S. Haggerty, W. R. Cannon, in: Laser-Induced Chemical Processes, J. I. Steinfeld (ed.), Plenum Press New York, 1981, 165 -241
[2] P. R. Buerki, Ph.D. thesis, University of Berne, Switzerland, 1991, and references therein
[3] P. R. Buerki, S. Leutwyler, Nanostructured Materials 4, 1994, 577 - 582
[4] X. Li, Y. Nakata, H. Nagai, M. Suzuki, Nanostructured Materials, 10, 1998, 1173 - 1187
[5] P. R. Buerki, LowG 6/2, 1995, 16 - 19 (Intospace GmbH, Hannover, Germany)
[6] U. Ott, Nature 364, 1993, 25 - 33

S88-29

A COMPACT, TUNABLE NEAR-UV SOURCE FOR QUANTITATIVE MICROGRAVITY COMBUSTION DIAGNOSTICS

K. A. Peterson and D. B. Oh, Southwest Sciences, Inc. 1570 Pacheco St., Suite E-11, Santa Fe, NM 87505. peterson@swsciences.com, dboh@swsciences.com

INTRODUCTION

There is a need for improved optical diagnostic methods for use in microgravity combustion research. Spectroscopic methods with fast time response that can provide absolute concentrations and concentration profiles of important chemical species in flames are needed to facilitate the understanding of combustion kinetics in microgravity. Although a variety of sophisticated laser-based diagnostics (such as planar laser induced fluorescence, degenerate four wave mixing and coherent Raman methods) have been applied to the study of combustion in laboratory flames, the instrumentation associated with these methods is not well suited to microgravity drop tower or space station platforms.

Important attributes of diagnostic systems for such applications include compact size, low power consumption, ruggedness, and reliability. We describe a diode laser-based near-UV source designed with the constraints of microgravity research in mind. Coherent light near 420 nm is generated by frequency doubling in a nonlinear crystal. This light source is single mode with a very narrow bandwidth suitable for gas phase diagnostics, can be tuned over several cm^{-1} and can be wavelength modulated at up to MHz frequencies.

We demonstrate the usefulness of this source for combustion diagnostics by measuring CH radical concentration profiles in an atmospheric pressure laboratory flame. The radical concentrations are measured using wavelength modulation spectroscopy (WMS)[1] to obtain the line-of-sight integrated absorption for different paths through the flame. Laser induced fluorescence (LIF) measurements are also demonstrated with this instrument, showing the feasibility of simultaneous WMS absorption and LIF measurements with the same light source.

LIF detection perpendicular to the laser beam can be used to map relative species densities along the line-of-sight while the integrated absorption available through WMS provides a mathematical constraint on the extraction of quantitative information from the LIF data. Combining absorption with LIF – especially if the measurements are made simultaneously with the same excitation beam – may allow elimination of geometrical factors and effects of intensity fluctuations (common difficulties with the analysis of LIF data) from the analysis.

THE NEAR-UV LIGHT SOURCE

We have developed a tunable, wavelength modulated near-UV source based on single pass frequency doubling of a modulated near-IR diode laser. Figure 1 shows a schematic of the

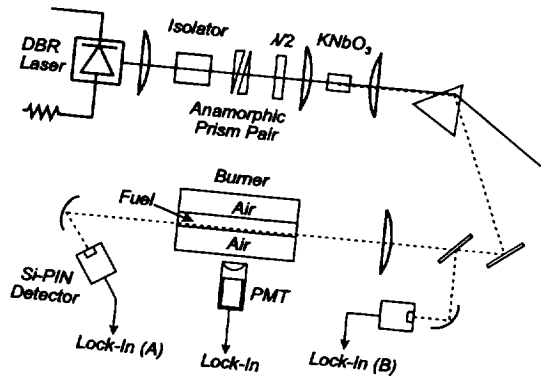

Figure 1 - Experimental schematic for UV generation and flame measurements.

experimental arrangement. The diode laser beam is collimated, passed through an optical isolator, circularized with an anamorphic prism pair, and focused into a 7 mm long, A-cut, $KNbO_3$ crystal (CASIX). A half-wave plate before the crystal matches the input polarization of the pump beam to the crystal orientation. The $KNbO_3$ crystal is mounted on a thermo-electric (TE) cooling stage in a N_2 purged housing for temperature-tuned, non-critical phase matching operation near 10°C. The generated near-UV beam is collimated and separated from the residual near-IR beam with a CaF_2 prism. 100 μW of near-UV light is produced from 120 mW of near-IR.

The frequency of the residual near-IR beam is monitored to 0.01 cm^{-1} with a scanning interferometer and the output of the DBR laser is tuned by adjusting its temperature and injection current. Modulation of the diode laser injection current results in a corresponding wavelength modulation of the near-UV beam. For the measurements described below, a 50 kHz modulation frequency was used. A linear current sweep was also applied to tune the center wavelength across the absorption line during wavelength modulation.

The entire laser and optical set up required for generating the near-UV light has a 24 by 6 inch footprint using standard optical mounts. This can be reduced by using miniature mounts and by adding additional mirrors to "fold" the layout. Once the optics and crystal temperature are adjusted for optimal UV generation, the UV power remains constant. Thus, fixed or locking mounts can be used for rugged instrumentation.

CH RADICAL DETECTION

The CH radical was chosen due to its importance in hydrocarbon flame chemistry, its role in soot formation, and its use as a marker of flame fronts. Rotationally-resolved transitions of the $A\ ^2\Delta \leftarrow X\ ^2\Pi$ band near 430 nm and the $B\ ^2\Sigma^- \leftarrow X\ ^2\Pi$ band near 385 nm have been assigned[2] and are utilized by many workers using LIF techniques.[3-6] The $R_2(8)$ (23,460.81 cm^{-1}) line in the (0,0) band of the CH $A\ ^2\Delta \leftarrow X\ ^2\Pi$ transition was chosen for the present study. In addition to several CH lines in this (0,0) band, the frequency-doubled laser can access some lines in the (1,1) band that would allow optical thermometry[7] in a future study.

As shown in Fig. 1, the 426 nm beam is directed along the flame front of a Wolfard-Parker slot burner, and is focused to ~250 μm diameter at the center and ~330 μm diameter on either side of the 4 cm long burner. The transmitted beam intensity is monitored with a UV-grade Si-PIN photodiode, and sent to a digital lock-in amplifier (SRS 830) for 2*f* detection at 100 kHz. A Schott BG-18 blue pass filter is used to reduce the amount of visible and near-IR flame luminescence reaching the detector. Phase-sensitive detection of LIF is made at 90 degrees to the excitation beam. A 3-element *f*/2.5 collection optic images a 2 mm segment of the region excited by the laser. A 1 nm fwhm bandpass filter centered at 431 nm is used to reduce the flame luminescence while detecting CH fluorescence. The PMT (Hamamatsu H5783) output is sent to a lock-in amplifier for 2*f* detection of LIF at 100 kHz. A reference beam is created by a 50/50 beam splitter before the burner and used to subtract étalon and common mode noise from the absorption measurements in the dual channel lock-in.

Figure 2 shows spectra from (a) direct absorption, (b) 2*f* absorption detection, and (c) 2*f* LIF detection at 2 mm above the burner surface in an ethylene/air flame. Fuel and air flow rates are 9.7 and 19.4 $cm^{-3}s^{-1}$, respectively, at an atmospheric pressure of 590 torr and ambient temperature. The

peak CH absorbance at this height measured by direct absorption is 7.5×10^{-4} with a S/N of 5:1. Assuming a uniform 2000 K flame temperature along the 4 cm long flame front, and using reported CH electronic transition moments and rotational transition probabilities,[8] we estimate a peak CH mole fraction of 3 ppm. The 2*f* LIF spectrum shown in Fig. 2c is taken with the same detection bandwidth and averaging time as the 2*f* absorption spectrum in Fig. 2b. The LIF S/N is excellent and the 2*f* LIF detection scheme is effective in removing interference from flame luminescence. There is sufficient fluorescence signal using the ~50 μW excitation beam to perform higher resolution imaging using improved imaging optics and a linear array detector. As Fig. 3 shows, the use of modulated detection methods provides significant noise reduction relative to unmodulated detection methods. It is also clear that S/N ratios are limited by residual étalon fringes and not source or detector noise.

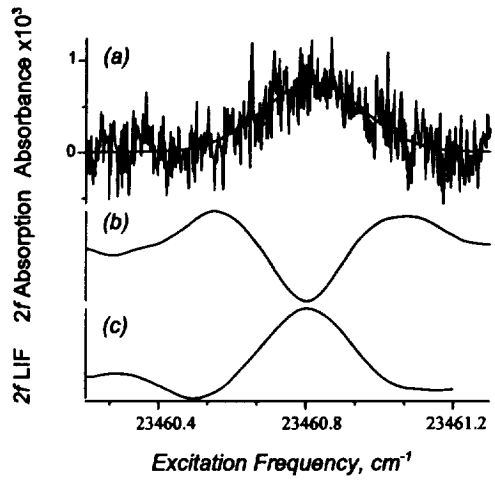

Figure 2 - (a) Direct absorption (b) 2*f* absorption (c) 2*f* LIF detection of CH in an ethylene/air diffusion flame.

Figure 3 shows CH concentration profiles at flame heights of 2 and 4 mm above the burner surface for ethylene/air and methane/air diffusion flames with equivalent fuel/air mass ratios. These profiles are constructed from the maxima of 2*f* absorption spectra along different lines-of-sight obtained by moving the burner laterally across the UV laser beam at a fixed height. A zero mm lateral position corresponds to the center of the burner and 4 mm is the position of the fuel/air interface at the burner surface. The peak absorbance decreases and shifts further away from the burner center as the height in the flame increases. The peak CH mole fraction in the methane/air flame at 2 mm is 2/3 that in the ethylene/air flame.

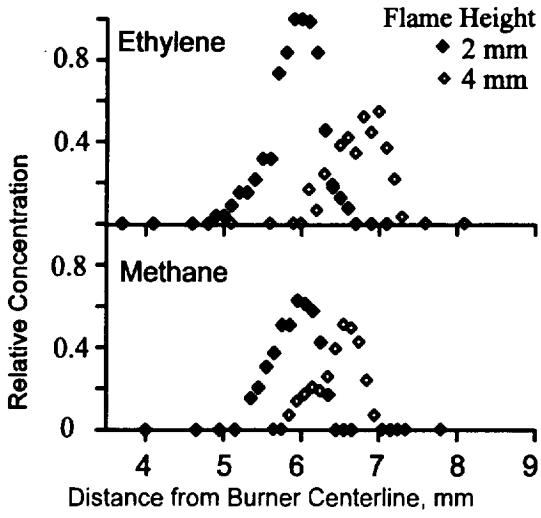

Figure 3 - CH concentration profiles measured by 2*f* WMS at for different fuels and flame heights.

These peak CH mole fractions fall within the 0.08 ppm to 2 ppm range estimated by Norton and Smyth,[5] from LIF measurements on a methane/air diffusion flame using a similar burner and flow rates, but at a 9 mm height. They observe similar trends in CH concentration profiles with changing height in the flame. These mole fractions are significantly less than the 100 ppm or larger values reported by others.[4] The accuracy of these concentration determinations can be improved in the future by incorporating optical thermometry to measure local flame

temperatures simultaneously with 2*f* WMS and LIF.

Figure 4 compares the 2*f* absorption signal for a line-of-sight across the flame fronts, obtained by turning the burner 90 degrees, with one taken at the same height, but parallel to the diffusion flame front. The "perpendicular" spectrum is magnified by a factor of 20 and is an average of 1,500 sweeps, while the "parallel" spectrum is an average of 200 sweeps. The upper spectrum shows an S/N of about 3:1 with an absorbance amplitude of 5×10^{-5}. The baseline noise stems from residual, incomplete subtraction of background étalons. Absorbance detection limits of 10^{-6} are routinely achievable with WMS when care is taken to eliminate laser source noise and optical étalons from the system.[1] Laser source noise is not observed with the present apparatus. We expect to reduce étalon fringes with improvements to the optical components (such as AR coatings, non-parallel optical faces and, if needed, active étalon suppression) and obtain detection limits approaching 10^{-6} without background subtraction.

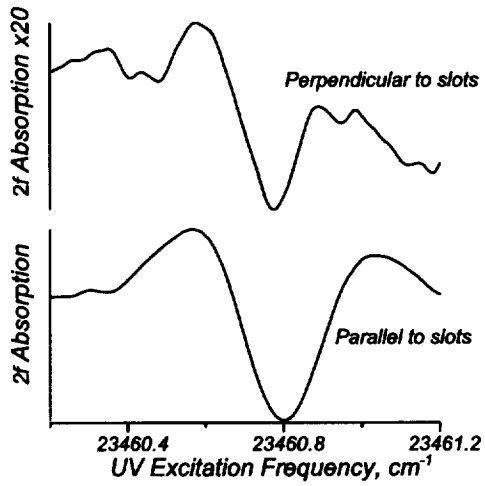

Figure 4 - 2*f* absorption spectra of CH acquired perpendicular and parallel to the flame front.

In conclusion, the feasibility of detecting combustion radicals with simultaneous phase-sensitive, spatially resolved LIF and line-of-sight WMS absorption measurements has been demonstrated in an atmospheric pressure diffusion flame. The WMS absorption measurements afford a quantitative measure of the integrated absorbance along the line-of-sight with much greater sensitivity than direct absorption measurements. Extending this technique to monitoring other important combustion radical species is currently limited by the availability of single frequency, high power pump diode lasers and suitable nonlinear crystals. By increasing near-infrared laser power though power amplifiers and tripling or quadrupling diode laser outputs,[9] accessing other UV to VUV wavelengths is possible and would allow measurement of OH, NO, SO_2 and other species. In addition, this diode laser-based approach is suitable for demanding applications such as microgravity drop-tower experiments where compact, rugged and energy efficient instrumentation is required.

This work was supported by the NASA Lewis Research Center under contract NAS3-98044. We thank Dr. Nancy Piltch of NASA GRC for helpful suggestions.

1) Bomse, D. S.; Stanton, A. C.; Silver, J. A. *Appl. Opt.* **1992**, *31*, 718.
2) Moore, C. E.; Broida, H. P. *J. Res. of NBS-A* **1959**, *63A*, 19.
3) Lensberger, K. J.; Dreyer, M. J.; Copeland, R. A. *Appl. Opt.* **1988**, *27*, 3679.
4) Allen, M. G.; Howe, R. D.; Hanson, R. K. *Opt. Lett.* **1986**, *11*, 126.
5) Norton, T. S.; Smyth, K. C. *Combust. Sci. and Technol.* **1991**, *76*, 1-20.
6) Garland, N. L.; Crosley, D. R. *J. Quant. Spectrosc. Radiat. Transfer* **1985**, *33*, 591.
7) Raiche, G. A.; Jeffries, J. B. *Appl. Opt.* **1993**, *32*, 4629-4635.
8) Luque, J.; Crosley, D. R. *J. Chem. Phys.* **1996**, *104*, 2146.
9) Koplow, J. P.; Kliner, D. A. V.; Goldberg, L. *Appl. Opt.* **1998**, *37*, 3954.

HYPERSPECTRAL IMAGING OF FLAME SPREAD OVER SOLID FUEL SURFACES USING ADAPTIVE FABRY-PEROT FILTERS

W.T. Rawlins, W.J. Marinelli, and M.G. Allen

S89-25

Physical Sciences Inc.
20 New England Business Center
Andover, MA 01810

Introduction

Investigations of the dynamics of flame spread over combustible surfaces in microgravity are critical to spacecraft fire safety, as well as for the understanding of fundamental fire phenomena. In the absence of gravity-induced buoyancy and forced convection, heat transfer between the flame and the surface is dominated by conductive and radiative mechanisms.[1] The detailed understanding of these mechanisms requires direct, quantitative observations of the spatial propagation and radiative fluxes of key flame product species such as CO_2 and H_2O. These observations can be performed non-intrusively in a microgravity combustion experiment by observing spatially and spectrally resolved infrared emission from the product molecular species. Additional flame species which can potentially be observed in this manner include CO, N_2O, OH, NO, hydrocarbon vapor, and soot particles. The species-specific band structures of the molecular emissions enable discrimination between gas phase, particulate, and hot surface contributions to the observed emission. In addition, the observed band shapes and intensities can be analyzed quantitatively to determine species abundances, temperatures, and optical thickness effects. Such measurements are critically important for evaluating unsteady combustion models.

We have recently initiated a research program to implement our previously developed Adaptive Infrared Imaging Spectrometer (AIRIS) instrument concept for high-speed, wavelength-tunable, and quantitative spatial imaging of mid-infrared (2 to 5 μm) flame and fuel surface emission in microgravity combustion experiments. AIRIS is a compact, wavelength-scanning spectral imager based on the use of a low-order Fabry-Perot interferometer coupled to an infrared detector array. We plan a four-year project to (1) demonstrate and optimize the AIRIS prototype instrument and quantitative infrared spectroscopic methods for normal-gravity laboratory flames, (2) design the integration of AIRIS with planned reduced-gravity experiments on unsteady flame propagation, and (3) conduct reduced-gravity flight tests using the prototype AIRIS filter. In this effort, we will collaborate closely with the SIBAL (Solid Inflammability Boundary at Low Speed) research team at NASA/Glenn and Case Western Reserve University.[2]

Infrared Emission and Flame Spread

In addition to observing the phenomenological spread of the flame in microgravity, it is important to observe the production and spread of the key combustion product species CO_2, H_2O, CO, hydrocarbons, and soot particles. CO_2 and H_2O are responsible for much of the heat transfer to the fuel surface through infrared radiation and conduction, the gas phase hydrocarbons provide the impetus for continued combustion, and CO, CO_2, and soot particles are deleterious

combustion products which remain in the air after extinction of the flame. Because these species are all at high temperatures in the combustion zone, their characteristic thermal infrared emissions are reasonably strong. Thus imaging infrared emission spectroscopy in the readily accessible 2 to 5 μm spectral region offers considerable promise for spatially resolved, non-intrusive detection of these species and their temperatures.

While the particulates and the hot fuel surface exhibit spectrally continuous grey-body emission, the gas phase molecular species radiate in specific vibration-rotation bands whose wavelengths depend on the unique internal vibrational energy structure of each molecule. The high-temperature radiative strengths for the most prominent bands of H_2O, CO_2, and CO are illustrated in Figure 1, as computed from a well-validated high-temperature empirical band model.[3] Depicted are the H_2O ν_3 (asymmetric stretch mode) and ν_2 (bend mode) bands centered at 2.7 and 6.3 μm, respectively, the CO_2 $\nu_1+\nu_3$ (combination symmetric + asymmetric stretch) and ν_3 (asymmetric stretch mode) bands centered at 2.7 and 4.3 μm, respectively, and the CO(Δv=1) fundamental band centered near 4.7 μm. The variations of the computed band shapes and strengths with temperature illustrate how spectrally resolved infrared emission can be used to determine both temperatures and concentrations. The observed spectral shapes of the molecular bands can be used to determine the gas phase species temperatures, while the absolute intensities at known temperatures are proportional to the species concentrations integrated along the line of sight.[4] Using the AIRIS spectrometer, we will scan through these bands to obtain spectrally

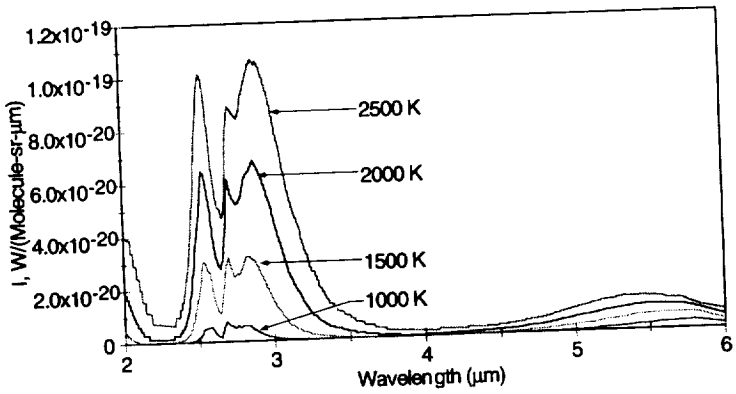

(a) H_2O in the 2 to 6 μm spectral region

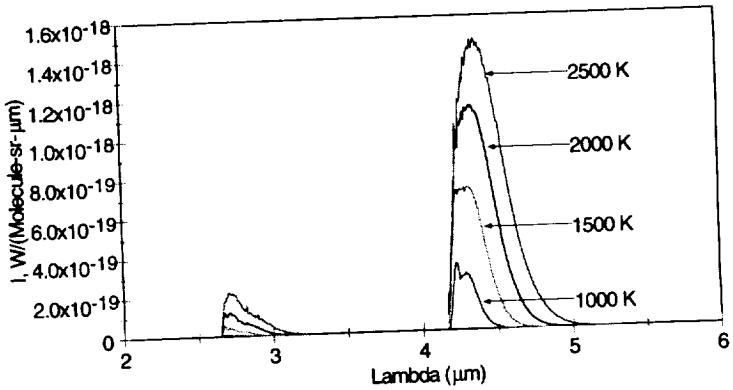

(b) CO_2 in the 2 to 6 μm spectral region

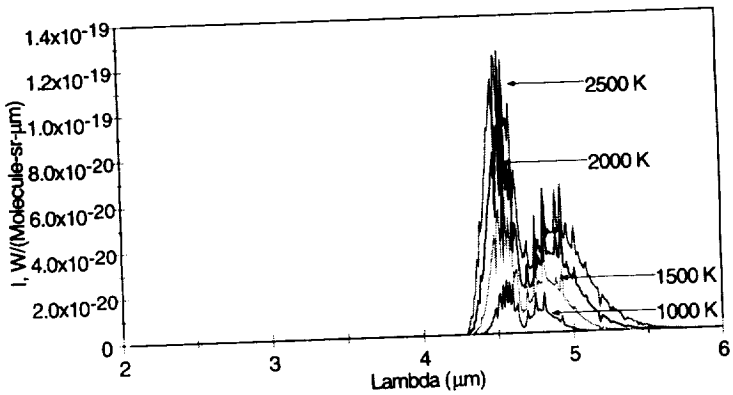

(c) CO in the 2 to 6 μm spectral region

Figure 1. Computed band strengths and band shapes for high-temperature infrared emission.

scanned 2-D images showing the concentration and temperature distributions of the radiating species.

AIRIS and Hyperspectral Imagery

The AIRIS spectrometer combines advanced infrared camera technology with an imaging, tunable Fabry-Perot etalon filter. This combination allows software control of the transmission bandpass over a broad wavelength range with a spectral resolution better than 1% of the central wavelength. This capability can be used to select wavelength bands of the combustion-generated species and scan them spectrally to determine band shapes, intensities, and spectral background corrections such as particulate and fuel surface radiation. AIRIS can be repositioned in wavelength at framing rates approaching 1 kHz, and can thus acquire a broad range of spectral data on the time scale of a microgravity flame spread experiment.

Unlike conventional Fabry-Perot interferometers, AIRIS utilizes mirror spacings which are comparable to the desired transmission wavelength. In a Fabry-Perot interferometer, light is selectively transmitted by constructive interference through the faces of two partially reflecting parallel mirrors, forming a concentric ring pattern for an image of a monochromatic source in the far field. The central spot contains a spatially continuous image of the scene. For a system which operates in low order (i.e., small mirror spacings) and restricts the full-angle field of view sufficiently, only the central spot is observed, and a spatially continuous, wide-field monochromatic image is produced.

The prototype AIRIS instrument is diagrammed in Figure 2. The instrument is currently configured to operate in the 3.5 to 5.1 μm wavelength range, and will be extended into the 2 to 3.4 μm region as part of this program. The device employs a tunable interferometer module with capacitance micrometry mirror position measurement and piezoelectric mirror actuators which are interfaced to a microprocessor-based control system. We have previously interfaced a number of InSb focal plane arrays with this filter design, including those from Cincinnatti Electronics (160 x 120) and Amber Engineering (128 x 128, 256 x 256), at framing rates up to 1 kHz. Wavelength calibrations are performed with an infrared HeNe laser (3.39 μm) to establish parallelism and an FTIR spectrometer to measure spectral resolution and free spectral range. Absolute radiometric calibrations are performed with a high-temperature, variable-aperture blackbody source.

Summary

This paper discusses quantitative infrared emission spectroscopic methods for the analysis of combustion product concentrations and temperatures, and the application of this method to microgravity flames using a hyperspectral Fabry-Perot imaging technique. We plan to develop this non-intrusive measurement method for investigations of flame spread in microgravity and reduced gravity environments. Although specifically focussed toward implementation on a solid fuel flame spread experiment, the IR imaging spectrometer will be widely applicable to other microgravity combustion experiments, such as diffusion and premixed flame structure, soot formation, and droplet combustion investigations.

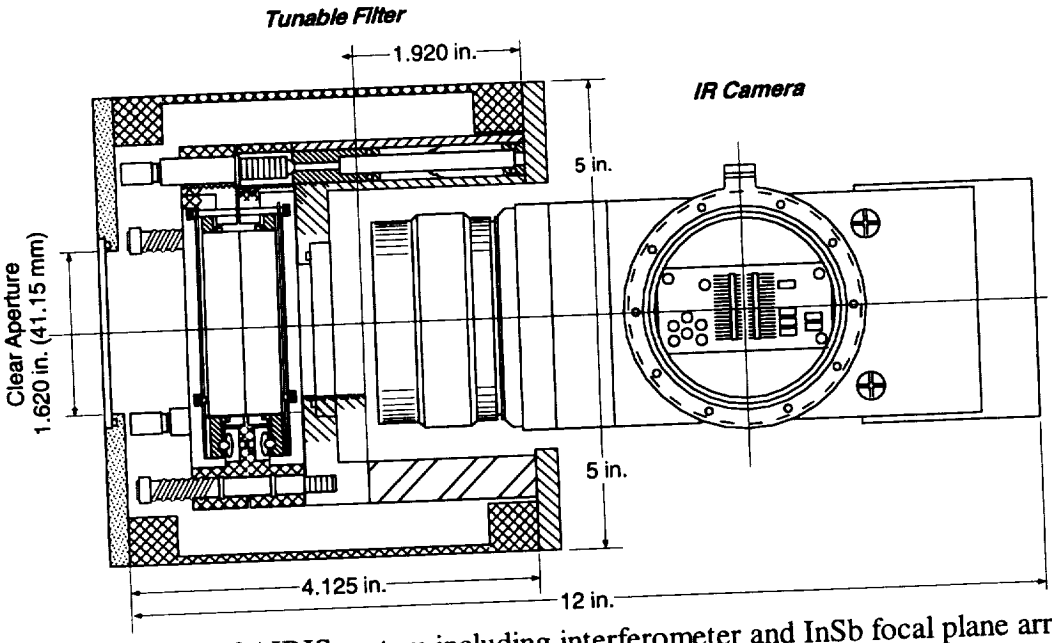

Figure 2. Layout of AIRIS system including interferometer and InSb focal plane array.

References

1. Law, C.K., and Faeth, G.M., "Opportunities and challenges of combustion in microgravity," Prog. Energy Combust. Sci. 20, pp. 65-113, 1994.

2. J.S. T'ien, K.R. Sacksteder, P.V. Ferkul, H. Bedir, H.-Y. Shih, P.S. Greenberg, R.D. Pettegrew, N. Piltch, and D. Frate, "Solid Inflammability Boundary at Low Speed (SIBAL) (Abstract) Proceedings of the Fourth International Microgravity Combustion Workshop, NASA Conference Publication 10194, National Aeronautics and Space Administration, 1997, pp. 399-404.

3. Ludwig, C.B., Malkmus, W., Reardon, J.E., and Thompson, J.A.L., "Standard Infrared Radiation Model (SIRRM), Volume 1: Development and Validation," U.S. Air Force Rocket Propulsion Laboratory, AFRPL-TR-81-54, Edwards AFB, CA, August 1981.

4. Parker, T.E., Miller, M.F., McManus, K.R., Allen, M.G., and Rawlins, W.T., "Infrared emission from high-temperature $H_2O(\nu_2)$: A diagnostic for concentration and temperature," AIAA J. 34, 500, 1996.

PARTICLE-IMAGE VELOCIMETRY IN MICROGRAVITY LAMINAR JET DIFFUSION FLAMES*

P. B. Sunderland[1], P. S. Greenberg[2], D. L. Urban[2], M. P. Wernet[3], and W. Yanis[1]
[1]NCMR, [2]Microgravity Combustion Branch, [3]Optical Instrumentation Technology Branch
NASA Glenn Research Center
21000 Brookpark Rd.
Cleveland OH 44135

590-29

INTRODUCTION

This paper discusses planned velocity measurements in microgravity laminar jet diffusion flames. These measurements will be conducted using Particle-Image Velocimetry (PIV) in the NASA Glenn 2.2-second drop tower. The observations are of fundamental interest and may ultimately lead to improved efficiency and decreased emissions from practical combustors. The velocity measurements will support the evaluation of analytical and numerical combustion models.

There is strong motivation for the proposed microgravity flame configuration. Laminar jet flames are fundamental to combustion and their study has contributed to myriad advances in combustion science, including the development of theoretical, computational and diagnostic combustion tools. Nonbuoyant laminar jet flames are pertinent to the turbulent flames of more practical interest via the laminar flamelet concept (Bilger 1976; Urban et al. 1998). The influence of gravity on these flames is deleterious: it complicates theoretical and numerical modeling, introduces hydrodynamic instabilities, decreases length scales and spatial resolution, and limits the variability of residence time.

Whereas many normal-gravity laminar jet diffusion flames have been thoroughly examined (including measurements of velocities, temperatures, compositions, sooting behavior and emissive and absorptive properties), measurements in microgravity gas-jet flames have been less complete and, notably, have included only cursory velocity measurements. It is envisioned that our velocity measurements will fill an important gap in the understanding of nonbuoyant laminar jet flames.

REVIEW OF PAST WORK

The first experimental observations of nonbuoyant jet diffusion flames were reported by Cochran and co-workers (Edelman et al. 1972 and references cited therein). This work, and subsequent studies by Bahadori and co-workers (Bahadori et al. 1990, 1993 and references cited therein), were mostly confined to measurements of luminous flame shapes. Sunderland et al. (1999) sought to measure true stoichiometric shapes of both buoyant and nonbuoyant jet diffusion flames. Faeth and co-workers extensively characterized twenty-one flames in the Laminar Soot Processes (LSP) flight experiment (Urban et al. 1998). There have been two other flight experiments which considered laminar jet diffusion flames: Turbulent Gas-Jet Diffusion Flames (TGDF; Bahadori et al. 1997) and Enclosed Laminar Flames (ELF; Lee et al. 1997). Other recent ground-based studies of gas-jet flames are discussed in Agrawal et al. (1997), VanDerWege et al. (1997), Kato et al. (1998), Sitzki et al. (1998), and Walsh et al. (1999).

Despite these studies, the characterization of microgravity laminar jet flames remains incomplete. Measurements to date have included shapes, temperatures, soot properties, radiative

* Presented at the Fifth International Microgravity Combustion Workshop, Cleveland, 1999.

emissions and compositions. Technological barriers associated with microgravity experimentation have largely precluded the measurement of gas velocities in gas-jet flames.

Laminar jet diffusion flames have been the subject of extensive analysis. Burke and Schumann (1928) conducted the seminal analytical work on these flames. Improvements to their model were many years in the coming, and either neglected the influence of gravity (e.g. Klajn and Oppenheim 1982), or incorporated its effects by neglecting viscous dissipation (e.g. Roper 1977). No simplified model has incorporated both buoyant acceleration and viscous dissipation; thus none can be fully evaluated with observations of normal-gravity flames.

Most gas-jet models invoke one of three velocity approximations: constant velocity (Burke and Schumann 1928; Villermaux and Durox 1992); uniform acceleration without viscous dissipation (Roper 1977; Markstein and De Ris 1984; Saito et al. 1986); and viscous dissipation without buoyancy (Kanury 1975; Spalding 1979; Klajn and Oppenheim 1982; Kuo 1986). Among these, only the last type can be validated experimentally, and this can be accomplished only through observations of nonbuoyant flames. Because the inclusion of buoyancy exceeds the capabilities of all analytical and many numerical models, the proposed velocity measurements are essential to model validation.

PLANNED TEST CONDITIONS

We will study methane and ethane flames burning in quiescent air. Testing will emphasize flames which approach steady state quickly and which have light soot loading, in particular flames with relatively small burners, pressures and fuel flowrates.

For these tests, we will build a new rig fashioned after the general-purpose combustion rigs. The test chamber will be a 25 cm ID by 53 cm high cylindrical pressure vessel certified for operation from vacuum to 3 atm. Chamber access will be facilitated by an endplate secured with a v-band clamp. Four chamber windows will allow flexible optical access. A fuel plumbing system will be included which allows for fuel storage and seeding, precise flow metering, and rapid flow initiation and termination. The rig will contain the standard drop tower batteries, microprocessor controller and data-acquisition systems. The optical breadboard will be 41 cm by 51 cm and will allow shock isolation if necessary.

PLANNED PIV MEASUREMENTS

Laboratory-based development of Particle-Image Velocimetry (PIV) is in progress. These experiments should resolve issues related to: i) laser-power requirements, ii) imaging configuration and optical collection efficiency, iii) particle seed selection and delivery, and iv) data acquisition and processing.

The first three issues are closely coupled. While the inherent sensitivity of the imaging array ultimately determines the signal-strength requirement, the faceplate levels are strongly influenced by field of view, seed-particle size and index of refraction, and collection numerical aperture. Since volume, mass, and power consumption are strictly confined in microgravity facilities, the minimization of laser power is paramount.

It is fortunate that both velocities and their gradients are small in the present test flames. In the intended regime, scattering intensity is roughly proportional to particle diameter squared, allowing diagnostic limitations to be compensated for with increased particle size. Microgravity seeding presents a unique challenge. Conventional seeders employing packed or fluidized beds involve large amounts of sedimented material, whose behavior is generally unpredictable and difficult to

control without gravity. The present approach combines cyclonic and turbulent entrainment and has been successfully demonstrated in previous microgravity Laser-Doppler Velocimetry measurements.

Space and power constraints introduce challenges to the PIV system design. Compactness, for example, motivates short focal length optics. Large numerical apertures are desirable since they increase collection efficiency and decrease required source strength. A balance is needed, however, since both field angle and aperture-dependent aberrations will degrade the determination of particle positions. Calculations and scaling analyses of existing configurations indicate that commercially available lasers can provide the required source strength in a configuration suited to the 2.2-second drop tower, enabling medium to high collection f/number operation and control of aberration.

Data acquisition and processing are being approached through a combination of commercial and in-house resources. A commercial system for image acquisition and storage will provide required triggers for synchronizing the laser source and imaging array. A frame-straddling CCD camera will allow cross-correlation data reduction. This method is optimal since it provides directionally-resolved velocity vectors, no self-correlation peak, and hence no restriction on minimum particle displacement. The commercial system also provides on-line data visualization, which is valuable during evaluations of diagnostics. Custom software has been developed to implement the cross-correlation analysis (Wernet, 1995). This software provides image-gain scaling, region-of-interest processing, fuzzy-logic data validation, and real-time graphical display of processed vector maps.

ACKNOWLEDGMENTS

This research is sponsored by the Microgravity Research Division of the NASA Office of Life and Microgravity Sciences and Applications. Discussions with H. D. Ross are gratefully acknowledged.

REFERENCES

Agrawal, A. K., Gollahalli, S. R., and Griffin, D. (1997), "Study of Buoyancy Effects in Diffusion Flames Using Rainbow Schlieren Deflectometry," Fourth International Workshop on Microgravity Combustion, p. 117.

Bahadori, M. Y., Edelman, R. B., Stocker, D. P., and Olson, S. L. (1990), "Ignition and Behavior of Laminar Gas-Jet Diffusion Flames in Microgravity," *AIAA J.* 28:236-244.

Bahadori, M. Y., Hegde, U. and Stocker, D. P. (1997), "Structure of Microgravity Transitional and Pulsed Jet Diffusion Flames," Fourth International Workshop on Microgravity Combustion, Cleveland, May 19-21, pp. 179-184.

Bahadori, M. Y., Stocker, D. P., Vaughan, D. F., Zhou, L., and Edelman, R. B. (1993), "Effects of Buoyancy on Laminar, Transitional, and Turbulent Gas Jet Diffusion Flames," in *Modern Developments in Energy, Combustion and Spectroscopy*, (F. A. Williams et al., eds.), Pergamon Press, pp. 49-66.

Bilger, R. W. (1976), "The Structure of Diffusion Flames," *Combust. Sci. Technol.* 13:155-170.

Burke, S. P., and Schumann, T. E. W. (1928), "Diffusion Flames," *Ind. Eng. Chem.* 20:998-1004.

Edelman, R. B., Fortune, O. F., Weilerstein, G., Cochran, T. H., and Haggard, J. B. (1972), "An Analytical and Experimental Investigation of Gravity Effects upon Laminar Gas Jet-Diffusion Flames," *Fourteenth Symposium (International) on Combustion*, The Combustion Institute, Pittsburgh, pp. 399-412.

Kanury, A. M. (1975), *Introduction to Combustion Phenomena*, Gordon and Breach, Amsterdam, p. 241.

Kato, H., Kunieda, S., Enomoto, H., Okai, K., Kaneko, T., Chauveau, C., Gokalp, I., Sato, J., Tsue, M., and Kono, M. (1998), "Effects of Co-flowing Air on Behavior of Gas Jet Diffusion Flames under Normal- and Micro-gravity Fields," Drop Tower Days, JAMIC, Sapporo, Japan, pp. 73-75.

Klajn, M., and Oppenheim, A. K. (1982), "Influence of Exothermicity on the Shape of a Diffusion Flame," *Nineteenth Symposium (International) on Combustion*, The Combustion Institute, Pittsburgh, pp. 223-235.

Kuo, K. K. (1986), *Principles of Combustion*, Wiley, New York, p. 366.

Lee, Y. G., Chen, L. -D., Brooker, J. E. and Stocker, D. P. (1997), "Structure and Stability of Burke-Schumann Diffusion Flames," Fourth International Workshop on Microgravity Combustion, Cleveland, May 19-21, pp. 111-114.

Markstein, G. H., and De Ris, J. (1984), "Radiant Emission and Absorption by Laminar Ethylene and Propylene Diffusion Flames," *Twentieth Symposium (International) on Combustion*, The Combustion Institute, Pittsburgh, pp. 1637-1646.

Roper, F. G. (1977), "The Prediction of Laminar Jet Diffusion Flame Sizes: Part I. Theoretical Model," *Combust. Flame* 29:219-226.

Saito, K., Williams, F. A., and Gordon, A. S. (1986), "Effects of Oxygen on Soot Formation in Methane Diffusion Flames," *Combust. Sci. Technol.* 47:117-138.

Sitzki, L., Tittmann, K., Tischer, S., Rau, H., and Grabski, R. (1998), "The Shape of Hydrogen, Methane, Propane and n-Butane Diffusion Flames under Microgravity," 36th AIAA Meeting, paper 98-0565.

Spalding, D. B. (1979), *Combustion and Mass Transfer*, Pergamon Press, New York, p. 170.

Sunderland, P. B., Mendelson, B. J., Yuan, Z. –G., and Urban, D. L. (1999), "Shapes of Buoyant and Nonbuoyant Laminar Jet Diffusion Flames," *Combust. Flame* 116:376-386.

Urban, D. L., Yuan, Z. –G., Sunderland, P. B., Linteris, G. T., Voss, J. E., Lin, K. –C., Dai, D., Sun, K., and Faeth, G. M. (1998), "Structure and Soot Properties of Nonbuoyant Ethylene/Air Laminar Jet Diffusion Flames," *AIAA J.*, 36:1346-1360.

VanDerWege, B. A., O'Brien, C. J. and Hochgreb, S. (1997), "Application of Shear Plate Interferometry to Jet Diffusion Flame Temperature Measurements," Fourth International Microgravity Combustion Workshop, p. 141.

Villermaux, E., and Durox, D. (1992), "On the Physics of Jet Diffusion Flames," *Combust. Sci. Technol.* 84:279-294.

Walsh, K. T., Long, M. B., Tanoff, and Smooke, M. D. (1999), "Experimental and Computational Study of Coflow Laminar Diffusion Flames in a Microgravity Environment," 37th AIAA Meeting.

Wernet, M.P. (1995), "Fuzzy Inference Enhanced Information Recovery From Digital PIV using Cross-Correlation Combined With Particle Tracking," Proceedings of the SPIE Conference on Optical Techniques in Fluid, Thermal and Combusting Flows, San Diego CA, July 9-14.

S91-36

DIODE LASER VELOCITY MEASUREMENTS BY MODULATED FILTERED RAYLEIGH SCATTERING

J. J. Mach, P. L. Varghese, and J. J. Jagodzinski, Center for Aeromechanics Research, Department of Aerospace Engineering & Engineering Mechanics, The University of Texas at Austin, Austin, Texas 78712, varghese@mail.utexas.edu

INTRODUCTION

The ability of solid-state lasers to be tuned in operating frequency at MHz rates by input current modulation, while maintaining a relatively narrow line-width, has made them useful for spectroscopic measurements. Their other advantages include low cost, reliability, durability, compact size, and modest power requirements, making them a good choice for a laser source in micro-gravity experiments in drop-towers and in flight. For their size, they are also very bright. In a filtered Rayleigh scattering (FRS) experiment[1,2,3] a diode laser can be used to scan across an atomic or molecular absorption line, generating large changes in transmission at the resonances for very small changes in frequency. The hyperfine structure components of atomic lines of alkali metal vapors are closely spaced and very strong, which makes such atomic filters excellent candidates for sensitive Doppler shift detection and therefore for high-resolution velocimetry. In the work we describe here we use a Rubidium vapor filter, and work with the strong D_2 transitions at 780 nm that are conveniently accessed by near infrared diode lasers.

The low power output of infrared laser diodes is their primary drawback relative to other laser systems commonly used for velocimetry. However, the capability to modulate the laser frequency rapidly and continuously helps mitigate this. Using modulation spectroscopy and a heterodyne detection scheme with a lock-in amplifier, one can extract sub-microvolt signals occurring at a specific frequency from a background that is orders of magnitude stronger. The diode laser modulation is simply achieved by adding a small current modulation to the laser bias current. It may also be swept repetitively in wavelength using an additional lower frequency current ramp.

THEORY

When the laser beam is scattered from a flow the Rayleigh (and Mie) scattered light is Doppler shifted according to the equation:

$$\Delta\nu_{Doppler} = \frac{V}{\lambda_o}\,[\boldsymbol{i}_V \bullet (\boldsymbol{i}_S - \boldsymbol{i}_L)] \approx \frac{V}{\lambda_o} \qquad (1)$$

The factor containing unit vectors in brackets arises from the geometry of the experiment and is of order unity. If the unshifted beam ($V=0$) is set on the edge of a particular hyperfine component of Rb, then in a moving gas ($V\neq 0$) the Doppler effect shifts the scattered light to a new frequency that is attenuated differently by the atomic filter. Velocity fluctuations are thus converted to intensity fluctuations in principle. In practice, a normalizing scheme is needed to account for the fact that the intensity of the scattered signal itself fluctuates because of fluid density fluctuations or because of variations in the density of small particulates carried in the flow. Ambient light interferences can be a problem because the Rayleigh signal is weak particularly when using a cw (continuous wave) solid-state laser.

To improve detectability in the MFRS technique we perform frequency modulation absorption spectroscopy[4] using the Rayleigh scattered light as a light source. Conventional modulation absorption spectroscopy is used to distinguish a weak absorption on a relatively

strong laser signal. In our work we use it to detect a relatively strong absorption but on a weak signal. Synchronous detection provides very high rejection of interferences, so weak signals and ambient light are much less of a problem. Additionally, the modulation of the laser frequency that is needed for MFRS also provides a simple means of stabilizing the laser frequency and improving the measurement precision still further.

EXPERIMENTAL SETUP

Figure 1 is a schematic diagram of an MFRS experimental set-up. A small portion of the laser beam is split off to a reference arm containing a Rb cell. The modulation spectrum recorded by the detector (A) in this arm provides an absolute frequency reference. The major portion of the beam is focused into the flow being studied. The Rayleigh and Mie scattered signal is collected and split into two beams via a 50/50 beam splitter. One beam is passed to a reference detector (B), the second part is filtered through another Rb-cell before being detected on detector C. The ratio of the two signals gives the fractional transmission and thus removes the dependence on density of scatterers in the flow. The probe beam is set at 135° from the flow direction, while the scattered light collection axis is 45° from the flow, i.e. at 90° to the laser beam, all in the plane of the optical table on which the experiment is run. If two velocity components are measured simultaneously a second set of collection optics is located directly opposite the first. The measurement volume of approximately $0.2mm^3$ is at the intersection of the laser and the focus of the collection optics. In preliminary experiments we made measurements in a supersonic jet of CO_2 that forms a fine fog that serves as a Rayleigh-Mie scattering source.

The system may be operated in one of two modes. In the first mode the laser is scanned across several hyperfine components so as to record a portion of the spectrum. The displacement between the derivative spectra, recorded simultaneously in the reference and signal arms, gives the Doppler shift and thus the flow velocity. One advantage of this mode is that one can dispense with the reference detector (B) in the signal arm provided the mean scattering density is constant and the time constant of the detection scheme is long enough to average out density fluctuations. The disadvantage is that the temporal resolution is limited both by the need to average out such fluctuations, and by the need to scan the laser. One velocity measurement is obtained per scan in this mode. In the second mode the laser is operated at a fixed frequency and the magnitude of the normalized derivative provides a direct measure of the velocity and its fluctuations. Here the reference beam is required to normalize scattering density fluctuations. This signal also provides a measure of Rayleigh cross-section weighted density fluctuations, which gives density directly in flows of fixed composition. For reacting flows specially tailored mixtures can be used so that the scattered signal directly provides mixture fraction[5] or temperature.[6] In this mode the temporal resolution is limited by the averaging time constant of the synchronous detection scheme but the laser frequency must be stabilized to prevent drifts. However, the modulation scheme offers a simple and convenient way of doing this using a feedback signal generated in the reference arm.

RESULTS

Preliminary experiments have been made to validate the MFRS concept using the sweep mode of velocity measurement. The Doppler shift is determined from a cross-correlation between the shifted and unshifted signal traces, with the frequency scaling determined from the known separation of the hyperfine components. The local jet velocities inferred from the measurements were 300 m/s with a variation of ±5% that is largely due to unsteadiness of the condensing jet.

A simple feedback stabilization of the laser has also shown itself to be very effective. The

frequency stability was measured by setting the laser to a frequency on the edge of a narrow Rb peak and monitoring the value of the reference lock-in output. Without feedback the laser frequency jittered about ±11 MHz, and drifted by 78 MHz over a span of 8 s. These translate to an uncertainty in velocity of 9 and 43 m/s respectively for this experimental configuration. There was a marked improvement in laser stability with feedback, and the jitter was reduced to ±290 kHz with a drift of 1.2 MHz over 8 s. Laser frequency drifts would then only contribute an uncertainty in velocity of ±0.16 m/s under these conditions. An optimized feedback control loop should improve the frequency precision by more than an order of magnitude so we can probably reduce the velocity error associated with laser frequency drift to negligible levels. Frequency stabilization of diode lasers via feedback is a well-established technology[7,8] and diode lasers have been stabilized to less than 1 kHz.[9]

CONCLUSIONS

Velocity measurements with an inexpensive prototype MFRS system have been made in a jet of condensing CO_2. The use of modulation spectroscopy techniques and precise feedback stabilization of the diode laser show promise of providing high-resolution continuous velocity measurements with a diode laser system.

Future work will involve implementing the fixed frequency technique, to obtain continuous velocity measurements, and extension to unseeded flows. The addition of a second detection arm opposite the first will allow for simultaneous measurement of two velocity components with a single laser beam, which would be significantly less complex than most other two-axis laser velocimetry techniques. Finally, in collaboration with Prof. Linne of the Colorado School of Mines, we wish to extend the technique to simultaneous multi-point velocity measurements along a line using the demodulating linear detector arrays they are developing.

ACKNOWLEDGMENTS

This project has been sponsored by the Texas Advanced Technology Program under grant 003658-454, and by the National Science Foundation under Grant CTS-9871249. Additional support for the development of an MFRS velocimeter for micro-gravity experiments has been approved by NASA in the Microgravity Combustion Science Program under NRA-97-HEDS-01.

REFERENCES

1. R. Miles and W. Lempert, "Two-dimensional Measurement of Density, Velocity, and Temperature in Turbulent High-Speed Air Flows by UV Rayleigh Scattering," *Applied Physics B* **51**, 1990, pp. 1- 7.
2. J. A. Lock, R. G. Seasholtz, and W. T. John, "Rayleigh-Brillouin scattering to determine one-dimensional temperature and number density profiles in a gas flow field, *Applied Optics* **31**, pp. 2839-2848 (1992).
3. D. Hoffman, K.-U. Münch, and A. Leipertz, "Two-dimensional temperature determination in sooting flames by filtered Rayleigh scattering," *Optics Letters* **21**, 1996, pp. 525-527.
4. J. Silver, "Frequency-modulation spectroscopy for trace species detection: theory and comparison among experimental methods" *Applied Optics* **31**, 707 (1992).
5. J. F. Driscoll, R. W. Schefer, and R. W. Dibble, *Nineteenth Symposium (International) on Combustion*, p. 477, The Combustion Institute, 1983.
6. D. A. Everest, J. F. Driscoll, W. J. A. Dahm, and D. A. Feikema, "Images of the Temperature Field and Temperature Gradients to Quantify MixingRates within a Non-Premixed Turbulent Jet Flame," *Combustion and Flame* **101**, 58-68 (1995)

7. C. J. Nielsen and J. H. Osmunden, "New Approach Towards Frequency Stabilization of Linewidth-Narrowed Semiconductor Lasers," *Electronics Letters* **19**, pp. 644-646 (1983).
8. H. Tsuchida and Y. Mitsuhashi, "Frequency Stabilisation of a Modulated Semiconductor Laser," *Electronics Letters* **23**, pp. 1147-1148 (1987).
9. Y. C. Ching and T. M. Shay, "450Hz Relative Frequency Stability in an AlGaAs Laser," *Electronics Letters* **23**, pp. 1044-1045 (1987).

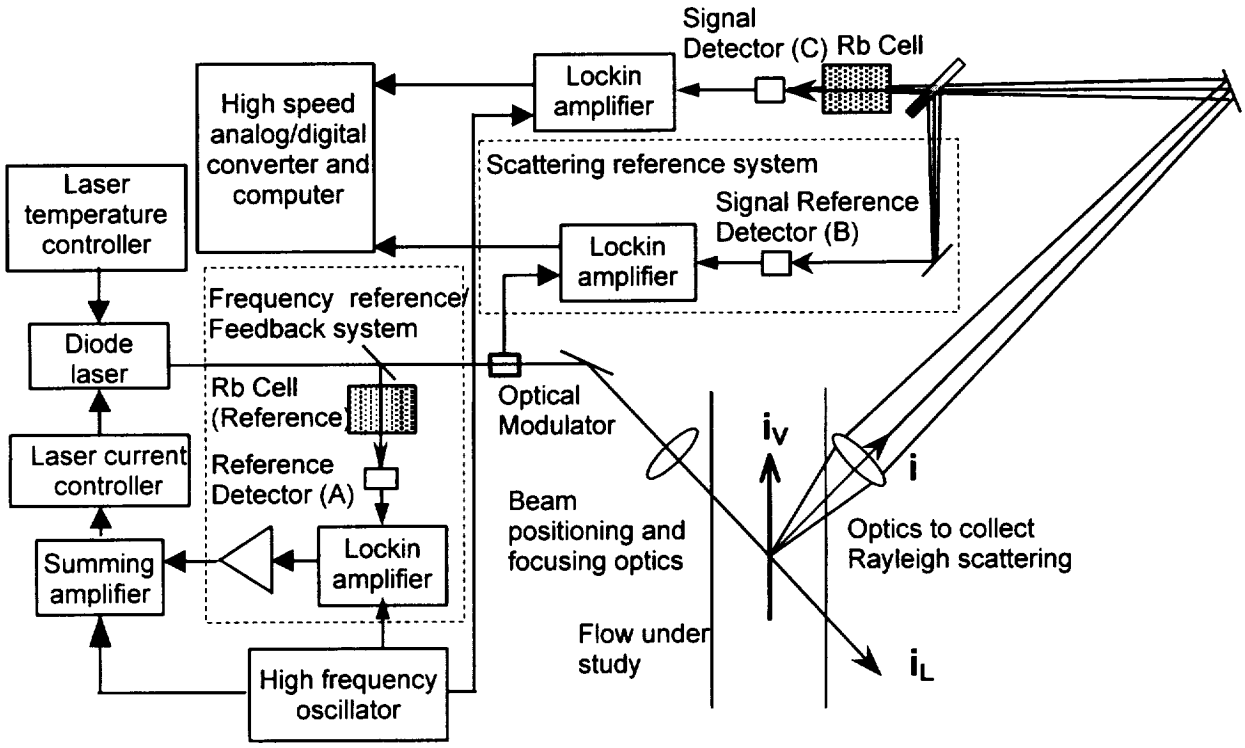

Fig. 1 Schematic diagram of experimental arrangement

OMIT THIS PAGE

Propellants and Rockets

INITIAL TEST FIRING RESULTS FOR SOLID CO/GOX CRYOGENIC HYBRID ROCKET ENGINE FOR MARS ISRU PROPULSION APPLICATIONS

Eric E. Rice, Christopher P. St.Clair, Martin J. Chiaverini , William H. Knuth,
Robert J. Gustafson and Daniel J. Gramer

ABSTRACT

ORBITEC is developing methods for producing, testing, and utilizing Mars-based ISRU fuel/oxidizer combinations to support low cost, planetary surface and flight propulsion and power systems. When humans explore Mars we will need to use *in situ* resources that are available, such as: energy (solar); gases or liquids for life support, ground transportation, and flight to and from other surface locations and Earth; and materials for shielding and building habitats and infrastructure. Probably the easiest use of Martian resources to reduce the cost of human exploration activities is the use of the carbon and oxygen readily available from the CO_2 in the Mars atmosphere. ORBITEC has conducted preliminary R&D that will eventually allow us to reliably use these resources. ORBITEC is focusing on the innovative use of solid CO as a fuel. A new advanced cryogenic hybrid rocket propulsion system is suggested that will offer advantages over LCO/LOX propulsion, making it the best option for a Mars sample return vehicle and other flight vehicles. This technology could also greatly support logistics and base operations by providing a reliable and simple way to store solar or nuclear generated energy in the form of chemical energy that can be used for ground transportation (rovers/land vehicles) and planetary surface power generators. This paper describes the overall concept and the test results of the first ever solid carbon monoxide/oxygen rocket engine firing.

INTRODUCTION

To enable cost-effective, *in situ* production of Mars atmosphere-derived oxidizers (oxygen) and fuels (carbon monoxide) work needs to be achieved in the development of processes to form the propellants into a usable form and work needs to be achieved in the demonstration of their use and performance of the propellants in applications involving rocket propulsion, ground-based rovers that use IC or turbine engines, and electric power generation systems. It is believed that by using the baseline C/O system, in the proper fuel form (CO gas, solid) that significant economic dividends can be achieved for the HEDS enterprise. The production of oxygen and carbon monoxide through solid state electrolysis appears to be well in hand by K. R. Sridhar at the University of Arizona. Hardware is now being prepared to fly to Mars for an ISRU demo. Diane Linne of NASA/GRC is a proponent of a LCO/LOX propulsion system and has begun testing with a flight-weight chamber. However, a propulsion system study recently reported by JPL was not favorable to rocket performance of ISRU - LCO/LOX, because of the heavy tank needed to store the LCO under the guidelines used in the study. However, with our significant innovative work and the successful hot firing demonstrations of cryogenic solid hybrid rocket engines for NASA and the USAF, including SH_2, SOX, SCH_4, and SC_2H_2, the concept of a solid CO fuel grain is recommended to alleviate the heavy weight tank problem.

CO gas can be directly frozen to a uniform solid hybrid fuel grain below the triple point temperature (68 K) by using subcooled LOX as the freezing fluid and oxidizer in a cryogenic hybrid engine. The heavy tank associated with LCO is eliminated and a much lighter propulsion system can now be developed that will be the most simple and low-cost approach. Mars-produced fuels and oxidizers will enhance and/or enable a variety of Mars exploration missions by

providing a very cost-effective supply of propellants. The establishment of practical feasibility could result in an absolutely significant cost savings to our exploration programs.

INITIAL TEST FIRING AND RESULTS

On January 29, 1998, ORBITEC performed the first ever test firing of a solid CO/GOX propellant combination in the ORBITEC Mark-II Cryogenic Hybrid Rocket Engine. Ideal performance using the GRC CEA performance code is shown in Figure 1 for an expansion ratio of 100 and a chamber pressure of 500 psia. A schematic of the ORBITEC Mark-II Cryogenic Hybrid Rocket Engine is shown in Figure 2. 100 grams of solid CO was frozen onto the inside of the cylindrical chamber of the engine. LHe was used to freeze and cool the CO for the test. The freezing pressure was on the order of 1 Torr. The freezing process took 29 minutes; however, it could have been faster if we had increased the CO flow rate. Based on previous experience, we estimate that the CO was approximately 10 K just prior to the test firing. The grain appeared slightly green in color and looked uniform and smooth. Video of the formation and firing were taken and recorded. A gaseous H/O ignitor was used that provided a hydrogen-rich hot gas to the grain as the GOX flow was initiated. The ignition was smooth. The chamber pressure during the burn is shown in Figure 3. The pressure steadily increased as the firing progressed. Based upon comparison to other firings using other propellants, thermocouple data showed that it was very hot – indicating a close to an optimum burn. The oxygen flow rate was controlled to a steady flow of 6 grams per second. Figure 4 shows the estimated O/F ratio. At the beginning of the burn the O/F ratio was 0.7; at the end of the burn the O/F ratio was about 0.4. The estimated C* efficiency was ~83%. The calculated average O/F ratio was 0.57 (ideal is 0.5 for maximum performance, as shown in Figure 1). We expect to be able to control the O/F ratio to the desired level in the next generation engine. Figure 5 summarizes ORBITEC's regression rate data for various solid cryogens, including solid carbon monoxide. The regression rate for SCO is about an order of magnitude higher than conventional fuels/oxidizers and about a factor of 2 less than SCH_4/GOX.

CONCLUSIONS

The conclusions reached from the first SCO/GOX test are: SCO can be easily and quickly formed in a solid grain that looks structurally sound; SCO burns very well with GOX – it has been one of the smoothest burning cryogenic solids that we have tested; the pressure change with time was primarily due to the increase in area as the grain regressed -- the increase in grain temperature is also believed to be a contributor; the optimum O/F ratio was achieved; and the test shows great promise for the SCO/LOX propellant combination for use in a Mars Sample Return mission and a wide variety of other Mars exploration applications.

ACKNOWLEDGEMENTS

The initial work on this propellant combination was supported by ORBITEC IR&D. The basic cryogenic hybrid rocket engine hardware used in the testing was developed through work sponsored by the USAF/AFRL and the NASA/GRC. Follow-on work is currently planned as part of the NASA Microgravity Combustion Science Program, with technical support from NASA/GRC.

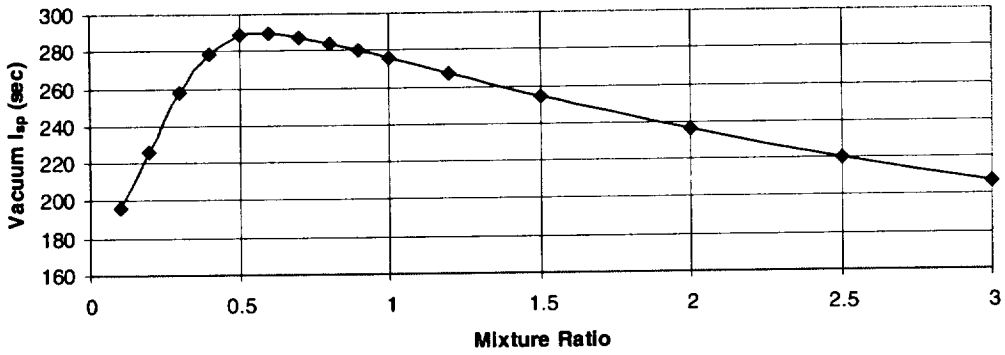

Figure 1. Solid CO/LOX Theoretical I_{sp} vs O/F Ratio for e=100, Pc- 500 psia

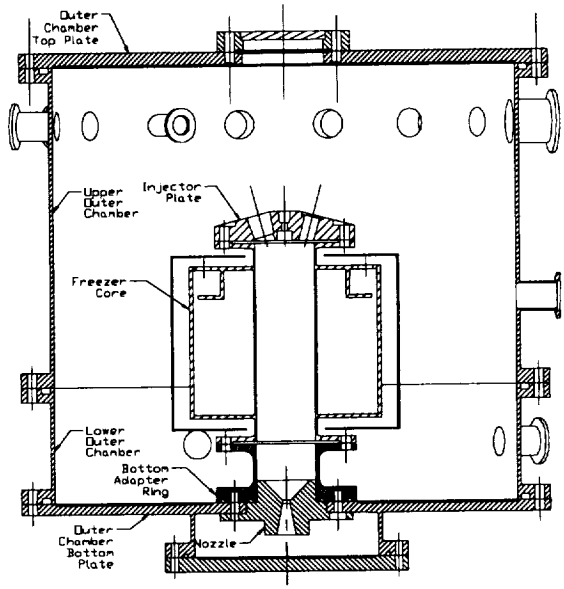

Figure 2. ORBITEC's Mark II Cryogenic Hybrid Rocket Engine

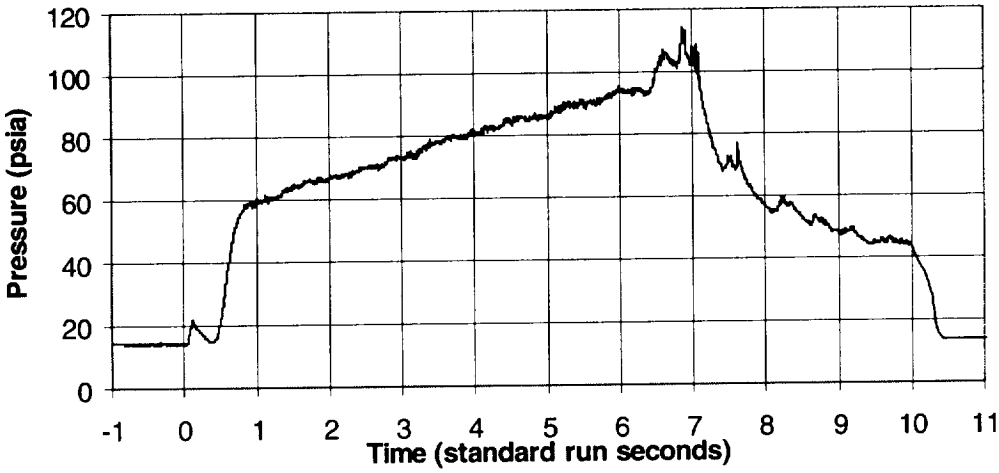

Figure 3. SCO/GOX Combustion Chamber Pressure Plot for SCO/GOX Static Firing

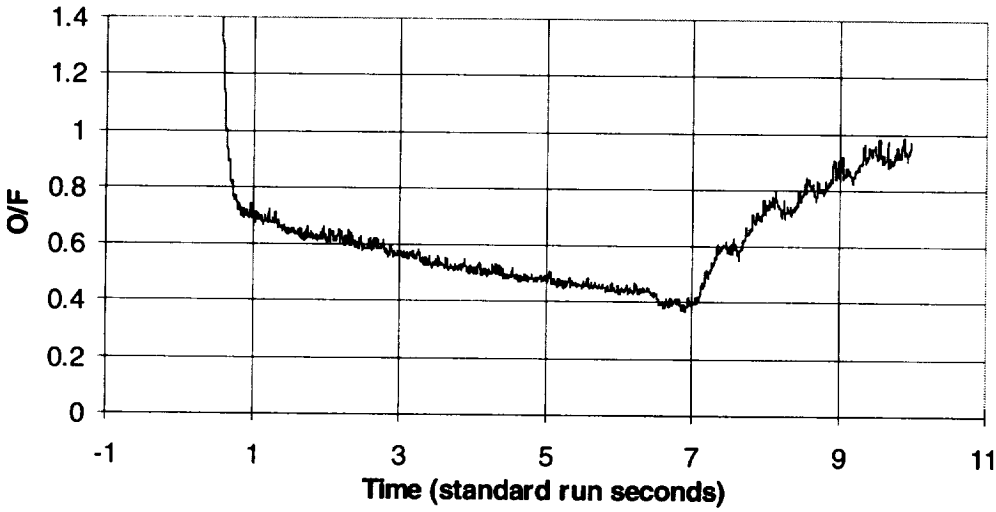

Figure 4. Estimated O/F Ratio for SCO/GOX Static Firing

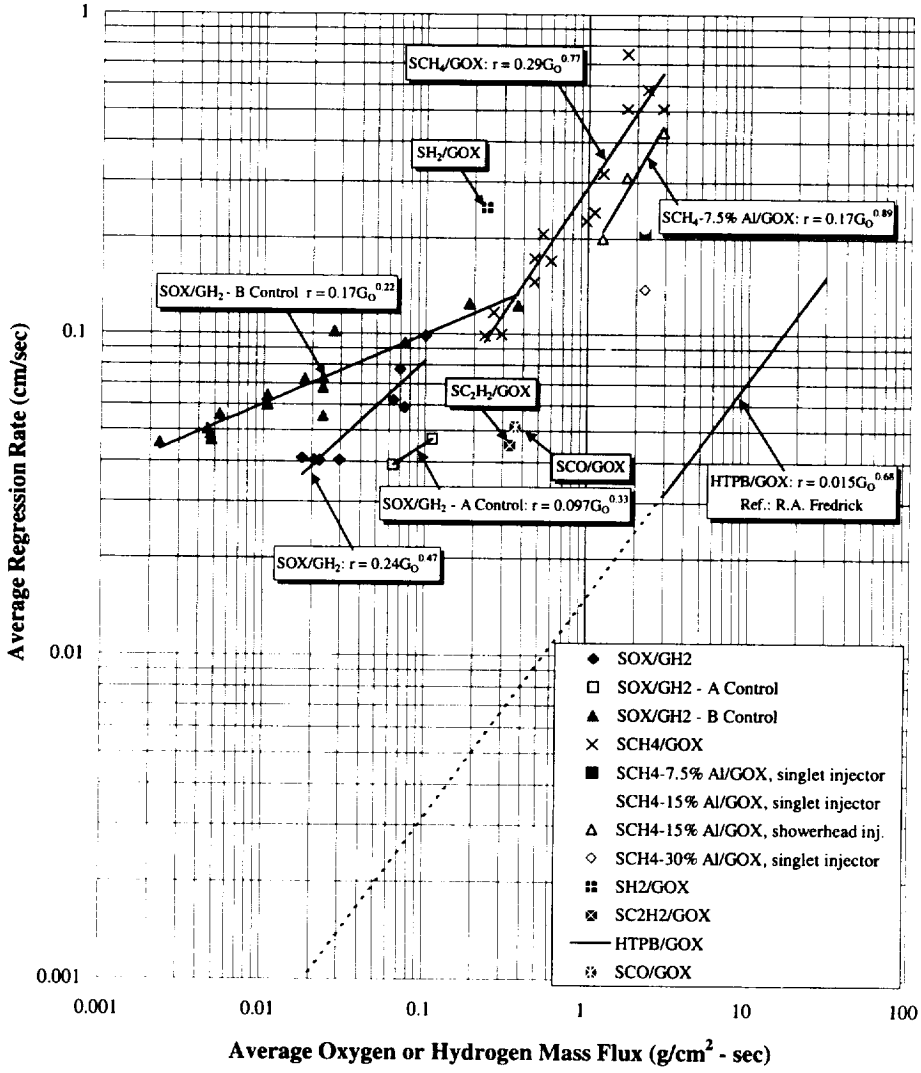

Figure 5. ORBITEC's Composite Regression Rate Data for Cryogenic Solid Propellants

S93-28

COMBUSTION OF HAN-BASED MONOPROPELLANT DROPLETS IN REDUCED GRAVITY

B. D. Shaw, MAE Department, University of California, Davis, CA 95616

INTRODUCTION

The objective of this research is to study combustion of monopropellant droplets and monopropellant droplet components in reduced-gravity environments so that spherical symmetry is strongly promoted. The experiments will use hydroxylammonium nitrate (HAN, chemical formula NH_3OHNO_3) based monopropellants. This class of monopropellant is selected for study because of its current relevance and also because it is relatively benign and safe to work with.

For some background, HAN is a major constituent in a class of liquid monopropellants that have many attractive characteristics and which display phenomena that differ significantly from other liquid monopropellants [1]. They are composed primarily of HAN, H_2O and a fuel species, often triethanolammonium nitrate (TEAN). HAN-based propellants have attracted attention as liquid gun propellants (e.g., [1]), and are attractive for NASA spacecraft propulsion applications [2]. A representative propellant is LPG 1845. This mixture has a HAN-to-TEAN molar ratio of 7 and is 16.8% H_2O by weight. This propellant is stoichiometric to N_2, CO_2 and H_2O, and has an adiabatic flame temperature of about 2800 K. At pressures below about 6 atm, combustion cannot be sustained. Experiments have shown that these liquid monopropellants cannot be ignited at atmospheric pressure, are non-detonable, and are essentially benign regarding health and safety risks, making them reasonably safe to work with.

Previous research on HAN-based propellants, which has all been performed in normal gravity, has shown that combustion of HAN-based mixtures proceeds sequentially (see, e.g., [3]). Condensed-phase HAN decomposition occurs first, releasing some heat and substantial amounts of N_2, H_2O, N_2O, NO, and NO_2. [3,4]. HAN decomposition gasifies at least some of the liquid water, and molten salt droplets of the fuel species are then thought to be formed; these droplets react primarily with gaseous oxides of nitrogen (which result from HAN decomposition), releasing most of the heat of combustion. While providing valuable information, previous research has not been able to accurately determine surface regression rates of HAN-containing liquids. In addition, only limited studies have been reported on TEAN reactions, and no studies of the behaviors of TEAN (or other fuel) droplets have been reported.

In this research, experimental and theoretical studies will be performed on reduced-gravity combustion of liquid monopropellant droplets based on HAN. The research will involve studying combustion of HAN/water droplets, HAN/TEAN/water droplets, TEAN particles, and TEAN/water droplets. Droplets/particles initially in the mm size range will be studied at pressures up to 30 atm. These pressures are directly applicable to spacecraft thruster applications [2]. The samples will be placed in Ar environments with various amounts of N_2, O_2, NO_2 and N_2O. The experimental studies will utilize reduced gravity to strongly promote spherically symmetrical combustion. This will allow observations of burning rates and flame structures to be made without the complicating effects of buoyant and forced convection (especially in regimes where ordinary strand burner results are strongly influenced by hydrodynamic instabilities, rendering interpretation of experimental data difficult [5,6]).

This research will yield information on the fundamental combustion mechanisms of HAN-based liquid propellants. The experimental studies will allow for accurate determination of fundamental data on deflagration rates, gas-phase temperature profiles, transient gas-phase flame behaviors, the onset of bubbling in droplets at lower pressures, and the low-pressure deflagration limit. The theoretical studies will provide rational models of deflagration mechanisms of HAN-based liquid propellants. Besides advancing fundamental knowledge, the proposed research should aid in applications (e.g., spacecraft thrusters and liquid propellant guns) of this unique class of monopropellants.

EXPERIMENTAL RESEARCH

This research will involve studying combustion characteristics of droplets/particles initially in the mm size range. A drop rig will be constructed at UC Davis and used at the NASA Lewis 2.2 Sec Drop Tower. The design of this drop rig will be primarily based upon the droplet combustion test rigs that are presently in use at the NASA Lewis Research Center. However, for these experiments, the pressure vessel will be modified to allow pressures up to 30 atm to be achieved. Pressures in this range are representative of pressures which apply to spacecraft thrusters [2]. A schematic of major components within and around the pressure vessel is shown in Fig. 1. This vessel will be mounted on a drop frame with imaging, electronic and fluid handling systems.

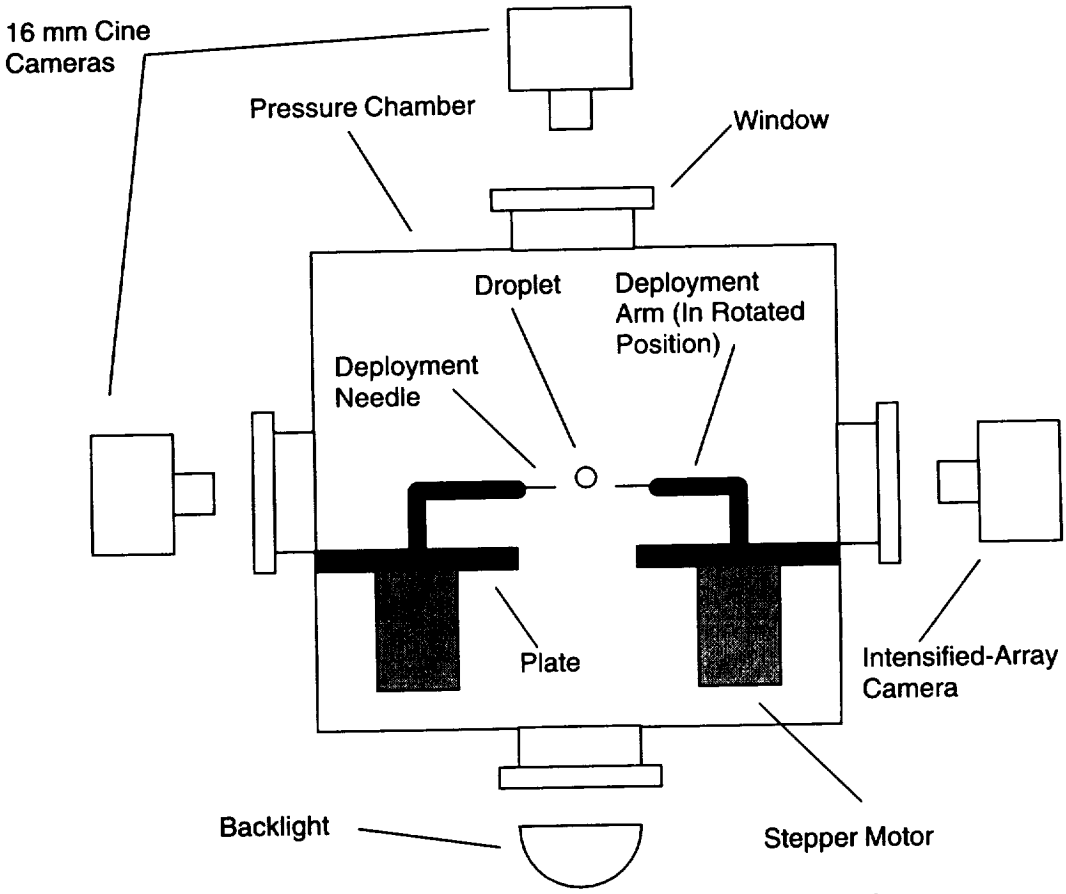

Figure 1. Schematic diagram of the pressure vessel and associated apparatus.

As shown in Fig. 1, orthogonal views will be used. One view will be used to image droplets and the other view will be used to image flames. The droplet view, which will be backlit, will utilize a high-speed camera to capture transient droplet behaviors. The flame view will not be backlit, and two cameras will actually be used to image flames. A 16 mm cine camera (or high-speed video camera) will be used to image gas-phase combustion behaviors, and an intensified-array CCD camera will be used to image OH emissions. Not shown in Fig. 1 is the ignition system, the fuel delivery system, and a thermocouple rake that will be used to measure gas-phase temperatures.

The expected combustion behavior for a HAN/TEAN/water droplet is shown in Fig. 2. It is expected that HAN decomposition will occur in a thin liquid layer near the regressing droplet surface. Surface bubbling may occur as the heat release from HAN decomposition vaporizes

water and the HAN decomposition products bubble out of solution; some water droplets may also be formed, as should TEAN droplets [3]. These TEAN droplets may eventually react with oxides of nitrogen from the HAN decomposition [3]. For droplets that do not have TEAN, it is expected that the liquid-phase processes will be similar, but that there will not be appreciable chemical reactions occurring in the gas phase.

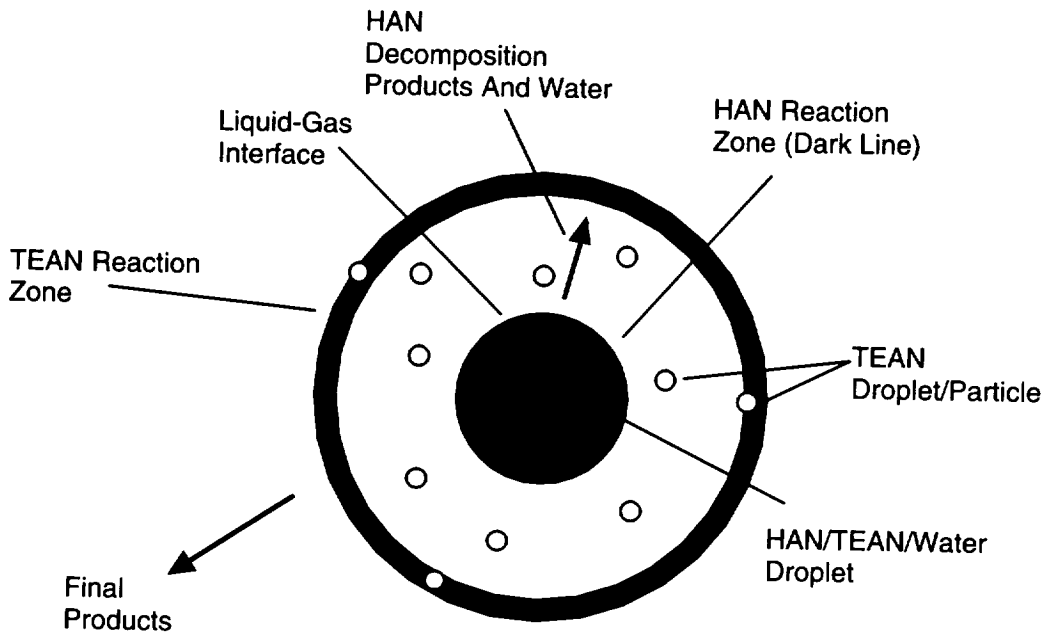

Figure 2. Schematic diagram of expected HAN/TEAN/water droplet combustion behaviors.

At the present time, there are no data on combustion behaviors of TEAN droplets. While condensed-phase HAN decomposition does not involve appreciable effects of species diffusion and is essentially of a premixed character [4], TEAN droplet combustion may be strongly influenced by species diffusion. One possible scenario is that TEAN is vaporized from the droplet surface, with TEAN vapor being transported outwards where it reacts with oxides of nitrogen in a gas-phase reaction zone. This scenario is similar to conventional bipropellant droplet combustion, where gas-phase diffusion flames may predominate. Alternatively, it may be that TEAN vaporization is negligible such that appreciable chemical reactions occur in the condensed phase or on the surface. It is also possible that TEAN decomposition might occur at or near the droplet surface, with decomposition products burning in the gas phase in a diffusion flame mode [7]. The proposed experiments will provide needed information on TEAN droplet combustion characteristics.

In the experiments, the pressure range 1 to 30 atm will be explored. While HAN-based liquid mixtures are not expected to burn at pressures lower than roughly about 6 atm, TEAN droplets and particles may burn at all pressures (if sufficient oxidizer is present). The propellants to be considered will include HAN/water mixtures with HAN molarities ranging from about 3 to 13, HAN/TEAN/water mixtures corresponding to practical fuels as well as mixtures with more or less HAN or TEAN than is required for stoichiometry, TEAN/water mixtures, and TEAN particles. In this way, influences of variations in mixture properties can be explored more fully. In addition, O_2 will sometimes be added to the ambient. This is because shock tube studies [7] have suggested that TEAN reacts significantly more slowly with oxides of nitrogen than with O_2. Adding O_2 may show that it is advantageous to burn monopropellants containing TEAN in the presence of oxygen.

Unsupported (free) droplets and droplets supported with ≈ 10 μm silicon carbide fibers will be burned within the pressure chamber. Data to be obtained will include transient droplet and gas-phase flame diameters, the occurrence of liquid bubbling inside droplets, the low-pressure deflagration limit, influences of fuel species on liquid consumption rates, and gas thermal profiles. Normal-gravity comparison experiments will also be performed at UC Davis using the reduced-gravity apparatus.

THEORETICAL RESEARCH

The theoretical efforts will be essentially divided into two efforts. The first effort will be an extension of the research that led to the publication of Ref. [4]. Rational theoretical models (based on existing solid propellant deflagration theory or new models to be developed) will be applied to HAN-based liquid propellants. Theoretical models that are consistent with experimental data will be selected or developed. Influences of phenomena such as nonequilibrium vaporization, two-phase flow, gas solubility in liquids, the presence of a fuel species (e.g., TEAN) and chemical reactions downstream of the HAN decomposition zone will be considered. These phenomena may possibly influence decomposition rates in the HAN decomposition zone, and will certainly influence downstream gas-phase combustion of TEAN (or another fuel) that might be present.

The second effort will be directed towards developing models of TEAN droplet combustion. After the TEAN experiments have been completed and the basic physics have been observed, efforts will be directed towards developing simplified models which describe spherically-symmetrical combustion of TEAN droplets, e.g., droplet surface regression rates, flame radii, and gas temperatures. An emphasis of this research will be to develop simplified analytical models.

ACKNOWLEDGEMENTS

The financial support of NASA is gratefully acknowledged. The Technical Monitor for this research is Dr. D. Dietrich.

REFERENCES

1. Klein, N., Report ARBRL-02471, Ballistic Research Laboratory (1983).
2. Jankovsky, R. S., AIAA Paper 96-2863.
3. Klein, N. and Leveritt, C. S., "The Ignition and Combustion of Liquid Gun Propellants," 22nd International Annual Conference on ICT. Published by Fraunhofer-Inst fuer Treib- und Explosivstoffe, Pfinztal-Berghausen, Ger. p. 49.1 (1991).
4. Shaw, B. D. and Williams, F. A., 24th Symposium (Int'l.) on Combustion, p. 1923 (1992).
5. Vosen, S. R., Combust. Sci. Tech. 68: p. 85 (1989).
6. Vosen, S. R., Combust. Flame 82: p. 376 (1990).
7. Beyer, R. A., CPIA Publication 557, Volume I, p. 605 (1990).

S94-27

COMPUTATIONAL AND EXPERIMENTAL STUDY OF ENERGETIC MATERIALS IN A COUNTERFLOW MICROGRAVITY ENVIRONMENT

Mitchell D. Smooke[1], R. A. Yetter[2], T. P. Parr[3], D. M. Hanson-Parr[3] and M. A. Tanoff[4], [1]Department of Mechanical Engineering, Yale University, New Haven, CT 06520-8284, [2]Department of Mechanical and Aerospace Engineering, Princeton University, Princeton, NJ 08544-5263, [3]Weapons Division, Naval Air Warfare Center, China Lake, CA 93555-6100, [4]W. K. Kellogg Institute, Battle Creek, MI 49016-3232

INTRODUCTION

Ground based (normal gravity) combustion studies can provide important information on the processes by which monopropellants and composite systems burn. The effects of gravitational forces, however, can often complicate the interpretation of the models and the implementation of experiments designed to help elucidate complex issues. We propose to utilize a combined computational/experimental approach in a microgravity environment to understand the interaction of oxidizer-binder diffusion flames in composite propellants. By operating under microgravity conditions we will be able to increase the length scales and suppress the gravitational forces on melting binders such that increased resolution of both major and minor species will be possible thus reducing the demands placed on both the computational and diagnostic tools. Results of a detailed tranport/finite rate chemistry model will be compared with nonintrusive optical diagnostic measurements of the structure and extinction of diffusion flames in which oxidizers such as ammonium perchlorate (AP) and ammonium dinitramide (ADN) are counterflowed against realistic binders such as hydroxyl-terminated polybutadiene (HTPB) and 3,3-bis(azidomethyl)oxetane (BAMO). The work proposed herein represents a collaborative effort among the research groups at Yale University, Princeton University and the Combustion Diagnostics Laboratory at the Naval Air Warfare Center in China Lake, CA.

RESEARCH PROJECT DESCRIPTION

Many solid rocket propellants are based on a composite mixture of ammonium perchlorate (AP) oxidizer and polymeric binder fuels. In these propellants, complex three-dimensional diffusion flame structures between the AP and binder decomposition products, dependent upon the length scales of the heterogeneous mixture, drive the combustion via heat transfer back to the surface. Changing the AP crystal size changes the burn rate of such propellants. Large AP crystals are governed by the cooler AP self-deflagration flame and burn slowly, while small AP crystals are influenced more by the hot diffusion flame with the binder and burn faster. This allows control of composite propellant ballistic properties via particle size variation. While the ultimate goal in composite propellant modeling is the ability to carry out a full three-dimensional computation that includes the random distribution of oxidizer crystals in the fuel matrix binder, such a study is beyond our current computational and modeling capabilitites. Although previous measurements of AP/binder diffusion flames undertaken in planar two-dimensional sandwich configurations have yielded insight into the controlling flame structure [1,2], there are several drawbacks that make comparison with modeling difficult. The flames are two-dimensional in structure making modeling much more complex computationally than with one-dimensional propellant systems, such as RDX self- and laser-supported deflagration [3]. The melting of the binder can interfere with the composite propellant diffusion flame. This can complicate the interpretation and the implementation of experiments designed to help elucidate complex issues. Also, the length scales in the two-dimensional composite experimental configuration are extremely small – the majority of the heat release occurs in a region only

100 to 200 microns off the surface. It is much too difficult from a diagnostic viewpoint to resolve the combustion processes occurring within this region.

The counterflow configuration greatly spreads the heat release region allowing spatial resolution of the chemical kinetic process in the AP/binder diffusion flame. This provides an excellent geometric configuration within which AP/binder diffusion flames can be studied both experimentally and computationally. However, when a realistic binder, such as HTPB, or other oxidizers, such as ADN, burn, the surface melts forming a thick viscous layer which can flow, drip, or puddle making it virtually impossible to employ the counterflow oxidizer-binder configuration at normal gravity. Only a few binders, such as PBAN, do not form significant surface melt layers. PBAN, however, is an outdated binder system and modern binders, such as HTPB, and especially energetic thermoplastic binders such as BAMO, melt easily. Not only will the low gravity environment preclude melting binder and energetic material surface layers from dripping or otherwise flowing, but the adverse effects of buoyancy on the flame structure will be removed as well, allowing more accurate comparison with the model. Previous ground based experiments were severely limited in the range of strain rates that could be studied by the effects of buoyancy [4]. Low strain rates are selected by using large separation distances between the fuel and oxidizer flows (there is no independent control over the flow speeds; the AP regresses according to heat feedback from the flame and the fuel velocity must be chosen to place the stagnation plane in the proper location). In the AP/methane experiments the AP regression rate decreased with low strain rates leading to very low gas velocities. This, coupled with the larger length scale, leads to buoyancy affecting the flame structure. The negative buoyancy of the cold fuel compared to hot AP decomposition products causes the AP gases to expand radially and the stagnation plane to be pushed lower. This seriously distorts the flame structure for large separation distances required for low strain rates ($Gr/Re^2 = 2.5$ for d = 10 mm). With the experimental strain rate limited on the high end by heat loss to the burner and on the low end by the effect of buoyancy, the ground based experiments were limited to essentially a single strain rate. Investigation of flame structure and extinction under varying strain rates is a vital technique to exercise and validate the kinetic database upon which the model is based. The low gravity counterflow system experiments proposed here will allow a much wider range of strain rates to be studied.

We plan on investigating the modeling of counterflow diffusion flames in which oxidizers such as AP and ADN are counterflowed against a polymeric fuel binder such as HTPB and BAMO. The results of the computational model will be compared with a series of experimental measurements on the ground and in a low gravity environment. Ground based experiments will make use of advanced laser diagnostics to measure species and temperature profiles. These will include the planar laser induced fluorescence, emission spectroscopy, and Raman scattering used in the previous laboratory AP/methane counterflow experiments. The ground tests will make use of the few binders that don't form extensive melt layers, such as PBAN. After a period of ground-based verification of the techniques, experiments in microgravity will be undertaken. The experimental methods to be employed in microgravity must be simpler than those used in the ground tests. The laser used for the ground tests requires 11 kW of power, 1.5 gal/min of cooling, and takes up over 30 cubic feet of space making it incompatible with any of the ground based low gravity test facilities. The diagnostics for low gravity tests will be carefully chosen to be compatible with existing microgravity facilities and to best evaluate the effects of buoyancy on the flames. The initial technique verification will take advantage of our previous ground-based measurements of oxidizer-fuel diffusion flames.

The proposed apparatus for studying solid oxidizer-solid fuel counterflow diffusion flames in microgravity is illustrated in Figure 1. It consists of an oxidizer pellet (AP in this case) and binder are held at a controllable separation via a quick change pellet

holder cartridge. The surface positions are held constant during regressive deflagration by a spring load from below and tension wire across the surface. This simple technique has been successfully used on RDX and HMX combustion (which burn much faster) and can keep the surface at a constant position to within less than 100 micrometers.

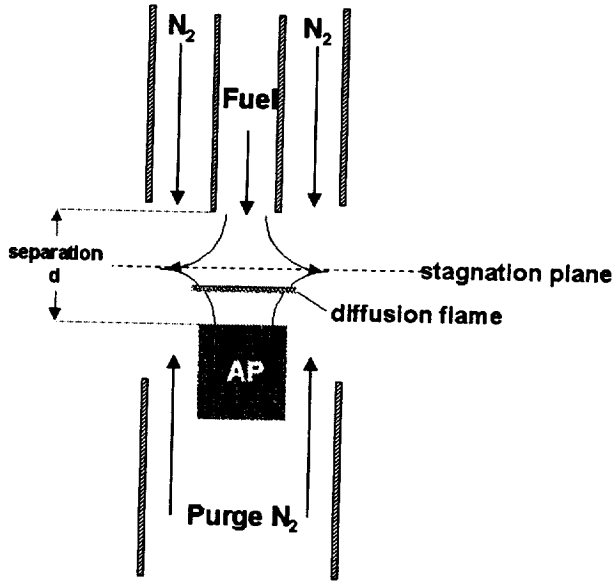

Figure 1 – Schematic of experimental configuration for ethylene vs. AP counterflow flame system.

A color video camera with a macro lens will be used to monitor the flame and provide images of its structure. This camera is gateable for the particle tracking velocimetry (PTV). A UV-Visible gated intensified camera with UV macro lens will be used to acquire 2D images of selected chemiluminescent species (such as CN, NH, CH, C_2, OH, etc.). This camera can also be used for PTV. Quantitative species concentration data will be obtained using line resolved UV-Visible absorption spectroscopy. A xenon lamp will be used as a light source with the beam being formed into a sheet which passes through the flame perpendicular to the surfaces of the binder and oxidizer. Spectral fitting of certain absorption bands, such as OH, may afford limited temperature profiling as well.

In ground based experiments the temperature was measured on the fuel side using radiation corrected thermocouples and on the oxidizer side with OH rotational population distributions measured using PLIF (see Figure 2). The thermocouples were found to disturb significantly these sensitive flames and the PLIF is not compatible with microgravity facilities. The combustion group at Yale has developed a flight capable temperature imaging technique based on Rayleigh scattering, but this is not likely to work in the counterflow solid flames. The solid fuel/oxidizer inevitably leads to particulates in the flame and Mie scattering from the particulates would overwhelm the Rayleigh signal. In addition, binders such as HTPB burn with very sooty flames leading to Mie scattering from soot. During the first year of the program we will attempt to develop a flight capable diagnostic for gas temperatures that is applicable to these experiments.

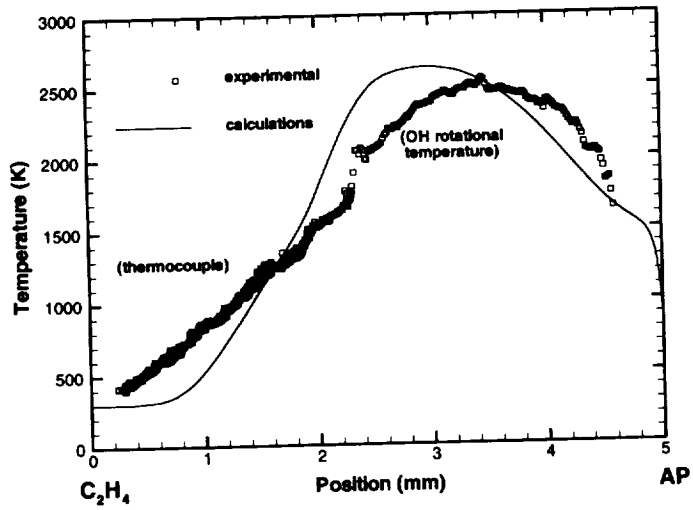

Figure 2 – Comparison between experimentally measured and calculated temperature profiles for the fuel vs. AP counterflow flame.

ACKNOWLEDGEMENTS

This work has been approved for support by NASA (contract number and start date to be determined). The technical monitor is Dr. David L. Urban.

REFERENCES

1. Parr, T. P. and Hanson-Parr, D. M., "AP Diffusion Flame Structure", *Proceedings of the 33rd JANNAF Combustion Meeting*, Monterey, CA, November 1996.

2. Parr, T. P. and Hanson-Parr, D. M., *Twenty-Sixth Symposium (International) on Combustion*, The Combustion Institute, Pittsburgh, PA, 1997, p. 1981.

3. Prasad, K., Yetter, R. and Smooke, M. D., "An Eigenvalue Method for the Determination of Burning Rates for RDX Monopropellants," *Comb. Sci. and Tech.*, **124**, p. 35, (1997).

4. Illincic, N., Tanoff, M., Smooke, M., Yetter, R., Parr, T., and Hanson-Parr, D., "Modeling AP Combustion in Gaseous Environments," *Proceedings of the 34th JANNAF Combustion Meeting, 1997.*

Combustion Synthesis

S95-29

Formation of Carbon Nanotubes in a Microgravity Environment

J. M. Alford and M.D. Diener, TDA Research, Inc., 12345 W.52 Ave., Wheat Ridge, CO 80033

Introduction

The scientific objective of this investigation is to determine how microgravity processing can improve the production and morphology (size and length) of single-walled carbon nanotubes (SWNTs).

Single-walled carbon nanotubes were discovered in 1991 as an outgrowth of research into fullerene ("Buckyball") molecules. SWNTs are, in essence, single fullerene molecules that have been stretched until their length is millions of times their diameter. The evolution of a fullerene into a single-walled nanotubes is shown in Figure 1. Researchers soon discovered that SWNTs possess many remarkable properties[1]. They represent the strongest known type of carbon fiber and form the ideal basis for new composite materials. Calculations show that a carbon nanotube-based cable could have one hundred times the strength of steel while having just one-sixth of the weight. Such a cable, for example, would make an ideal space tether. Carbon fiber composites made from nanotubes would save significant weight in spacecraft and aircraft structures. In addition to their mechanical properties, nanotubes have interesting electronic properties, which are dependent upon the tubes morphology. Some tubes have conducting electronic structures and can be envisioned as molecular quantum wires, while others are semiconducting and can be used to fabricate the world's smallest "single molecule" transistors.

Because of their potential as new materials, there is currently a large interest in the synthesis and characterization of carbon nanotubes. In fact, nanotube science has become one of the worlds most rapidly advancing areas of research. However, most investigations have concentrated on determining the physical properties of the tubes; very little is known about the fundamental processes involved in nanotube formation. The current nanotube synthesis processes are poorly understood and can only produce small, gram quantities of nanotubes that are less than ~100 microns in length. Because of these limitations, nanotubes have remained largely a laboratory curiosity. If industrial amounts of tubes 10-100 times longer, 1-10mm, could be efficiently produced, then commercial applications in new composite materials would become much more favorable. The key to developing better production processes is to gain a better understanding of the nanotube formation process.

There are several methods for the production of single-walled carbon nanotubes. The two most common processes are the carbon arc and laser ablation method. Both processes rely on catalytic

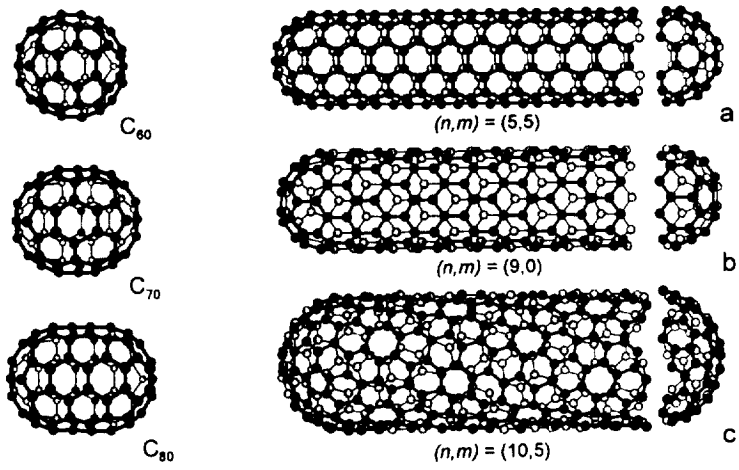

Figure 1. Stretching of C_{60} by adding 10 carbon atoms around the belt eventually produces tube (a). Some larger tubes with their fullerene endcaps are shown in (b) and (c).

growth of the nanotubes from carbon vapor in the presence Co/Ni or other transition metal catalysts. Although some types of multi-wall nanotubes grow from surfaces, the growth of single-walled nanotubes occurs primarily in the gas phase. As the carbon and metal catalyst vapors cool, they condenses into small sub-nanometer sized clusters that continually collide and grow. When the metal carbide cluster becomes saturated with carbon, the carbon re-crystallizes or grows out of the particle as a nanotube. The metal particle remains on the head of the tube and channels the remaining carbon it encounters into the tube. A schematic of this process is shown in Figure 2. Although conceptionally simple, very little detailed modeling of this process has been performed, and it remains unclear what factors have the largest effect on nanotube growth and the ultimate

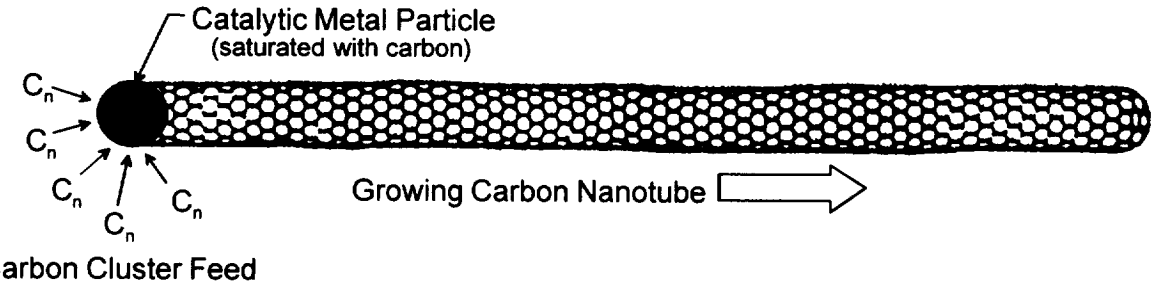

Figure 2. Catalytic growth of a SWNT.

length that can be attained.

The formation of single-walled nanotubes is a gas phase process that is similar to the formation of soot during combustion processes. Buoyancy is known to have a large effect on soot formation, and we hypothesize that the same is also true for nanotube formation. Both the arc and laser process vaporize carbon in a high temperature plasma which induces a strong convective flow in the apparatus. (Nanotubes are currently produced at 1 atm. where the sublimation point of carbon is ~3367 °C). In the laser apparatus, convection currents due to buoyancy can be directly observed in the laser plume. Currents are also readily seen in arc reactors and explain why the quality of nanotube deposits varies greatly depending on their position in the apparatus. The formation of a nanotube is undoubtedly a strong function of the time/temperature/concentration history of the growing tube and its precursors. Buoyancy produces an uncontrolled environment that makes estimation (and hence further optimization) of these critical factors difficult if not impossible. Microgravity conditions will provide a much more controlled environment for measurement, modeling, and optimization of these parameters. In addition, the time available for incorporation of carbon into the growing nanotube will be increased, allowing for enhanced growth of the nanotubes.

Experimental

In this project we have planned a series of systematic experiments to investigate the effect of buoyancy on nanotube growth. We estimate that the 100 um long tubes produced by the arc and laser methods are formed in less than 100 msec., and therefore, the weightless time needed for the experiments will depend more on the amount of material desired rather than on the time required for nanotube formation. Proof-of-principle experiments should therefore be readily accomplished using drop tower experiments, and we are currently designing a carbon nanotube reactor that can be dropped from the NASA LeRC 2.2 second microgravity drop tower. The proposed reactor

will utilize a metal doped carbon wire that can be evaporated either resistively or used to form a small arc following its release from the tower. A simplified schematic is shown in Figure 3. In spirit, this machine is similar to that developed by R.E. Smalley for the production of SWNTs

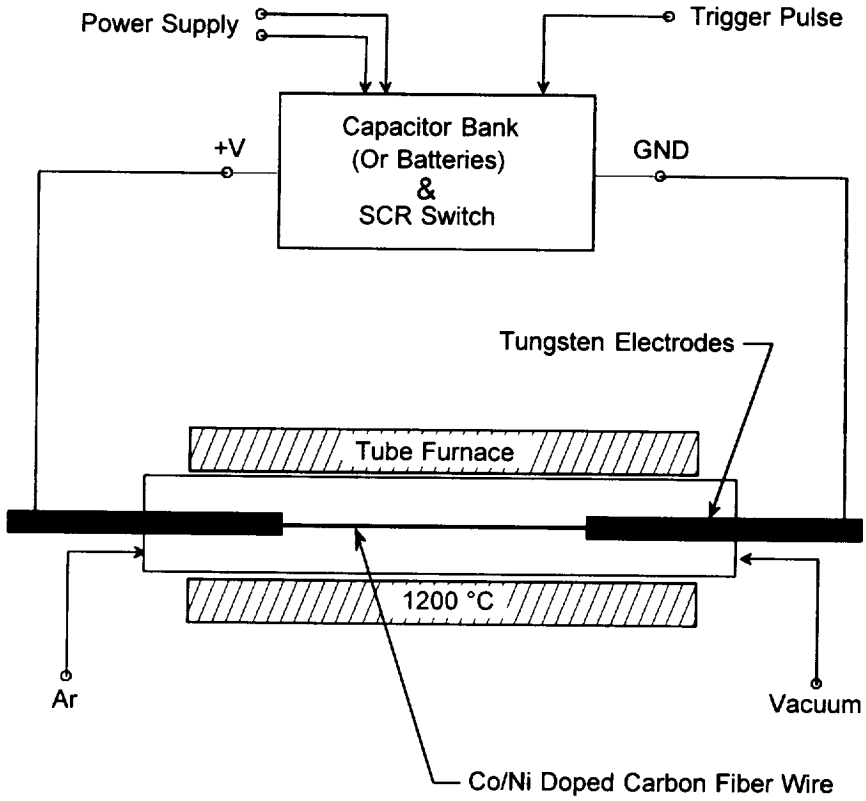

Figure 3. Schematic for the evaporating wire nanotube apparatus.

using the laser vaporization of graphite. In this case, we have replaced the laser pulse with a pulse of electric current capable of evaporating the wire.

After performing an experiment, the soot in the reaction chamber will be collected and analyzed using both scanning electron microscopy (SEM) and transmission electron microscopy (TEM). Because the samples will be small (10mg), they will be collected by washing the inside of the apparatus with a solvent such as ethanol, and then deposited from solution onto the microscope sample grids.

Once good single-walled nanotubes are produced under 1g conditions, the experiments will be reproduced on the drop tower. Nanotubes grown in the 1g and microgravity environment will then be compared using transmission electron microscopy to determine how the absence of buoyancy effects their yield, growth, and structure.

Summary

Nanotube science has become one of the worlds most rapidly advancing areas of research. However, most investigations have concentrated on determining the physical properties of the tubes; very little is known about the fundamental processes involved in nanotube formation. The

gas phase process for single-walled nanotube formation is very similar to many sooting combustion processes and most of the fundamental kinetic and transport processes involved are expected to be similar. By eliminating the uncontrolled effects of buoyancy, we believe that microgravity experiments could substantially increase the fundamental knowledge of nanotube formation and lead to the development of both better nanotubes and production processes.

References

The following review and references therein provide a good introduction into the current issues in carbon nanotube production and their applications.

1) Yakobson, B. I. and R.E. Smalley (1997), "Fullerene Nanotubes, $C_{1,000,000}$ and Beyond", *American Scientist* **85**, pp. 324-337.

S96-26

Synthesis of graphite encapsulated metal nanoparticles and metal catalyzed nanotubes

R. L. Vander Wal[1] and V. P. Dravid[2]; [1]NCMR at NASA-Lewis, Cleveland OH 44135, [2]Northwestern University, Evanston IL 60208.

INTRODUCTION

This work focusses on the growth and inception of graphite encapsulated metal nanoparticles and metal catalyzed nanotubes using combustion chemistry. Deciphering the inception and growth mechanism(s) for these unique nanostructures is essential for purposeful synthesis [1-8]. Detailed knowledge of these mechanism(s) may yield insights into alternative synthesis pathways or provide data on unfavorable conditions. Production of these materials is highly desirable given many promising technological applications [9-17].

SIGNIFICANCE

The technological promise of these materials stems from their unique structure. In graphite encapsulated metal nanoparticles, the protective graphite coating provides immunity to most environments while allowing retention of their magnetic properties [4,7,9,10]. Interest in the iron group metals is particularly high because they can be encapsulated in metallic form as single magnetic domains [9]. Such encapsulated ferromagnetic metals should have interesting properties and commercially valuable applications, ranging from magnetic data storage and ferrofluids to biomedical applications [10]. Metal catalyzed nanotubes can be used as supports for metal catalysts which are deposited upon the surface [11]. Because of their mesoscopic structure, nanotubes may exhibit quantum effects arising from their small diameter, < 10 nm [15]. Theoretical calculations of their electronic structure indicate that single-walled nanotubes are either metallic conductors, or semiconductors, depending on the diameter and helicity of the individual tubes [16]. Filled with metals or semiconductors, nanotubes may well provide components for nanoscale electrical or electronic devices such as amplifiers, switches or electrical-mechanical converters [17].

To-date, the primary vehicles for synthesis of these novel materials has been an electric arc discharge or high temperature furnace. While possessing great potential for new discoveries, a shared deficit of traditional methods is the occurrence of several simultaneous processes coupled through buoyancy. The proposed experiments seek to eliminate this shortcoming by controlled experiments in microgravity. The advantage that microgravity confers is the independent control of temperature and residence times, variables normally coupled and controlled by buoyancy, for synthesis of these nanostructures.

OBJECTIVE

The proposed work seeks to vary metal nanoparticle residence times in controlled temperature and chemical environments. Systematic variation of these parameters will be used to achieve different levels of encapsulation or nanotube growth. These measurements are expected to also lead to identification of optimum gas-phase parameters for synthesis of carbon encapsulated metal nanoparticles or fullerenic nanotubes as judged by characterization of their

morphology, chemistry and crystallography. As a secondary objective, the kinetics of the encapsulation process and nanotube growth will be sought.

APPROACH

Hydrocarbon flames will be used to supply the carbon source. Variation of the stoichiometry and flame temperature will be used to control the local gas-phase chemistry. Both the species available for decomposition for metal carbide formation and the temperature govern the growth rate and quality of the graphitic layers associated with the nanostructure. These same parameters are also central to graphitic layer plane growth of carbon aerosols (soot) via molecular addition of small PAHs and other hydrocarbons (such as acetylene). Judicious control of these parameters can not only alleviate deposition of amorphous carbon but also facilitate formation of regular graphitic layers in these novel structures through termination of energetically unfavorable dangling bonds. Additionally, an alternative pathway for regular graphitic layer plane formation is available for catalytically inactive metals via the repetitive addition of acetylene and small PAHs, analogous to soot growth via the celebrated HACA mechanism [18].

The first stage of the research will focus on production of metal nanoparticles.

Particle and aggregate size will be controlled through variation of metal precursor concentration, particle residence time, dilution after particle formation and electrostatic charging.

The next stage will investigate the overlap between metal particle production and hydrocarbon decomposition. Traditionally, significant overlap exists in these processes. These multiple concurrent processes are particularly important for synthesis of graphite-metal nanostructures. Variation of the degree of overlap will be sought to determine if concurrent hydrocarbon decomposition/deposition upon the nucleating metal particle (hence partial carbide formation) can alter the particle growth process or level of aggregation. In all cases, the hydrocarbon will be a minor component in the metal precursor/diluent (carrier) + hydrocarbon mixture. This will ensure that metal nucleation dominates any metal particle catalyzed nanostructure growth process. Tests for effects of partial carbide formation will subsequently be made for conditions identified as fruitful and nonfruitful for purposeful nanostructure growth.

A series of fuel mixtures and temperatures will be used to create a broad range of chemical environments. The range of fuel mixtures will be used to systematically vary the C/H ratio of the fuel mixture. Concentrations within an inert carrier will be varied to achieve different growth rates. Post-synthesis treatment via oxidation will be considered to remove amorphous carbon deposits. Material samples for TEM analysis will be collected through sampling of the nanostructures. A combination of TEM, HRTEM imaging, diffraction and analytical nanoscale spectroscopies will be used to provide morphological, structural, chemical and electronic information about these unique graphitic-metal nanostructures.

ACKNOWLEDGEMENTS

This work is supported under NASA cooperative agreement NCC3-544.

REFERENCES

1. Seraphin, S., J. Electrochem. Soc. 142:290 (1995).
2. Saito, Y., Carbon 33:979 (1995).
3. Seraphin, S., Zhou, D. and Jiao, J., J. Appl. Phys. 80:2097 (1996).
4. Host, J. J., Teng, M. H., Elliott, B. R., Hwang, J.-H., Mason, T. O. Johnson, D. L. and Dravid, V. P., J. Mater. Res. 12:1268 (1997).
5. Lin, X., Wang, X. K., Dravid, V. P., Chang, R. P. H. and Ketterson, J. B., J. Appl. Phys. 64:181 (1994).
6. Setlur, A. A., Lauerhass, J. M., Dai, J. Y. and Chang, R. P. H., Appl. Phys. Lett. 69:345 (1996).
7. Jiao, J., Supapan, S., Wang, X. and Withers, J. C., J. Appl. Phys. 80:103 (1996).
8. Dai, J. Y., Lauerhaas, J. M., Setlur, A. A. and Chang, R. P. H., Chem. Phys. Lett. 258:547 (1996).
9. Seshadri, R., Sen, R., Subbanna, G. N., Kannan, K. R., and Rao, C. N. R., Chem. Phys. Lett. 231:308 (1994).
10. a) McHenry, M. E., Majetich, S. A., Artman, J. O., DeGraef, M. and Staley, S. W., Phys. Rev. B49:11358 (1994). b) McHenry, M. E., Majetich, S. A. and Kirkpatrick, E. M., Mater. Sci. Eng. A204:19 (1995).
11. Planeix, J. M., Coustel, N., Coq, B., Brotons, V., Kumbhar, P. S.,Dutartre, R., Gneste, P., Bernier, P. and Ajayan, P. M., J. Am. Chem. Soc. 116:7935 (1994).
12. Ajayan, P. M., Ebbesen, T. W., Ichihashi, T., Iijima, S., Tanigaki, K. and Hiura, H., Nature 362:522 (1993).
13. Rodriguez, N. M., Kim, M. S., Downs, W. B. and Baker, R. T. K., in Carbon Fibers, Filaments and Composites, (J. L. Figueiredo, C. A. Bernaardo, R. T. K. Baker and K. J. Huttinger eds.) NATO ASI Series (Kluwer Academic Publishers, Dordrecht, The Netherlands, 1987) Vo. 177.
14. Treacy, M. M. J., Ebbesen, T. W. and Gibson, J. M., Nature 381:678 (1996).
15. Murakami, Y., Shibata, T., Okuyama, K., Arai, T., Suematsu, H. and Yoshida, Y., J. Phys. Chem. Solids, 54:1861 (1993).
16. Saito, R., Fuijita, M., Dresselhaus, G. and Dresselhaus, M. S., Appl. Phys. Lett. 60:2204 (1993).
17. Proceedings of the Electrochemistry Society, San Francisco, CA, USA 22-27 May 1994 eds: K. M. Kadish, and R. S. Ruoff. Electrochemical Society, Pennington, NJ p. 1414.
18. Frenklach, M., Wang, H. and Rabinowitz, M. J., Prog. Energy Combust. Sci. 18:47 (1992). b. Frenklach, M. and Wang, H., Twenty-Third Symposium (International) on Combustion, The Combustion Institute p. 1559 (1990).

597-29

THE EFFECTS OF GRAVITY ON COMBUSTION AND STRUCTURE FORMATION DURING SYNTHESIS OF ADVANCED MATERIALS*

A. Varma, A. Pelekh and A. Mukasyan
Department of Chemical Engineering
University of Notre Dame
Notre Dame, IN 46556

Introduction

Combustion in a variety of heterogeneous systems, leading to the synthesis of advanced materials [1-4], is characterized by high temperatures (2000-3500 K) and heating rates (up to 10^6K/s) at and ahead of the reaction front. These high temperatures generate liquids and gases which are subject to gravity-driven flow. The removal of such gravitational effects is likely to provide increased control of the reaction front, with a consequent improvement in control of the microstructure of the synthesized products. Thus, microgravity experiments can lead to major advances in the understanding of fundamental aspects of ***combustion*** and ***structure formation*** under the extreme conditions of the combustion synthesis wave. In addition, the specific features of microgravity environment allow one to produce ***unique materials***, which cannot be obtained under terrestrial conditions.

The general ***goals*** of the current research are: 1) to improve the understanding of fundamental phenomena taking place during combustion of heterogeneous systems, 2) to use low-gravity experiments for insight into the physics and chemistry of materials synthesis processes, and 3) based on the obtained knowledge, to optimize processing conditions for synthesis of advanced materials with desired microstructures and properties.

This research follows logically from the results of investigations we have conducted in the framework of our previous grant (NASA NAG 3-1644, Combustion Science) on gravity influence on ***combustion synthesis*** (CS) of gasless systems. Prior work, by others and by us, has clearly demonstrated that gravity plays an important role during combustion synthesis of materials. The immediate tasks for the future are to ***quantitatively*** identify the nature of observed effects, and to create accurate ***local kinetic models*** of the processes, which can lead to a control of the microstructure and properties of the synthesized materials. In summary, this is the ***value*** of the proposed research. Based on our prior work, we focus on the following fundamental aspects of combustion and structure formation under the unique condition of ***microgravity***.

Investigation of New Phenomena in Gasless Combustion of Low Density Mixtures

Our preliminary results show that gravity significantly influences the combustion behavior of heterogeneous reaction mixtures. For example, in the Ni+Al system under 1-g, the combustion front propagates with an average velocity U_c ~1.6 cm/s, while in microgravity U_c was about 5 cm/s, that is more than ***3 times higher*** than in normal gravity [5]. Also, we observed that during combustion of loose Ni/Al cladded particles, the combustion front propagates much more steadily under microgravity [6]. The data demonstrate that in 1-g, the width of distribution

* Work funded under NASA Grant NAG3-2213

of the instantaneous velocities is ***large*** (σ_U ~0.4cm/s), while in microgravity σ_U is ***4 times smaller*** (~0.1cm/s; see also Fig.1).

These dramatic changes in combustion behavior may be explained by a ***change*** in the primary ***mechanism of heat transfer*** in the heterogeneous reaction medium. This may take place in the following cases of gasless CS [7]: (i) high sample density, where heat conduction through the essentially poreless medium controls the wave propagation process; (ii) very high porous mixtures, where radiation becomes the main mechanism of heat transfer. We believe that the latter condition was achieved under μg in the experiments discussed above. A detailed study of these new phenomena, which can be observed only in μg conditions, will improve the fundamental understanding of combustion mechanism in heterogeneous systems. Two types of mixtures will be investigated: cladded powders, where contact between reactants occurs ***within each*** particle, and mixtures of elemental powders, where ***interparticle*** contacts are necessary for the reaction.

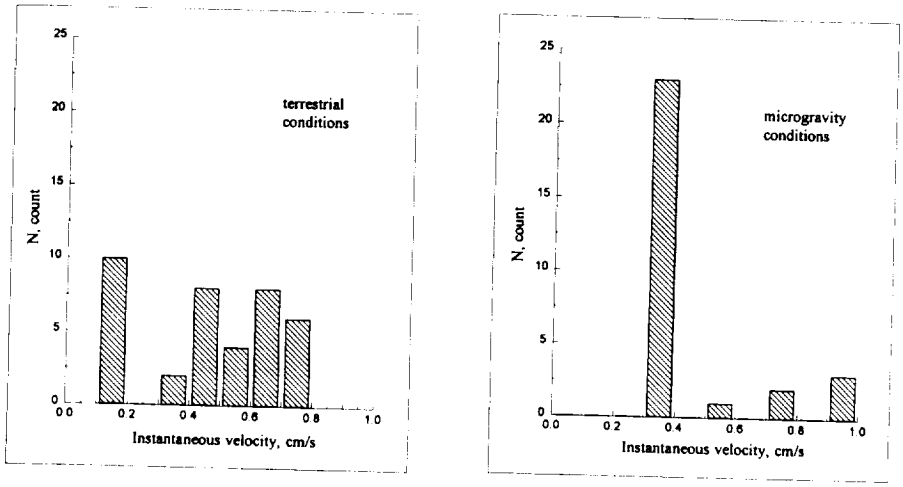

Figure 1. Distribution of instantaneous combustion velocity during reaction in Ni/Al cladded particle system.

Influence of Gravity on Solid Particle Growth in Melts during Combustion Synthesis

We have shown experimentally that in a variety of systems (e.g. Ti-C-Ni, Ti-B-Ni-Al), fine (< 0.1μm) initial grains of solid products (TiC, TiB_2) form quickly (< 0.1s) in melts (Ni, Al) of the reaction zone, followed by relatively long (minutes) process of structure transformations which take place at high temperatures reached during combustion synthesis [6,8]. The growth rate of these grains is ***4 times smaller*** in μg as compared to 1-g, thus yielding final product with finer grains that provide superior mechanical properties (Fig.2; see also [9]).

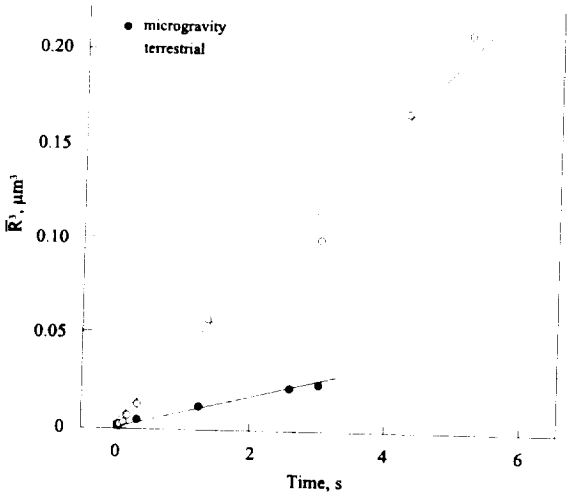

Figure 2. Evolution of TiB_2 grain size (R) during combustion synthesis of (Ti+2B)-(3Ni+Al) system in different gravity conditions.

It is known that when solid and liquid phases coexist for some period, microstructural changes can occur following two different mechanisms [10]. In one, larger particles grow at the expense of smaller ones, so as to lower the free energy of a system (***Ostwald ripening effect***), and in the second, grain growth is controlled by the process of

solid particle ***coalescence*** following collision of the particles. It is interesting that in ***both*** cases, the cube of particle radius is proportional to time of coarsening (Fig.2). Thus, the observed differences in growth rates of solid grains (e.g. TiB_2) in liquid matrix (e.g. Ni_3Al) in 1-g and μg conditions can be explained by the influence of gravity on these mechanisms. Indeed, both mechanisms of particle coarsening require mass transport (diffusion) from one grain to another, which can be influenced by gravitationally induced flow (natural convection) of liquid between particles.

Based on the ***hypothesis*** that these mechanisms govern structure formation during CS in many systems, a systematic study is planned to understand the fundamentals and to control the particle growth phenomenon. Precise microgravity experiments will be conducted for this purpose. Several industrially important composites will be investigated (TiC-Ni; TiB_2-Ni_xAl, where x=1 or 3).

References

1. Munir, Z.A., and Anselmi-Tamburini, U., "Self-Propagating Exothermic Reactions: The Synthesis of High-Temperature Materials By Combustion," *Mater. Sci. Reports*, **3**, 277 (1989).
2. Merzhanov, A.G., "Self-Propagating High-Temperature Synthesis: Twenty Years of Search and Findings," In *Combustion and Plasma Synthesis of High-Temperature Materials*, edited by Z. A. Munir and J. B. Holt, New York: VCH Publishers, 1 (1990).
3. Moore, J.J., and Feng, H.J., "Combustion Synthesis of Advanced Materials," *Prog. Mater. Sci.*, **39**, 243 (1995).
4. Varma A., Rogachev A.S., Mukasyan A.S., Hwang S., "Combustion Synthesis of Advanced Materials: Principles and Applications" , *Advances in Chemical Engineering*, **24**, 79 (1998).
5. Mukasyan A.S., Pelekh A., Varma A., Rogachev A.S., and Jenkins A., " The Effects of Gravity on Combustion Synthesis in Heterogeneous Gasless Systems ", *AIAA Journal*, **35**, 1821 (1997).
6. Mukasyan A.S., Pelekh A., Varma A.,"Combustion Synthesis in Gasless Systems under Microgravity Conditions", *J. Mater. Synth. Proc.*, **5**, 391 (1997).
7. Hwang, S., Mukasyan, A.S., Rogachev, A.S., and Varma, A., "Combustion Wave Microstructure in Gas-Solid Systems: Experiments and Theory," *Combust. Sci. Tech.*, **123**, 165 (1997).
8. Varma A., Mukasyan A.S., Pelekh A., "The Effects of Gravity on Combustion and Structure Formation during Combustion Synthesis in Gasless Systems," *International Microgravity Combustion Workshop,* NASA, Cleveland, Ohio, 31 (1997).
9. Evans A.G., *Ceramic Containing Systems: Mechanical Aspects of Interfaces and Surfaces*, Noyes Publications, Park Ridge, N.J. (1986).
10. German R.M., *Liquid Phase Sintering*, Plenum Press, New York (1985).

Laminar Diffusion Flames

S78-25

NUMERICAL STUDY OF BUOYANCY AND DIFFERENTIAL DIFFUSION EFFECTS ON THE STRUCTURE AND DYNAMICS OF TRIPLE FLAMES

J.-Y. Chen[1] and T. Echekki [2], [1]6163 Etcheverry Hall, University of California at Berkeley, Berkeley, CA 94720, jychen@newton.me.berkeley.edu, [2]Combustion Research Facility, Sandia National Labs., Livermore, CA 94550, techekk@ca.sandia.gov.

INTRODUCTION

Triple flames arise in a number of practical configurations where fuel and oxidizer are partially premixed, such as in the base of a lifted jet flame (e.g., Phillips, 1965; Chung and Lee, 1991). Past experimental studies, theoretical analyses, and numerical modeling of triple flames suggested the potential role of triple flames in stabilizing turbulent flames and in promoting flame propagation (Buckmaster and Matalon 1988; Hartley and Dold, 1991; Kioni, et al, 1993; Lee et al, 1994; Ruetsch, et al 1995; Domingo and Vervisch, 1996). From recent numerical simulations of laminar triple flames, a strong influence of differential diffusion among species and heat on the triple flame structure has been gradually appreciated (Vedarjan and Buckmaster, 1998; Plessing et al, 1998; Daou and Linan, 1998; Echekki and Chen, 1998). This paper reports preliminary numerical results on the influence of gravity and differential diffusion effects on the structure and dynamics of triple flames with a one-step global irreversible chemistry model.

NUMERICAL SIMULATION

As a first step, Direct Numerical Simulations (DNS) of triple flames have been conducted using a one-step irreversible reaction between fuel and oxidizer for revealing the salient features of triple flames subject to different conditions. The one-step chemical model is described by

$$F+O \rightarrow P, \tag{1}$$

where the stoichiometric coefficients are unitary for simplicity. The reaction rate has the Arrhenius form

$$\dot{w} = A\rho Y_F \rho Y_O \exp\left(-\frac{T_a}{T}\right), \tag{2}$$

where T_a is the activation temperature and A is the pre-exponential factor. With the non-dimensional temperature (θ), heat release parameter (α), Zeldovich number (β), and reduced pre-exponential factor (Λ),the above reaction rate can be expressed as

$$\dot{w} = \Lambda\rho Y_F \rho Y_O \exp\left(-\frac{\beta(1-\theta)}{1-\alpha(1-\theta)}\right), \tag{3}$$

where $\theta = (T-T_0)/(T_f-T_0)$, $\alpha = (T_f-T_0)/T_f$, $\beta = \alpha T_a/T_f$, and $\Lambda = A\exp(-\beta/\alpha)$ with T_f being the adiabatic flame temperature at the stoichiometric and T_0 being the inlet temperature. The compressible Navier-Stokes equations along with the conservation equations for reactants are solved in a two-dimensional domain. Spatial derivatives are approximated by a sixth-order compact difference algorithm and the equations are integrated in time with a third-order Runge-Kutta scheme. Boundary conditions are specified using the Navier-Stokes Characteristic Boundary Conditions (NSCBC) (Poinsot and Lele, 1992). A uniform inflow velocity is prescribed at the bottom of the computational domain (See Fig. 1). An outflow boundary condition is

specified at the top and non-reflective boundary conditions are imposed on all sides. The mass fraction distributions of fuel and oxidizer at the inflow boundary are specified as

$$Y_F = \frac{1}{2}\left[1 - erf(\frac{x}{W})\right] \quad \text{and} \quad Y_O = \frac{1}{2}\left[1 + erf(\frac{x}{W})\right], \tag{4}$$

where *erf* is the error function, x is the horizontal coordinate with zero at the middle, and W is the characteristic mixing width. In this study, we assign α=0.85, β=8, and the mixing width being four times of the planar laminar flame thickness at equivalence ratio of 1. The DNS were carried out with a uniform grid of 121x241 (vertical x horizontal).

RESULTS AND DISCUSSIONS

The computed flame structure of a typical triple flame is illustrated in Figure 1 showing the temperature field, the fuel consumption rate, an overlay of reaction rate and temperature contours, and the fuel concentration. The arrows represent the local velocity vectors and their lengths are proportional to the magnitude. Several salient features of a triple are seen in the result and they are consistent with past experimental and numerical results. First, the reaction zone consists of three branches: one rich premixed branch on the left, one lean premixed branch on the right, and a diffusion flame in the middle. Second, the burning rate is most intensive at the joint of the three branches designated as the triple flame tip. Third, under the current condition, the propagating velocity at the triple flame point, V_f, is higher than that of a planar laminar flame, V_{sl}. Fourth, the flow field upstream of the triple flame exhibits a divergent pattern. The flow decelerates before the triple flame because of flow divergence effects and it accelerates above the triple flame tip as dilatation effect becomes dominant.

The above results serve as a base line for comparison with triple flames under the influence of gravity and differential diffusion. Figure 2 presents such a comparison of fuel consumption rates under the influence of gravity and differential diffusion. The color scales correspond to values normalized by the maximum. The gravity force is pointed downward in the figure. The Froude number based on the mixing width and the laminar flame speed under normal gravity is assigned unity. While the Lewis number (thermal diffusivity/mass diffusivity) of oxidizer is kept at unity, the Lewis number of fuel is changed from 1 to 0.4 and 2.0 to illustrate the differential diffusion effects. As revealed in the figure, buoyancy enhances the flow acceleration above the triple flame tip as density decreases by a factor of about 6.5. In comparison with the triple flame at zero gravity, buoyancy reduces the size of triple flame and decreases the propagation speed. The effect of Lewis number is shown in the lower two plots revealing that the shape of reaction zone becomes asymmetric when the Lewis number of fuel deviates from unity. The propagating speed decreases when the Lewis number is greater than one and increases when the Lewis number is less than one. This trend is consistent with the results from laminar premixed flame studies. The combined effects of Lewis number and gravity force with realistic chemistry will be investigated in future work.

ACKNOWLEDGMENTS

This work is currently supported by NASA Lewis Center Microgravity Combustion Sciences under the technical monitoring of Uday Hegde.

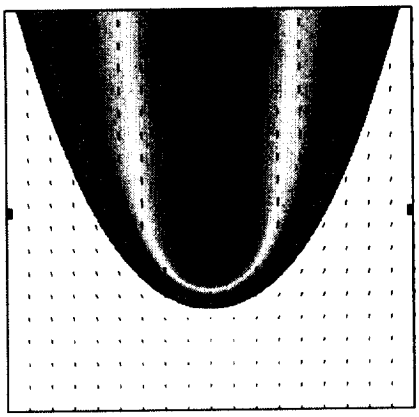

Temperature

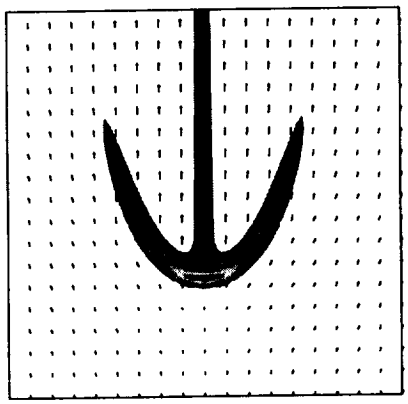

Fuel consumption rate

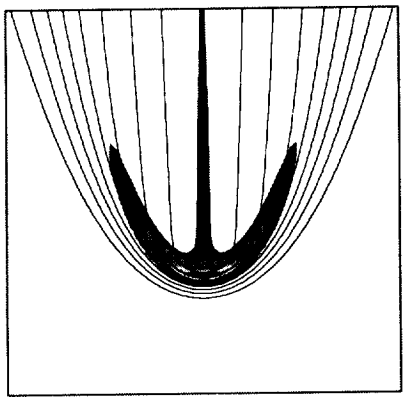

Fuel Consumption rate overlaid by constant temperature contours

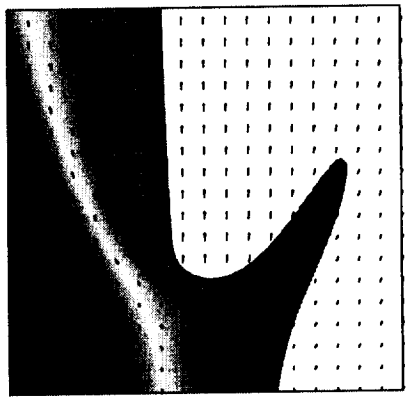

Fuel mass fraction

Figure 1: Results from Direct Numerical Simulation (DNS) of a triple flame with one-step global chemical reaction revealing salient characteristics

REFERENCES

Buckmaster, J. and Matalon, M. 22nd *Symposium (Int.) on Combustion,* pp. 1527-1535, 1988.
Chung, S.H. and Lee, B.J. , *Combust. Flame*, 86:62-72. (1991).
Daou, J, and Linan, A, *Combustion Theory and Modeling*, 2:449-477 (1998).
Echekki, T. and Chen, J.H., *Combust. Flame*, 114:231-245 (1998).
Hartley, L.J. and Dold, J.W., *Combust. Sci. and Tech* 80:23-46 (1991).
Kioni, P.N., Rogg, B., Bray, N.C., and Linan, A., *Combust. Flame* 95:276-290 (1993).
Lee, B.J., Kim, J.S., and Chung, S.H., *25th Symposium (Int.) on Combustion,* pp. 1175-1181, 1994.

Poinsot, T and Lele, S., *J. Computational Physics*, 101:104-129 (1992).
Phillips, H., *10th Symposium (Int.) on Combustion*, pp.1227-1283, 1965.
Ruetsch, G.R., Vervisch, L. and Linan, *A., Phys. Fluids*, 7(6):1447-1454 (1995).
Domingo, P., and Vervisch, L., *26th Symposium (Int.) on Combustion*, pp.233, 1996.
Plessing, T., Terhoeven, P., Peters, N., and Mansour, M.S., *Combust. Flame* 115:335-353 (1998).
Vedarjan, T.G., and Buckmaster, J., *Combust, Flame* 114:267-273 (1998).

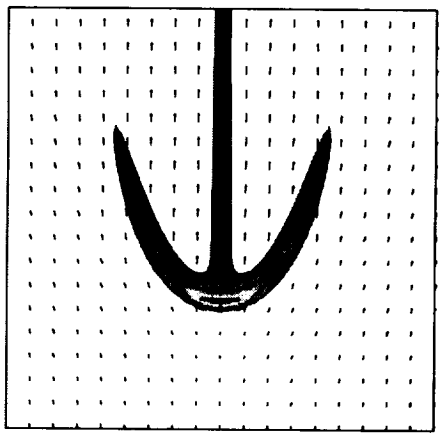

Le=1.0 Zero Gravity
V_f/V_{sl}=1.92

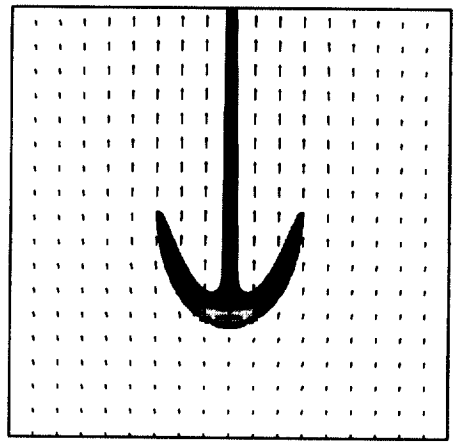

Le=1.0 Gravity Force Pointed Downward
V_f/V_{sl}=1.26, Fr=1.0

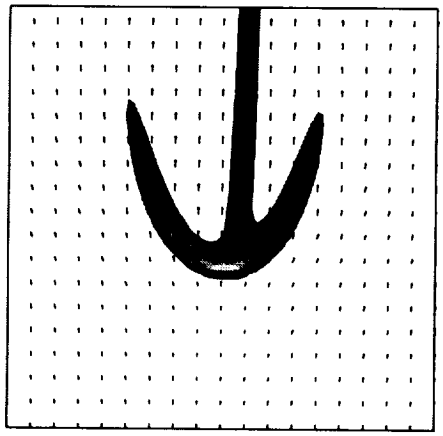

Le=2.0 Zero Gravity
V_f/V_{sl}=1.20

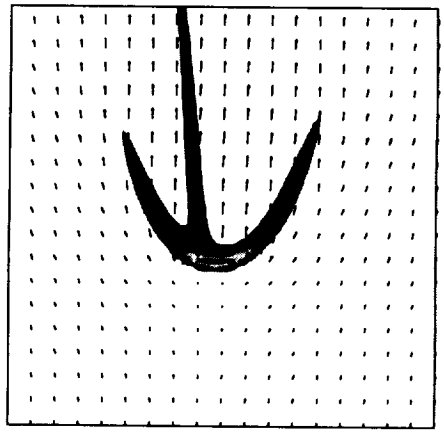

Le=0.4 Zero Gravity
V_f/V_{sl}=3.07

Figure 2: Results from Direct Numerical Simulation of triple flames with one-step global chemical reaction showing the influence of gravity force and differential diffusion.

Studies on the Behavior of Highly Preheated Air Flames in Microgravity

Ashwani K. Gupta
University of Maryland
Department of Mechanical Engineering
College park, MD 20742
e-mail: akgupta@eng.umd.edu

599-29

Summary

This study is directed at examining the global flame behavior of highly preheated air flames under microgravity conditions using methane, ethane and propane as the fuels. Specific focus will be on determining the global flame features, time resolved spatial emission of OH, CH and C_2 from flames, spatial distribution of flame flicker, flame radiation and spatial distribution of temperature (using micro-thermocouples and optical pyrometer) and vibrational temperature (calculated by comparing two different C_2 bands) as affected by microgravity, combustion air preheat temperature, fuel type and flame equivalence ratio. Highly preheated air combustion is extremely important in practice as it can reduce fuel consumption by up to about 30%, reduce the equipment size, and reduce pollutants emission (including NO_x and CO_2) and by about 20-30% without any adverse effect on thermal loading or performance of the system. In order to explore the potential of highly preheated low oxygen concentration air combustion we propose to examine the fundamental differences in the behavior of these flames at normal and microgravity conditions as compared to the flames obtained with normal temperature air or slightly preheated air.

The flowing gas mixture of N_2 and O_2 at room temperature will be preheated to any temperature up to about 1200° C in an experimental facility. This degree of air preheat in the furnace is commensurable with that used in many regenerative furnaces. The fuel maintained at near room temperature, will be injected into the combustion chamber. The facility will allow controlled variation of the air preheat temperature, fuel type, injector geometry, O_2 concentration in air and mixture stoichiometry in the test section of the combustion chamber. The test section will be optically accessible for providing the desired optical diagnostics of the flames. The methane fuel simulates well the behavior of natural gas fueled flames while propane fuel simulates LPG and most liquid fueled flames without the added complexity of droplet formation and evaporation. The choice of ethane fuel is due to the availability of flame behavior with normal air at room temperature under microgravity conditions, in addition to the role of type of hydrocarbon fuel. Flame plume behavior is available with the above three fuels at reduced gravity using normal room temperature air. We propose to examine the flame behavior with unheated, moderately heated and highly preheated air having normal (21% oxygen) and low oxygen concentration (down to about 2%) at microgravity conditions.

Specific measurements to be made here at normal or microgravity conditions include: flame size and shape, vibrational flame temperature, time resolved spatial emission of OH, CH and C_2 , spatial distribution of flame flicker and flame heat flux. This data will then be analyzed to determine the role of microgravity on the flame behavior. The systematic data to be obtained here will allow most desirable flame characteristics to be achieved with a given fuel at any equivalence ratio, including the case of ultra fuel-lean combustion conditions. In some applications high flame radiations are important while in others a blue flame is desired. Our studies will provide means of controlling the flame signatures and flame radiation in addition to providing a database for model validation and model development.

NEAR-LIMIT, HIGH-PRESSURE SPHERICAL FLAME PROPAGATION IN MICROGRAVITY

5/0029

C. K. Law, S. D. Tse, and D. L. Zhu
Department of Mechanical and Aerospace Engineering
Princeton University, Princeton, NJ 08544 USA

Overview

Recognizing that combustion processes within internal combustion engines take place in elevated pressure environments, that most fundamental information on the aerothermochemistry of flames were obtained at substantially lower pressures, and that the chemical reaction mechanisms which govern the various flame processes are inherently nonlinear which can cause non-monotonic variations of the combustion responses with pressure, the proposed program aims to obtain fundamental understanding and useful data on flame propagation, extinction, and stability, and to assist in the compilation of comprehensive reaction mechanisms applicable to pressures up to 60 atmospheres. The vehicle of study is the spark-ignited outwardly-propagating spherical flame in a pressurized environment. The need to conduct the experiment in microgravity arises from the interest in limit phenomena especially those associated with ultra-lean combustion, and the observation that buoyancy tends to significantly distort the flame from spherical symmetry for weakly-burning flames in elevated pressure environments.

The proposed program on near-limit and limit phenomena at elevated pressures consists of the following inter-related projects, each with its own focus and objectives: (1) Determination of the laminar flame speeds of conventional gaseous fuels by experimentally measuring the stretch-affected propagation speeds of the spherical flame and systematically subtracting out the stretch effect. (2) Determination of the corresponding Markstein times which represent the flame responsivity to influences of aerodynamic stretching and mixture nonequidiffusion. (3) Determination of the extinction limits of these aerodynamically-stretched flames, and computational assessment of the role of radiative loss in extinction and the possible extension of the fundamental flammability limits by stretch. (4) Investigation of the characteristics of the Landau-Darrieus and diffusional-thermal flamefront instabilities, including their interactions and the influence of flame wrinkling on the flame propagation rate. (5) Re-compilation of existing chemical kinetic mechanisms by using the high-pressure flame speed data as optimization points, so as to extend their applicability to higher pressure ranges.

The experiment, initially to be conducted in the drop tower, will involve optical imaging of the expanding flamefront, from which the instantaneous flame speed and stretch rate can be determined when the flame is smooth, and the nature of flamefront instability can be studied when it is wrinkled. From these data, the laminar flame speeds, the Markstein times, and the extinction states can be determined. Re-compilation of the chemical kinetic mechanism will adopt state-of-the-art optimization technique. Computational simulation and analytical modeling using detailed/simplified chemistry and transport will also be conducted, in parallel with the experimentation, in order to identify the controlling diffusive and chemical kinetic processes and factors which influence the various combustion responses.

It is anticipated that successful completion of the proposed program will represent a significant advance in our understanding of the aerodynamics and chemical kinetics of flames at high pressures.

Proposed Program

Before presenting the proposed program, it is useful to first emphasize that while the practical motivation for the proposed high-pressure research is for its relevance to internal combustion engines, there are also compelling fundamental reasons which indicate that the dependence of the various combustion responses on pressure can be very nonlinear due to the underlying chemical kinetics, and as such simple scaling is not expected to yield meaningful results. To illustrate such an influence, let us consider the well-known H-O_2 chain mechanism: (R1) $H + O_2 \rightarrow OH + O$; (R2) $H + O_2 + M \rightarrow HO_2 + M$. Here (R1) is a temperature-sensitive two-body branching reaction while (R2) is a temperature-insensitive three-body termination reaction. As such, while increasing pressure is expected to generally increase the overall reaction rate because of the dominance of (R1), the rate of increase could be substantially slowed down by (R2) because third-body reactions are favored over two-body reactions at higher pressures. Indeed, it has been found that, for sufficiently weak flames such that (R1) is slow, (R2) can become dominating and therefore lead to a slowing down of the mass burning rate of the flame with increasing pressure. The effect is particularly strong for weak flames, which is quite contrary to what is conventionally assumed. With decreasing burning rate, the flame also becomes thicker instead of thinner, and will have significant implications on the modeling of turbulent flames.

With the above illustration serving as background for the complex and nonlinear effects of pressure on the burning intensity, we now outline the proposed research for the various projects.

Determination of Laminar Flame Speeds

Ever since the recent recognition that stretch effects on measured flame speeds need to be subtracted out before the laminar flame speed s_u^o of a combustible mixture can be determined with fidelity, extensive amount of data have been collected for the s_u^o of a variety of fuels. Most of the experimental determinations have utilized the counterflow burner, although satisfactory elevated-pressure data could only be taken for pressures below six or seven atmospheres. The difficulty is that the flow becomes unstable as its Reynolds number increases with increasing pressure, and various constraints would lead to the pressure limit observed. A completely different approach is therefore needed for the high pressure studies. This has led to the present choice of the spark-ignited, outwardly-propagating flame in an enclosed chamber. Recent studies by Faeth and by Smith, at pressures slightly above atmospheric, have demonstrated the viability and versatility of this method in the determination of stretch-compensated laminar flame speeds.

The ability to determine s_u^o as discussed above implicitly assumes that the flame surface is smooth, although theoretical and experimental results have demonstrated that instabilities in the form of cells can spontaneously develop over the flame surface. There is, however, a good reason to believe that there could exist sufficient time during flame propagation before these instabilities are developed. Furthermore, the positive stretch associated with the outwardly-propagating flame also tends to suppress the development of instability. It is therefore reasonable to anticipate that

instabilities will develop only after the flame has attained a certain size and the stretch has reduced below a certain value. By then, we will have already gathered enough data to allow for the flame speed determination.

Determination of Markstein Times

It was recognized quite early that most of the laboratory and practical flames are subjected to stretch which can be manifested through flow nonuniformity, flame curvature, and flame unsteadiness.

Comprehensive theories for stretched flames have shown that the single most important parameter characterizing the dynamics of stretched flames is the Markstein time τ. Indeed, while it is well-established that the laminar flame speed s_u^o is a thermochemical property of a combustible mixture, characterizing the propagation of the one-dimensional unstretched flame, it is less well recognized that the Markstein time is another thermochemical property of the mixture which, together with s_u^o, characterizes the propagation of the stretched flame. As such, the Markstein time τ is of the same degree of importance as the laminar flame speed s_u^o in flame modeling because almost all practical flames are stretched. Thus the objective of this project is to conduct such a determination, for both atmospheric and high pressures because reliable values of this parameter are lacking. The determination is actually quite straightforward because each linear fitting between the stretched flame speed and the stretch rate yields the laminar flame speed as the y-intercept and the Markstein time as the slope.

Stretch-Affected Flammability Limits

Recognizing that the fundamental flammability limit is defined on the basis of the freely-propagating one-dimensional planar flame, and that most flames are aerodynamically stretched, it is then of interest to determine the extent to which the fundamental flammability limit can be modified by stretch. For example, if stretch increases the burning intensity of a flame, then a mixture which is beyond the limit based on the planar configuration could still be rendered to be flammable due to stretch. Thus the relevant limit depends on the application, which in most situations involves the initiation and outward propagation of spherical flames.

Experiments will therefore be conducted to map these stretch-affected flammability limits, at atmospheric pressure as well as elevated pressures. Computational simulation will also be conducted, allowing for radiative loss.

Flamefront Instabilities

Premixed flames are subjected to three sources of instability, namely the Rayleigh-Taylor instability due to density stratification in a gravity field, the Landau-Darrieus, hydrodynamic instability due to thermal expansion across the flame, and diffusional-thermal instability due to mixture nonequidiffusion.

In our microgravity experiments, we shall first determine the state at which the Landau-Darrieus and diffusional-thermal instabilities are triggered. The subsequent evolution of the cells will be imaged to identify their characteristic sizes, rates of growth, and the nature of the chaos for the diffusional-thermal cells and the extent of regularity for the Landau-Darrieus cells. We

shall simultaneously perform computational "simulation" of the phenomena, but probably only for two-dimensional flows. One-step overall reaction will be used, although with the overall activation energy extracted from the planar, one-dimensional flame.

We shall also study the enhancement of the global flame propagation speed of the wrinkled flame surface due to the increased flame surface area. Guided by analysis, we shall attempt to develop some meaningful correlation between the experimental wrinkled flame propagation speed and the cell size.

Input to the Development of Chemical Kinetic Mechanisms

An important benefit of an accurate value of s_u^o is that it can be used in the development of the chemical kinetic mechanisms of fuel/oxidizer systems. Because of the complexity of these mechanisms, the adequacy of a given mechanism is assessed by its ability to quantitatively describe as many combustion experiment/phenomena as possible. Typical of these are the ignition delay times from shock tube experiments, ignition and extinction limits from well-stirred reactors, species evolution profiles from flow reactors, ignition and extinction limits of laminar premixed and diffusion flames, and the laminar burning velocities. Furthermore, since there exist sufficient unknowns and flexibility in the data base, the reliability of individual mechanisms is only limited to the thermodynamic parametric ranges (*e.g.* mixture concentrations and pressure) of the data base upon which the mechanisms are "calibrated." Because of the intrinsic nonlinearity of the kinetic processes, application of the mechanism beyond the range of calibration could lead to quantitatively as well as qualitatively erroneous results. In this regard we note that the laminar flame speed data used in the calibration of several existing mechanisms are mainly around atmospheric pressure.

Thus the primary objective of this project is to use the high-pressure laminar flame speed data to re-assess and most likely modify existing kinetic mechanism of gaseous fuels. The method to be adopted for the optimization and compilation of kinetic mechanisms is the same as that used for the GRI-Mech. The first fuel to be studied is hydrogen because of its relative simplicity. Following this, methane, propane and other C_2 to C_4 compounds will also be studied. The potential complication from the development of flamefront instability can be mostly circumvented by changing the nature and concentration of the inert so as to modify the mixture Lewis number and steer the flame response away from developing instability. Since the role of the laminar burning velocities here is simply as a carrier of the chemical information instead of its actual utility in simulating burning conditions in practical situations, the proposed manipulation is acceptable.

5101-29

GRAVITY EFFECTS ON PARTIALLY PREMIXED FLAMES

Ishwar K. Puri[1] and Suresh K. Aggarwal[2], University of Illinois at Chicago
Department of Mechanical Engineering, Chicago, Illinois 60607-7022
[1](ikpuri@uic.edu), [2](ska@uic.edu).

INTRODUCTION

Partially premixed flames can be established by design by placing a fuel-rich mixture in contact with a fuel-lean mixture, but these flames also occur otherwise in many practical systems. For instance, initially nonpremixed combustion may involve regions of local extinction followed by partial premixing and re-ignition [1]. Likewise, partial premixing is an important process in nonpremixed flame liftoff phenomena, since the reactants can mix slightly prior to ignition [2, 3]. Nonuniform evaporation in spray flames can also result in local fuel-rich regions in which burning occurs in the partially premixed mode and the technique of lean direct injection used to achieve stable combustion and reduced pollutant levels involves regions of partially-premixed combustion. In addition, unwanted fires can originate in a partially premixed mode when a pyrolyzed or evaporated fuel forms an initial fuel-rich mixture with the ambient air.

Under normal-gravity conditions the flame heat release produces both flow dilatation and buoyancy effects in partially premixed flames. Gas expansion due to the heating causes downstream motion normal to the flamefront. The buoyant gases accelerate the flow in an opposite direction to the gravity vector, causing air entrainment that enhances the fuel-air mixing and, consequently, influences the upstream region. While it is possible to minimize gravitational effects in a premixed flame by isolating buoyancy effects to the lower-density post-flame region or plume, it is not so straightforward to do so in nonpremixed flames. Several investigations have established that partially premixed flames can contain two (even, three) reaction zones (e.g., Refs. 4-8), one with a premixed-like structure and the other consisting of a transport-limited nonpremixed zone (in which mixing and entrainment effects are significant). For these reasons it is important to understand the interac-

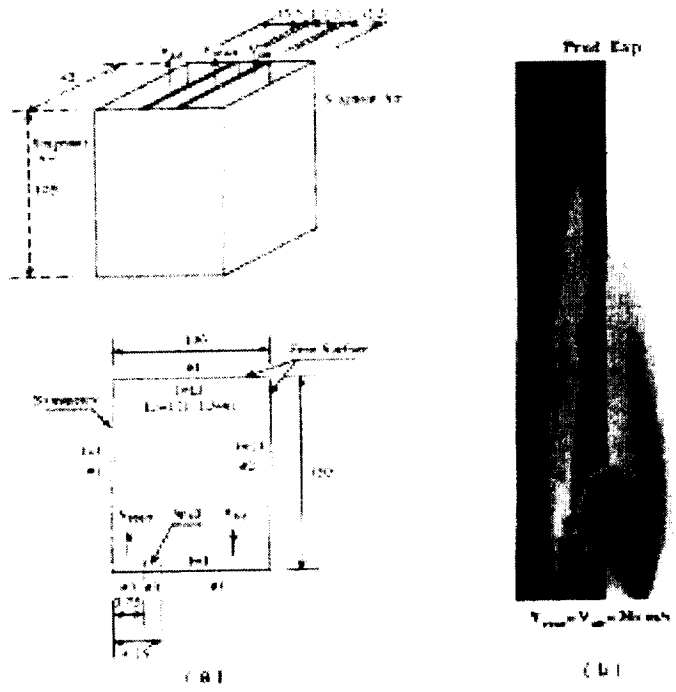

Figure 1: (a) Schematic diagram of the burner and computational domain. (b) Comparison of the simulated heat release with the C_2-chemiluminescence image for a 1-g flame established at $\phi = 2$, and $V_{reac} = V_{air} = 30$ cm s^{-1}.

tion between flow dilatation and buoyancy effects in partially premixed flames. This investigation compares the results obtained from numerical computations of two-dimensional partially premixed methane-air flames established under both normal and zero gravity conditions.

This investigation pertains to partially premixed flames established on a rectangular Wolfhard-Parker slot burner that is schematically depicted in Fig. 1(a) and described elsewhere [9]. A fuel-rich mixture is introduced from the inner slot, and air from either side of it. Identical two-dimensional flames are established on either side of the centerline.

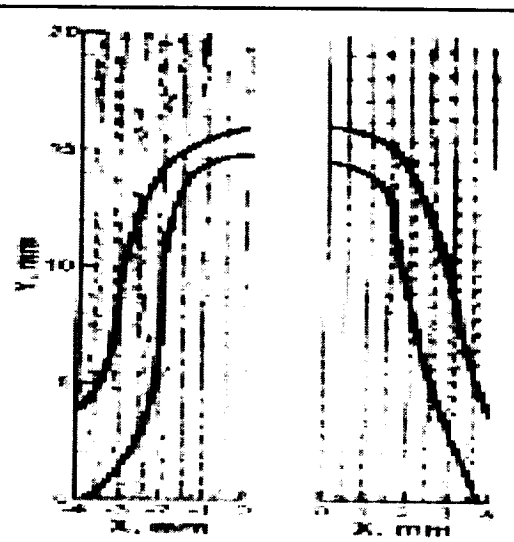

Figure 2: Comparison of the measured and predicted velocity vectors for the flame. The corresponding flame interfaces are superimposed.

The combustion process is simulated by employing a detailed numerical model based on the solution of time-dependent governing equations for a two-dimensional reacting flow. Further details about the numerical procedure and the treatment of boundary conditions are provided in earlier publications [10-12]. A relatively detailed 17-species, 52-step C_1-mechanism is used to represent the CH_4-air chemistry [13].

RESULTS AND DISCUSSION

The simulations are validated by comparing the predicted heat release profile with the experimentally obtained chemiluminescent emission due to excited-C_2^* free radical species from a representative flame established under normal gravity conditions (cf. Fig. 1(b)). Images of the (1,0) C_2 Swan band (at a wavelength of 473 nm [27]) are obtained through a narrow wavelength interference filter (470 ± 10 nm). The emission can be interpreted as a signature of chemical reaction and heat release [9, 14-16], since the excited C_2^* free radical species is short-lived, a good indicator of the reaction zone and its light intensity is known to vary linearly with the volumetric heat release. The chemiluminescence images are directly proportional to the C_2^* formation rates and, thus, serves as a qualitative rate measure of the flame chemistry [15].

Figure 1(b) contains a comparison between the predicted heat release rate and the experimentally-obtained emission image for a representative 1-g methane-air flame established at an equivalence ratio $\phi = 2$, and air and reactant velocities (respectively, V_{air} and V_{reac}) of 30 cm s^{-1}. Both the simulated heat release and the C_2^*-emission signal are confined to two relatively thin sheet-like reaction zones, one each on the rich and lean sides of the flow. The simulation and experiment show excellent agreement with respect to the spatial location of the reaction zones. Combustion proceeds in two distinct separated reaction zones, one an inner premixed flame and the other an outer nonpremixed flame. The highest temperatures occur in the outer flame. The chemistry is frozen in the region between the inner and outer reaction zones despite the high temperatures there due to a local scarcity of hydroxyl radicals that are required to oxidize the intermediate species CO and H_2, which are formed in the inner (premixed-like) reaction zone.

The computed velocity field is compared with measurements obtained using particle image velocimetry. Figure 2 compares the measured and computed velocity vectors in the 1-g flame discussed in the context of Fig. 1(b). The flame interface separates smaller velocity magnitudes on the reactant side from larger values on the partially burned side in both sets of data. The measured and predicted results are in excellent agreement. Flow dilatation due to the inner flame heat release causes the velocity vectors to move away from the centerline. The experimental data are sparse in some post-flame regions, since dilatation reduces the particle seed densities in those areas considerably. Consequently, there is some discrepancy in the comparison in the post-flame region due to experimental uncertainties.

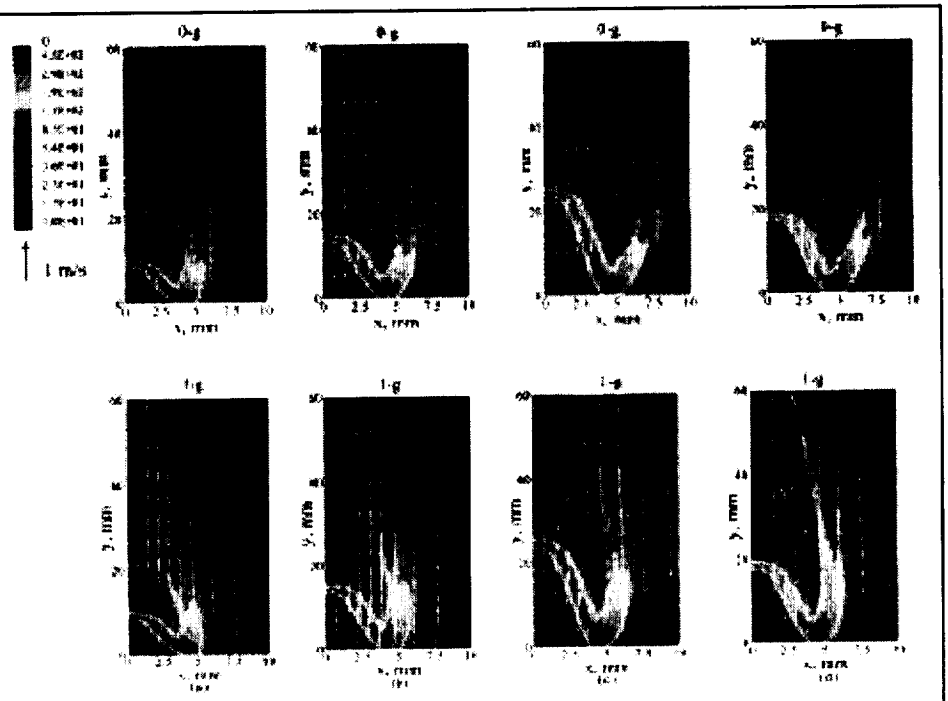

Figure 3: Heat release rate contours and velocity vector plots for several normal- and zero-gravity flames (for all of the cases V_{air} = 30 cm/s): (a) V_{reac} = 20 cm/s, ϕ = 2.0; (b) V_{reac} = 30 cm/s, ϕ = 2.0; (c) V_{reac} = 50 cm/s, ϕ = 2.0; and (d) V_{reac} = 30 cm/s, ϕ = 2.5.

Figure 3 depicts the normal- and zero-gravity flame structures for different values of V_{reac} and ϕ. For both the 1-g and 0-g flames, the inner and outer reaction zone heights increase as either or both of the reactant velocity and the equivalence ratio are increased. The dependence of the inner flame height on the reactant velocity is attributable to the residence time, since the chemical reaction time essentially depends only on the equivalence ratio. Consequently, the premixed reaction zone moves to increasingly higher axial locations as V_{reac} is raised. On the other hand, the chemical reaction time also increases as ϕ is increased and, consequently, the inner flame height increases. The increase in the outer flame height with larger reactant velocities is attributed to two factors: (1) Due to the strong synergistic interactions between the two flames, the outer flame height increases with the inner flame height; (2) Larger values of V_{reac} enhance the advection fluxes of CO and H_2 (that are provided by the inner reaction zone and serve as intermediate fuels) that move the outer flame farther downstream in the axial direction.

The presence of gravity reduces the spatial separation between the inner and outer reaction zones and, thereby, enhances the interaction between these regions. While the inner flame characteristics are essentially unaffected by gravity, the outer flame shows a strong sensitivity to grav-

ity. For all the cases considered, the presence of gravity makes the outer flame more compact, taller, and closer to the inner flame. In addition, the outer flames exhibit weaker reaction rates at their tips at zero-gravity as compared to their 1-g counterparts. This is apparently caused by the relatively enhanced diffusive fluxes downstream of the inner premixed zone compared to the reduced advection fluxes in the outer region for the 0-g flames.

While the advection of H-atoms in the region of the inner reaction zone is similar for both the 1- and 0-g flames, it is markedly dissimilar in the region of the outer reaction zone. Therefore, buoyant transport enhances radical advection into the outer reaction zone. In contrast, the flux of radical species into the outer reaction zone of the zero-gravity flame is smaller and, consequently, the reactant residence times are larger in the outer zone of that flame. The advective flux of the various species in the region contained between the inner and outer reaction zones is much larger at normal gravity and, consequently, the separation between the inner and outer reaction zones is smaller at 1-g. In general, buoyancy effects increase the advection of all species. Therefore, the 1-g flames exhibit larger emission of unburned intermediates, such as CO and H_2.

REFERENCES

1. Peters, N., Twentieth Symposium (International) on Combustion, The Combustion Institute, pp. 353-360, 1984.
2. Smooke, M. D., Seshadri, K., and Puri, I. K., Twenty-second Symposium (International) on Combustion, The Combustion Institute, pp. 1555-1563, 1988.
3. Rogg, B., Behrendt, F., and Warnatz, J., Twenty-first Symposium (International) on Combustion, The Combustion Institute, Pittsburgh, 1986, p. 1533.
4. Yamaoka, I., and Tsuji, H. Fifteenth Symposium (International) on Combustion, The Combustion Institute, Pittsburgh, 1974, p. 737.
5. Seshadri, K., Puri, I., and Peters, N., *Combust. Flame* 61:237-249 (1985).
6. Law, C. K., Li, T. X., Chung, S. H., Kim, J. S., and Zhu, D. L., *Combust. Sci. Tech.* 64:199-232 (1989).
7. Shu, Z., Aggarwal, S. K., Katta, V. R., and Puri, I. K., *Combust. Flame* 111: 276-295 (1997).
8. Shu, Z., Aggarwal, S. K., Katta, V. R., and Puri, I. K., *Combust. Flame* 111: 296-311 (1997).
9. Shu, Z., Krass, B. J., Choi, C. W., Aggarwal, S. K., Katta, V. R., and Puri, I. K., Twenty-seventh Symposium (International) on Combustion, Boulder, Colorado, August 2-7, 1998.
10. Katta, V. R., Goss, L. P., and Roquemore, W. M., *Combust. Flame* 96: 60-74, (1994).
11. Takahashi, F., and Katta, V. R., *AIAA J. Propulsion Power* 11 (1995).
12. Aggarwal, S. K., Park, T. W., and Katta, V. R., *Combust. Sci. Tech.* 113: 429-438 (1996).
13. Peters, N., in Reduced Kinetic Mechanisms for Applications in Combustion Systems, Lecture Notes in Physics, N. Peters and B. Rogg (Eds.), Springer-Verlag, Vol. m15, 1993, pp. 3-14.
14. Brandon, Y., and Samaniego, J.-M., *Combust. Sci. Tech.* 84:81–89 (1992).
15. McManus, K., Yip, B., and Candel, S., *Exptl. Thermal Fluid Sci.* 10:486–502 (1995).
16. Najm, H. N., Paul, P. H., Mueller, C. J., and Wyckoff, P. S., *Combust. Flame* 113:312–332 (1998).

S102-25

REACTION KERNEL STRUCTURE AND DIFFUSION FLAME STABILIZATION

Fumiaki Takahashi[1] and Vedha Nayagam[2]
[1]University of Dayton Research Institute, Dayton, Ohio
[2]National Center for Microgravity Research on Fluids and Combustion, Cleveland, Ohio

INTRODUCTION

The attachment of a diffusion flame to solid or liquid surfaces is of fundamental and practical importance because of its relation to flame holding by bodies in combustion chambers and fire spread through condensed fuels for both terrestrial and space applications. Although simple diffusion flames formed in a gaseous fuel jet or over a flat fuel surface in a parallel oxidizing stream have long been studied as model combustor flames and fires, a flame-holding, or standing, mechanism has not been fully understood. The objectives of this research are to reveal the structure of the flame stabilizing region (flame base) of laminar two-dimensional (2D) jet diffusion flames and steady-state flat-plate burner flames in microgravity and to develop a unified flame stabilization mechanism common to these flames. The roles of inhibitors, particle dynamics, and boundary layer structure in flame stabilization will also be addressed during the project.

RESEARCH MOTIVATION

In diffusion flames, transport processes are, in general, rate determining, yet partial fuel-air premixing in the quenched (dark) space near the surfaces auguments reaction processes. Early investigators [1] postulated that "there must be a sort of flame velocity in this premixed zone at the base which causes the combustion processes to propagate downwards along the flame front against the gas stream, thus preventing the flame from lifting." A correlation was obtained [2] between the velocity of the flow entrained into the flame base at lifting and the maximum burning velocity for hydrogen flames. However, the flame structure measurements [3] in a small (~a few mm square) stabilizing region of rim-attached, laminar flames of methane revealed a premixed zone which was too narrow for a premixed flame to propagate.

Recent observations by two-color particle image velocimetry (PIV) (Fig. 1) and computations (Fig. 2) of the stabilizing region of methane flames [4] have led to a hypothesis: In normal Earth-gravity, the oxidizing flow is induced due to buoyancy even in still air, and the highest reactivity (heat-release or oxygen-consumption rate) spot, or *reaction kernel*, is formed in the flame base at relatively low flame temperatures by back-diffusion of radical species against the incoming oxygen-abundant flow. The calculated peak heat-release rate or oxygen-consumption rate depends almost linearly on the velocity at the reaction kernel for both jet and flat-plate diffusion flames. Therefore, the reaction kernel provides a stationary ignition source to incoming reactants, sustains combustion, and thus stabilizes the trailing diffusion flame.

In microgravity, however, no buoyancy-induced flow exits in a quiescent environment, and thus, diffusion is the only transport mode and limits the reaction rates [5]. Flame stabilization mechanisms in this regime remain largely unstudied. By decreasing the velocity of the approach air flow under microgravity, the structure of the flame-stabilizing region and a transition from the convective-diffusive mode to the pure diffusion mode can be studied systematically.

RESEARCH APPROACH

Ground-based experiments will be conducted under normal Earth- and low-gravity conditions using the 2.2-s drop tower and, occasionally, the 5.18-s zero-gravity facility. A small 2D diffusion flame burner (Fig. 3), which can be configured as a free jet, wall jet, porous flat-plate, and backward facing step—essential features in combustion systems and fires—will be placed in an air duct (Fig. 4). An intensified charge-coupled device with an interference filter will capture images of the chemiluminescence emissions from OH or CH radicals. Two-color PIV using pulsed xenon flashlamps and color filters will measure the velocity field and provide flow visualization information. Interferometry [6] will measure the temperature distributions. The 2D burner possesses a great advantage for emission imaging and interferometry: a long optical path and simple deconvolution process. The diagnostic measurements are made in a small stabilizing region to obtain high-resolution data. Methane, ethylene-nitrogen, and hydrogen-nitrogen mixtures are the fuels. The air and fuel velocities are major parameters.

The numerical code (UNICORN) to be used was developed by Katta et al. [7] and validated against measurements and flow visualization of various diffusion and premixed flame phenomena; i.e., extinction, ignition, vortex-flame interactions, and attachment mechanisms [4, 8, 9]. Time-dependent governing equations consist of mass continuity, axial and radial momentum conservation, energy conservation, and species conservation equations with the ideal-gas equation of state. Body-force term caused by the gravitational field is included. The momentum equations are integrated using an implicit QUICKEST scheme. The transport coefficients are estimated using molecular dynamics and mixture rules. The enthalpy of each species is calculated from polynomial curve-fits. The semi-detailed chemistry model [10] for 24 species and 81 elementary steps is used.

REFERENCES

1. Gaydon, A. G., and Wolfhard, H. G., *Flames—Their structure, radiation and temperature,* 4th Ed., Chapman and Hall, London, 1979, p. 39.
2. Takahashi, F., Mizomoto, M., Ikai, S., Futaki, N., Lifting Mechanism of Free Jet Diffusion Flames, *Twentieth Symposium (International) on Combustion,* 1985, p. 295.
3. Takahashi, F., Mizomoto, M., and Ikai, S., Structure of The Stabilizing Region of a Laminar Jet Diffusion Flame, *J. Heat Transfer* **110**, 182 (1988).
4. Takahashi, F., Schmoll, W. J., and Katta, V. R., Attachment Mechanisms of Diffusion Flames, *Twenty-Seventh Symposium (International) on Combustion,* 1998, in press.
5. Dietrich, D. L., Ross, H. D., and T'ien, J. S., Candle Flames in Microgravity, Third Microgravity Combustion Workshop, 1995, p. 31.
6. Urban, D. L., Goldmeer, J. S., and Yuan, Z., Interaction Between Flames on Parallel Solid Surfaces, Forth Microgravity Combustion Workshop, 1997, p. 429.
7. Katta, V. R., Goss, L. P., and Roquemore, W. M., Numerical Investigations of Transitional H_2/N_2 Jet Diffusion Flames, *AIAA J.* **32**, 84 (1994).
8. Takahashi, F., and Katta, V. R., Unsteady Extinction Mechanisms of Diffusion Flames, *Twenty-Sixth Symposium (International) on Combustion,* 1996, p. 1151.
9. Roquemore, W. M., and Katta, V. R., Role of Flow Visualization in the Development of UNICORN, *Proceedings of VSJ-SPIE98,* Yokohama, Japan, Paper No. KL310, 1998.
10. Peters, N., Flame Calculations with Reduced Mechanisms—An Outline, *Reduced Kinetic Mechanisms for Applications in Combustion Systems,* Springer-Verlag, Berlin, 1993, p. 3

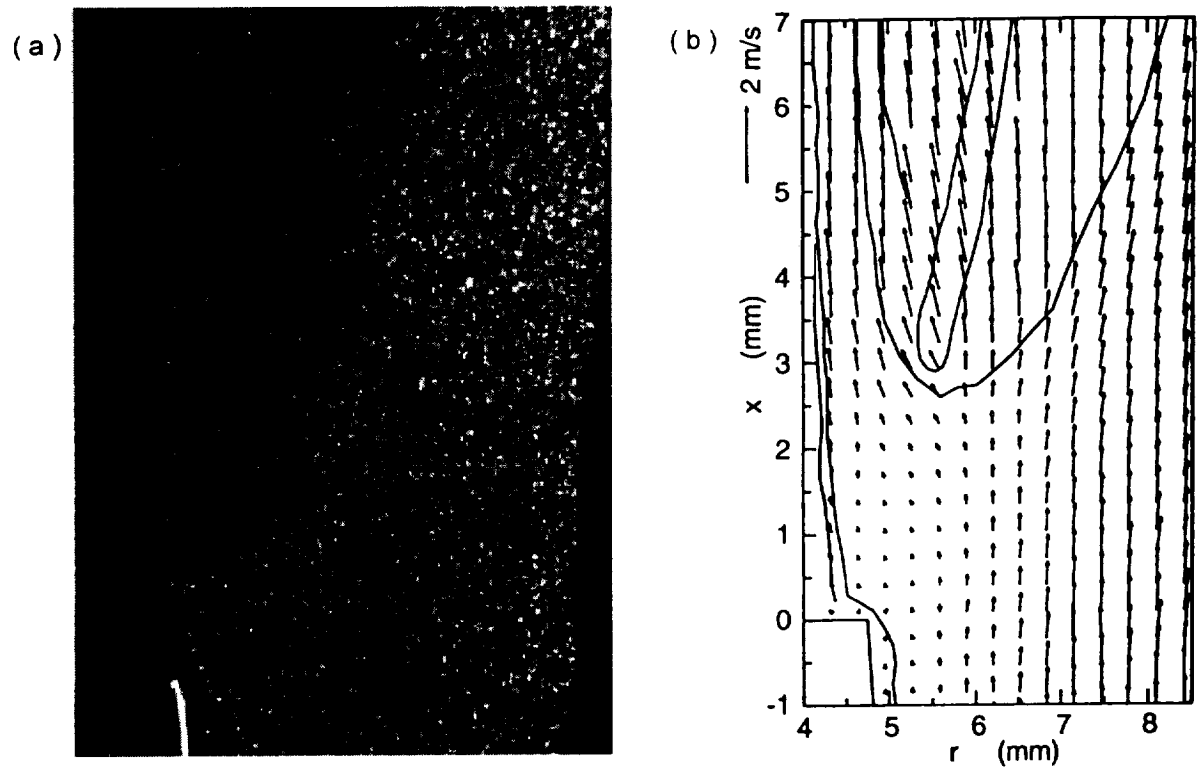

Fig. 1 (a) A two-color PIV photograph and (b) measured velocity vectors of the stabilizing region of methane jet diffusion flames. d = 9.45 mm., U_a = 0.72 m/s, U_j = 1.8 m/s. [4]

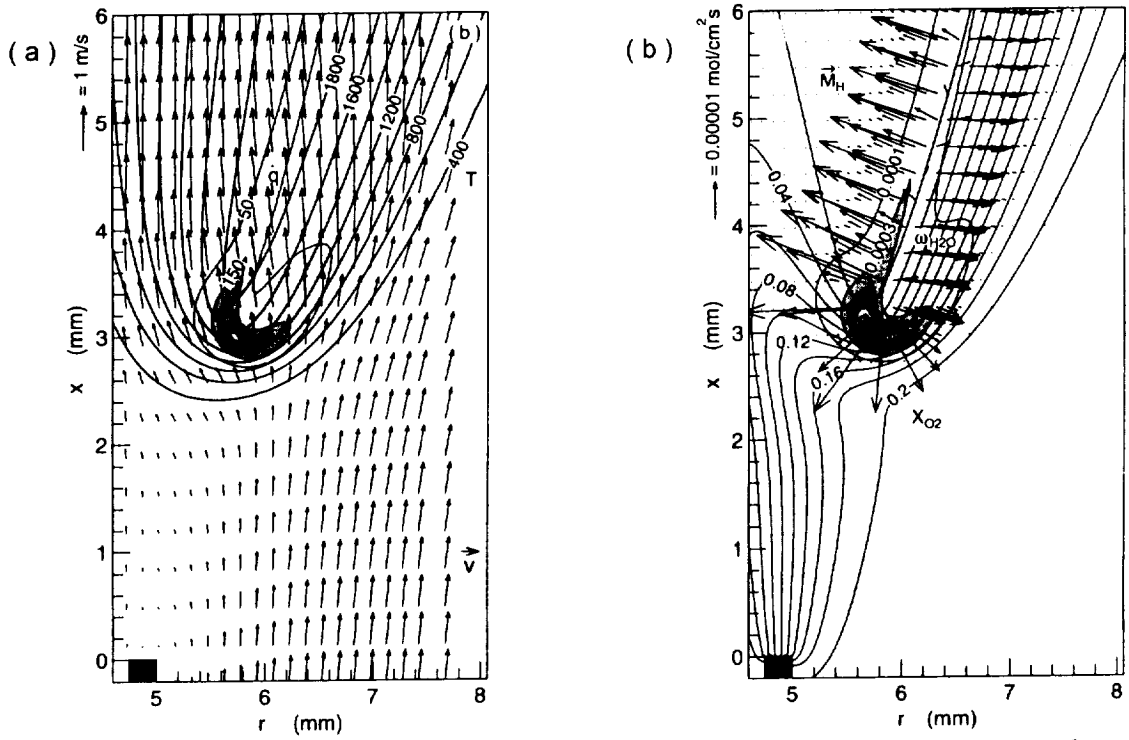

Fig. 2 Calculated (a) velocity vectors, isotherms (unit, K), and heat-release rate (J/cm^{3}s); and (b) molar flux vectors of H, mole fraction of oxygen, and water vapor production rate (mol/cm^{3}s) in a methane jet diffusion flame. d = 9.5 mm., U_a = 0.72 m/s, U_j = 1.7 m/s. [4]

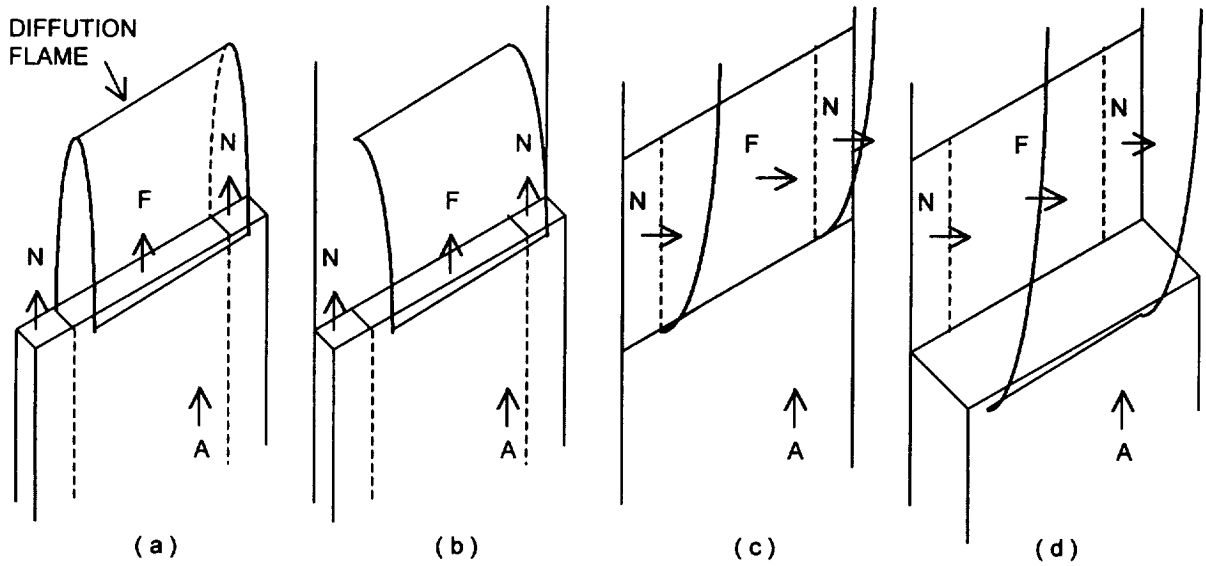

Fig. 3 The diffusion flame burner configurations. (a) Slot burner, (b) slot burner with a plate, (c) flat-plate burner, and (d) flat-plate burner with a step. F: fuel, A: air, and N: nitrogen.

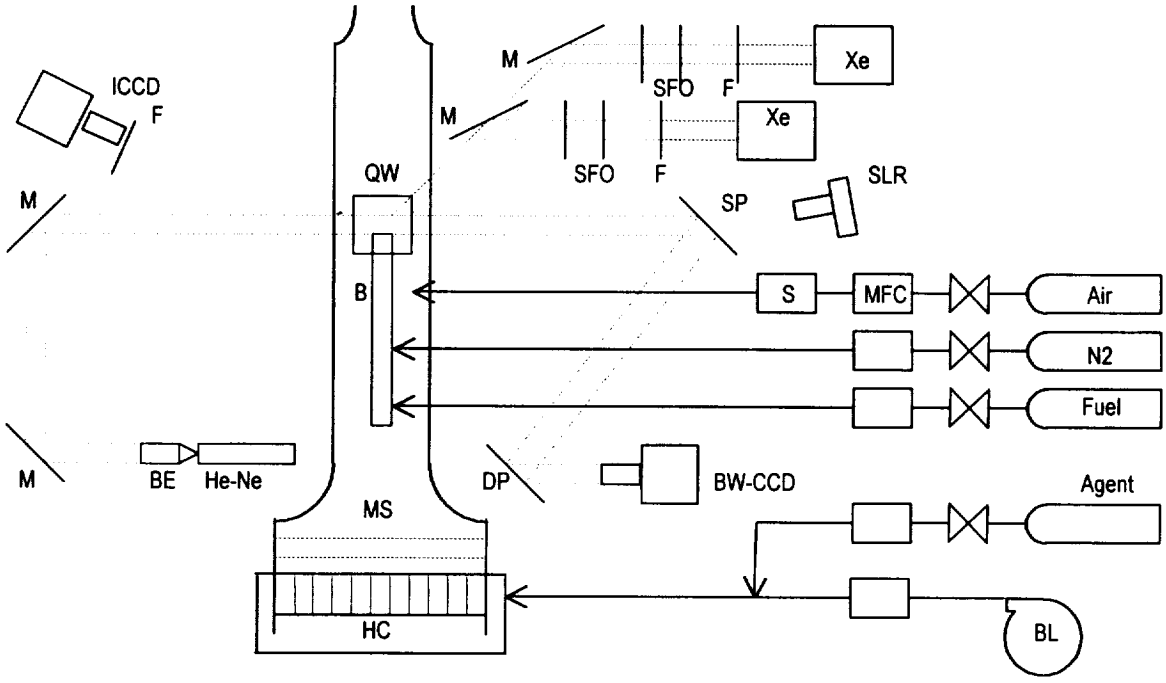

Fig. 4 Experimental apparatus. Flow system—BL: air blower, HC: honeycomb, MS: mesh screen, B: burner, QW: quartz window, MFC: mass flow controller, S: seeder. Interferometer—He-Ne: laser, BE: beam expander, M: mirror, SP: shear plate, DP: diffuse plate, BW-CCD: monochrome camera. PIV—Xe: xenon lamp, F: filter, SFO: sheet-forming optics, SLR: 35-mm camera, C-CCD: color camera. Emission—ICCD: intensified camera.

Turbulent Flames

5/03-25

INVESTIGATION OF STRAIN / VORTICITY AND LARGE-SCALE FLOW STRUCTURE IN TURBULENT NONPREMIXED JET FLAMES

N. T. Clemens, Department of Aerospace Engineering and Engineering Mechanics, The University of Texas at Austin, Austin, TX 78712.

BACKGROUND AND MOTIVATION

Our study will use the microgravity environment to investigate the underlying flow structure of turbulent nonpremixed round jet flames. In particular, we aim to investigate the large-scale turbulent structure using planar laser Mie scattering (PLMS), and the strain rate and vorticity fields using particle image velocimetry (PIV). This work is motivated by recent studies in our laboratory that have led to several interesting observations of nominally momentum-driven turbulent nonpremixed planar flames. First of all, the organized large-scale turbulent structures that are observed in nonreacting planar jets may be substantially modified or suppressed in nonpremixed planar jet flames.[1] Furthermore, a recent study using PIV and planar laser-induced fluorescence of OH has shown that in transitional and turbulent nonpremixed planar jet flames the presence of the flame seems to greatly influence the underlying vorticity and strain fields, as compared to nonreacting jets.[2] For example, the reaction zones in the jet flames are strongly correlated with regions of high vorticity. A related study has demonstrated that vorticity is not correlated in the same way with either iso-scalar surfaces or scalar dissipation layers in nonreacting planar jets.[3] Furthermore, the relationship between strain and the reaction zone appears to be modified by the presence of high levels of heat release. In particular, the strain rate field in planar jet flames exhibits a preferred direction of principal compressive strain that apparently is related to strong shear across the reaction zone.[3] This preferred direction of strain was not observed in nonreacting jets.

One of the major problems encountered when conducting these types of studies is that it is difficult to know to what extent buoyancy influences the results. Therefore, the microgravity environment provides us with an excellent opportunity to explore these issues without the complicating effects of buoyancy. This is particularly the case when studying flames that are transitional between laminar and turbulent states. For example, the strong correlation of vorticity with the reaction zone (discussed above) was observed in both transitional and turbulent planar flames, but the effect was stronger for the transitional case. To date, the reason for the presence of the vorticity-reaction zone correlation is not known, although vorticity production via baroclinic torque is a likely cause. The microgravity environment will allow us to specifically determine whether the vorticity is produced by baroclinic torque resulting from the flame density gradient acting with the hydrostatic pressure gradient.[4] Additional details of the planned experiments are provided below.

APPROACH

We will conduct a study of the turbulent structure of nonpremixed jet flames that will be performed under both microgravity and standard gravity conditions. The microgravity experiments will allow us to investigate the fundamental structure of momentum dominated flames, while comparisons with standard gravity flames will allow us to infer how weak

buoyancy effects modify this basic structure.

The microgravity experiments will be conducted in the NASA Lewis 2.2-second droptower. A schematic diagram of a preliminary drop box design is shown in Figure 1. The jet flame will likely be generated using a 3 mm diameter tube flowing hydrogen or methane diluted with an inert to reduce the flame length. So that higher Reynolds numbers can be achieved without liftoff, a pilot flame will be used. Both the PLMS and PIV measurements will use a stationary Nd:YAG system available at NASA Lewis whose light is delivered to the box via fiber optic cable. The laser beam will be formed into a sheet on one side of the drop box and then directed to the flame using a mirror. The flame itself will be located on the other side of the box, so that there is sufficient distance to form the laser sheet. Alumina particles will be seeded into the jet fluid using a fluidized bed. For the PIV measurements it will probably be necessary to seed particles into the outer flow, particularly for regions near the flame base; however, without a coflow this will be problematic. The external flow seeding will probably be accomplished using some type of localized injection of a low momentum particle-laden stream into the outer flow. We expect that this will be an issue that will require substantial development work. For both the PLMS and PIV experiments, the particle scattering will be captured using a 1k x 1k CCD camera (Kodak ES1.0). For PIV this camera will operate in a frame-straddling mode where each image is placed in a different frame, thus removing any directional ambiguity and reducing particle dropout in low velocity regions. We expect that the output from the camera will be sent to a stationary computer via a fiber-optic transmission cable.

The proposed study will be aimed at a thorough exploration of the issues identified in the first section. In particular, we will investigate two primary aspects of flame structure: 1) the characteristics of the large-scale turbulent structure, and 2) the structure of the underlying strain and vorticity fields. The large-scale structure will be investigated both qualitatively and statistically using large ensembles of PLMS images. Specifically, we will seek to address how the large-scale turbulent structure of momentum dominated jet flames differs from that of isothermal jets, and how this structure is modified under weakly buoyant conditions. Furthermore, the strain and vorticity fields will be investigated using the PIV measurements. We will specifically address issues such as whether the strong correlation between vorticity and the reaction zone -- previously observed in transitional and turbulent flames at standard gravity -- is due to gravity-induced baroclinic torque. Furthermore, it will be possible to investigate the evolution of the underlying strain field as the jet transitions from laminar to turbulent. Under standard gravity conditions, it is difficult to do this as buoyancy effects typically dominate at the lower Reynolds numbers. Finally, the microgravity environment will allow us to isolate particular effects, such as finite rate chemistry, on the flame structure, in a way that either would be impossible, or at least less than definitive, at standard gravity conditions.

ACKNOWLEDGEMENT

This work will be supported under the NASA Microgravity Combustion Science Program.

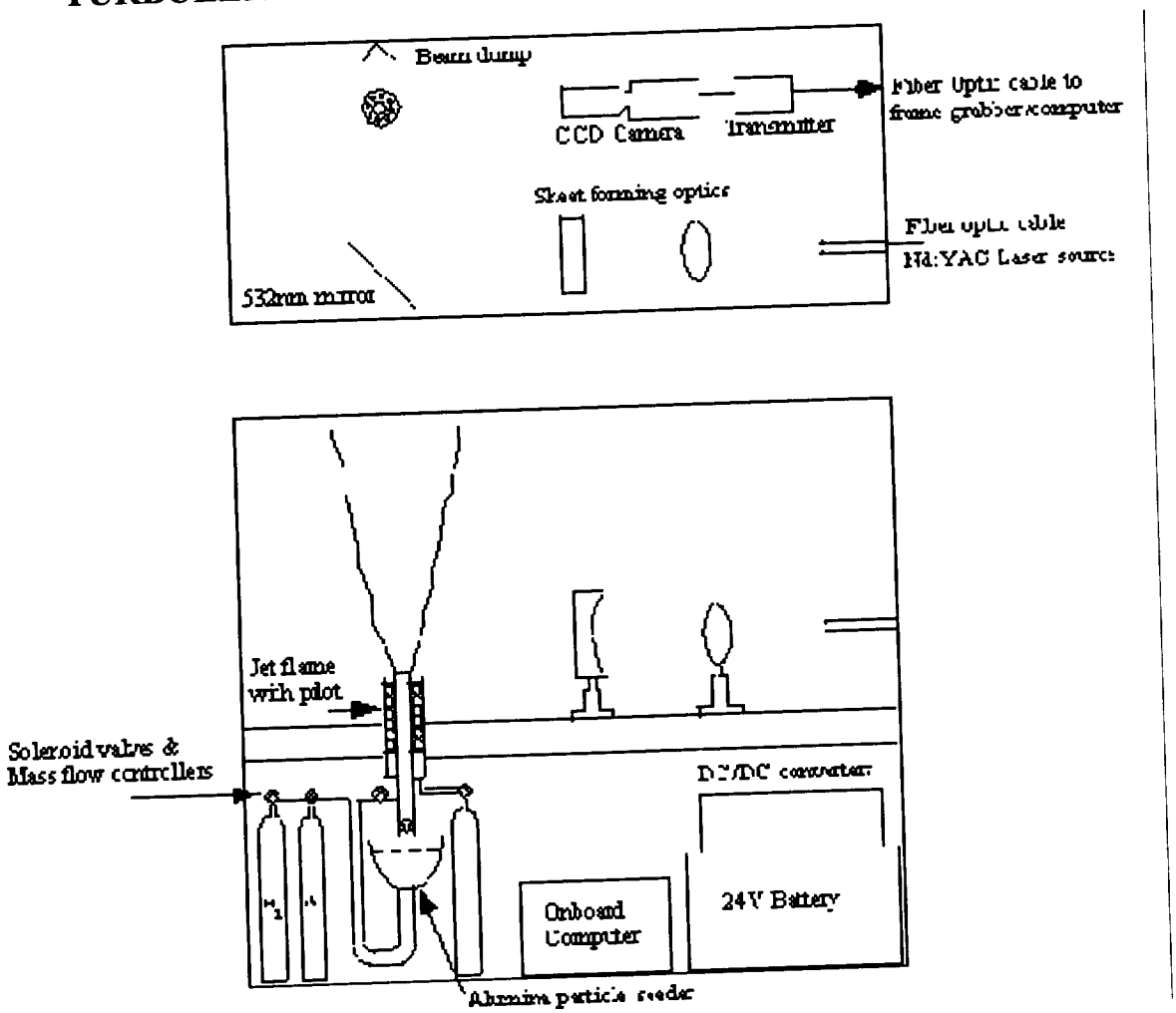

Figure 1. Preliminary design of the drop box that will be used for studies of turbulent nonpremixed round jet flames in the NASA Lewis 2.2-second droptower. (Please excuse the poor conversion of the figure to PDF format.)

REFERENCES

1. Rehm, J.E. and Clemens, N.T., "The large-scale turbulent structure of planar jet diffusion flames," *Combustion and Flame*, Vol. 116, pp. 615-626, 1999.

2. Rehm, J.E. and Clemens, N.T., "The relationship between vorticity/strain and reaction zone structure in turbulent nonpremixed planar jet flames," Twenty-Seventh Symposium (International) on Combustion, pp. 1113-1120, 1998.

3. Rehm, J.E. and Clemens, N.T., "The association of strain/vorticity/dilatation and reaction zone structure in turbulent nonpremixed planar jet flames," AIAA paper 99-0676, January, 1999.

4. Chen, L-D, Roquemore, W.M., Goss, L.P., and Vilimpoc, V., "Vorticity Generation in Jet Diffusion Flames," *Combustion Science and Technology*, Vol. 77, pp. 41-57, 1991.

S104-29

LARGE EDDY SIMULATION OF GRAVITATIONAL EFFECTS ON TRANSITIONAL AND TURBULENT GAS-JET DIFFUSION FLAMES

L.Y.M. Gicquel, F.A. Jaberi and P. Givi, Department of Mechanical and Aerospace Engineering, State University of New York at Buffalo, Buffalo, NY 14260-4400

OBJECTIVE

The objective of this work is to assess the influence of gravity on the compositional and the spatial structures of transitional and turbulent hydrocarbon flames with nonpremixed reactants. This is an entirely ground-based research in which we plan to utilize a recently developed methodology termed the "filtered mass density function" (FMDF) [1] for large eddy simulation (LES) of turbulent reactive flows. The novelty of the methodology is that it allows for "reliable" LES of turbulent flames at a small fraction of the computational cost of direct numerical simulation (DNS). It also allows for inclusion of "realistic physics;" this has been difficult in the majority of previous contributions via DNS [2,3]. Moreover, it facilitates detailed analysis of the compositional structure and the evolution of the flame which are not possible via "Reynolds averaged simulation" (RAS) [4].

The flow configuration is that of a gas-jet in which a fuel is issued from a jet into a coflowing (or stagnant) stream of an oxidizer. The importance of buoyancy in such a diffusion flame is well recognized [5]. However, presently there are very few large scale computational strategies which can include all of the important physical intricacies of turbulent combustion in this configuration. The LES/FMDF methodology will be used in conjunction with realistic representations of the chemical kinetics effects; thus replicating a "genuine" flame via numerical simulations. The simulated results will be utilized for: (i) capturing the unsteady evolution of the flame and the influence of buoyancy-induced flow on the "spatial" flame structure, (ii) determining the statistical flame behavior at varying gravity levels and orientations, (iii) elucidating the "compositional structure" of the flame at microgravity, and (iv) analyses of the data set recently made available by the Microgravity Science and Application Division of the NASA Headquarters [6,7].

FORMULATION

Large eddy simulation involves the spatial filtering [8]: $\langle f(\mathbf{x},t)\rangle_\ell = \int f(\mathbf{x}',t)\mathcal{H}(\mathbf{x}',\mathbf{x})d\mathbf{x}'$, where $\mathcal{H}$ denotes the filter function, $\langle f(\mathbf{x},t)\rangle_\ell$ represents the filtered value of the transport variable $f(\mathbf{x},t)$. In variable density flows it is more convenient to consider the Favre filtered quantity, $\langle f(\mathbf{x},t)\rangle_L = \langle \rho f\rangle_\ell / \langle \rho\rangle_\ell$. For spatially & temporally invariant and localized filter functions, $\mathcal{H}(\mathbf{x}',\mathbf{x}) \equiv H(\mathbf{x}'-\mathbf{x})$ with the properties [8], $H(\mathbf{x}) = H(-\mathbf{x})$, and $\int_{-\infty}^{\infty} H(\mathbf{x})d\mathbf{x} = 1$. The FMDF is proposed to be implemented via two formulations: (I) to consider only the

subgrid scale (SGS) scalar quantities, (II) to consider the SGS velocity-scalar quantities.

To summarize formulation I, Let $\boldsymbol{\phi}(\mathbf{x},t)$ denote the scalar array. The joint "filtered mass density function" (FMDF) is defined as $F_L(\boldsymbol{\psi};\mathbf{x},t) \equiv \int_{-\infty}^{+\infty} \rho(\mathbf{x}',t)\zeta\left[\boldsymbol{\psi},\boldsymbol{\phi}(\mathbf{x}',t)\right] H(\mathbf{x}'-\mathbf{x})d\mathbf{x}'$ with $\zeta\left[\boldsymbol{\psi},\boldsymbol{\phi}(\mathbf{x},t)\right] = \delta[\boldsymbol{\psi}-\boldsymbol{\phi}(\mathbf{x},t)] \equiv \prod_{\alpha=1}^{\sigma} \delta[\psi_\alpha-\phi_\alpha(\mathbf{x},t)]$, where δ denotes the delta function, σ is the number of scalar variables, and $\boldsymbol{\psi}$ denotes the composition domain of the scalar array. The term $\zeta[\boldsymbol{\phi},\boldsymbol{\psi}(\mathbf{x},t)]$ is the "fine-grained" density [9], and the FMDF is the mass weighted spatially filtered value of the fine-grained density which provides all the statistical information pertaining to the subgrid values of the scalar field. With this formulation, however, the resolved hydrodynamic field must be simulated by other means. For that we will make use of procedures which are well-established in the LES of non-reacting flows. The need for closures associated with the velocity-velocity and velocity-scalar fluctuations is avoided by formulation II in which the joint velocity-scalars FMDF, $\mathcal{F}_L(\mathbf{V},\boldsymbol{\psi};\mathbf{x},t) = \int_{-\infty}^{+\infty} \rho(\mathbf{x}',t)\xi\left[\mathbf{V},\mathbf{U}(\mathbf{x}',t),\boldsymbol{\psi},\boldsymbol{\phi}(\mathbf{x}',t)\right] G(\mathbf{x}'-\mathbf{x})d\mathbf{x}'$ with $\xi\left[\mathbf{V},\mathbf{U}(\mathbf{x},t),\boldsymbol{\psi},\boldsymbol{\phi}(\mathbf{x},t)\right] = \prod_{k=1}^{3} \delta[v_k-u_k(\mathbf{x},t)] \prod_{\alpha=1}^{\sigma} \delta[\psi_\alpha-\phi_\alpha(\mathbf{x},t)]$. In the transport equation for the joint velocity-scalar FMDF the terms associated with SGS convection, buoyancy, and chemical reaction are represented in a closed form. The transport equation for the FMDF is obtained by following the same procedure as that used in PDF methods [9]. The derivation procedure is rather lengthy [1,10] and is not presented here.

NUMERICAL SIMULATIONS

The most convenient means of solving the FMDF transport equation is via the "Lagrangian Monte Carlo" procedure. In this procedure, the FMDF is represented by an ensemble of computational "stochastic elements" (or "particles") which are transported in the "physical space" by the combined actions of large scale convection and diffusion (molecular and subgrid). In addition, transport in the "composition space" occurs due to chemical reaction and SGS mixing. These are represented by the stochastic differential equations (SDEs) $dX_i(t) = \mathcal{D}_i(\mathbf{X}(t),t)dt + \mathcal{E}(\mathbf{X}(t),t)d\mathcal{W}_i(t)$, $d\phi_\alpha^+(t) = \mathcal{R}_\alpha(\boldsymbol{\phi}^+,t)dt$ where X_i is the Lagrangian position of the particles, $\mathcal{D}$ and $\mathcal{E}$ are known as the "drift" and "diffusion" coefficients, and $\mathcal{W}_i$ denotes the Wiener process [11]. ϕ_α^+ denotes the scalar value of the particle with the Lagrangian position vector X_i. The PDFs of the stochastic processes $(X_i(t),\ \phi_\alpha^+(t))$ are governed by the Fokker-Planck equation.

For the numerical solution of the hydrodynamic field in formulation I, we will use a high-order accurate finite difference procedure based on the "compact parameter" scheme [12]. All the finite difference operations will be performed on fixed grid points. The transfer of information from the fixed finite difference points to the location of the Monte Carlo particles will be conducted via interpolation. In formulation II, the Monte Carlo procedure will also be applied to the velocity field. In this case, obviously, additional SDEs must be considered. With this joint FMDF formulation, the effects of small scale convection appear in a closed form, thus eliminating the need for the SGS viscosity and diffusivity as needed in formulation I. In this regard, the FMDF scheme is expected to be more flexible (and more powerful) than the conventional LES even for non-reacting flow simulations. The computational advantage is that the interpolation procedure as discussed above is not required since the Monte Carlo elements carry information pertaining to both the composition and the velocity. We plan

to start with the Langevin equations proposed by Pope [13] for the velocity field. This procedure is reasonably well developed in RAS and its relation to second order turbulence closures is well understood. We will consider several of the "Ornstein-Uhlenbeck" [11] type closures as suggested in RAS [13].

PLAN

We will consider the jet-flame configuration in which the fuel is issued with a velocity U_{in} and temperature T_{in} from a jet of width d into a co-flowing stream of oxidizer with the velocity $U_{ou} = rU_{in}$, $0 \leq r \leq 1$ and temperature T_{ou} in an environment in which the gravity vector is $\mathbf{g}$, with varying levels. For this flow configuration, the hydrodynamic parameters which characterize the flame structure are the Reynolds number, the Froude number and the Richardson number. Assessment of the spatial structure of the flame is rather straightforward. The primary quantities to be considered are the velocity components, the mass fractions of the major & the radical species, and the temperature. The unsteady spatial-temporal $(\mathbf{x} - t)$ evolution of these quantities and their time-sampled (Reynolds averaged) values can be readily constructed from the LES results. The statistical quantities are the means & the covariance (the first two joint moments) and the joint PDFs. The most obvious influence of gravity on the spatial structure is on the flame height. In some of the cases, because of enormous computational requirements (even in LES), we will not be able to capture the full flame height by three-dimensional (3D) simulations at high Reynolds numbers. While consideration of high Reynolds numbers is possible by LES, it is not possible to consider a large enough computational domain in 3D which fully encloses the flame. In order to have a "rough estimate" of this influence of gravity we will perform 2D simulation for which we can consider a larger domain. The construction of the compositional structure requires data analyses in the domain of the "mixture fraction." This includes consideration of both the "scattered" data and the "conditional statistics," such as the conditional averages and the conditional PDFs.

Another ambitious but hopefully feasible component of our proposed research is model assessment by comparison of LES results with experimental and, to a limited extent, DNS data. Microgravity experimental data are compiled by NASA [6], including the results obtained by Bahadori *et al.* [14,15] and Hegde *et al.* [16,17]. These results portray the spatial flame structure and include some of the lower order statistical moments (such as the streamwise variation of the mean values along the jet centerline). Comparisons with these data would be useful in determining how the "trends" can be captured by LES. Further detailed comparisons in portraying the compositional structure will be done with consideration of other data as currently available. The comparison with DNS data will be of only a limited set of 2D simulations to concentrate on issues for which experimental data are not sufficient. DNS provides a convenient means of furnishing such "exact" results.

References

[1] Colucci, P. J., Jaberi, F. A., Givi, P., and Pope, S. B., *Phys. Fluids*, **10**(2):499–515 (1998).

[2] Libby, P. A. and Williams, F. A., editors, *Turbulent Reacting Flows*, Academic Press, London, England, 1994.

[3] Givi, P., In Libby and Williams [2], chapter 8, pp. 475–572.

[4] Libby, P. A. and Williams, F. A., editors, *Turbulent Reacting Flows, Topics in Applied Physics*, Vol. 44, Springer-Verlag, Heidelberg, 1980.

[5] Glassman, I., *Combustion*, Academic Press, Inc., San Diego, CA, 3rd edition, 1986.

[6] NASA, *Microgravity Science and Applications, Program Tasks and Bibliography for FY 1996*, NASA Technical Memorandum 4780, 1996.

[7] NASA, *Proceedings of the Fourth International Microgravity Combustion Workshop*, NASA Conference Publication 10194, Cleveland, OH, 1997.

[8] Aldama, A. A., Filtering Techniques for Turbulent Flow Simulations, *Lecture Notes in Engineering*, Vol. 49, Springer-Verlag, New York, NY, 1990.

[9] Pope, S. B., *Prog. Energy Combust. Sci.*, **11**:119–192 (1985).

[10] Colucci, P. J., Ph.D. Thesis, Department of Mechanical and Aerospace Engineering, State University of New York at Buffalo, Buffalo, NY, 1998.

[11] Karlin, S. and Taylor, H. M., *A Second Course in Stochastic Processes*, Academic Press, New York, NY, 1981.

[12] Carpenter, M. H., in Morton, K. W., editor, *Twelfth International Conference on Numerical Methods in Fluid Dynamics, Lecture Notes in Physics*, Vol. 371, pp. 254–258, Springer-Verlag, New York, NY, 1990.

[13] Pope, S. B., *Ann. Rev. Fluid Mech.*, **26**:23–63 (1994).

[14] Bahadori, M. Y., Stocker, D. P., Vaughan, D. F., Zhou, L., and Edelman, R. B., in Williams, F. A., Oppenheim, A. K., Olfe, D. B., and Lapp, M., editors, *Modern Developments in Energy, Combustion and Spectroscopy*, chapter 4, pp. 49–66, Pergamon Press, New York, NY, 1993.

[15] Bahadori, M. Y., Hegde, U., and Stocker, D. P., In *Proceedings of the Fourth International Microgravity Combustion Workshop* [7], pp. 179–184.

[16] Hegde, U., Zhou, L., and Bahadori, M. Y., *Combust. Sci. and Tech.*, **102**:95–113 (1994).

[17] Hegde, U., Yuan, Z., Stocker, D. P., and Bahadori, M. Y., In *Proceedings of the Fourth International Microgravity Combustion Workshop* [7], pp. 185–190.

S105-29

AN EXPERIMENTAL INVESTIGATION OF FULLY-MODULATED, TURBULENT DIFFUSION FLAMES IN REDUCED GRAVITY

J.C. Hermanson,[1] H. Johari,[1] J.E. Usowicz,[1] D.P. Stocker,[2] T. Nagashima,[3] and S. Obata[4]

[1]Mechanical Engineering Department, Worcester Polytechnic Institute, 100 Institute Road, Worcester MA 01609 (jherm@wpi.edu), [2]NASA Glenn Research Center, MS 500-115, 21000 Brookpark Road, Cleveland, OH 44135, [3]Department of Aeronautics and Astronautics, Tokyo University, Tokyo, Japan, [4]Aerospace Engineering Department, National Defense Academy, Yokosuka, Japan

INTRODUCTION

Pulsed combustion appears to have the potential to provide for rapid fuel/air mixing, compact and economical combustors, and reduced exhaust emissions. The ultimate objective of this program is to increase the fundamental understanding of the fuel/air mixing and combustion behavior of pulsed, turbulent diffusion flames by conducting experiments in microgravity.

In this research the fuel jet is fully-modulated (i.e., completely shut off between pulses) by an externally controlled valve system. This can give rise to drastic modification of the combustion and flow characteristics of flames,[1-3] leading to enhanced fuel/air mixing mechanisms not operative for the case of acoustically excited or partially-modulated jets.[4] In addition, the fully-modulated injection approach avoids the strong acoustic forcing present in pulsed combustion devices, significantly simplifying the mixing and combustion processes.

Relatively little is known of the behavior of turbulent flames in reduced-gravity conditions, even in the absence of pulsing. The goal of this Flight-Definition experiment (PUFF, for PUlsed-Fully Flames) is to establish the behavior of fully-modulated, turbulent diffusion flames under microgravity conditions. Fundamental issues to be addressed in this experiment include the mechanisms responsible for the flame length decrease for fully-modulated, turbulent diffusion flames compared with steady flames, the impact of buoyancy on the mixing and combustion characteristics of these flames, and the characteristics of turbulent flame puffs under fully momentum-dominated conditions.

EXPERIMENTAL APPROACH

As part of this program, developmental experiments in the laboratory and in ground-based reduced-gravity facilities will be conducted using a cylindrical combustor. The basic combustor configuration will consist of a single fuel jet nozzle 1-2 mm in diameter located on the combustor centerline. The gaseous fuel jet flow will be fully-modulated by a solenoid valve driven by an electronic controller to provide for a range of injection times and duty cycles (the jet-on fraction of each cycle). The pulsing frequency, f, is directly related to the duty cycle, α, and the injection time, τ_i, by $f = \alpha/\tau_i$. The mean fuel velocity during injection will give Reynolds numbers ranging from 3000 to 10,000. A slow air co-flow will be established in the combustor space surrounding the jet nozzle to properly ventilate the flame. An annular pilot flame or other type of ignitor will provide a continuous ignition source for the pulsed fuel jet.

Four types of diagnostic techniques will be employed in the experiments for the quantitative measurement of flame length, fuel/air mixing, combustion temperatures, and exhaust emissions. First, video imaging will be used to study the turbulent structure of the pulsed flames and to determine the corresponding flame lengths. Second, fine-wire thermocouple probes and thermopile detectors will be used to determine temperatures and radiant emissions. Third, planar

laser imaging of particles seeded into the co-flow or fuel jet will allow the determination of the amount of air entrained by the fully-modulated, turbulent flame puffs. Finally, gas sampling, combined with gas chromatography, will be employed to establish emissions levels and to determine combustion efficiency. It should be pointed out that not all of these diagnostics are appropriate for a given ground-based reduced-gravity test platform (e.g., drop tower, aircraft).

Experiments conducted in the laboratory provide a set of baseline results for the behavior of fully-modulated turbulent diffusion flames at normal gravity. Tests at reduced gravity will be conducted in the NASA GRC 2.2-second Drop Tower. These tests will provide some indication of the behavior of fully-pulsed flames in reduced gravity, and will also serve to identify candidate pulsed flames for further detailed study (times well in excess of 5 seconds are required to completely establish a stationary, fully-modulated flame condition.[5]) The jet and co-flow will be initiated and the flame ignited before or immediately after the drop.

If appropriate, selected test cases will be further studied in the NASA KC-135 parabolic-trajectory aircraft, based on the candidate experiments identified in the 2.2-second Drop Tower. The longer duration (~20s) of reduced gravity available on the aircraft will allow briefly the establishment of a stationary pulsed injection configuration for imaging and limited measurements. Specifically, the aircraft experiments would include *in-situ* gas sampling, at selected intervals in the pulsing cycle, and subsequent analysis by gas chromatography.

NUMERICAL MODELING (U. TOKYO/NDA)

The combustion characteristics of fully-modulated diffusion flames are also being investigated by unsteady, 3-dimensional, Navier-Stokes numerical calculations using a 2-equation, q-ω turbulence model. The model will provide the essential physical quantities, such as temperature, air entrainment, and flame puff celerity for comparison with the experimental results.

RESULTS TO DATE – COMBUSTION

Preliminary experiments have been conducted at WPI at normal gravity in the laboratory.[1,2] An in-line solenoid valve was used to fully-modulate the gaseous fuel flow to nozzles ranging in diameter from 3.2 to 9.9 mm. The valve cycle was varied over frequencies from 0.5 to 10 Hz and duty cycles, ranging from $\alpha = 0.08$ to 0.93. The fuel consisted of either natural city gas or ethylene. The maximum steady-state nozzle exit Reynolds numbers were 5500 for natural gas fuel and 20,000 for ethylene, and the experiments were conducted at one atmospheric pressure with unheated fuels. A small pilot flame was used to ensure jet ignition. The luminous flame emission was recorded using a video camcorder to determine the flame shape and allow the quantitative measurement of the flame length.

For short injection times and short duty cycles, widely-spaced puff-like structures were observed, as shown in Fig. 1a for natural gas. These puff-like structures exhibited a flame length reduction of nearly 50% compared with the corresponding steady-state cases. For relatively longer injection times, narrower, longer, "cigar-shaped" flames were observed. A representative image of a cigar-shaped, flame with ethylene fuel is presented in Fig. 1b. The flame lengths of these cigar-shaped flames were generally comparable to those of the corresponding steady-state cases.

Whether a fully-modulated jet gives a flame structure more puff-like or cigar-shaped can be characterized in terms of a parameter $P \equiv [(4V_0/\pi d^2)/d]^{1/3}$. This parameter relates the volume of the injected fuel (V_0) to the nozzle exit area ($\sim d^2$). For the case of widely-spaced, compact puffs the maximum flame length can be shown[2,3] to depend linearly on P.

The flame length normalized by nozzle diameter, *L/d,* is plotted in Fig. 2a,b versus the parameter P and the duty cycle, for the case of ethylene and natural gas fuel, respectively. An increase in normalized flame length with P for the lowest value of duty cycle ($\alpha \approx 0.1$) is evident for both fuels. This corresponds to the widely-spaced puff case with the linear scaling of the flame length with P mentioned above. For ethylene (Fig. 2a), deviation from linearity is apparent for values of $P > 12$, which also roughly corresponds to the end of the transition between puff-like structures and cigar-shaped flames. The relatively lower maximum injection volume for the natural gas case was evidently not sufficient to reach this transition.

For both fuels the flame length tends to increase with the duty cycle for a given value of P. This is most evident for the natural gas case (Fig. 2b). As the duty cycle increases, the discrete fuel puffs give way to more closely-packed, interacting puffs which exhibit mixing and combustion characteristics more similar to those of steady-state flames. The change in flame length with duty cycle is relatively less for cigar-shaped flames ($P > 12$ for ethylene). Much of the data scatter is likely due to variations in injection pulse shape with changes in frequency and duty cycle.

RESULTS TO DATE - JET ENTRAINMENT

Determination of the amount of air entrained into pulsed, turbulent fuel jets is crucial to this research effort. The utility of using planar laser imaging of seed particles in the co-flow is being explored for this purpose. In addition to providing concentration information in the jet, this method allows for visualization of the streaklines and flow patterns in the co-flow stream.

In these non-reacting flow tests, a 1.36 mm-diameter jet nozzle is situated on the centerline of a wind tunnel (15 × 15 cm cross section). The tunnel air flow is uniformly seeded with oil smoke upstream of the test section. The seeded smoke in the test section is illuminated by a laser light sheet and imaged by a progressive-scan CCD camera. These images are then reduced to determine jet concentration based on the changing density of seed particles entrained into the jet.

An image of a steady jet over a downstream extent of roughly 30 *x/d* is shown in Fig. 3. Streaklines in the co-flow can be clearly seen in the figure. Radial profiles of jet concentration over a range of downstream distance are shown in Fig. 4. The concentration information was extracted from the average of 200 individual images. Research is continuing to improve the method to allow the effective imaging of fully-modulated jets.

ACKNOWLEDGEMENT

This work is sponsored by NASA Glenn Research Center under Agreement NCC3-673.

REFERENCES

[1]Hermanson, J.C., Dugnani, R., and Johari, H., AIAA paper 98-0561, 1998.

[2]Johari, H. and Motevalli, V., *Combustion Science and Technology*, 94 (1-6), 229-245, 1993.

[3]Hermanson, J.C., Dugnani, R., and Johari, H., submitted to *Comb. Sci. Tech.,* 1999.

[4]Lovett, J.A. and Turns, S.R., *AIAA Journal* 28(1), 38-46, 1990.

[5]Bahadori, M.Y., Stocker, D.P., Vaughan, D.F., and Zhou, L, *Second International Microgravity Combustion Workshop*, Cleveland, OH, 91-104, September, 1992.

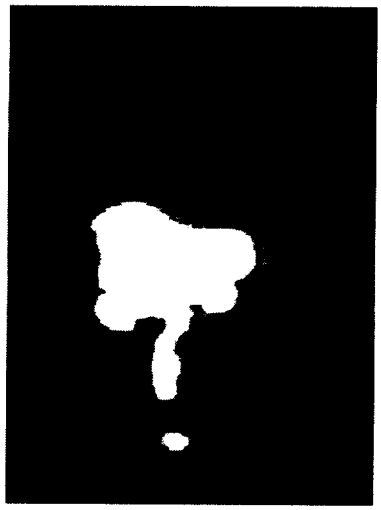

Fig. 1a: Puff-like flame. *Re = 5,500, d = 9.9 mm, τ_i = 25 ms, α = 0.11.*

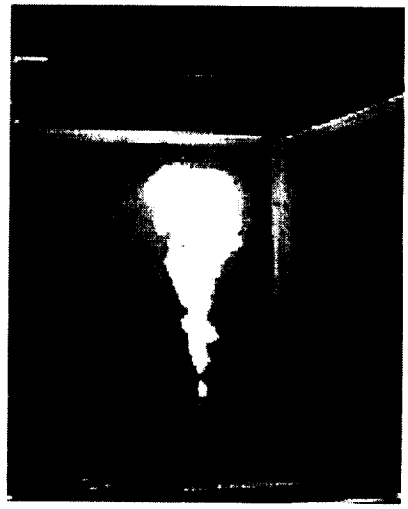

Fig. 1b: Cigar-shaped flame. *Re = 20,000, d = 3.2 mm, τ_i = 50 ms, α = 0.11.*

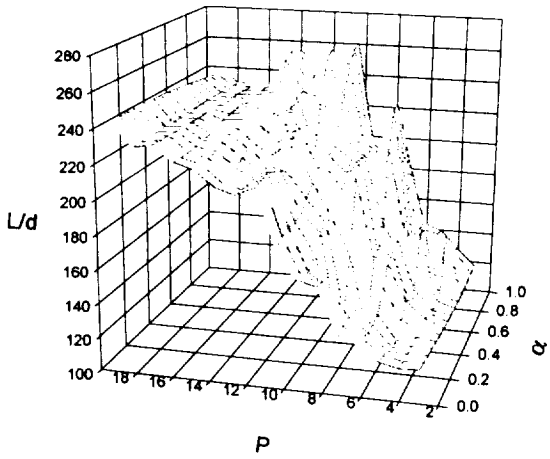

Fig. 2a: Flame length for ethylene.

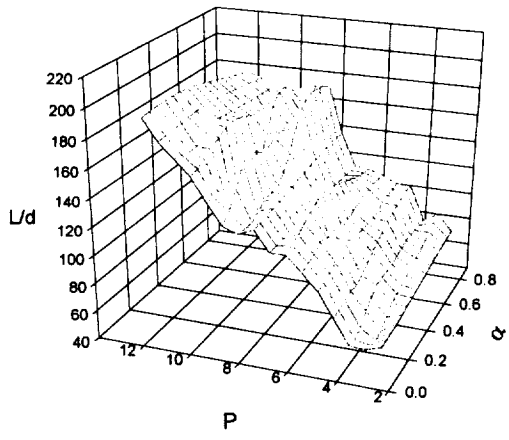

Fig. 2b: Flame length for natural gas.

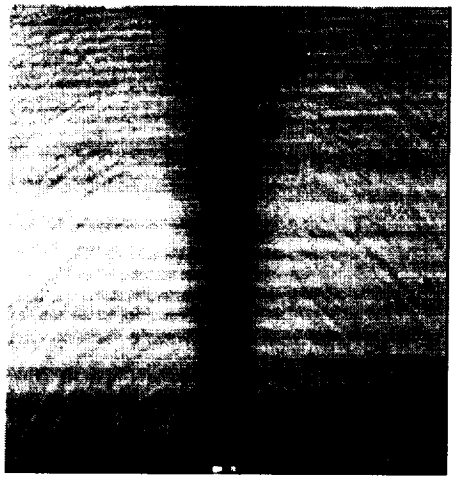

Fig. 3: Steady turbulent jet with co-flow seeding. *d = 1.36 mm , Re = 6680.*

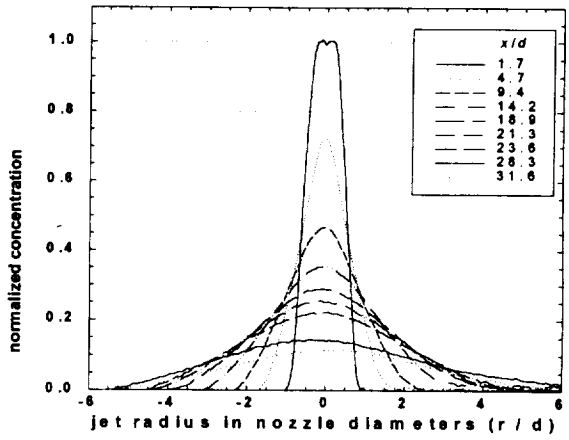

Fig. 4: Normalized jet concentration. *d = 1.36 mm , Re = 6680.*

Droplet Combustion

5/54-25

DYNAMICS OF DROPLET EXTINCTION IN SLOW CONVECTIVE FLOWS

V. Nayagam[1], J. B. Haggard, Jr.[2], and F. A. Williams[3]. [1]National Center for Microgravity Research, [2]NASA Glenn Research Center, Cleveland, Ohio.[3] University of California San Diego, La Jolla, California.

INTRODUCTION

The classical model for droplet combustion predicts that the square of the droplet diameter decreases linearly with time. It also predicts that a droplet of any size will burn to completion over a period of time. However, it has been known for some time that under certain conditions flames surrounding a droplet, in a quiescent environment, could extinguish because of insufficient residence time for the chemistry to proceed to completion. This type of extinction that occurs for smaller droplets has been studied extensively in the past. Large droplets, on the other hand, exhibit a different type of extinction where excessive radiative heat loss from the flame zone leads to extinction. This mode of "radiative extinction" was theoretically predicted for droplet burning by Chao et al. (1990) and was observed in recent space experiments (Dietrich et al., 1996; Nayagam et al., 1998) in a quiescent environment (see e.g., Fig.1).

Thus far, the fundamental flammability limit prescribed by radiative extinction of liquid droplets has been measured only under quiescent environmental conditions. In many space platforms, however, ventilation systems produce small convective flows and understanding of the influences of this convection on the extinction process will help better define the radiative extinction flammability boundaries (T'ien, 1990, 1997). Boundaries defined by experiments and captured using theoretical models could provide enhanced fire safety margin in space exploration as well as improve our fundamental understanding. Also, systematic, controlled investigation of convective effects will help in interpretations of burning-rate data obtained during free-floated droplet combustion experiments with small residual velocities.

PLANNED RESEARCH

This is a new project that is just getting underway. The primary objective of the planned research is to investigate the effects of slow convection on radiative extinction of liquid fuel droplets. Experimentally, quantitative data on flame extinction dynamics for typical non-sooting, (e.g., methanol) and sooting (e.g., n-heptane) fuel droplets will be obtained for a range of convective velocities at different oxygen concentrations and ambient pressures. Figure 2 shows typical flame views of n-decane droplets burning in air at normal atmospheric pressure for various Reynolds numbers in microgravity. These images were obtained from a recent fiber-supported droplet combustion experiment (FSDC-2) carried out in the Glovebox facility onboard the Space Shuttle (Nayagam and Calvert, 1998). In the works planned here use is to be made of an experimental apparatus similar to that of the Droplet Combustion Experiment (DCE) with few minor modifications, thus minimizing the development costs. The DCE apparatus has a fiber-support capability, but flow control needs to be added to provide the slow convective flow. Theoretically we propose to describe the radiative extinction using asymptotic techniques and to develop generalized flammability maps for the entire range of droplet combustion regimes possible in a microgravity environment. Our theoretical approach will be based on the works of Tarifa and

Crespo (1972), who employed perturbation techniques (ratio of gas to liquid density being the small perturbation parameter) to investigate the effects of small convection during droplet combustion in the limit of infinitely fast chemistry, and the analysis of Sohrab et al. (1982), where radiative extinction of diffusion flames in the presence of gas-phase radiation is described. The theoretical effort thus is essentially an extension of previously available mathematical tools extended to the present problem. An approach of this nature while minimizing the development time provides techniques to correlate the experimental data in a generalized fashion. Detailed numerical model development is not currently planned. The results of this study, however, could be compared to the 2-d, axisymmetric droplet combustion code under development in another project funded by NASA (Lee et al. 1996) if opportunity arises.

REFRENCES

Chao, B. H., Law, C. K., and T'ien, J. S., "Structure and extinction of diffusion flames with flame radiation," Twenty-Third Symposium (International) on Combustion, The Combustion Institute, Pittsburgh, 1990, pp. 523-531.

Dietrich, D. L., Haggard, J.B., Jr., Dryer, F. L., Nayagam, V., Shaw, B. D. and Williams, F. A., *Twenty-sixth Symposium (International) on Combustion*, The Combustion Institute, Pittsburgh, PA, 1996.

Lee, C. J., Tomboulides, Marchese, A. J., Yetter, R. A.,Dryer, F. L., and Orsag, S. A., "Droplet combustion in a low Reynolds number flow environment," Eastern States Section Meeting of the Combustion Institute, December, 1996.

Nayagam, V., Haggard, J. B., Jr., Colantonio, R. O., Marchese, A. J., Dryer, F. L., Zhang, B., and Williams, F. A., "N-heptane droplet combustion in oxygen-helium mixtures at atmospheric pressure," AIAA Journal, Vol. 36, No.8, 1998, pp. 1369-1378.

Nayagam, V., and Calvert, M. E., "Forced Convective Burning of Two-droplet n-Decane Linear Arrays in Microgravity," Proceedings of the 1998 Technical Meeting of the Central Sates Section of the Combustion Institute, Lexington, KY, pp. 87-91.

Shorab, S. H., Linan, A., and Williams, F. A., "Asymptotic theory of diffusion flame extinction with radiant loss from the flame zone," 1982, *Combst. Sci. Tech.* **27**, 143-154.

Tarifa, C. and Crespo, A., "Droplet combustion at high pressures with unsteady effects," Air Force Office of Scientific Research, Office of Aerospace Research. Grant F61052-69-C-0035. Final Report, 1972.

T'ien, J. S., "The possibility of a reversal of material flammability ranking from normal gravity to microgravity," Combustion and Flame, 1990, Vol. 80, pp. 35-357.

T'ien, J. S., "Radiative extinction of diffusion flames - A review," Asia-Pacific Conference on Combustion, Osaka, Japan, May 12-15, 1997.

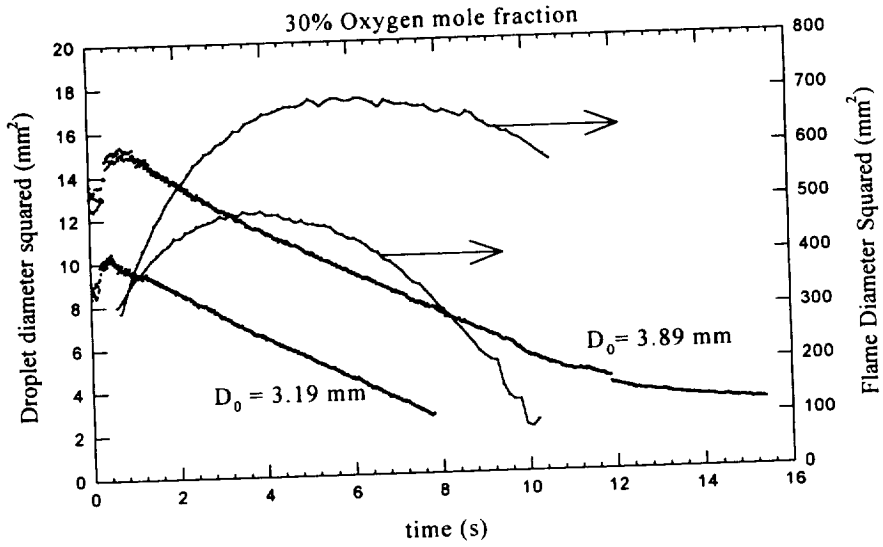

Figure 1. Diffusive and radiative extinction of n-heptane droplets in oxygen-helium (30%-70%) environment at 1-atm pressure.

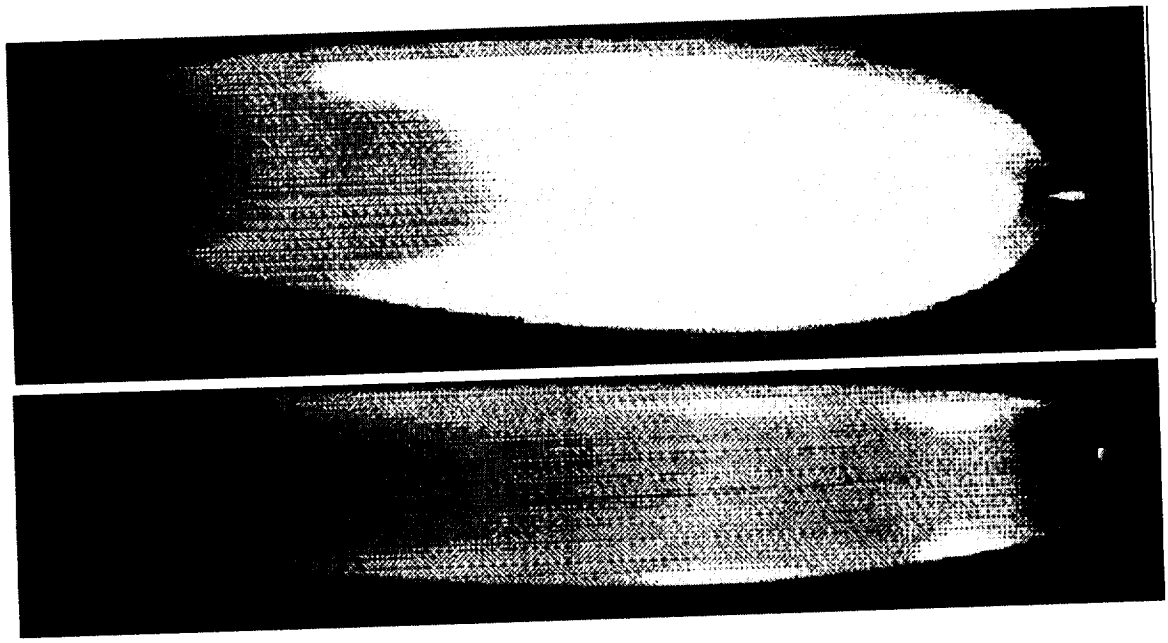

Figure 2. N-Decane droplets burning in air at 1-atm. pressure under microgravity for Reynolds number, Re=28 (top) and Re=73 (bottom).

S107-25

COMBUSTION OF INDIVIDUAL BUBBLES AND SUBMERGED GAS JETS IN LIQUID FUELS

Daniel E. **Rosner,** Yale University, Dept. Chemical Engineering and *Center for Combustion Studies,* New Haven, CT 06520-8286 USA (E-mail: *daniel.rosner@qm.yale.edu*)

INTRODUCTION

Motivated by industrial "submerged flame" reactor experience, in which oxygen gas jets were ignited in liquid crude oil to synthesize acetylene and ethylene (see Fig. 1, below), we propose a sequence of fundamental microgravity and ground-based experiments, as well as ancillary theoretical studies, on the combustion of oxygen(-containing) *bubbles* in liquid fuels---especially transparent liquid hydrocarbons. We demonstrate below that the detailed study of the combustion of large spherical bubbles is best carried out in a microgravity environment and that useful single-bubble data *can* probably be obtained in existing drop-tower facilities.

The broad **objectives** of this new research program† may be summarized as follows:

- To exploit the microgravity environment and modern analytical/numerical/experimental techniques to carefully study a rather unexplored mode of *liquid fuel combustion----ie.*, the transient combustion of an isolated spherical gaseous *oxidizer bubble*
- To use microgravity-derived insights, ancillary theoretical/numerical studies and new ground-based laboratory studies of combustion in bubble columns and submerged jets to provide a more rational basis to ultimately design improved "submerged gas jet combustors" for use in ground-based synthesis-oriented chemical industry, especially when the liquid "fuel" (feedstock) is difficult to "atomize" (because of its viscosity or "chemical aggressiveness")
- To open up a relatively virgin branch of *bubble dynamics* dealing with *intra-bubble chemical reactions.* This can be later extended to more complex systems such as oxidizer bubbles in more energetic fuels (such as hydrazine or molten aluminum), or, conversely, *fuel* vapor pockets in non-cryogenic and cryogenic liquid *oxidizers*

Ironically, fundamental studies of this neglected branch of combustion should, as byproducts, shed valuable new light on many apparently different modes of combustion or bubble-contacting devices including, perhaps, the combustion of *foams* containing air.

PREMISE

An interesting and potentially useful yet neglected mode of liquid fuel combustion is that associated with the consumption of one/more near-spherical oxidizer vapor *bubbles*. However, because of the large density difference between the liquid fuel and the vapor, even for transparent fuels with large surface tensions, such studies are not readily done in a ground-based laboratory due to gravitationally-induced bubble distortion or bubble breakaway and rise through the liquid. Moreover, because the total diffusion-controlled combustion time will scale with the *square* of the initial bubble diameter, while the ignition time will scale *linearly* with $d_{b,o}$, there is an incentive to study rather large bubbles to minimize the inevitable effects of asymmetric ignition transients. These facts, combined with an interest in hydrocarbon fuels with low surface tension, make the *microgravity* environment *very* attractive for such fundamental combustion studies. Of course, bubble *reactors* are common in ground-based chemical industry (*eg.*, partial oxidations of liquid hydrocarbons (say, *p*-xylene) to produce polymer pre-cursors (say, terephthalic acid).*in solution*; see, *eg.*, Godbole and Shah (1986)), and instructive experiments on bubble *combustion* (*eg.*, a single column of ignited oxidizer bubbles rising in a liquid fuel-filled channel) are planned as part of this program However, the pricipal focus of this program will be the design of ancillary *microgravity* single bubble combustion experiments, initially for the drop-tower environment.

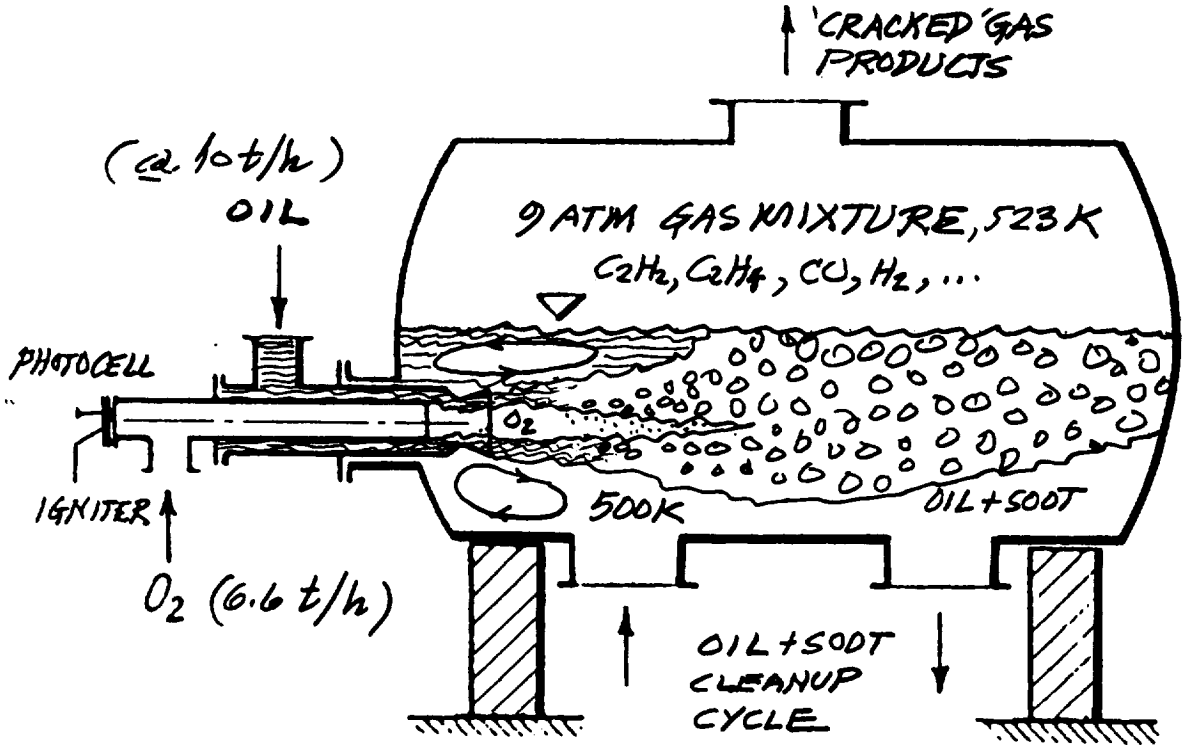

Fig. 1 Principal features of the BASF "submerged flame" acetylene synthesis reactor (adapted from Friz (1968))

REVIEW OF RELEVANT RESEARCH

Acetylene Synthesis *via* a "Submerged Flame" in Crude Oil

From the vantage point of this program, a very interesting and potentially instructive *precedent* † is the BASF "partial combustion" method for making acetylene at *ca.* 10% yield using pressurized oxygen gas bubbling through hot *liquid* petroleum ("crude" oil). Figure 1 shows the principal features of this so-called "submerged flame" reactor. We note that, in contrast to ordinary liquid fuel 'spray' combustors, in this relatively unfamiliar class of chemical synthesis reactors the (difficult to "atomize") liquid fuel/feedstock is the *continuous* (not dispersed) phase! In this case the fuel bath not only supplies the fuel for combustion energy release in the vapor phase, it also supplies the pyrolysis precursor (to produce acetylene and ethylene) and the quenching medium†. A significant fraction of the inevitable byproduct soot is also captured by this oil bath, which then becomes suitable as a slurry fuel for supplementary (on-site) power generation or process heat. Evidently, a pilot scale unit producing *ca.* 40 tons/day of acetylene was operational in Milan, Italy in 1974 (Bauer and Taglieber(1975); see, also: Friz (1968)) and it would be fascinating to gain access to the (primitive?) design procedures (perhaps in part *via* the patent literature) used to guide the selection of equipment dimensions and operating conditions. Even today, virtually no fundamental information necessary to rationally design such submerged gas jet combustors can be found in the open* literature. Needless to say, very much less was known/published in the *pre-1968* period!

† Contrast this with the better-known (and somewhat higher yield) *pre-vaporization*, rich premixed-then-quenched combustion route to acetylene synthesis (see, *eg.*, Rosner (1997)).

* High speed submerged oxygen jets (called *tuyures* or "lances") are widely used in metallurgical processing, including modern steelmaking (see, *eg.*, Ohashi(1992))

Fully Transient Combustion of an Isolated Fuel Droplet

Not surprisingly, the "unit" liquid fuel combustion problem of greatest fundamental interest here shares many features in common** with the now-classical and much more familiar "inverse"¶ problem of transient liquid *fuel droplet* combustion near its critical pressure (see, *eg.*, Rosner and Chang(1973)). Indeed, our recommended "heirarchical" theoretical attack on the bubble combustion problem would exploit approximations/methods now familiar from earlier fuel droplet studies----starting with the approximations of unit Lewis number and high Damkohler number (intra-bubble diffusion flame sheet) in the first year and culminating with more kinetically realistic numerical models to incorporate the essential features of acetylene formation and soot formation on the fuel-rich side of the laminar diffusion flame.

PLANS

Ground-Based Research: *Experiments*

The density ratio disparity responsible for the need for a microgravity environment to study this type of liquid fuel combustion is also responsible for the happy fact that the time to consume an *oxygen bubble* will be much smaller than the time required to consume fuel droplets of comparable initial size! This means that, while ordinary *drop towers* provide inadequate time to study many features of large single *fuel droplet* combustion, they are expected to provide adequate time for bubble combustion experiments for many, if not all, interesting fuels/conditions. Also:

- By exploiting transparent viscous fuels or fuels with rather high surface tension, and possibly exploiting downward convection, it may be possible to perform useful preliminary studies of electrical spark-ignited combustion in small single bubbles (1st and 2d y). Of immediate interest will be measurements of bubble diameter *vs.* time and the time to extinguish reaction (and associated chemiluminescence) within the bubble
- In the 2d year we are planning studies of bubble "trains" (or columns) from a single vertical oxygen gas cylindrical source at the base of a 'quiescent' (baffled) fuel channel with provision to ignite bubbles at the moment of breakaway. Video records of bubble dynamics will be combined with flame luminosity and exit gas composition measurements. Results will be compared with theoretical expectations to assess convective effects for rising bubbles over a range of sizes. All important effects of ignition/combustion on the observed bubble dynamics/stability will be recorded and contrasted with the corresponding behavior of non-ignited bubbles under otherwise identical conditions.
- Potentially instructive ancillary experiments are also contemplated. One would be the use of an isothermal liquid ("reactive liquid-liquid-extraction") analog---*viz.* rising liquid droplets in a host immiscible liquid with a diffusion-controlled reaction of a dilute solute taking place within the rising droplet. Another would be the ability of the host fluid to capture an aerosol (*eg.*, suspended soot) initially uniformly distributed within a rising gas bubble.

Ground-Based Research: *Theory*

Our approach to theory development will be "heirarchical", and, at each stage of the proposed program, theoretical predictions will guide the experimental designs and goals. Conversely, new experimental results will guide the evolution of the theory, probably in presently unforseen ways.

Our first year studies will exploit approximations/methods now familiar from earlier fuel droplet studies----starting with the approximations of unit Lewis number and high Damkohler number (intra-bubble diffusion flame sheet) (*cf.* Rosner and Chang(1973)). Of principal immediate interest will be the evolution of bubble radius and intra-bubble diffusion flame radius, and the total

**A significant difference is that while the classical fuel droplet envelope flame combustion problem can often be simplified *via* a quasi-steady (QS-) approximation, this will never be justified for ordinary intra-bubble combustion
Perhaps closer to the present case is the behavior of a LOX droplet in an environment of hydrogen vapor----relevant to the analysis of high-performance cryogenic liquid propellant thrustors (Deplanque and Sirignano (1993)).

time required to consume the oxygen inventory of the original bubble*. In subsequent years the most restrictive assumptions will be successively "relaxed", especially those dealing with variable thermophysical properties, heat loss to the fuel bath, dissolution of combustion product(s) in the fuel

bath, multi-component fuels, and non-unity Lewis number effects. By the third year, more computationally intensive analyses ("numerical experiments") will be carried out to deal with homogeneous chemical kinetic effects, especially those relevant to bubble "extinction", and acetylene+ ethylene formation. By the fourth year, we propose incorporating a kinetically realistic *soot* model on the fuel-rich side of the laminar diffusion flame, allowing for the thermophoretically driven soot "loss" to the surrounding liquid fuel, and any soot formed even *after* the oxygen initially present in the bubble has been consumed. These predictions would be compared to observed acetylene and soot "yields", including, if possible, BASF experience.

REFERENCES

Bauer, K.G., and Taglieber, K., "Neuentwicklungen beim Tauchflammenverfahren", *Chemie-Ing. Techn.* **47** Jahrg. 1975, p. 385

Clift, R., Grace, J.R. and Weber, M.E. (1978), **Bubbles, Drops and Particles**, Academic Press, NY

Deplanque, J.P. and Sirignano, W.A. (1993) "Numerical Study of the Transient Vaporization of an Oxygen Droplet at Sub- and Supercritical Conditions", *Int. J. Heat Mass Transfer* **36** (2) 303-314

Friz, H. (1968), "Neuere Entwicklungen der Acetylen-Herstellung bei der BASF", *Chem. Ing. Tech.* **40** Jahrg. 1968 Heft 20, pp. 999-1004; see, also, Bauer, K.G.(1969),"Acetylene From Crude Oil Makes Debut in Italy", *Chem. Eng.* Feb.10; p 82

Godbole, S.P. and Shah,Y.T.(1986), "Design and Operation of Bubble Column Reactors", Ch.39 in *Encyclopedia of Fluid Mechanics*, Vol. **3:** Gas/Liquid Flows, pp 1216-1239, Gulf Publishing Co., Houston TX

Gomez, A. and Rosner, D.E. (1993), "Thermophoretic Effects on Particles in Counterflow Laminar Diffusion Flames", *Comb. Sci. Tech.* **89** 335-362

Labowsky, M.J. and Rosner, D.E. (1978)," Conditions for 'Group' Combustion of Droplets in Fuel Clouds", Proc. Symp. **Evaporation/Combustion of Fuel Droplets**, ACS *Adv. Chem Ser*, No. 166, 63-69

Ohashi, N. (1992), "Modern Steelmaking", *American Scientist*, **80**, 540-555

Rosner, D.E.(1967), " On Liquid Droplet Combustion at High Pressures", *AIAA J.*, **5** (1), 163-166

Rosner, D.E. and Chang, W.S. (1973), "Transient Evaporation and Combustion of a Fuel Droplet Near its Critical Temperature", *Comb. Sci. Techn.* 7, 145-158

Rosner, D.E. (1972), "Liquid Droplet Vaporization and Combustion", Section 2.4 of Harrje, D.T. ed. (*loc.cit.*) NASA SP 194, pp 74-100

Rosner, D.E. (Fall 1997) " Combustion Synthesis and Materials Processing", *Chem Eng. Educ.* , Amer. Soc. Engrg. Educ., pp 228-235

Rosner D.E. (1986) **Transport Processes in Chemically Reacting Flow Systems**, Butterworths-Heinemann (Stoneham, MA); 3d printing 1990

Rosner, D.E., Mackowski, D.W., and Garcia-Ybarra, P.(1991) "Size- and Structure Insensitivity of the Thermophoretic Transport of Aggregated 'Soot' Particles in Gases", *Comb. Sci. Tech.* 80 (1-3) 87-101

*Clearly a decisive dimensionless parameter governing the performance of submerged flame reactors will be a Damkohler number based on the *ratio* of the mean bubble *residence time* to this particular time (to consume the initial O2 inventory); see, by analogy, page 442 of Rosner (1986) for fuel spray combustors.

5108-29

ACOUSTICALLY FORCED, CONDENSED PHASE FUEL COMBUSTION UNDER MICROGRAVITY CONDITIONS

O. I. Smith[1], A. R. Karagozian[2], H.-C. Kim[3], and C. Ghenai[4]
Department of Mechanical and Aerospace Engineering, UCLA
48-121 Engineering IV, Los Angeles, CA 90095-1597
[1]osmith@seas.ucla.edu [2]ark@seas.ucla.edu [3]heonchan@seas.ucla.edu [4]cghenai@seas.ucla.edu

INTRODUCTION

The focus of this project is on understanding and quantifying the effects of external acoustical perturbations on combustion of condensed fuels under microgravity conditions. The issue of acoustic excitation of flames in microgravity is especially pertinent to understanding the behavior of accidental fires which could occur in spacecraft crew quarters and which could be affected by pressure perturbations as result from ventilation fans or engine vibrations. While in normal gravity, studies have long shown that there can be a significant increase in fundamental reaction and transport processes with the imposition of an external acoustical field[1], under reduced gravity, the elimination of natural convection means the effect of acoustic excitation could be far more pronounced on flame behavior.

Experiments as well as numerical computations will be performed in this study. The geometry of the combusting fuel droplet has been selected. While it is widely recognized that single droplet combustion is a problem well suited for fundamental microgravity studies[2], the spherical geometry here is selected purely for experimental and numerical convenience. We plan to examine combustion of very large droplets, such that curvature effects are relatively unimportant. Hence we expect the results of this study to apply as well to condensed fuel combustion in other geometries.

BACKGROUND

In a gravitational field, studies have long shown that there can be a significant increase in fundamental heat and mass transfer rates from reactive surfaces with the imposition of an external acoustical field. Yet as seen by Saito, et al.[1], evaporative or combustion rate constants for a fuel droplet can increase substantially when the droplet is situated at a pressure antinode, but when the droplet is located at a pressure node, there may be little appreciable change in the evaporation or combustion rates. Theoretical models of evaporating droplets and burning char particles[3] similarly indicate the potential for transport enhancement under specific conditions of acoustic excitation.

While extensive experiments have been conducted pertaining to microgravity droplet combustion and associated phenomena[2], to our knowledge the behavior of burning droplets exposed to acoustic forcing in microgravity has not been studied. In fact, it was only recently that the acoustically excited, *non-reacting* droplet problem in microgravity was studied experimentally during a Shuttle flight[4], focusing on dynamic surface tension. Excellent correspondence was found between observed (transient) droplet shapes and numerical predictions[5] using the boundary integral method.

PLANNED MICROGRAVITY EXPERIMENTS

As noted, the experimental component of the proposed study will examine the burning characteristics of droplets which are exposed to acoustical excitation within a low- or microgravity

environment. Most of the tests are to be conducted in a low-g aircraft flying in a parabolic trajectory. Although the aircraft microgravity conditions are far from perfect (e.g., due to "g-jitter" effects), they will clearly introduce only negligible errors when there are high enough levels of acoustic forcing. However, a limited number of preliminary experiments will be conducted in the NASA Lewis drop towers to validate the method used for fixing droplet diameter and to determine the range of acoustic forcing levels where valid aircraft data may be expected.

The droplet and flame are to be centered on the axis of a cylindrical acoustic waveguide in the experiment. Acoustic waves are to be excited by a speaker, with the waveguide tuned to produce standing waves by adjusting the position of the speaker and/or termination. We plan to use a 90 cm waveguide, corresponding to a half wave at 200 Hz in air at 300K. The droplet could be located at the midpoint, or at the velocity antinode (pressure node) for 200 Hz excitation, but could be situated away from the pressure node at higher frequencies, mimicking the more typical practical situation in which acoustic forcing results in perturbation of both pressure and velocity. Since the diameter of the waveguide is much larger than that of the droplet, the latter essentially sees plane waves.

We intend to work with fuel droplets of diameters near 2 mm. Because the selection of the spherical fuel droplet geometry is done purely for experimental and numerical convenience in examining the effects of acoustic perturbation on μg diffusion flames, such large droplets are an appropriate choice for the present study. Similar reasoning was used in prior microgravity droplet experiments[4] in which 25 mm, non-reactive droplets in an acoustic field were examined.

In the proposed studies the droplet is to be attached at the end of a quartz capillary through which fuel is fed. We propose to test several fuels of differing volatility and sooting properties (n-heptane, methanol, and diethylether), some of which have been extensively studied under reduced gravity conditions without forcing[6,7]. We recognize that the presence of the capillary will alter the burning rate from that in the absence of the capilliary, yet the capillary itself should not play any significant role in the comparison of acoustically excited vs. non-excited external conditions for the droplet.

The fuel flow rate here is to be adjusted so as to maintain the burning droplet at a constant diameter. In order to accomplish this, we plan to use an inexpensive semiconductor diode laser to backlight the droplet. The droplet shadow would then be magnified and imaged onto a diode array, first passing through a laser line filter to block most of the emission from the flame. The output from the diode array would be preprocessed and sent to a microprocessor based controller, where the size of the droplet shadow may be compared with a setpoint so that the fuel flow rate may be adjusted accordingly. This dynamic control of the fuel droplet diameter will be tested experimentally in one of the NASA Lewis drop towers.

The full experiment of the acoustically excited, burning droplet will be conducted in both the Lewis 5s drop tower (for concept testing) and in NASA low-g aircraft. Locations of the flame front and the soot shell[8] are to be monitored by two intensified CCD cameras. Radiation from the flame will impinge on a 300 nm short pass interference filter oriented at 45 degrees to the axis of the waveguide. The filter will also serve as a type of beamsplitter, reflecting radiation with $\lambda \geq 300$ nm into one camera and transmitting radiation with $\lambda \leq 300$ nm to a second camera. Camera one captures radiation in the visible and IR, which could be dominated by blackbody emission from the soot shell where one is present. Radiation below 300 nm would be dominated by chemiluminescence from electronically excited hydroxyl radicals.

Pressure disturbances resulting from acoustic excitation can produce distortions in droplet shape from the spherical geometry, as seen in non-reactive experiments[4,5]. We plan to limit the acoustical forcing intensity in the proposed experiments to a small enough magnitude (< 100 dB) so that the droplet shape is not strongly distorted. The primary reason for this imposed limitation is that the diode array will allow us to monitor images in only one dimension. Alterations in the shape of the soot shell and flame (via chemiluminescence of OH) will be detected, however.

PLANNED COMPUTATIONAL STUDIES

There have been extensive modeling efforts directed toward representation of the single burning droplet in microgravity in the absence of acousic perturbation, with differing degrees of complexity in the reaction kinetics used[2,6,7], in representation of soot generation and behavior[9,10], and in the representation of radiative effects. While models for the burning droplet exposed to acoustic disturbance have not been developed, to our knowledge, models for the acoustically excited, spherical, burning char particle with simplified kinetics[3] and for a deformed non-reactive drop in an acoustic field under normal microgravity conditions[5] have relevance to the present study. The highly successful calculations of Shi and Apfel[5] for a deformed drop in an acoustic field indicate that, for certain forcing frequencies and large sound pressure levels, the droplet aspect ratio can deviate significantly from unity. Shi and Apfel used the boundary integral technique to resolve the droplet shape, and obtained excellent correspondence with experimental results in microgravity[4].

For the acoustically disturbed, burning droplet in microgravity, periodic deformations (local stretching) of the diffusion flame surrounding the droplet are likely to occur for even low levels of acoustic forcing, while deformations in the droplet shape will depend on the level of acoustic excitation. Hence while the experimental component of the present study will limit sound pressure levels to magnitudes for which the droplet will remain roughly spherical (< 100 dB), the computational studies will consider acoustic disturbances which may be so large as to deform the droplet shape, as done in non-reactive studies[4,5].

Accurate representation of the acoustically perturbed, burning droplet will require accurate resolution of characteristic phenomena thought or known to be important, including complex reaction kinetics, presences of the soot shell and associated radiative effects, and deformation of the flame and possibly the droplet itself. We expect to perform the modeling effort here with a multi-pronged approach, with increasing degrees of complexity incorporated into the computations.

First, we are in the process of developing a one-dimensional (spherically symmetric) model for the problem with an imposed oscillatory pressure and velocity field, assuming the droplet to remain spherical but with the possibility of the flame responding to the pressure field through oscillations in the radial direction. Alternative reaction mechanisms will be incorporated for the several types of fuel droplets to be examined in the experimental studies. Professor Dryer's group at Princeton has kindly provided CHEMKIN input data for kinetic mechanisms associated with methanol and n-heptane reactions[6,7], to be incorporated in the present modeling. The effect of the relative position of the droplet with respect to the spatial distribution of the pressure magnitude will be explored. Different levels of numerical resolution of the flame front, ranging from first order upwinding to third order essentially-non-oscillatory (ENO) spatial integration, will be performed. Added degrees of complexity in the reaction process, including models for soot formation, as in prior studies[9,10], will also be explored.

The second level of modeling will continue to incorporate a spherical droplet but with the pos-

sibility of a two-dimensional, longitudinally symmetric (deformed) burning fuel droplet exposed to the longitudinal acoustic forcing. Here it is expected that a higher order scheme for resolution of the flame front (with a relatively coarse grid) will be used, as is possible with ENO methods. As described above, different levels of complexity in the reaction kinetics and in the soot model will be examined, and results will be compared directly with experimental observations.

The final level of modeling will examine the possibility of deformation of the droplet as well as the diffusion flame resulting from the acoustic perturbations. As done in the non-reactive droplet model of Shi and Apfel[5], the acoustical radiation pressure field acting on the droplet will include components which apply "suction" in one direction and "squeezing" in the opposite direction. The resulting exterior pressure field may then be characterized in terms of an incident wave and a wave scattered by the droplet surface. The droplet surface deformation will be solved using either the boundary integral technique or level set methods. Depending on the results of the first two levels of modeling, increased degrees of complexity in the reaction kinetics and soot representation will be included.

References

[1] Saito, M., Sato, M., and Suzuki, I., *Fuel, 73*, 349, 1994.

[2] Law, C. K. and Faeth, G. M., *Prog. Energy Combust. Sci., 20*, 65, 1994.

[3] Ha, M. Y. and Yavuzkurt, S., *Combust. Flame, 86*, 33, 1991.

[4] Apfel, R. E., et al., *Phys. Rev. Lett., 78(10)*, 1912, 1997.

[5] Shi, T. and Apfel, R. E., *Phys. Fluids, 7*, 1545, 1995.

[6] Marchese, A.J., Nayagam, N.V., Colantonio, R., and Dryer, F.L., *26th Symp. (Int.) on Comb.*, 1209, 1997.

[7] Nayagam, V., Haggard, J.B. Jr., Colantonio, R.O., Marchese, A.J., Dryer, F.L., Zhang, B.L., and Williams, F.A., *AIAA J., 36*, 1369, 1998

[8] Jackson, G. S., Avedisian, C. T., and Yang, J. C., *Int. J. Heat Mass Trans., 35*, 2017, 1992.

[9] Said, R. , Garo, A., and Borghi, R., *Combust. Flame, 108*, 71, 1997.

[10] Moss, J. B., Stewart, D. C., and Syed, K. J., *22nd Symp. (Int.) on Comb.*, 413, 1988.

OMIT THIS PAGE

Soot Processes

5109-29

EFFECTS OF STRUCTURE AND HYDRODYNAMICS ON THE SOOTING BEHAVIOR OF SPHERICAL MICROGRAVITY DIFFUSION FLAMES*

P. B. Sunderland[1], R. L. Axelbaum[2], and D. L. Urban[1]
[1]NASA Glenn Research Center, Cleveland
[2]Department of Mechanical Engineering, Washington University, St. Louis

INTRODUCTION

Recent experimental, numerical and analytical work has shown that the stoichiometric mixture fraction (Z_{st}) can have a profound effect on soot formation in diffusion flames (Du and Axelbaum, 1995, 1996; Lin and Faeth, 1996a, 1996b, 1998; Chao *et al.*, 1999). These findings were obtained at constant flame temperature (T_{ad}), employing the approach described in Du and Axelbaum (1995, 1996). For example, a fuel mixture containing 1 mole of ethylene and 11.28 moles of nitrogen burning in pure oxygen ($Z_{st} = 0.78$) has the same adiabatic flame temperature (2370 K) as that of pure ethylene burning in air ($Z_{st} = 0.064$). An important finding of these works was that at sufficiently high Z_{st}, flames remain blue as strain rate approaches zero in counterflow flames, or as flame height and residence time approach infinity in coflowing flames. Lin and Faeth (1996a) coined the term *permanently blue* to describe such flames.

Two theories have been proposed to explain the appearance of permanently-blue flames at high Z_{st}. They are based on (1) hydrodynamics (Sugiyama, 1994, Lin and Faeth, 1996a, 1996b) and (2) flame structure (Du and Axelbaum, 1995; Chao *et al.*, 1999). Previous experimental studies in normal gravity are not definitive as to which, if either, mechanism is dominant because both hydrodynamics and structure suppress soot formation at high Z_{st} in coflowing and counterflowing diffusion flames. Figure 1 illustrates the hydrodynamic effect. In counterflow flames with $Z_{st} < 0.5$ (Figure 1a) streamlines at the flame sheet are directed toward the fuel. Newly formed soot is convected into richer regions, favoring soot growth over oxidation. For $Z_{st} > 0.5$ (Figure 1b) convection at the flame is toward the oxidizer, thus enhancing soot oxidization. Thus, in counterflow flames, hydrodynamics causes soot to be convected towards the oxidizer at high Z_{st}, which suppresses soot formation.

Axelbaum and co-workers maintain that while the direction of convection can impact soot growth and oxidation, these processes alone cannot cause permanently-blue flames. Soot growth and oxidation are dependent on the existence of soot particles and the presence of soot is invariably accompanied by yellow luminosity (Du *et al.*, 1988). Soot-particle inception, on the other hand, arises from gas-phase reactions and its dependence on flow direction is weak, similar to that of other gas-phase reactions in flames. For example, when the flame moves across the stagnation plane no significant changes in flame chemistry are observed. Furthermore, since the soot-inception zone has a finite thickness, soot has been produced in counterflow flames with $Z_{st} > 0.5$ (Du and Axelbaum, 1995). As shown in Figure 2 and described in greater detail in Du and Axelbaum (1995), for large Z_{st} the fuel concentration decreases and oxygen concentration increases in the soot forming regions of the flame. This yields a shift in the OH profile toward the fuel side of the flame, and this shift can dramatically influence soot inception because it essentially narrows the soot inception zone. Soot-free (permanently-blue) conditions can be realized when the structure of the flame is adjusted to the extent that significant oxidizing species

* Presented at the 5th Microgravity Combustion Workshop, Cleveland, 1999.

exist on the fuel side of the flame at temperatures above the critical temperature for soot inception, ca. 1250 K.

In previously considered flames it was impossible to independently vary flame structure and convection direction. In contrast, spherical diffusion flames (which generally require microgravity) allow both properties to be varied independently. We altered structure (Z_{st}) by exchanging inert between the oxidizer and the fuel and we independently varied convection direction at the flame sheet by interchanging the injected and ambient gases.

In this work we established four flames: (a) ethylene issuing into air, (b) diluted ethylene issuing into oxygen, (c) air issuing into ethylene, and (d) oxygen issuing into diluted ethylene. Z_{st} is 0.064 in flames (a) and (c) and 0.78 in flames (b) and (d). The convection direction is from fuel to oxidizer in flames (a) and (b) and from oxidizer to fuel in flames (c) and (d). Under the assumption of equal diffusivities of all species and heat, the stoichiometric contours of these flames have identical temperatures and nitrogen concentrations.

EXPERIMENTAL

The experiments were conducted in the NASA Glenn 2.2-second drop tower using a general-purpose combustion rig. The porous burner is a 6.4 mm diameter sphere with a 1.6 mm hole to its center and was sintered from 10 micron stainless steel particles. The sphere was supported and fed by a 1.6 mm stainless steel tube. All tests were conducted in quiescent ambient gas at 98 kPa. The present tests involved the following gases: ethylene, oxygen, synthetic air (21±0.02% oxygen by volume in nitrogen) and diluted ethylene (8.14±0.02% ethylene by volume in nitrogen). Purities of the individual gases were 99.999% (nitrogen and oxygen) and 99.9% (ethylene.) Nitrogen mixtures were prepared gravimetrically. Uncertainties in the flowrates (at the 95% confidence level) are estimated at 5%. Ignition was accomplished in microgravity. The flames were imaged through the chamber window (BK7) using a color CCD camera (Panasonic WV-CL352). Soot formation in diffusion flames commences at 1250 K (Sunderland *et al.*, 1995), at which temperature it emits visible light. Thus, diffusion flames that create soot necessarily emit yellow luminosity, and experiments have shown that the onset of yellow emissions is an effective means of determining soot inception limits in hydrocarbon diffusion flames (Du *et al.*, 1988). Testing in normal gravity has confirmed our video system to be sensitive to the presence of even trace quantities of soot in flames.

RESULTS AND DISCUSSION

Figure 3 shows color images of four flames that represent the four configurations considered. Each flame has an ethylene consumption rate of 1.51 mg/s. At least ten flames of each configuration were observed in order to confirm repeatability. The flames grow in size during the 2.2-s tests but appear to approach steady shapes prior to test completion. The approximate final diameters of the flames are marked in the figures; these were determined from contours of peak blue emissions (where visible). The flames shown in Figure 3 depict typical end-of-drop conditions. Flames in Figures 3b-d had little color variation throughout the 2.2-second tests while those in Figure 3a displayed a slowly decreasing yellow luminosity.

Figure 3a shows a flame of ethylene injecting into ambient air. This flame has a yellow interior surrounded by a well-defined blue corona. Figure 3b shows a flame of diluted ethylene issuing into ambient oxygen, which is pure blue and very bright. Figure 3c shows a flame of air issuing into ethylene, which is entirely yellow and the brightest observed. Finally, Figure 3d

shows a flame of oxygen issuing into diluted ethylene, which has a dim blue interior surrounded by a bright blue corona and which produces no soot.

The color images indicate that the sootiest flame involves air injecting into ethylene (Figure 3c). This is expected since both flame structure (small Z_{st}) and direction of convection (toward the fuel) promote soot formation. The soot formed in the fuel-rich region of this flame is convected into even richer regions, thus favoring soot growth and precluding soot oxidation. When we maintain the same Z_{st} as that of Figure 3c but reverse the convection direction, we obtain the flame of Figure 3a. The presence of soot in this flame indicates that when convection is toward the oxidizer, soot inception is not eliminated. Soot growth is suppressed and oxidation is enhanced but some regions of the flame are clearly yellow. On the other hand, a comparison of Figure 3c with Figure 3d reveals that for the same convection direction, increasing Z_{st} eliminates all soot even though convection would transport soot particles into the fuel rich region of the flame. Thus flame structure has a profound impact on soot formation. Finally, the flame involving diluted ethylene injecting into oxygen (Figure 2b) is soot free. In this case both structure ($Z_{st} = 0.78$) and convection direction (toward oxidizer) impede soot formation.

In summary, microgravity flames are uniquely capable of allowing independent variation of flame structure (i.e., stoichiometric mixture fraction, Z_{st}, through inert orientation) and direction of convection across the flame sheet while maintaining constant flame temperature. For these flames, structure was found to have a profound effect on soot production. Soot-free conditions were observed at high Z_{st} ($Z_{st} = 0.78$) and sooting conditions were observed at low Z_{st} ($Z_{st} = 0.064$) regardless of convection direction. Convection direction has a smaller impact on soot, with soot formation suppressed when convection at the flame sheet is directed toward the oxidizer.

ACKNOWLEDGMENTS

This work is sponsored by the Microgravity Research Division of the NASA Office of Life and Microgravity Sciences and Applications, with J. E. Brooker serving as Project Scientist. C. B. Lundquist assisted with the drop tests and H. D. Ross and S. A. Gokoglu provided helpful input.

REFERENCES

Chao, B. H., Liu, S. and Axelbaum, R. L. (1999), *Comb. Sci. Tech*, submitted.

Du, D. X., Axelbaum, R. L., and Law, C. K. (1988), *Twenty-Second Symposium (International) on Combustion,* The Combustion Institute, Pittsburgh, p. 387.

Du, J . and Axelbaum, R. L. (1995), *Combust. Flame* 100:367.

Du, J., and Axelbaum, R. L. (1996), *Twenty-Sixth Symposium (International) on Combustion,* The Combustion Institute, Pittsburgh, p. 1137.

Lin, K. C. and Faeth, G. M. (1996a), *J. Prop. Power* 12:691.

Lin, K. C. and Faeth, G. M. (1996b), *J. Prop. Power* 12:10.

Lin, K. C. and Faeth, G. M. (1998), *Combust. Flame* 115:468.

Sugiyama, G. (1994), *Twenty-Fifth Symposium (International) on Combustion,* The Combustion Institute, Pittsburgh, p. 601.

Sunderland, P. B., Köylü, Ü. Ö., and Faeth, G. M. (1995), *Combust. Flame* 100:310.

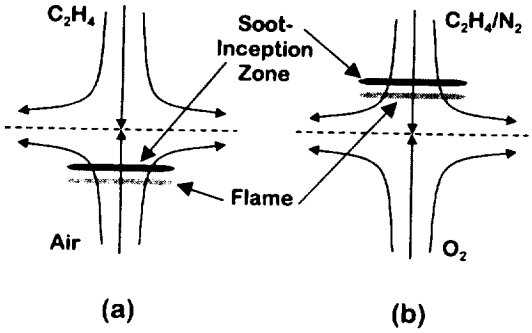

FIGURE 1 Schematic representation of counterflow flames with (a) $Z_{st} < 0.5$ such that the flame is on the oxidizer side of the stagnation plane and the flow is from the soot inception region toward the fuel source and (b) $Z_{st} > 0.5$ such that the flame is on the fuel side of the stagnation plane and the flow is from the soot inception region toward the oxidizer source.

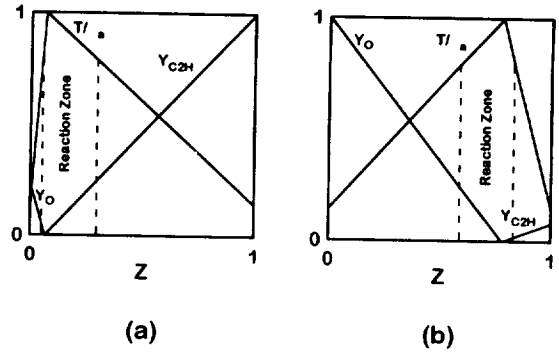

FIGURE 2 Plot of temperature (T) and major gas mass fractions (Y) versus mixture fraction (Z) for diffusion flames with (a) $Z_{st} = 0.064$ and (b) $Z_{st} = 0.78$. Reproduced from Du and Axelbaum (1995).

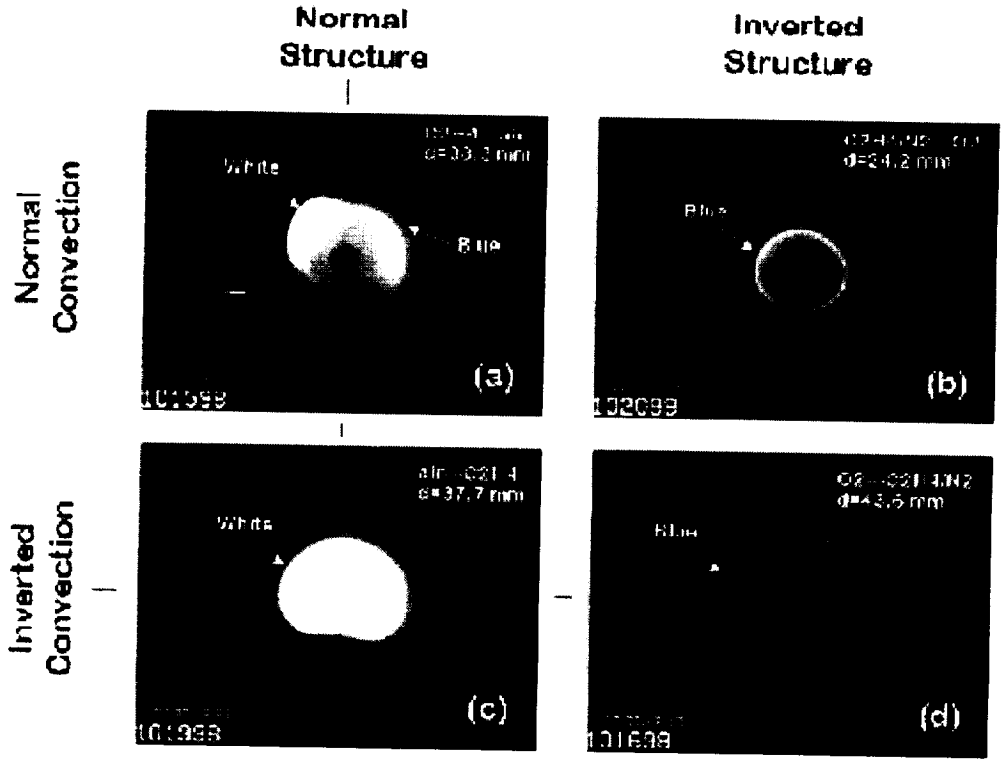

FIGURE 3 Color images of representative flames: (a) ethylene (1.51 mg/s) issuing into air, $Z_{st} = 0.064$, f1.4; (b) diluted ethylene (19 mg/s) issuing into oxygen, $Z_{st} = 0.78$, f1.4; (c) air (22 mg/s) issuing into ethylene, $Z_{st} = 0.064$, f6; (d) oxygen (5.2 mg/s) issuing into diluted ethylene, $Z_{st} = 0.78$, f6. The scale is revealed by the 6.4 mm spherical burner and by the noted approximate flame diameters, d. The ethylene consumption rate is 1.51 mg/s in all four cases.

S110-25

CARBON MONOXIDE AND SOOT FORMATION IN INVERSE DIFFUSION FLAMES

L.G. Blevins[1], G. W. Mulholland[1], R.W. Davis[2]
[1]National Institute of Standards and Technology, Building and Fire Research Laboratory,
100 Bureau Drive, Stop 8653, Gaithersburg, MD 20899-8653 USA
linda.blevins@nist.gov, george.mulholland@nist.gov
[2]National Institute of Standards and Technology, Chemical Science and Technology Laboratory,
100 Bureau Drive, Stop 8360, Gaithersburg, MD 20899-8360 USA
ronald.davis@nist.gov

INTRODUCTION

The objective of this project is to study carbon monoxide (CO) and soot formation in laminar, inverse diffusion flames (IDFs). The IDF is used because it is a special case of underventilated combustion. The microgravity environment is crucial for this study because buoyancy-induced instabilities impede systematic variation of IDF operating conditions in normal gravity. The project described in this paper is just beginning, and no results are available. Hence, the goals of this paper are to establish the motivation for the research, to review the IDF literature, and to briefly introduce the experimental and computational plan for the research.

MOTIVATION

Between 1972 and 1993, 73,000 people died in accidental fires in America.[1] Nearly seventy percent died from smoke inhalation, and many of them died from fires which progressed beyond flashover, the rapid change of a fire from a developing state to a fully-involved state. Flashover occurs when high-temperature fuel-rich gases accumulate within a room and ignite at a doorway or window where they mix with fresh air.[2] Carbon monoxide and soot are two hazardous components of the smoke that forms during the resulting underventilated combustion period. Hence, it is important to study the ways that these substances form in underventilated conditions.

While studies of underventilated, turbulent flames with various fuels have clearly established the importance of CO formation during underventilated burning,[3] the local conditions leading to CO (and soot) formation in these flames are difficult to deduce because theoretical predictions of turbulent reacting flows are difficult. Studying laminar flames provides a greater opportunity to predict local conditions and correlate them with global CO (and soot) measurements. This is the approach planned for the present project.

The planned research focuses on laminar IDFs because the IDF is related to the underventilated normal diffusion flame (NDF). In an IDF, the positions of the air and fuel streams are interchanged relative to a NDF. Hence, while a NDF is established at the interface between a fuel jet surrounded by air, an IDF is established at the interface between an air jet surrounded by fuel. The IDF and the underventilated NDF are related in that CO and soot which form on the fuel side of the flame can potentially escape without passing through the hot oxidative reaction zone. In the IDF, these fuel-formed species may be convected axially along the outer edge of the flame and bypass the flame tip entirely. In an underventilated NDF, these species may convect axially along the inner edge of the flame and pass through the open portion of the flame tip. In a sense, the IDF is an extreme case of the underventilated NDF, and allows the present study to focus on the type of fuel-formed species which bypass the hot oxidation zone in an underventilated flame.

LITERATURE REVIEW

The present authors are aware of only one past study of the CO and soot amounts produced by underventilated, *laminar* flames.[4] In this experimental study of NDFs, it was discovered that the ratio of volumetric CO concentration to carbon dioxide (CO_2) concentration was about one to two in the exhaust of underventilated methane (CH_4) and ethene (C_2H_4) NDFs over a range of operating conditions. In addition, the soot from these flames was more organic and agglutinated than that typically emitted from overventilated NDFs. The CO and soot yields were *not* correlated as expected based on overventilated flame studies. This study established the need for further research on the details of CO and soot formation during underventilated burning.

Compared to the vast NDF literature, relatively few studies have been performed using the IDF configuration.[5-22] The first studies of IDFs were published by Arthur and coworkers in the 1950s.[12-15] These authors performed extensive testing on IDFs burning with air and coal gas, CH_4, C_2H_4, propane (C_3H_8), and benzene. They discovered that the soot from IDFs was stickier and more viscous than that from normal flames, and that the hydrogen (H_2) content of the IDF soot was higher than that of NDF soot.[13] This soot structure is qualitatively similar to that discovered in underventilated NDFs.[4] In some cases, because Arthur *et al.* found that IDFs were difficult to stabilize between pure air and pure fuel, they studied flames between central O_2 jets and surrounding mixtures of (fuel + N_2).[12] Several years later, in 1979, Walker reported that, for air/natural gas flames, the IDF tip was more rounded than the NDF tip, the IDF was less luminous than the NDF, and the IDF soot was visible only near the flame tip.[11] This structure is shown schematically in Fig. 1 and in excellent color photographs in Refs 7 and 8.

Kent and Wagner performed a 1984 study of air/C_2H_4 IDFs surrounded by a glass tube.[8] They reported that their flames were stabilized by strong, buoyancy-induced recirculation zones in the annular region between the flame and the glass tube. Hence, it became apparent that IDFs formed between pure air and pure fuel were not independently stable over a wide range of operating conditions. Wu and Essenhigh addressed this issue in 1984.[5] They published stability maps of air/CH_4 IDFs obtained by systematically varying fuel and air inlet velocities. They found five types of flames, ranging from unstable, buoyancy-sensitive blue flames at very low fuel and air velocities, to stable, weak blue flames at low air and moderate fuel velocities, to stronger blue flames with orange-yellow caps at higher air velocities. Interestingly, these authors reported the existence of an unoxidized "pool" of CO and H_2 at the IDF tip.

When Sidebotham and Glassman published a 1992 study of air/C_2H_4 IDFs, they used a heavily-diluted fuel stream (92% N_2) and an oxygen-enriched air stream (36% O_2).[6] These authors determined that CO was formed on the fuel side of the temperature peak and did not penetrate across the reaction zone into the central air jet. They also found that the CO diffused radially outward into the surrounding fuel stream. They stated that the outwardly-diffusing CO could possibly quench in the cool fuel stream and be swept out of the flame as a net emission. Hence, this scenario, along with the flame-tip CO "pool" found by Wu and

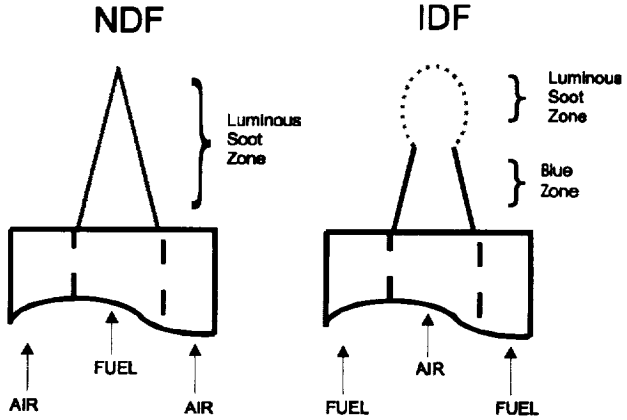

Fig. 1. Schematic showing visible appearance of sooting normal diffusion flame (NDF) and sooting inverse diffusion flame (IDF).

Essenhigh, supports a hypothesis that IDFs will emit large amounts of unoxidized CO, in a manner which is similar to underventilated NDFs.[4]

In 1994, Makel and Kennedy studied air/ C_2H_4 IDFs stabilized by a H_2 pilot flame.[9] They found that the integrated axial soot volume fraction in each flame increased and leveled off to a constant value with increasing axial distance, in contrast to the increasing and then decreasing trend measured in C_2H_4/air overventilated NDFs.[24] The IDF soot volume fractions presumably did not decrease because the soot did not pass through an oxidizing zone at the flame tip. This supports the hypothesis that IDF soot follows a pathway which is similar to that followed by underventilated NDF soot (i.e., it is not fully oxidized before exiting the flame).

Kang *et al.* published a 1997 study of air/C_3H_8 IDFs with diluted fuel (70% N_2) and oxygen-enriched air (40% O_2).[10] These authors demonstrated that the soot in an IDF experiences a temperature-time history similar to that of soot in a counterflow flame with the flame on the oxidizer side of the stagnation plane. They coined the phrase "soot formation flame" to describe these types of flames, as opposed to the phrase "soot formation-oxidation flame," which was used to describe NDFs and counterflow flames established on the fuel side of the stagnation plane.

The studies discussed above demonstrated that (1) buoyancy-induced instabilities impede systematic variation of pure IDF operating conditions in normal gravity, and (2) IDF CO and soot formation is similar to that in underventilated NDFs. The use of microgravity should eliminate the buoyancy-induced instabilities and allow a systematic study of underventilated-flame CO and soot formation.

To the present authors' knowledge, only two groups have previously studied microgravity IDFs.[25,26] Law *et al.* studied IDF structure in a low-pressure (1/4 atm) chamber.[25] These authors stabilized a burner-supported, spherical IDF by issuing a mixture of 10% O_2 and 90% N_2 through a porous sphere into a still environment containing H_2 mixed with about 2% CH_4. These authors did not report visible soot in their flames. Sunderland *et al.* found than drop-tower stabilized spherical IDFs of air issuing into C_2H_4 produced large amounts of soot which exited the flame without passing through the hot oxidation zone.[26] It is interesting to note that low-flow-rate CH_4/air and C_3H_8/air NDFs established in the NASA 2.2-Second Drop Tower had open tips similar to underventilated flames.[27,28]

RESEARCH PLAN

The specific project tasks are (1) to attempt to stabilize IDFs in a series of 2.2-second drop-tower experiments and capture the events with a video camera for assessment of their stability, (2) to gain an understanding of CO and soot formation in IDFs by analyzing the post-combustion products of CH_4 and C_2H_4 flames under normal and low gravity conditions, (3) to use a fiber-optic-coupled CO sensor to monitor the IDF tips during microgravity combustion, and (4) to model the flow field and soot particle temperature-time histories in both normal and low gravity conditions using an existing NIST computer program.[29] Post-flame amounts of CO and soot will be collected and measured. The soot will be analyzed for organic and graphitic content, for carbon and hydrogen content, and for primary sphere size, agglomerate size, and structure. The fiber-optic CO sensor will be based on near-infrared tunable diode laser absorption. The computer code features a particle transport model which includes the effects of inertial, thermophoretic, and gravitational forces.[30] The local computed flow conditions will be combined with the measured CO and soot information to gain insight into the conditions leading to the formation of these species during underventilated combustion.

ACKNOWLEDGMENTS

This research is supported by NASA Contract No. C-32069-J, with Dr. Peter Sunderland as technical contact and Dr. Kurt Sacksteder as technical monitor.

REFERENCES

1. Hall, J.R., Jr., "Burns, Toxic Gases, and Other Hazards Associated with Fires: Deaths and Injuries in Fire and Non-Fire Situation," NFPA, Quincy, MA, December 1996, p. 8.
2. Quintiere, James G., *Principles of Fire Behavior*, Delmar, Albany, NY, 1998, p. 170.
3. Pitts, W.M., *Prog. Energy and Combust. Sci.* 21:197 (1995).
4. Leonard, S., Mulholland, G.W., Puri, R., and Santoro, R.J., *Combust. Flame* 98:20 (1994).
5. Wu, K.T., and Essenhigh, R. H., *Twentieth Symposium (International) on Combustion*, The Combustion Institute, Pittsburgh, PA, 1984, p. 1925.
6. Sidebotham, G.W., and Glassman, I., *Combust. Sci. Technol.* 81:207 (1992).
7. Sidebotham, G.W., and Glassman, I., *Combust. Flame* 90: 269 (1992).
8. Kent, J.H., and Wagner, H.Gg., *Z. Phys. Chem (Munich)* 139:59 (1984).
9. Makel, D.B., and Kennedy, I.M., *Combust. Sci. Technol.* 97: 303 (1994).
10. Kang, K.T., Hwang, J.Y., Chung, S.H., and Lee, W., *Combust. Flame* 109:266 (1997).
11. Walker, J., *Scientific American* 241:192 (1979).
12. Arthur, J.R., and Napier, D.H., *Fifth Symposium (International) on Combustion*, The Combustion Institute, Pittsburgh, PA (1955), p. 303.
13. Arthur, J.R., Kapur, P.K., and Napur, D.H., *Nature* 169:372 (1952).
14. Arthur, J.R., and Littlejohn, R.F., *Nature* 169:288 (1952).
15. Arthur, J.R., Commins, B.T., Gilbert, J.A.S., Lindsey, A.J., and Napier, D.H., *Combust. Flame* 2:267 (1958).
16. Perthius, E., *Combust. Flame* 6:54 (1962).
17. McClure, H.H., Neely, W.J., and Elliott, J., *Chem. Eng. Prog.* 61:52 (1965).
18. Stansel, D.M., Laurendeau, N.M., and Senser, D.W., *Combust. Sci. Technol.* 104:207 (1995).
19. Partridge, W.P., Jr., and Laurendeau, N.M., *Fuel* 74: 1424 (1995).
20. Clausing, E.M., Senser, D.W., and Laurendeau, N.M., *Combust. Flame* 110:405 (1997).
21. Takagi, T., Xu, Z., and Komiyama, M., *Combust. Flame* 106:252 (1996).
22. Zhu, W., and Pratsinis, S.E., *AIChE Journal* 43:2657 (1997).
23. Partridge, W.P., Reisel, J.R., and Laurendeau, N.M., *Combust. Flame* 116:282 (1999).
24. Santoro, R.J., Semerjian, H.G., and Dobbins, R.A., *Combust. Flame* 51:203 (1983).
25. Law, C.K., Sung, C.J., and Zhu, D.L., *Fourth International Microgravity Combustion Workshop*, NASA Conference Publication 10194, 1997, p. 69.
26. Sunderland, P. B., Axelbaum, R. L., and Urban, D. L., "Effects of Structure and Hydrodynamics on the Sooting Behavior of Spherical Microgravity Diffusion Flames," Fifth Microgravity Combustion Workshop, 1999.
27. Bahadori, M.Y., Edelman, R.B., Stocker, D.P., and Olson, S.L., "Ignition and Behavior of Laminar Gas-Jet Diffusion Flames in Microgravity," *AIAA Journal* 28:236 (1988).
28. Hegde, U., Zhou, L., and Bahadori, M.Y., *Combust. Sci. Technol.* 102:95 (1994).
29. Davis, R.W., Moore, E.F., Chen, L.-D., Roquemore, W.M., Vilimpoc, V., and Goss, L.P., *Theoretical and Computational Fluid Dynamics* 6:113 (1994).
30. Burns, T.J., Davis, R.W., and Moore, E.G., *Aerosol Science and Technology* 27:1 (1990).

5111-25

Flow/Soot-Formation Interactions in Nonbuoyant Laminar Diffusion Flames

Z. Dai and G. M. Faeth
Department of Aerospace Engineering
The University of Michigan
Ann Arbor, MI48109-2140

INTRODUCTION

Nonpremixed (diffusion) flames are attractive for practical applications because they avoid the stability, autoignition, flashback, etc. problems of premixed flames. Unfortunately, soot formation in practical hydrocarbon-fueled diffusion flames reduces their attractiveness due to widely-recognized public health and combustor durability problems of soot emissions. For example, more deaths are attributed to the emission of soot (15,000-60,000 deaths annually in the U.S. alone) than any other combustion-generated pollutant (ref. 1). In addition, continuum radiation from soot-containing flames is the principle heat load to combustor components and is mainly responsible for engine durability problems of aircraft and gas turbine engines (ref. 2). As a result, there is considerable interest in controlling both soot concentrations within flames and soot emissions from flames. Thus, the objective of the present investigation is to study ways to control soot formation in diffusion flames by manipulating the mixing process between the fuel and oxidant streams. In order to prevent the intrusion of gravity from masking flow properties that reduce soot formation in practical flames (where effects of gravity are small), methods developed during past work (ref. 3) will be exploited to minimize effects of buoyant motion.

It is widely recognized that fast mixing is an effective way to reduce soot formation in diffusion flames (refs. 2-9). This idea has evolved empirically from the notion that residence times at fuel-rich conditions should be kept small to minimize soot growth. Several studies, however, suggest that the mechanism of fast mixing is important as well, and that soot formation can be reduced by causing velocities normal to the flame sheet to be sufficiently large and directed from the fuel-rich toward the fuel-lean side of the flame (ref. 9). Present considerations of this issue will be limited to laminar diffusion flames that are widely accepted to provide reasonable model flame systems for practical turbulent flames through the application of laminar flamelet concepts (ref. 9).

Appropriate mixing to control soot, with velocities normal to the flame sheet directed toward the fuel-lean side, can be provided by increasing air-stream velocities relative to fuel stream velocities, i.e., providing enhanced air-stream velocities as sketched in Fig. 1. This configuration involves a nonturbulent coflowing jet diffusion flame having uniform air and fuel velocities at the base of the flame. Typical streamlines, the locus of the flame sheet and the soot-containing regions are shown for conditions where air-stream velocities, u_a, are smaller (retarded) and larger (enhanced) than fuel-stream velocities, u_f. Soot particles are too large to diffuse like gas molecules and are mainly convected at the local velocity of the flow field. Then for retarded air-stream velocities, entrainment due to the higher velocity fuel stream causes the streamlines to

cross the flame sheet toward the fuel side. As a result, soot particles nucleate near the fuel-rich side of the flame sheet and are convected away from the flame sheet, yielding long residence times at fuel-rich conditions so that soot particle growth is enhanced. As a result, these soot particles become large and are difficult to oxidize completely when they reach the fuel-lean portions of the flame, which enhances soot emission. In contrast, when the air-stream velocity is enhanced, entrainment from the higher-speed air-stream causes streamlines to cross the flame toward the air side. This implies that soot particles begin to nucleate in the cool core of the fuel-rich side of the flame and then are immediately drawn across the flame to the fuel-lean region where they are readily oxidized because they have little time to grow at fuel-rich conditions. Thus, enhanced air-stream velocities intrinsically reduce residence times for soot growth compared to soot oxidation and offer a convenient way to control soot in nonpremixed flames (ref. 9).

Effects of velocities normal to the flame sheet on soot processes in laminar diffusion flames have been studied using coflowing and opposed-jet diffusion flames (ref. 9). Typical results for coflowing-jet diffusion flames are illustrated in Fig.2. These results involve laminar smoke point fuel flow rates, Q_f, as a function of the air/fuel-stream velocity ratios, u_a/u_f, at the base of 1,3-butadiene/air flames, however, results for other fuels are similar (ref.10). Combustion was observed at low-pressures in order to minimize effects of buoyancy on air/fuel-stream velocity ratios (ref. 11). Increasing air/fuel-stream velocity ratios clearly increases Q_f which implies increased resistance to the formation of soot, particularly at low pressure where changes of burner exit velocity ratio due to the intrusion of gravity are smallest. This behavior clearly supports the soot suppression argument discussed in connection with Fig.1.

Many practical combustor designs to minimize soot emissions appear to exploit effects of enhanced air-stream velocities as well (refs. 2, 7, 9), however, the effectiveness of the approach is neither widely recognized nor understood, which inhibits effective exploitation of this technology. No attempt has been made to assess capability to predict the properties of the resulting soot-free blue flames either, even though such flames are of substantial practical value. Based on these observations, the main objectives of the present investigation are as follows:

(i) Measure flame structure and soot properties of weakly-buoyant laminar jet diffusion flames in order to quantify effects of enhanced air (oxidant) stream velocities on soot processes and on the conditions to achieve soot-free (permanently blue) flames.

(ii) Complete numerical simulations corresponding to the conditions of the experiments using detailed transport and reaction mechanisms and focusing on computationally tractable soot-free flames.

Similar to past work (ref. 10) the study is limited to laminar diffusion flames as an experimentally and computationally tractable model of practical turbulent diffusion flames through laminar flamelet concepts (refs. 3 and 9).

EXPERIMENTAL METHODS

A sketch of the test apparatus appears in Fig. 3. Methods used are similar to past studies of soot-containing laminar jet diffusion flames in this laboratory (ref. 11). The flames operate at low pressures within a windowed chamber to reduce effects of buoyancy. Measurements include

dark-field photographs, soot volume fractions by laser extinction, soot temperatures by multiline emission, soot structure by thermophoretic sampling and TEM, gas compositions by sampling and gas chromatography, gas velocities by laser velocimetry and gas temperatures for soot free conditions by extrapolating results for various-sized thermocouples.

Test conditions include various coflow velocities similar to Fig.2. The use of swirl velocities to achieve larger enhanced air-stream velocities without blowoff is also of interest.

COMPUTATIONAL METHODS

Computations of flame structure will be undertaken using methods similar to past work. Notably, chemical mechanisms for soot-free hydrocarbon/air flames are substantially simplified compared to soot-containing flames so that multidimensional computations, particularly for the boundary-layer like flames to be studied, remain tractable. Results to be sought include predictions of flame shapes and insight about conditions at the onset of soot formation.

ACKNOWLEDGEMENTS

This research is sponsored by NASA grant NCC3-661 under the technical management of Z.-G. Yuan of the National Center for Microgravity Research, NASA Glenn Research Center, Cleveland Ohio.

REFERENCES

1. Hilts, P.J., The New York Times, New York, p. 1, 19 July 1993.
2. Bahr, D.W., in Gas Turbine Combustion Design Problems (A.H. Lefevre, ed.), Hemisphere Publishing, Washington, 1979, p.205.
3. Urban, D.L., et al., AIAA J. 36:1346 (1998).
4. Lefebvre, A.H., Fifteenth Symposium (International) on Combustion, The Combustion Institute, Pittsburgh, 1974, p.1169.
5. Lefebvre, A.H., Gas Turbine Combustion, Hemisphere Publishing Co., New York, 1983, p.463.
6. Jones, R.E., Prog. Energy Combust. Sci. 4:78 (1978).
7. Haynes, B.S. and Wagner, H.G., Prog. Energy Combust. Sci. 7:229 (1981).
8. Glassman, I., Twenty-Second Symposium (International) on Combustion, The Combustion Institute, Pittsburgh, 1988, p. 295.
9. Faeth, G.M., Roth, G. and Gunderson, M., Modern Developments in Propulsion and Combustion (G.D. Roy, ed.), Taylor & Francis, Washington, 1999. P. 359.
10. Lin, K.-C. and Faeth, G.M., J. Prop. Power 12:10 (1996).
11. Sunderland, P.B., Koylu, U.O. and Faeth, G.M., Combust. Flame 100:310 (1995).

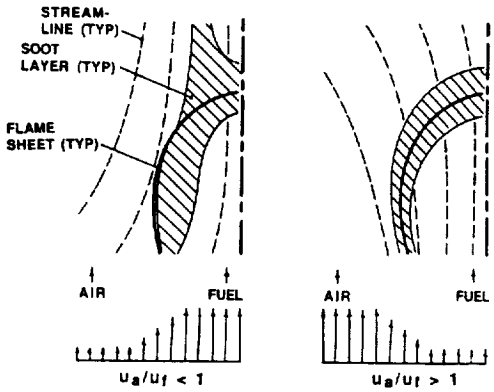

Fig.1 Effect of air-stream velocities on flame properties.

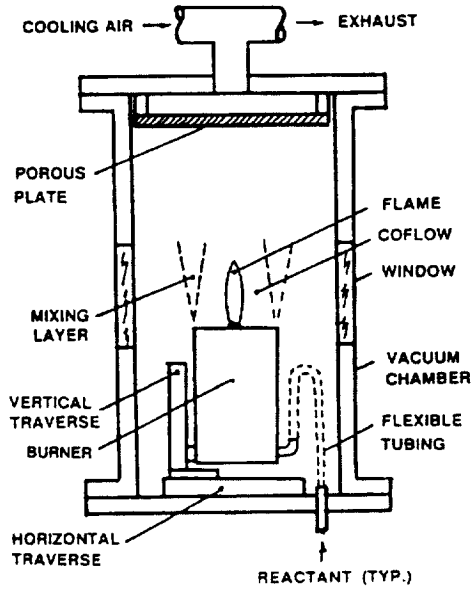

Fig.2 Laminar smoke point properties.

Fig.3 Sketch of test apparatus.

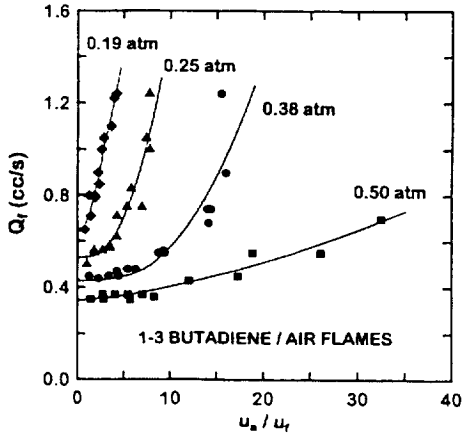

5/12-25

THE IMPACT OF BUOYANCY AND FLAME STRUCTURE ON SOOT, RADIATION AND NO_X EMISSIONS FROM A TURBULENT DIFFUSION FLAME

I. M. Kennedy[1], W. Kollmann[1] and R. L. Vander Wal[2], [1]Department of Mechanical and Aeronautical Engineering University of California Davis CA 95616, [2] NCMR at NASA-Lewis Research Center, 21000 Brookpark Rd., Cleveland OH 44135.

INTRODUCTION

It is hypothesized that the spatial structure of a turbulent diffusion flame plays an important role in determining the emissions of radiative energy, soot and NO_x from a combustor. This structure, manifested in the two point statistics, is influenced by buoyancy. Radiation, soot and NO_x emissions are the cumulative result of processes that occur throughout a flame. For example, radiation fluxes along a line of sight can be found from summing up the contributions from sources in individual pockets of hot soot that emit, and from sinks in cold soot that absorb. Soot and NO_x are both the results of slow chemistry and are not equilibrium products. The time that is available for production and burnout is crucial in determining the eventual emissions of these pollutants.

Turbulence models generally rely on a single point closure of the appropriate time averaged equations. Hence, spatial information is lost and needs to be modeled using solution variables such as turbulence kinetic energy and dissipation rate, often with the assumption of isotropy. However, buoyancy can affect the physical structure of turbulent flames and can change the spatial extent of soot bearing regions.

Theoretical comparisons with models are best done in the limit of infinite Froude number because the inclusion of buoyancy in flow models introduces significant uncertainties. Hence, LII measurements of soot, measurements of radiation fluxes from soot, Particle Imaging Velocimetry (PIV) of the flow field and measurements of post flame NO_x will be carried out on the NASA Lewis 2.2 sec drop tower and eventually on the parabolic flight aircraft. The drop rig will be a modified version of a unit that has been successfully used at Lewis in the past.

PLANNED EXPERIMENTS

Diffusion flames at atmospheric pressure will be established on a 0.51 mm I.D. nozzle (length/diameter > 20) with a pilot diffusion flame. A regulator and fine control valve will be adjusted using a mass flow meter to deliver a known fuel flow rate. The ethylene or acetylene flow through the central gas-jet tube will be about 1000 sccm giving a typical Reynolds number of around 4,000 while the fuel flow for the laminar coannular pilot flame will be roughly 10 sccm. The choice of fuel will be determined by the amount of soot that is formed under the chosen operating conditions and the performance of the LII and PIV systems.

The experiments will use the 2.2s drop rig currently being constructed by Dr. Vander Wal under an Advanced Technology Development Program funded by NASA Headquarters through the Microgravity Research Division (MRD). The LII configuration builds upon experience with a previous system.

Particle Imaging Velocimetry (PIV) has been demonstrated within the 2.2 sec drop tower

facility using a pulsed Nd:YAG and video camera. Image analysis was performed using custom software developed at NASA-Lewis. Current capabilities are being upgraded to allow variable interpulse time separation of the two laser pulses. For turbulent flow Reynolds numbers ranging from 2000 - 10000, time separations between the two laser pulses to achieve reasonable spatial resolution range from 50 - 10 μsec. Dual digital cameras and associated data storage and processing device are being tested for use in either the 2.2 sec or aircraft facilities.

MODELING

The main research issues are as follows.

(1) The effect of buoyancy on the correlations determining radiative heat transfer. These effects are essentially contained in the *pdf* of temperature and concentrations along a line of sight and include the associated length scales.

(2) The effect of buoyancy on the correlations determining soot production, burnout and transport as well as NOx. The effects of turbulence on soot are contained in the *pdf* of temperature and the variables describing the formation and burnout of soot. The turbulent transport of soot requires the associated second order moments.

The main research tool is LES simulation of turbulent reacting and non-reacting flows and the evaluation of the results with the aim to establish an improved closure model to predict radiative heat transfer, soot and NO_x. The direct numerical simulation of reacting turbulent flows is not feasible at the present. Hence, LES simulations will be used to compute the correlations involved in buoyant and micro-gravity turbulent jet flames.

Computational modeling will make use of soot models and radiation models that have been developed by the group at UC Davis. A Large Eddy Simulation (LES) of a round jet will be modified to include a sub grid scale model for chemical reaction, including soot formation and NO chemistry in a simple form. LES is able to capture the spatial structure of the flow and the results will be compared with the measurements of the flow field and soot distribution at 1g and μg. The predicted emissions of soot and NO_x will be compared with the measurements.

Work on the LES simulation method consisting of an accurate Navier-Stokes solver and a dynamic LES model has begun and the first step devoted to the accurate Navier-Stokes solver has been successfully concluded. The primitive variables formulation of the compressible Navier-Stokes equations in cylindrical coordinates was set up in dimensionless form consistent with the zero Mach number limit such that the incompressible equations are recovered without singularities. The equations were discretized using a Fourier spectral method in azimuthal direction and high order finite difference methods in the other two spatial directions. The solver allows the choice of second to eighth order for first and second derivatives as explicit central difference operators or third to ninth order upwind-biased differences. High order filters are used to provide the numerical dissipation to stabilize the system. Runge-Kutta type time integration methods with minimal storage requirements were implemented and the third and fourth order version are currently avialable in the solver. The simulation of turbulent flows requires the ability to prescribe time dependent boundary conditions for spatially evolving flows. Hence, the proper form of boundary conditions for compressible flows in domains with entrance and exit sections was established. The current version of the solver has been tested for non-reacting compressible flows at subsonic Mach numbers. Spatially developing round jet flows with and

without swirl have been simulated for axisymmetric and three-dimensional flows at Reynolds number Re=4000 and the reference Mach number Ma = 0.4.

The first case is the spatially developing axisymmetric flow generated by a round pipe exit with the Reynolds number Re=4000 based on the entrance conditions and the reference Mach number Ma = 0.4. The semi-infinite flow domain is mapped onto the standard domain using two-parameter exponential maps. The number of grid points was n_r x n_z= 121 x 295 with uniform spacing in the image domain. The spatial derivatives were discretized using sixth order central finite difference operators and the fourth order accurate Runge-Kutta time integrator was applied. The initial conditions were extended throughout the flow field and disturbances for the axial velocity were introduced at the entrance boundary.

Selected results at two times are shown to illustrate the flow development. The azimuthal vorticity plots show the development of the vortical structures in the flow field. Figure 1 shows the isolines of the azimuthal vorticity at t = 16.9394; the flow direction is from left to right. Several vortex rings have been formed at this time. The leading vortex, which results from the first merging process, is accelerated in axial direction by the induced velocity on the downstream part of the initial vortex region and is not visible in the figure. The second vortex ring, visible as the flattened structure at the right side of Fig.1, is also the result of merging as is the third ring (middle ring in figure. Vortex merging and subsequent acceleration increases the axial distance between the merged vortices and precludes further interaction with the next upstream vortex ring. The development of the flow shows that the roll up into vortex rings upstream of the merged rings becomes more crowded as the spacing between the rings decreases due to the reduced influence of the merged rings as seen in Fig.2. The third and fourth rings (counted from the left) are beginning to merge and this process is continued establishing the growth rate of the jet. The isotherms in Fig.3 are the lines of constant disturbance temperature where the absolute (dimensionless) temperature is 1+T(r,z,t). They reflect the presence of vortex ring structures.

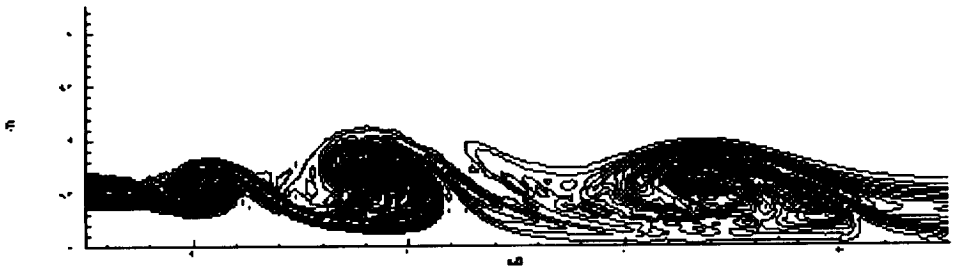

Fig. 1 Vorticity in jet at an early time

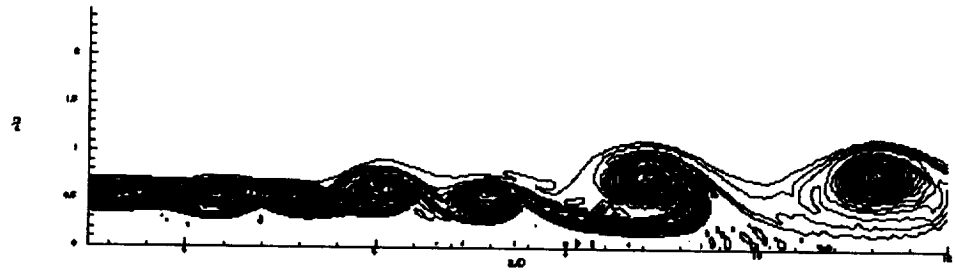

Fig. 2 Vorticity in jet at later time

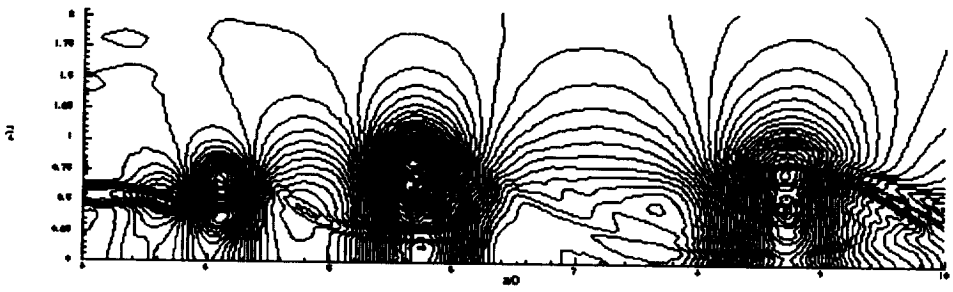

Fig. 3 Isotherms in jet

ACKNOWLEDGEMENTS

This work is supported by the NASA Microgravity Combustion Program. RVW acknowledges support under NASA cooperative agreement NCC3-544.

S113-25

KINETICS AND STRUCTURE OF SUPERAGGLOMERATES PRODUCED BY SILANE AND ACETYLENE

G. W. Mulholland[1], A. Hamins[1], and Y. Sivathanu[2], [1] The National Institute of Standards and Technology, 100 Bureau Dr. STOP 8653, Gaithersburg, MD 20899-8653, george.mulholland@nist.gov, [2] En'Urga Inc., Business and Technology Center, 1291-A, Cumberland Ave., West Lafayette, IN 47906, sivathan@enurga.com.

INTRODUCTION

The evolution of smoke in a laminar diffusion flame involves several steps (Smyth and Miller, 1987). The first step is particle inception/nucleation in the high-temperature fuel-rich region of the flame followed by surface growth and coagulation/coalescence of the small particles. As the primary spheres grow in size and lose hydrogen, the colliding particles no longer coalesce but retain their identity as a cluster of primary spheres, termed an agglomerate. Finally, in the upper portion of the flame, the particles enter an oxidizing environment which may lead to partial or complete burnout of the agglomerates.

Currently there is no quantitative model for describing the growth of smoke agglomerates up to superagglomerates with an overall dimension of 10 μm and greater. Such particles are produced during the burning of acetylene and fuels containing benzene rings such as toluene and polystyrene. In the case of polystyrene, smoke agglomerates in excess of 1 mm have been observed "raining" out from large fires.

Evidence of the formation of superagglomerates in a laminar acetylene/air diffusion flame has been recently reported (Sorensen *et al.*, 1998). Acetylene was chosen as the fuel since the particulate loading in acetylene/air diffusion flames is very high. The photographs in Figure 1 were obtained by Sorensen using a microsecond xenon lamp of the "stream" of soot just above the flame.

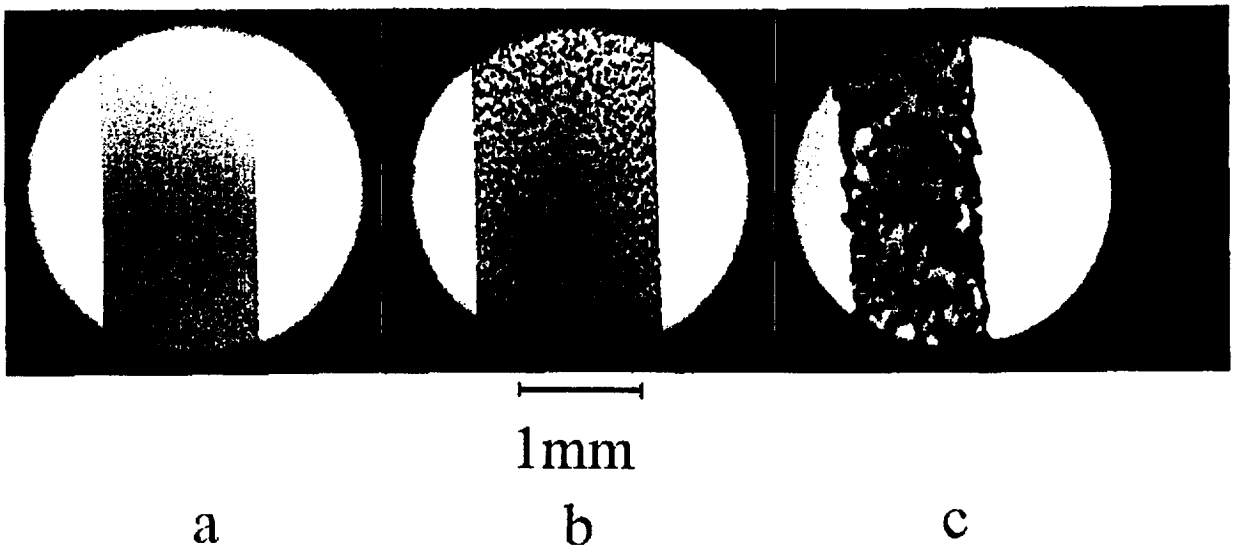

Figure 1. Soot gelation in a premixed acetylene/air flame.

For low flow rates of acetylene, only submicrometer soot clusters are produced and they give rise to the homogeneous appearance of the soot stream in Fig. 1(a). When the flow rate is increased to 1.7 cm^3/s, soot clusters up to 10 μm are formed and they are responsible for the graininess in Fig. 1(b), and at a flow rate of 3.4 cm^3/s, a web of interconnected clusters as large as the width of the flame is seen (Fig. 1(c)). This interconnecting web of superagglomerates is described as a gel state by Sorensen *et al* (1998). This is the first observation of a gel for a gas phase system. It was observed that this gel state immediately breaks up into agglomerates due to buoyancy induced turbulence and gravitational sedimentation.

RESEARCH PLAN

The plan is to study the evolution of these superagglomerate structures to the gelation stage in a microgravity environment. As pointed out above, the gel structure observed at 1-g in acetylene flames is short lived. There is a combination of flow effects and ultimately gravitational settling that will limit the existence of this structure. It is not possible to observe such a for more than a few ms at 1-g. In a microgravity environment, there are excellent prospects for studying such structures for extended periods. The gravity induced flows will be absent, sedimentation will be absent, and the time scale for physical agglomeration is extended by the much slower dilution effect of the surrounding gases. We propose to take advantage of the microgravity conditions to better quantify the growth of superagglomerates and the gel state and to determine the initial partilce volume fraction and time required to reach the gel state.

We will focus much of the effort on a silicon based fuel. We propose to burn silane and look at the evolution of the "white" silica smoke. There are a number of advantages to this system over hydrocarbon fuels for studying agglomeration. First, the silica particles produced are a major product of combustion with the yield easily computed from the flow of silane. That is, one silane molecule produces one SiO_2 molecule. For carbonaceous fuels, the smoke is a secondary combustion product and the yield can not be predicted. Secondly, the initial particle volume fraction can be simply controlled by the concentration of nitrogen mixed with the silane. Thirdly, the particulate volume fraction can be adjusted to values as much as a factor of 10 higher than carbonaceous smokes. Fourthly, the oxidation step is the same as the formation step for silica so there is no loss of particulate mass, while in a carbonaceous system part or even all of the smoke produced can be burned out. Finally, silane autoignites upon mixing with air so that an igniter is not needed.

To carry out this study we will use three optical methods plus thermophoretic collection of the particles. The superagglomerates will be directly imaged using microsecond flash photography. Secondly, a small-angle light scattering instrument will be developed for measuring the radius of gyration of the soot agglomerates as a function of time. We are not aware of any instrument currently available that can provide continuous particle sizing for agglomerates as large as 100 μm. Thirdly, the radiant flux from the flame will be measured as a function of fuel flow for both silane and acetylene to determine the radiant fraction of the heat release rate and to correlate with particulate loading. Finally, the agglomerates will be collected thermophoretically and by filtration for determining structure and primary sphere size by electron microscopy as well as the density and yield of the agglomerates.

A schematic diagram of the agglomeration chamber that will be used to obtain and hold very high levels of silica and carbon agglomerates at different temperatures is shown in Fig. 2. The cell will be designed so that one side of the container will serve as a release diaphragm. Silane

premixed with nitrogen (to control the temperature and particle loading) is introduced through a tube at the bottom of the burner. The tube has a fast acting solenoid valve to meter the amount of silane introduced into the agglomeration chamber. The valve is specifically designed for silane because of the reactivity of silane with oxygen. Air is introduced through a solenoid valve before the silane. As silane is introduced into the chamber, it undergoes a fast exothermic reaction and the products of combustion (silica particulate and water vapor) are formed and persist at microgravity conditions as a cloud within the chamber. It is expected that 1 s to 2 s will be adequate time to test the silane burner under microgravity conditions and that 10 s to 20 s will allow adequate time for the formation and collection of the superagglomerates under microgravity conditions. Thus, experiments are planned for both the 2.2 s Drop Tower and for the KC-135 aircraft. Depending on the concentration and amount of silane introduced into the system, the agglomerate size will increase and a gel structure ultimately form. Some tests will also be carried out using acetylene to study the formation of superagglomerate carbon particles. In this case an igniter will be added to the facility.

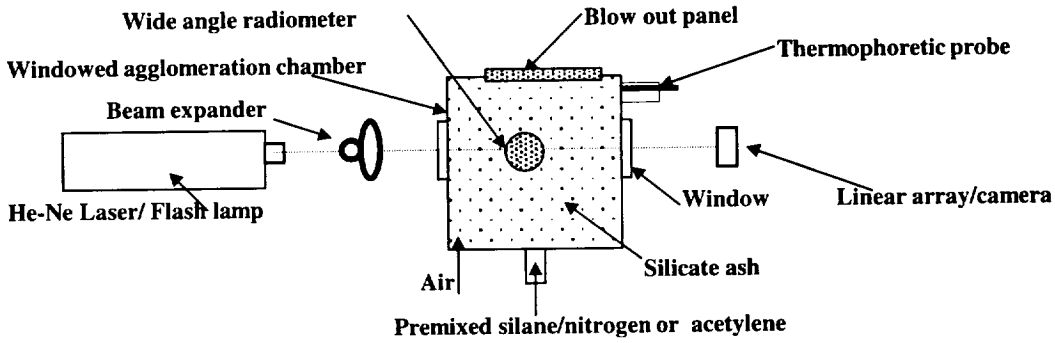

Figure 2. Burner/chamber configuration for formation of superagglomerate.

COMPUTER SIMULATION

Agglomeration occurs when diffusing primary particles collide and stick together, forming doublets, which in turn collide with primary particles as well as doublets, leading to larger and larger irregularly shaped clusters. Mulholland *et al.* (1988) simulated this process by distributing 8000 primary particles at random positions in a cubic box The diffusive motion of a particle of mass m is described by Langevin equations (Chandrasekhar, 1943)

$$d\vec{r}/dt = \vec{v}; \quad m\, d\vec{v}/dt = -m\beta\vec{v} + \vec{f} \tag{1}$$

where $\vec{r}$ and $\vec{v}$ are the position and velocity of the particle, β^{-1} is the momentum relaxation of the agglomerate, and $\vec{f}$ is a random force related to β by the fluctuation-dissipation theorem

$$\left\langle \vec{f}(t_0) \bullet \vec{f}(t_0 + t) \right\rangle = 6\beta m k_B T \delta(t) \tag{2}$$

Here k_B is Boltzmann's constant, T is the absolute temperature of the medium in which the agglomeration process is taking place, and $\delta(t)$ is the Dirac delta function. The free molecular condition corresponds to the particle relaxation time, β^{-1}, long compared to the time for the particle to move one diameter in the absence of drag force resulting from the gas molecules..

The diffusive motion of the particles is supplemented by the condition that if any two particles touch, they stick forming a larger, rigid cluster. The cluster continues to diffuse according to the Langevin equation but with a changed mass. This growth process is known in the fractal literature as cluster-cluster aggregation.

Previous simulations focused on conditions appropriate to a low density agglomeration process. At the time of this earlier study the anomalously large agglomeration rate obtained for a large initial volume fraction was discarded as unphysical for a low density system; however, ***this high density condition is appropriate for simulating gelation***

A previously developed computer code will be adapted for current generation computers, which will allow calculation on systems with as many as 80,000 primary spheres. This will correspond to a maximum cell size of about 10 μm compared to a maximum size of about 3 μm in the previous studies. The time dependence of the average cluster size and of the intensity weighted average radius of gyration will be computed and the behavior near the gel point assessed. These results will be compared with the measured time dependence of the radius of gyration based on the small angle light scattering experiments. While the cluster size at the gel point will be much larger for the experimental system, it is anticipated that a scaling relation will be found from the computer simulation for the behavior near the gel point

The direction of the modeling will be led by the experiments. The size and structure observed for the agglomerates will be important as inputs to the modeling. For example, if there is evidence from the electron microscopy of restructuring of the agglomerates to a higher fractal dimension, the sticking condition of the clusters will be adapted to simulate this effect.

POTENTIAL IMPACT

The gel produced by the aerosol route has the potential for being an ultra low-density material. One intriguing application for such a material is as a filter media, since it has a small particle size yet a high porosity. A second impact of this study is a better understanding of the differences between hydrocarbon combustion and burning with silicon. This is important for appreciating the fire safety advantages of silicon containing materials for aerospace applications, including space travel.

ACKNOWLEDGEMENT

This study is funded by by NASA's Microgravity Research Division Ground-based Research Plan.

REFERENCES

Chandrasekhar, S., 1943, *Rev. Mod. Phys.*, vol. 15, 1.

Mulholland, G. W., Samson, R. J., Mountain, R.D., and Ernst M.H., 1988, "Cluster Size Distribution for Free Molecular Agglomeration," *J. Energy and Fuels*, vol. 2, 481.

Smyth, K.C., and Miller, J.H., 1987, "Chemistry of Molecular Growth Processes in Flames," *Science*, vol. 236, pp. 1540.

Sorensen, C. M., Hageman, W. B., Rush, T. J., Huang, H., and Oh. C., 1998, "Aerogelation in a Flame Soot Aerosol,"*Phys. Rev. Lett*, vol. 80, 1782.

Heterogeneous Diffusion Flames

S/14-25

INTERNAL HETEROGENEOUS PROCESSES IN ALUMINUM COMBUSTION

E. L. Dreizin, AeroChem Research Laboratory, The Titan Corp.
P.O. Box 2229, Princeton NJ 08843 (E-mail: edreizin@titan.com)

INTRODUCTION

This paper discusses the aluminum particle combustion mechanism which has been expanded by inclusion of gas dissolution processes and ensuing internal phase transformations. This mechanism is proposed based on recent normal and microgravity experiments with particles formed and ignited in a pulsed micro-arc[1-4].

Figure 1 summarizes recent experimental findings on the three stages observed in Al particle combustion in air and shows the burning particle radiation, trajectory (streak), smoke cloud shapes, and quenched particle interiors. During stage I, the radiation trace is smooth and the particle flame is spherically symmetric. The temperature measured using a three-color pyrometer is close to 3000 K. Because it exceeds the aluminum boiling point (2730 K), this temperature most likely characterizes the vapor phase flame zone rather than the aluminum surface. The dissolved oxygen content within particles quenched during stage I was below the detection sensitivity (about 1 atomic %) for Wavelength Dispersive Spectroscopy (WDS). After an increase in the radiation intensity (and simultaneous decrease in the measured color temperature from about 3000 to 2800 K[3]) indicative of the transition to stage II combustion, the internal compositions of the quenched particles change. Both oxygen-rich (~ 10 atomic%) and oxygen-lean (<1%) regions are identified within the particles using back-scattered electron imaging and WDS[3]. During stage II, oscillations are observed in particle radiation and the flame and smoke cloud are distorted from their original spherically-symmetric shape. In stage III, particle radiation continues to exhibit oscillations, but its radiation intensity drops and remains at a nearly constant level. The measured temperature decreases to about 2300 K[3]. Also, larger changes in particle velocities are observed, and oxide caps are found on quenched particle surfaces.

While these results showed the correlation between the aluminum particle combustion behavior and the evolution of its internal composition, the change from the spherically symmetric to asymmetric flame shape occurring upon the transition from stage I to stage II combustion could not be understood based only on the fact that dissolved oxygen is detected in the particles. The connection between the two phenomena appeared even less significant because in earlier aluminum combustion studies carried in O_2/Ar mixtures, flame asymmetry was not observed as opposed to experiments in air or O_2/CO mixtures [5,6]. It has been proposed that the presence of other gases, i.e., hydrogen[7], or nitrogen[8,9] causes the change in the combustion regime.

RESULTS OF THE MICROGRAVITY AND NORMAL GRAVITY EXPERIMENTS

One of the most widely accepted hypotheses is that flame asymmetry develops when convective and buoyant flows disturb the originally spherically symmetric diffusion flame adjacent to the molten aluminum particle [10,11]. In order to explore this hypothesis, experiments on single aluminum particle combustion were conducted in a microgravity environment[2,3]. Nearly motionless aluminum particles were produced, ignited and burned under conditions where buoyant and convective flows are greatly reduced as compared to those existing in normal gravity laboratory experiments. The crucial result of the microgravity experiments was that flame asymmetry developed in the aluminum particle flame

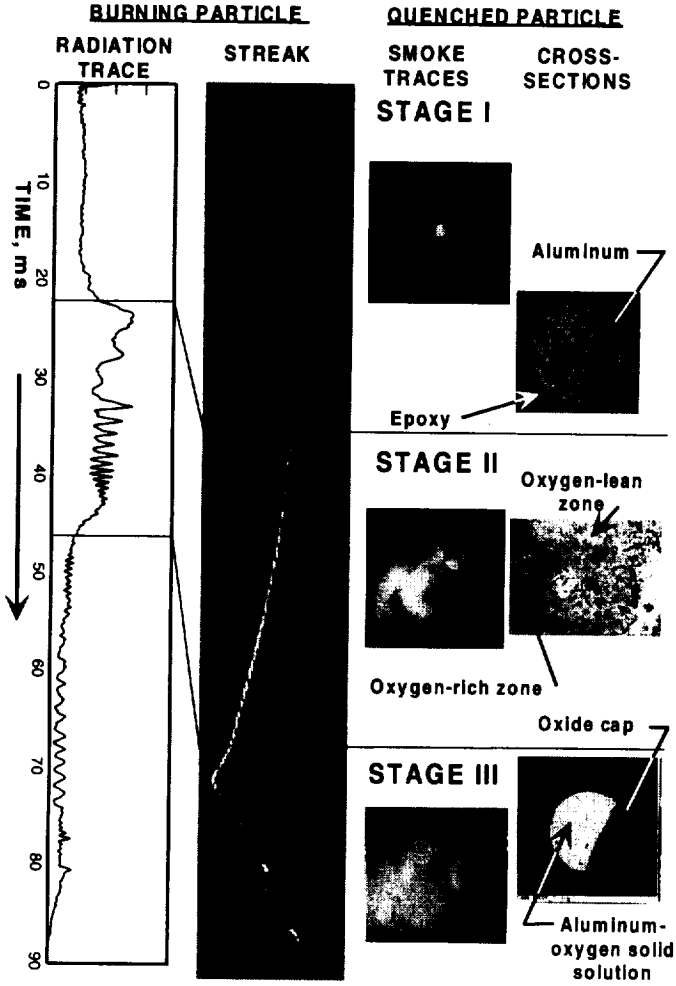

Fig.1. Aluminum particle radiation, streak, smoke traces, and particle cross-sections interior during aluminum particle combustion in air[1-3]

in the same way as in normal gravity. Thus, buoyant and convective flows were found not to be the primary reason for the transition from symmetric to asymmetric burning.

Subsequent experiments[4] focused on identifying conditions under which asymmetric combustion could develop. Particles of 90 and 250 μm diameter were produced and ignited in pure O_2, N_2/O_2, Ar/O_2, and He/O_2 gas mixtures. Brightness oscillations indicative of asymmetric particle burning developed reproducibly in the N_2/O_2 gas mixtures, consistent with the previous observations[1-3]; similar brightness oscillations developed occasionally in pure O_2 and both Ar/O_2 and He/O_2 mixtures. The oxygen-rich and oxygen-lean phases were detected in the interiors of all the partially burned particles independent of the gas environment. Oxide caps were found on the surfaces of particles burning in all the environments; however the size of the oxide caps detected on the particles quenched in the Ar/O_2 and He/O_2 mixtures was markedly smaller than that found in the N_2/O_2 gas mixtures. Therefore, in all of these environments, oxygen is transported to and absorbed by the burning aluminum particle. The rate of this process and, as a result, the total amount of absorbed oxygen and size of the oxide caps depend on the gas environment. One likely mechanism for the oxygen transport to the particle surface is diffusion and thermophoresis of oxygen-containing molecules produced in the vapor phase flame. Estimates for equilibrium oxygen-containing gas phase species showed that significant amounts of NO are produced in air in addition to Al_2O, AlO, and Al_2O_2 produced in all the gas environments. It was shown[4] that this NO could account for an enhanced transport of oxygen from the flame zone to the particle surface in air, as compared to the other environments.

COMBUSTION MECHANISM

A proposed overall mechanism linking phase changes occurring in burning aluminum particles with the observed stages in its combustion is described below. It uses the available experimental results and the aluminum-oxygen phase diagram [12,13] shown schematically in Fig. 2. Aluminum

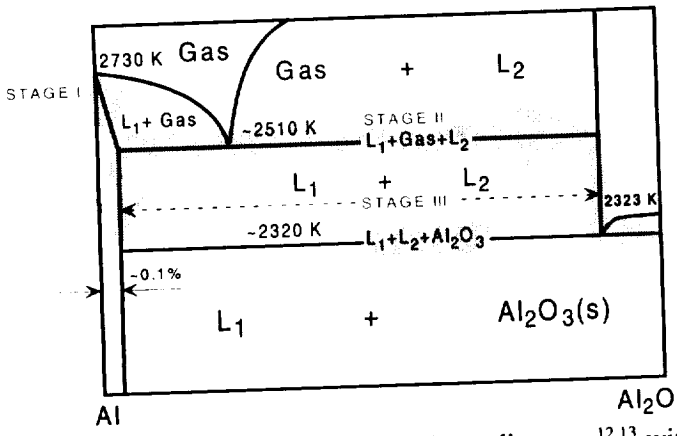

Fig. 2. Aluminum-oxygen binary phase diagram [12,13] with paths of processes occurring during different stages of aluminum particle combustion.

ignites at a temperature approaching or exceeding melting point of the natural Al_2O_3 layer (2323 K) [6]. Because the adiabatic flame temperature for aluminum is very high (e.g., it is greater than 3500 K for aluminum flame in air), the particle rapidly self-heats to the aluminum boiling point, 2730K (onset of stage I combustion, see Fig. 2). A spherical vapor-phase flame develops in which condensed Al_2O_3 forms as a result of the multi-step aluminum gas phase oxidation[9]. Part of the high temperature gaseous oxides produced in the flame including Al_2O, AlO, Al_2O_2, and NO species are transported (via diffusion and thermophoresis) back to aluminum surface[4] and provide the oxygen source for the heterogeneous aluminum-oxygen reactions. The phase diagram, Fig. 2, indicates that molten aluminum can dissolve up to about 0.1 at. % of oxygen producing a liquid L_1. Therefore, a uniform Al-O (L_1) solution forms within burning particle in the first stage of its combustion. The phase diagram shows that the oxygen solubility in L_1 increases when the temperature decreases. The solution boiling temperature decreases from 2730 K (pure Al) to 2510 K (saturated L_1) as the concentration of oxygen dissolved in L_1 increases. At 2510 K, the phase diagram shows a three-phase equilibrium between L_1, gas, and an oxygen-rich liquid L_2. Stage II combustion begins when a new liquid phase, L_2, starts to form as a result of heterogeneous reaction between saturated L_1 and oxygenated species:

$$L_1 + (Al_2O + AlO + Al_2O_2 + NO)^{gas} \xrightarrow{2510K} L_1 + L_2 + N_2^{gas} \qquad (1)$$

Production of L_2 precursors (and L_2) produces non-uniformity both inside and on the surface of the particles because L_1 and L_2, are immiscible[12]. This non-uniformity in oxygen distribution within the burning particles correlates with the oxygen-rich and oxygen-lean zones detected within particles quenched during stage II combustion. The boiling point of L_2 is around 3250 K, much higher than that of L_1 (2510 K) and thus, even though the amount of the new phase produced is very small because of the much higher oxygen content in it, the aluminum evaporation rate decreases dramatically above each small island of L_2 or its precursor. This non-uniformity in the aluminum evaporation results in the asymmetry in the aluminum particle flame observed during stage II combustion. The bulk of the particle still is the oxygen-lean phase, L_1, and it continues to boil because of the heat flux from the vapor phase combustion zone. Therefore, during stage II combustion while reaction (1) is ongoing, the particle temperature is maintained at 2510 K. Eventually, when the particle size decreases, the heat flux from the flame becomes smaller than that required to boil L_1 and the temperature drops. Stage III combustion begins when the particle temperature decreases from the L_1 boiling point and the combustion rate drops rapidly because of the sudden decrease in the aluminum vaporization rate. When the temperature decreases to 2323 K, the phase diagram predicts a monotectic phase transition:

$$L_1 + L_2 \xrightarrow{2323\ K} Al_2O_3 + L_1 \quad (2)$$

As a result of this reaction, solid aluminum oxide precipitates from a mixture of two liquids. This transformation proceeds at a constant temperature and Al_2O_3 grows heterogeneously from the inclusions of L_2 formed during stage II. Because the two liquids L_1 and L_2 are immiscible and have different densities, spinning of the burning particle triggered during stage II by the non-uniform aluminum evaporation separates the two liquids. This results in the formation of one large oxide lobe rather than a number of smaller oxide inclusions.

The above mechanism allows one to qualitatively interpret phenomena observed by different researchers in aluminum particle combustion experiments. There also are noteworthy implications for higher pressure aluminum combustion, e.g., in aluminized propellants. While reaction (2) occurs at 2323 K independent of pressure, the temperature of the Gas-L_1-L_2 equilibrium (1) increases at higher pressures[13]. It is thus probable, that the boiling point of aluminum or L_1 will not be reached when there are significant radiative heat losses at high temperatures and pressures. This means that the gas region separating the oxygen-lean and oxygen-rich phases in the Al-O diagram at the 1 atm aluminum combustion temperatures will be replaced by a condensed phase region in which dissolved oxygen concentration will change in a wide range. At high pressures, the mechanism of aluminum combustion is thus predicted to become more similar to the combustion mechanisms of metals that burn primarily on the surface at 1 atm, e.g., Zr.

Acknowledgments: This work was supported by NASA Contract No. NAS3-27259.

REFERENCES

1. Dreizin, E.L., *Combust. Flame*, 105:541-556 (1996).
2. Dreizin, E.L., *NASA Conference Publication 10194*, pp. 49-54 (1997)
3. Dreizin, E.L., *Combust. Flame*, 116:323-333 (1999)
4. Dreizin, E.L., *Combust. Flame*, in press (1999), AeroChem TP 562
5. Prentice, J.L., (Ed.), *NWC TP 5162*, Naval Weapons Center, China Lake, CA, 1971
6. Price, E.W., in *Fundamentals of Solid Propellant Combustion* (K.K.Kuo and M. Summerfield, Eds.), AIAA, New York, 1984, pp. 479-514
7. Drew, C.M., Gordon, A.S., and Knipe, R.H., *Heterogeneous Combustion* 15:17 (1964)
8. Boborykin, V.M., Gremyachkin, V.M., Istratov, A.G., Kolesnikov-Svinaryov, V.I., Kuznetsov, G.P., Leypunskiy, O.I., and Puchkov, V.M., *Fizika Gorenia i Vzryva*, 11:22-29 (1975) (in Russian)
9. Bucher, P., Yetter, R.A., Dryer, F.L., Parr, T.P., Hanson-Parr, D.M., and Vicenzi, E.P., *Twenty-Sixth Symposium (Int'l) on Combustion*, The Combustion Institute, Pittsburgh, 1997, pp. 1899-1908
10. Brooks, K.P. and Beckstead, M.W., *Journal of Propulsion and Power* 11:769-780 (1995)
11. Turns, S.R., Wong, S.C., and Ryba, E., *Combust. Sci. Tech.*, 54:299 (1987)
12. Massalski, T.B., Okamoto, H., Subramanian, P.R., and Kacprzak, L. (Eds) *Binary Alloy Phase Diagrams*. ASM Publ., Materials Park, OH, 1990
13. Levinskiy, Y.V., *P-T-X Binary Phase Diagrams of Metal Systems*, Moscow, Metallurgia, (1990) (In Russian)

S7.25-25

INTERFEROMETER DEVELOPMENT FOR STUDY OF INTERACTIONS BETWEEN FLAMES ON PARALLEL SOLID SURFACES

J. S. Goldmeer[1], D. L. Urban[2], and Z.G. Yuan[3], [1]National Research Council, [2]NASA GRC, [3]National Center for Microgravity Research, 21000 Brookpark Road, Cleveland OH 44135.

INTRODUCTION

The interactions between flames spreading over parallel solid sheets of paper are being studied in normal gravity and in microgravity. This geometry provides interesting opportunities to study the interaction of radiative and diffusive transport mechanisms on the spread process. These transport mechanisms are changed when the flame interacts with other flames. Most practical heterogeneous combustion processes involve interacting discrete burning fuel elements, consequently, the study of these interactions is of practical significance. Owing largely to this practical importance, flame interactions have been an area of active research, however microgravity research has been largely limited to droplets [1,2]. Consideration of flame spread over parallel solid surfaces has been limited to 1-g studies [3,4,5].

To study the conductive transport in these flames, an interferometer system has been developed for use in the drop tower. The system takes advantage of a single beam interferometer: Point Diffraction Interferometry (PDI) [6] which uses a portion of the light through the test section to provide the reference beam. Like other interferometric and Schlieren systems, it is a line of sight measurement and is subject to the usual edge and concentration effects. The advantage over Schlieren and shearing interferometry systems is that the fringes are lines of constant index of refraction rather than of its gradient so the images are more readily interpreted. The disadvantage is that it is less able to accommodate a range of temperature gradients.

INTERFEROMETER HARDWARE

The interferometer [7] uses a 200 micron optical fiber pig-tailed to a 0.9 mW laser diode (635 nm) to create a point source at the cleaved fiber tip. The diverging laser beam is collimated into an 8 cm diameter beam by an achromatic lens (0.31 m focal length), passes through the test section, and is focused on a PDI disk by a second achromatic lens. The interference pattern is imaged with an 80-200mm f4 lens mounted to a black and white CCD camera. A color CCD camera is used to capture flame images. The PDI disk is a commercially available product produced by Ealing Electro-Optics Inc. that consists of a circular diffraction hole (~100 nm) centered in a semi-absorbing thin film (~1mm diam.). A portion of the beam passes through the film with some attenuation, but is otherwise unchanged. Light passing through the center pinhole, creates a spherical diffraction wave that acts as the reference beam. The interaction of the reference (diffracted) wavefront and the incident (test) wavefront generates an interferogram. For ease of interpretation of the interferograms, the interferometer is used in infinite fringe mode where the fringes are contours of constant optical path length. For a two dimensional system at constant pressure, with ideal gases of constant composition, these fringes are identically isotherms. If the system is axisymmetric, the fringes must be deconvoluted.

EXPERIMENTAL RESULTS

Comparisons of interferometry measurements to thermocouple measurements were made to validate the performance of the PDI system. In the first set of tests, the PDI system was used to

measure temperature profiles generated by a heated vertical flat plate and a heated vertical circular cylinder. As can be seen in Figure 1, the interferometer results agree well with the thermocouple measurements and with the predicted values.

Comparisons of PDI and thermocouple measurements in flames were made in two-dimensional and axisymmetric steady geometries. The PDI temperatures were compared with data taken with a 76 micron OD, type S thermocouple (Platinum / Platinum-10% Rhodium) that has a measurement uncertainty of ±0.25% K; this corresponds to an uncertainty of ±5 K at a temperature of 1800 K.

A two-dimensional flame was produced using methanol evaporating from a vertical sheet of ceramic insulation material [8]. The insulation board was 5.1 cm wide by 10.2 cm tall by 0.32 cm deep and was supported in an aluminum frame. Ten milliliters of methanol were applied to the lower half of the board prior to each test. Multiple tests were conducted with the thermocouple probe to ensure that the thermal profile was steady. The thermocouple profiles were taken at the sample mid-plane, 0.9 cm from the leading edge of the aluminum frame (0.25 cm from the leading edge of the insulation board). This elevation was chosen to examine a flame that was qualitatively similar to the leading edge of a spreading flame. To limit heat conduction effects, the thermocouple was inserted horizontally, parallel to the sample surface

A comparison of the interferogram of the flame with a visible flame image is shown in Figure 2. Note that the closed fringes (those that do not end at the wall, but appear to loop around) appear at the same location as the visible flame. Figure 3 is a comparison of the PDI and thermocouple temperature profiles. The thermocouple data for these tests were corrected for radiative losses using the method of Ang, et al.[8]. The error bars on the PDI data represent the width of the fringes; the center of the fringe was assumed to be the location of the fringe temperature. At the peak temperature, the thermocouple and PDI profiles vary by less then 2%. At the wall, the PDI and thermocouple data differ by 20%.

The flame temperatures were calculated from the fringe data using gas properties for air (a reasonable approximation at the leading edge). The decrease in the flame temperature (from the peak to the wall) was achieved by reducing the absolute magnitude of the fringe numbers. The maximum fringe order was taken to be the center of the closed fringes. Thus, the fringe numbers increase from the ambient to the peak and then decrease towards the wall. The difference between the PDI and thermocouple temperatures at the wall could be caused by the fact that the PDI was measuring the gas phase temperature next to the wall while the thermocouple was influenced by the wall temperature. Similar comparisons were made with good results for a dilute methane laminar gas jet diffusion flame.

Figure 4 contains interferograms for downward flame spread over Kimwipe fuel at different pressures in 1-g in 30% oxygen/nitrogen. As is evident in the images, the width of the thermal field changes with pressure. This effect is consistent with the change in the thermal diffusivity with pressure. These interferograms were used to calculate the conducted heat transport to the paper surface ahead of the leading edge of the flame where the gas composition is predominantly air. This conductive transport was used to estimate the rate at which the thermal field would propagate if conduction was the sole mechanism for the measured increase in the temperature of the solid fuel (equivalence of the temperature of the gas at the surface and the surface was assumed). In the equation, the RHS is the gas phase conductive heat flux to the sample surface

$$U_F \left(\frac{1}{2} \rho \tau \right) C_S (T_{VAP} - T_{REF}) = \int_0^L k(y) \left(\frac{dT}{dx} \right)_{x=0} dy$$

which is balanced with the LHS which is the sensible heat in the solid. These results are presented in Figure 5. The spread rate based upon the conducted flux is about 30% lower than the measured spread rate. Reasons for the discrepancy include radiative transport to the fuel. Further work will examine this difference in more detail.

ACKNOWLEDGMENTS

This research is sponsored by the Microgravity Research Division, of the NASA Office of Life and Microgravity Sciences and Applications.

REFERENCES

1. Dietrich, D. L. and J. B. Haggard. 1992. Combustion of Interacting Droplet Arrays in a Microgravity Environment. Second International Microgravity Combustion Workshop, NASA CP 10113, 317-323.
2. Mikami, M., H. Kato, J. Sato, and M. Kono. 1994. Interactive Combustion of Two Droplets in Microgravity. Presented at 25 Symposium (International) on Combustion, Irvine CA.
3. Emmons, H. W., and T. Shen. 1971. Fire Spread in Paper Arrays, Thirteenth Symposium (International) on Combustion 917-926.
4. Kurosaki, Y., A. Ito and M. Chiba. 1979. Downward Flame Spread Along Two Vertical, Parallel Sheets of Thin Combustible Solid. Seventeenth Symposium (International) on Combustion 1211-1220.
5. Itoh, A., and Y. Kurosaki. 1985. Downward Flame Spread along Several Vertical, Parallel Sheets of Paper. Combustion and Flame 60:269-277.
6. Smartt, R.N. 1979. Special Applications of the Point-Diffraction Interferometer, SPIE Vol. 192, 35-40.
7. Goldmeer, J.S., D. L. Urban and Z. G. Yuan. Application of a Point Diffraction Interferometer for Measuring Flame Temperatures, AIAA Journal, submitted.
8. Ang, J., et al. 1988. Temperature and Velocity Profiles in Sooting Free Convection Diffusion Flames, AIAA Journal 26:323-329.

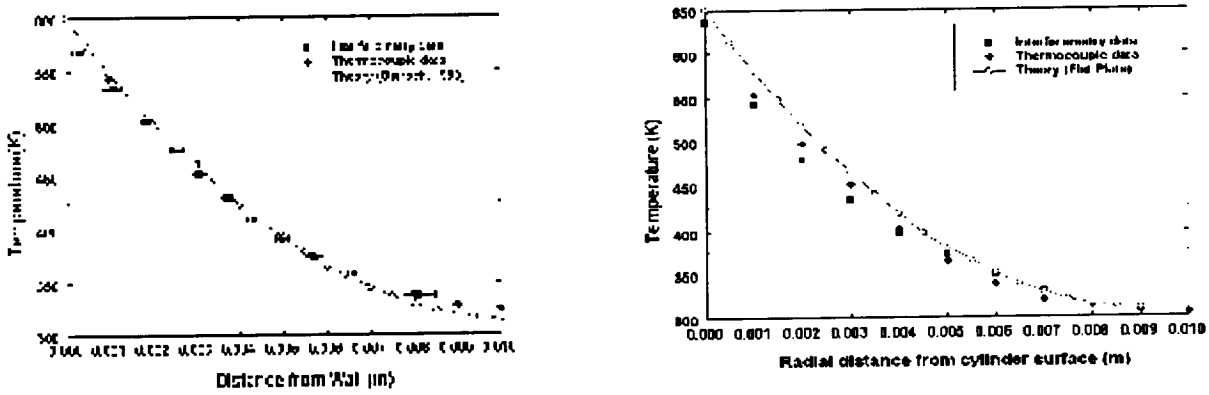

Figure 1. Comparison of experimental and theoretical temperature profiles generated by a heated vertical flat plate(left) and a heated cylinder (right). The error bars on the interferometry data represent the width of each fringe; the fringe temperature is assumed to be at the center of each fringe.

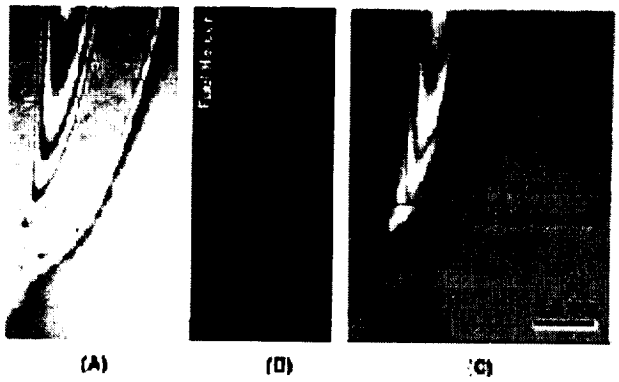

Figure 2 - Fringe image (A), visible flame image (B), and combined visible flame/fringe images (C) for a two-dimensional methanol flame. The bright white region in image (C) is the visible (blue) flame.

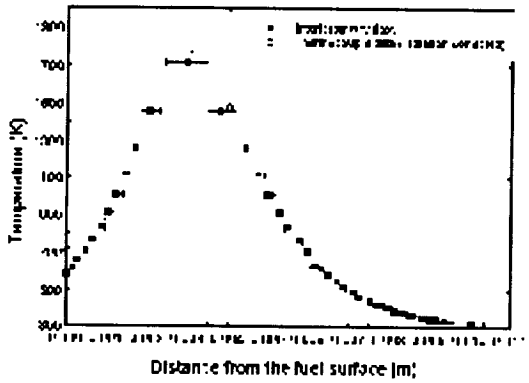

Figure 3 - Comparison of PDI and thermocouple temperature profiles for the two-dimensional methanol flame in Figure 2. The error bars on the interferometry data represent the width of each fringe; the fringe temperature is assumed to be at the center of each fringe.

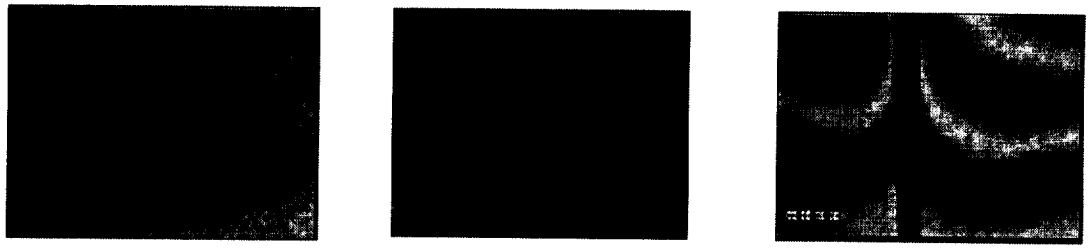

Figure 4. Interferograms for normal gravity, downward flame spread (1-g) in 30% O2/ Balance N2. All three images are at the same scale: 1.75 cm (width) x 1.38 cm(height) From the left, pressure = 0.50 Atm, 0.25 Atm., and 0.10 Atm.

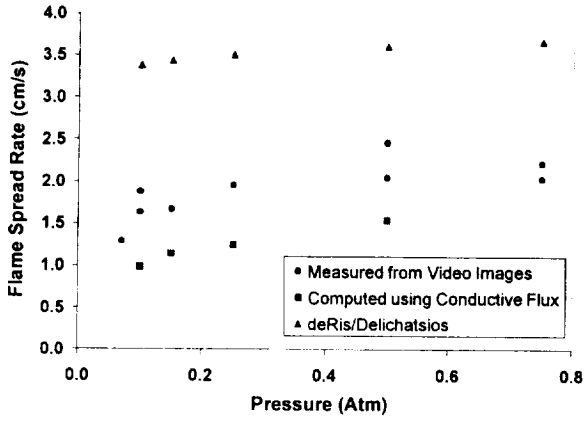

Figure 5. Comparison of the calculated spread rate (based upon the conducted transport measured from the interferograms) with the measured and theoretical spread rates.

S116-25

Low Stretch Diffusion Flames over a Solid Fuel

S. L. Olson[1] and J.S. T'ien[2], [1]NASA Glenn Research Center, Lewis Field mail stop 500-115, Cleveland,OH 44135, sandra.olson@lerc.nasa.gov; [2]Dept. of Mech. And Aerospace Engr., Case Western Reserve Univ., Cleveland, OH, 44106, jst2@po.cwru.edu.

INTRODUCTION

A unique new way to study low gravity flames in normal gravity has been developed. To study flame structure and extinction characteristics in low stretch environments, a normal gravity low-stretch diffusion flame is generated using a cylindrical PMMA sample of varying large radii.

Foutch and T'ien[1] used the radiative loss as well as a densimetric Froude number to characterize the blowoff (small Da) and quenching extinction (large Da) boundaries in stagnation-point diffusion flames under various convective conditions. An important conclusion of this study was that the shape and location of the extinction boundary, as well as a number of important flame characteristics, were *almost identical* for the buoyant, forced, and mixed convective environments they modeled. This theory indicates it should be possible to understand a material's burning characteristics in the low stretch environment of spacecraft (induced by fans and crew movements) by understanding its burning characteristics in an equivalent Earth-based stretch environment (induced by normal gravity buoyancy). Similarly, the material's burning characteristics in Lunar or Martian stretch environments (induced by partial gravity buoyancy) can be assessed.

Equivalent stretch rates can be determined as a function of gravity, imposed flow, and geometry. A generalized expression for stretch rate which captures mixed convection includes both buoyant and forced stretch is defined[1] as $a = a_f(1+ a_b^2/a_f^2)^{1/2}$. For purely buoyant flow, the equivalent stretch rate is $a_b = [(\rho^e-\rho^*)/\rho_e]\ [g/R]^{1/2}$ [1,2]. For purely forced flow, the equivalent stretch rate is characterized by either $a_f = 2U_\infty/R$ for a cylinder[1,3], or $a_f=U_{jet}/d_{jet}$ for a jet impinging on a planar surface[4,5]. In these experiments, the buoyant stretch is varied through R, the radius of curvature, but the buoyant stretch could also be varied through g, the gravity level. In this way the effect of partial gravity, such as those found on the Moon (1/6 g) or Mars (1/3 g) can be captured in the definition of flame stretch.

NORMAL GRAVITY RESULTS

A concept of the experimental apparatus is shown in Figure 1. The fuel sample was hung from the ceiling to avoid flow disturbances from the support structure. The apparatus was enclosed in a large double layered screen cage to eliminate room drafts while allowing free flow of air around the sample. An exhaust vent was recessed in the ceiling above the sample to remove combustion products while minimizing disturbances to the natural convective stagnation point flow below the sample. Sample probes, cameras, thermocouples, and other diagnostics were introduced on cantilevered extension arms through small openings in the wire screens for minimal disturbance.

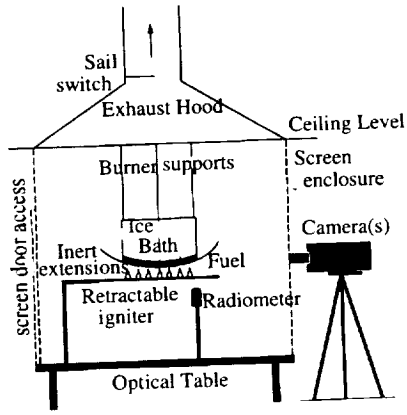

Figure 1 Experiment layout

SURFACE REGRESSION RATES

Figure 2 captures the surface regression rates for PMMA over the full range of flammability in air, from blowoff at high stretch, to quenching at low stretch, observed for the first time in this work.. The solid line drawn through the central portion of the data ($3<a<100\ s^{-1}$) has a slope of unity, which indicates regression is proportional to stretch. This relationship is different from classical theory where regression is proportional to $a^{1/2}$. The high stretch data[4] actually follows classic theory. The deviation from this classic theory has been predicted for low stretch when radiative loss is included[1]. This figure assumes the existence of a direct relationship between forced stretch [6], and buoyant stretch [7], and the excellent correlation between these different methods of stretch generation shows that this assumption is reasonable.

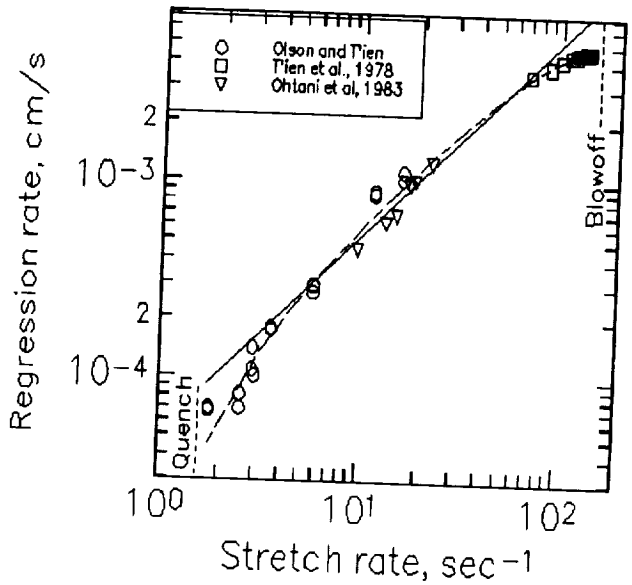

Figure 2: Surface regression rate measurements as a function stretch rate. Data spans from blowoff extinction at high stretch rate to quenching extinction at low stretch rate. Line through linear portion of data (away from limits) has a slope of unity.

In Figure 2, the stretch rate below which uniform flame burning was not achieved is $3\ s^{-1}$, where departure from the linear correlation occurs. Similarly, the overall extinction limit is marked simply as a Quench limit, which means that flames could not sustain at these large radii (low stretch rates). In the low stretch region between these limits, a new flamelet phenomenon is observed, which is believed to be a new regime of near-limit unstable flame behavior which occurs at low stretch. More detail on low stretch flamelets is reported in Olson [2].

SURFACE ENERGY BALANCE

Burning rate data and temperature measurements were used to evaluate each term of the surface energy balance at the solid surface, written as shown in the equation to the right. The first term on the left-hand side is the conductive heat flux to the surface, the second term on the left is the net flame radiative flux absorbed by the solid (radiative influx minus reflected and transmitted flux). The first term on the right-hand side is the conductive heat flux into the solid interior, the second term is the energy needed for pyrolysis of the solid, and the last term is the surface radiative loss.

$$\lambda_g \frac{\partial T_g}{\partial y} + q''_{rad} = \lambda_s \frac{\partial T_s}{\partial y} + \dot{m}'' L_v + \epsilon\sigma(T_s^4)$$

To determine overall trends, the terms of the surface balance are compared as ratios. The ratio $F_{reutilization}$, is the fraction of gas-to-surface net heat flux used to vaporize more fuel, and another ratio, F_{loss}, is the fraction of gas-to-surface net heat flux that is lost to the solid interior and radiated from the system. In this way, $F_{loss}+F_{reutilization}=1$. ϕ, the fraction of gas-to-surface net heat flux that is conducted in depth, is defined for comparison with Yang and T'iens' theory [8].

$$F_{reutilization} = \frac{\dot{m}''L_v}{\lambda_g \frac{\partial T_g}{\partial x} + q''_{rad}} \qquad F_{loss} = \frac{\lambda_s \frac{\partial T_s}{\partial x} + \epsilon\sigma(T_s^4)}{\lambda_g \frac{\partial T_g}{\partial x} + q''_{rad}} \qquad \phi = \frac{\lambda_s \frac{\partial T_s}{\partial x}}{\lambda_g \frac{\partial T_g}{\partial x} + q''_{rad}}$$

These ratios are plotted in Figure 3 as a function of stretch rate, using the data in Table 1. They represent the pseudo-steady period for the one-dimensional flames and typical values for the flamelets. Fractional heat losses increase as flame stretch is reduced. At the onset of flamelets at $3s^{-1}$, only 15% of the net heat flux is reused to vaporize more fuel; 85% of it is lost. At the Quench limit, only 10% of the heat flux is reused; 90% of it is lost. The value of ϕ at the Quench limit of a=2 s^{-1} agrees well with the value of ≈0.45 predicted by Yang and T'ien [8] for the same stretch rate in air. It is interesting to note that over the range of stretch rates studied, that in-depth solid-phase losses are comparable to surface radiative losses.

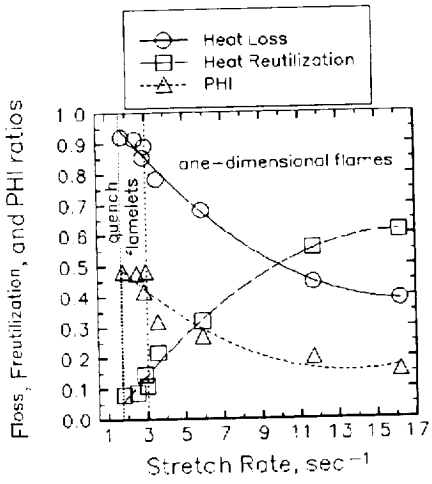

Figure 3: Loss, Reutilization, and PHI ratios as a function of stretch rate.

The fractional losses are increasing at low stretch, but the losses themselves are not increasing, but actually remain fairly constant over the range of conditions studied. Instead, the net heat flux from the gas-phase to the surface decreases dramatically with decreased stretch, as shown in Fig.11. What changes significantly is the heat release in the gas phase - the reaction rate is decreasing. The limiting factor in the reaction rate is hypothesized here to be the oxygen transport to the flame in this low stretch (low convective) environment, just as it was hypothesized in low velocity flame spread [9]. Flamelet phenomena at very low stretch, where the flame breaks up into pieces and becomes multi-dimensional, is viewed as the flame's method of enhancing oxygen flow to the flame, through increased local curvature (stretch).

PRELIMINARY DROP TOWER RESULTS

Drop tower testing is underway using the Combustion Tunnel drop rig, a droppable wind-tunnel capable of low velocity forced flow[9]. Cylindrical samples approximately 2 cm in radius were ignited in normal gravity and dropped after stable burning of the sample was achieved. Preliminary results of microgravity gas-phase flame standoff distances agree well with normal gravity flame standoff distances.

The data are shown in Figure 3, and indicate that the normal gravity buoyant stretch prior to drop is approximately 20 s^{-1} for all tests. During the drop, stable flame standoff distances were obtained for stretch rates above 3 s^{-1}. Below that, the flame was not stable during the short drop, in reasonable agreement with normal gravity experiments below 3 s^{-1} which exhibited unstable flamelets.

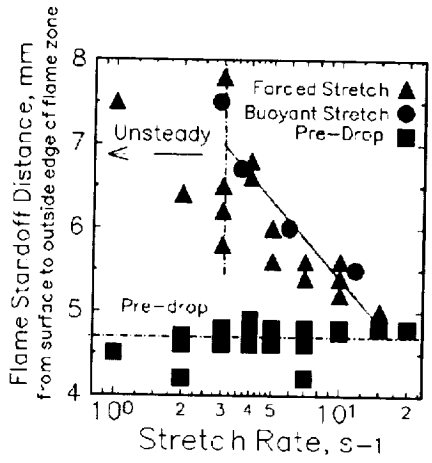

Figure 4 Preliminary drop tower forced convective stretch flame standoff distance measurements compared to buoyant stretch flame standoff distances.

SUMMARY

Experiments on buoyant low stretch stagnation point diffusion flames over a solid fuel (PMMA) cylinder were conducted over a range of radii from 2.5-200 cm, or 2-16 sec^{-1} stretch. These experiments were the first conducted in normal gravity at such low stretch for a large-scale solid fuel. The results are consistent with characteristics of low-gravity, low-stretch flames. The only clear gravitational effect noted was the fuel dripping, which was inconvenient but did not change the overall trends provided by the experiment. These experiments have demonstrated that low gravity flame characteristics can be generated in normal gravity through proper use of scaling. Based on this work, it may be feasible to apply this concept toward the development of an earth-bound method of evaluating materials flammability in various gravitational environments from normal gravity to microgravity, including the effects of partial gravity low stretch rates such as those found on the Moon (1/6g) or Mars (1/3g).

REFERENCES

[1]Foutch, D.W., and T'ien, J.S., 1987; *AIAA Journal*, Vol. 25, No. 7, pp. 972-976.
[2]Olson, S.L.; 1997; *Ph.D. Dissertation*, Case Western Reserve University.
[3]Tsuji, H.., *Prog. Energy Combust. Sci.*, V. 8, pp. 93-119, 1982.
[4]T'ien, J.S., Singhal, S.N., Harrold, D.P., and Prahl, J.M.,, *Combustion and Flame*, Vol. 33, pp. 55-68, 1978.
[5]Pellett, G.L. et all,. *Combustion and Flame*, V. 112, pp. 575-592, 1998.
[6]T'ien, J.S., Singhal, S.N., Harrold, D.P., and Prahl, J.M.; 1978; *Combustion and Flame*, Vol. 33, pp.55-68.
[7]Ohtani, H., Akita, K., and Hirano, T., 1983; *Combustion and Flame*, Vol. 53, pp. 33-40.
[8]Yang, C. T., and T'ien, J.S., 1998, *Journal of Heat Transfer*, Vol. 120, pp. 1055-1063.
[9]Olson, S.L.; 1991; *Combustion Science and Technology*, 76,4-6, pp. 233-249.

5117-29

A STUDY OF CANDLE FLAME IN MICROGRAVITY

X. Q. Zhang[1], W. F. Du[1], M. G. Wei[1], W. J. Kong[1], and Y. Hua[2]
[1]Institute of Engineering Thermophysics, Chinese Academy of Sciences.
P. O. Box 2706, Beijing 100080, China. Email: ietcazxq@public.east.cn.net,
[2]Macroenergy Lab., P. O. Box 2706, Beijing 100080, China.

INTRODUCTION

Candle flame is one of the most interesting topics in microgravity combustion and has been extensively studied to illustrate the characteristics of a non-propagating, steady-state, pure diffusion flame. Many important results were obtained, such as flame shape, size, color and structure that are quite different in microgravity from those in normal gravity[1-4]. Candle flame in normal gravity is tear-drop-like shape and bright yellow color, however in microgravity it becomes spherical (or hemispherical) and dim blue respectively. In order to have further information of these differences, a series of experiments have been conducted in the existing drop tower at National Microgravity Laboratory (NML), Chinese Academy of Sciences (CAS). Some of the experimental observations will be presented here briefly.

EXPERIMENTAL APPARATUS

All the experiments were conducted in the existing drop tower at NML, CAS. This drop tower is 22meters tall. The effective drop distance is about 18 meters. Two operation modes are used in this drop tower. One is free fall mode that can provide 1.7sec microgravity test time. The another is lift-up/free fall mode that can provide about 2.8sec. microgravity test time. A dual drop capsule (drag shield and experiment package) is used in this facility. The residual acceleration of the experiment package is less than $10^{-4}g_0$. The candles used in the experiments are commercial products with about 2mm wick diameter and 10mm candle diameter. The experiment package is a cubic chamber with 74cm long, 44cm width and 29cm thick. The volume of the chamber is about 94 liter. A differential interferometer (Fig.1) was developed for measuring the candle flame temperature both in normal gravity and in microgravity. This is one of the objectives of the present study. If we can measure the candle flame temperature in microgravity, presumably it will provide very useful information to interpret at least partly why the candle flame color in microgravity is dim blue. The ignition system was a coiled 250μm aluminum alloy wire heated with a current of approximately 4 amperes. For all the experiments the ignition was done in normal gravity about 30 sec before the experiment began. Two video cameras were used to record the interferogram of the candle flame and the regular image of the candle flame respectively at the rate of 25 frames/sec.

EXPERIMENTAL RESULTS AND DISCUSSION

The experiments were performed at three different oxygen concentrations. The oxygen volume concentrations were 25%, 21% and 19%. The candle was ignited in normal gravity. Then about 30 seconds later it got into microgravity environment. This arrangement is for studying the transient behavior of the candle flame from normal gravity to microgravity. The transient behavior can be seen from Fig. 2-4. Two aspects of the transient behavior will be discussed here. One is the variation in flame shape. The flame shape varies from tear-drop-like to hemispherical very quickly. The transient process takes about 0.2 sec. It is much faster than the variation in flame color. Flame shape depends mainly on aerodynamic feature of the combustion process and flame color depends mainly on chemistry and transport feature of the combustion process. From these experimental observations it is clear that the response of the aerodynamic feature of flame

on gravity is much more sensitive than the response of the chemistry and transport feature of flame on gravity. The chemistry feature is closely related to the supplement of fuel and oxygen. The supply of fuel is based on the capillary action that will not be affected by gravity, so the supply of fuel is almost no difference between in normal gravity and in microgravity. But the supply of oxygen will be quite different in microgravity from that in normal gravity. In normal gravity the fresh air (oxygen) is supplied by convection and diffusion, but the convection plays dominant role. In microgravity the fresh air is supplied by diffusion only. Obviously the supply of fresh air in microgravity is much weaker than that in normal gravity. Meanwhile due to the absence of convection in microgravity the escape of combustion products from the flame zone will be dominated by diffusion only. All these differences will result in weakening the chemical reaction in microgravity, and this change is a gradually progressing transient process. Accordingly, the variation in flame color is much slower than the variation in flame shape in microgravity. Similar transient process can also be seen from Fig.4. During the recovery process the experiment package went back from microgravity to normal gravity. Both the flame shape and the flame color immediately went back to tear-drop-like shape and bright yellow color respectively.

The candle flame temperature measured by using the differential interferometer is shown in Fig. 5. It can be seen that the candle flame temperature in dim blue region is about 1200K. It is lower than 1300K which is the threshold temperature of soot formation. These results might partly verify the question why the microgravity candle flame color is dim blue.

One more interesting question raised from our experimental observations is whether indeed the dim blue color is a symbol of candle flame in microgravity. A series of experiments with oxygen concentrations (25%, 21% and 19%) were arranged to study this problem. It can be seen from Fig. 2-4 that the candle flame keeps bright yellow color throughout the whole experiment with oxygen concentration 25%. However the candle flame first is bright yellow color and then becomes dim blue gradually in the experiments with oxygen concentration 21%. The candle flame color very quickly becomes dim blue in the experiment with oxygen concentration 19%. It is of interest to point out that the candle flame becomes blue relatively faster in the experiment with less dense oxygen concentration. From these experimental observations one might have such impression that candle flame color in microgravity, either yellow or blue, is closely related to the oxygen concentration. Candle flame color, or temperature, depends mainly on the chemical reaction rate. Candle flame in microgravity is a non-propagating, steady-state, pure diffusion flame. The transport rates are driven by diffusion alone in microgravity and are therefore much smaller than the rates in normal gravity which are driven by both buoyant convection and diffusion. So the chemical reaction rate will be lower in microgravity than those in normal gravity. This is why the color of candle flame in microgravity becomes blue. But if the transport rates are relatively fast enough to maintain the chemical reaction with moderate rates. For instance, if the oxygen concentration is large enough the color of candle flame will presumably keep yellow all the time even in microgravity. The preliminary experimental observations have already show the possibility. The capability of our drop tower is limited. The microgravity test time is only 2.8sec. It is too short to verify the speculation. Experiments with much longer microgravity test time are in preparation. Numerical simulation has also been in progress.

REFERENCES

1. Ross, H., Sotos, R. and T'ien, J.S. (1991). "Observations of Candle Flames Under Various Atmospheres in Microgravity". *Combust. Sci. Tech.*. 75, pp.155-160.
2. Dietrich, D. L., Ross, H. D. and T'ien, J. S. (1995). "Candle Flames in Microgravity". Third International Microgravity Combustion workshop, Cleveland, Ohio.
3. Dietrich, D. L., Ross, H. D., Frate, D. T., T'ien, J. S. and Shu, Y. (1997). "Candle Flames in Microgravity". Fourth International Microgravity Combustion Workshop. NASA CP-10194.
4. King, M. K. and Ross, H. D. (1998). "Overview of the NASA Microgravity Combustion Program". *AIAA J.* 36, pp.1337-1345.

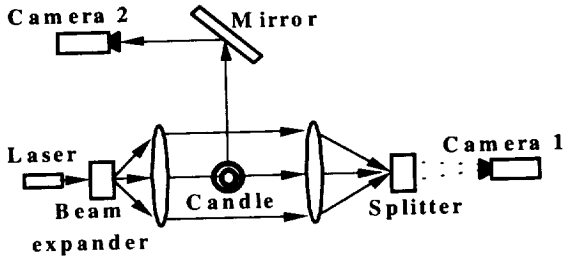

Fig.1 The schematic of differential interferometer apparatus for the measurement of candle flame temperature field

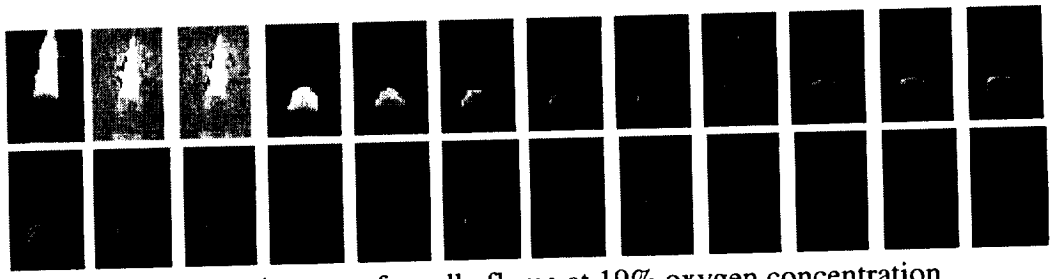

Fig. 2 The images of candle flame at 19% oxygen concentration

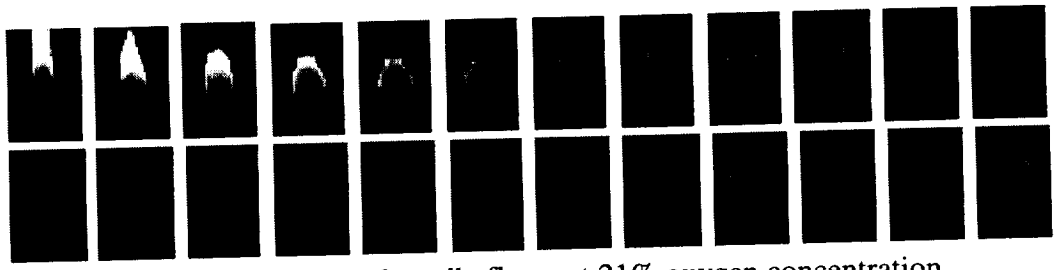

Fig. 3 The images of candle flame at 21% oxygen concentration

Fig. 4 The images of candle flame at 25% oxygen concentration

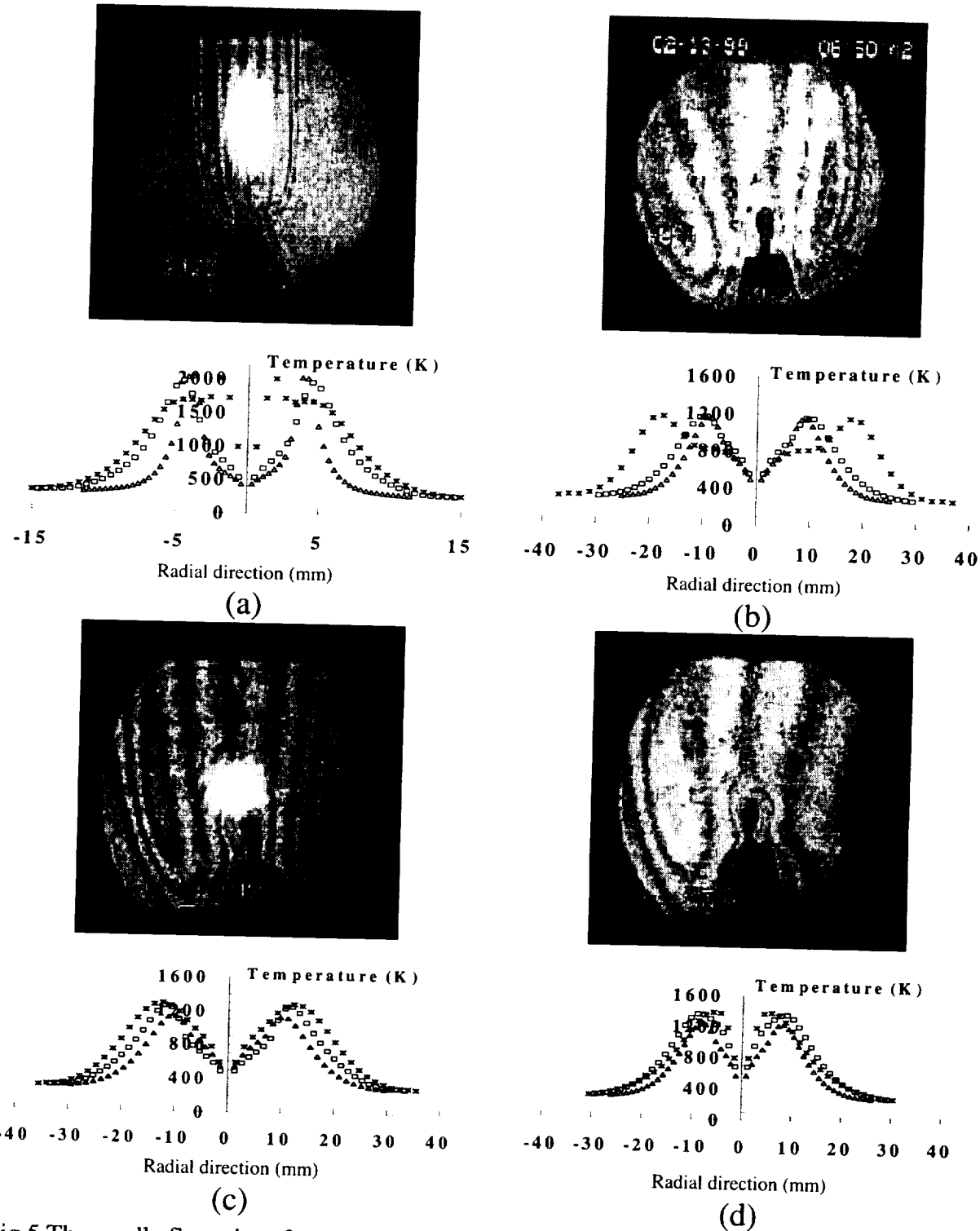

Fig.5 The candle flame interferogram and corresponding temperature distributions of different cross-sections with * --0cm, --1cm, and Δ -- 2cm over the candle tip under conditions of the normal gravity with 21% O_2 (case a) and microgravity with 19% O_2 (case b), 21% O_2 (case c) and 25%O_2 (case d)

OMIT THIS PAGE

Body Force Effects on Flames

S118-29

Electrical Aspects of Flames in Microgravity Combustion

D. Dunn-Rankin and B. Strayer
Mechanical and Aerospace Engineering
University of California Irvine, California 92697-3975.
F. Weinberg and F. Carleton
Department of Chemical Engineering and Chemical Technology
Imperial College of Science, Technology, and Medicine, London, England.

INTRODUCTION

A principal characteristic of combustion in microgravity is the absence of buoyancy driven flows. In some cases, such as for spherically symmetrical droplet burning, the absence of buoyancy is desirable for matching analytical treatments with experiments. In other cases, however, it can be more valuable to arbitrarily control the flame's convective environment independent of the environmental gravitational condition. To accomplish this, we propose the use of ion generated winds driven by electric fields to control local convection of flames. Such control can produce reduced buoyancy (effectively zero buoyancy) conditions in the laboratory in 1-g facilitating a wide range of laser diagnostics that can probe the system without special packaging required for drop tower or flight tests. In addition, the electric field generated ionic winds allow varying gravitational convection equivalents even if the test occurs in reduced gravity environments.

THEORY

The force per unit volume, F, due to buoyancy is given by:

$$F = (\rho - \rho_0)g \approx -\rho_0 g$$

where ρ is the density of the hot gas, g is the acceleration due to gravity, and subscript 0 represents ambient conditions. Balancing this force with that of a wind induced via flame ions mobilized by an applied electric field, produces the relation:

$$\int g(\rho - \rho_0)dx = \int \rho_0 g\left(\frac{T_0}{T} - 1\right)dx = \int \frac{j}{K}dx$$

where K is the mobility of the charge carrier and j is the current density. The current density is related to the imposed field strength. This effect is not electrostatic. The ions do not accelerate in the electric field but transfer their additional momentum to the neutral gas during the collision that follows each mean free path transit. Around the flame, the negative charge carriers tend to be electrons. Electrons do not affect the convective flow substantially because their high mobility ensures they have a relatively low concentration. Hence it is necessary to consider only the positive charge carriers (Lawton and Weinberg, 1969).

EXPERIMENTAL APPARATUS

In the study we used a simple diffusion flame geometry by placing a permeable wire gauze as cathode below a downward facing burner anode--1.7mm o.d. metal capillary (Fig. 1). We increase the electric potential between the anode and cathode until a point of balance is reached. The visual indication of when the point of balance has been achieved is that the flame becomes spherical and symmetrical around the capillary mouth and this is accompanied by its enlargement, the fading of luminosity, and a tendency to extinguish. At a methane flow rate of 0.3cc/s, the

point of balance occurs for a mean field strength of about 100kV/m (approximately 2.4kV over and electrode separation of 2.45cm).

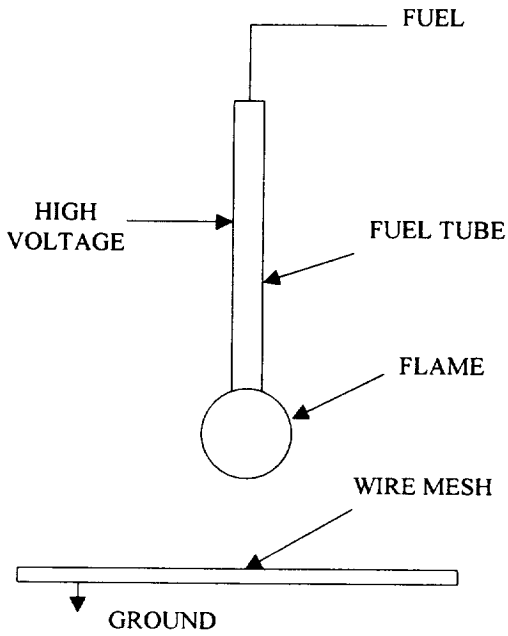

Figure 1. Schematic of the capillary diffusion flame controlled by an electric field

PRELIMINARY RESULTS

The electric field configuration necessary to counteract buoyant flow is greatly simplified for flames that are small relative to the electrode separation, and this technique has been successfully demonstrated for small gas diffusion flames. In these demonstrations, microgravity equivalent conditions could be maintained for longer than 5 seconds (a time equal to that available in a drop tower of over 100 meters). The microgravity condition was indicated by spherical flame shape, a reduction in overall flame luminosity, and a spread in the thermal gradient structure surrounding the flame (Fig. 2) (Carleton and Weinberg, 1996 and Carleton et al., 1998).

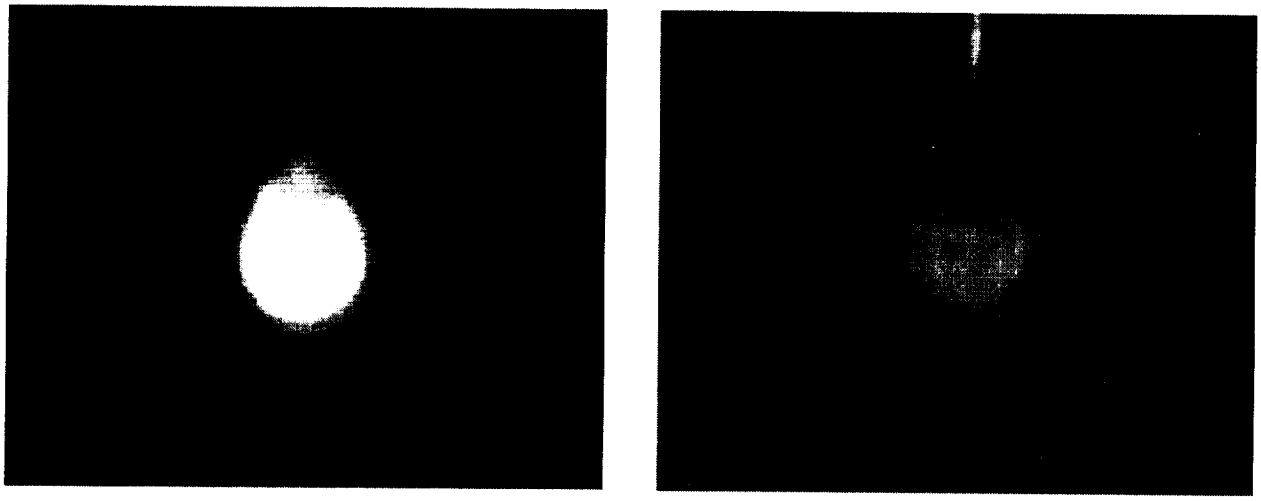

Figure 2. Images of flame under normal gravity and reduced gravity with applied electric field

APPLICATIONS OF ELECTRIC FIELDS

Electric field driven flames have not been the subject of intensive ground-based research of late in part because one can rely on buoyancy driven convection, compressed gas, or mechanically driven convection to dominate the flame behavior at 1-g. In space, however, besides allowing a new mechanism for flame control where other convection sources are absent or expensive, an ion driven wind may have some further advantages. We intend to explore these potential advantages by studying four specific topics involving the applications of electric field in microgravity combustion science.

(1) *Labtop zero-g.* Electric fields can be use to counter buoyancy in 1-g so that ground based-diagnostics can be tested, evaluated, and synthetic zero-g combustion can be probed more intensely than is currently possible in space or drop-tower facilities.

(2) *Gravity ranges.* A range of g conditions can be simulated. While zero-g is an academically interesting situation, there can be further information gleaned from flames at negative g, higher the 1-g, or at intermediate g conditions.

(3) *Flame Control.* Fundamental studies of combustion control are hampered by the convective delay times (i.e. the time it takes for a change in the upstream flow conditions to be felt at the flame) and by buoyancy (i.e. the buoyant convection acts as an upset in the system). Actuating convection at the flame front (the ion source) should allow for improved feedback control response.

(4) *Fire Safety.* It is possible to produce sufficient ion wind to extinguish flames. At 1-g, this extinguishment mechanism is not particularly effective because of the robust flames fed by buoyant convection. At zero-g, this may not be the case, and it is worth investigating the extent to which ion winds can be used to control fires. In addition, electrostatic spraying methods can be used at zero-g to introduce liquid fire suppressants into the gas stream feeding the fire.

ACKNOWLEDGMENTS

The authors would like to acknowledge the support from the National Aeronautics and Space Administration Office of Life & Microgravity Sciences & Applications Microgravity Research Division.

REFERENCES

Carleton, F.B., Dunn-Rankin, D., and Weinberg, F.J. "The Optics of Small Diffusion Flame in Microgravity," 27th International Symposium on Combustion, Boulder, Colorado (1998).

Carleton, F.B. and Weinberg, F.J. "Simulation of microgravity by the application of electric field to flame," Joint meeting of the Portuguese, British, Spanish, and Swedish Sections of The Combustion Institute, April 1-4, Madeira, p.8.5.1 (1996).

Lawton, J. and Weinberg, F.J. *Electrical Aspects of Combustion,* Clarendon Press, Oxford (1969).

S11925

SIMULATION OF COMBUSTION SYSTEMS WITH REALISTIC *g*–JITTER

William E. Mell[1], Kevin B. McGrattan[1], Howard R. Baum[1]

[1]Mail Stop 8640, National Institute of Standards and Technology, Gaithersburg, MD 20899

INTRODUCTION

A number of facilities are available for microgravity combustion experiments: aircraft, drop tower, sounding rocket, space shuttle and, in the future, the international space station (ISS). Acceleration disturbances or *g*–jitter about the background level of reduced gravity exist in all the microgravity facilities. While *g*–jitter is routinely measured, a quantitative comparison of the quality of *g*–jitter among the different microgravity facilities has not been compiled. Low frequency *g*–jitter (< 1 Hz) has been repeatedly observed to disturb a number of combustion systems [1]. Guidelines regarding tolerable levels of acceleration disturbances for a given combustion system have been developed for use in the design of ISS experiments. The validity of these guidelines, however, remains unknown.

In this project, recently funded by NASA, a transient, fully three-dimensional simulation code will be developed to simulate the effects of realistic *g*–jitter on a number of combustion systems. Acceleration disturbances of realistic orientation, magnitude and time dependence will be included in the simulation. Since this is a newly funded project with code development just underway no simulation results will be presented. Instead, first a short review of the relevant background concerning *g*–jitter will be given followed by a section on the proposed technical approach.

BACKGROUND

Many experimental studies and to a lesser degree numerical studies of microgravity combustion have been reported (e.g., ref [5]). Low frequency *g*–jitter (< 1 Hz) has been repeatedly observed to affect a number of combustion systems (including candles, gas jets and flame balls) [1]. To date, only a few quantitative studies have considered the effects of *g*–jitter on combustion (e.g., [2,3,4]). Also, the numerical studies to date are limited in sense that they are not three–dimensional and, therefore, can not account for the complex orientation of realistic *g*–jitter. The *g*–jitter is categorized into three types of acceleration disturbances [6]: quasi–steady accelerations which vary little over periods longer than one minute; oscillatory accelerations which are periodic with a characteristic frequency; and transient accelerations which are nonperiodic and typically have a duration of less than one second. It is important to assess the relevance of *g*–jitter for a proposed combustion experiment in order to choose the appropriate microgravity facility (aircraft, drop tower, sounding rocket, space shuttle, planned international space station). Also, on the space shuttle the amount of *g*–jitter depends on crew activity and scheduled events involving shuttle equipment [6, 7]. An experiment which is deemed to be sensitive to *g*–jitter from these activities should be appropriately scheduled [7].

Struk *et al.* [3] measured variations in the gravity level aboard NASA Lewis Research Center's DC-9 aircraft for experimental rigs which were either attached to the frame of the aircraft or free–floated. For experiments attached to the airframe, reduced *g* levels oscillated between $\pm 0.02\ g_e$ along the vertical axis (ceiling to floor) over a 4 s time period, $\pm 0.01\ g_e$ along the lateral axis (wing–tip to wing–tip) and remained steady at $-0.01\ g_e$ along the longitudinal axis; reduced gravity level duration was 18 s to 20 s. Here g_e is normal gravity. For the free-floated experiments the acceleration level was much smaller, between $\pm 5 \cdot 10^{-4}\ g_e$ along each of the axes. However,

reduced gravity levels lasted for only a maximum of 7 s since time was spent positioning the experimental rig. Note that for experiments attached to the airframe the orientation of the g–jitter was such that numerical simulations of g–jitter effects in this scenario need to be three-dimensional – even if the experimental geometry is not.

Droplets of various sizes were burned on the DC-9 to test the hypothesis of a large diameter extinction limit. The g–jitter effects corrupted the experiments which were attached to the airframe. Both increased soot production and non-spherical flame shapes were associated with g–jitter. Fortunately, the time period of the free-floated experiments was sufficiently long for visible flame extinction to be observed – in support of a large diameter extinction limit.

Using numerical simulations, Kaplan *et al.* [2] and Long *et al.* [4] considered g–jitter effects on axially–symmetric jets. Kaplan *et al.* [2] simulated a laminar ethylene–air noncoflowing jet diffusion flame to better understand the dynamics and behavior of heavily sooting flames in a variety of gravity environments. The g–jitter was investigated by applying a sinusoidal acceleration in the axial direction of amplitude 0.01 g_e and frequency 1 Hz. The flame height was found to oscillate with the 1 Hz frequency. Long *et al.* [4] simulated a coflowing methane/air jet with g varying between $\pm$ 0.01 g_e. The flame structure was found to be insensitive to these levels of acceleration. The differing results of these two studies, in regard to the influence of g–jitter, imply that the relevance of g–jitter is problem dependent and should be assessed for each combustion system.

The quality of the reduced acceleration levels in the DC-9 aircraft (for experiments attached to the airframe) represents the low end among the microgravity facilities. In the significantly lower mean acceleration–level environment of the space shuttle, disturbances to flames have also occurred. For example, premixed flame–ball experiments were conducted during the operation of the fine attitude control thrusters (vernier reaction control system thrusters) and repeated during a period of free drift [1]. Maximum g levels of approximately $7 \cdot 10^{-5}$ g_e along the z–axis due to the thrusters were measured during the experiment. Radiometer measurements clearly showed the experiments were influenced by the operation of the thrusters.

The ultimate input of the many possible acceleration disturbances and their affect on a combustion experiment is unknown. A code that can accurately simulate the effects of the variety of possible g–jitter input on a given combustion experiment would be a valuable resource for both experimental planning and the development of maximum acceptable acceleration levels for different combustion scenarios.

TECHNICAL APPROACH

Although some investigators could simulate certain aspects of g–jitter effects with their own code, there is a need for a more general approach with a code designed for the investigation of the full spectrum of g–jitter effects. This is especially clear when one sees that many microgravity combustion codes are too specialized to realistically simulate g–jitter effects. For example, as was seen above, g–jitter can occur in all three directions. Most simulation codes, however, are one– or two–dimensional (e.g., axially-symmetric). Moreover, enclosure effects are often neglected, but can play a major role in g–jitter phenomena.

The proposed simulation code will be three–dimensional and include enough geometric flexibility to account for the presence of an enclosure. Given current workstation capabilities it is not possible to perform transient, three–dimensional direct numerical simulations with multi–step chemistry and/or fully developed turbulence in physical domains similar in size to microgravity experiments. Instead, suitable, but simple, combustion models (e.g., flame sheet or highly

reduced, finite rate, second order, global Arrhenius kinetics) will be used. The minimum requirement of these models is that g–jitter effects are reliably simulated. To do this it is essential to have the collaboration of experimental investigators.

The authors have assisted in the design of a numerical algorithm used to investigate flame spread on cellulosic samples in a microgravity environment [8,9,10,11,12]. Many of the techniques from this code will be carried over into the proposed code, as well as techniques used by the large eddy simulation (LES) model presently used at NIST to study fires [13,14]. The idea is to combine the combustion physics of the flame spread code with the numerical efficiency and flexibility (in terms of the use of direct solvers and the ability to accommodate a variety of domain geometries, respectively) of LES code. This flexibility will allow experimentalists to vary the location of diagnostic equipment and check for unwanted effects on the flow field.

At solid surfaces, a no-flux condition must be maintained and thermal boundary conditions enforced. This is simple if the solid surface corresponds to the edge of the computational grid, but is not so simple if it is internal. A technique has been developed to enforce the no-flux condition (as well as all other appropriate boundary conditions) at all solid surfaces. Using this method the solid surfaces defining the boundaries of the experimental domain and the diagnostic and experimental equipment can be defined and modified for rectangular or cylindrical domains with internal boundaries approximately aligned with computational grid.

Regarding spatial resolution, consider a middeck glovebox which has a working volume of 45 cm wide, 30 cm deep and 25 cm high. Even for the worst case scenario, where the entire volume was simulated, a 1.25 million grid cell calculation would have grid cell dimensions of three millimeters. Flame spread calculations based on finite rate chemistry that actually resolve the flame structure have required approximately 0.6 mm spatial resolution [11]. Thus, a three millimeter grid simulation would be of moderate spatial resolution more appropriate to a mixture fraction based combustion model [15]. This resolution is expected to be adequate for experimental design (e.g., effects of diagnostic apparatus on the flow field). The spatial resolution applied to the combustion problem can be easily increased by not requiring that the simulation include the entire experimental domain. For some combustion scenarios, therefore, it may be necessary to determine g–jitter effects by simulating, at relatively high resolution, a subvolume of the experimental domain which encompasses the flame under study.

As mentioned above, the authors have been involved in the development and execution of a three–dimensional code which simulates transition from ignition to flame spread [11,12] in microgravity. This is an ongoing project (RITSI) in NASA's microgravity combustion program. Given our familiarity with this project (both the simulation code and the experimental results) we plan to initially focus the development of the code for g–jitter effects on this combustion experiment. This will help us to more quickly identify the physical mechanisms involved in g–jitter effects and the necessary requirements of the simulation code. Extending the capabilities of the simulation code to other combustion systems will done at a later stage in the project.

ACKNOWLEDGMENTS

This study is supported by the NASA Microgravity Science Program under the Inter-Agency Agreement No.C-32070-J.

REFERENCES

1. Howard Ross, NASA Lewis Research Center, personal communication.
2. Kaplan, C.R., Oran, E.S., Kailasanath, K. and Ross, H.D., "Gravitational Effect on Sooting Diffusion Flames," *26th Intnl. Symp. on Comb.*, Combustion Institute, New York, 1996, pp. 1301–1309.
3. Struk, P.M., Dietrich, D.L. and T'ien, J.S., "Large Droplet Combustion Experiment Using Porous Spheres Conducted in Reduced Gravity Aboard an Aircraft – Extinction and the Effects of g–jitter," *Microgravity Sci. Technol.*, Vol. 9, No. 2, 1996, pp. 106–116.
4. Long, M., Walsh, K. and Smooke, M., "Computational and Experimental Study of Laminar Diffusion Flames in a Microgravity Environment," NASA Conference Publication 10194, *Proceedings of the Fourth International Microgravity Combustion Workshop*, Cleveland, OH, May 19–21, 1997, pp. 123–128.
5. NASA Conference Publication 10194, *Proceedings of the Fourth International Microgravity Combustion Workshop*, Cleveland, OH, May 19–21, 1997.
6. DeLombard, R., "Compendeum of Information of Interpreting the Microgravity Environment of the Orbiter Spacecraft," *NASA Technical Memorandum 107032*, Lewis Research Center, Cleveland, OH, August, 1996.
7. DeLombard, R., McPherson, K., Moskowiz, M. and Hrovat, K., "Comparison Tools for Assessing the Microgravity Environment of Missions, Carriers and Conditions," *NASA Technical Memorandum 107446*, Lewis Research Center, Cleveland, OH, April, 1997.
8. Nakabe, K., McGrattan, K.B., Kashiwagi, T. Baum, H.R., Yamashita, H. and Kushida, G., "Ignition and Transition to Flame Spread Over a Thermally Thin Cellulosic Sheet in a Microgravity Environment," *Combust. Flame,* **98**: 361-374 (1994)
9. McGrattan, K.B., Kashiwagi, T., Baum, H.R. and Olson, S.L., "Effects of Ignition and Wind on the Transition to Flame Spread in a Microgravity Environment," *Combust. Flame,* **106**: 377-391, 1996.
10. Kashiwagi, T., McGrattan, K.B., Olson, S.L., Fujita, O., Kikuchi, M. and Ito, K., "Effects of Wind on Localized Radiative Ignition and Transition to Flame Spread in Microgravity," *26th Intnl. Symp. on Combust.*, 1345-1352, 1996.
11. Mell, W.E. and Kashiwagi, T., "Dimensional Effects on the Transition from Ignition to Flame Spread in Microgravity," *27th Intnl. Symp. on Combust.*, Combustion Institute, New York, to appear.
12. Kashiwagi, T., Mell, W.E., Baum, H.R. and Olson, S., "Ignition, transition, flame spread in multidimensional configurations in microgravity," *Fifth International Microgravity Combustino Workshop*, May 18–20, 1999, Cleveland, OH.
13. Baum, H.R., McGrattan, K.B. and Rehm, R.G., "Three Dimensional Simulations of Fire Plume Dynamics," *Fire Safety Science – Proceedings of the Fifth International Symposium*, IAFSS, Boston, pp. 511–522, 1997.
14. McGrattan, K.B., Baum, H.R. and Rehm, R.G., "Large Eddy Simulations of Smoke Movement," *Fire Safety Journal*, **20**, March 1998, pp. 161-178.
15. Mell, W.E., McGrattan, K.B. and Baum, H.R., "Numerical simulation of combustion in fire plumes," *26th Intnl. Symp. on Combust.*, Combustion Institute, New York, 1996, pp. 1523–1530.

5120-29

FLAME SPREAD AND EXTINCTION IN PARTIAL-GRAVITY ENVIRONMENTS

K. R. Sacksteder,[1] P. V. Ferkul,[2] and J. S. T'ien[3]

[1] Microgravity Science Division, NASA Glenn Research Center, 21000 Brookpark Road, Cleveland, OH 44135, kurt.sacksteder@grc.nasa.gov, [2] National Center for Microgravity Research, NASA Glenn Research Center, 21000 Brookpark Road, Cleveland, OH 44135, [3] Department of Mechanical and Aerospace Engineering, Case Western Reserve University, Cleveland, OH 44106

INTRODUCTION

Considerable progress has been made in understanding the mechanisms of spreading flames under certain conditions, nearly all under the influence of normal Earth gravity. Recently, several investigators have studied some aspects of flame spread in purely forced flows in microgravity. However, very few have considered (especially experimentally) purely-buoyant flow influences, using gravity as a variable. In addition to the scientific interest in understanding how variable gravity affects flame spread in purely-buoyant flow, prospective human exploration of the Moon and Mars provides an incentive to obtain practical knowledge for use in fire-safety related engineering and mission operations in those partial-gravity environments.

The purpose of this research effort is to conduct a focused experimental effort to observe the behavior of flames spreading both upward (concurrent flow) and downward (opposed flow) over thin fuels in partial-gravity environments, and to extend an existing numerical model of flame spread to predict flammability and flame spread behavior in these two regimes. A significant aspect of the experimental effort is to use a special device to improve the simulated partial-gravity environment achievable aboard reduced-gravity aircraft facilities.

FLAME STRUCTURE

The structure of a flame spreading over a solid fuel in the presence of a flow can be divided into three zones. The flame encounters the incoming flow in the *flame stabilization zone* where upstream diffusion must balance convective effects to sustain the flame position. Underlying this convective-diffusive balance are chemical kinetics which, under different circumstances, may be finite either with respect to reactant residence time in the flame stabilization zone or because of heat-loss rates from the flame. Nearby in the *pyrolysis zone*, fuel is vaporized by heat supplied by the flame, then transported to the flame by Stefan flow, diffusion (primarily in opposed flows), and convection (primarily in concurrent flows).

In the *fuel preheat zone* the solid is heated from an initial temperature to the temperature where pyrolysis begins. In opposed-flow spreading the fuel is preheated by upstream diffusion, aided in some instances by radiation. Since fuel preheating in opposed-flow spreading requires the same convective-diffusive balance needed for flame stabilization in the flow, these two zones overlap, simplifying the characterization of the flame (only one length scale is involved). In concurrent-flow spreading the fuel is preheated by convection and radiation, generally downstream and separated from the stabilization zone. The stabilization and preheat zones may propagate at different rates, allowing flames to grow, accelerate or become turbulent. Transport and chemistry occur over multiple length scales, complicating the characterization of the flame.

The magnitude of the relative velocity between the flame and oxidizer flow affects flame spread speed and flame extinction phenomena generally because of convective transport rates of heat, reactants (oxygen and vaporized fuel) and combustion products - especially where convective

transport is comparable to rates of heat and mass diffusion, chemical reactions in the solid and gas, and radiative interactions between the fuel, the flame and the surroundings. Increasing flow velocities tend to compress the convective-diffusive flame stabilization and opposed-flow fuel-preheat zones but to lengthen and accelerate concurrent flow flames. Low-speed flows provide a regime for flame spreading where these length scales may be closer in size; and the flow remains laminar even in concurrent flow. Under the influence of normal Earth gravity, access to low speed flow near a spreading flame is limited because of gravity-induced buoyant convection.

Since forced flows are primarily independent of the flame while buoyant flows are closely coupled, distinct flow patterns result that affect flame structure and the transport mechanisms that control flame spread characteristics and flammability boundaries. Experimental comparisons of flame spread in purely-buoyant and purely-forced flows of controllable velocity can be achieved using reduced-gravity environments. While some observations of flame spread in purely-forced flows in microgravity exist,[1,2,3] only our experiments in partial-gravity environments, summarized below, provide observations of flames in reduced-speed, purely-buoyant flows.[4]

From a theoretical standpoint, though, computed results based on *two-dimensional* models of steady flame spread in concurrent flow are available for both the forced and buoyant cases.[5,6] A comparison can be made between cases where the flow velocities in the flame stabilization zones are similar (approximately 7 cm/sec). In the forced-flow case, the flow velocity increases because of thermal expansion then decreases because of viscosity, with diverging streamlines downstream. In the buoyant case, the flow accelerates continuously to a much greater speed downstream. The streamlines first deflect away from the centerline due to thermal expansion, but then are drawn toward the fuel surface as a result of the buoyant acceleration. These different downstream flow patterns result in different flame shapes and sizes. In the forced-flow case the flame is shorter and wider while the flame is longer and closer to the surface for the buoyant-flow case. Consequently, the buoyant flame has a longer pyrolysis zone and a higher spread rate than the forced-flow flame despite the fact that in the stabilization zone the flows are similar.

In contrast, opposed-flow flame spreading occurs in the convective-diffusive flame stabilization and fuel preheating zones. Hence, when the forced and buoyant velocities are similar there, the two cases will have a similar flame spread rate.[7]

FLAME SPREAD AND EXTINCTION IN LOW-SPEED FLOWS

Purely forced flows in microgravity environments have been used to predict[8,9,5] and demonstrate a flammability boundary (in terms of atmospheric oxygen content vs. flow velocity) with a "U" shape for non-spreading flames,[10] and for flames spreading in opposed[1] and concurrent[2] flows. The shape of the boundary suggests two merging branches with distinct limiting mechanisms, viz. a residence-time limit (i.e., a minimum Damkohler number) in higher-speed flows and a radiative-quenching branch in lower-speed flows. A similar flammability boundary for downward burning in purely-buoyant flow in variable gravity has been suggested by two modeling efforts, one focusing on enhanced oxygen atmospheres,[7] the other on flame radiation losses.[11]

Flame spreading experiments in purely-buoyant opposed flow have been conducted using NASA parabolic aircraft to obtain partial-gravity accelerations.[4] Thin tissue samples were ignited to burn downward in oxygen fractions from 13% to 21% (balance nitrogen) in one atmosphere and simulated gravity levels of 0.05 to 0.60 g/g_{Earth}. Figure 1 shows the downward burning test conditions and indicates the approximate flammability boundary. The plot includes

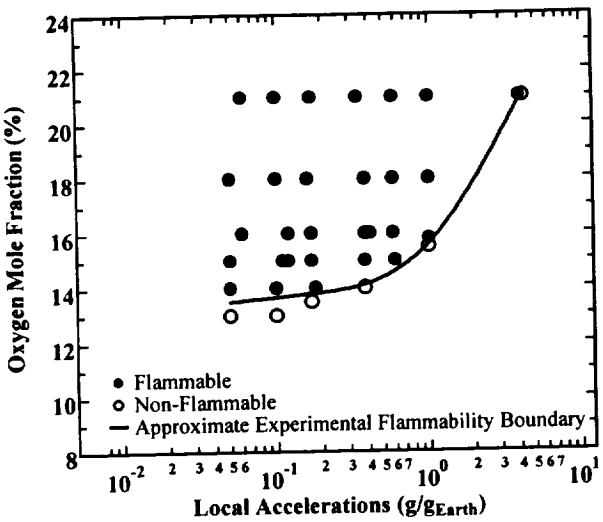

Figure 1 Flammability Boundary for Downward Burning of Thin Cellulose Sheets in Purely Buoyant Flows

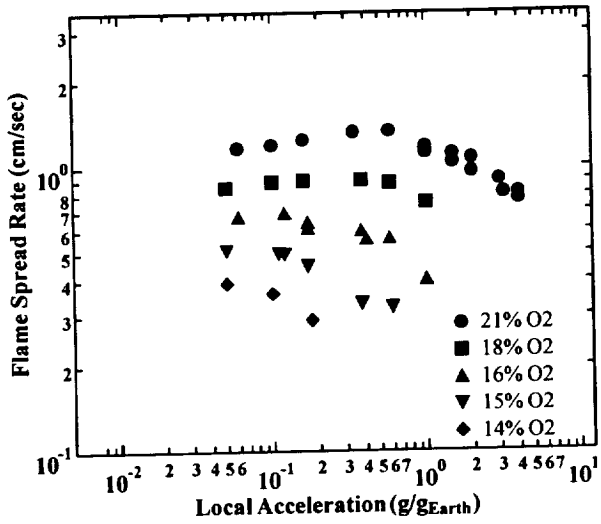

Figure 2 Downward Flame Spread Rates for Thin Cellulose Sheets in Purely Buoyant Flows

high-gravity centrifuge data obtained for a similar fuel.[12] As the gravity level (and therefore the buoyant-flow velocity) is reduced, the test material becomes flammable at lower atmospheric oxygen fractions; consistent with other Damkohler number limited flammability boundaries.[12,13] Figure 2 shows the measured flame-spread rates of the tests indicated by Fig. 1. Spread rates at 18% and 21% oxygen increase with reductions in gravity from the flammability limit condition, but reach a maximum value and fall with further reductions in gravity. The change in slope of the spread rate curves is consistent with an increasing influence of radiative losses as the buoyant flow speed is reduced.[5-11] Correlation of these spread rate data with Damkohler number and radiative effects has been successful,[4,14] but the expected low-speed radiative quenching limit has not yet been observed. Further clarification of these radiative effects await access to lower but finite (and steady) levels of partial gravity.

IMPROVED AIRCRAFT-BASED REDUCED-GRAVITY ENVIRONMENT

Until recently, reduced-gravity aircraft testing was limited by the presence of seemingly random acceleration noise, called g-jitter, measured to be on the order of 10^{-2} g/g_{Earth}. The Canadian Space Agency has developed technology for the reduction of g-jitter experienced by aircraft experiments. Their Large Microgravity Isolation Mount, LMIM, has demonstrated reductions to the order of 10^{-4} g/g_{Earth} for up to 10 seconds. A new version of the LMIM is being developed in conjunction with this flame spread research to accommodate larger experiments and provide simulations of steady, selectable gravity levels between 10^{-4} and 10^{-2} g/g_{Earth}.

With this capability, we will extend reduced-gravity aircraft useage for partial-gravity experiments below 0.05 g/g_{Earth}. First, a low-speed quenching branch may be observed, completing the opposed-flow flammability boundary suggested in Fig. 1, and the direct comparisons between flames spreading in purely-forced and purely-buoyant flows are to be completed. Moreover, in this extended partial-gravity regime, new studies of concurrent-flow (upward) flame spreading are to be conducted, complementing purely-forced concurrent-flow flame spreading tests we are pursuing in another program. Upward burning studies in partial

gravity will establishing a direct link between normal-gravity material flammability screening tests and reduced-gravity material behavior.

ACKNOWLEDGEMENT

The authors are grateful for the support of this work by NASA Headquarters Microgravity Research Division.

REFERENCES

1. Olson, S.L., Ferkul, P.V., and T'ien, J.S., "Near-Limit Flame Spread over a Thin Solid Fuel in Microgravity," *Twenty-Second Symposium (International) on Combustion*, The Combustion Institute, pp. 1213-1222 (1988).
2. Grayson, G. D., Sacksteder, K. R., Ferkul, P. V., and T'ien, J. S., "Flame Spreading Over a Thin Solid in Low Speed Concurrent Flow: Drop Tower Experimental Results and Comparison with Theory," *Microgravity Science and Technology*, vol.VII, no. 2, pp. 187-195 (1994).
3. Ramachandra, P.A., Altenkirch, R.A., Bhattacharjee, S., Tang, L., Sacksteder, K.R., and Wolverton, M.K., "The Behavior of Flames Spreading over Thin Solids in Microgravity," *Twenty-Fifth Symposium (International) on Combustion, Combustion and Flame*, Vol. 100, pp. 71-84 (1995).
4. Sacksteder, K. R. and T'ien, J. S., "Buoyant Downward Diffusion Flame Spread and Extinction in Partial-Gravity Accelerations," *Twenty-Fifth Symposium (International) on Combustion*, The Combustion Institute, pp. 1685-1692 (1994).
5. Jiang, C.-B., "A Model of Flame Spread Over a Thin Solid in Concurrent Flow with Flame Radiation," Ph.D. Thesis, Case Western Reserve University, Cleveland, Ohio (1995).
6. Jiang, C.-B., T'ien, J.S., and Shih, H.Y., "Model Calculation of Steady Upward Flame Spread Over a Thin Solid in Reduced Gravity," *Twenty-Sixth Symposium (International) on Combustion*, The Combustion Institute, pp. 1353-1360 (1996).
7. West, J., Bhattacharjee, S., and Altenkirch, R.A., "A Comparison of the Roles Played by Natural and Forced Convection in Opposed-Flow Flame Spreading," *Combustion Science and Technology*, Vol. 83, pp. 233-244 (1992).
8. T'ien, J. S., "Diffusion Flame Extinction at Small Stretch Rates: The Mechanism of Radiative Loss," *Combustion and Flame*, vol. 65, pp. 31-34 (1986).
9. Ferkul, P. V. and T'ien, J. S., "A Model of Low-Speed Concurrent Flow Flame Spread Over a Thin Solid," *Combustion Science and Technology*, Vol. 99, pp. 345-370 (1994).
10. Foutch, D.W., "Size and Shape of Solid Fuel Diffusion Flames in Very Low Speed Flows," M.S. Thesis, Case Western Reserve University, *NASA CR-179576* (1987).
11. Chen, C.H., and Cheng, M.C., "Gas-Phase Radiative Effects on Downward Flame Spread in Low Gravity," *Combustion Science and Technology*, 97, pp. 63-83 (1994).
12. Altenkirch, R. A., Eichorn, R., and Shang P. C., "Buoyancy Effects on Flames Spreading Down Thermally Thin Fuels," *Combustion and Flame*, Vol. 37, pp. 71-83 (1980).
13. Fernandez-Pello, A. C. and Hirano, T., "Controlling Mechanisms of Flame Spread," *Combustion Science and Technology*, vol. 32, pp. 1-31 (1983).
14. Sacksteder, K. R., Pettegrew, R. D. and T'ien, J. S., "Flame Spreading over Thin Fuel Samples in Partial-Gravity Environments," 36th AIAA Aerospace Sciences Meeting, AIAA-98-0567 (1998).

OMIT TO END

AUTHOR INDEX

Workshop Check-In and Late Registration: Monday, May 17th, 5:00-7:00 pm, and Tuesday, May 18th, beginning 7:00 am

Tuesday, May 18th

8:00	Plenary Chair: D. Urban. Welcoming Remarks: Don Campbell, Jack Salzman, Simon Ostrach, Chung K. Law, and Merrill King Keynote Address: Kathryn Clark, Senior Scientist, International Space Station	
9:45	Break	
	Flammability/ Extinction Chair: T. Kashiwagi Ballroom East	Laminar Flames Chair: P. Sunderland Ballroom West
10:00	1 T'ien, James S.	10 Ronney, Paul D.
10:25	2 Dryer, Fred L.	11 Miller, Fletcher J.
10:50	3 Egolfopoulos, Fokion N.	12 Faeth, Gerard M.
11:15	4 Altenkirch, Robert A.	13 Abbud-Madrid, Angel
11:40	5 Nayagam, Vedha	14 Kawakami, Tadashige
12:05	Lunch	
	Flammability/ Extinction Chair: R. Friedman Ballroom East	Particle Clouds/ Dusts Chair: TBD Ballroom West
1:15	6 Fernandez-Pello, A. Carlos	15 Egolfopoulos, Fokion N.
1:40	7 Sanchez-Tarifa, Carlos	16 Jarosinski, Jozef
2:05	8 Atreya, Arvind	17 Lee, John H.S.
2:30	9 Ivanov, Anatoliy	18 Gokalp, Iskender
2:55	Break	
	Combustion Synthesis and Soot Chair: R. VanderWal Ballroom East	Flame Stability Chair: M. Smooke Ballroom West
3:15	19 Faeth, Gerard M.	25 Buckmaster, John
3:40	20 Howard, Jack B.	26 Wichman, Indrek S.
4:05	21 Axelbaum, Richard L.	27 Matalon, Moshe
4:30	22 Moore, John J.	28 Margolis, Stephen B.
4:55	23 Matkowsky, Bernard J.	29 Pearlman, Howard
5:20	24 Sytschev, Alexander Evgen'evich	30 Kailasanath, Kazhikathra
6:00	Social Hour/Cash Bar, until 7:30	

Wednesday, May 19th

8:00	Plenary Keynote Address: To Be Announced	
9:15	Break	
	Laminar Flames Chair: S. Gokoglu Ballroom East	Combustion Diagnostics Chair: P. Greenberg Ballroom West
9:30	31 Law, Chung K.	41 Silver, Joel A.
9:55	32 Fendell, Frank	42 Koenig, Jens
10:20	33 Dietrich, Daniel	43 Fernandez-Pello, A. Carlos
10:45	34 Sohrab, Siavash H.	44 Kane, Daniel J.
11:10	35 Torero, Jose L.	45 Massoli, Patrizio
11:35	36 Butler, Kathryn M.	46 Misra, Prabhakar
12:00	Lunch	
	Laminar Flames Chair: D. Stocker Ballroom East	Metals Combustion Chair: J. Howard Dolder-Hassler Room
1:15	37 Chen, Lea Der	47 Branch, Melvyn C.
1:40	38 Joulain, Pierre	48 Dreizin, Edward L.
2:05	39 Long, Marshall B.	49 Meinkoehn, Dirk
2:30	40 Agrawal, Ajay K.	50 Assovskiy, Igor G.
2:55	Break	
3:15	Poster Session, until 5:30 Ballroom West Papers 81 - 120 Flammability and Extinction, Combustion Diagnostics, Propellants and Rockets, Combustion Synthesis, Laminar Diffusion Flames, Turbulent Flames, Droplet Combustion, Soot Processes, Heterogeneous Diffusion Flames, Body Force Effects on Flames	
6:15	Shuttle Buses between Sheraton and Great Lakes Science Center - Service Begins	
6:30	Reception, IMAX Movie and Dinner at the Great Lakes Science Center - Speaker: Dr. Shannon Lucid, Shuttle/Mir Astronaut	

Thursday, May 20th

8:00	Plenary - Chair: H. Ross. NASA Research Announcement and Plans for the International Space Station: Merrill King, David Urban, Karen Weiland (NASA) Space Station Utilisation Initiatives of the European Space Agency ESA/ESTEC: Ewald Kufner (ESA)	
9:15	Break	
	Droplet and Particle Combustion Chair: R. Santoro Ballroom East	Turbulent Combustion Chair: Z. Yuan Dolder-Hassler Room
9:30	51 Williams, Forman A.	57 Bahadori, M. Yousef
9:55	52 Cheliah, Harsha K.	58 Hegde, Uday
10:20	53 Shaw, Benjamin D.	59 Cheng, Robert K.
10:45	54 Choi, Mun Young	60 Driscoll, James F.
11:10	55 Avedisian, C. Thomas	61 Dahm, Werner J. A.
11:35	56 Tanabe, Mitsuaki	62 Elghobashi, Said
12:00	Lunch Speaker to be announced	
	Flame Spread Chair: P. Ferkul Ballroom East	Sprays and Droplet Arrays Chair: K. Weiland Dolder-Hassler Room
1:30	71 Altenkirch, Robert A.	63 Dietrich, Daniel L.
1:55	72 Ross, Howard D.	64 Ruff, Gary A.
2:20	73 Sirignano, William A.	65 Nomura, Hiroshi
2:45	74 Tashtoush, Ghassan	66 Yoshizaki, Takuo
3:10	Break	
	Flame Spread Chair: S. Olson Ballroom East	High Pressure Combustion Chair: J. Sung Dolder-Hassler Room
3:30	75 Kashiwagi, Takashi	67 Williams, Forman A.
3:55	76 Ronney, Paul D.	68 Kadota, Toshikazu
4:20	77 Fujita, Osamu	69 Kobayashi, Hideaki
4:45	78 Nagata, Harunori	70 Gokalp, Iskender